(NASA-TM-X-61008) LAUNCH VEHICLE NO. 3 FLIGHT EVALUATION (NASA) 231 p

N79-76261

Unclas
00/15 11086

[redacted] 43

MSC-G-R-65-2 (NASA)
Supplemental Report 2

No. 6 [redacted] (CATEGORY)
[redacted]

# GEMINI LAUNCH VEHICLE

GEMINI

# LAUNCH VEHICLE NO. 3

# FLIGHT EVALUATION (U)

Engineering Report 13227-3

Published by National Aeronautics and Space Administration, Manned Spacecraft Center, Houston, Texas as Supplement 2 to the Gemini Program Mission Report GT-3, MSC-G-R-65-2 (NASA)

May 1965

PREPARED BY

MARTIN COMPANY

UNDER CONTRACT NUMBER
AF 04(695)-394
PRIORITY DX-A2

FOR

SPACE SYSTEMS DIVISION
AIR FORCE SYSTEMS COMMAND
UNITED STATES AIR FORCE
Los Angeles, California

CLASSIFICATION CHANGE
To UNCLASSIFIED
By authority of GDS-GP-4
Changed by L. Shirley Date 10-75
Classified Document Master Control Station, NASA
Scientific and Technical Information Facility

[redacted]

This document contains information affecting the National Defense of the United States within the meaning of the Espionage Laws, Title 18, U.S.C., Sections 793 and 794, the transmission or revelation of which in any manner to an unauthorized person is prohibited by law.

Group 4
Downgraded at 3-year intervals; declassified after 12 years. DOD DIR 5200.10.

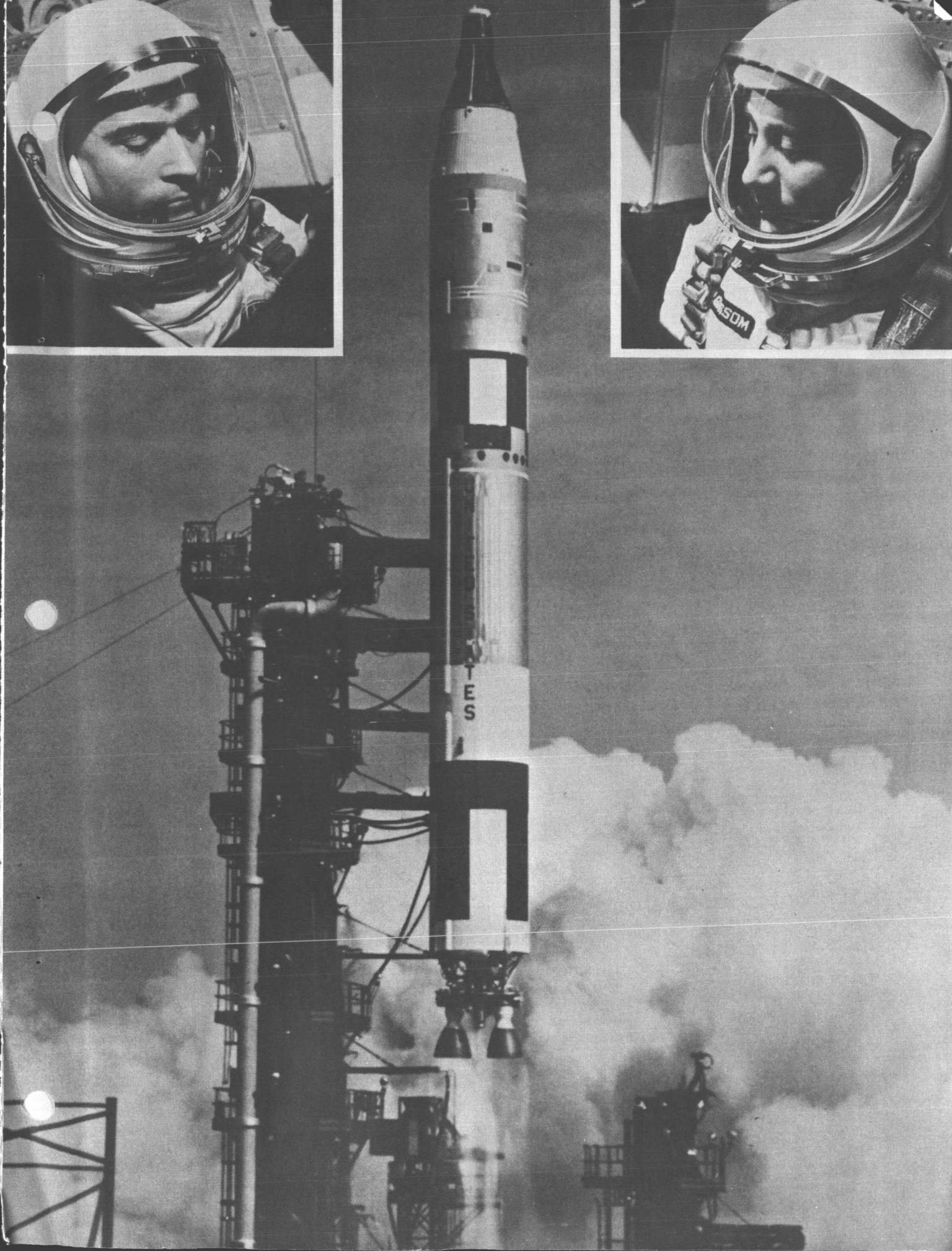
ASOM

C68-3662

ER 13227-3 ~~CONFIDENTIAL~~ May 1965

GEMINI LAUNCH VEHICLE

GEMINI

# LAUNCH VEHICLE NO. 3

# FLIGHT EVALUATION (U)

Approved by

L. J. Rose
Assistant Technical Director
Test Evaluation

W. D. Smith
Technical Director

NOTICE — THIS DOCUMENT CONTAINS INFORMATION AFFECTING THE NATIONAL DEFENSE OF THE UNITED STATES WITHIN THE MEANING OF THE ESPIONAGE LAWS, TITLE 18, U.S.C., SECTIONS 793 AND 794, ITS TRANSMISSION OR THE REVELATION OF ITS CONTENTS IN ANY MANNER TO AN UNAUTHORIZED PERSON IS PROHIBITED BY LAW.

GROUP 4
Downgraded at 3 year intervals; declassified after 12 years

Prepared by

Baltimore

For

~~CONFIDENTIAL~~

## FOREWORD

This report has been prepared by the Gemini Launch Vehicle Program Test Evaluation Section of the Martin Company, Baltimore Division. It is submitted to the Space Systems Division, Air Force Systems Command, in compliance with Contract AF04(695)-394.

This report presents the results of the performance evaluation of the Gemini Launch Vehicle used on the GT-3 mission and is published as Supplement 2 to the NASA Gemini Program Mission Report GT-3, MSC-G-R-65-2.

# CONTENTS


| | | Page |
|---|---|---|
| | Foreword | ii |
| | Summary | vii |
| I. | Introduction | I-1 |
| II. | Systems Performance | II-1 |
| | A. Trajectory Analysis | II-1 |
| | B. Payload Capability | II-42 |
| | C. Staging | II-42 |
| | D. Weight Statement | II-45 |
| III. | Propulsion System | III-1 |
| | A. Engine Subsystem | III-1 |
| | B. Propellant Subsystem | III-19 |
| | C. Pressurization Subsystem | III-65 |
| | D. Environmental | III-68 |
| IV. | Flight Control System | IV-1 |
| | A. Stage I Flight | IV-1 |
| | B. Stage II Flight | IV-9 |
| | C. Post-SECO Flight | IV-13 |
| V. | Hydraulic System | V-1 |
| | A. Stage I | V-1 |
| | B. Stage II | V-5 |
| VI. | Guidance Systems | VI-1 |
| | A. Radio Guidance System Performance | VI-1 |

CONTENTS (continued)


| | | Page |
|---|---|---|
| | B. Spacecraft Inertial Guidance System Ascent Performance | VI-6 |
| VII. | Electrical System | VII-1 |
| | A. Configuration | VII-1 |
| | B. Countdown and Flight Performance | VII-1 |
| VIII. | Instrumentation System | VIII-1 |
| | A. Airborne Instrumentation | VIII-1 |
| | B. Landline Instrumentation | VIII-3 |
| IX. | Range Safety and Ordnance Systems | IX-1 |
| | A. Command Control Receivers | IX-1 |
| | B. MISTRAM System | IX-2 |
| | C. Ordnance System | IX-3 |
| X. | Malfunction Detection System | X-1 |
| | A. Configuration | X-1 |
| | B. System Performance | X-1 |
| XI. | Crew Safety | XI-1 |
| | A. Prelaunch Simulations | XI-1 |
| | B. Slow Malfunctioning Monitoring | XI-10 |
| XII. | Airframe System | XII-1 |
| | A. Structural Loads | XII-1 |
| | B. Vibration Environment | XII-35 |
| | C. Structural Integrity Program | XII-37 |
| | D. Longitudinal Vibrations (POGO) | XII-53 |

CONTENTS (continued)


| | | Page |
|---|---|---|
| XIII. | AGE and Facilities | XIII-1 |
| | A. Mechanical AGE | XIII-1 |
| | B. Electrical AGE | XIII-1 |
| | C. Master Operations Control Set (MOCS) | XIII-2 |
| | D. Pad Damage | XIII-2 |
| XIV. | Reliability | XIV-1 |
| | A. Environmental Criteria | XIV-1 |
| | B. Probability Estimates | XIV-2 |
| XV. | Range Data | XV-1 |
| | A. Data Disposition | XV-1 |
| | B. Film Coverage | XV-5 |
| XVI. | Prelaunch and Countdown Operations | XVI-1 |
| | A. Prelaunch Summary | XVI-1 |
| | B. Countdown Summary | XVI-2 |
| XVII. | Configuration Summary | XVII-1 |
| | A. Launch Vehicle Systems Description | XVII-1 |
| | B. Major Components | XVII-12 |
| XVIII. | References | XVIII-1 |

## SUMMARY

On 23 March 1965, Gemini-Titan No. 3 (GT-3) was launched successfully from Complex 19, Cape Kennedy, Florida. Launch vehicle/spacecraft separation was completed 359.386 seconds after liftoff. Spacecraft re-entry was successful after completion of three orbits.

The countdown was picked up at 0700 hours, Greenwich Mean Time (GMT) and proceeded to T-35 minutes (1325 hours GMT), at which time a 24 minute hold was initiated due to a minor leak. The count was resumed at 1349 hours GMT and continued without incident through liftoff at 1424 hours GMT. The insertion into Earth orbit was accomplished with greater precision than that demonstrated on GT-1, and insertion parameters were well within specified limits. All test objectives for the launch vehicle were achieved.

Stages I and II engines operated satisfactorily throughout powered flight. Stage I burning time was 155.805 seconds with shutdown initiated by oxidizer depletion. The Stage II engine was terminated by a guidance command after 181.314 seconds. The redundant engine shutdown system (RESS) was flown for the first time on GLV-3 with satisfactory results.

The flight control system (FCS) maintained satisfactory vehicle stability during Stages I and II flight. The roll and pitch programs were executed properly. During peak wind disturbances, vehicle rates never exceeded 1 deg/sec and the maximum attitude error was 1.7 degrees. The maximum rate and attitude that occurred during staging did not exceed 2 deg/sec and 1.8 degrees, respectively.

The radio guidance system (RGS) performance was satisfactory. The rate and pulse beacons properly maintained lock throughout flight. Pitch and yaw commands were received by the decoder and properly transmitted to the FCS. The SECO signal was properly transmitted by the decoder.

The hydraulic system operated satisfactorily during launch operations and flight.

The electrical system functioned as designed throughout the launch countdown and flight. Power transfer to airborne batteries was comparatively smooth and liftoff occurred without incident.

All channels of the PCM and FM instrumentation systems functioned properly throughout flight, resulting in 100% data acquisition. The landline instrumentation system functioned satisfactorily prior to and up to

liftoff. All airborne instrumentation hold functions monitored in the blockhouse remained within specification throughout the countdown.

The ordnance system umbilical dropweight release, propulsion system prevalves, explosive launch nuts and stage separation nuts operated as designed. The performances of the Advanced Communications, Inc., command control receivers and the General Electric MISTRAM transponder were satisfactory.

Malfunction detection system (MDS) performance during preflight checkout and flight was satisfactory. There were no switchover commands during the flight.

The flight environment encountered by GT-3 was within the launch vehicle design requirements. Flight loads were well within the structural capabilities of the launch vehicle.

The longitudinal oscillation (POGO) was the lowest measured and was considered insignificant by the astronauts. At Station 280, the peak value was 0.13 g zero-to-peak at a frequency of 13.5 cps.

The crew safety monitoring operation was excellent. The only monitoring action required during flight was to inform RETRO of a buildup in negative lateral velocity that occurred between LO + 80 seconds and BECO for possible impact on the Stage I ground tracking.

The precount operation progressed with no problems. The AGE and facilities operated without incident during the countdown.

Engine blast and heat damage to the launch stand was minor and less than that from the GT-1 and GT-2 launches.

GLV-3 Primary Test Objectives and Results

| | Objective | Flight Results |
|---|---|---|
| P-1 | Evaluate GLV system performance in placing a Manned Gemini spacecraft into prescribed orbit | Orbit insertion was within the predicted tolerances for V, h and $\gamma$; GLV system performance was satisfactory |
| P-2 | Evaluate the second-stage redundant engine (gas generator) shutdown system (RESS) including effect on SECO cutoff impulse | RESS operated as designed; post-SECO cutoff impulse was less than that on GLV-1 and GLV-2 |
| P-3 | Evaluate and verify satisfactory performance of the malfunction detection system (MDS) and associated flight malfunction monitoring operations at MCC | MDS operated as planned; slow malfunction monitoring operations at MCC were performed satisfactorily |
| | GLV-3 Secondary Test Objectives and Results | |
| S-1 | Demonstrate ability to load propellants to the weight and temperature limits imposed by payload performance and GLV requirements | Achieved; tanks were loaded to within required tolerances of weight and temperature |
| S-2 | Evaluate launch countdown time and procedure for applicability in support of the rendezvous missions | One minor hold (24 minutes) was experienced; procedures were accomplished on schedule |
| S-3 | Evaluate GLV longitudinal oscillation during flight | Maximum vibration was 0.13 g zero-to-peak at LO + 140 seconds (Station 280) |
| S-4 | Evaluate GLV bending moments and aerodynamic heating effects during powered flight | Structural loads were well within design capability; maximum skin temperature was 258.5° F at Station 377 |
| S-5 | Qualitatively evaluate the secondary flight control system (FCS) with available instrumentation | The secondary FCS was capable of maintaining stabilized flight should it have been required to assume control |

# I. INTRODUCTION

This report presents an evaluation of the systems performance of Gemini Launch Vehicle No. 3 (GLV-3) during the launch and flight of Gemini-Titan No. 3 (GT-3) from Complex 19, Cape Kennedy Test Center, Florida, on 23 March 1965.

GT-3 was the first manned flight in the Gemini program, with astronauts V. I. Grissom and J. W. Young aboard the spacecraft. The GT-3 three-orbit mission was completed successfully. The next Gemini mission (GT-4) will be a four-day orbital flight.

The GT-3 vehicle was comprised of a two-stage GLV, essentially the same as GLV-2, and a spacecraft. The spacecraft was injected into an elliptical orbit of 87/121 nautical miles. R

Significant events experienced by, and tests performed on, GLV-3 at Complex 19, ETR, are summarized in Fig. I-1.

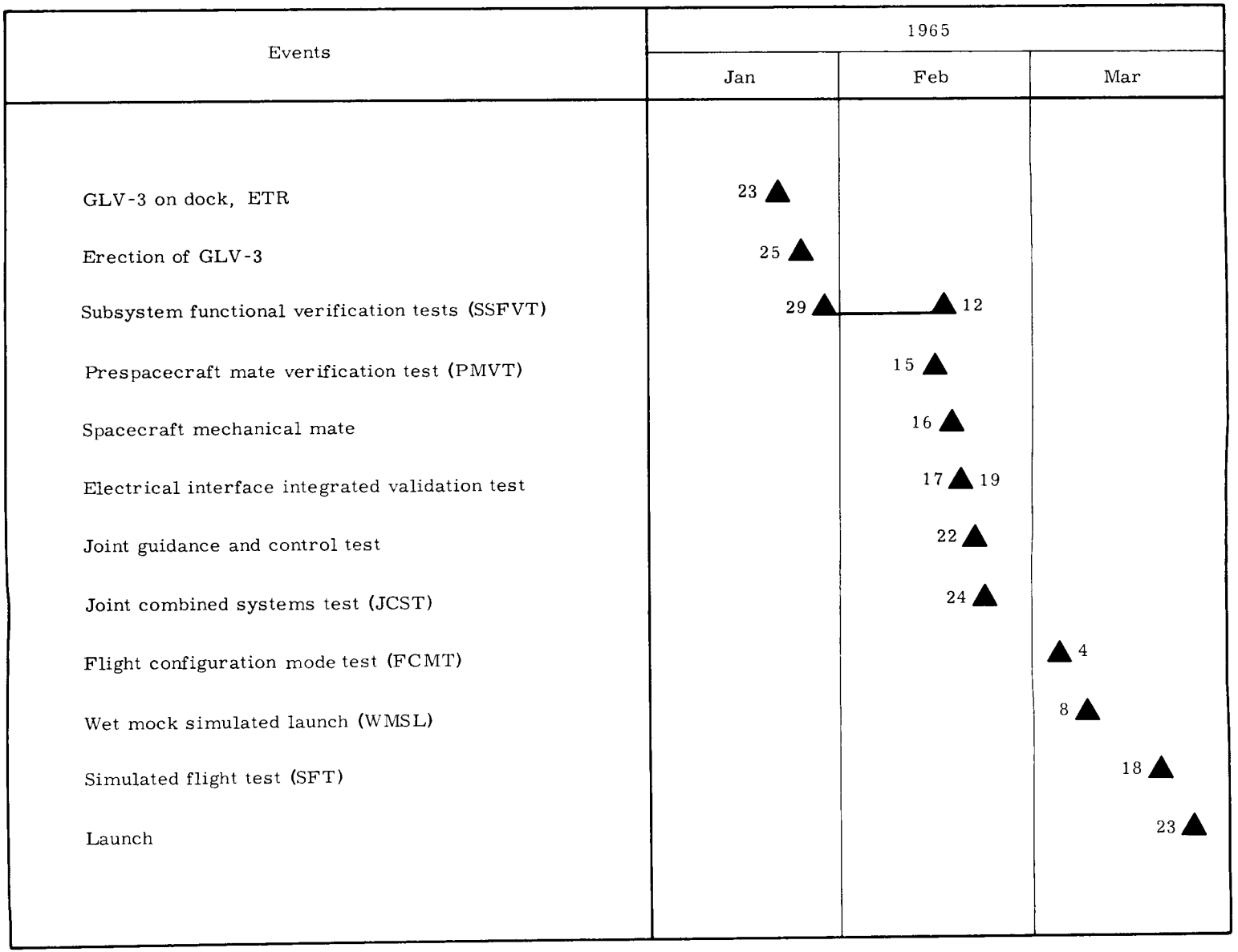


Fig. I-1. GT-3 Events Schedule at ETR

# II. SYSTEMS PERFORMANCE

## A. TRAJECTORY ANALYSIS

### 1. Orbit Insertion

Insertion of the GT-3 spacecraft into earth orbit was accomplished with greater precision than was demonstrated on GT-1. During the ascent portion of this flight, the launch vehicle performed as expected and met insertion requirements within the allowable tolerance limits.

A comparison of the predicted and observed insertion conditions is given in Table II-1. In this table and in all succeeding references to a predicted trajectory, the data are derived from the last prelaunch nominal trajectory computed by the Martin Company. This final predicted trajectory is an updated version of that appearing in Ref. 1. The observed trajectory parameters are those derived from the MOD III-G radar data which have been fully corrected for refraction and systematic biases, and smoothed.

TABLE II-1

Comparison of Insertion Conditions (SECO + 20 Seconds)

| Parameter | Planned Nominal | Observed | Observed Minus Planned | Total Tolerance |
|---|---|---|---|---|
| Inertial velocity (fps) | 25,698.4 | 25,688 | -10.4 | ±52.28 |
| Inertial flight path angle (deg) | -0.0048 | -0.0323 | -0.0275 | ±0.338 |
| Altitude (naut mi) | 87.408 | 87.612 | +0.204 | ±0.626 |

### 2. Derivation of Trajectory Uncertainties

Table II-1 contains the total allowable tolerance for the prime insertion conditions. These tolerances have been computed in the following manner:

Total tolerance = preliminary tolerance + $3\sigma$ data error

where

Preliminary tolerance =

$$\sqrt{(\text{vehicle perturbations})^2_{\text{MB-1046}} + (\text{RGS dispersion})^2}$$

The MOD III-G data errors which were obtained from Ref. 6 are listed in Table II-2. The preliminary tolerances for BECO and SECO + 20 seconds are shown in Table II-3. The error values shown in Table II-2 should be multiplied by three when used for computation of total tolerance. The data errors included here represent the total uncertainties based on nominal systematic bias estimates (a priori) and actual random bias error estimates. In accordance with all other trajectory data contained herein, the reference system used is AFMTC Coordinate System No. 1.

TABLE II-2

Total Uncertainties on Fully Corrected and Smoothed MOD III-G Radio Guidance and Instrumentation System

| Parameter | BECO | SECO | SECO + 20 Sec |
|---|---|---|---|
| $\sigma_{X_F}$, downrange position (ft) | 11.4 | 102.4 | 121.1 |
| $\sigma_{Y_F}$, cross-range position (ft) | 26.0 | 47.2 | 70.1 |
| $\sigma_{Z_F}$, vertical position (ft) | 20.6 | 295.8 | 584.4 |
| $\sigma_{\dot{X}_F}$, downrange velocity (fps) | 0.27 | 1.32 | 2.58 |
| $\sigma_{\dot{Y}_F}$, cross-range velocity (fps) | 0.24 | 1.05 | 2.39 |
| $\sigma_{\dot{Z}_F}$, vertical velocity (fps) | 0.40 | 11.14 | 32.37 |
| $\sigma_R$, geocentric radius (ft) | 20.8 | 290.2 | 570.1 |
| $\sigma_V$, inertial velocity (fps) | 0.14 | 2.40 | 7.3 |
| $\sigma_\gamma$, inertial flight path angle (deg) | 0.003 | 0.024 | 0.071 |

## 3. Geodetic and Weather Parameters

Pertinent geodetic parameters and surface weather conditions which existed at the time of launch are shown in Table II-4.

## TABLE II-3

Preliminary Tolerance at BECO and at SECO + 20 Seconds

| Performance Parameter | Nominal ① Value | 3σ Nominal Dispersions | | |
|---|---|---|---|---|
| | | Vehicle ② Perturbations | RGS ③ Dispersions | RSS of RGS and Perturbations |
| BECO | | | | |
| Time (sec)⑤ | 154.27 | ±3.90 | N/A | ±3.90 |
| Geocentric radius (ft) | 21,119,526 | ±12,741 | N/A | ±12,741 |
| Cross range (ft) | -825 | ±15,513 | N/A | ±15,513 |
| Ground range (naut mi) | 49.85 | ±3.12 | N/A | ±3.12 |
| Cross-range velocity (fps) | -34.84 | ±386 | N/A | ±386 |
| Inertial flight path angle (deg) | 19.514 | ±2.59 | N/A | ±2.59 |
| Inertial velocity (fps) | 9889.3 | ±169 | N/A | ±169 |
| SECO + 20 Seconds | | | | |
| Time (sec)⑤ | 358.57 | ±7.39 | ±0.081 | ±7.39 |
| Geocentric radius (ft)④ | 21,438,514 | ±1,554 | ±1,408 | ±2,096 |
| Cross range (ft) | -37,297 | ±72,055 | ±498 | ±72,057 |
| Ground range (naut mi) | 540.13 | ±15.49 | ±1.7592 | ±15.59 |
| Cross-range velocity (fps)④ | -408.59 | ±22.98 | ±9.91 | ±25.03 |
| Inertial flight path angle (deg) | -0.0048 | ±0.0540 | ±0.113 | ±0.125 |
| Inertial velocity (fps)④ Redundant shutdown system (RESS) | 25,698.4 | ±18.53 | ±24.1 | ±30.38 |

NOTES:

① Martin GLV Trajectory 06-GT-3, dated 23 March 1965.

② MB-1046, SCN-6 (Ref. 10)

③ Ref. 11

④ Performance Incentive Parameter (Ref. 12)

⑤ Times from liftoff

N/A = Not applicable

[redacted]

TABLE II-4

Geodetic and Weather Conditions at Launch

| | |
|---|---|
| **Location** | |
| Site | Complex 19 |
| Site coordinates: latitude (deg) | 28.507 N |
| longitude (deg) | 80.554 W |
| Pad orientation (deg) | 84.91 true azimuth |
| **Weather** | |
| Ambient pressure (psi) | 14.83 |
| Ambient temperature (° F) | 73 |
| Dew point (° F) | 64 |
| Relative humidity (%) | 74 |
| Surface wind: speed (fps) | 24 |
| direction (deg) | 150 true azimuth |
| Max winds aloft: speed (fps) | 172 |
| direction (deg) | 291 |
| altitude (ft) | 41,000 |
| Cloud cover | None |
| **Reference Coordinate System No. 1** | |
| Type | AFMTC coordinate System No. 1 |
| Origin | Center of launch ring Complex 19 |
| Positive X-axis | Downrange along flight azimuth |
| Positive Z-axis | Away from earth on a geodetic radius |
| Positive Y-axis | Forms a right-hand orthogonal system |
| Reference ellipsoid | Fischer |
| **Launch** | |
| Initial flight azimuth (deg) | 72 true |
| Roll program (deg) | 12.9 |

[redacted]

## 4. Flight Plan

A primary test objective for GLV-3 was to place the Gemini spacecraft into an elliptical earth orbit with a perigee at 87 nautical miles and an apogee at 130 nautical miles.* Orbital insertion occurs at perigee with sufficient velocity overspeed to enable the spacecraft to coast to the desired apogee. To attain these desired conditions the following flight plan is employed.

A vertical rise is planned for the first 23.04 seconds, during which time a programmed roll rate of 1.25 deg/sec is initiated to roll the vehicle to the desired flight azimuth of 72 degrees. At this time, an open-loop pitch program is begun (via a three-step rate command) which terminates at 162.56 seconds. Guidance commands from the radio guidance system (RGS) are initiated at 168 seconds and continue until two seconds prior to SECO; however, velocity cutoff computations continue to SECO. A comparison of the planned and actual sequence of events is shown in Table II-5.

Analysis of the radar and camera data indicates a normal flight with only one anomaly--the unusually high BECO condition. The probable cause for this anomaly is discussed in a subsequent section.

Figure II-1 depicts a profile of the GT-3 flight superimposed on the range planning map and showing the proper orientation of the flight azimuth and position relative to local geography.

## 5. Trajectory Results

Trajectory and aerodynamic data derived from GT-3 flight are presented in Figs. II-2 through II-24. Atmospheric conditions obtained shortly after liftoff are presented in Figs. II-25 and II-26.

In almost all aspects, the flight trajectory was nearly as predicted with only one anomaly noted--the high BECO conditions. These dispersions have been investigated thoroughly in an effort to isolate the causes. Inspection of the GT-3 telemetry data indicates that all launch vehicle systems operated within their allowable tolerances and that the off-nominal BECO conditions were the result of an unusual combination of in-tolerance effects on the first-stage trajectory. Table II-6 provides a comparison of predicted and observed values of altitude, velocity and flight path angle for the GT-2 and GT-3 flights. Although only the geocentric radius was outside the expected tolerance for GT-3, all three parameters were larger than expected on both flights.

---

*Relative to Complex 19.

[redacted]

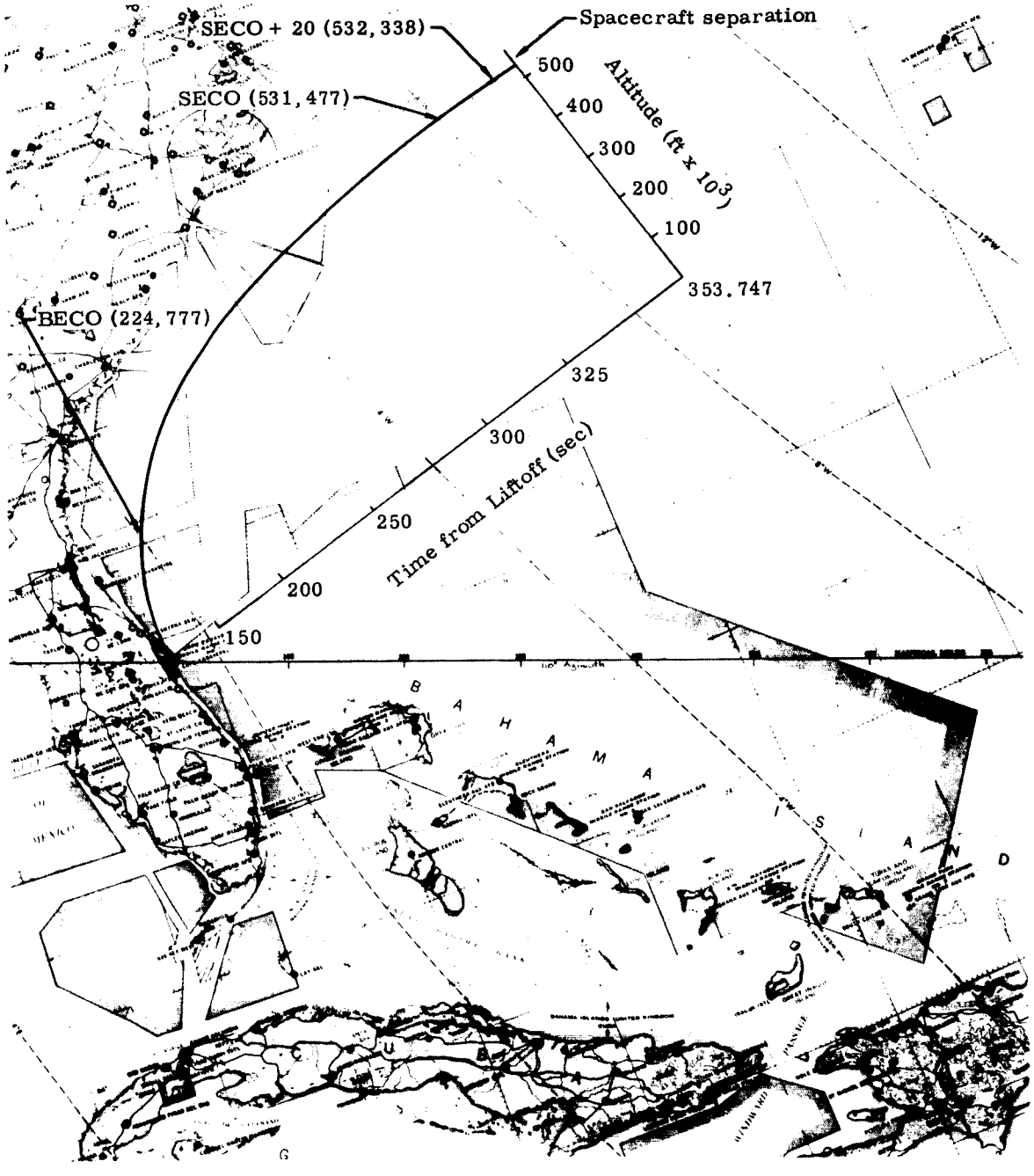


Fig. II-1. GT-3 Boost Flight Path Profile

[redacted]

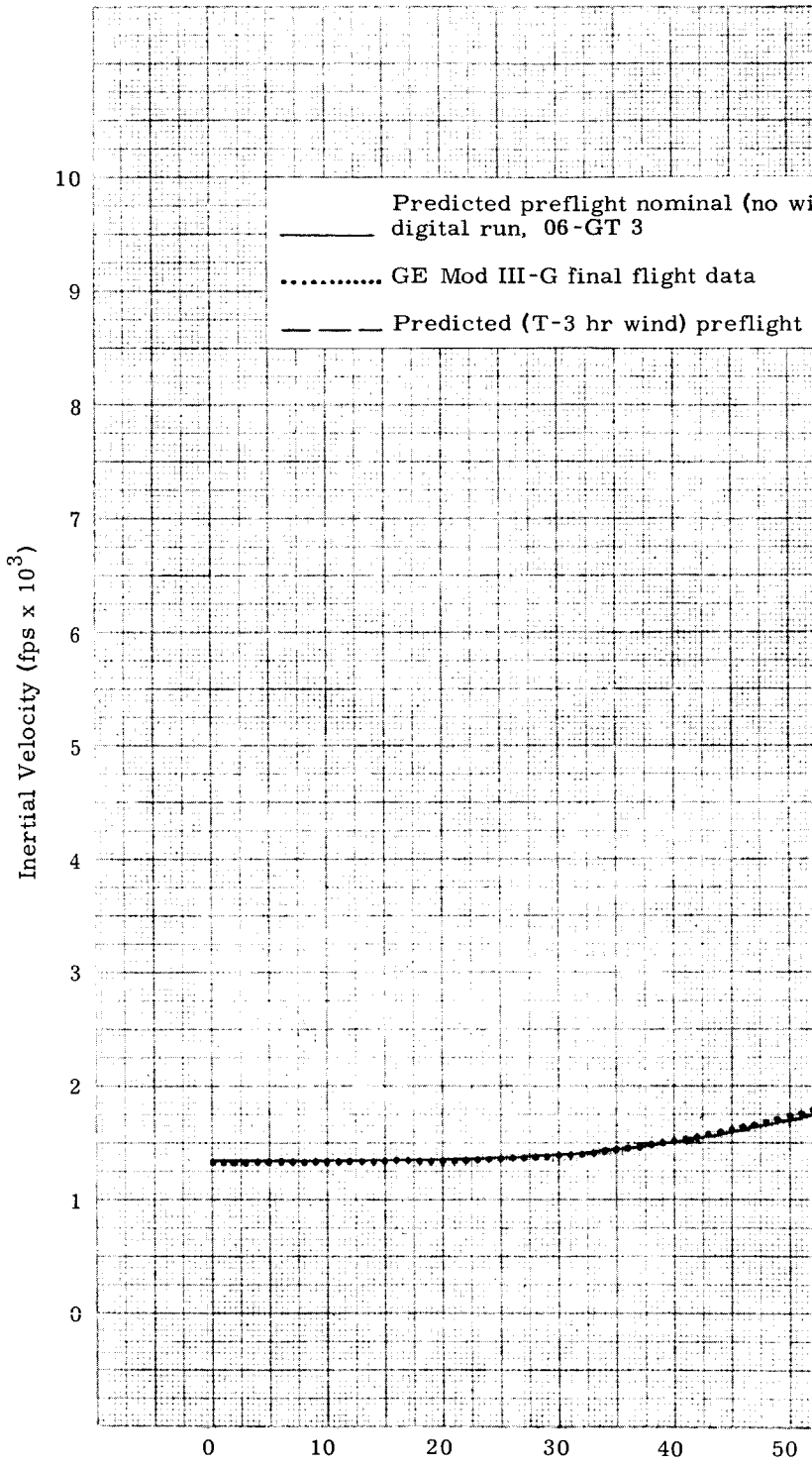
Predicted preflight nominal (no wi
digital run, 06-GT 3
GE Mod III-G final flight data
Predicted (T-3 hr wind) preflight
Inertial Velocity (fps x $10^3$)
10
9
8
7
6
5
4
3
2
1
0
0
10
20
30
40
50

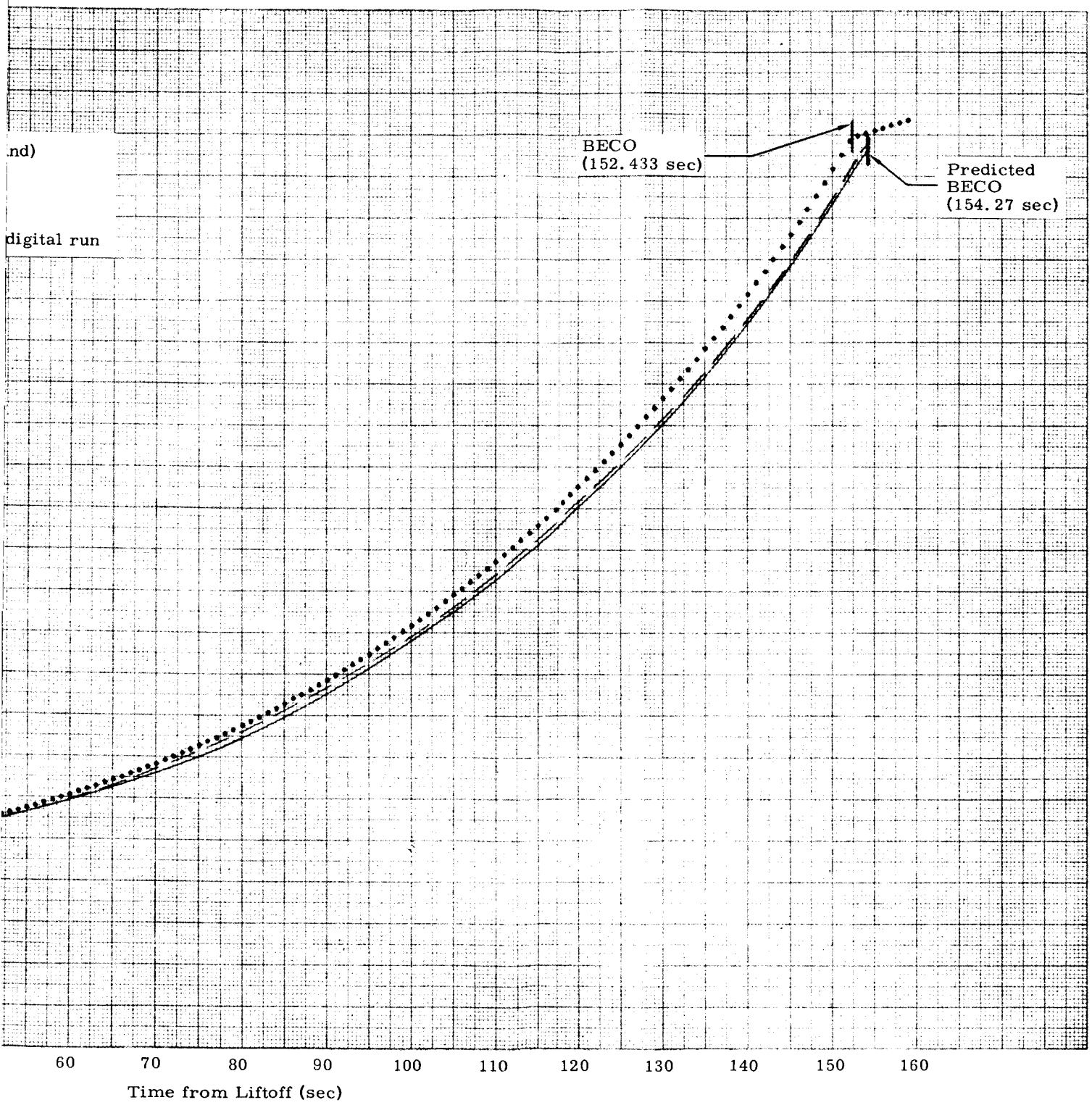


Fig. II-2. Inertial Velocity Versus Time: Stage I Flight

[redacted]

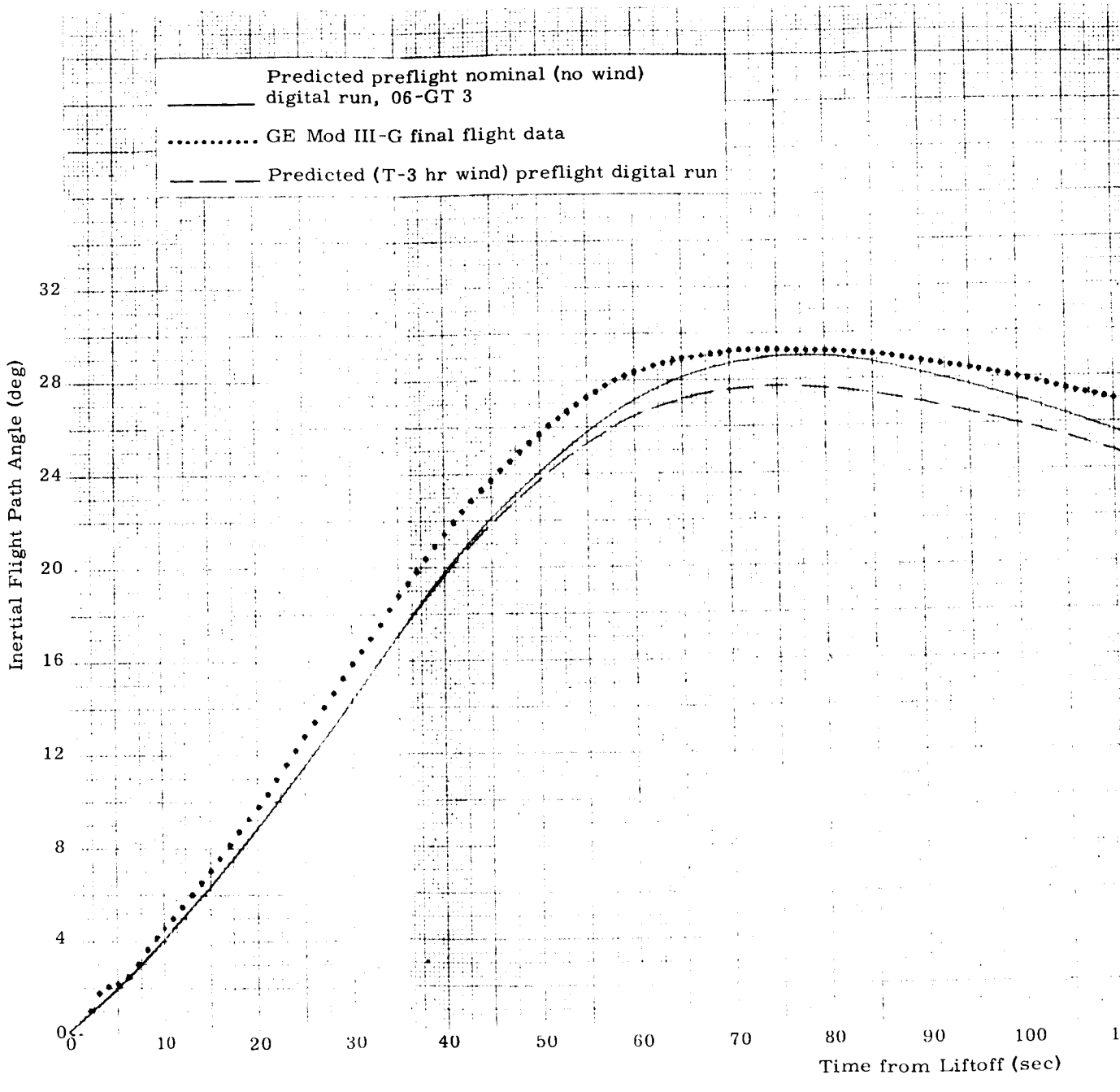


[redacted]

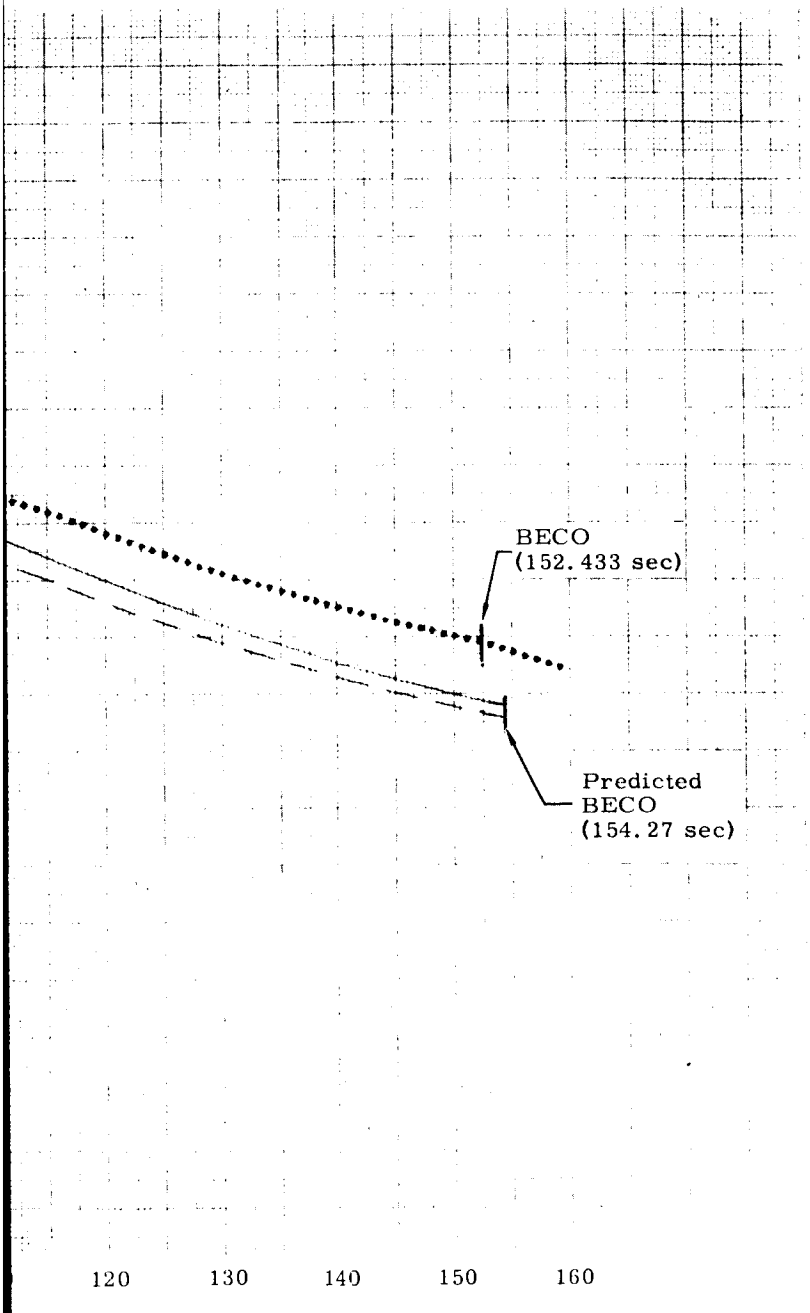


Fig. II-3. Inertial Flight Path Angle Versus Time: Stage I Flight

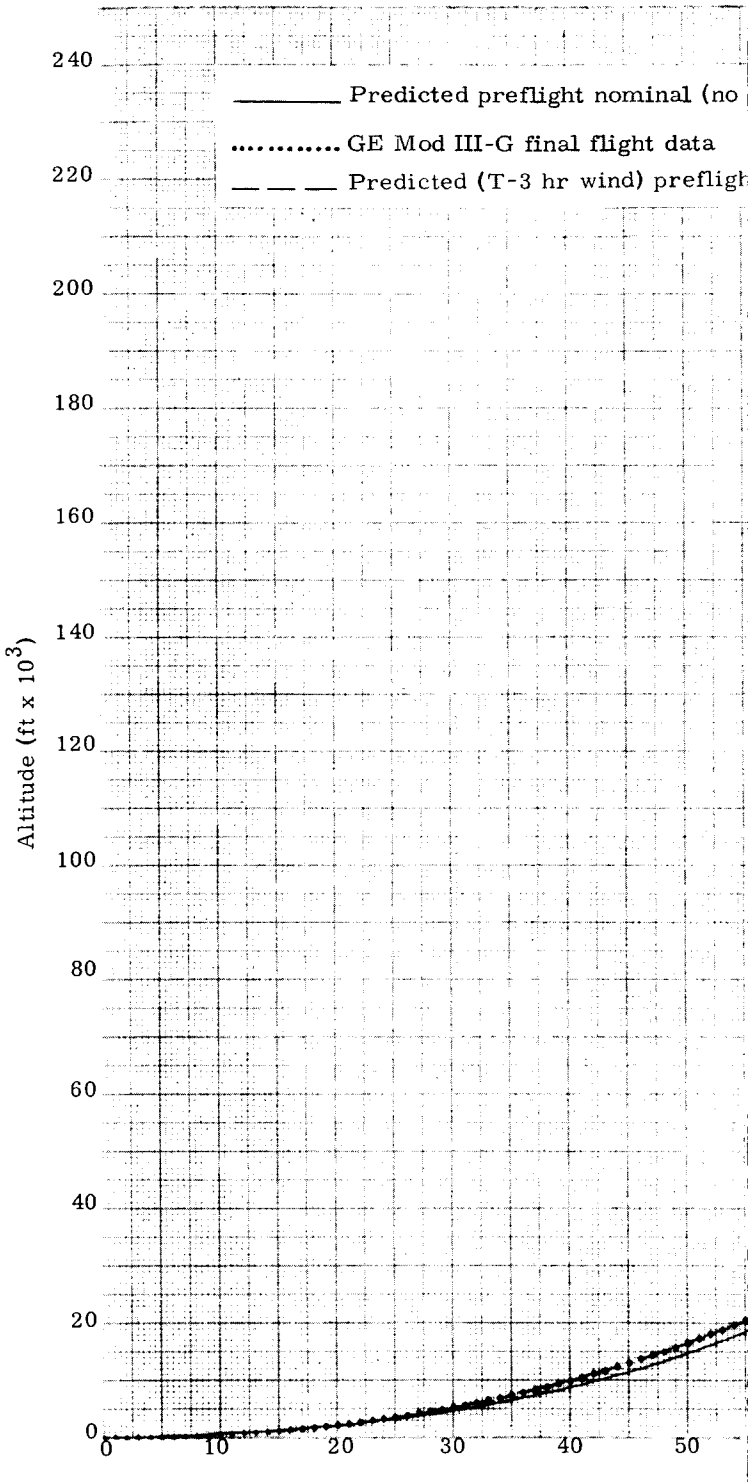
Predicted preflight nominal (no
GE Mod III-G final flight data
Predicted (T-3 hr wind) prefligh
Altitude (ft x $10^3$)
240
220
200
180
160
140
120
100
80
60
40
20
0
0
10
20
30
40
50

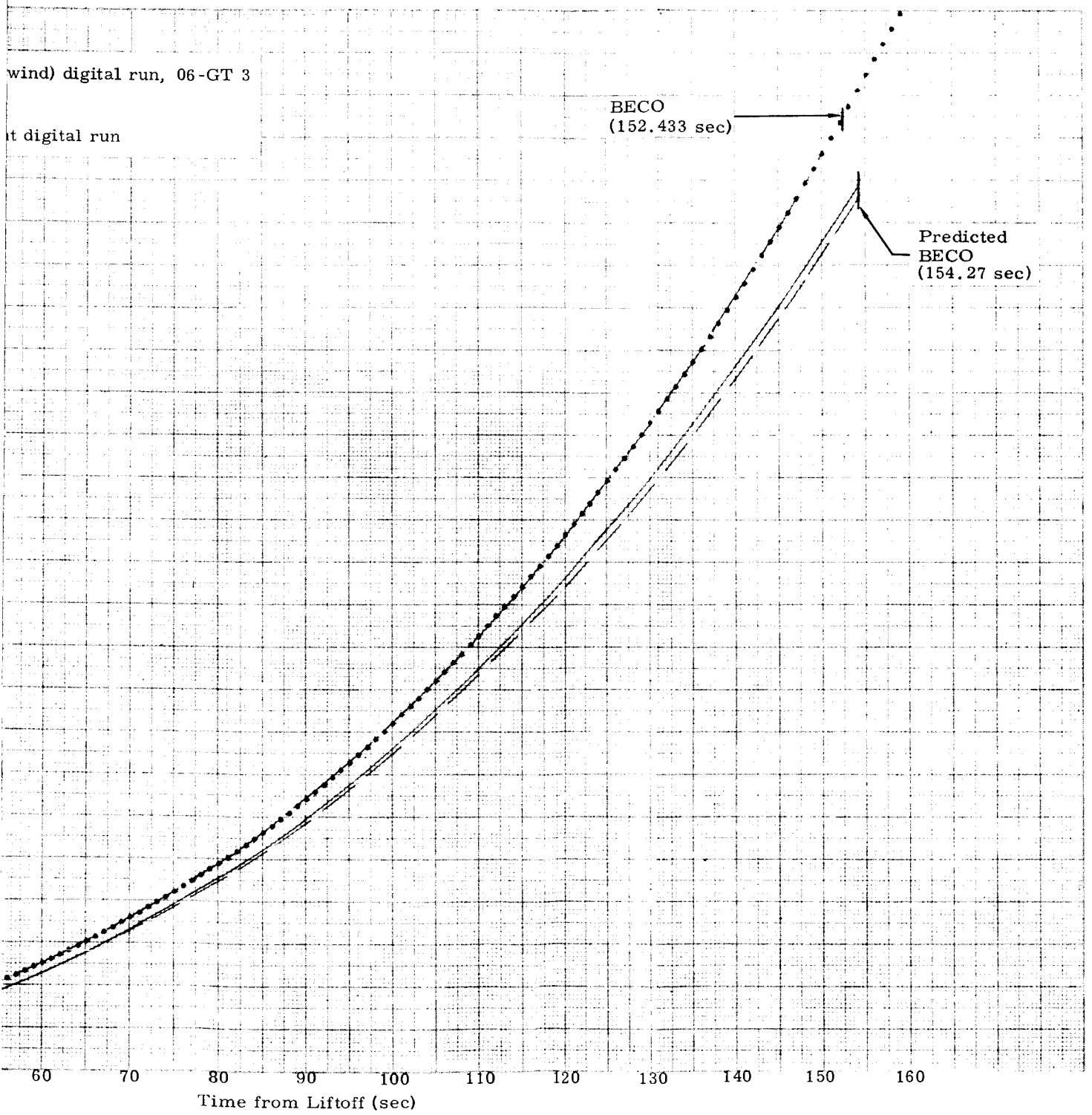


Fig. II-4. Altitude (h) Versus Time: Stage I Flight

[redacted]

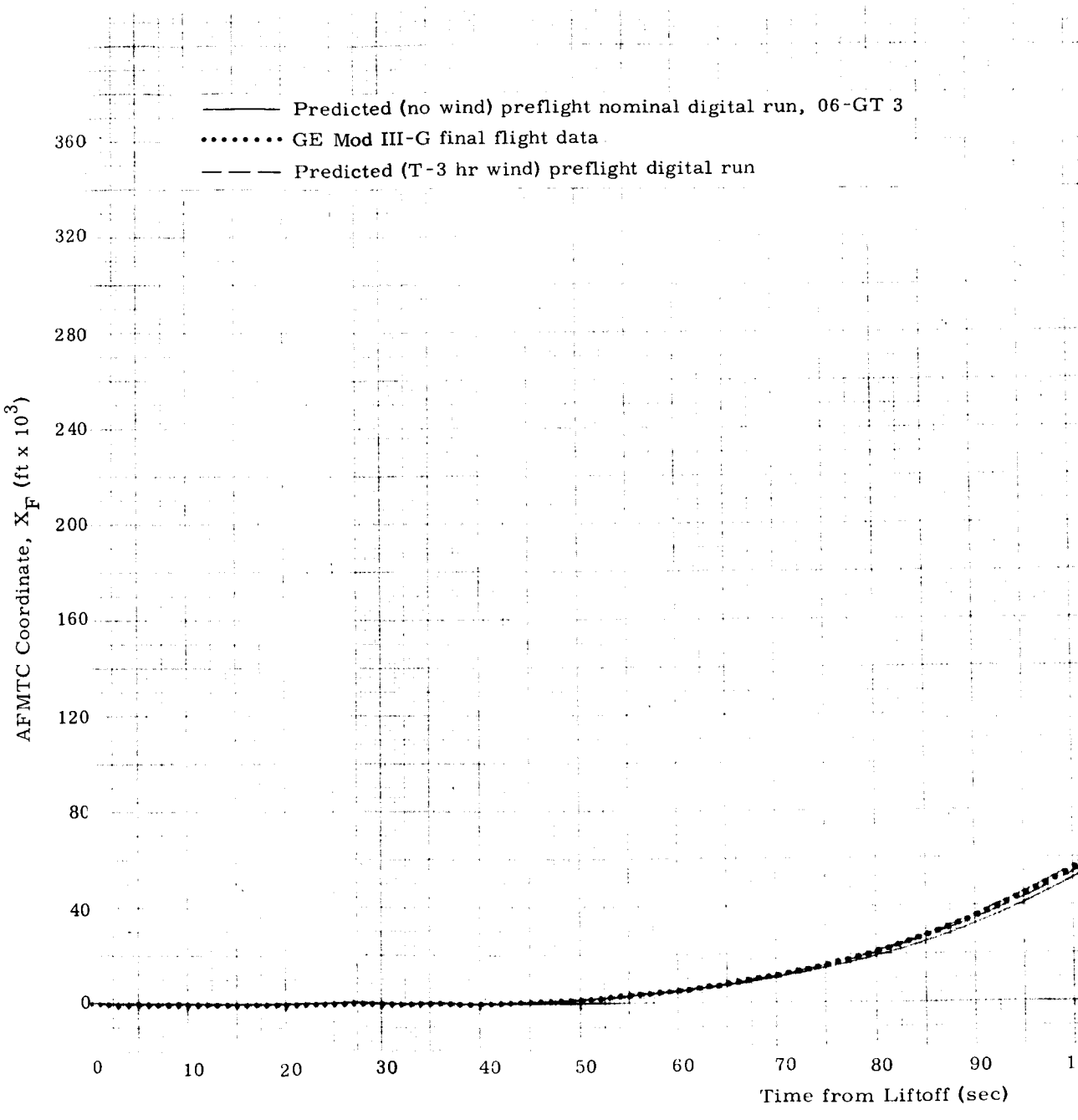


Fig. II-5. Downr

[redacted]

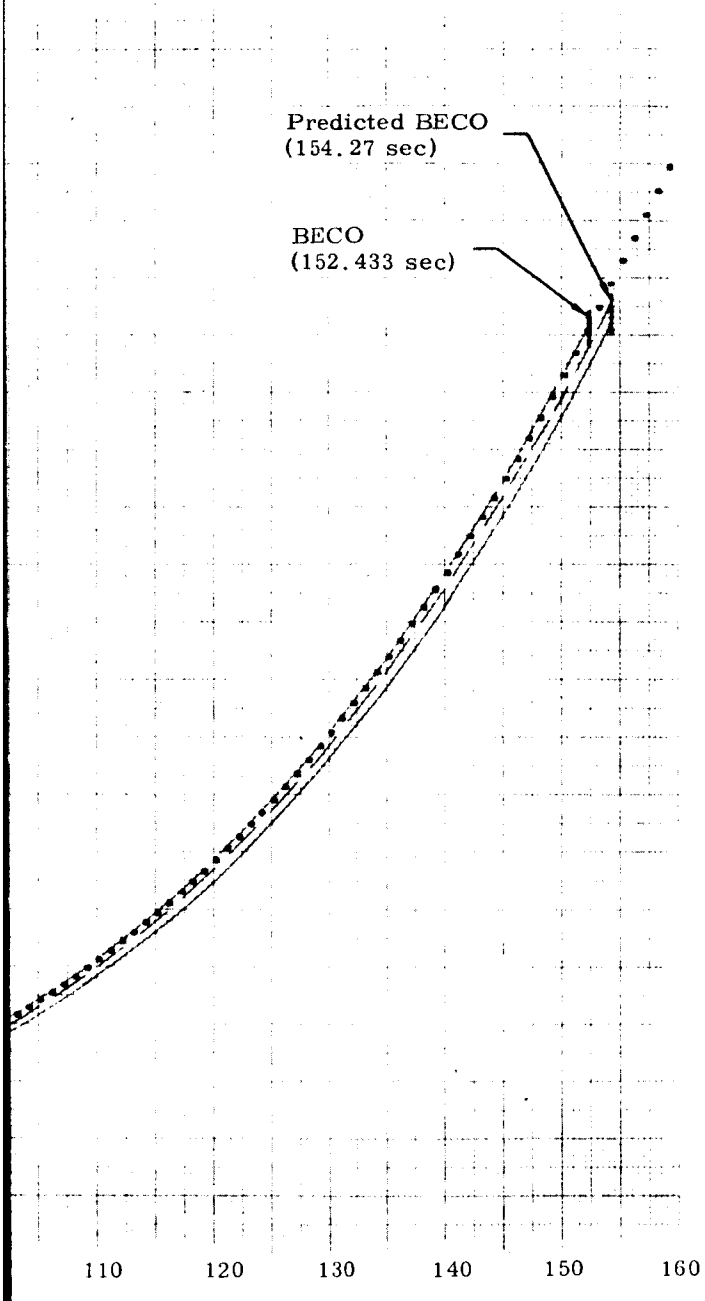


ge Position Coordinate ($X_F$) Versus Time: Stage I Flight

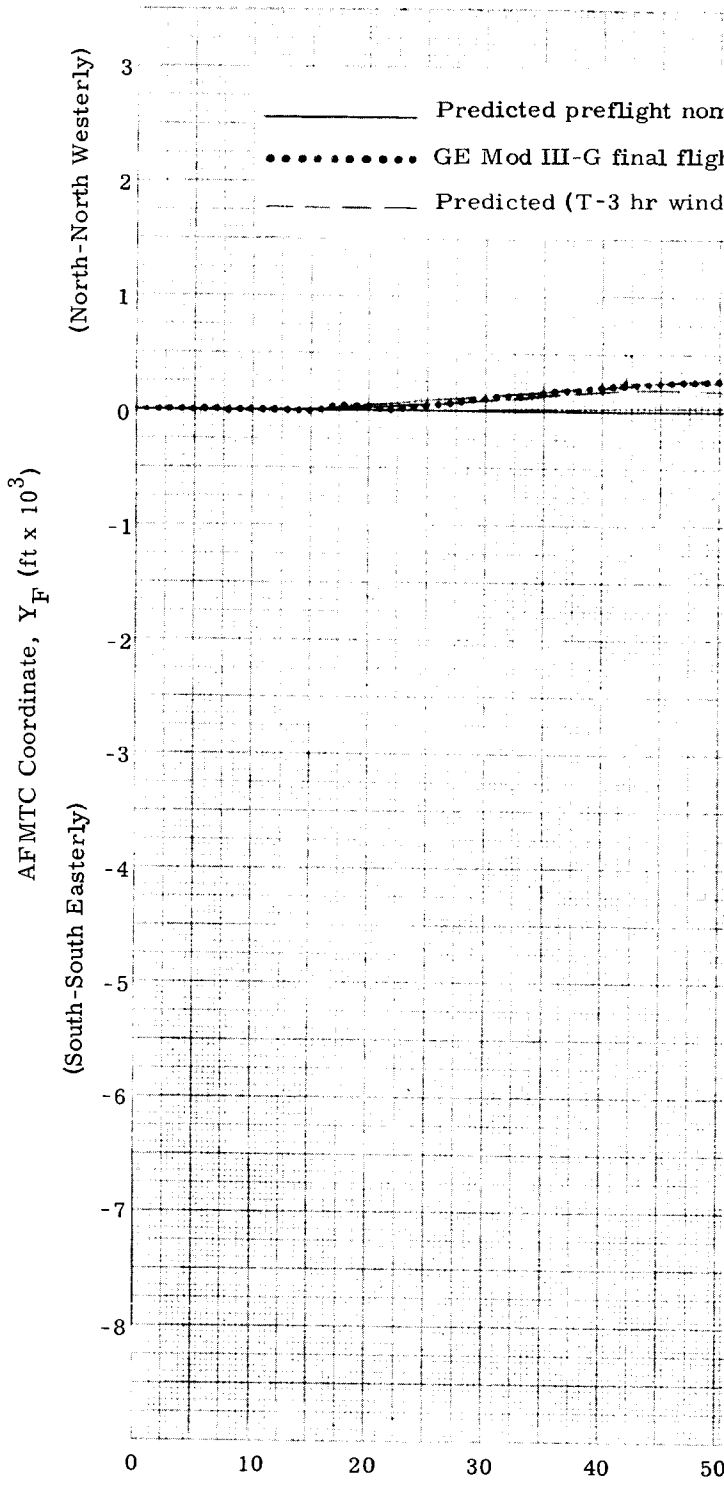
Predicted preflight nom
GE Mod III-G final fligh
Predicted (T-3 hr wind
AFMTC Coordinate, $Y_F$ (ft x $10^3$)
(North-North Westerly)
(South-South Easterly)
3
2
1
0
-1
-2
-3
-4
-5
-6
-7
-8
0
10
20
30
40
50

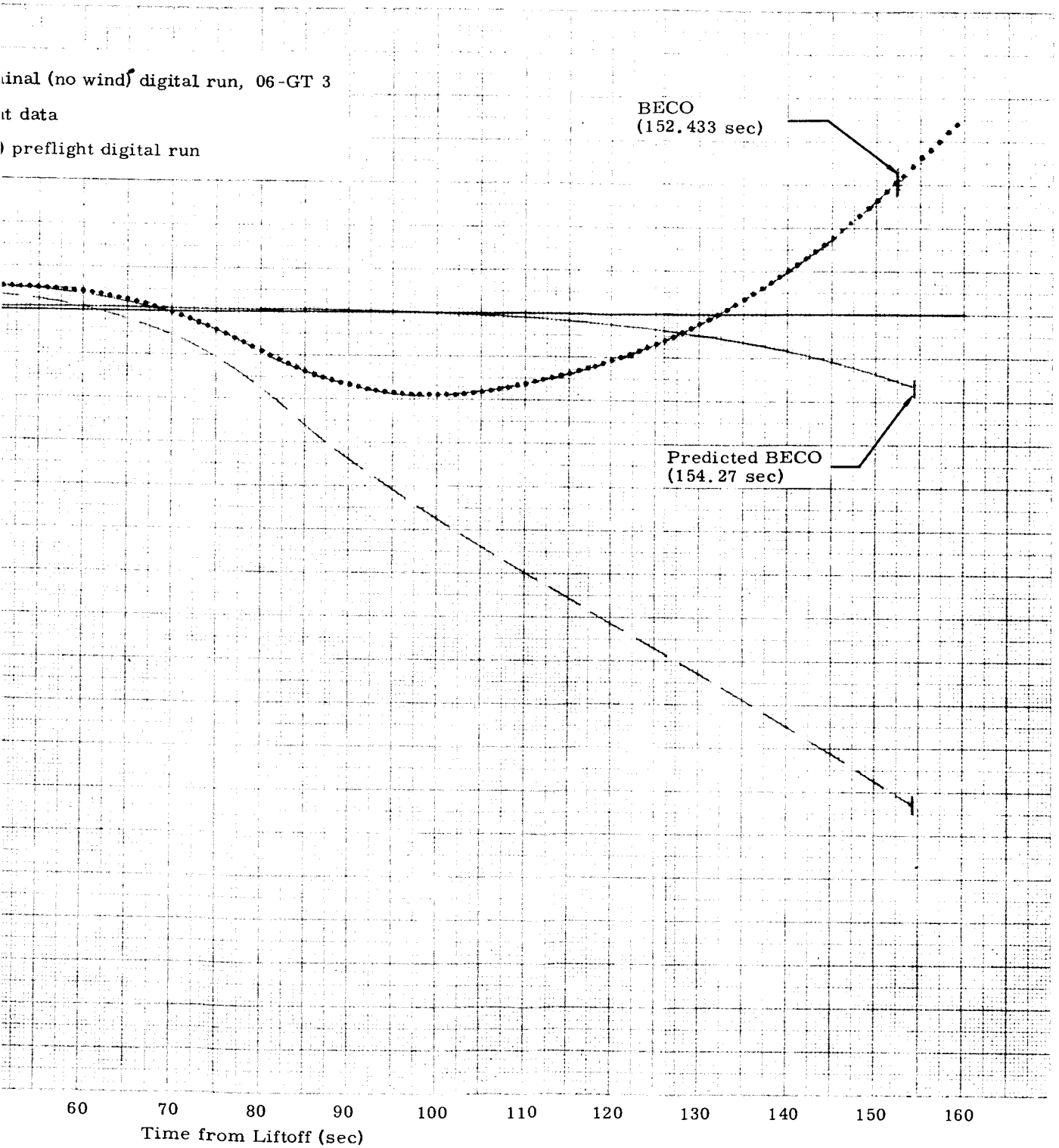


Fig. II-6. Cross-Range Position Coordinate ($Y_F$) Versus Time: Stage I Flight

[redacted]

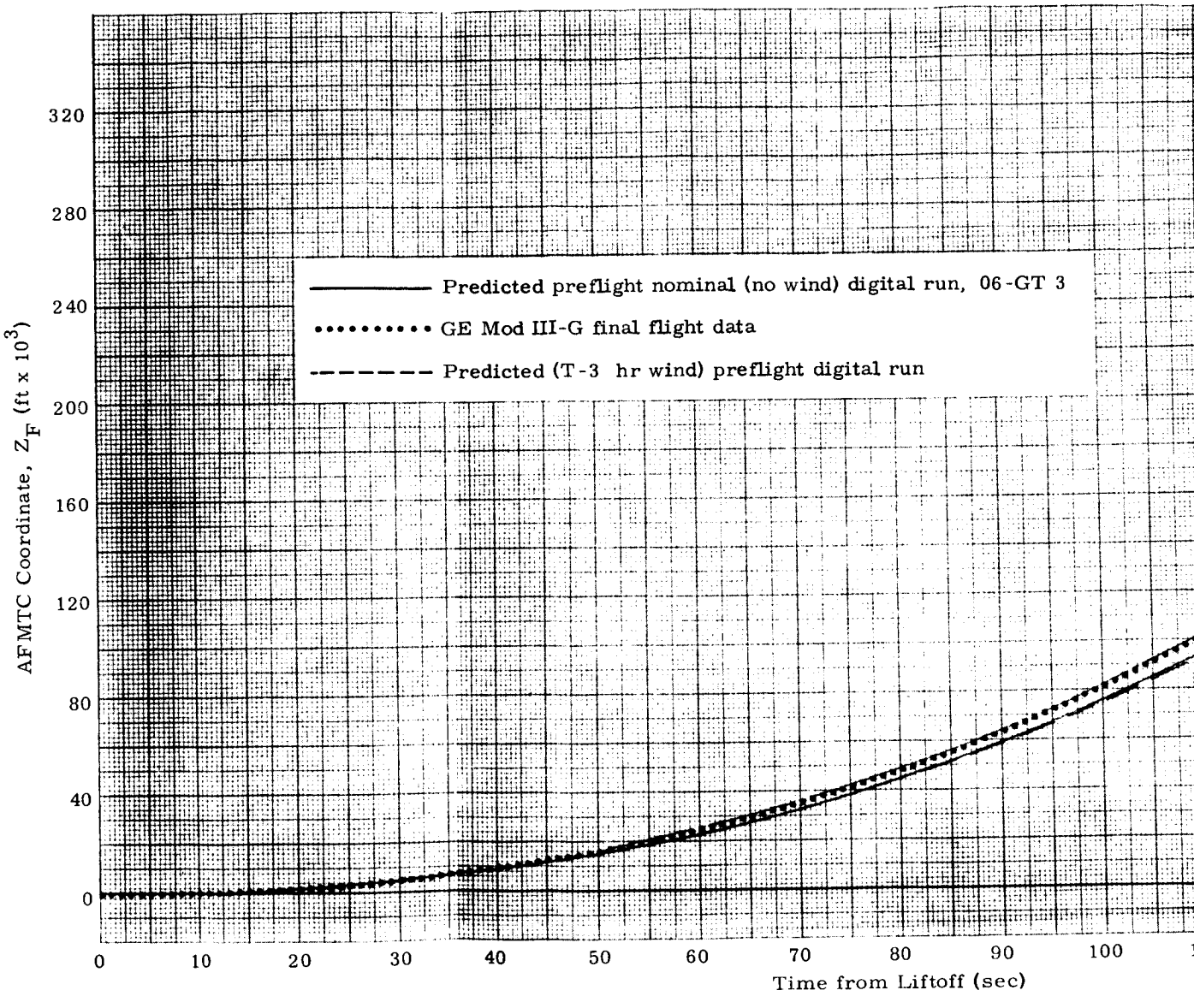


Fig. II-7. Ver

[redacted]

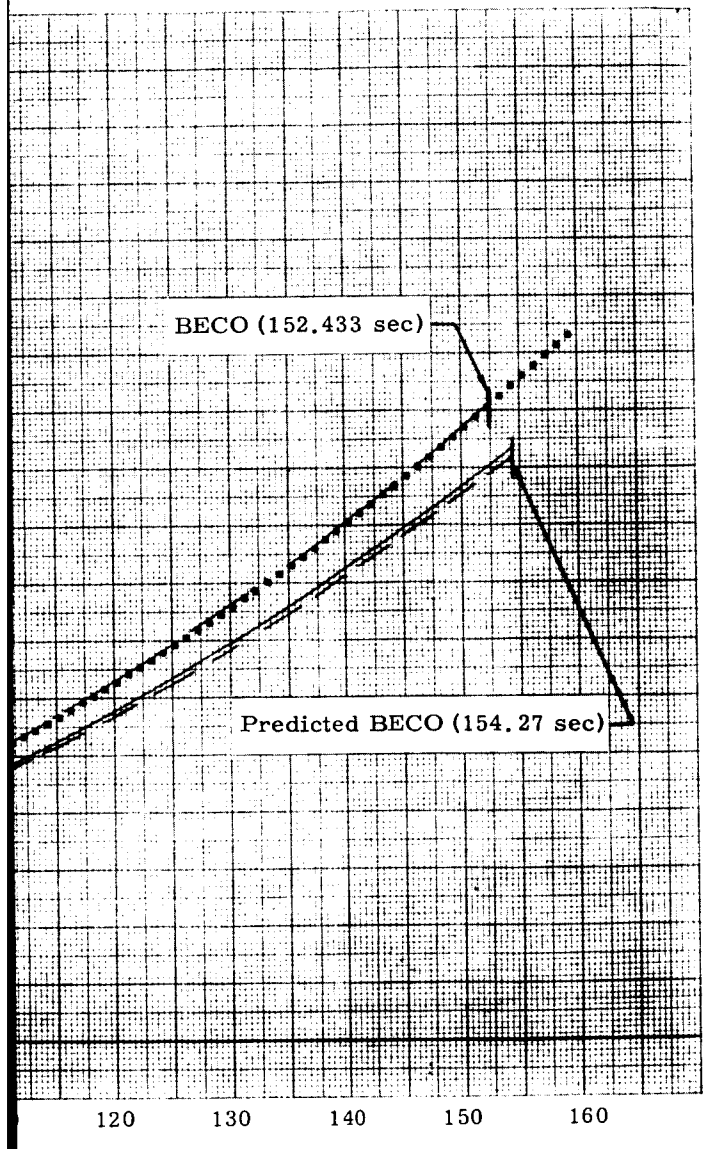


al Position Coordinate ($Z_F$) Versus Time: Stage I Flight

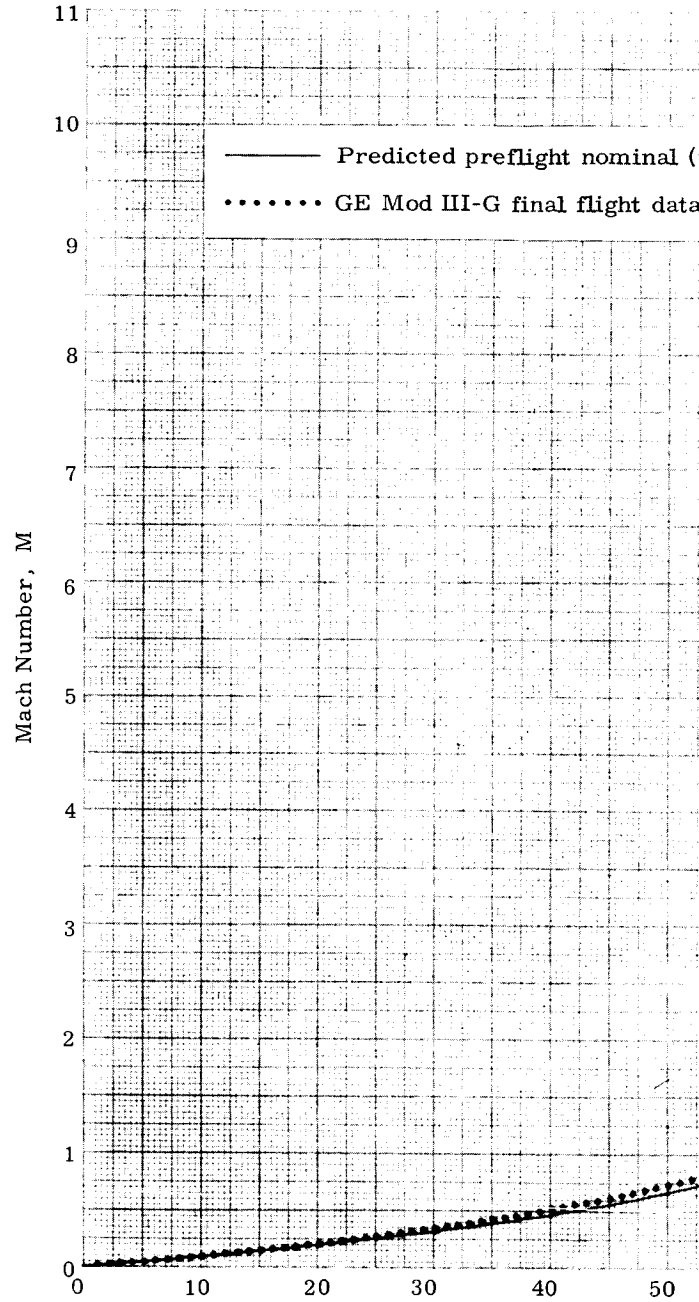
Predicted preflight nominal (
GE Mod III-G final flight data
Mach Number, M
0
1
2
3
4
5
6
7
8
9
10
11
0
10
20
30
40
50

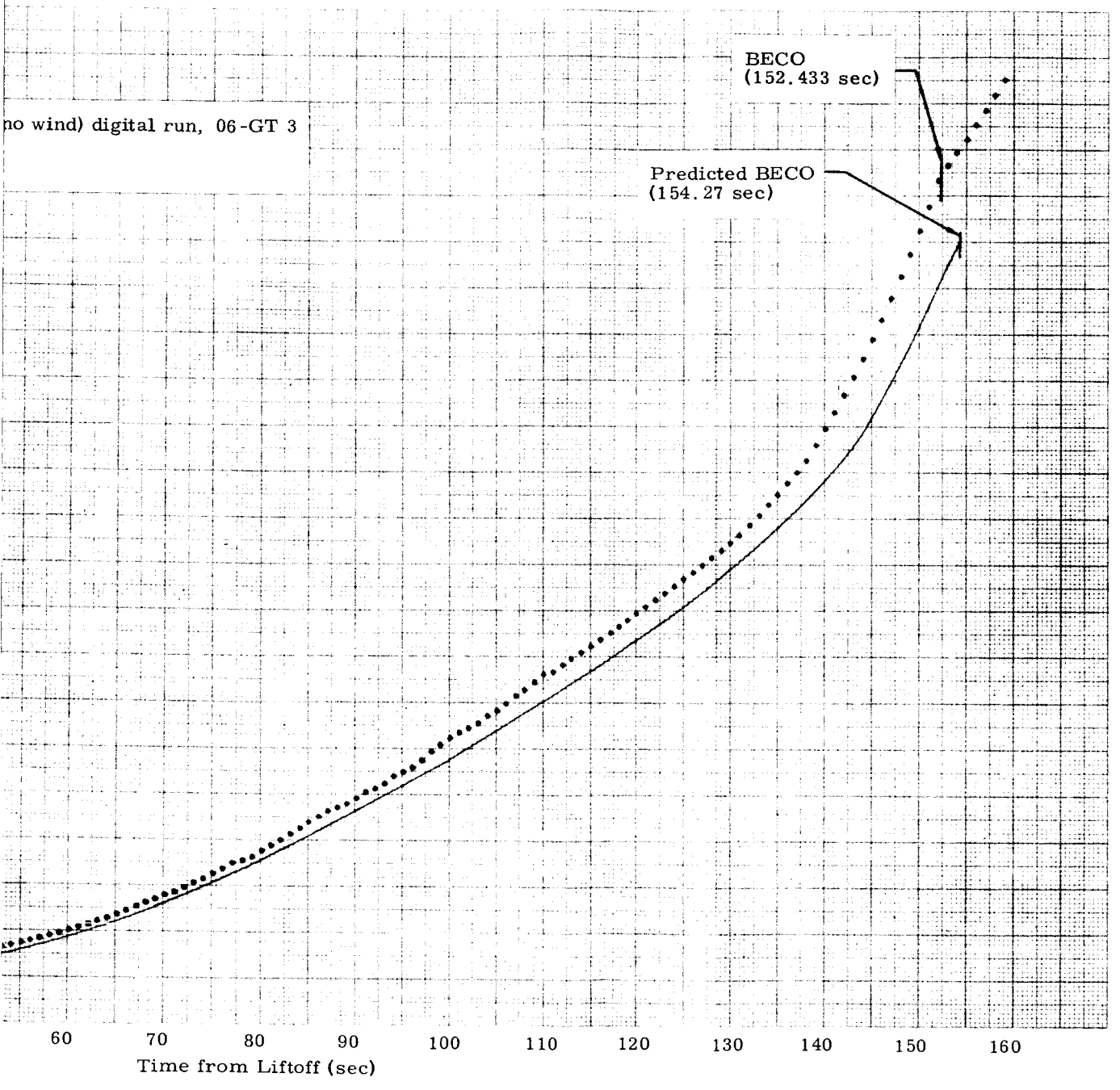


Fig. II-8. Mach Number (M) Versus Time: Stage I Flight

[redacted]

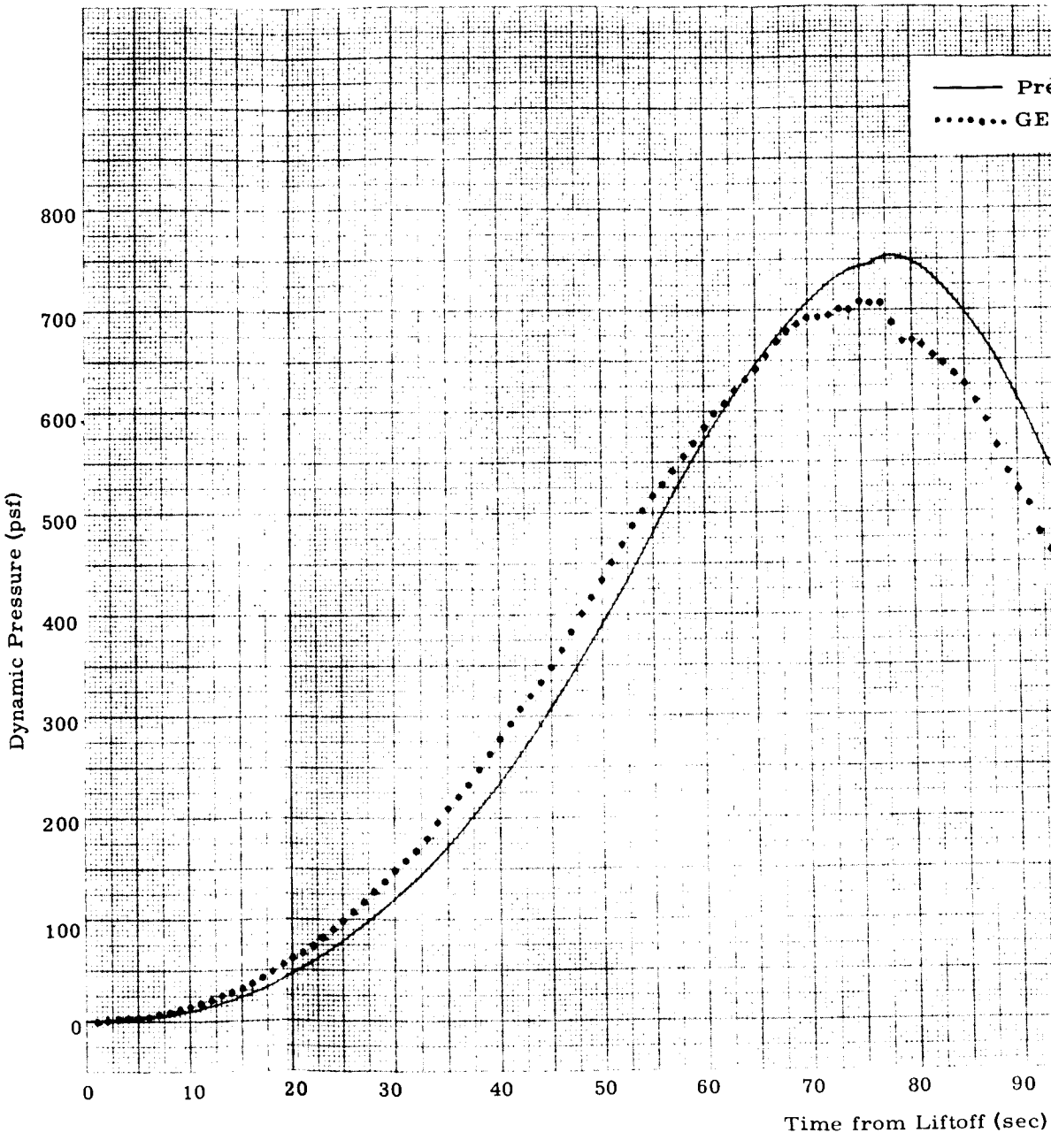


[redacted]

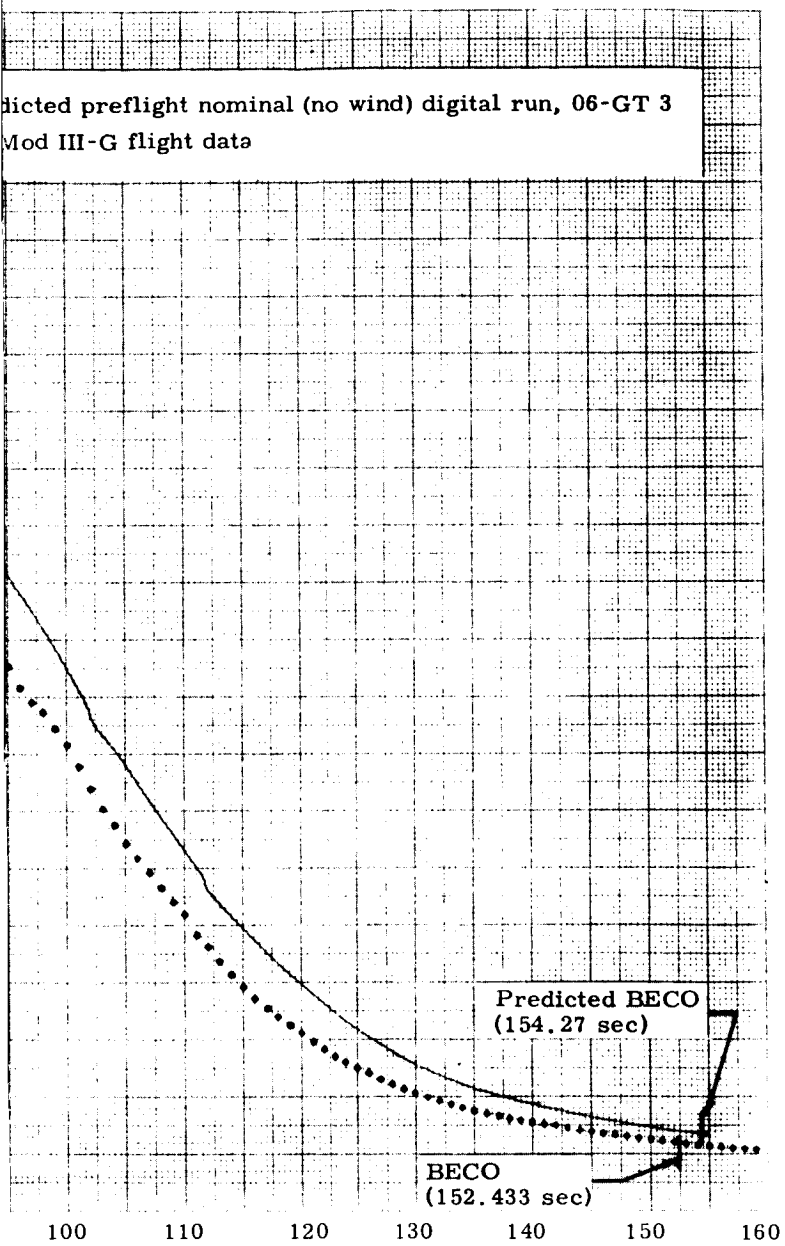


Fig. II-9. Dynamic Pressure (q) Versus Time: Stage I Flight

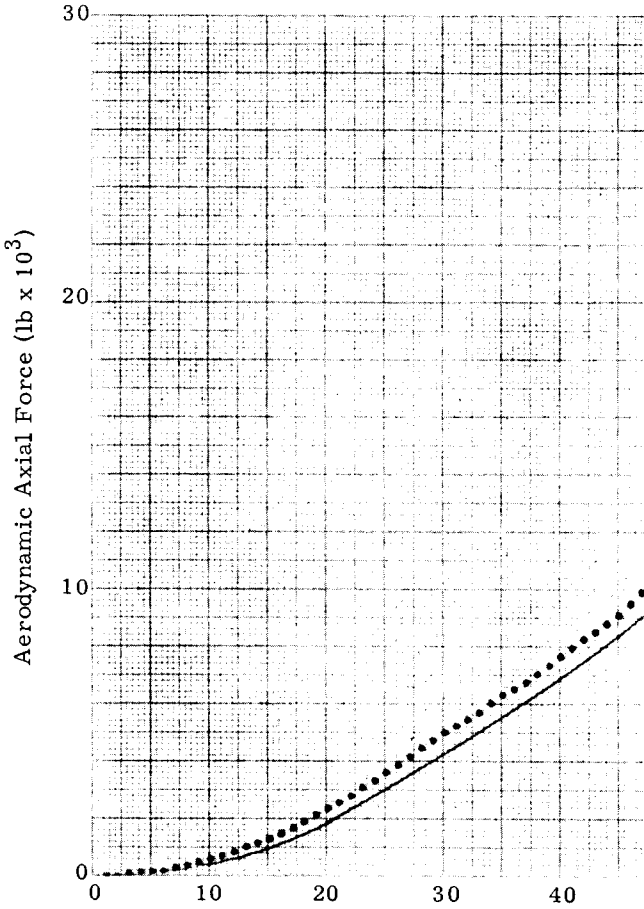
Aerodynamic Axial Force (lb x $10^3$)
30
20
10
0
0
10
20
30
40

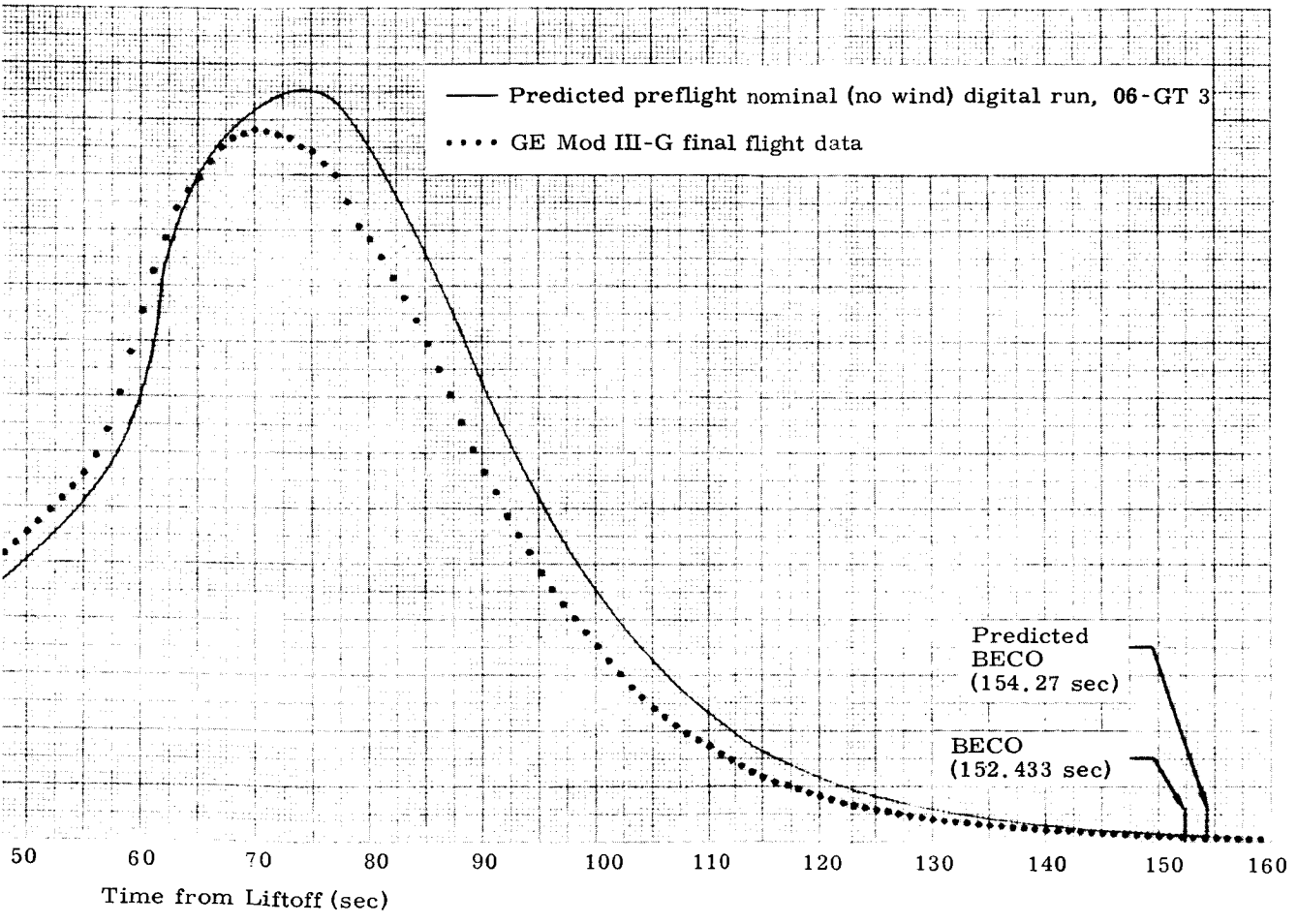


Fig. II-10. Axial Force Versus Time: Stage I Flight

[redacted]

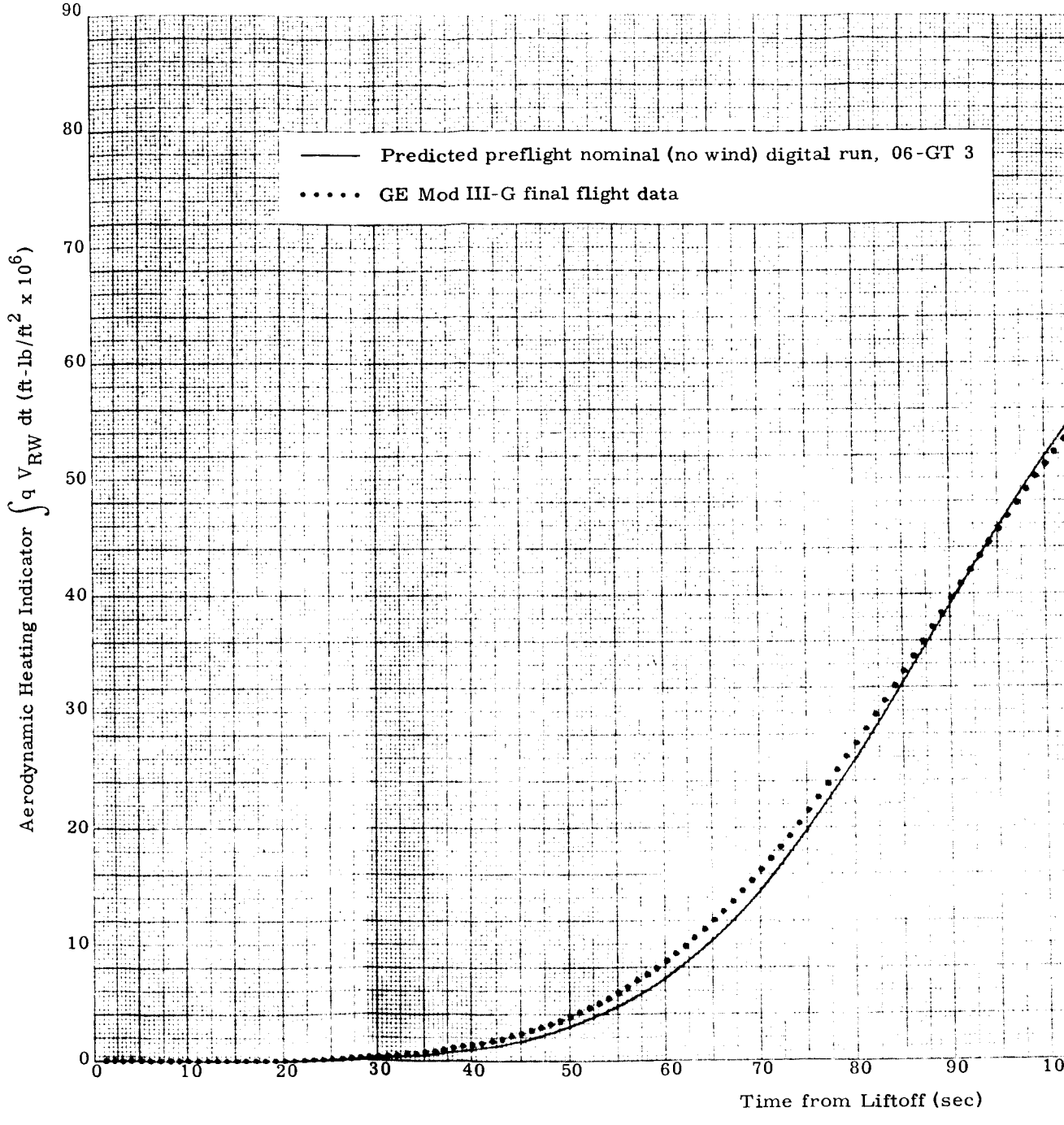


Fig. II-11. A

[redacted]

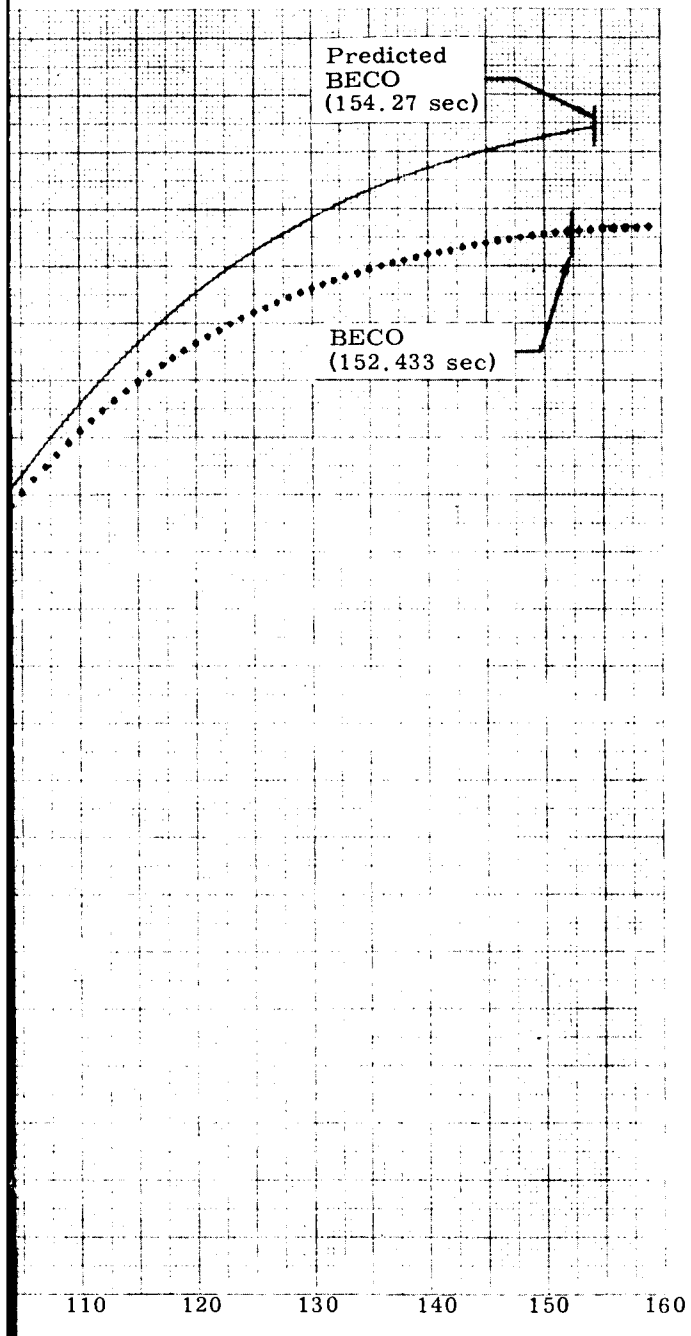


dynamic Heating Indicator Versus Time: Stage I Flight

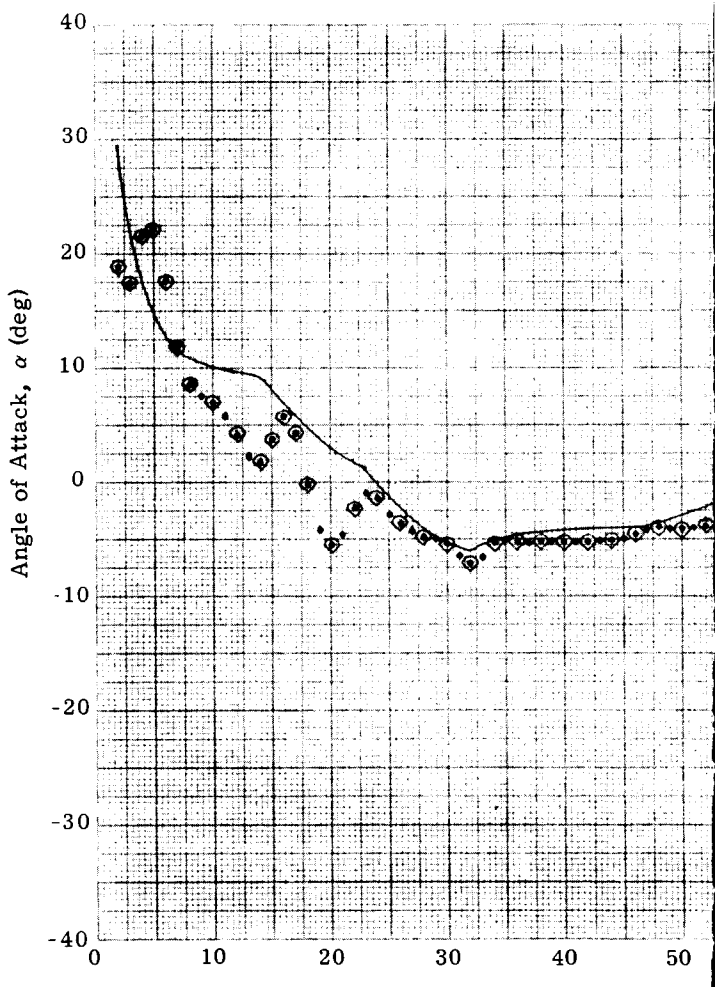
Angle of Attack, α (deg)
40
30
20
10
0
-10
-20
-30
-40
0
10
20
30
40
50

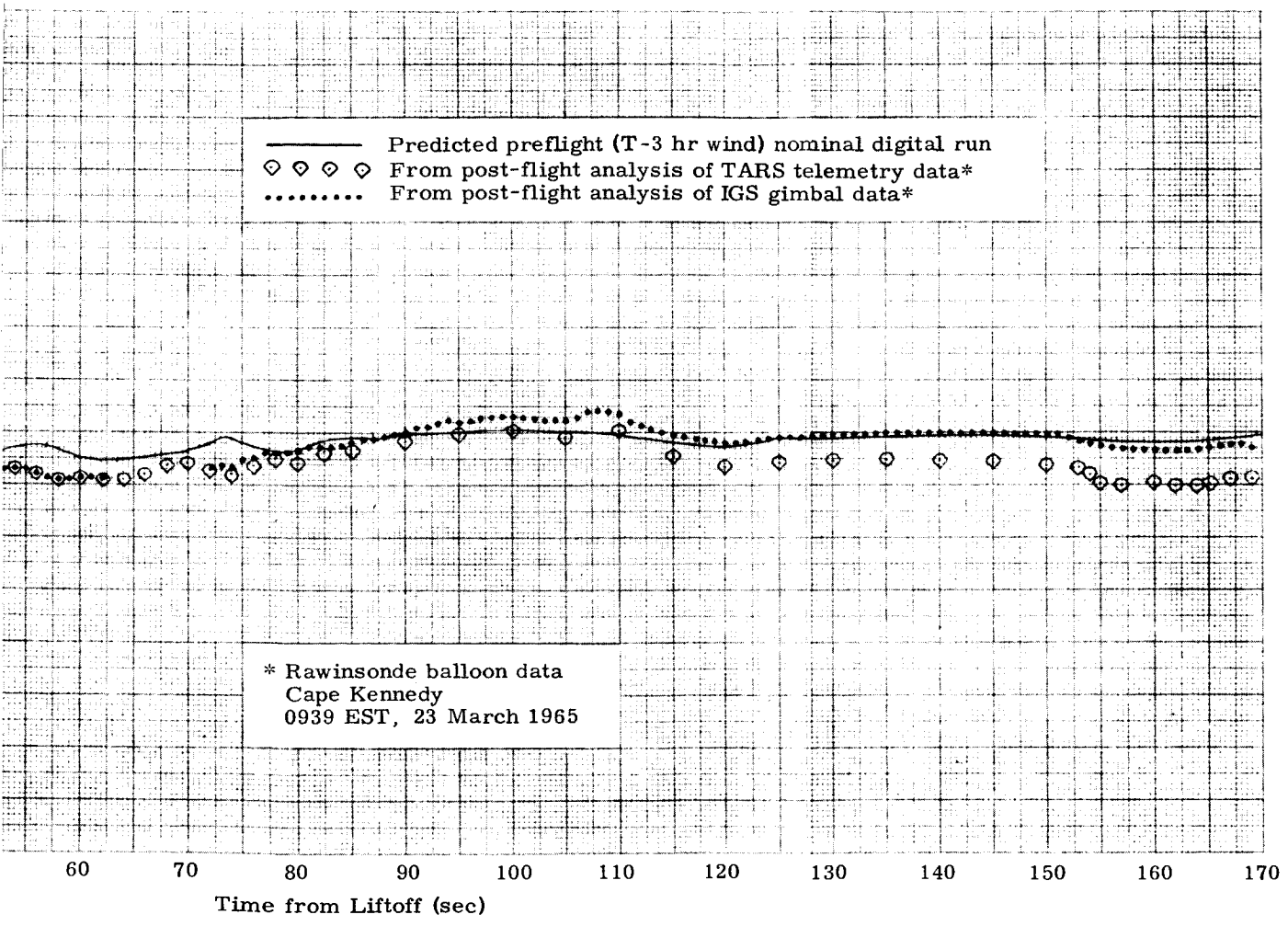


Fig. II-12. Stage I Angle of Attack History

[redacted]

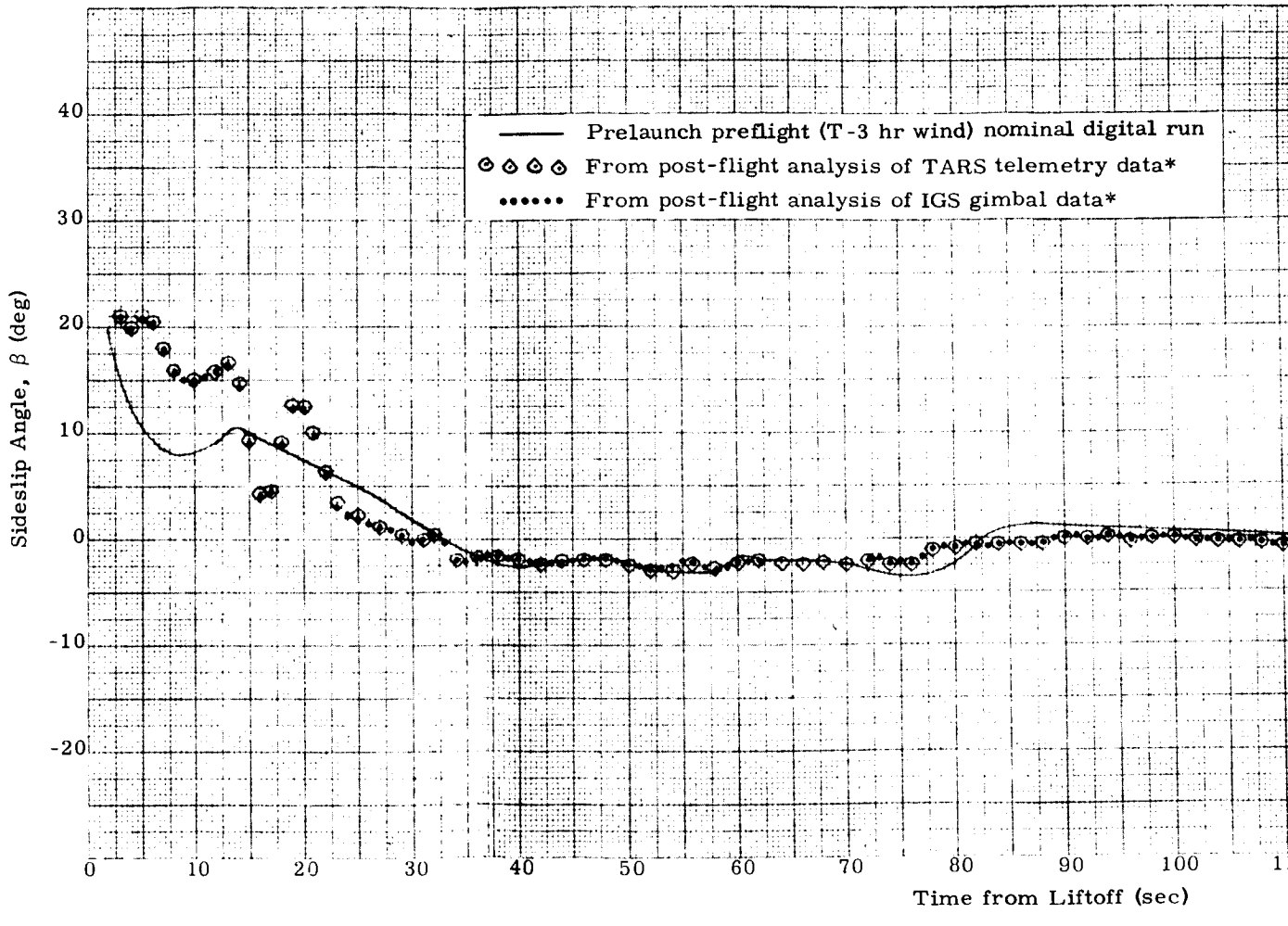


[redacted]

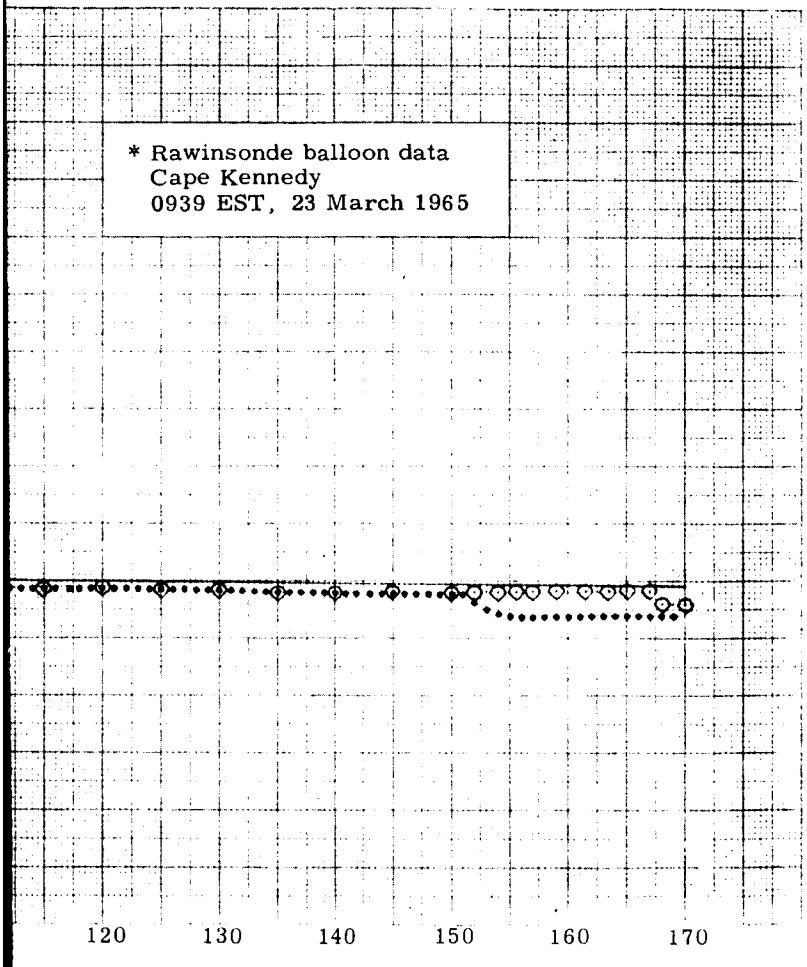


Fig. II-13. Stage I Angle of Sideslip History

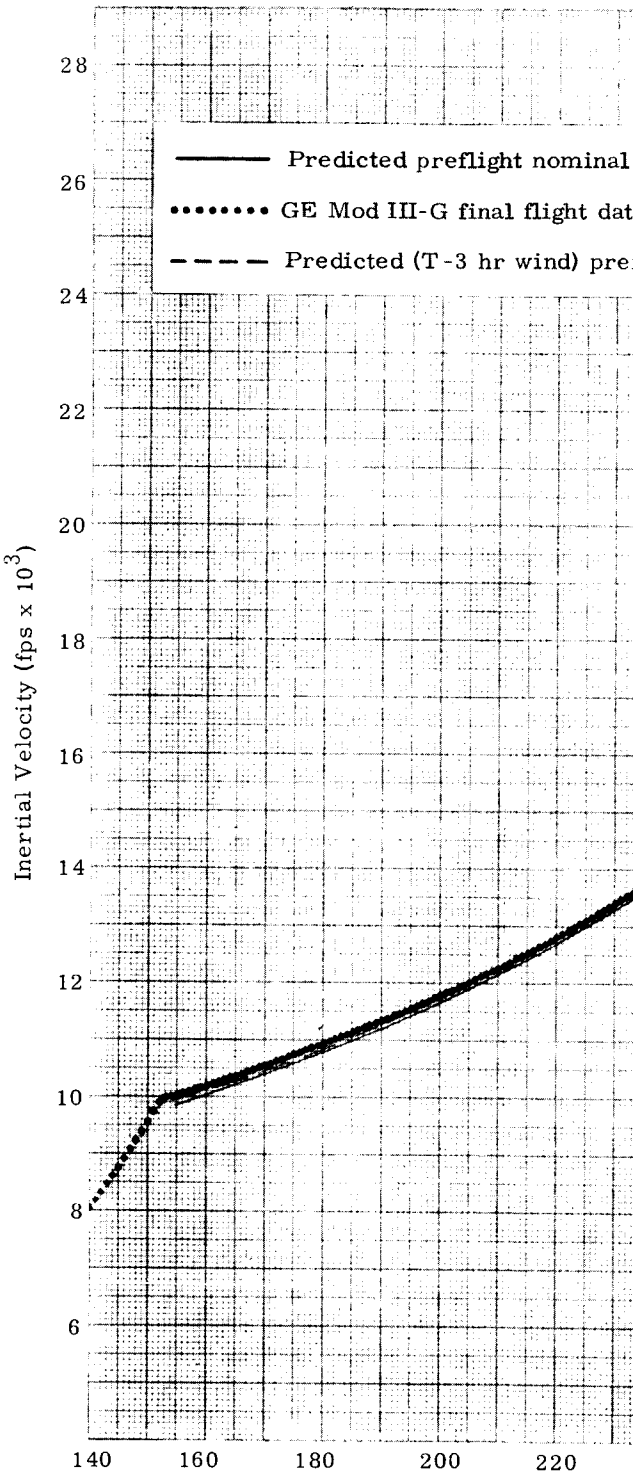
Predicted preflight nominal
GE Mod III-G final flight dat
Predicted (T-3 hr wind) pre
Inertial Velocity (fps x 10^3)
28
26
24
22
20
18
16
14
12
10
8
6
140
160
180
200
220

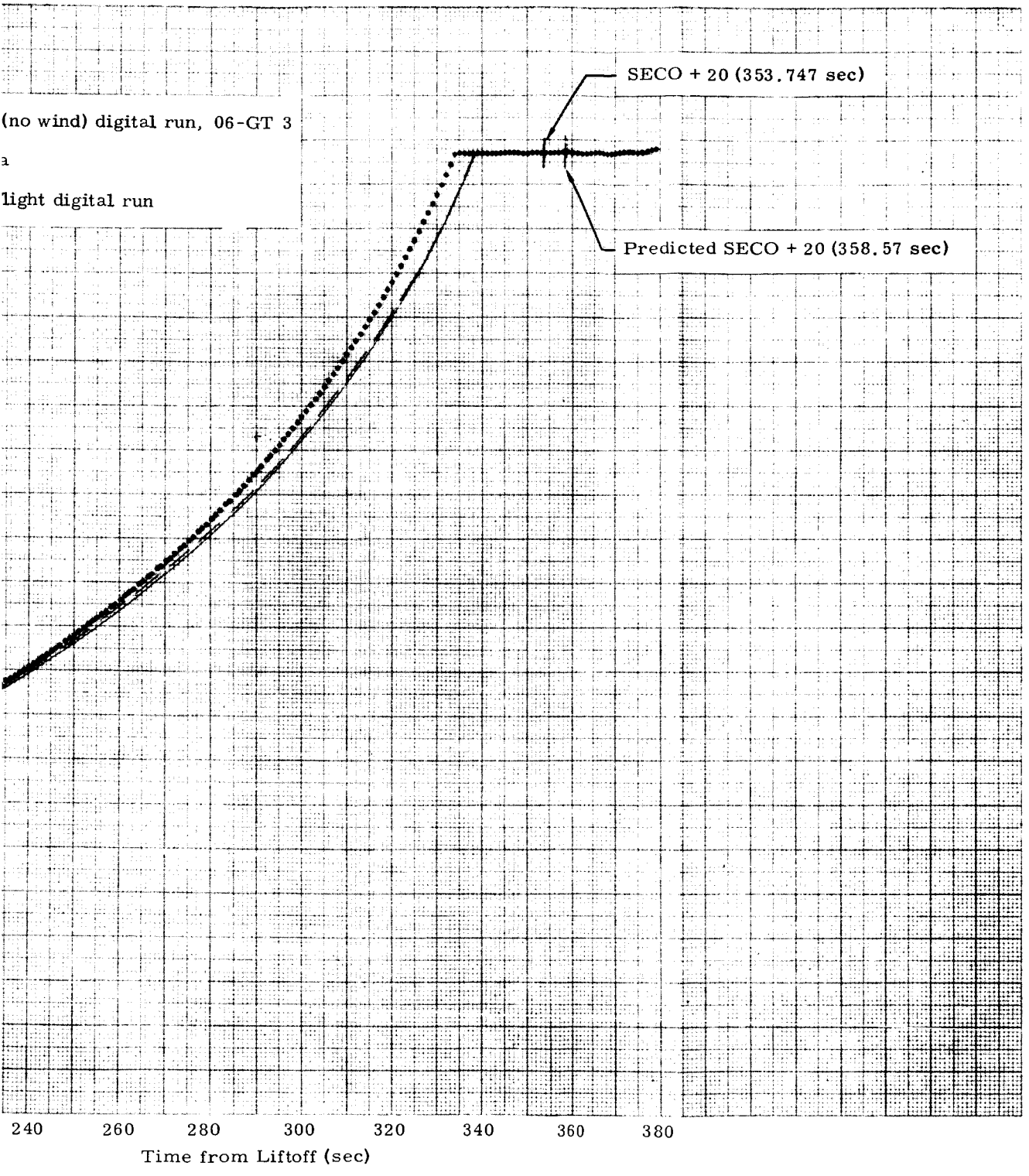


Fig. II-14. Resultant Inertial Velocity ($V_I$) Versus Time: Stage II Flight

[redacted]

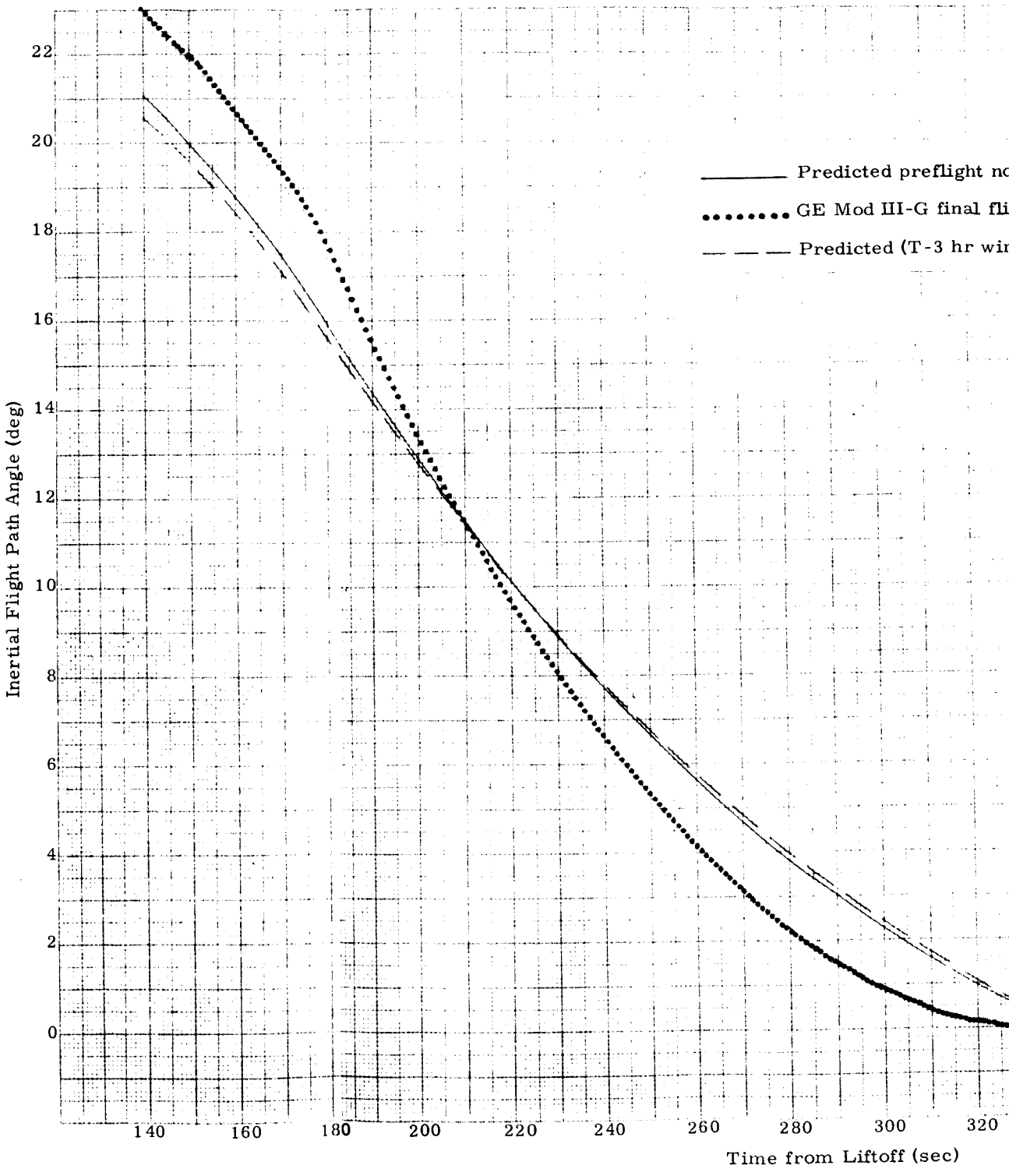


Fig. II-1

[redacted]

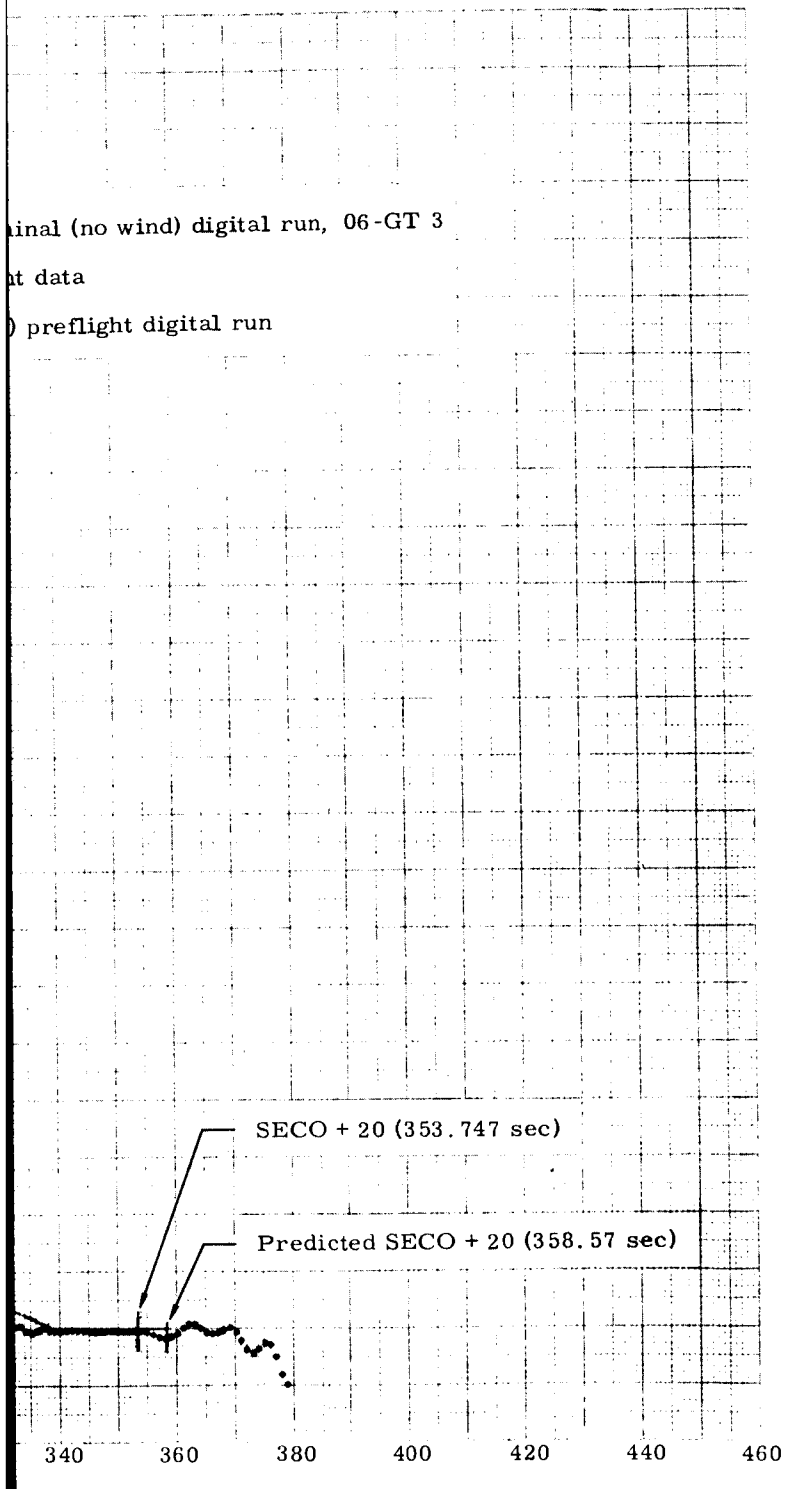


Inertial Flight Path Angle ($\gamma_I$) Versus Time: Stage II Flight

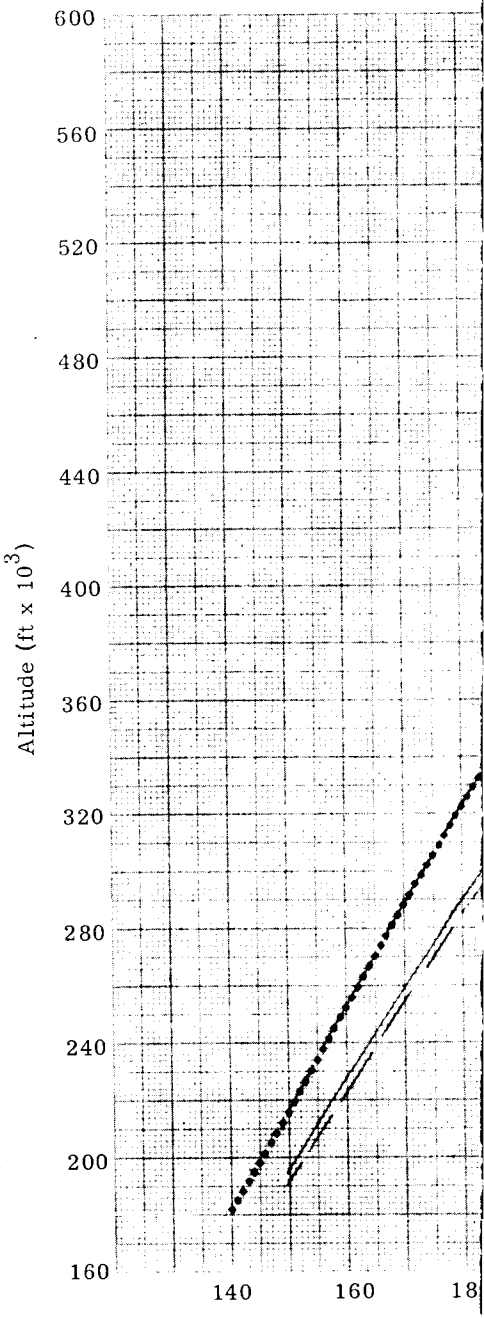
600
560
520
480
440
400
360
320
280
240
200
160
Altitude (ft x $10^3$)
140
160
18

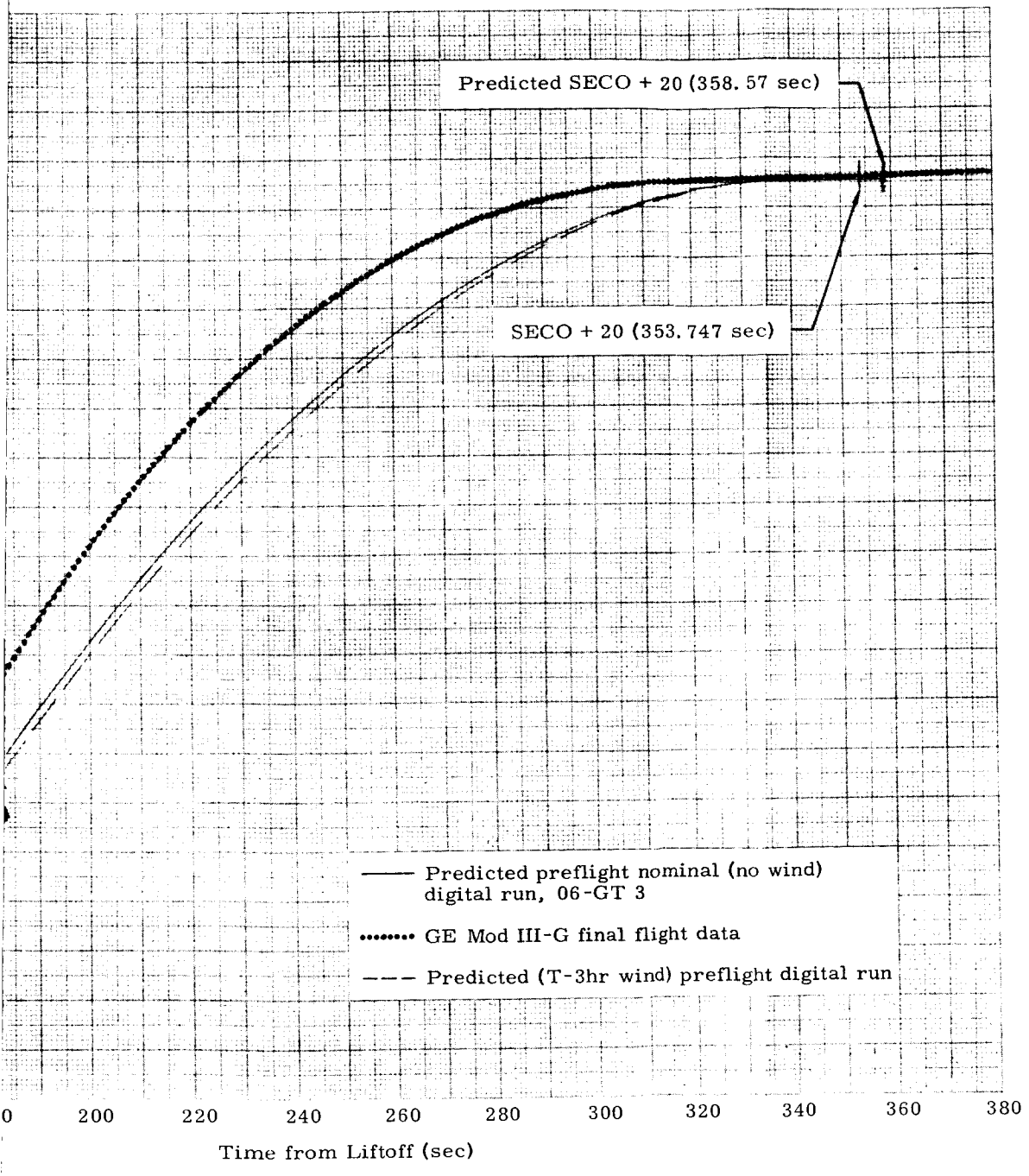


Fig. II-16. Altitude Versus Time: Stage II Flight

[redacted]

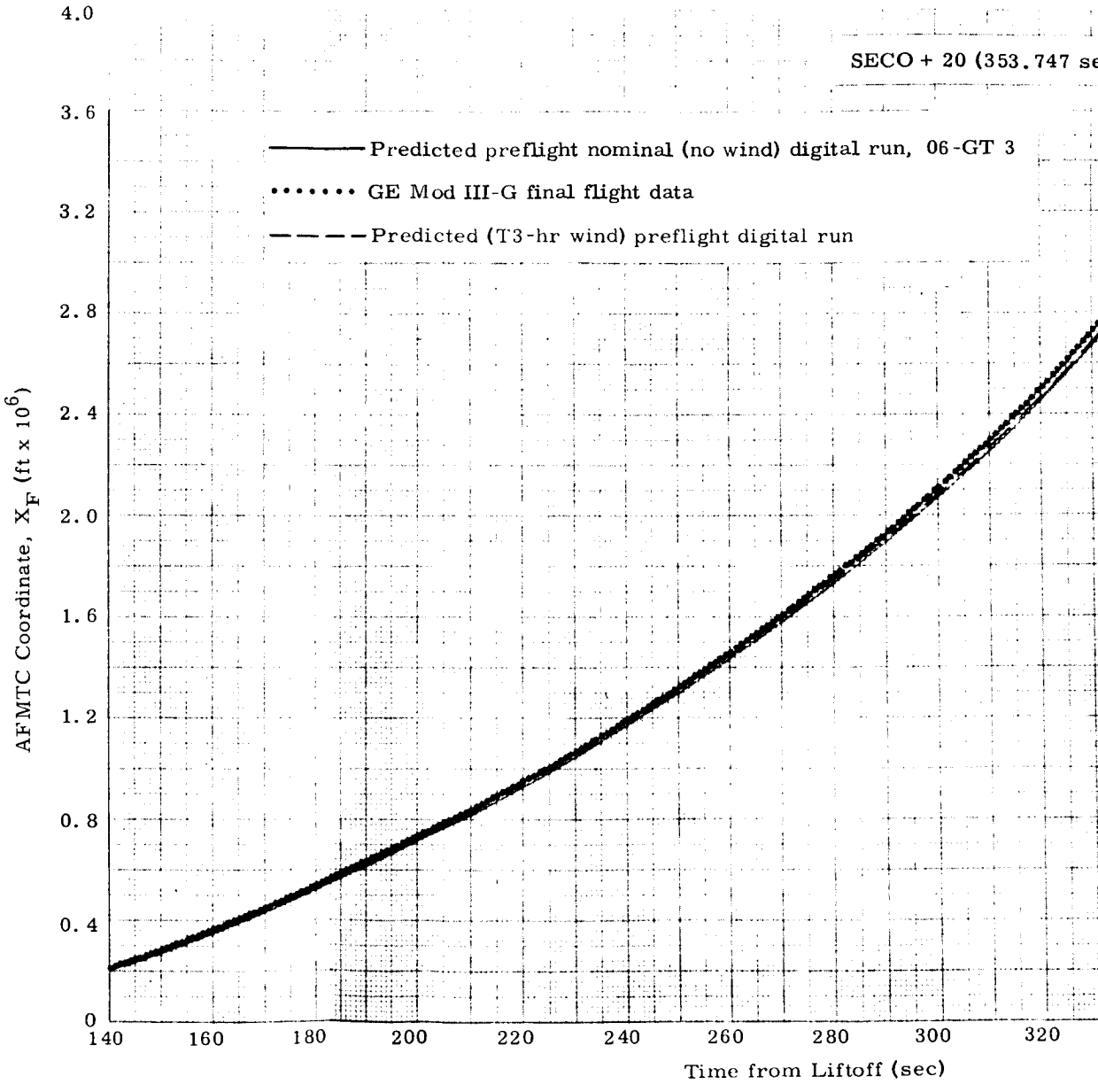


Fig. II-17. Downrange Pos

[redacted]

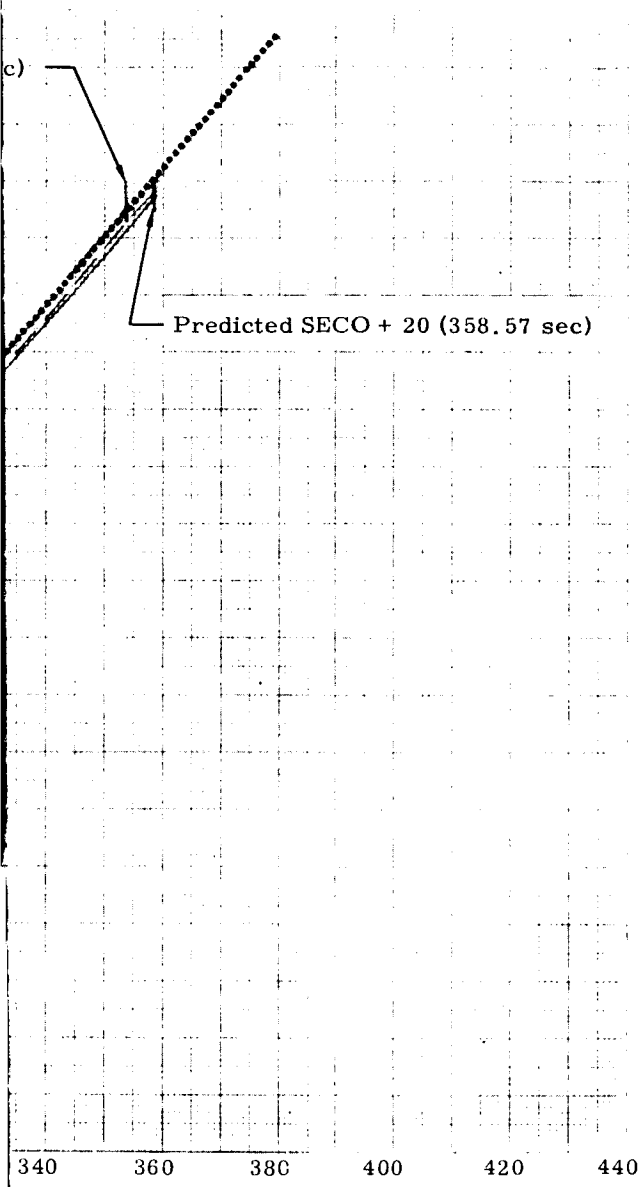


ion Coordinate ($X_F$) Versus Time: Stage II Flight

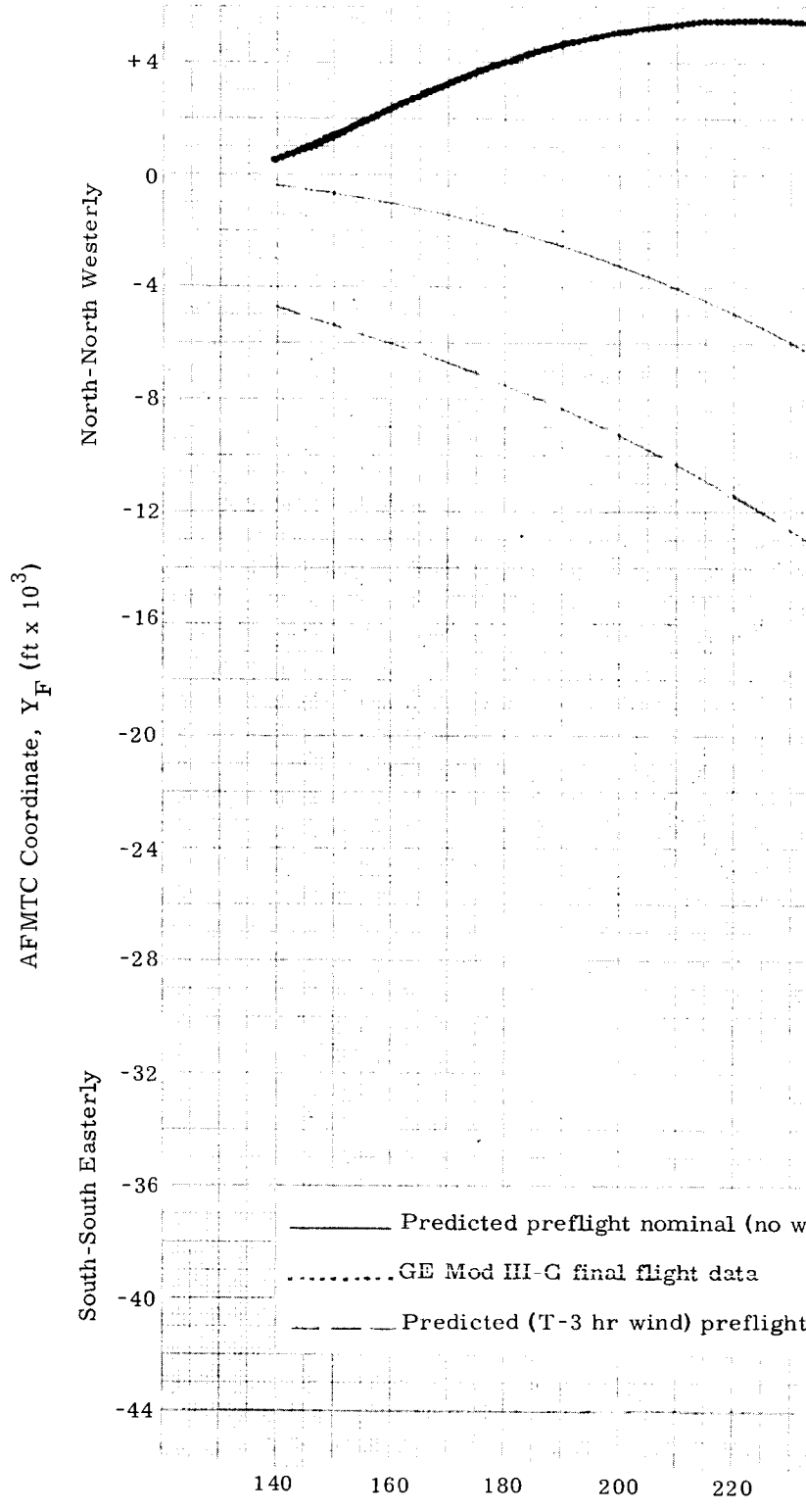
AFMTC Coordinate, $Y_F$ (ft x $10^3$)
North-North Westerly
South-South Easterly
+4
0
-4
-8
-12
-16
-20
-24
-28
-32
-36
-40
-44
140
160
180
200
220
Predicted preflight nominal (no w
GE Mod III-G final flight data
Predicted (T-3 hr wind) preflight

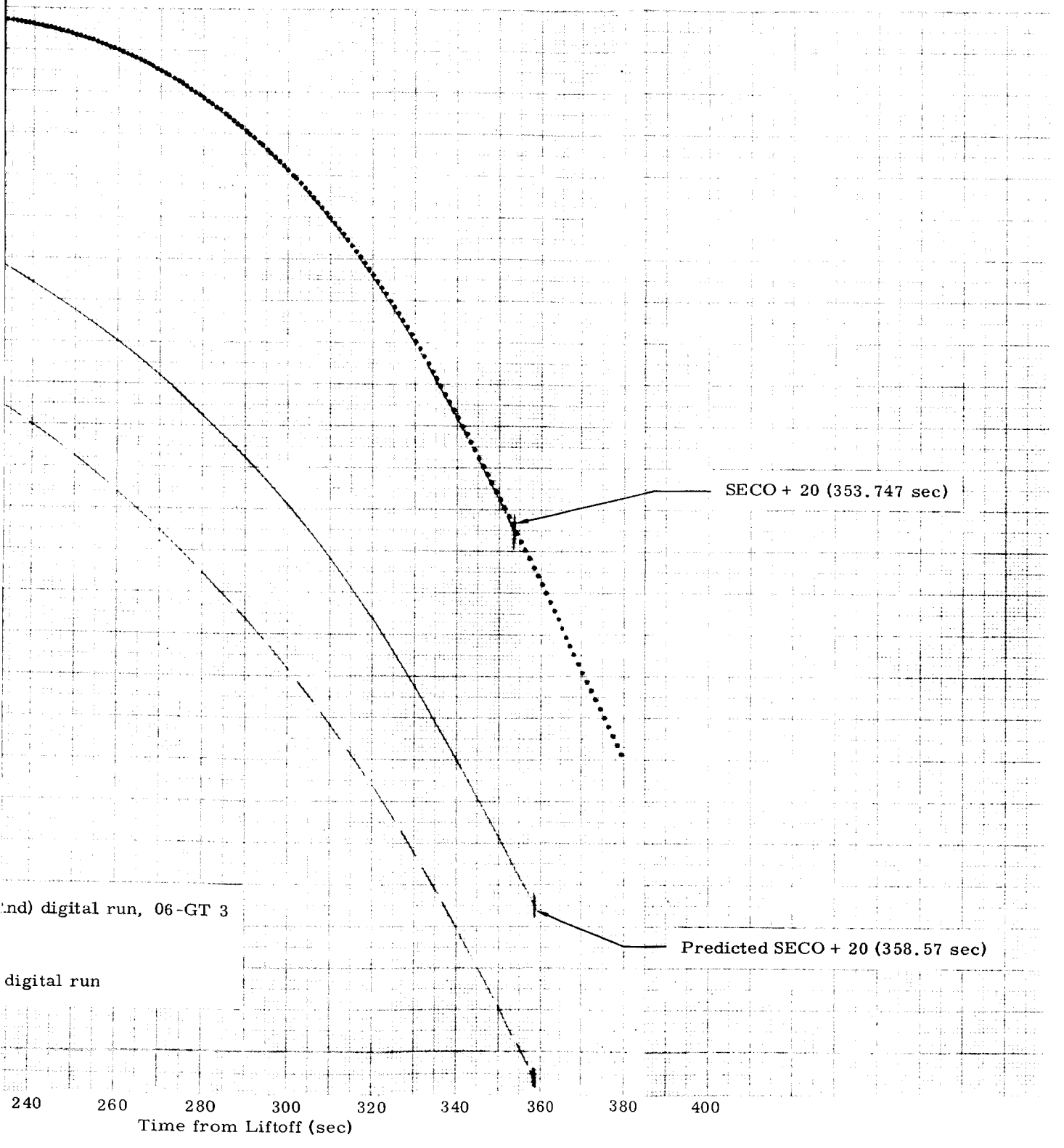


Fig. II-18. Cross-Range Position Coordinate ($Y_F$) Versus Time: Stage II Flight

CONFIDENTIAL

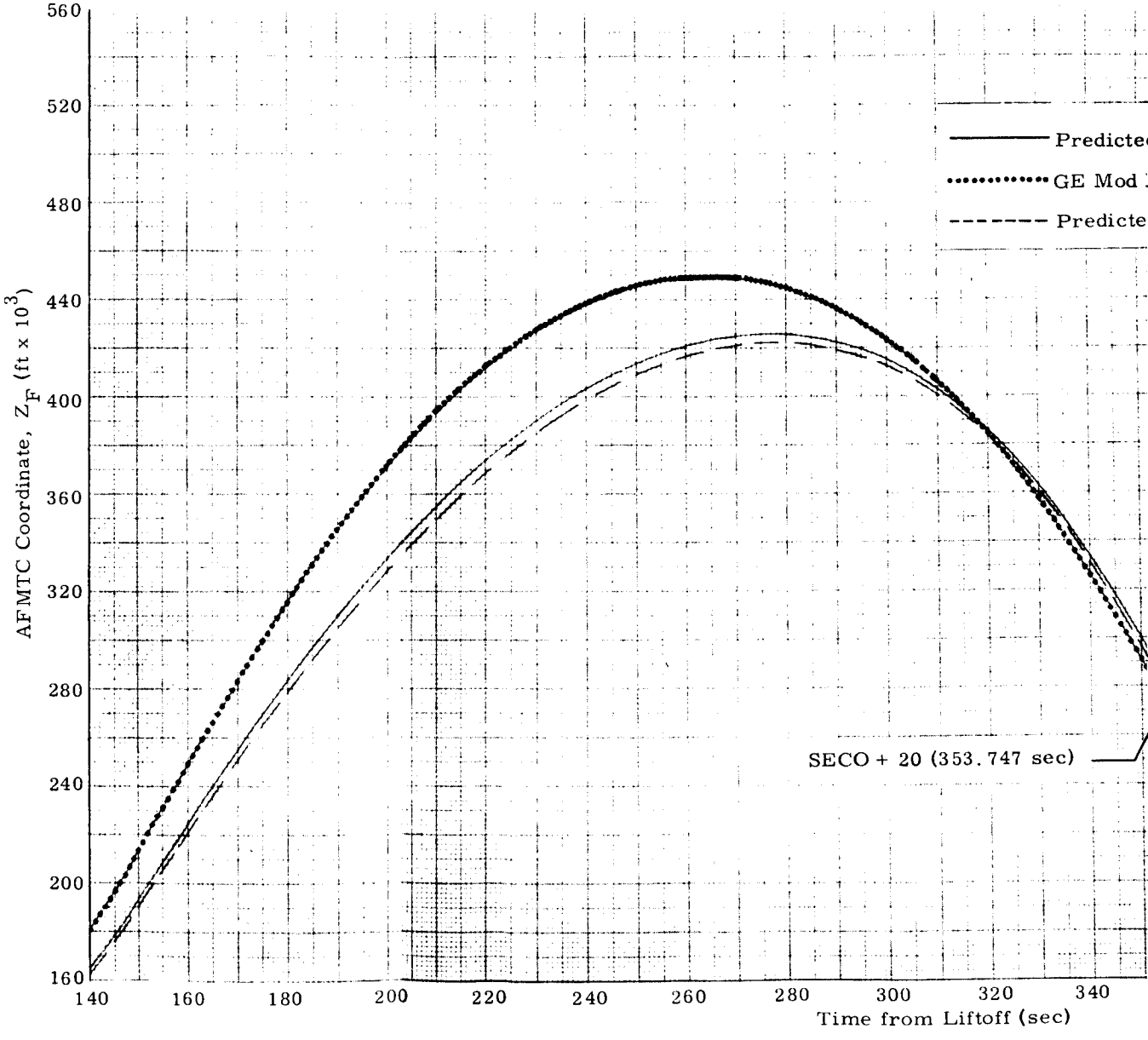


Fig. II-19. Ve

CONFIDENTIAL

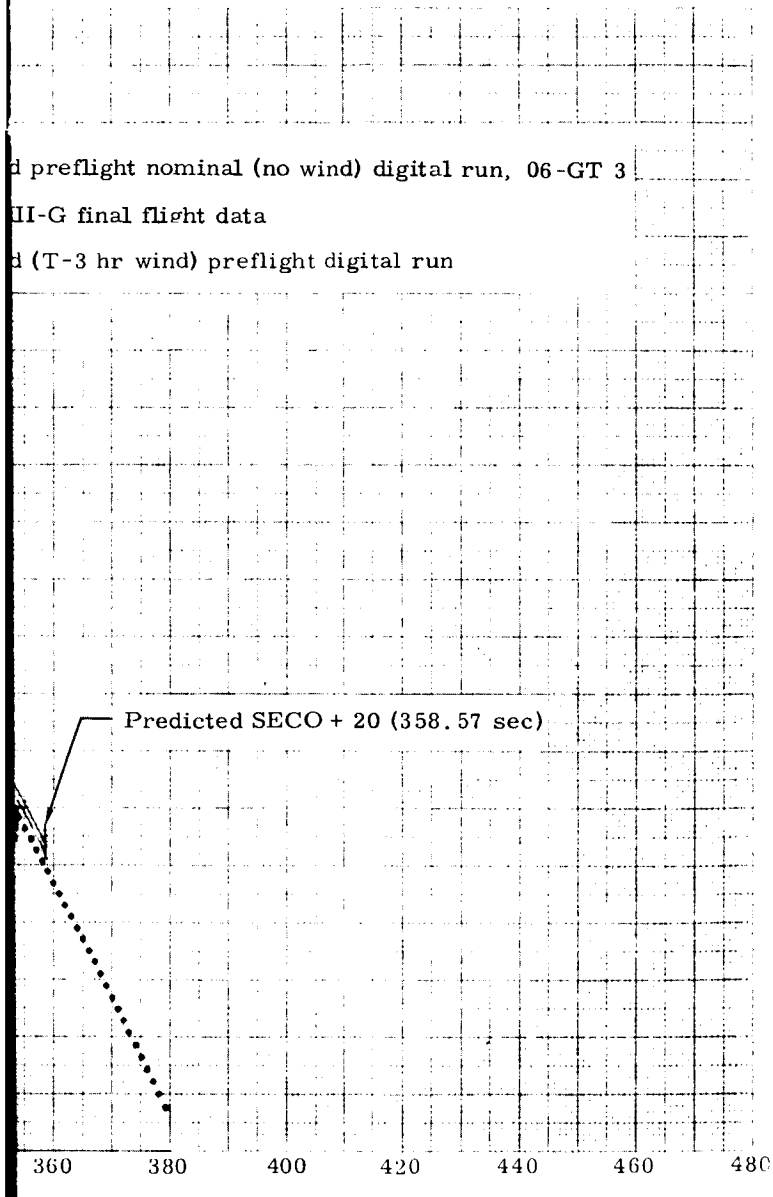


ical Position Coordinate ($Z_F$) Versus Time: Stage II Flight

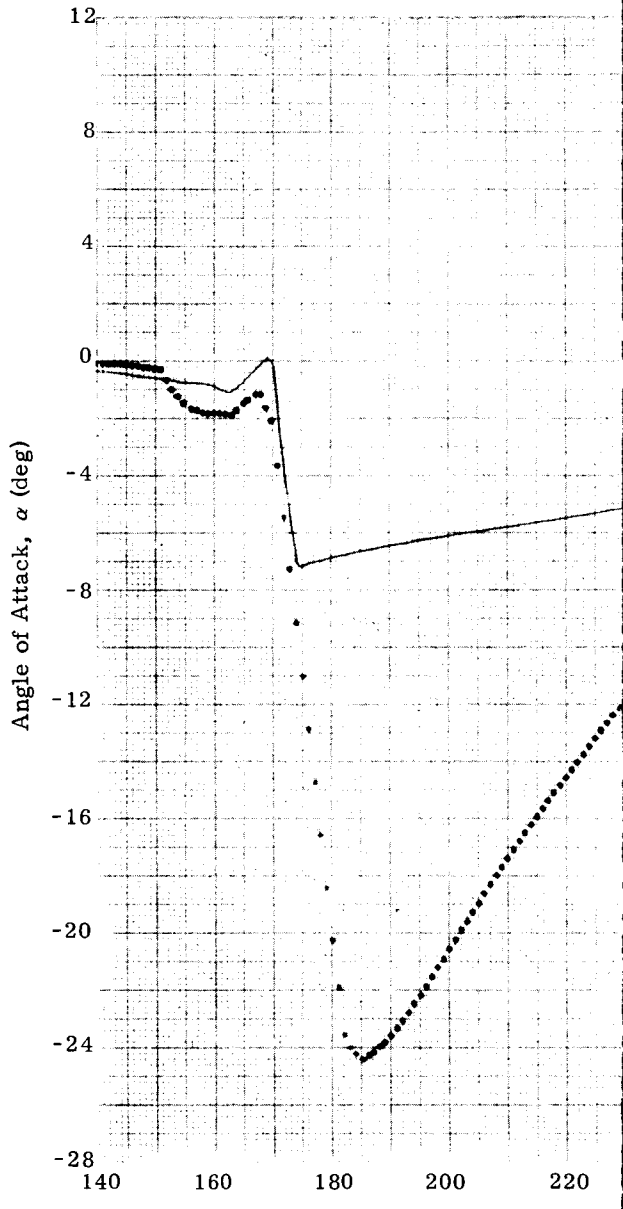
12
8
4
0
-4
-8
-12
-16
-20
-24
-28
Angle of Attack, α (deg)
140
160
180
200
220

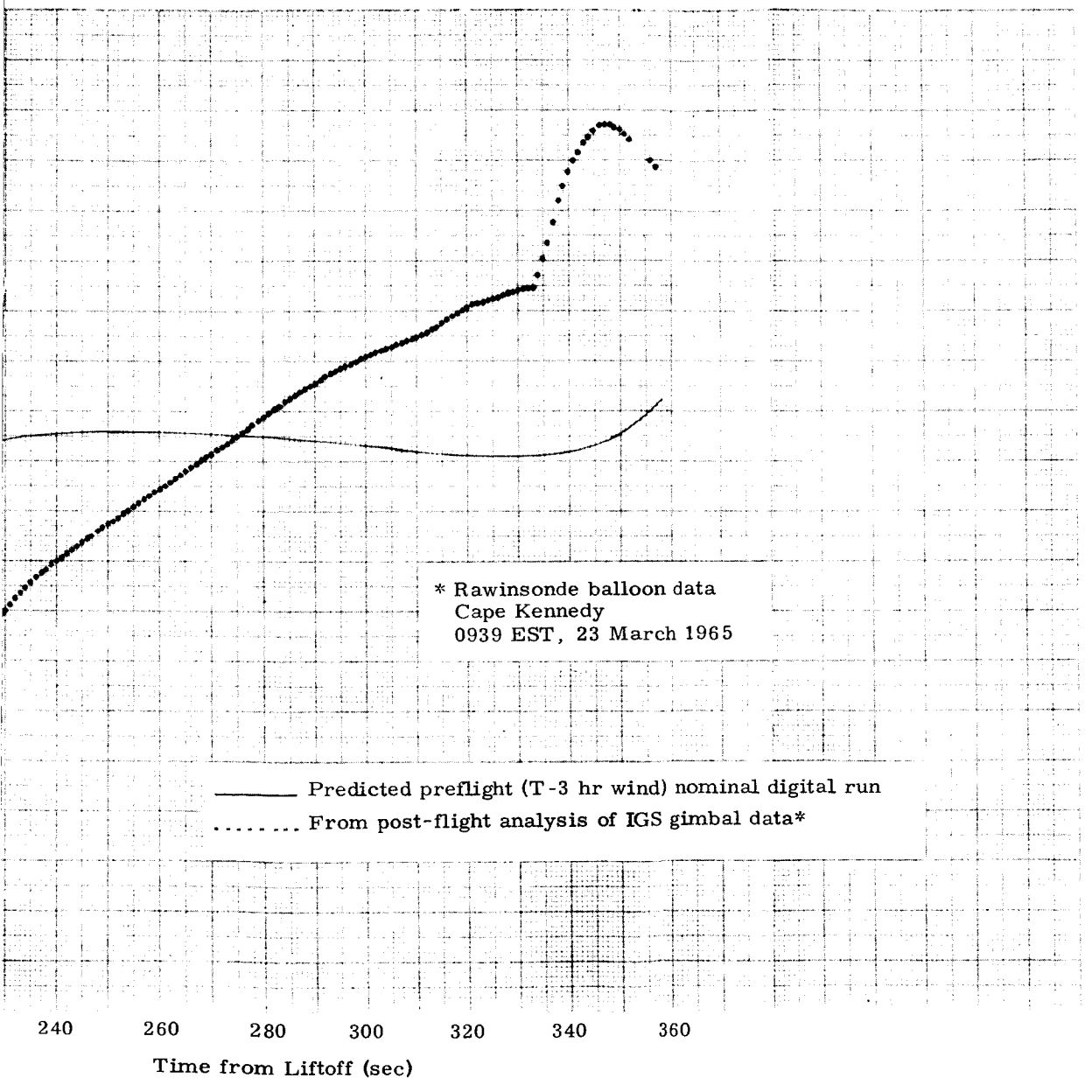


Fig. II-20. Stage II Angle of Attack History

CONFIDENTIAL

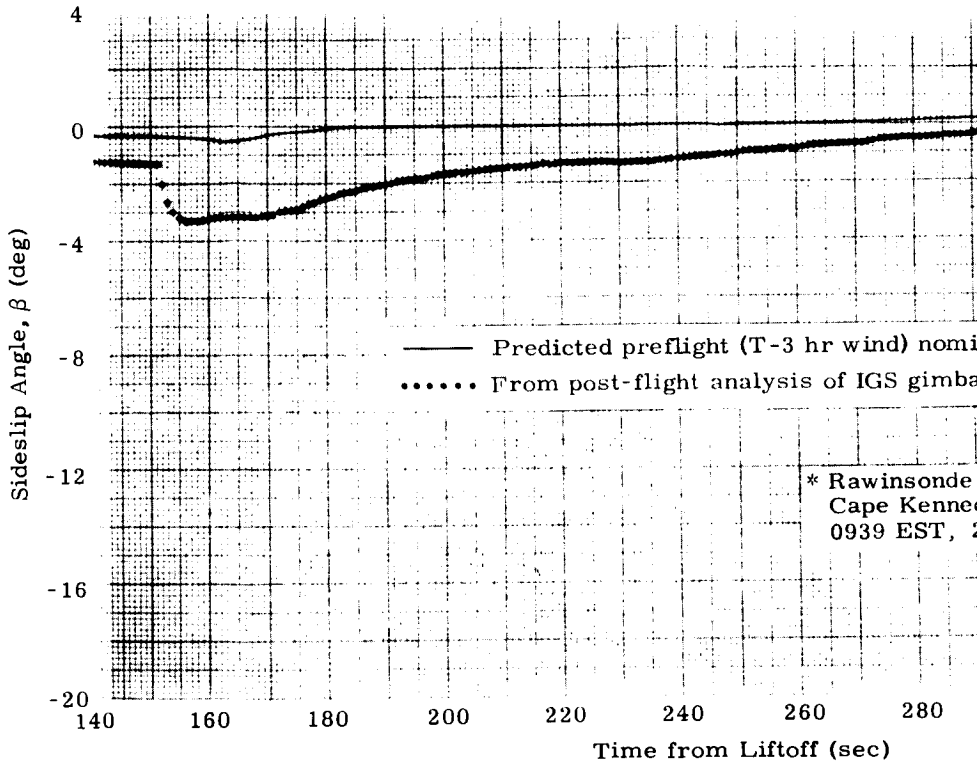


Fig. II-21. Angle of Sid

CONFIDENTIAL

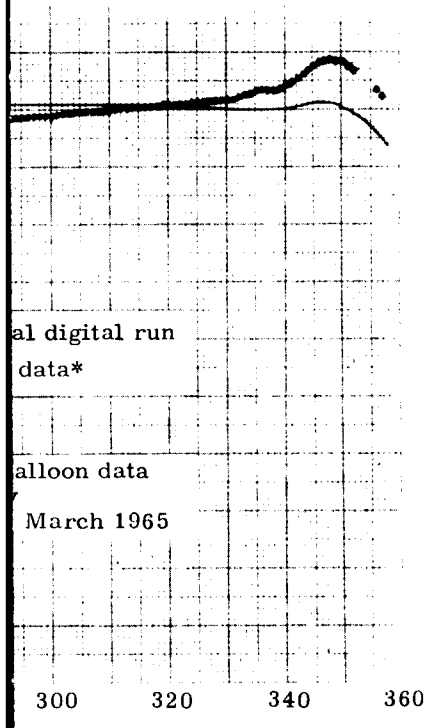


lip Versus Time: Stage II Flight

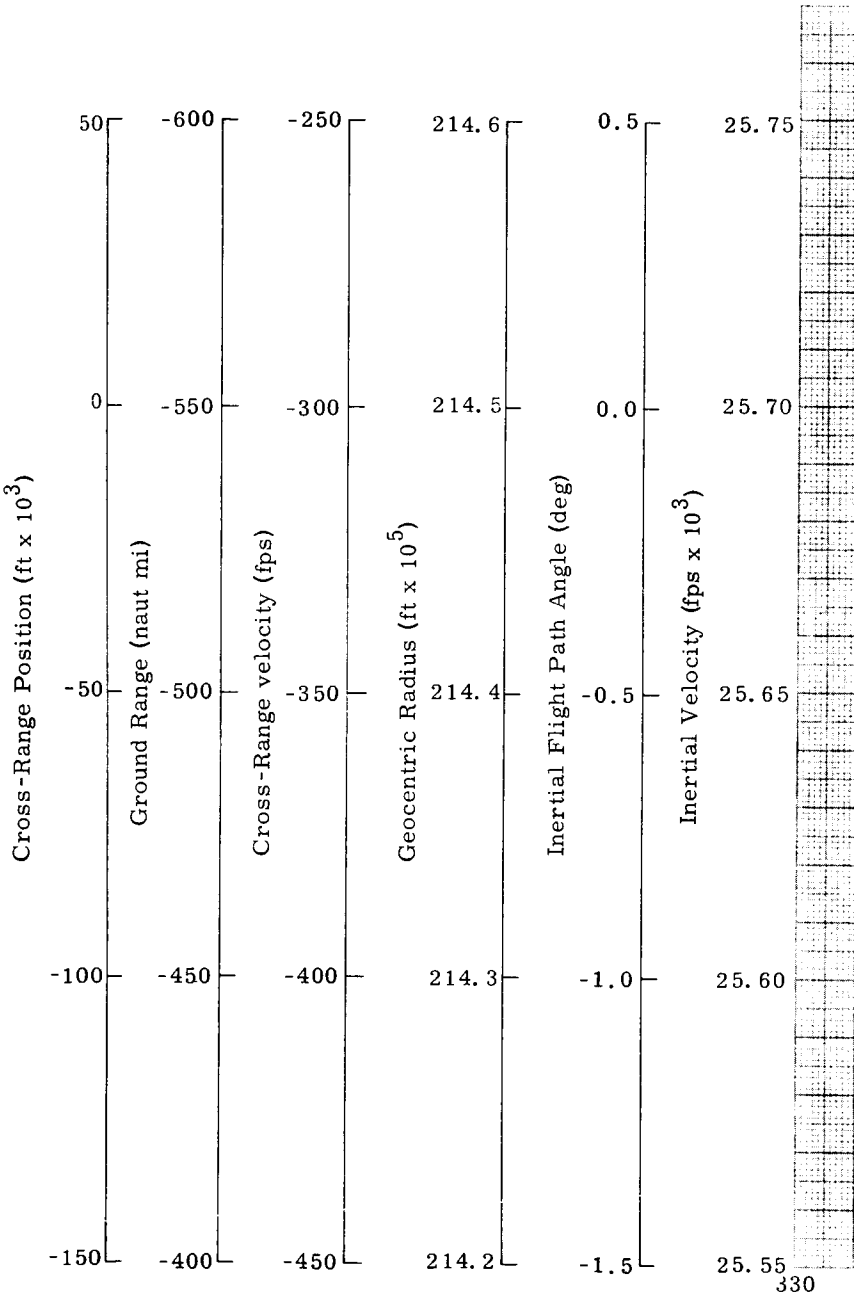
Cross-Range Position (ft x 10^3)
50
0
-50
-100
-150
Ground Range (naut mi)
-600
-550
-500
-450
-400
Cross-Range velocity (fps)
-250
-300
-350
-400
-450
Geocentric Radius (ft x 10^5)
214.6
214.5
214.4
214.3
214.2
Inertial Flight Path Angle (deg)
0.5
0.0
-0.5
-1.0
-1.5
Inertial Velocity (fps x 10^3)
25.75
25.70
25.65
25.60
25.55

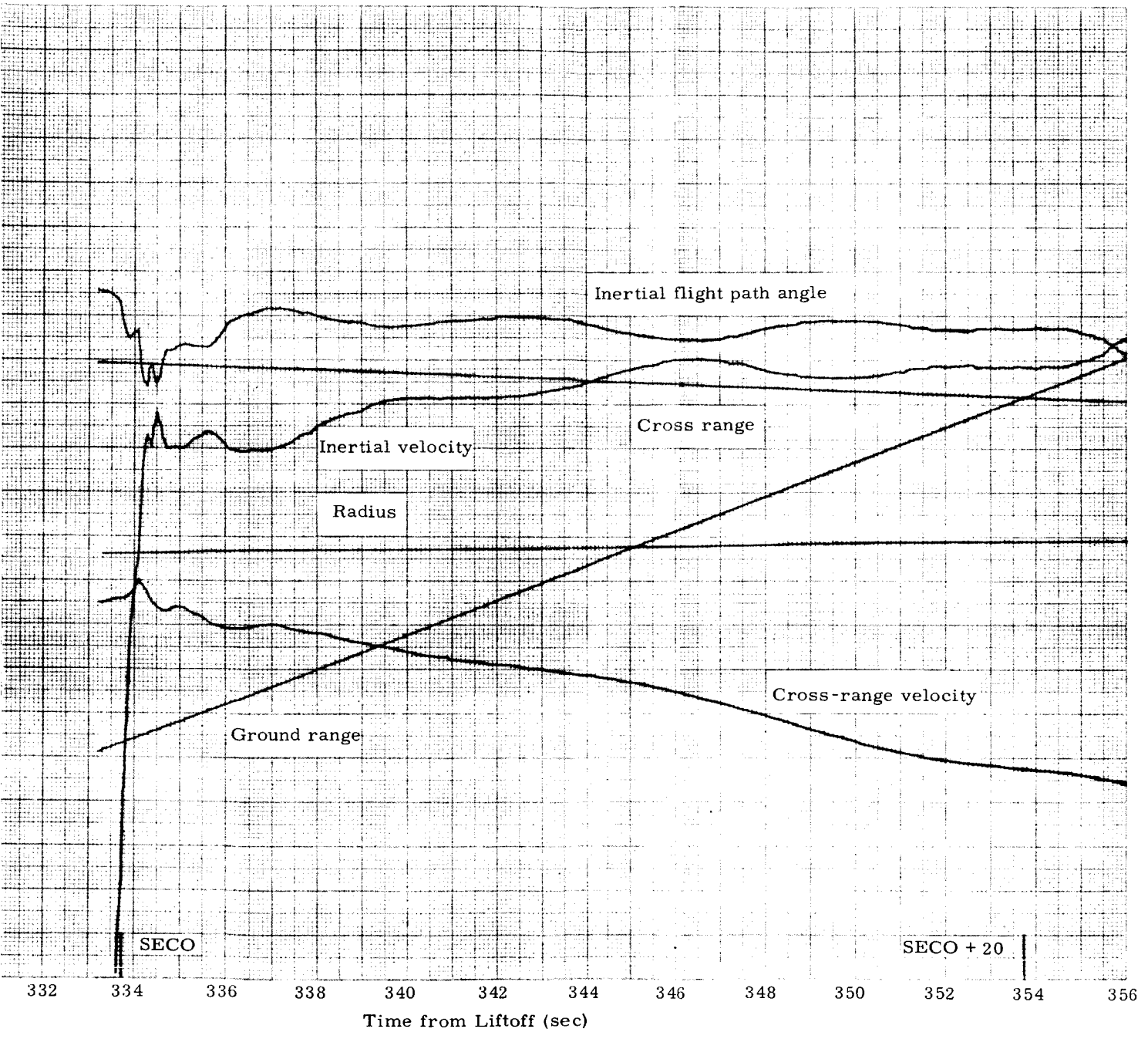


Fig. II-22. GE Mod III-G Flight Data from SECO to SECO + 20 Seconds

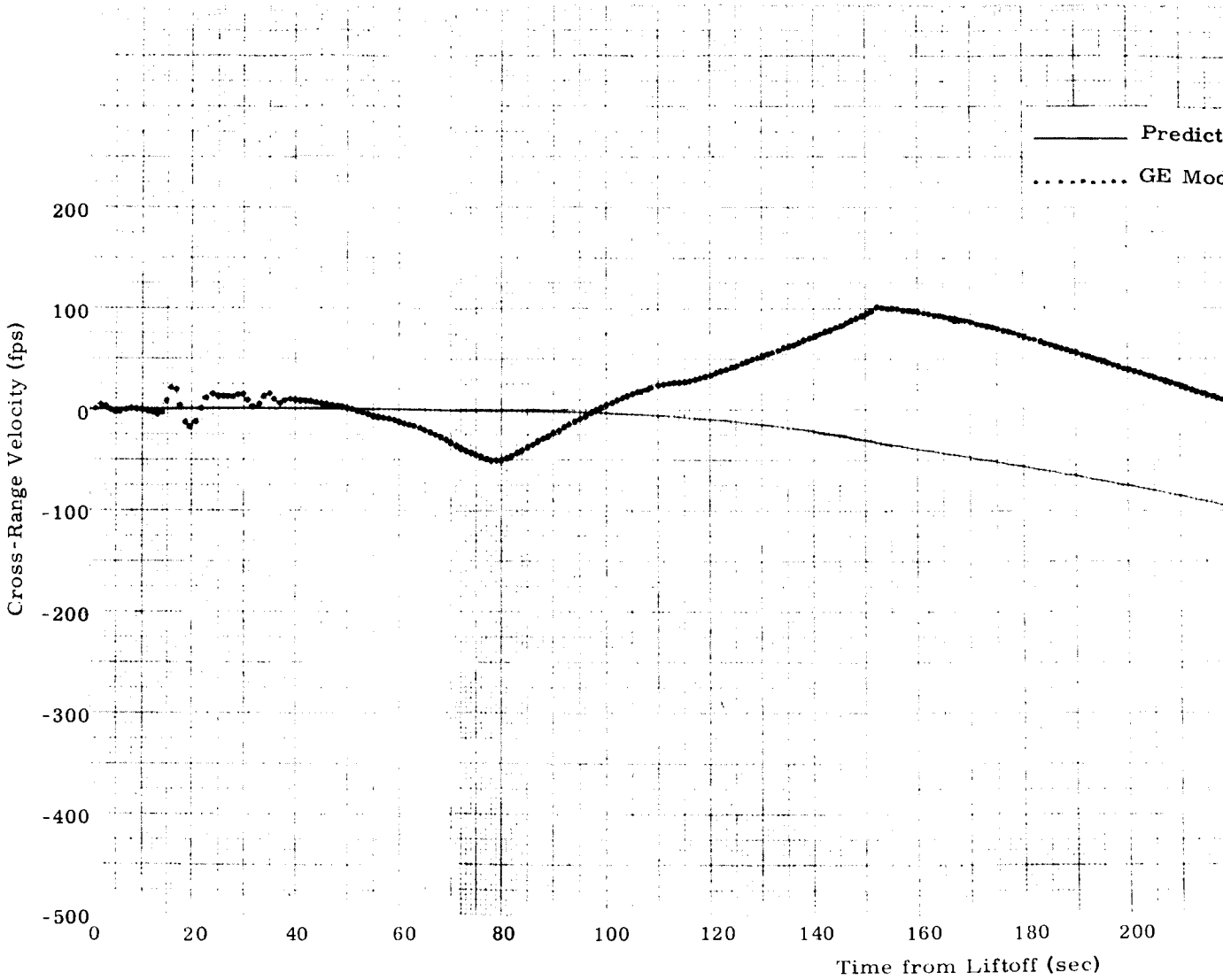
Predict
GE Mod
200
100
0
-100
-200
-300
-400
-500
Cross-Range Velocity (fps)
0
20
40
60
80
100
120
140
160
180
200
Time from Liftoff (sec)

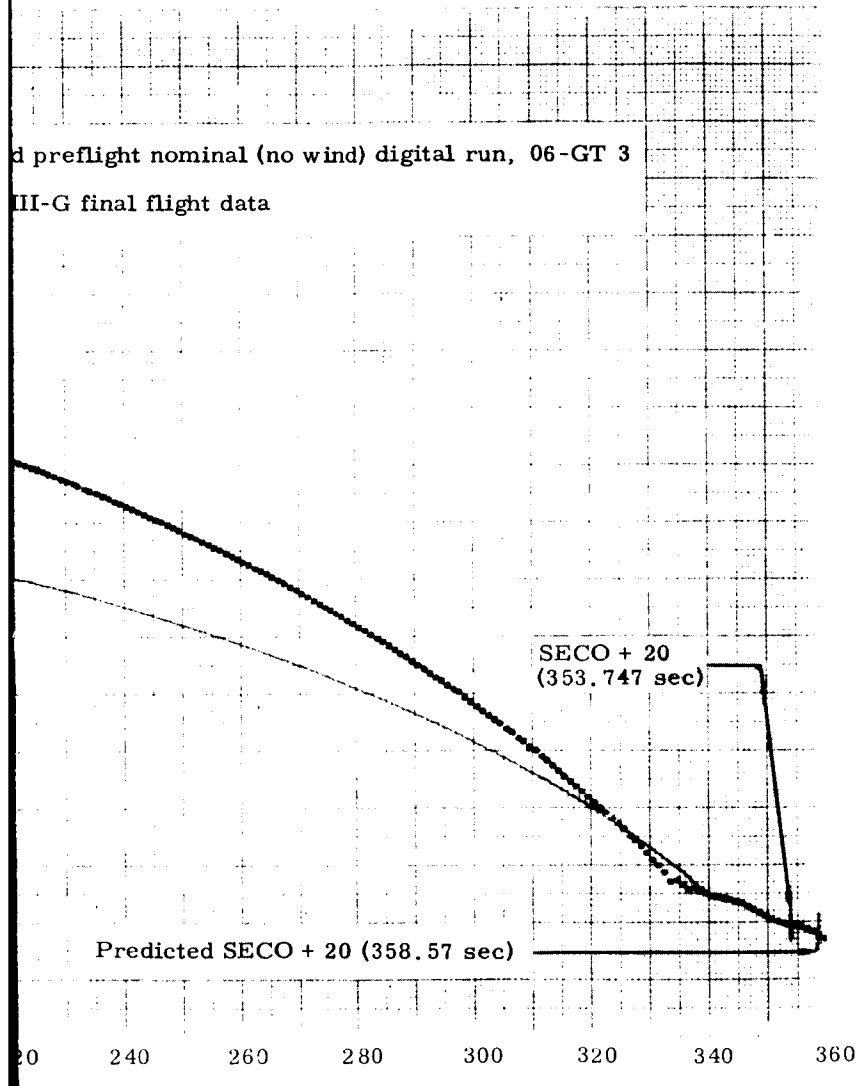


Fig. II-23. Cross-Range Velocity ($Y_F$) Versus Time

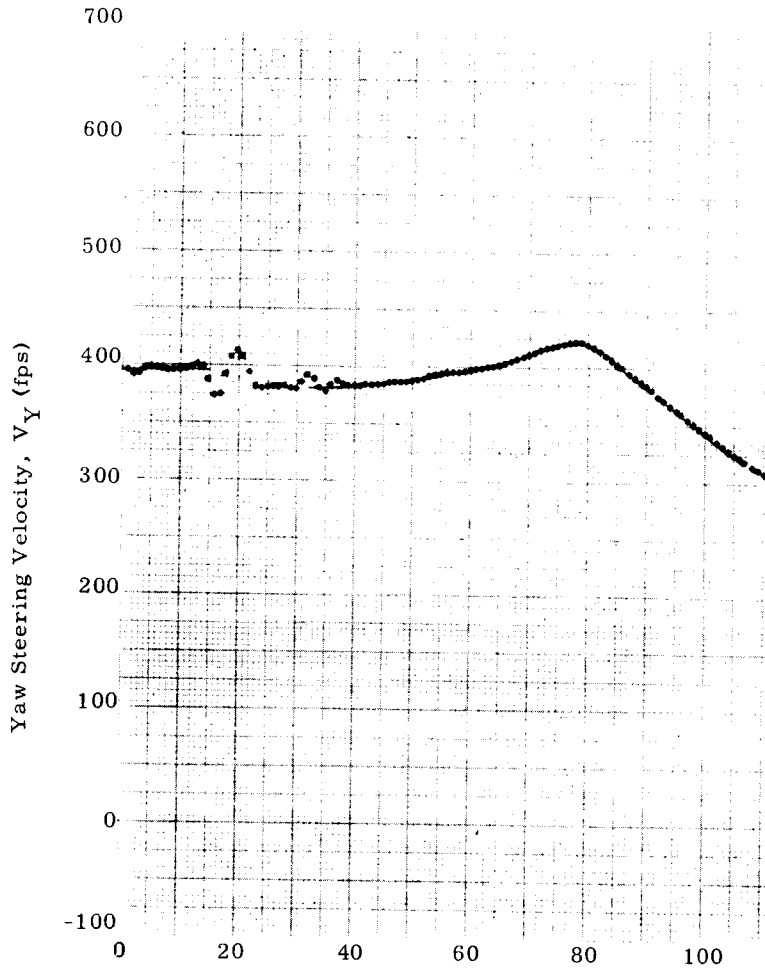
Yaw Steering Velocity, $V_Y$ (fps)
700
600
500
400
300
200
100
0
-100
0
20
40
60
80
100

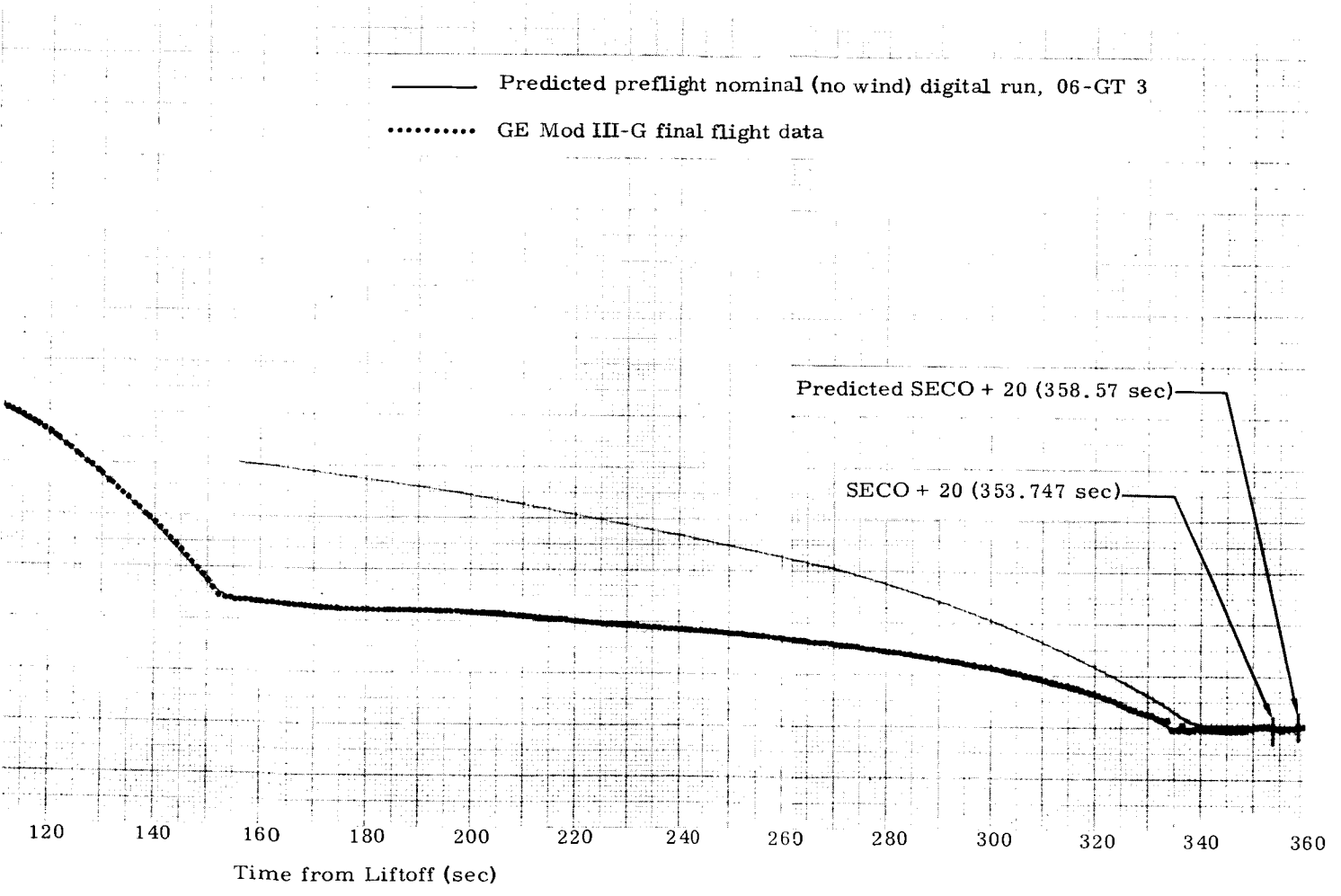


Fig. II-24. Yaw Steering Velocity ($V_Y$) Versus Time

[redacted]

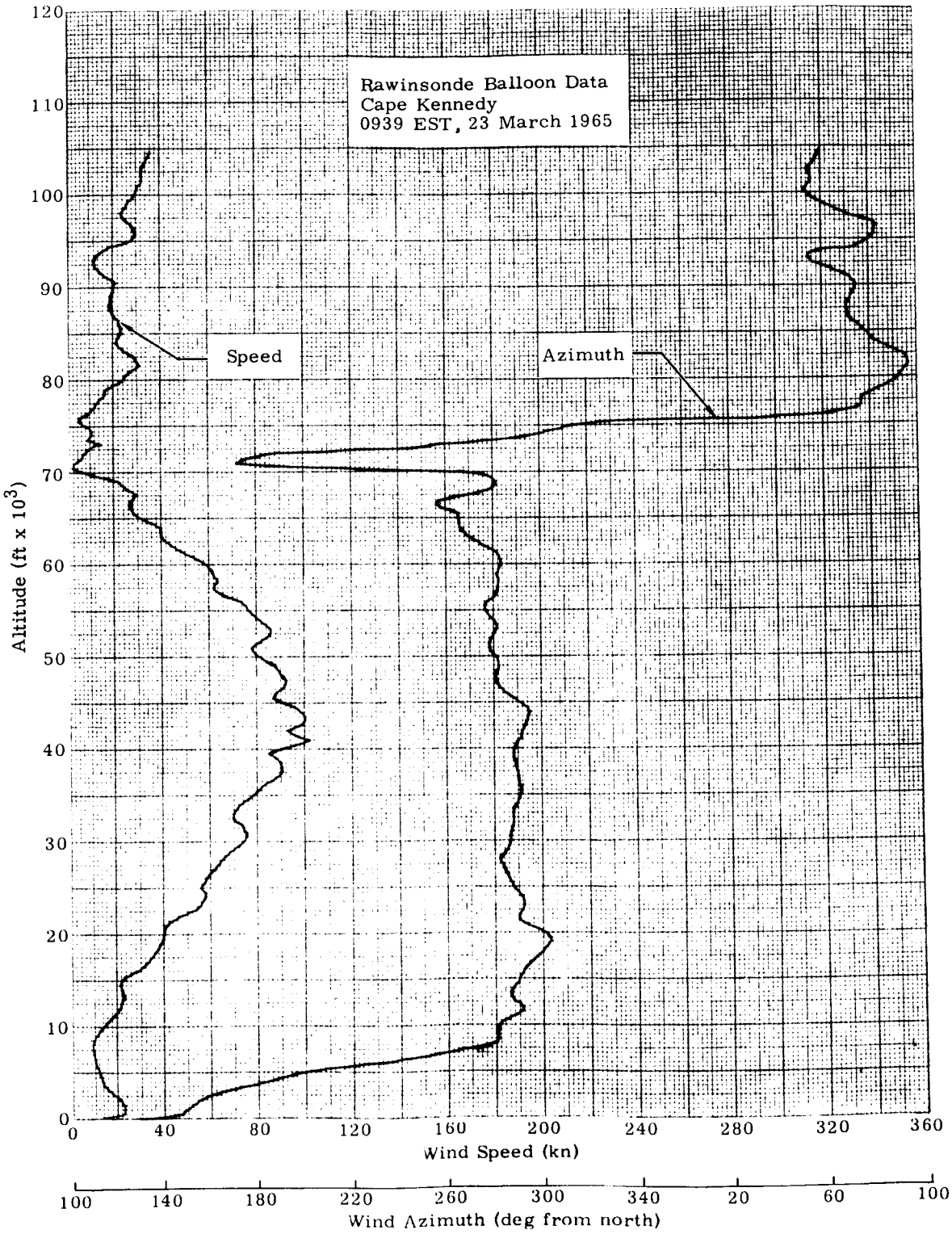


Fig. II-25. Wind Speed and Azimuth Versus Altitude

[redacted]

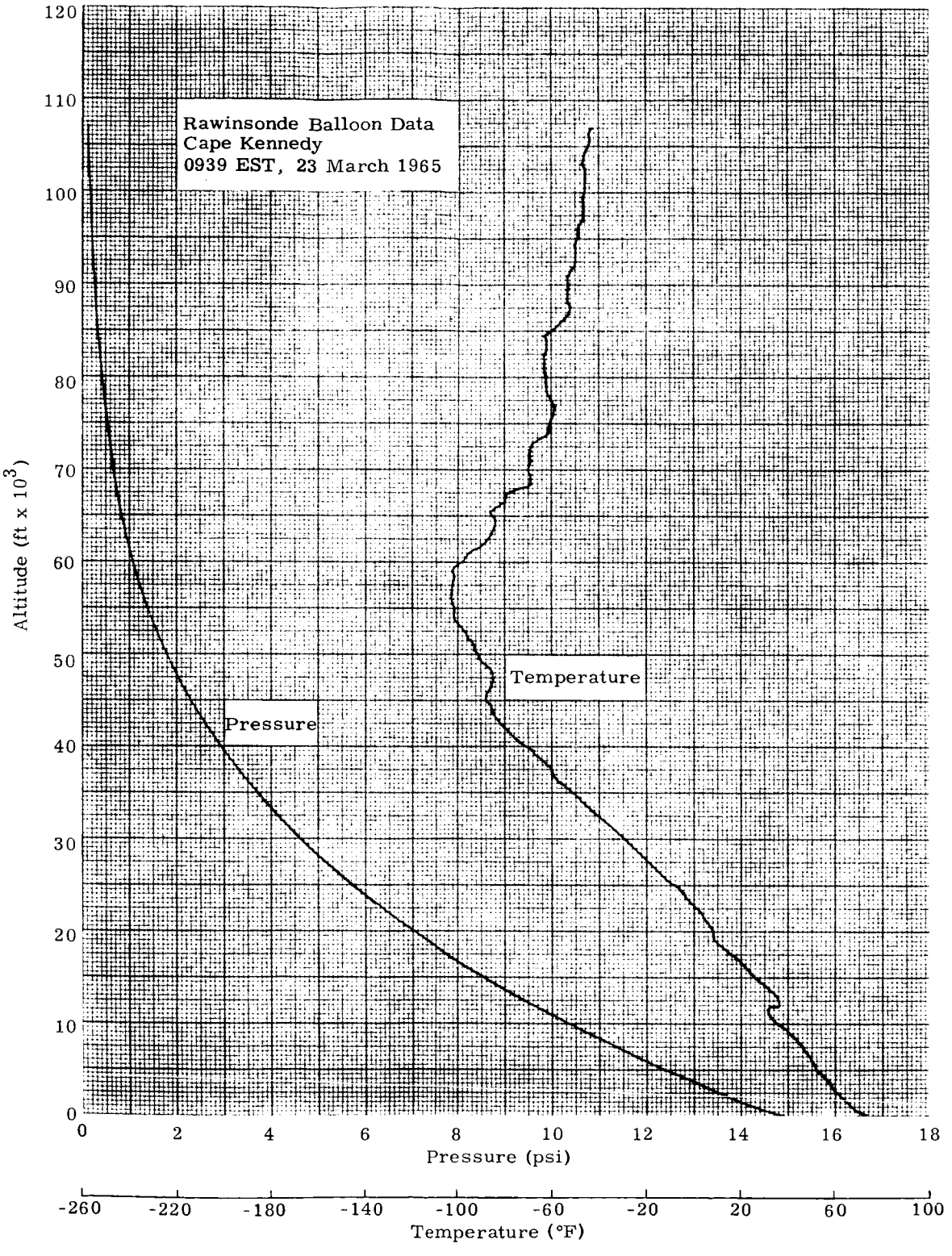


Fig. II-26. Ambient Temperature and Pressure Versus Altitude

[redacted]

TABLE II-5

GT-3 Flight Events Summary

| Meas | Event | GMT (hr-min-sec) | Time from Liftoff Actual | Time from Liftoff Planned* |
|---|---|---|---|---|
| 0800/0801 | Power transfer | 1422:31.1 | -88.96 | -90 |
| 2104 | $87FS_1$ (T-0) | 1423:56.692 | -3.372 | -3.37 |
| 0356 | Stage I S/A 1 MDTCPS make | 1423:57.609 | -2.455 | -2.27 |
| 0357 | Stage I S/A 2 MDTCPS make | 1423:57.700 | -2.364 | -2.27 |
| 2101 | TCPS S/A 1 and S/A2 | 1423:57.816 | -2.248 | -2.27 |
| 1169 | Launch nuts | 1423:59.9 | -0.16 | -0.2 |
| 4421 | First motion | 1423:59.986 | -0.078 | -0.11 |
| 4422 | Shutdown lockout (first motion) | 1424:00.000 | -0.064 | -0.11 |
| 4423 | Liftoff | 1424:00.064 | 0 | 0 |
| 0734 | Start roll program | 1424:10.20 | 10.14 | 10.16 |
| 0734 | End roll program | 1424:20.48 | 20.42 | 20.48 |
| 0732 | Start pitch program No. 1 | 1424:23.07 | 23.01 | 23.04 |
| 0732 | Stop pitch program No. 1 | 1425:28.28 | 88.22 | 88.32 |
| 0732 | Start pitch program No. 2 | 1425:28.28 | 88.22 | 88.32 |
| 0728 | FCS gain change No. 1 | 1425:44.88 | 104.82 | 104.96 |
| 0732 | Stop pitch program No. 2 | 1425:58.90 | 118.84 | 119.04 |
| 0732 | Start pitch program No. 3 | 1425:58.90 | 118.84 | 119.04 |
| -- | Start tape recorder | 1426:23.22 | 143.156 | 143.36 |
| 0735 | Staging enable (TARS discrete) | 1426:24.485 | 144.421 | 144.64 |
| 0741 | IPS staging arm timer | 1426:25.197 | 145.133 | 145.00 |
| 0356 | Stage I S/A 1 MDTCPS break | 1426:32.441 | 152.377 | 154.21 |
| 0357 | Stage I S/A 2 MDTCPS break | 1426:32.442 | 152.378 | 154.21 |
| 0032 | $87FS_2/91FS_1$ (BECO) | 1426:32.497 | 152.433 | 154.27 |
| 0502 | Start $PC_3$ rise | 1426:33.130 | 153.066 | 154.97 |
| 1085/1169 | Stage separation | 1426:33.155 | 153.091 | 154.97 |
| 0855 | Stage II MDFJPS make | 1426:33.148 | 153.084 | 155.17 |
| -- | Stop tape recorder | 1426:35.26 | 155.20 | 157.27 |
| -- | Start tape recorder playback | 1426:37.44 | 157.38 | 159.27 |
| 0732 | Stop pitch program No. 3 | 1426:42.38 | 162.32 | 162.56 |

[redacted]

TABLE II-5 (continued)

| Meas | Event | GMT (hr-min-sec) | Time from Liftoff | |
|---|---|---|---|---|
| | | | Actual | Planned* |
| 0740 | RGS enable | 1426:42.370 | 162.306 | 162.56 |
| 0755/0756 | First guidance command | 1426:48.346 | 168.282 | 168.25 |
| 0739 | Stage II shutdown enable | 1429:17.064 | 317.000 | 317.44 |
| 0777 | Guidance SECO | 1429:33.791 | 333.727 | 338.54 |
| 0519 | $91FS_2$ | 1429:33.811 | 333.747 | 338.57 |
| 0521 | Shutdown squib | 1429:33.836 | 333.772 | 338.59 |
| 0522 | Shutdown valve relay | 1429:33.846 | 333.782 | 338.59 |
| 0799 | ASCO | 1429:33.853 | 333.789 | 338.59 |
| 0855 | Stage II MDFJPS break | 1429:33.952 | 333.888 | 338.87 |
| AB-03 | Spacecraft separation | 1429:59.450 | 359.386 | 358.60 |

*GLV trajectory 06-GT-3, dated 23 March 1965.

NOTES: Burning time for Stage I = 155.805 sec
Stage II = 181.314 sec

It appears that, even with the limited amount of data available, a consistent set of contributing factors may be determined and their effects accounted for on future flights. A detailed examination of all possible factors contributing to BECO dispersions includes over 20 possible parameters. Some of these are relatively insignificant; however, those causing the greatest portion of the BECO deviation on the GT-3 flight are presented in Table II-7. Table II-7 is comprised of two parts. Part A consists of those items which can be measured to a fair degree of accuracy while Part B contains those items which can only be estimated due to the lack of suitable instrumentation. The amount of probable deviation for each parameter was obtained from post-flight evaluations wherever possible. The resulting incremental changes in time, altitude, velocity, and flight path angle were obtained from the dispersion analysis report (Ref. 8). Addition of these incremental changes results in a total apparent deviation which agrees reasonably well with the measured delta in each case. To check the validity of this method of combining dispersions, a composite digital trajectory utilizing all these parameters was computed. The results verify that the dispersions may be combined algebraically to obtain the desired result.

To summarize, the high BECO dispersion appears to be due primarily to winds, programmer error, and larger-than-expected engine thrust and specific impulse.

[redacted]

TABLE II-6

BECO Conditions for GT-2 and GT-3 Flights

| | Parameter | Predicted | Observed* | Apparent Delta | Expected** Tolerance |
|---|---|---|---|---|---|
| GT-2 | Inertial velocity (fps) | 9761 | 9916 | +155 | ± 169 |
| | Flight path angle (deg) | 21.18 | 22.85 | +1.67 | ± 2.58 |
| | Geocentric radius (ft) | 21,127,148 | 21,139,874 | +12,726 | ± 11,990 |
| | Time (sec) | 154.95 | 151.71 | -3.24 | ± 3.89 |
| GT-3 | Inertial velocity (fps) | 9889 | 9981 | +92 | ± 169 |
| | Flight path angle (deg) | 19.51 | 21.79 | +2.28 | ± 2.59 |
| | Geocentric radius (ft) | 21,119,526 | 21,134,377 | +14,856 | ± 12,741 |
| | Time (sec) | 154.27 | 152.43 | -1.84 | ± 3.90 |

*From MOD III final 10 pps data (smoothed and corrected).
**Nominal dispersion resulting from 3σ vehicle perturbations.

[redacted]

TABLE II-7

Factors Contributing to GT-3 BECO Dispersions

| | Δt (sec) | ΔAlt (ft) | ΔVel (fps) | Δγ (deg) |
|---|---|---|---|---|
| Measured parameters | | | | |
| Winds (1439 ZULU atmosphere) | 0 | -1,800 | +46 | -0.14 |
| Outage (408 lb) | +0.24 | +700 | +39 | -0.02 |
| Propellant loading (-559 lb) | -0.35 | +104 | -13 | +0.10 |
| Inert weight (+109 lb) | -- | -255 | -8 | -0.01 |
| Trend indications | | | | |
| Program error (-1.2%) | 0 | +3,040 | -28 | +0.65 |
| $I_{sp}$ (+2.53 sec) | +1.46 | +2,240 | +88 | -0.29 |
| Thrust (+2.09%) | -3.03 | +5,660 | +20 | +1.068 |
| Pitch engine misalignment (-0.065 deg) | -- | +930 | -10 | +0.233 |
| Pitch gyro drift (+16.3 deg/hr) | -- | +2,250 | -23 | +0.54 |
| Σ Apparent Δ (A and B) | -1.68 | +12,869 | +111 | +2.131 |
| Measured Δ (from Table II-6) | -1.84 | +14,856 | +92 | +2.28 |

On the basis of these reconstructions, it has been decided to use slightly increased values of thrust and $I_{sp}$ for the GT-4 preflight predicted trajectories. Thrust and $I_{sp}$ will be increased 8200 pounds and two seconds, respectively, from the engine acceptance test values as computed with the AGC thrust coefficient. As a result of the engine model changes, the TARS programmer pitch rates will be modified on GLV-4 to maintain a balanced pitch look-angle constraint.

BECO conditions and orbit insertion conditions are presented in Table II-8, and a complete list of data sources utilized in the trajectory analyses is contained in Table II-9.

## 6. Look Angles

Upon initiation of closed-loop guidance at LO + 168.3 seconds, the RGS commanded the maximum 2 deg/sec nose-down pitching rate for an interval of 12 seconds in order to correct for the high BECO position. This maneuver resulted in large negative angles of attack during this period as is shown in Fig. II-20. The attendant vehicle's pitch look angle (LAP) nearly exceeded the established 40-degree limit as is shown in Fig. II-27. In order to minimize the probability of exceeding the LAP boundary on GT-4, the Stage I open-loop pitch program will be revised.

[redacted]

## TABLE II-8

### GT-3 Predicted and Flight Performance

| BECO | Planned | Data Source: GE MOD III Actual | GE MOD III Difference | MISTRAM Actual | MISTRAM Difference | FPQ-6 (19.18) Actual | FPQ-6 (19.18) Difference |
|---|---|---|---|---|---|---|---|
| Time (sec) | 154.27 | 152.433 | -1.737 | 152.433 | -1.737 | 152.433 | -1.737 |
| Altitude (ft) | 209,921 | 224,777 | 14,856 | 225,055 | 15,134 | 225,023 | 15,102 |
| Ground range (naut mi) | 49.85 | 49.55 | -0.30 | 49.64 | -0.21 | 49.66 | -0.19 |
| Inertial velocity (fps) | 9,889 | 9,981 | +92 | 9,982 | -7 | 9,970 | +81 |
| Inertial flight path angle (deg) | 19.51 | 21.79 | 2.28 | 21.78 | 2.27 | 21.82 | 2.31 |
| Geocentric radius (ft) | 21,119,526 | 21,134,377 | 14,851 | 21,134,655 | 15,129 | 21,134,700 | 15,174 |
| Down range position, $X_F$ (ft) | 305, 845 | 304,230 | -1,615 | 304,700 | -1,145 | 304,954 | -891 |
| Cross range position, $Y_F$ (ft) | -825 | 1,546 | 2,371 | 1,512 | 2,337 | 1,548 | 2,373 |
| Vertical position, $Z_F$ (ft) | 207,676 | 222,559 | 14,883 | 222,828 | 15,152 | 222,870 | 15,194 |
| Down range velocity, $\dot{X}_F$ (fps) | 8,066 | 8,023 | -43 | 8,024 | -42 | 8,011 | -55 |
| Cross range velocity, $\dot{Y}_F$ (fps) | -35 | 100 | 135 | 98.9 | 133.9 | 97 | 132 |
| Vertical velocity, $\dot{Z}_F$ (fps) | 3,194 | 3,597 | 403 | 3,595 | 401 | 3,597 | 403 |
| Yaw steering velocity, $V_Y$ (fps) | 254 | 120 | -134 | 121 | -133 | 124 | -130 |

| SECO + 20 Seconds | Planned | GE MOD III Actual | GE MOD III Difference | MISTRAM Actual | MISTRAM Difference | FPQ-6 (3.18) Actual | FPQ-6 (3.18) Difference |
|---|---|---|---|---|---|---|---|
| Time (sec) | 358.57 | 353.747 | -4.823 | 353.747 | -4.823 | 353.747 | -4.823 |
| Altitude (ft) | 531,090 | 532,338 | 1,248 | 532,314 | 1,224 | 532,295 | 1,205 |
| Ground range (naut mi) | 540.13 | 531.21 | -8.92 | 531.53 | -8.60 | 531.47 | -8.66 |
| Inertial velocity (fps) | 25,698 | 25,688 | -10 | 25,680 | -18 | 25,703 | 5 |
| Inertial flight path angle (deg) | -0.0048 | -0.0323 | -0.0275 | -0.0399 | -0.0351 | -0.1120 | -0.1072 |
| Geocentric radius (ft) | 21,438,514 | 21,439,747 | 1,233 | 21,439,722 | 1,208 | 21,439,697 | 1,183 |
| Down range position, $X_F$ (ft) | 3,351,763 | 3,297,117 | -54,646 | 3,298,890 | 52,873 | 3,298,776 | 52,987 |
| Cross range position, $Y_F$ (ft) | -37,297 | -19,046 | 18,251 | -19,215 | 18,082 | -19,100 | 18,197 |
| Vertical position, $Z_F$ (ft) | 267,728 | 277,519 | 9,791 | 277,241 | 9,513 | 276,575 | 8,847 |
| Down range velocity, $\dot{X}_F$ (fps) | 24,081 | 24,080 | -1 | 24,076 | -5 | 24,088 | 7 |
| Cross range velocity, $\dot{Y}_F$ (fps) | -408 | -403 | 5 | -402 | 6 | -416 | -8 |
| Vertical velocity, $\dot{Z}_F$ (fps) | -3,795 | -3,742 | 53 | -3,712 | 83 | -3,782 | 13 |
| Yaw steering velocity, $V_Y$ (fps) | 2 | -0.7 | -2.7 | -1.2 | -3.2 | 0 | -2 |

[redacted]

TABLE II-9

Data Sources Utilized for Trajectory Analyses

| | | Flight Coverage (sec from LO) |
|---|---|---|
| **AFETR-Supplied Data** | | |
| Position, velocity and acceleration | FPS-16 radar: reduced by RCA | |
| | Station 3 (Grand Bahama) | +66 to +409 |
| | FPQ-6 radar: reduced by RCA | +19 to +341 |
| | Station 0 (Patrick AFB) | +353 to +380 |
| | Station 3 (Grand Bahama) | +87 to +422 |
| | Station 7 (Grand Turk) | +211 to +486 |
| | Station 19 (MILA) | +12 to +429 |
| Position, velocity, acceleration and attitude | Fixed camera: reduced by RCA | 0 to +22 |
| | Cine theodolite: reduced by RCA | +6 to +62 |
| Position, velocity and acceleration | MISTRAM: reduced by RCA | +45 to +379 |
| Position, velocity and acceleration | Best estimate of trajectory: reduced by RCA | +10 to +433 |
| **Goddard-Supplied Data (NASA)** | | |
| Position and velocity | GE/Burroughs: reduced by Burroughs | 0 to + 404 |
| | IP 7092: reduced by ETR | 0 to SECO +20 |
| | MSC-Supplied Data (NASA) | |
| IGS ascent parameters | Spacecraft guidance data reduced by Houston | 0 to +380 |
| **GE-Supplied Data** | | |
| Position and velocity | Mod III-G radar: reduced by GE | 0 to +394 |

~~CONFIDENTIAL~~

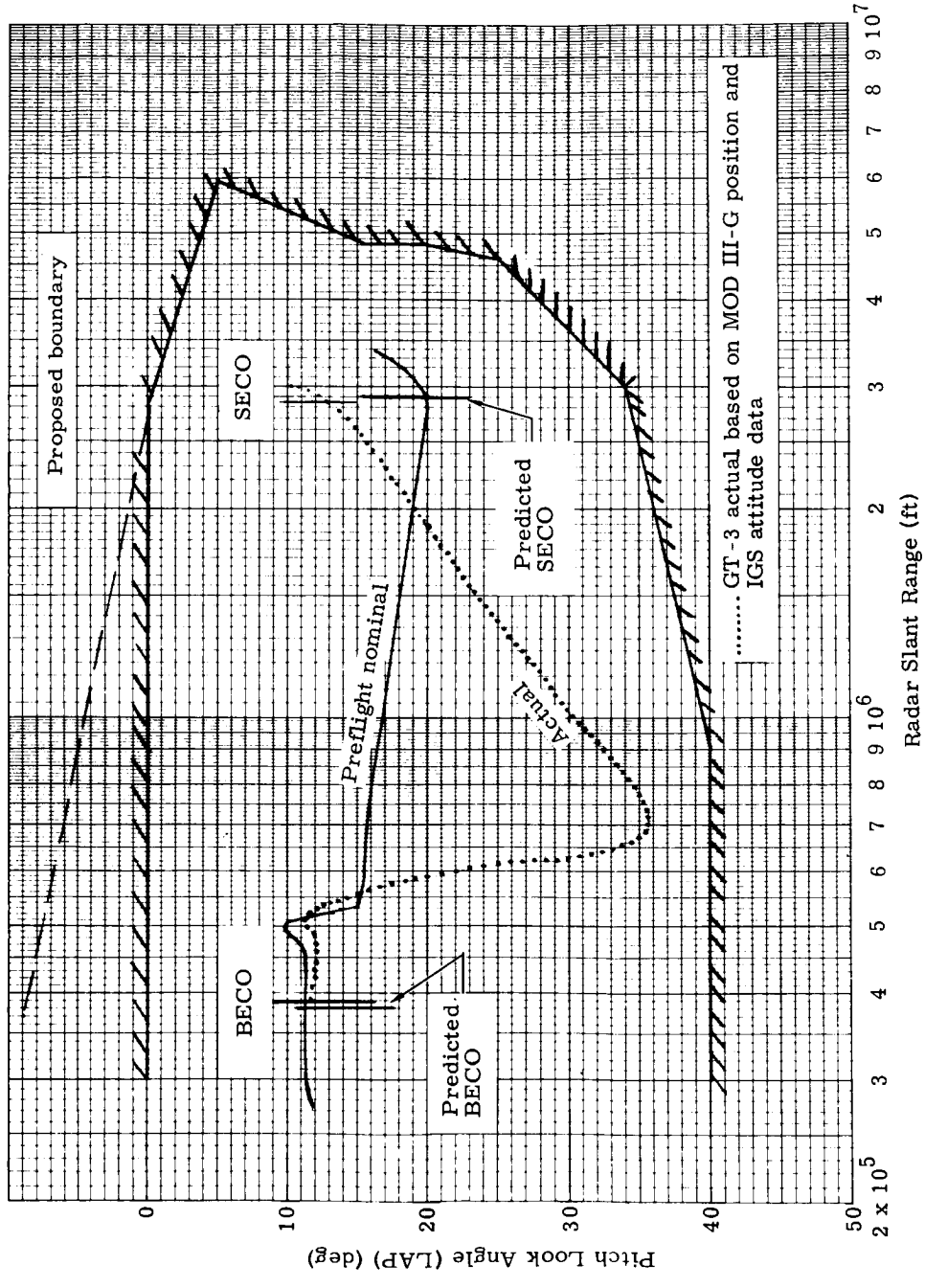


Fig. II-27. Permissible Pitch Look-Angle Envelope

~~CONFIDENTIAL~~

The yaw look angle (LAY) also came close to the established boundary as seen in Fig. II-28. From Ref. 8, the LAY 3σ dispersed value is +5.36 degrees; this compares with the maximum flight value of 5.44 degrees. The relative proximity of these values to the LAY boundary of +7 degrees suggests that the presently used simplified boundary is not adequate and should be better defined.

A reasonably good reconstruction of the flight value of the LAY at LO +160 seconds has been obtained from consideration of the LAY dispersion sensitivity parameters given in Ref. 8. The calculated LAY dispersions are shown in Table II-10.

TABLE II-10

Yaw Look Angle (LAY) Reconstruction at LO +160 Seconds

| Parameter | Δ LAY ~ (deg) | ΔYaw Steering Velocity, $V_Y$ (fps) |
|---|---|---|
| Winds (0939 EST, 3-23-65) | 0.65 | +19 |
| Stage I yaw engine misalignment (+0.1 deg) | 0.41 | -56 |
| Stage I roll engine misalignment (-0.15 deg) | 0.16 | -104 |
| Stage II yaw engine misalignment (-0.3 deg) | 1.35 | +3 |
| Thrust (+2.09%) | 0.12 | -2 |
| $I_{sp}$ (+2 sec) | +0.06 | -1 |
| ΣΔ (to be added to nominal) | +2.51 | - 141 |
| Nominal trajectory value | +2.61 | +252 |
| Σ total deviation in LAY | 5.12 | +111 |
| Flight value | 5.45 | +116 |

CONFIDENTIAL

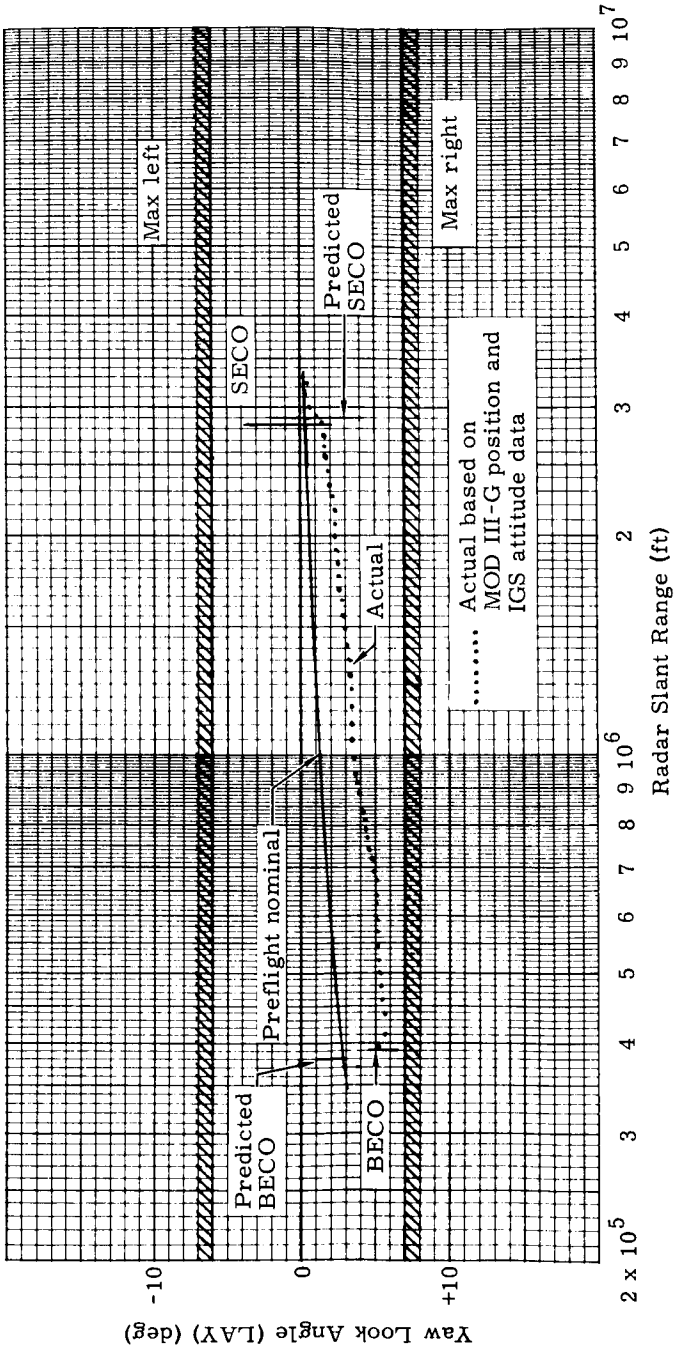


Fig. II-28. Permissible Yaw Look-Angle Envelope

CONFIDENTIAL

## 7. Maximum Dynamic Pressure

Table II-11 compares actual and planned aerodynamic parameters associated with the time of maximum dynamic pressure. As on GT-2, the Max q experienced was less than predicted (no wind nominal). It resulted from the quartering tail wind which reduced the relative velocity--hence, the dynamic pressure.

TABLE II-11

Aerodynamic Parameters at Maximum Dynamic Pressure

| Parameter | Planned* (nominal) | Actual** |
|---|---|---|
| Time from liftoff (sec) | 78 | 75.1 |
| Dynamic pressure (psf) | 754 | 708 |
| Mach number | 1.69 | 1.63 |
| Altitude (ft) | 42,469 | 42,234 |
| Relative wind velocity (fps) | 1,626 | 1,558 |
| Wind velocity (fps) | 0 | 94 |
| Wind azimuth (deg) | -- | 292 (true) |
| Total angle of attack (deg) | | 3.44 |

*Preflight digital simulation run No. 6, 3-22-65.

**GE Mod III-G flight data.

## 8. Angles of Attack and Sideslip

Predicted and actual histories of vehicle angles of attack and sideslip during powered flight are shown in Figs. II-12, -13, -20 and -21. The predicted values were obtained from the preflight digital computation using the T-3 hour winds. The actual values were derived from post-flight analyses of IGS and TARS telemetry data. The first-stage values are in fairly close agreement. However, at the beginning of closed-loop guidance, there is a large change in the actual angle of attack. This deviation from predicted was due to the maximum nose-down pitch command of 2 deg/sec for 12 seconds that was commanded to compensate for the off nominal (high) BECO conditions. A large negative angle of attack logically resulted.

## B. PAYLOAD CAPABILITY

Propellants remaining onboard after Stage II low level sensor uncover indicated that a burning time margin (BTM) of 3.7 seconds existed to a command shutdown. The total propellant margin was 1220 pounds and the corresponding payload capability was 1340 pounds. These values and the predicted nominal and minimum values appear in Fig. II-29.

## C. STAGING

Measured times of staging events (Table II-5) were within the times and tolerances predicted for this sequence with a Stage I oxidizer exhaustion shutdown. The time interval from staging signal ($87FS_2$/ $91FS_1$) to start of Stage II engine chamber pressure ($P_{c_3}$) rise was 0.620 second. This compares favorably with the nominal expected time of 0.70 ± 0.08 second. Stage separation occurred 0.025 second following start of $P_{c_3}$ rise; predicted time for this event, with both the reconstructed $P_{c_3}$ and telemetry $P_{c_3}$, was 0.010 second.

The time-distance relationship between the two stages during the staging process was established by using available telemetry data for engine thrusts and estimated values for vehicle weights, aerodynamic drag and the pressure force acting on Stage I. The thrust versus time histories used were derived from $P_c$ data shown in Chapter III for Stage I shutdown and Stage II buildup (as recorded and as reconstructed with ignition transient spike). Maximum stagnation pressure acting on the Stage I oxidizer tank dome was estimated to be 40 psia. Mass and air drag values used were:

| Vehicle | Mass (slugs) | Aerodynamic Drag (lb) |
|---|---|---|
| Stage I | 337 | 77 |
| Stage II | 2250 | 118 |

Figure II-30 is a plot of separation distance between the two stages as a function of time from $P_{c_3}$ rise. This graph shows that eight feet of separation (distance required for Stage II engine nozzle to clear the Stage I ring frame at the separation plane) was reached in 0.245 second based on the reconstructed $P_{c_3}$ rise and in 0.260 second based on measured $P_{c_3}$ data.[a]

[a]0.260 second was 0.0260 second. (Typographical error corrected by NASA GT-3 Mission Evaluation Team, August 11, 1965.)

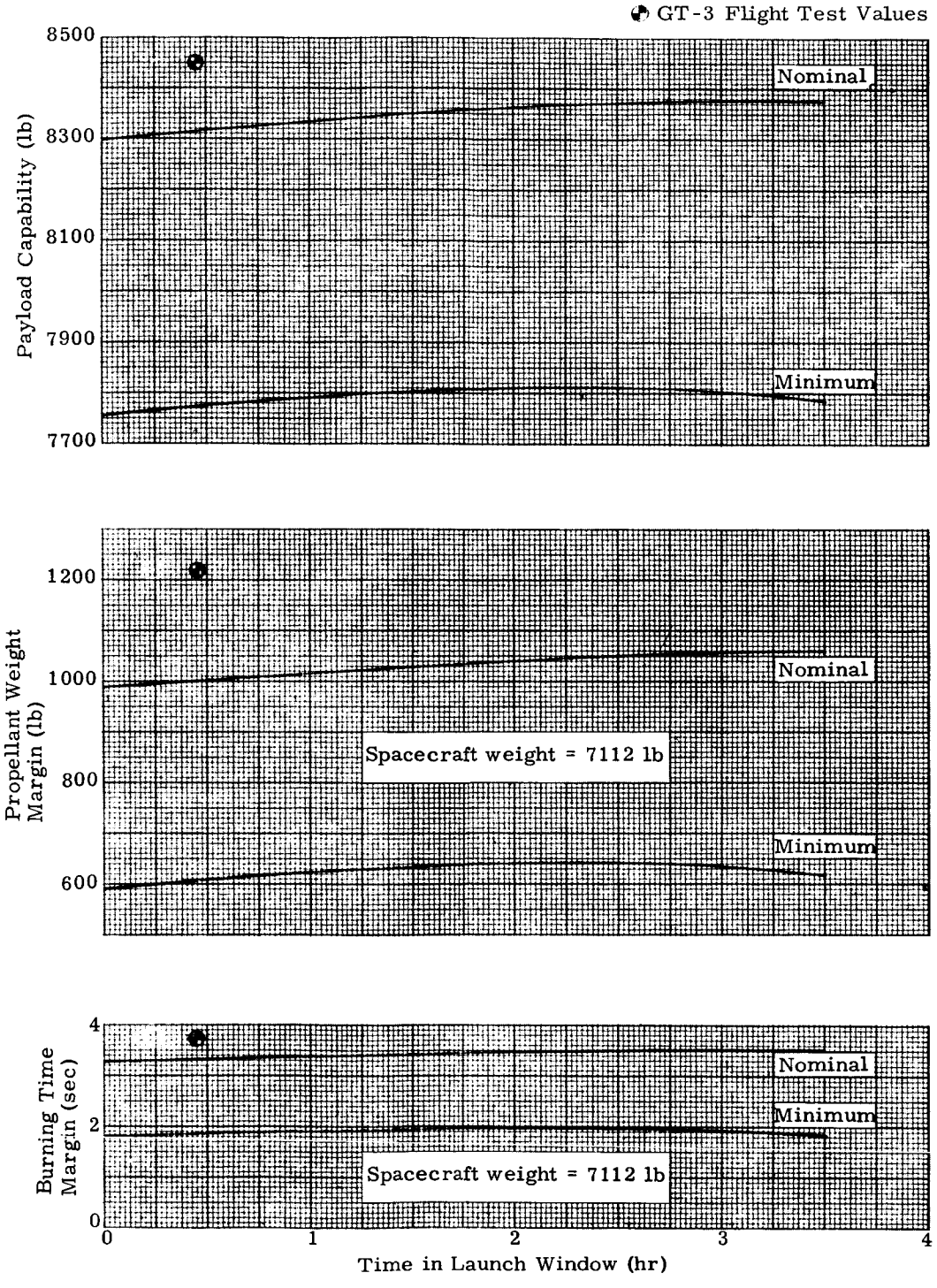


Fig. II-29. GLV-3 Payload Capability

~~CONFIDENTIAL~~

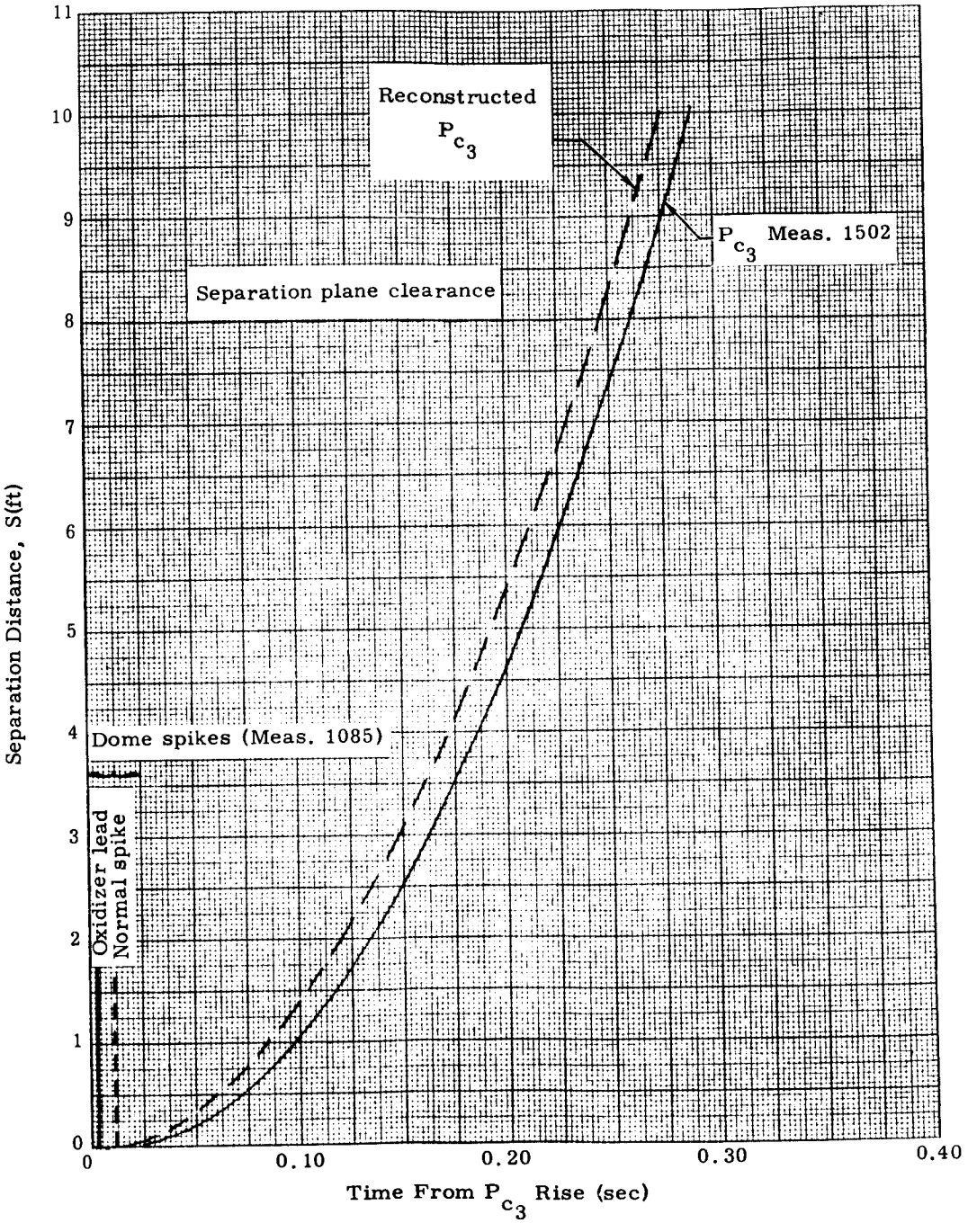


Fig. II-30. Estimated GT-3 Separation Distance Versus Time

~~CONFIDENTIAL~~

## D. WEIGHT STATEMENT

Table II-12 shows the GT-3 weight breakdown from launch to orbital insertion.

The post-flight weight report (Ref. 9) provides the background data for this summary. The report includes a list of dry weight empty changes at ETR and shows a derivation of weight empty from the actual vehicle weighing. Other items covered include the derivation of burn-out, BECO, SECO and shutdown weights; weight comparisons with the BLH data; and the center-of-gravity travel envelope as a function of burn time for the horizontal, vertical and lateral planes.

TABLE II-12

GT-3 Weight Summary

| | Step I | Step II | Step III | Stage Total |
|---|---|---|---|---|
| Loaded weight (lb) | 271,769 | 65,509 | 7,112 | 344,390 |
| Start and ground losses (lb) | -3,914 | | | |
| Liftoff weight (lb) | 267,855 | 65,509 | 7,112 | 340,476 |
| Propellant consumed to BECO (lb) | 256,963 | 11 | 3 | |
| Weight at BECO (lb) | 10,892 | 65,498 | 7,109 | 83,499 |
| Shutdown propellants (lb) | 44 | | | |
| Weight, Stage I burnout (lb) | 10,848 | 65,498 | 7,109 | 83,455 |
| Stage II engine start (lb) | 10,848 | 185 | | |
| Stage II liftoff (lb) | | 65,313 | 7,109 | 72,422 |
| Propellant consumed to SECO (lb) | | 58,322 | | |
| Ablative and Coolant Water (lb) | | 20 | 4 | |
| Stage II at SECO (lb) | | 6,971 | 7,105 | 14,076 |
| Shutdown propellant (lb) | | 157 | | |
| Weight at SECO +20 seconds (lb) | | 6,814 | 7,105 | 13,919* |

*Includes 1,220 pounds usable propellant (to fuel depletion).

# III. PROPULSION SYSTEM

## A. ENGINE SUBSYSTEM

The GLV-3 Stages I and II engines operated satisfactorily throughout the flight and met all test objectives. The Stage I burning time from $87FS_1$ was 155.805 seconds, and shutdown was initiated by oxidizer exhaustion. Stage II operation was terminated by guidance command after 181.314 seconds of burning time.

Several problems occurred during the countdown and flight, none of which adversely affected engine performance. These were as follows:

(1) A minor oxidizer leak was detected in the S/A 1 oxidizer pump discharge pressure transducer sensing line fitting shortly after Stage I oxidizer prevalve opening. The leak stopped after the fitting "jam" nut was backed off and retorqued, indicating that the leak occurred within the Natorque seal area.

(2) The Stages I and II engine flight performances (thrust and propellant flow rates) were higher than anticipated.

(3) Measurement 0029 (S/A 2 fuel bootstrap venturi inlet pressure) dropped below operating pressure briefly during Stage I flight, and Measurement 0517 (Stage II fuel bootstrap venturi inlet pressure) was erratic during Stage II flight. Valid data, however, were obtained from both measurements. The instrumentation anomalies are discussed in Chapter VIII.

Significant propulsion events are listed in Table III-1.

### 1. Stage I Engine (YLR87-AJ-7, S/N 1004)[a]

a. Configuration

The GLV-3 Stage I engine incorporated one significant hardware change since GLV-2; additional fire protection insulation was installed to provide more extensive thermal protection of critical engine parts and subsystems.

b. Engine start transient

The S/A 1 and S/A 2 spikes indicated 90% and 84%, respectively, of rated thrust, considerably higher than the engine model specification allowable of 75%. However, the GLV $P_c$ instrumentation system has characteristically exhibited undamped oscillations which mask true

[a]YLR87-AJ-7 was YLB87-AJ-7. (Typographical error corrected by NASA GT-3 Mission Evaluation Team, August 11, 1965.)

~~CONFIDENTIAL~~

TABLE III-1

Propulsion Events Summary

| Description of Event | Time from $FS_1$ | Time (GMT) |
|---|---|---|
| Start Stages I and II oxidizer loading | -15 hr 03 min | 23:21:00 |
| Stage II oxidizer loading completed | -14 hr 09 min | 00:15:00 |
| Stage I oxidizer loading completed | -13 hr 25 min | 00:59:00 |
| Start Stages I and II fuel loading | -10 hr 29 min | 03:35:00 |
| Stage II fuel loading completed | -10 hr 10 min | 04:14:00 |
| Stage I fuel loading completed | -09 hr 31 min | 04:33:00 |
| Stage I oxidizer prevalves opened | -2 hr 53 min | 11:31:00 |
| Tank ullage volumes pressurized to flight pressure | -3 hr 30 min | 10:53:00 |
| Oxidizer surge chamber adjustment set | -2 hr 05 min | 12:19:00 |
| Stage I fuel prevalves opened | -47 sec | 14:23:10 |
| Stage II prevalves opened | -35 sec | 14:23:22 |
| $87FS_1$ | 0 | 14:23:56.692 |
| S/A 1 MDTCPS make | $87FS_1$ + 0.917 | 14:23:57.609 |
| S/A 2 MDTCPS make | +1.008 | 14:23:57.700 |
| TCPS | +1.124 | 14:23:57.816 |
| Liftoff | +3.372 | 14:24:00.064 |
| Stage I oxidizer high level sensor uncover, average | +13.453 | 14:24:10.145 |
| Stage I fuel high level sensor uncover, average | +17.878 | 14:24:14.570 |
| Stage I fuel outage sensor uncover, average | +149.573 | 14:26:26.267 |
| Stage I oxidizer outage sensor, uncover, average | +152.580 | 14:26:29.272 |
| S/A 2 MDTCPS break | +155.749 | 14:26:32.441 |
| S/A 1 MDTCPS break | +155.750 | 14:26:32.442 |
| $87FS_2/91FS_1$ | +155.805 | 14:26:32.497 |
| Stage II MDFJPS make | $91FS_1$ + 0.651 | 14:26:33.148 |
| Stage II fuel high level sensor uncover, average | +17.010 | 14:26:49.507 |
| Stage II oxidizer high level sensor uncover, average | +58.486 | 14:27:30.983 |
| Stage II fuel outage sensor uncover, average | +178.414 | 14:29:30.911 |
| Stage II oxidizer outage sensor uncover, average | +175.149 | 14:29:27.646 |
| $91FS_2$ | +181.314 | 14:29:33.811 |
| Stage II MDFJPS break | +181.455 | 14:29:33.952 |

~~CONFIDENTIAL~~

transient performance such that the measured spike pressure is not representative of the actual pressure. Therefore, it is not possible to determine the true values for the ignition spikes. Except for the high ignition spikes, the Stage I start transients, as presented in Figs. III-1 and III-2, were normal. Significant engine start parameters are as follows:

| Parameter or Event | S/A 1 | S/A 2 |
|---|---|---|
| $87FS_1$ to initial $P_c$ rise (sec) | 0.76 | 0.82 |
| $P_c$ spike at ignition (psia) | 720 | 660 |
| $P_c$ step level (psia) | 440 | 390 |
| $P_c$ overshoot (psia) | None | None |

The start cartridge temperatures at launch were approximately 59° F for S/A 1 and 60° F for S/A 2, and were within the prescribed limits of 45° to 70° F.

c. Steady-state operation

Stage I engine steady-state flight performance was satisfactory throughout the flight, and no major anomalies occurred. Engine flight performance, however, was higher than predicted.

The engine performance was calculated from measured engine flight data using the MMB PRESTO program and the Stage I thrust coefficient relationship as modified by Martin. The thrust coefficient modification was based on flight history. Engine flight performance, calculated from measured internal engine parameters and using the Aerojet thrust coefficient relationship to determine thrust, did not match the vehicle trajectory performance. Analysis of all Gemini-Titan flights shows that in order to match the Stage I trajectory, an increase in reconstructed thrust and specific impulse of approximately 3400 pounds and 2.0 seconds, respectively, was required above the values calculated with the Aerojet thrust coefficient relationship. Martin therefore modified the thrust coefficient relationship to simulate flight experience, and this relationship was used for the GLV-3 post-flight analysis.

The average Stage I engine performance, integrated from liftoff to $87FS_2$, is compared with the preflight prediction in Table III-2.

Stage I engine performance (calculated) is presented in Fig. III-3. The preflight prediction is also shown in this figure for comparison.

[redacted]

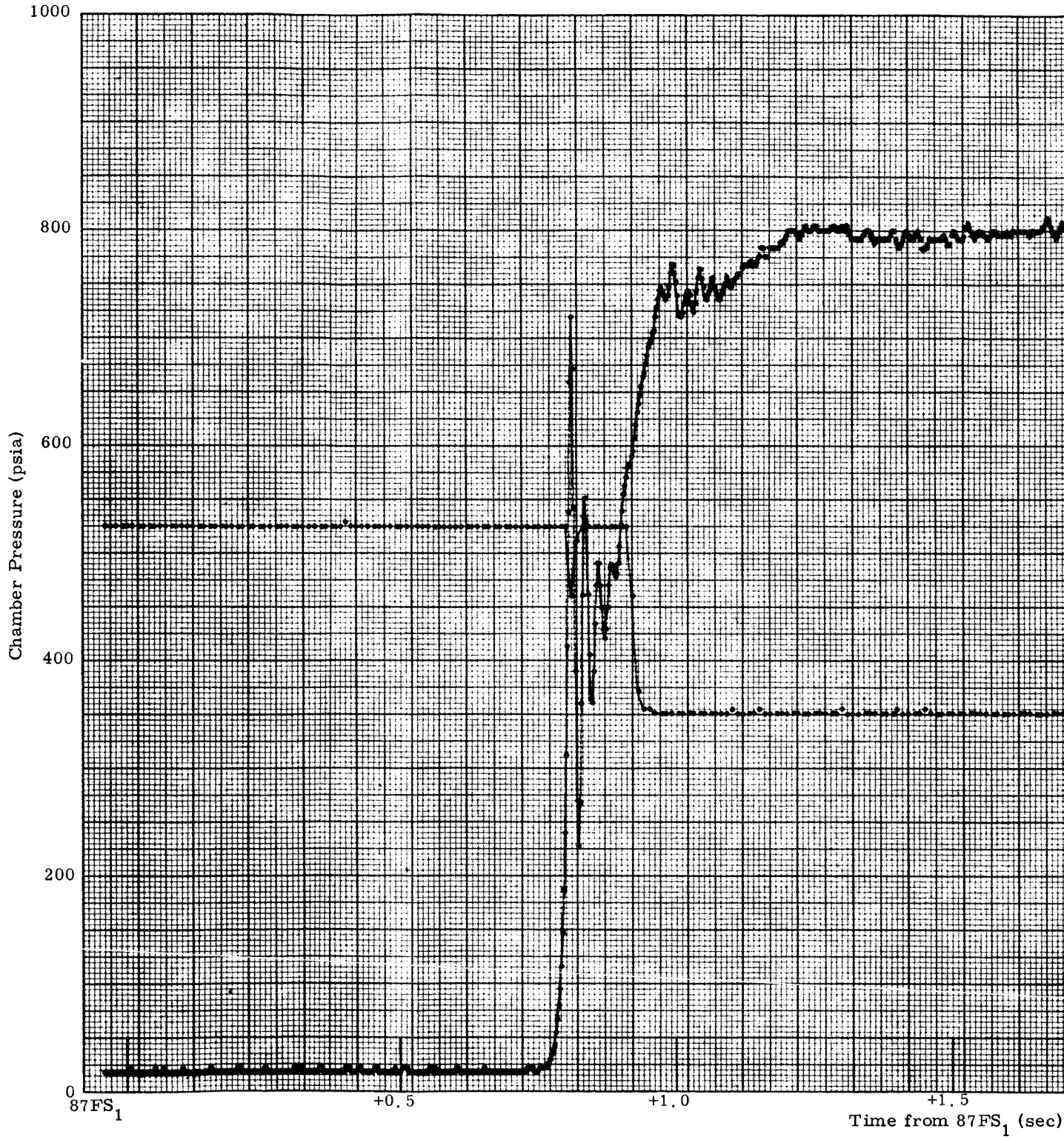


[redacted]

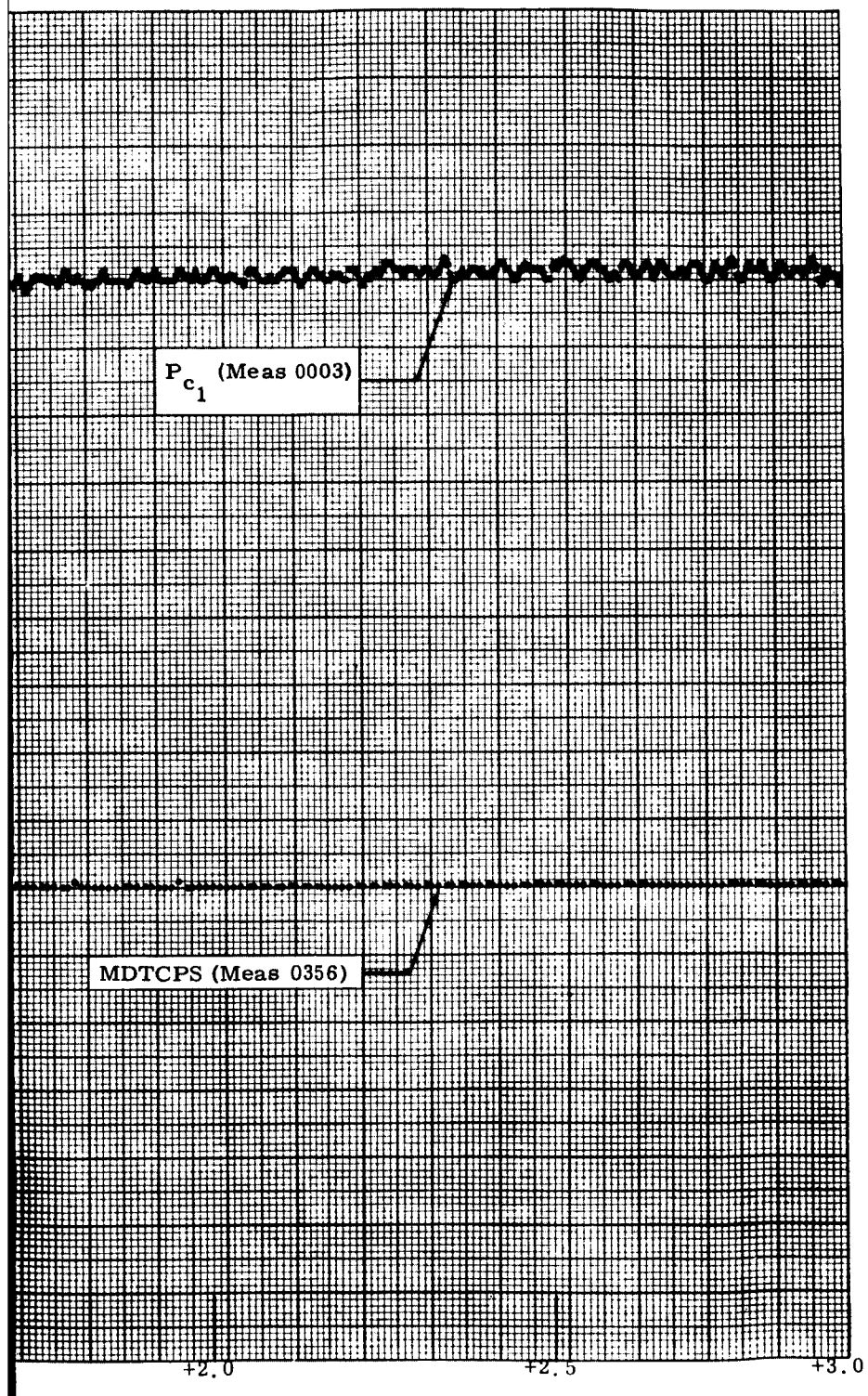


Fig. III-1. S/A 1 Start Transient

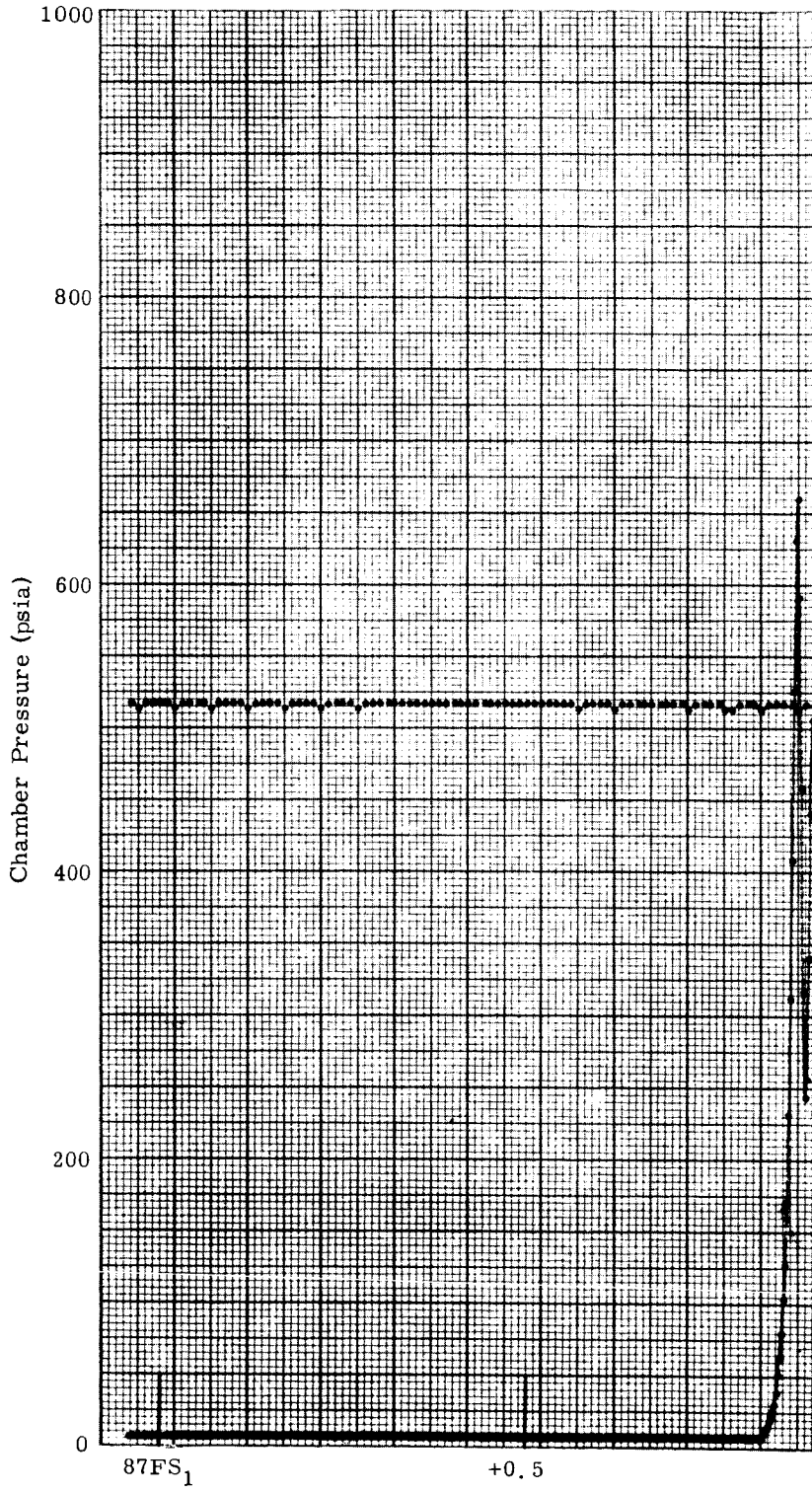
1000
800
600
400
200
0
Chamber Pressure (psia)
87FS1
+0.5

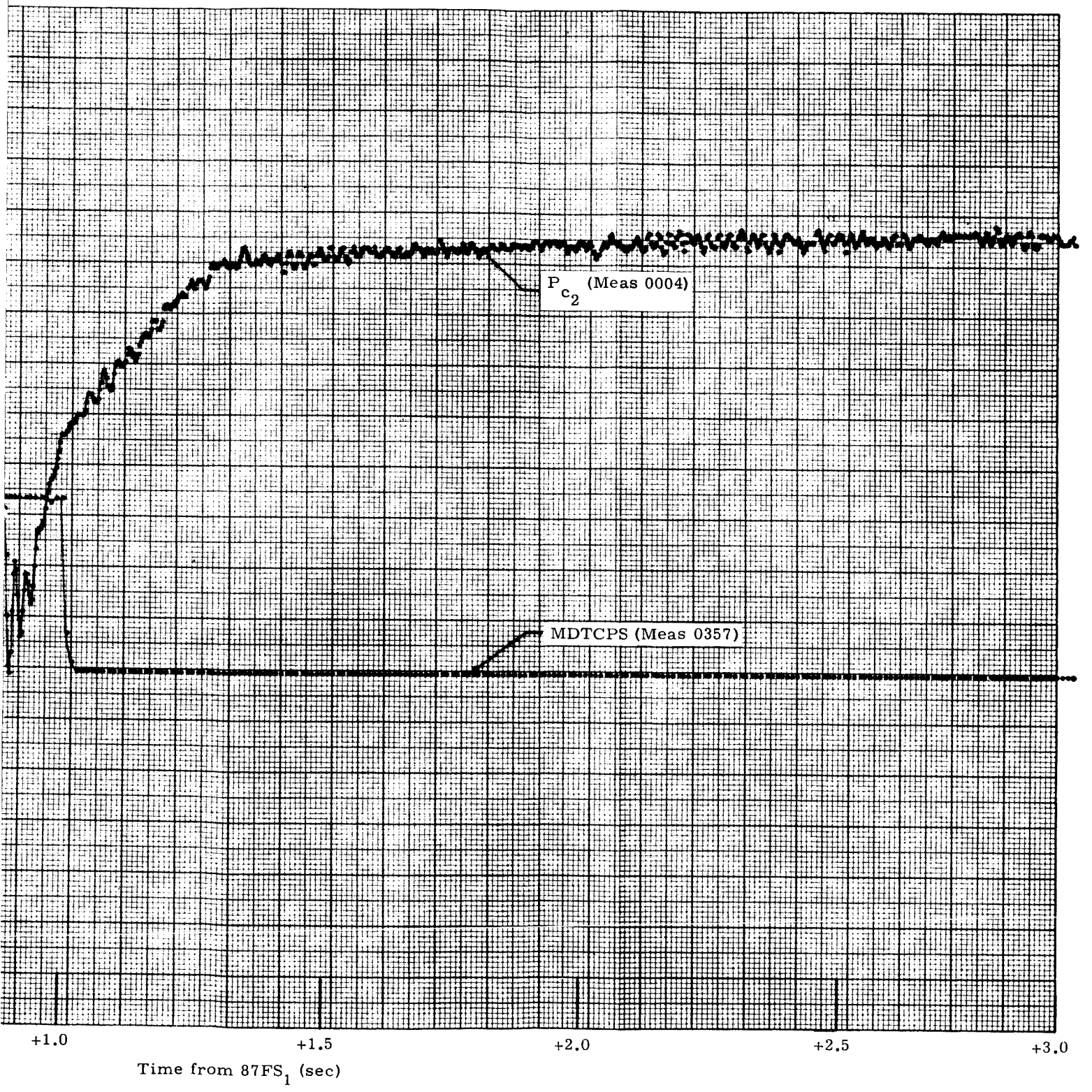


Fig. III-2. S/A 2 Start Transient

[redacted]

TABLE III-2

Predicted and Actual Engine Performance Parameters

| Parameter | Preflight Predicted Average* | Flight Average** | Percent Difference |
|---|---|---|---|
| Thrust, engine (lb) | 459,361 | 468,477 | +1.98 |
| Specific impulse, engine (sec) | 275.52 | 278.12 | +0.94 |
| Mixture ratio, engine | 1.9102 | 1.9037 | -0.34 |
| Oxidizer flow rate, overboard (lb/sec) | 1094.04 | 1103.97 | +0.91 |
| Fuel flow rate, overboard (lb/sec) | 573.24 | 580.45 | +1.26 |

* Performance predicted with Aerojet thrust coefficient relationship.

** Flight performance evaluated from flight data with Martin-modified thrust coefficient relationship.

Data from the new oxidizer pump inlet temperature probe (Meas 0024) were used in the post-flight analysis because of the excellent correlation with the bulk temperature probe data. The other oxidizer pump inlet temperature probe (Meas 0023) showed the characteristic temperature bias that has been observed on all Titan II and GLV flights.

Cyclic pressure oscillations were present in the fuel discharge pressure of S/A 1 and in the oxidizer discharge pressure of S/A 2. The cause of these oscillations, similar to those observed on GLV-2, has not yet been determined.

Stage I engine flight performance calculated at the $87FS_1$ + 57 second time slice, and corrected to standard inlet conditions, is compared in Table III-3 to the acceptance test data at the same time slice and standard inlet conditions. The acceptance test performance and the predicted flight performance at standard inlet conditions used in the predictions were calculated using the Aerojet thrust coefficient relationship. The flight performance at standard conditions was calculated with the same relationship to indicate the relative magnitude of the acceptance-to-flight performance changes. Also presented in Table III-3 is the engine performance calculated with the Martin-modified thrust coefficient relationship to provide a best estimate of the actual flight performance at standard inlet conditions.

[redacted]

R
Fuel Overboard Flow Rate, $\dot{W}_{fo}$ (lb/sec)
600
580
560
540
Oxidizer Overboard Flow Rate, $\dot{W}_{oo}$ (lb/sec)
1120
1100
1080
1060
1040
Engine Mixture Ratio
1.95
1.90
1.85
1.80
1.75
Engine Specific Impulse, $I_{sp_e}$ (sec)
290
285
280
275
270
265
260
255
Total Thrust, $F_T$ (lb x $10^3$)
490
480
470
460
450
440
430
420
410
0

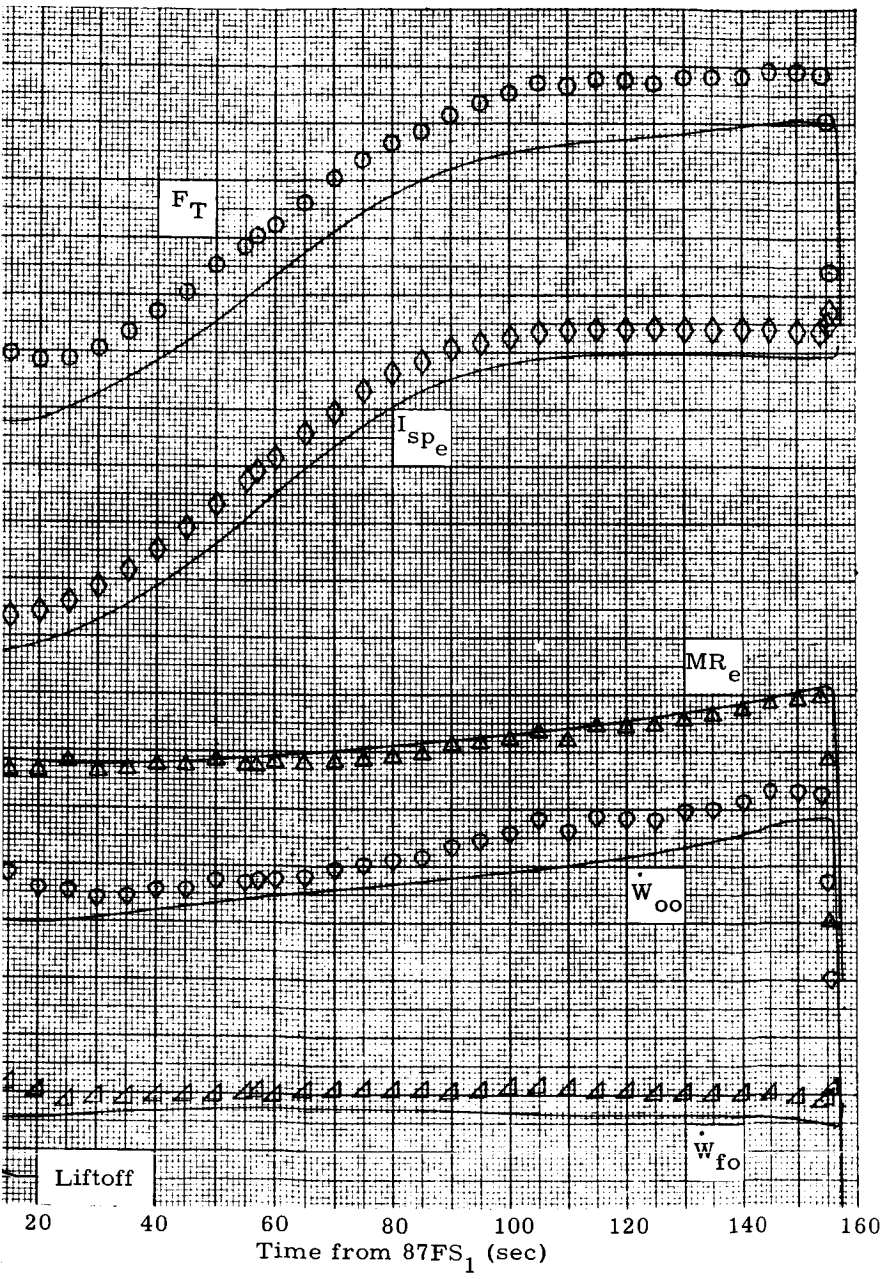


| Average Engine Performance Integrated from Liftoff to $87FS_2$ | | |
|---|---|---|
| Symbol | Preflight Prediction | Flight Average |
| $F_T$ | 459,361 | 468,477 |
| $I_{sp_e}$ | 275.52 | 278.12 |
| $MR_e$ | 1.9102 | 1.9037 |
| $\dot{W}_{oo}$ | 1094.04 | 1103.97 |
| $\dot{W}_{fo}$ | 573.24 | 580.45 |

Legend

——Preflight prediction

Flight performance symbols

⊙ $F_T$

◇ $I_{sp_e}$

△ $MR_e$

▽ $\dot{W}_{oo}$

◿ $\dot{W}_{fo}$

Fig. III-3. Stage I Engine Flight Performance

[redacted]

TABLE III-3

Performance Corrected to Standard Inlet Conditions

| Parameter | Acceptance Test* | Predicted Flight (includes 2450 lb thrust growth)* | Flight Performance** | Flight Performance*** |
|---|---|---|---|---|
| Thrust, engine (lb) | 433,680 | 436,130 | 439,511 | 442,899 |
| Specific impulse, engine (sec) | 258.77 | 258.77 | 259.35 | 261.35 |
| Mixture ratio, engine | 1.9261 | 1.9261 | 1.9119 | 1.9119 |
| Oxidizer flow rate, overboard (lb/sec) | 1102.83 | 1109.07 | 1112.34 | 1112.34 |
| Fuel flow rate, overboard (lb/sec) | 573.10 | 576.33 | 582.34 | 582.34 |

* Calculated with Aerojet thrust coefficient relationship as used in preflight performance predictions.

** Calculated with Aerojet thrust coefficient relationship to indicate magnitude of changes from acceptance-to-flight.

*** Calculated with Martin-modified thrust coefficient relationship to provide best estimate of actual flight performance at standard inlet conditions.

d. Shutdown transient

Stage I engine shutdown was initiated by oxidizer exhaustion; however, during the shutdown transient period, engine pressure data indicated that fuel exhaustion had also occurred. Figures III-4 and III-5 show the S/A 1 and S/A 2 chamber pressure decays.

Engine thrust at staging was approximately 16,000 pounds. Significant events during shutdown are as follows:

| Event | S/A 1 | S/A 2 |
|---|---|---|
| Time from $P_c$ decay to $87FS_2$ (sec) | 0.6 | 0.5 |
| $P_c$ at $87FS_2$ (psia) | 160 | 160 |
| Time from $87FS_2$ to data dropout (sec) | 0.75 | 0.75 |
| $P_c$ at data dropout (psia) | 35 | 20 |

e. Engine malfunction detection system (MDS)

The Stage I engine MDS operated satisfactorily throughout the flight. Pressure switch operation during the ignition and shutdown transients is depicted in Figs. III-1, III-2, III-4 and III-5.

[redacted]

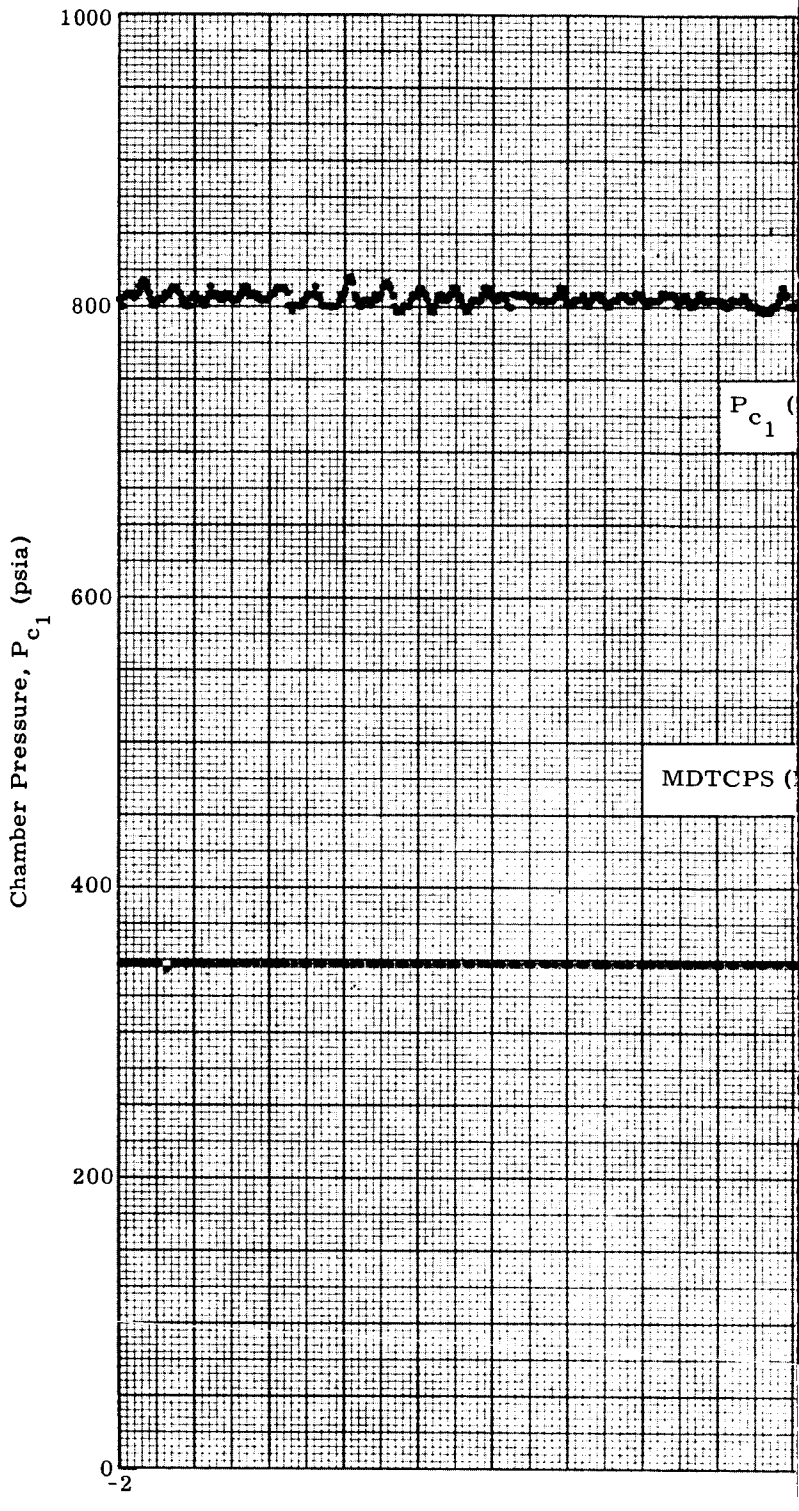
1000
800
600
400
200
0
-2
Chamber Pressure, $P_{c_1}$ (psia)
$P_{c_1}$ (
MDTCPS (

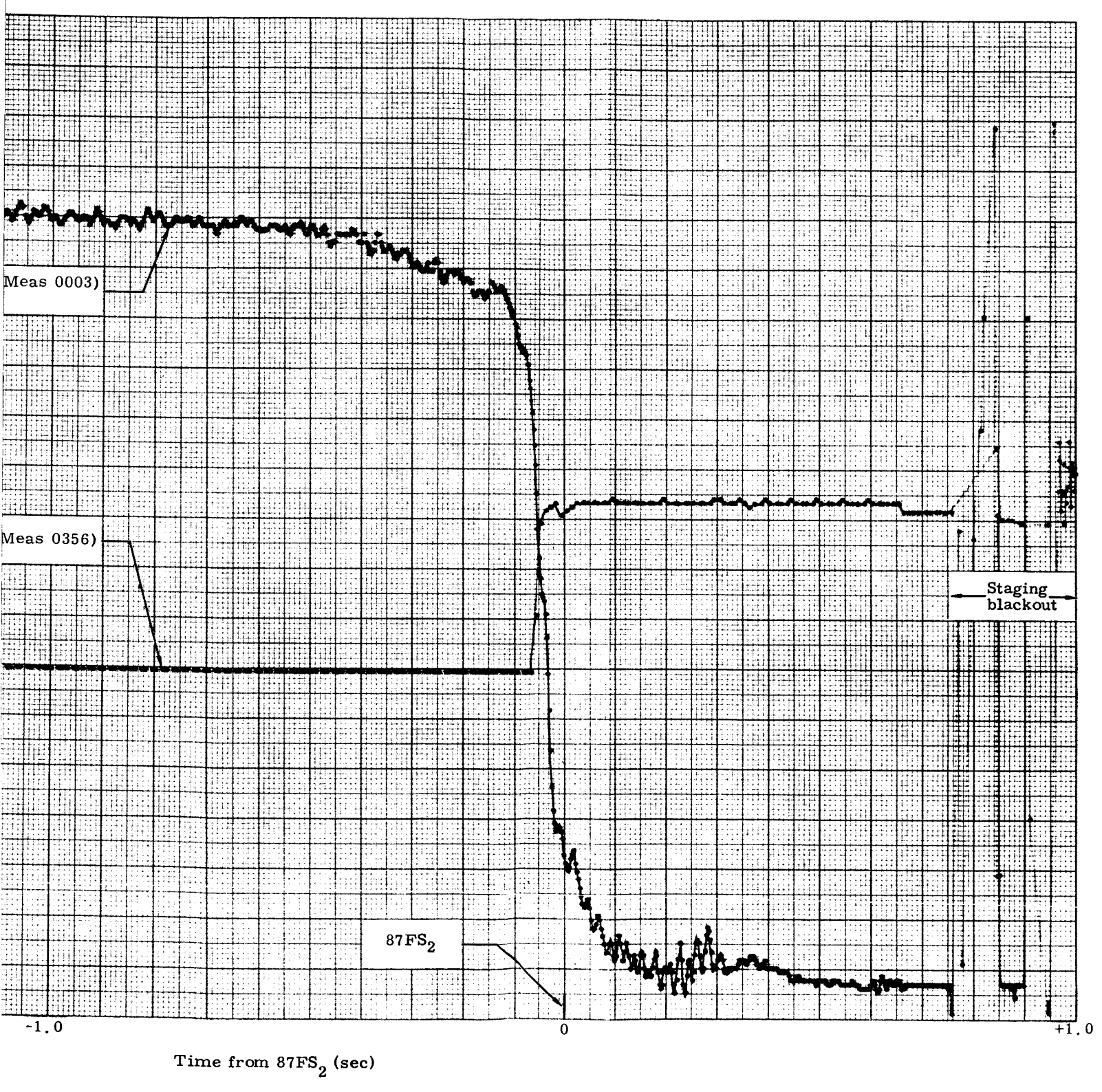


Fig. III-4. S/A 1 Shutdown Transient

[redacted]

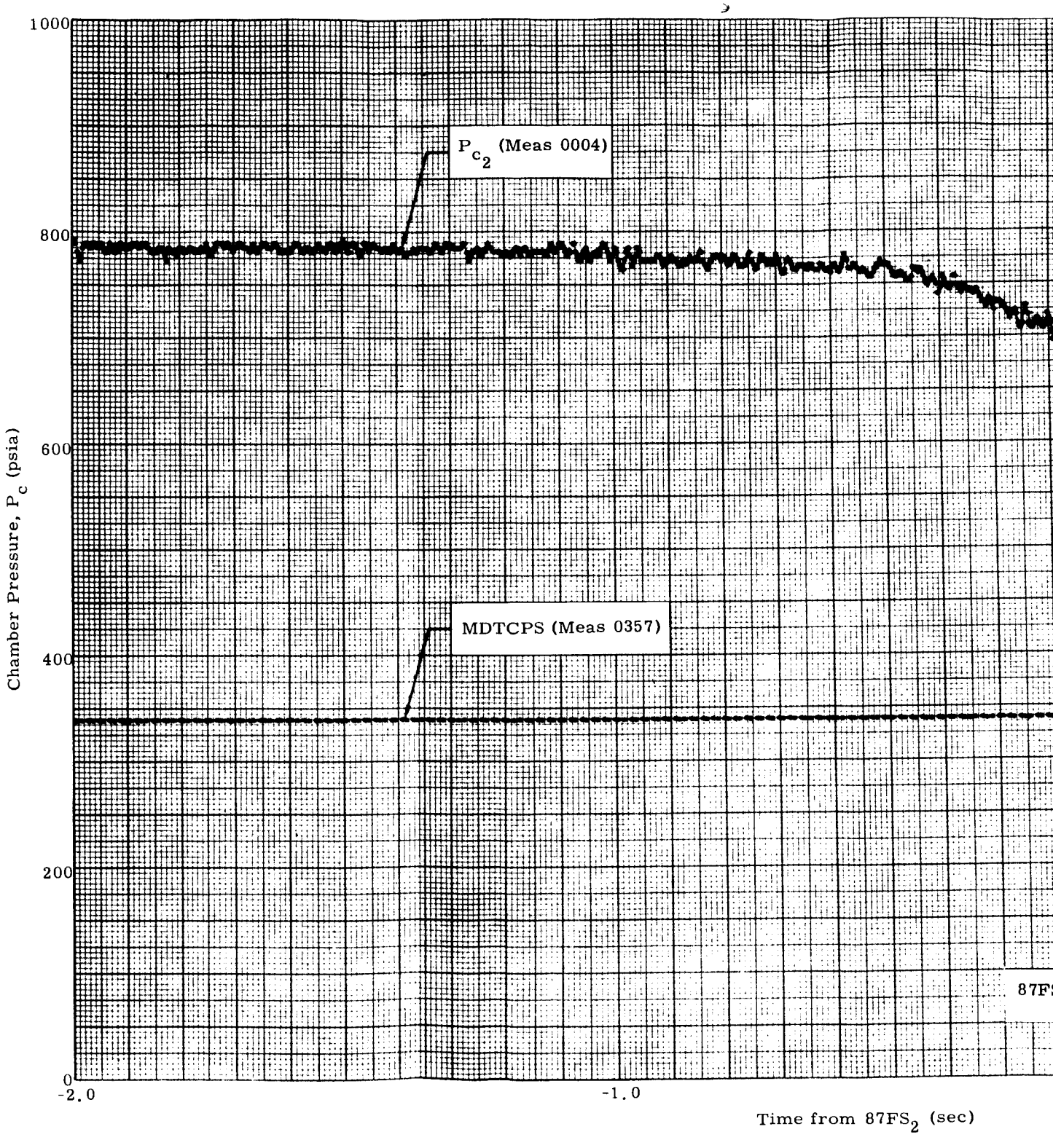


[redacted]

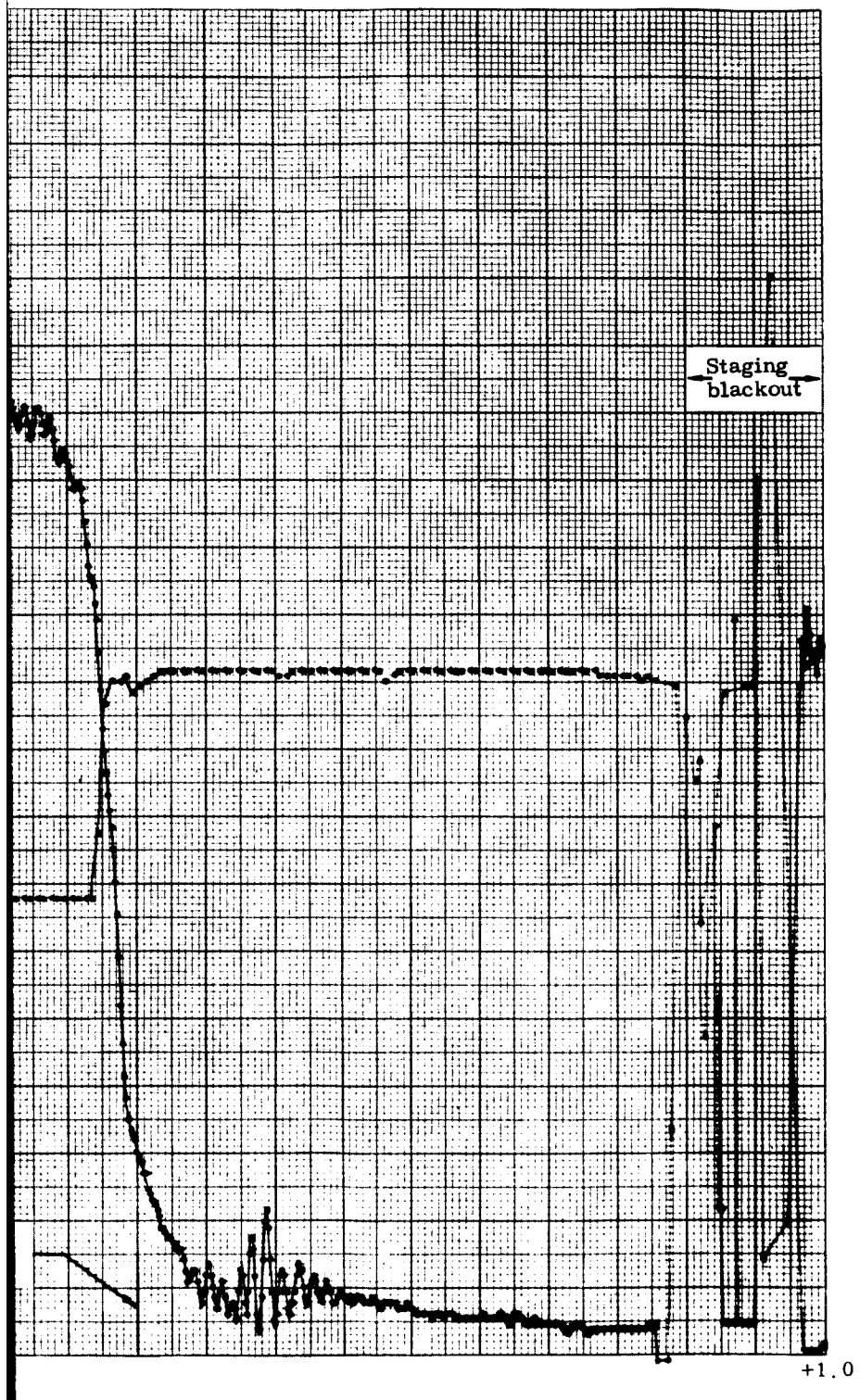


Fig. III-5. S/A 2 Shutdown Transient

The following summarizes the operation of the malfunction detection thrust chamber pressure switches (MDTCPS).

| Switch | Actuation at Ignition | | Actuation at Shutdown | |
|---|---|---|---|---|
| | Time (sec) | Pressure (psia) | Time (sec) | Pressure (psia) |
| $MDTCPS_1$ | $87FS_1 + 0.917$ | 590 | $87FS_2 - 0.056$ | 525 |
| $MDTCPS_2$ | $87FS_1 + 1.008$ | 585 | $87FS_2 - 0.056$ | 523 |

f. Engine prelaunch malfunction detection system (PMDS)

All PMDS switches actuated satisfactorily within the specified actuation times and pressures as shown in the following table:

| | TCPS | OPPS | FPDPS |
|---|---|---|---|
| Actuation time | | | |
| Measured (sec) | $FS_1 + 1.124$ | $FS_1 + 1.625$ | $FS_1 + 0.975$ |
| Required (sec)* | +2.2 | +2.2 | +2.2 |
| Actuation pressure | | | |
| Measured (psia) | ** | 430 | ** |
| Required (psia) | 600 to 640 | 360 to 445 | 46 to 79 (psid) |

* This time is 2.2 seconds after MOCS Sequencer T - 0 ($87FS_1$ -0.08).

** Not instrumented.

2. Stage II Engine (YLR91-AJ-7, S/N 2004)

a. Configuration

The GLV-3 Stage II engine configuration differed from the GLV-2 configuration only by the incorporation of the redundant engine shutdown system (RESS) to provide backup to normal engine shutdown. The RESS is actuated simultaneously with the normal method of shutdown (thrust chamber valve closure) for all modes of engine shutdown. RESS shutdown is accomplished by firing a squib-operated valve located in the gas generator oxidizer feedline which terminates oxidizer flow to the gas generator.

Incorporation of the RESS required the following changes:

(1) Revised thrust chamber oxidizer injector inlet line.

(2) Addition of a 1/2-inch normally open squib valve located in the oxidizer bootstrap line at the thrust chamber injector inlet elbow.

(3) Revised gas generator oxidizer feedline.

(4) Additional control harness installation.

(5) Additional instrumentation, including a squib valve position indicator and a vehicle RESS signal monitor.

(6) Associated wiring and mounting brackets.

b. Engine start transient

The stage II engine start transient was normal and is illustrated in Fig. III-6. A summary of significant start parameters is given in the following tabulation.

| | |
|---|---|
| $91FS_1$ to $P_c$ initial rise (sec) | 0.62 |
| $P_c$ ignition spike (psia) | 610 |
| $P_c$ step level (psia) | 520 |
| $P_c$ overshoot (psia) | 820 |

The start cartridge temperature recorded before liftoff was 57° F, which was within the 45° to 70° F specified range. Resistance of the gas generator oxidizer injector ($R_{OJGG}$), as determined from the gas generator injector and turbine inlet pressures at $91FS_1$ + 5 seconds, was approximately 1120 units--a normal value for an unclogged injector.

c. Steady-state operation

Stage II engine steady-state flight performance agreed favorably with preflight predictions. The average performance, as integrated over steady-state operation (from first steady-state to $91FS_2$), is compared with preflight predictions as follows:

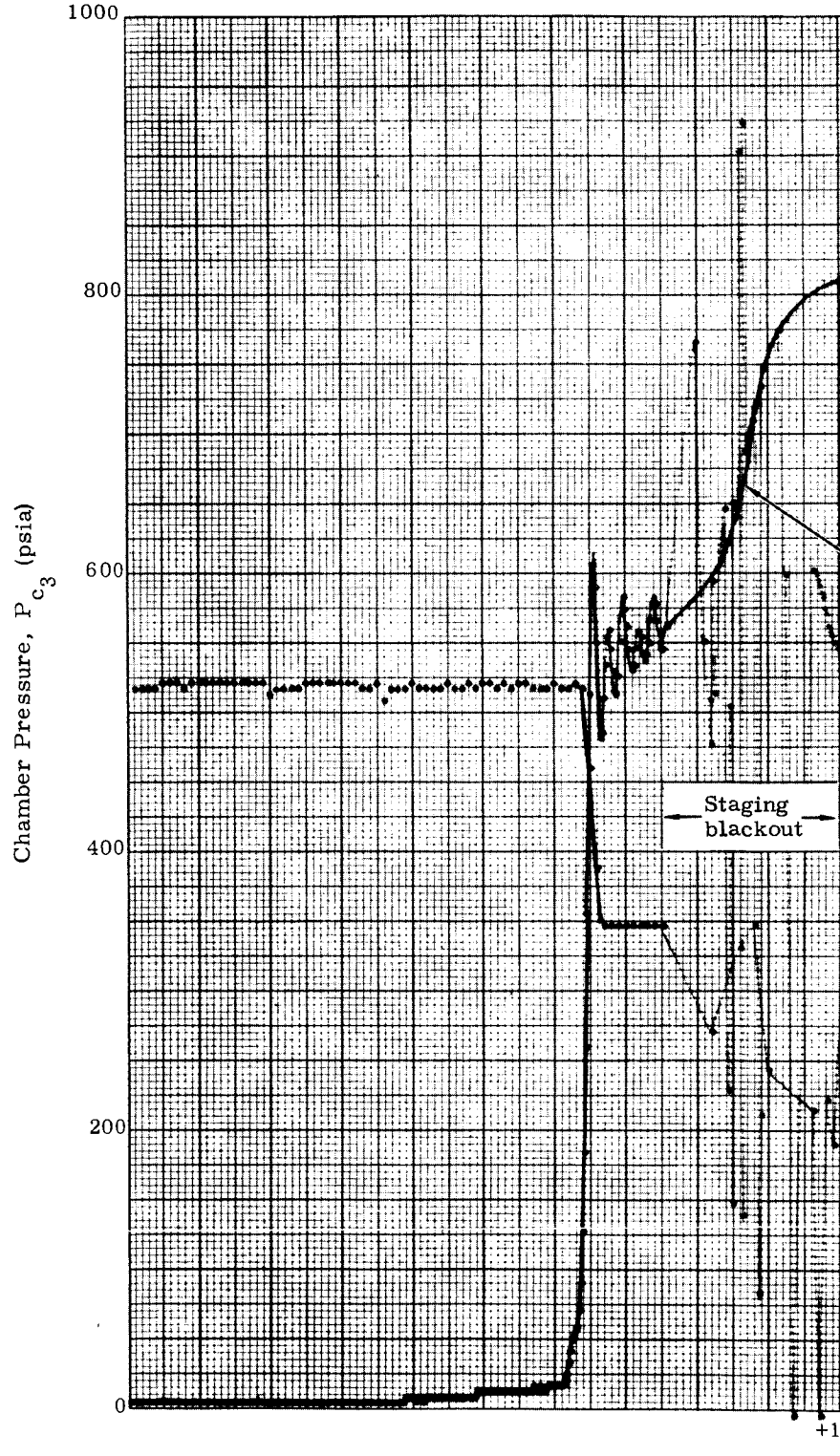
1000
800
600
400
200
0
Chamber Pressure, $P_{c_3}$ (psia)
Staging blackout
+1

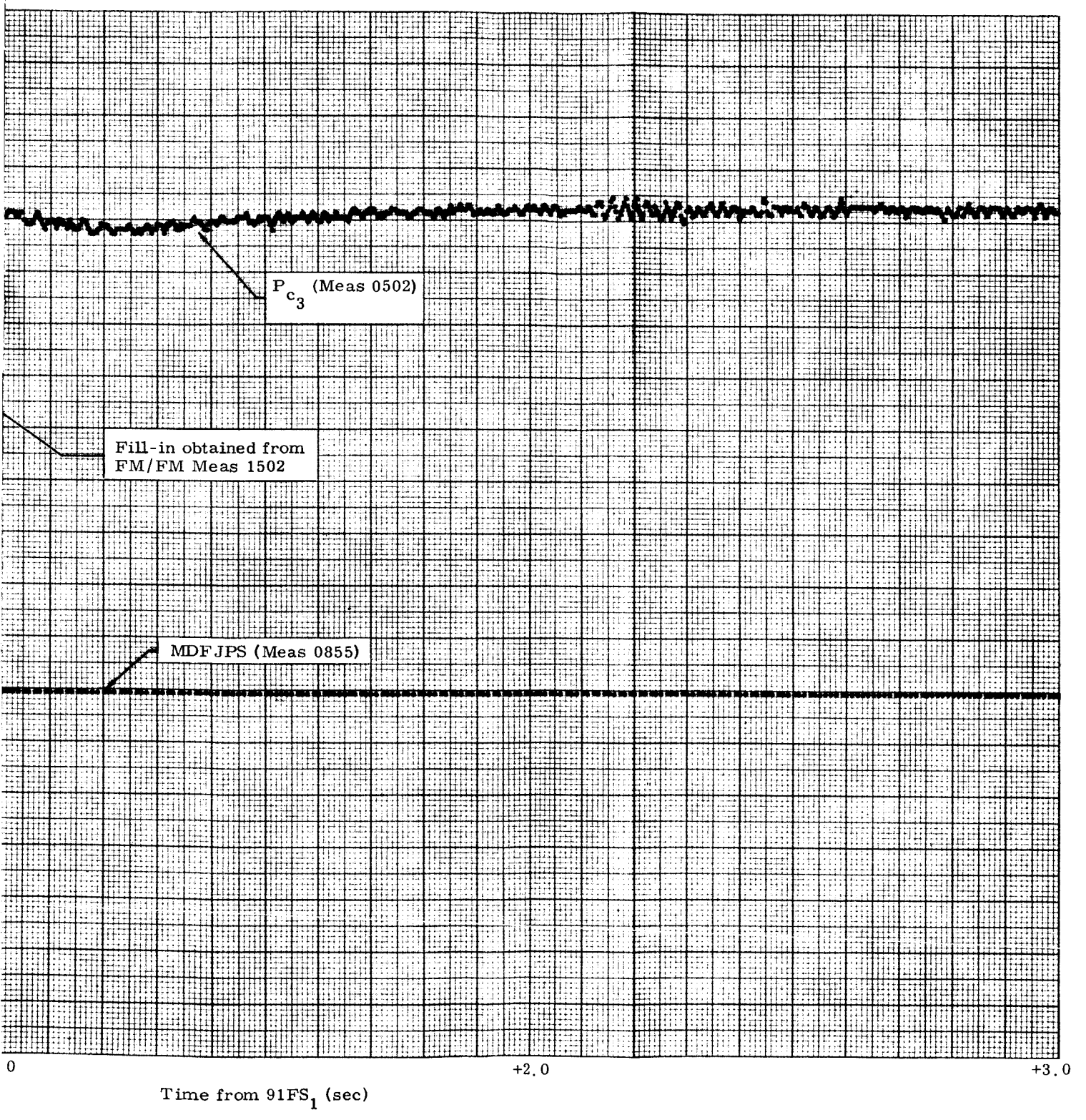


Fig. III-6. S/A 3 Start Transient

~~CONFIDENTIAL~~

Stage II Engine Steady-State Performance

| Parameter | Preflight Predicted Average | Flight Average | Percent Difference |
|---|---|---|---|
| Thrust, chamber (lb) | 98,694 | 100,547 | +1.88 |
| Specific impulse, engine (sec) | 310.13 | 310.64 | +0.16 |
| Mixture ratio, engine | 1.7476 | 1.7560 | +0.48 |
| Oxidizer flow rate, overboard (lb/sec) | 202.58 | 206.39 | +1.88 |
| Fuel flow rate, overboard (lb/sec) | 115.66 | 117.28 | +1.40 |

Engine flight performance was calculated with the Martin PRESTO program, and is shown in Fig. III-7 as a function of time from $91FS_1$. The preflight prediction is also presented in this figure for comparison.

Engine flight performance, corrected at the $91FS_1$ + 57 second time slice to standard inlet conditions, is compared to acceptance test data (also corrected to standard inlet conditions at the same time slice) in the tabulation which follows. The statistical ground test run-to-run thrust growth for Stage II of zero pounds was used in the preflight predictions. Therefore, the acceptance test data and predicted flight performance are identical.

The data show that the primary cause of the higher-than-predicted flight thrust and flow rates was an acceptance-to-flight thrust growth of 1603 pounds. This thrust growth was within the Titan II/Gemini-Titan flight experience.

Stage II Engine Performance Corrected to Standard Inlet Conditions

| Parameter | Acceptance Test and Predicted Flight | Flight Performance |
|---|---|---|
| Thrust, chamber (lb) | 98,522 | 100,125 |
| Specific impulse, engine (sec) | 309.46 | 310.38 |
| Mixture ratio, engine | 1.7796 | 1.7699 |
| Oxidizer flow rate, overboard (lb/sec) | 203.99 | 206.29 |
| Fuel flow rate, overboard (lb/sec) | 114.38 | 116.30 |

~~CONFIDENTIAL~~

Fuel Overboard Flow Rate, $W_{fo}$ (lb/sec)
125
120
115
110
105
100
Oxidizer Overboard Flow Rate, $\dot{W}_{oo}$ (lb/sec)
215
210
205
200
195
190
Engine Mixture Ratio, $MR_e$
1.85
1.80
1.75
1.70
Engine Specific Impulse, $I_{sp_e}$ (sec)
315
310
305
300
Chamber Thrust, $F_c$ (lb x $10^3$)
104
102
100
98
96
94
92
0
20
40

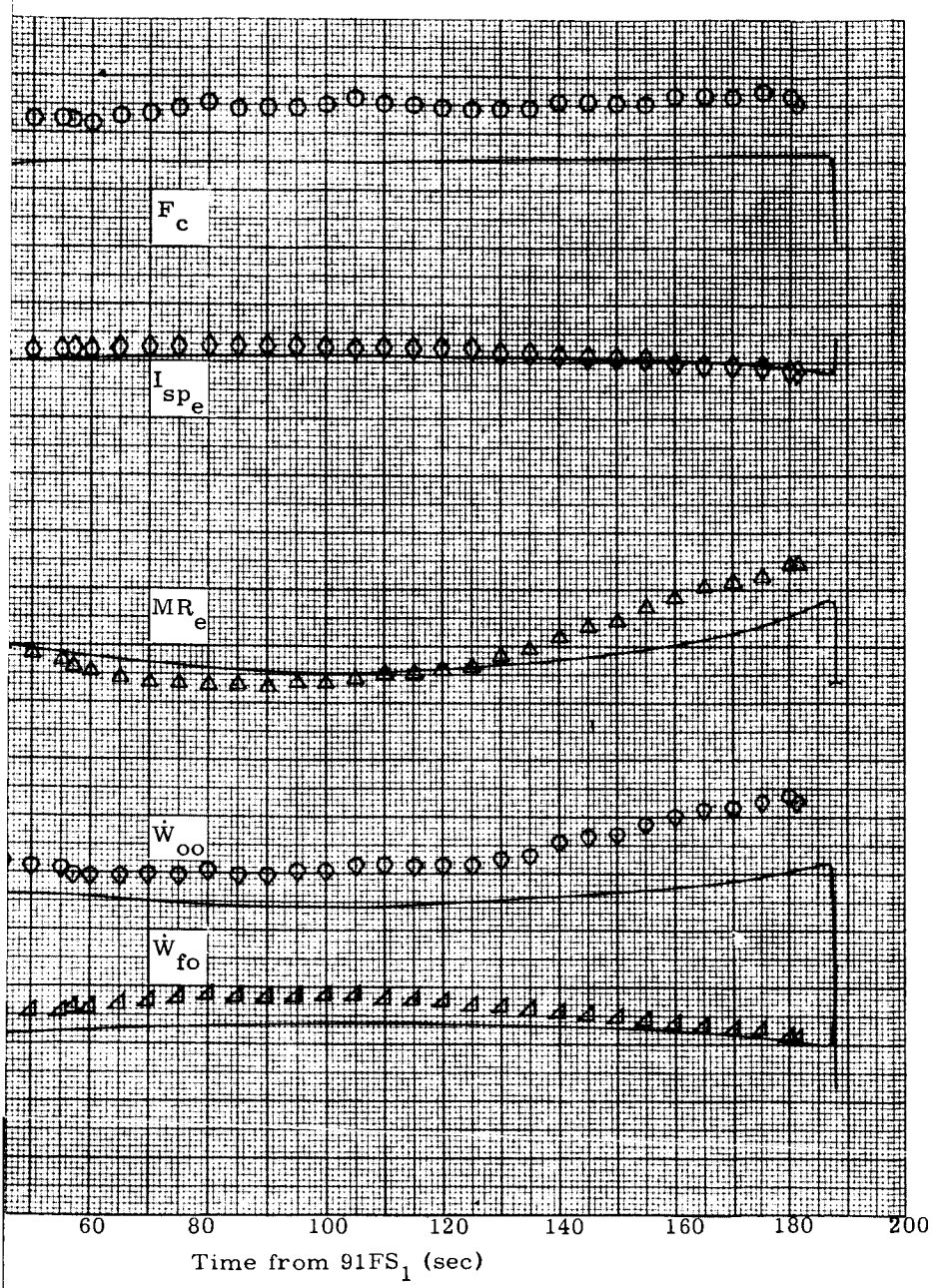


| Average Engine Performance Integrated from First Steady-State to $91FS_2$ | | |
|---|---|---|
| Symbol | Preflight Prediction | Flight Average |
| $F_c$ | 98,694 | 100,547 |
| $I_{sp_e}$ | 310.13 | 310.64 |
| $MR_e$ | 1.7476 | 1.7560 |
| $\dot{W}_{oo}$ | 202.58 | 206.39 |
| $\dot{W}_{fo}$ | 115.66 | 117.28 |

Legend
——— Preflight prediction
Flight performance symbols
⊙ $F_c$
◊ $I_{sp_e}$
△ $MR_e$
$\dot{W}_{oo}$
◿ $\dot{W}_{fo}$

Fig. III-7. Stage II Engine Flight Performance

[redacted]

d. Shutdown transient

Stage II engine shutdown was initiated by a guidance command. The shutdown sequence for GLV-3 included both the normal thrust chamber valve (TCV) method and the redundant system (RESS). The resulting shutdown transient was different than that previously experienced on GT-1 and GT-2. A description of the sequence of events during engine shutdown follows.

After initiation of engine shutdown by the guidance command, the squib valve (because of relays in the circuitry) was energized about 10 to 20 milliseconds after the pressure sequencing valve (PSV). Actuating the PSV initiated closure of the thrust chamber valves by venting the pressurized fuel overboard. Actuation of the RESS squib valve terminated oxidizer flow to the gas generator. A rapid decay in pump discharge pressures resulted from the loss of energy from the gas generator.

After the PSV had actuated, fuel discharge pressure was applied to the closing side of the fuel TCV actuator which closed the engine valves. However, TCV closing time was slightly extended due to lowered fuel discharge pressure, which resulted from the RESS squib valve actuation and the subsequent loss of energy to the pump.

With both shutdown systems operating, $P_c$ decay was initially more rapid than with the TCV shutdown alone. A comparison between the RESS/TCV shutdown transient of GLV-3 and the TCV shutdown of GLV-2 is presented in Figs. III-8 and III-9.

The calculated engine shutdown impulse (including the roll nozzle output) from $91FS_2$ (SECO) to $91FS_2$ + 20 seconds was 37,570 lb-sec compared to the prediction of 41,390 ± 7700 lb-sec. Calculation of shutdown impulse was made by utilizing $P_c$ data from $91FS_2$ to $91FS_2$ + 0.7 second (time of TCV closure) and low level accelerometer (±0.5 g) data from $91FS_2$ + 0.7 second to $91FS_2$ + 20 seconds. The impulse obtained from $P_c$ decay was 26,470 lb-sec; from accelerometer data 10,800 lb-sec was calculated. Total impulse from the roll control nozzle was 300 lb-sec. An average vehicle weight of 13,911 pounds was used with accelerometer data.

[redacted]

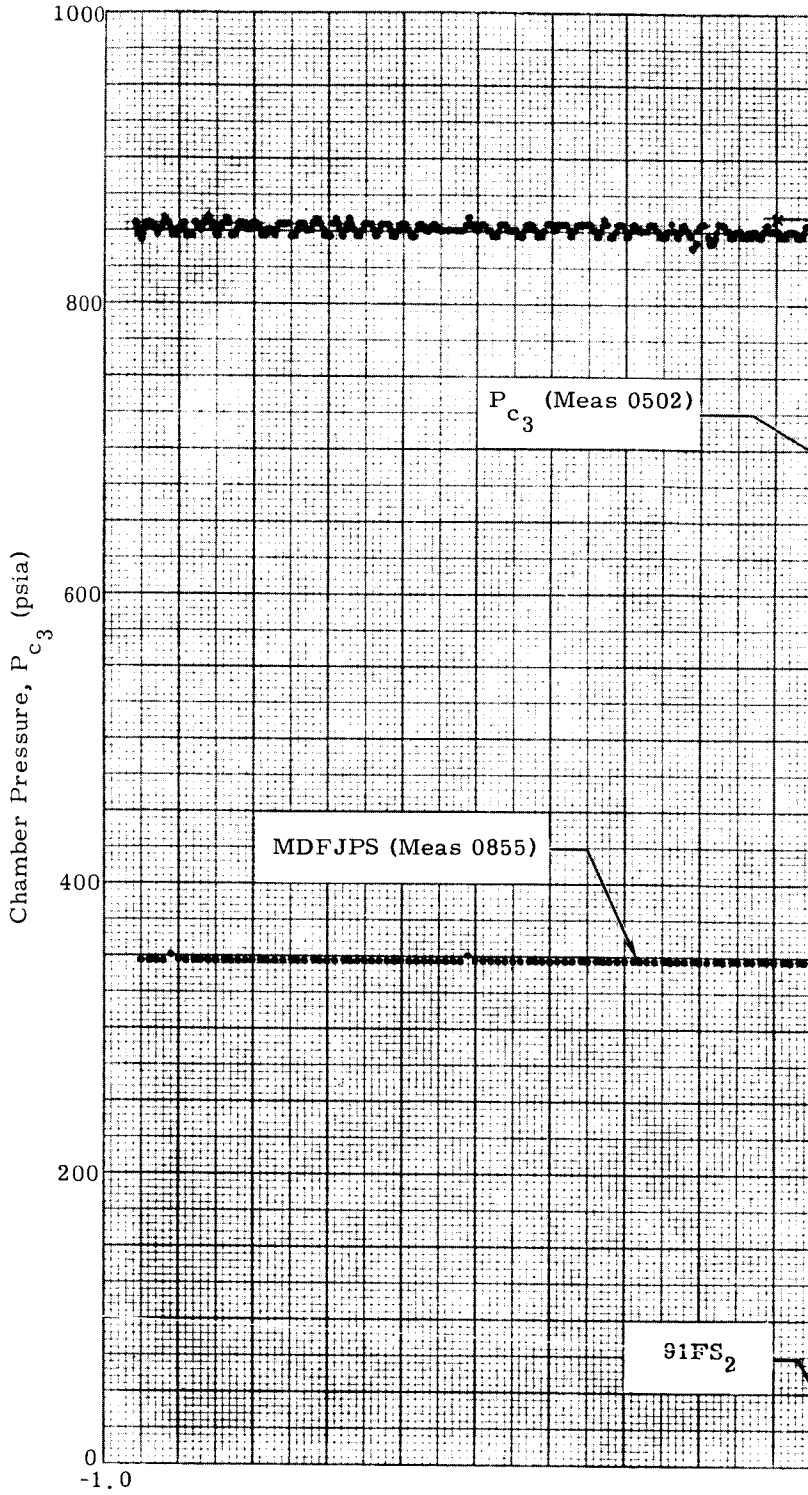
1000
800
600
400
200
0
-1.0
Chamber Pressure, $P_{c_3}$ (psia)
$P_{c_3}$ (Meas 0502)
MDFJPS (Meas 0855)
91FS$_2$

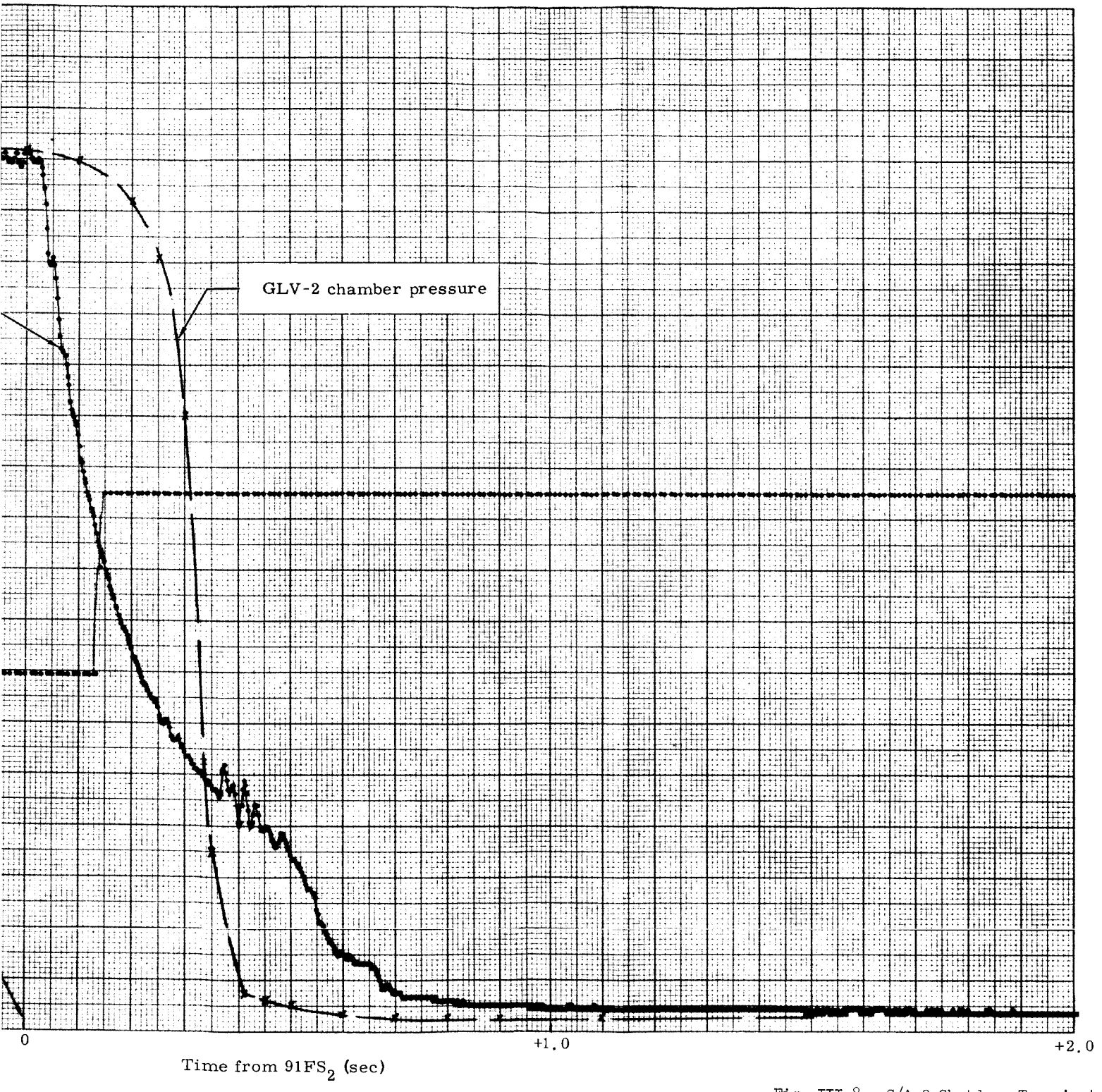


Fig. III-8. S/A 3 Shutdown Transient

[redacted]

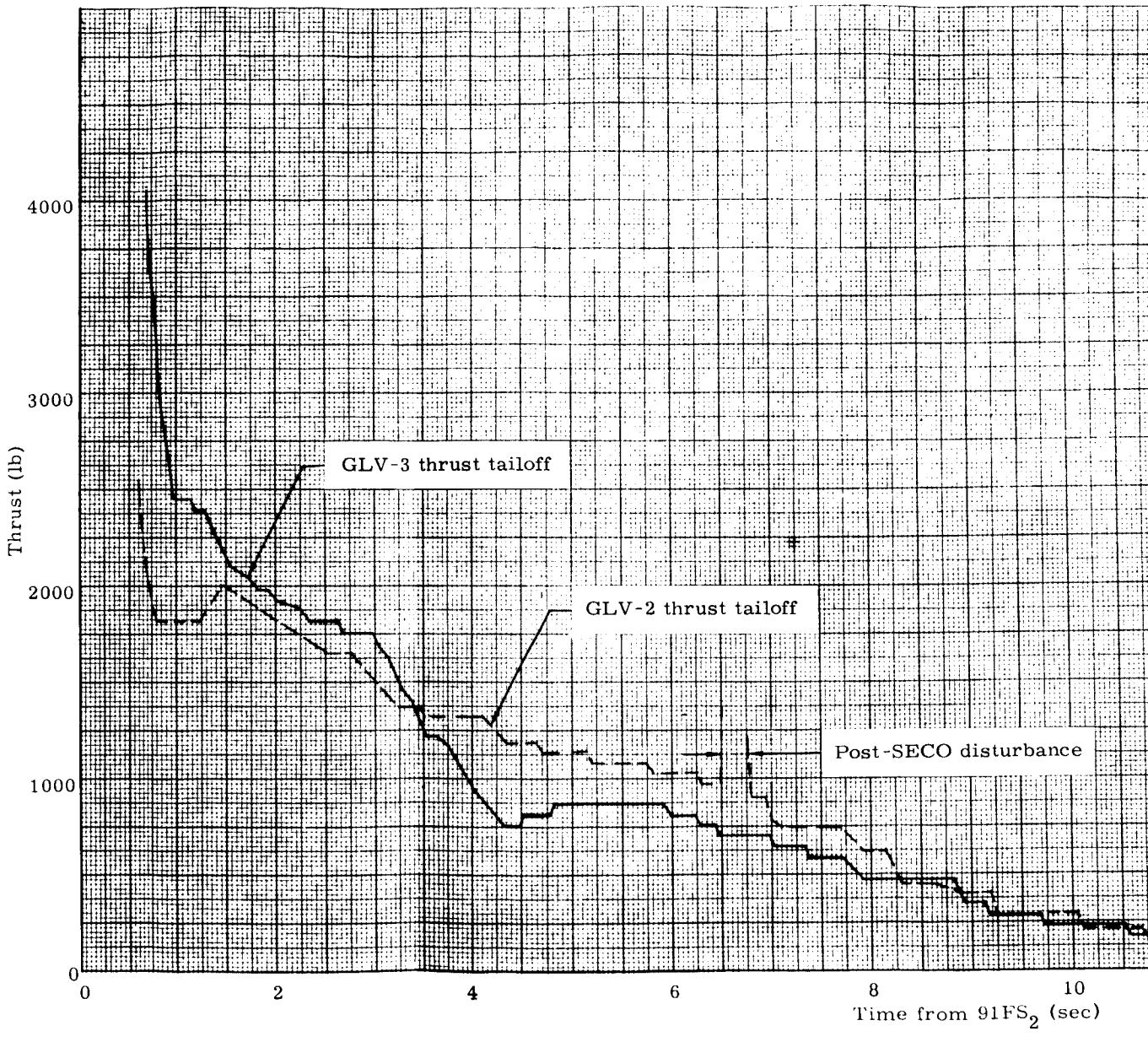


[redacted]

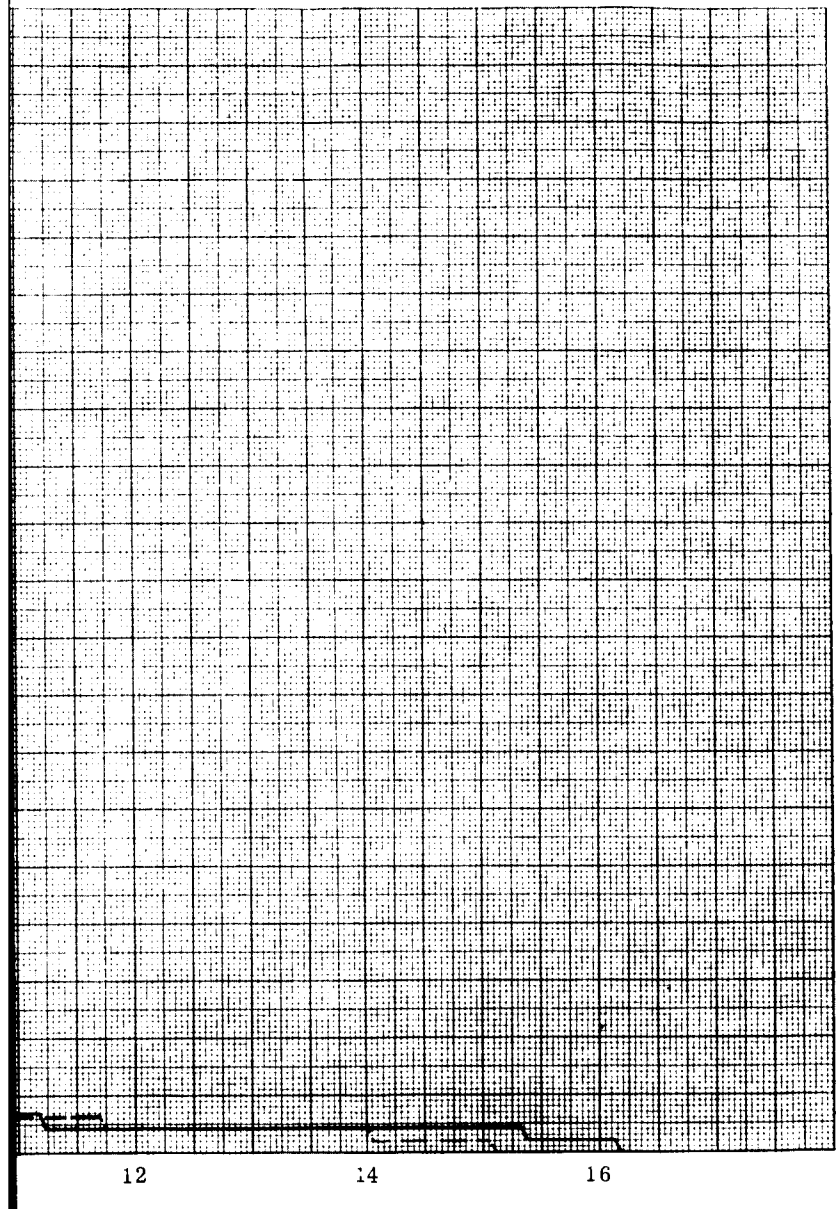


Fig. III-9. Stage II Engine Thrust Tail-Off

## B. PROPELLANT SUBSYSTEM

### 1. Propellant Loading

a. Wet mock simulated launch (WMSL) operation

Several problems were encountered during the WMSL test on GLV-3. Two abortive fuel loading attempts were made. On the first attempt, the Stages I and II fuel totalizers were recording data from the wrong flowmeters: Stage I fuel totalizer was recording Stage II fuel flowmeter and vice versa. This wiring error was corrected. On the second attempt, the umbilical tower fuel level sensors which are used to start the fuel totalizers were likewise reversed. This wiring error was also corrected. On the third attempt, a successful WMSL test was accomplished. Valid verification of fuel and oxidizer loads was obtained at Hi-Lite and satisfactory propellant temperatures were observed. In the course of this test, a discrepancy was observed wherein the Stage II fuel secondary totalizer was erroneous. Also, a leak was discovered in the Stage II oxidizer feedline after loading had been completed. Because of this leak, the Stage II oxidizer tank was unloaded and remained so during the WMSL countdown.

Following the WMSL, the Stage II oxidizer feedline leak was corrected by replacing the conoseal gasket which had been improperly installed. The Stage II fuel secondary counter was replaced.

A subsequent fuel and oxidizer tanking test demonstrated zero leakage at the conoseal connection, although an out-of-tolerance load condition at Hi-Lite on each fuel tank was noted. The fuel flowmeters were removed and returned to Martin-Denver and Wyle Laboratories for calibration checks. Testing at both facilities showed the meters to be very close to the initial calibration. Investigation of the out-of-tolerance condition is continuing.

b. Launch operation

The propellant loading system performed well for the GT-3 launch. A minor leak was discovered in the Stage II oxidizer fill and drain line pressure cap after oxidizer loading had been completed. The cap leak was attributed to a metal deposit on the Kynar seal inside the pressure cap. This metal prevented the seal from sealing properly on the seal surface of the airborne connector. The leak was stopped by replacing the airborne pressure cap. The cap leak also indicated that the disconnect poppet was likewise leaking. Leakage from the disconnect has been a chronic problem in the past and is attributed to variations in alignment of the poppet to the seal from one actuation to the next. Small poppet leaks can be tolerated by virtue of the redundant sealing feature provided by the pressure cap.

[redacted]

The propellant loading schedule is presented in Table III-4.

TABLE III-4

GT-3 Propellant Loading Schedule (22 March 1965)

| | Stage I Oxidizer | Stage I Fuel | Stage II Oxidizer | Stage II Fuel |
|---|---|---|---|---|
| Start (EST) | 18.21 | 22.35 | 18.21 | 22.35 |
| Hi-Lite (EST) | 19.47 | 23.26 | 19.00 | 23.09 |
| Complete (EST) | 19.59 | 23.33 | 19.15 | 23.14 |
| Flowmeters used in loading operation | | | | |
| | Stage I Oxidizer | Stage I Fuel | Stage II Oxidizer | Stage II Fuel |
| Serial No. | 199168 | 199169 | 199173 | 199170 |
| Part No. | 8315B4-10 | 8315B4-9 | 8315B4-12 | 8315B4-11 |

c. Load verification

Data from the propellant load verification tab run are presented in Table III-5.

TABLE III-5

Summary of Propellant Load Verification at Hi-Lite

| Tank | Hi-Lite Temperature (°F) | Flowmeter (lb) | Hi-Level Sensor (lb) | Difference (%) | Allowable Difference (%) |
|---|---|---|---|---|---|
| Stage I oxidizer | 25.4 | 160,220 | 160,100 | +0.070 | ±0.30 |
| Stage I fuel | 28.6 | 80,910 | 80,966 | -0.069 | ±0.25 |
| Stage II oxidizer | 26.3 | 26,710 | 26,763 | -0.198 | ±0.30 |
| Stage II fuel | 30.1 | 20,180 | 20,176 | +0.020 | ±0.25 |

All four propellant tanks were loaded to well within allowable tolerance at Hi-Lite.

[redacted]

d. Total propellant load

The total propellants loaded onboard at the completion of the loading operation, as determined by flowmeters, are listed in Table III-6. The flowmeter totalizer reading was corrected by subtracting the propellant vaporized, vented overboard and that remaining in the fill lines.

TABLE III-6

Total Mission Load

| Tank | Flowmeter Indicated (lb) | Requested (lb) |
|---|---|---|
| Stage I oxidizer | 171,689 | 171,676 |
| Stage I fuel | 90,457 | 90,440 |
| Stage II oxidizer | 38,160 | 38,165 |
| Stage II fuel | 21,956 | 21,959 |

e. Flight verification

The total propellant load, as reconstructed from flight data, is shown in Table III-7 which also compares it with the requested load and with the flowmeter indicated load. The total load, determined by a propellant inventory, used the time difference between uncover of the high level sensors and the outage level sensors. With these time differences and knowing the calibrated volume between sensors, an average flow rate was found.

The total integrated in-flight overboard propellant consumption was obtained from the engine analytical model using the average flow rates. All transient propellant consumptions and pressurization weights were calculated from measured flight data.

The flight reconstructed total loads, listed in Table III-7, represent the best estimate of total propellants loaded onboard.

[redacted]

TABLE III-7

Loads Comparison

| a. Comparison of Flight Reconstructed Load with Requested Load | | | |
|---|---|---|---|
| Tank | Reconstructed Load (lb) | Requested Load (lb) | Difference (%) |
| Stage I oxidizer | 171,474 | 171,676 | -0.117 |
| Stage I fuel | 90,445 | 90,440 | +0.005 |
| Stage II oxidizer | 38,225 | 38,165 | +0.157 |
| Stage II fuel | 21,991 | 21,959 | +0.145 |
| **b. Comparison of Flight Reconstructed Load with Flowmeter Load** | | | |
| Tank | Reconstructed Load (lb) | Flowmeter Indicated Load (lb) | Difference (%) |
| Stage I oxidizer | 171,474 | 171,689 | -0.125 |
| Stage I fuel | 90,445 | 90,457 | -0.013 |
| Stage II oxidizer | 38,225 | 38,160 | +0.170 |
| Stage II fuel | 21,991 | 21,956 | +0.159 |

f. Ullage volume

The initial ullage volumes shown in the following tabulation were obtained by calculating the total loaded volume in each tank, and subtracting this from the total calibrated tank volume. The propellant weight, as found by flight reconstruction, divided by the average in-flight density, is then the initial propellant volume to the thrust chamber valve. The average density was obtained by integrating flight temperatures from $FS_1$ to $FS_2$ and correcting for in-flight stratification.

[redacted]

| Initial Ullage Volume | | |
|---|---|---|
| Tank | Ullage Volume (cu ft) | Specification Minimum ($ft^3$) |
| Stage I oxidizer | 81.261 | 48 |
| Stage I fuel | 49.525 | 39 |
| Stage II oxidizer | 87.245 | 63 |
| Stage II fuel | 16.954 | 16 |

g. Propellant assay

Prelaunch data from the propellant assay laboratory report (sampled on F-2 day) for the oxidizer (nitrogen tetroxide) and fuel (50% hydrazine and 50% UDMH) are presented in Table III-8. Specification values are also listed. Good agreement is shown between the laboratory data and specification requirements. The density was determined by a pycnometer.

TABLE III-8

Propellant Assay Summary

| Fuel MIL-P-27402 (USAF) | Test | Requirement |
|---|---|---|
| Hydrazine | 50.8% | 51 ± 0.9% |
| UDMH | 48.1% | 46.9% min |
| $H_2O$ | 1.1% | 2.0% max |
| Total $N_2H_4$ + UDMH | 98.9% | 98% min |
| Solids | 0.4 mg/liter | 25 mg/liter |
| Particles on 50 mesh screen | 0 | 0 |
| Density (gm/cc) at 77° F | 0.8972 | -- |
| **Oxidizer MIL-P-26539 (USAF)** | **Test** | **Requirement** |
| Nitrogen tetroxide ($N_2O_4$) | 99.8% | 99.4% min |
| Chloride as NOCl | 0.003% | -- |
| $H_2O$ equivalent | 0.06% | 0.2% |
| Solids | 0.5 mg/liter | 10 mg/liter |
| Nonvolatile ash | 0.0004% | -- |
| Particles on 50 mesh screen | 0 | 0 |

## 2. Propellant Temperatures

a. Weather

A comparison of the F-45 day prediction, the F-1 day prediction, and the actual weather for the 23 March launch of GT-3 appears in Table III-10. The F-45 day prediction was made for an average March or April hot day. In the case of the F-1 day prediction, it can be seen that the predicted weather was in good agreement with the actual weather data.

b. Ready storage vessel temperature

The requested ready storage vessel (RSV) temperatures and the actual RSV temperatures are as follows:

| RSV System | Meas | Requested Temperature (°F) | Actual Temperature (°F) |
|---|---|---|---|
| Fuel | 4425 | 26 | 26.2 |
| Oxidizer | 4426 | 22 | 21.6 |

c. Flowmeter temperature

The propellant heating program predicts the temperature rise from the RSV to the flowmeter at the end of the precooling cycle. For GLV-3, the temperature rise was 1.8° F for oxidizer and 1.5° F for fuel.

The predicted flowmeter temperatures and the actual flowmeter temperatures that occurred at the end of the precooling cycle are shown in Table III-9.

TABLE III-9

Propellant Temperatures at Flowmeter

| System | Meas | Predicted Temperature (°F) | Actual Temperature (°F) | Delta Temperature (°F) |
|---|---|---|---|---|
| Stage I fuel | 4431 | 27.5 | 28.2 | +0.7 |
| Stage II fuel | 4432 | 27.5 | 28.0 | +0.5 |
| Stage I oxidizer | 4433 | 23.4 | 24.0 | +0.6 |
| Stage II oxidizer | 4434 | 23.4 | 24.7 | +1.3 |

## TABLE III-10

### Predicted and Actual Weather Conditions for GT-3 Launch

| Time EST (hr) | Dry Bulb Temperature (°F) | | | Dew Point Temperature (°F) | | | 53-Foot Elevation Wind Speed (fps) | | | Cloud Cover | | |
|---|---|---|---|---|---|---|---|---|---|---|---|---|
| | F-45 Day | F-1 Day | Actual | F-45 Day | F-1 Day | Actual | F-45 Day | F-1 Day | Actual* | F-45 Day | F-1 Day | Actual |
| 3-22-65 | | | | | | | | | | | | |
| 1800 | 79.0 | | 65.8 | 67.6 | | 60.0 | 10 | | 9 | 0.5 | | 0.6 |
| 1900 | 78.6 | | 66.9 | 67.0 | | 60.0 | 8 | | 10 | 0.5 | | 0.6 |
| 2000 | 76.9 | | 67.0 | 66.4 | | 61.0 | 7.5 | | 10 | 0.5 | | 0.6 |
| 2100 | 76.4 | 65.0 | 67.0 | 65.8 | 59.0 | 61.0 | 7 | 10 | 10 | 0.5 | 0.6 | 0.6 |
| 2200 | 75.9 | 65.0 | 67.3 | 65.4 | 59.0 | 61.0 | 7 | 10 | 7 | 0.5 | 0.5 | 0.5 |
| 2300 | 75.5 | | 67.2 | 65.0 | | 61.0 | 7 | | 7 | 0.5 | | 0.4 |
| 2400 | 75.0 | 65.0 | 67.0 | 64.6 | 60.0 | 61.0 | 6.5 | 10 | 9 | 0.5 | 0.5 | 0.5 |
| 3-23-65 | | | | | | | | | | | | |
| 0100 | 74.9 | | 67.0 | 64.4 | | 62.0 | 6.5 | | 7 | 0.5 | | 0.7 |
| 0200 | 74.6 | | 67.0 | 64.2 | | 62.0 | 6.5 | | 8 | 0.5 | | 1.0 |
| 0300 | 74.7 | 65.0 | 67.0 | 64.0 | 63.0 | 62.0 | 6.5 | 8 | 9 | 0.5 | 0.5 | 0.5 |
| 0400 | 74.6 | | 67.3 | 63.6 | | 62.0 | 6.5 | | 6 | 0.5 | | 0.4 |
| 0500 | 74.5 | | 67.5 | 63.7 | | 62.0 | 6.5 | | 7 | 0.5 | | 0.4 |
| 0600 | 74.4 | 66.0 | 67.3 | 63.6 | 63.0 | 63.0 | 6.5 | 8 | 5 | 0.5 | 0.6 | 0.6 |
| 0700 | 75.4 | | 67.0 | 64.9 | | 63.0 | 6.5 | | 5 | 0.5 | | 0.6 |
| 0800 | 77.2 | | 67.5 | 66.1 | | 64.0 | 8 | | 4 | 0.5 | | 0.6 |
| 0900 | 78.8 | 67.0 | 69.2 | 67.2 | 60.0 | 64.0 | 10 | 10 | 7 | 0.5 | 0.6 | 0.6 |
| 1000 | 80.0 | | 70.0 | 68.2 | | 64.0 | 11 | | 9 | 0.5 | | 0.5 |
| 1100 | 81.3 | | 69.8 | 68.8 | | 64.0 | 11.5 | | 9 | 0.5 | | 0.5 |
| 1200 | 82.1 | 69.0 | 71.5 | 69.2 | 59.0 | 64.0 | 12 | 12 | 11 | 0.5 | 0.5 | 0.5 |

*Actual wind velocity was taken at the 12-foot level because the 54-foot level was inoperative on Tower 700.

[redacted]

The propellant temperature rise during the loading operation caused by heat input from pump work is the difference between the flowmeter and RSV temperatures at the time that Hi-Lite is achieved. The temperature rise that occurred during the GT-3 loading operation is shown in Table III-11.

TABLE III-11

Propellant Temperature Rise During Loading

| System | Flowmeter Temperature (°F) | RSV Temperature (°F) | Temperature Rise (°F) |
|---|---|---|---|
| Stage I fuel | 28.3 | 26.7 | 1.6 |
| Stage II fuel | 27.5 | 26.6 | 0.9 |
| Stage I oxidizer | 25.4 | 22.9 | 2.5 |
| Stage II oxidizer | 25.0 | 21.8 | 3.2 |

The RSV and flowmeter temperatures recorded during loading are shown in Figs. III-10 and III-11.

d. Hi-Lite temperature

The requested and actual propellant temperatures at the time of high level sensor covering are presented in Table III-12.

TABLE III-12

Propellant Temperatures at Hi-Lite

| System | Meas | Requested Temperature (°F) | Actual Temperature (°F) | Delta Temperature (°F) |
|---|---|---|---|---|
| Stage I fuel | 4124 | 28.0 | 28.6 | +0.6 |
| Stage II fuel | 4601 | 29.1 | 30.1 | +1.0 |
| Stage I oxidizer | 4128 | 24.5 | 25.4 | +1.1 |
| Stage II oxidizer | 4604 | 26.2 | 26.3 | +0.1 |

The actual Hi-Lite temperatures were within the ±2° tolerance assigned to the requested values.

The increase in propellant temperatures during the loading operation caused by the heat transferred from the propellant tanks and from the fill lines which run from the flowmeter to the tanks is shown in Table III-13. Values are for the time at which the tank high level sensor was covered.

[redacted]

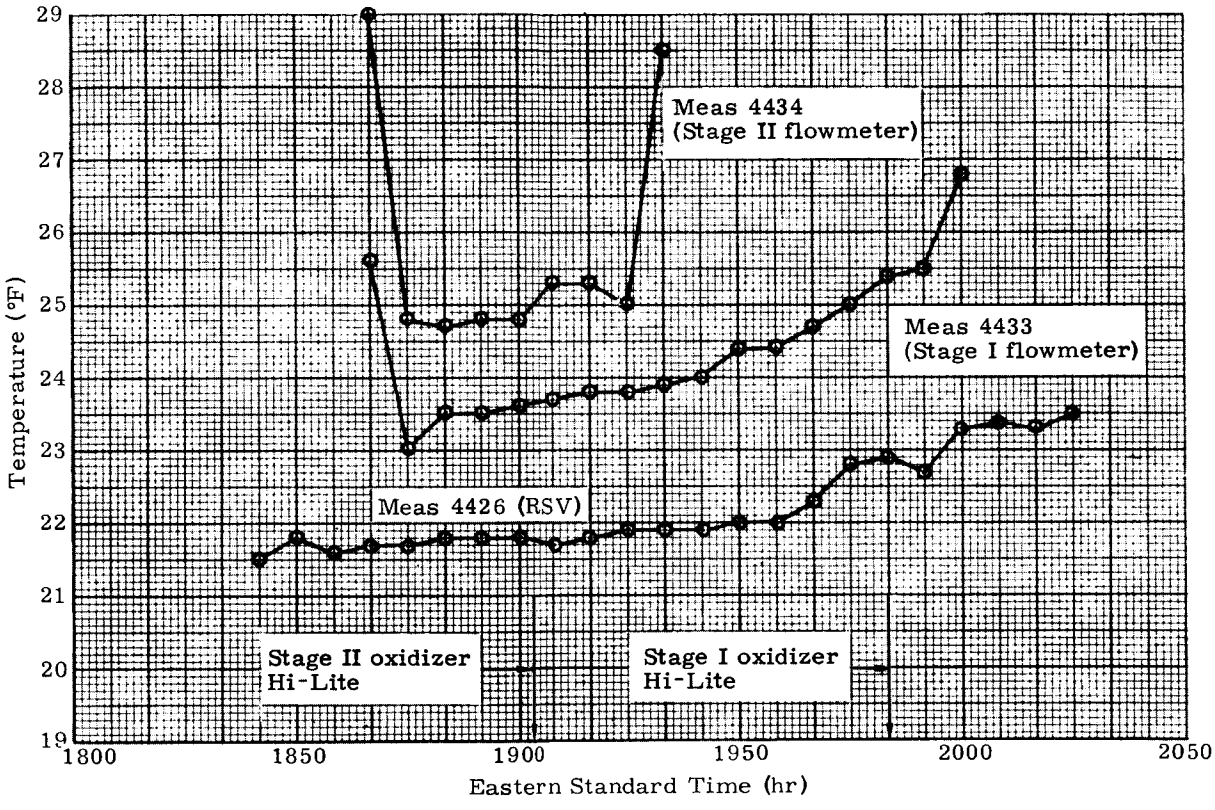


Fig. III-10. Oxidizer Temperatures During Loading

[redacted]

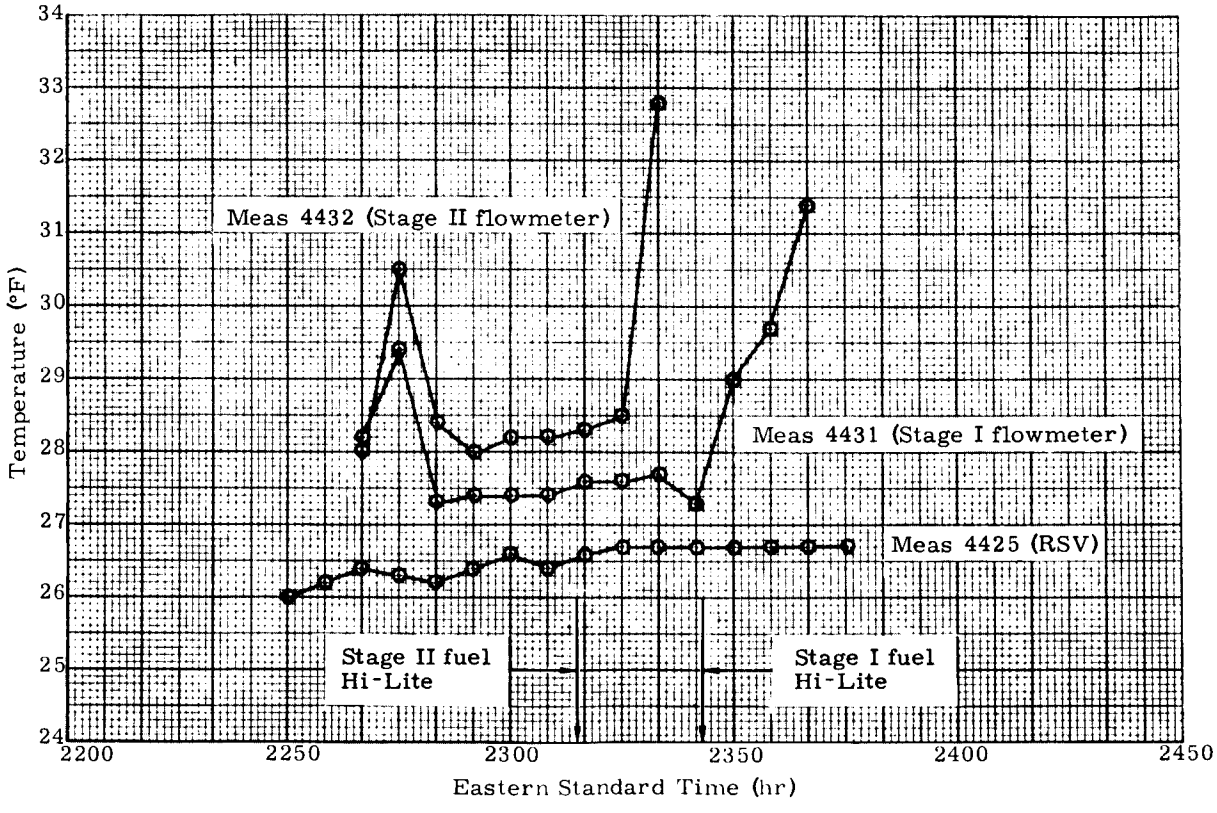


Fig. III-11. Fuel Temperature During Loading

[redacted]

TABLE III-13

Propellant Temperature Increase During Loading

| Tank | Flowmeter (°F) | Tank Hi-Lite (°F) | Temperature Rise (°F) |
|---|---|---|---|
| Stage I fuel | 28.3 | 28.6 | +0.3 |
| Stage II fuel | 27.5 | 30.1 | +2.6 |
| Stage I oxidizer | 25.4 | 25.4 | +0.0 |
| Stage II oxidizer | 25.0 | 26.3 | +1.3 |

e. Liftoff temperature

The propellant bulk temperatures at the time of liftoff are presented in Table III-14 (predicted values are also shown).

TABLE III-14

Propellant Bulk Temperatures at Liftoff

| Tank | F-45 Day Prediction (°F) | F-1 Day Prediction (°F) | Actual (°F) | Reconstructed (°F) |
|---|---|---|---|---|
| Stage I fuel | 38.2 | 44.2 | 44.0 | 41.5 |
| Stage II fuel | 38.3 | 40.8 | 41.3 | 40.2 |
| Stage I oxidizer | 38.9 | 46.4 | 43.9 | 44.1 |
| Stage II oxidizer | 42.7 | 48.0 | 44.8 | 46.7 |

The reconstructed temperatures were obtained using the propellant heating program. The position of these temperatures in the mixture ratio band is shown in Figs. III-12 and III-13.

Figures III-14, III-15, III-16 and III-17 show the variation of the F-1 day prediction, the reconstructed, and the actual propellant temperatures during the countdown for each propellant tank. The slight shift noted between 0300 and 0400 hours was caused by a paper change on the multipoint recorder. Corrective action will be taken to preclude this shift.

f. Suction temperatures

The flight pump inlet temperatures were in agreement with the predicted temperature profiles except for the Stage II oxidizer. These data are shown in Figs. III-18, III-19, III-20 and III-21. The discrepancy in the Stage II oxidizer was due to less stratification of the propellant

[redacted]

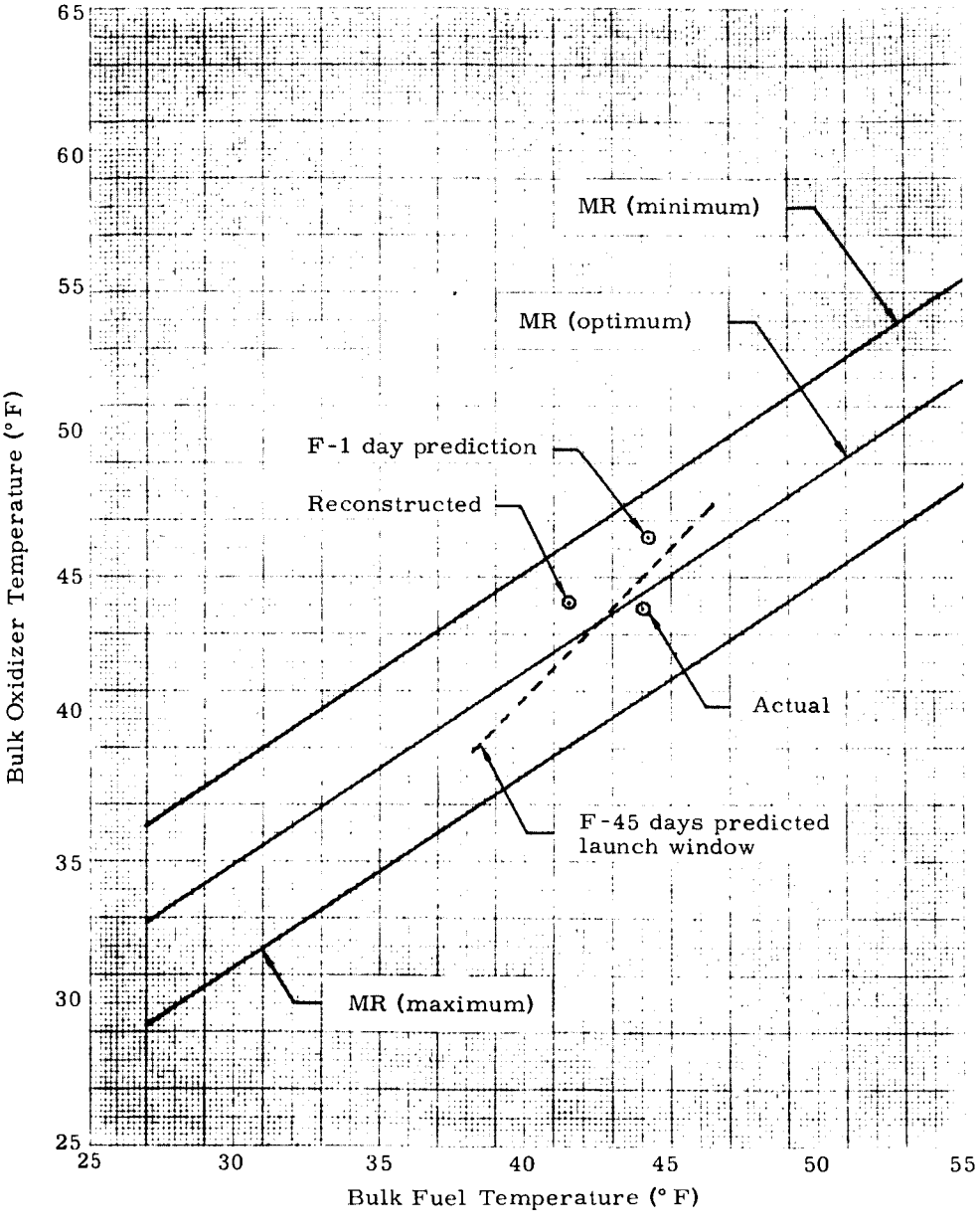


Fig. III-12. Propellant Bulk Temperatures at Liftoff, Stage I

[redacted]

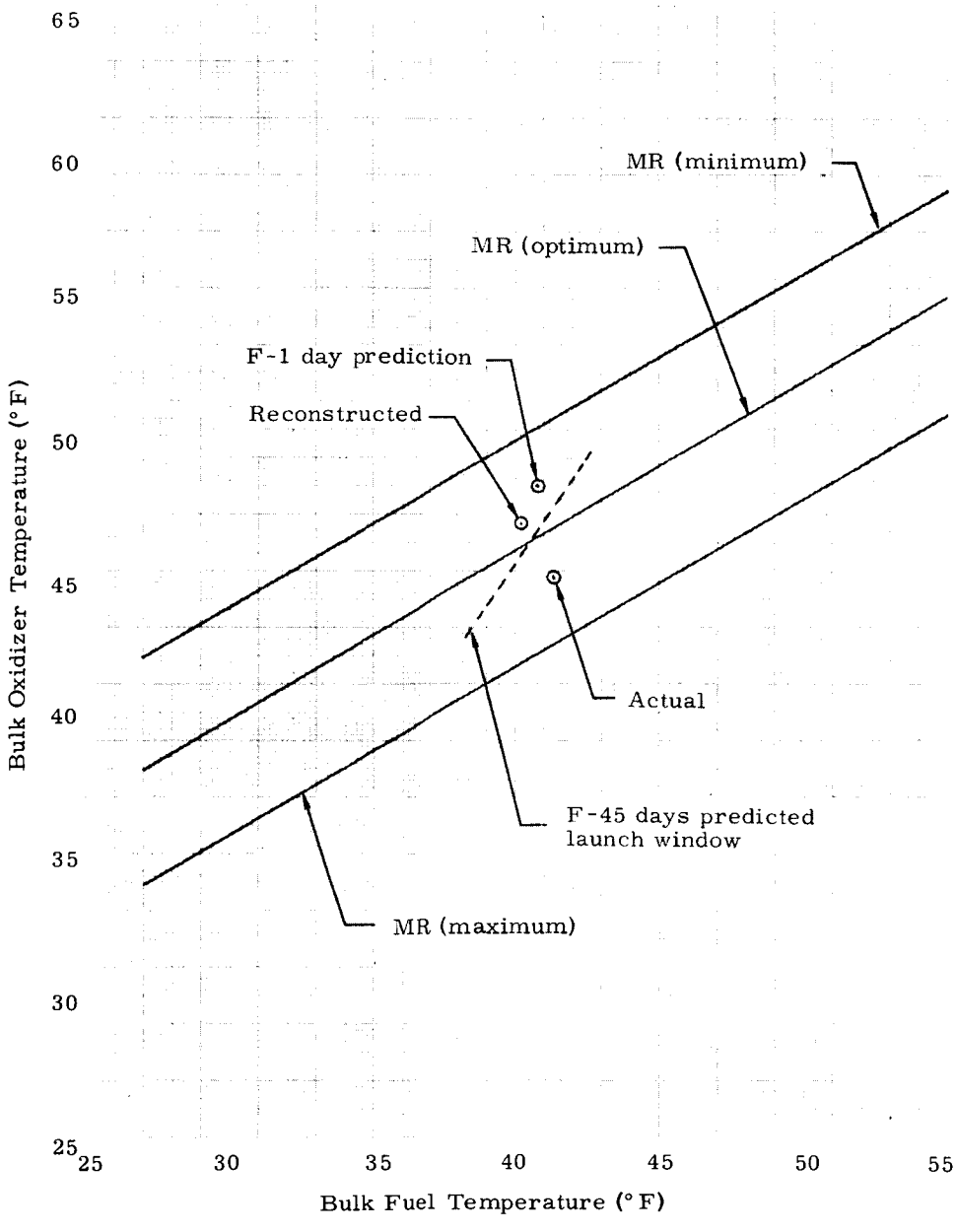


Fig. III-13. Propellant Bulk Temperatures at Liftoff, Stage II

[redacted]

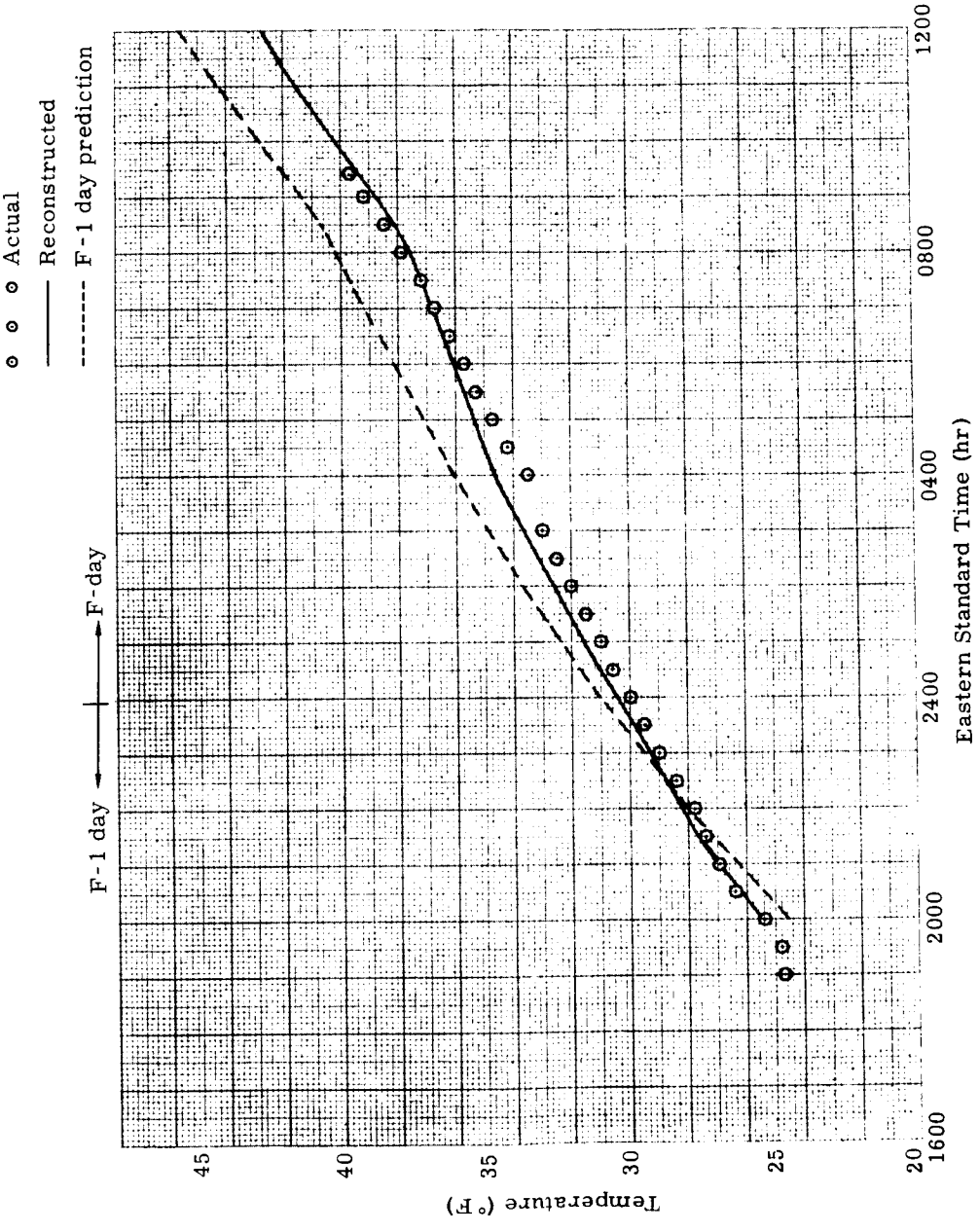


Fig. III-14. Stage I Oxidizer Tank Bottom Probe Temperature (Meas 4128)

[redacted]

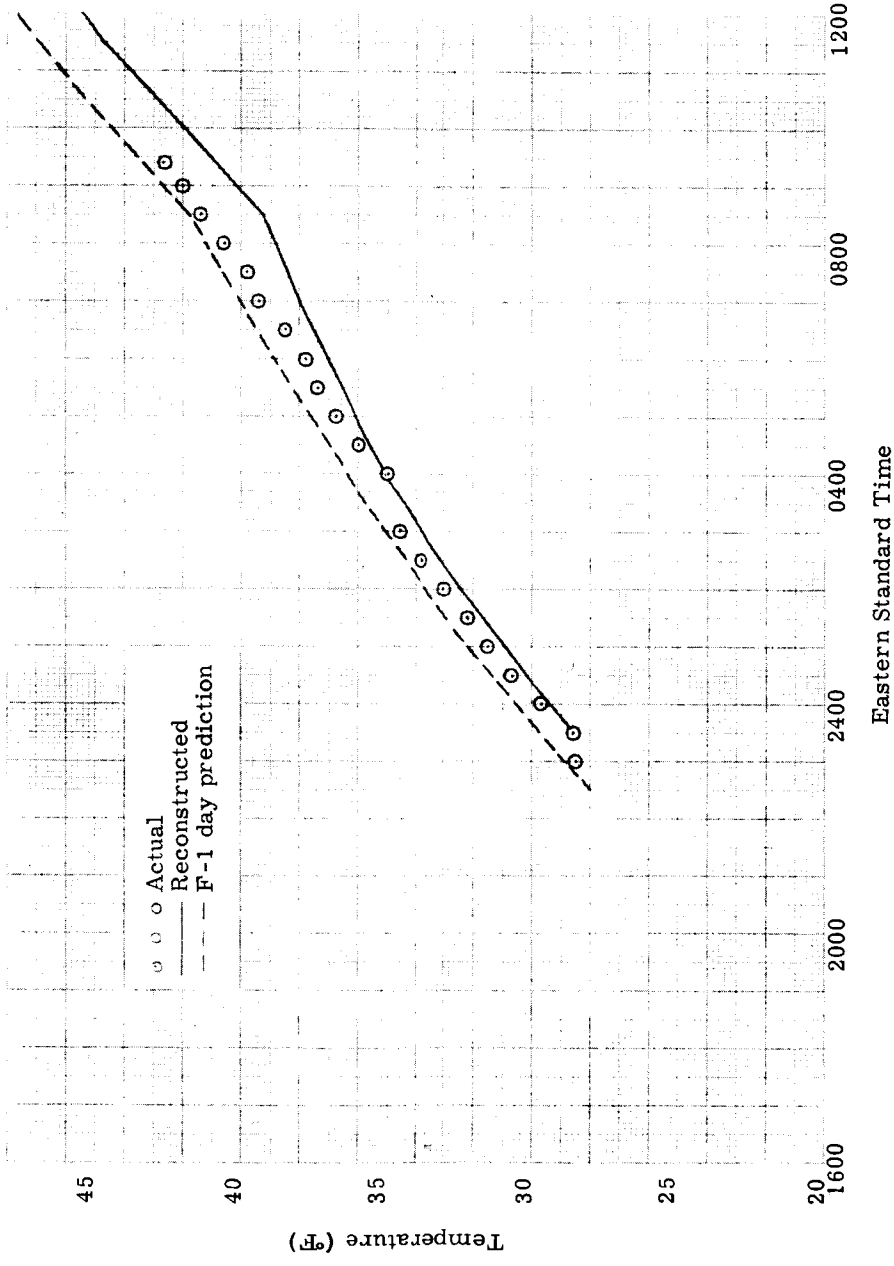


Fig. III-15. Stage I Fuel Tank Bottom Probe Temperature (Meas 4124)

[redacted]

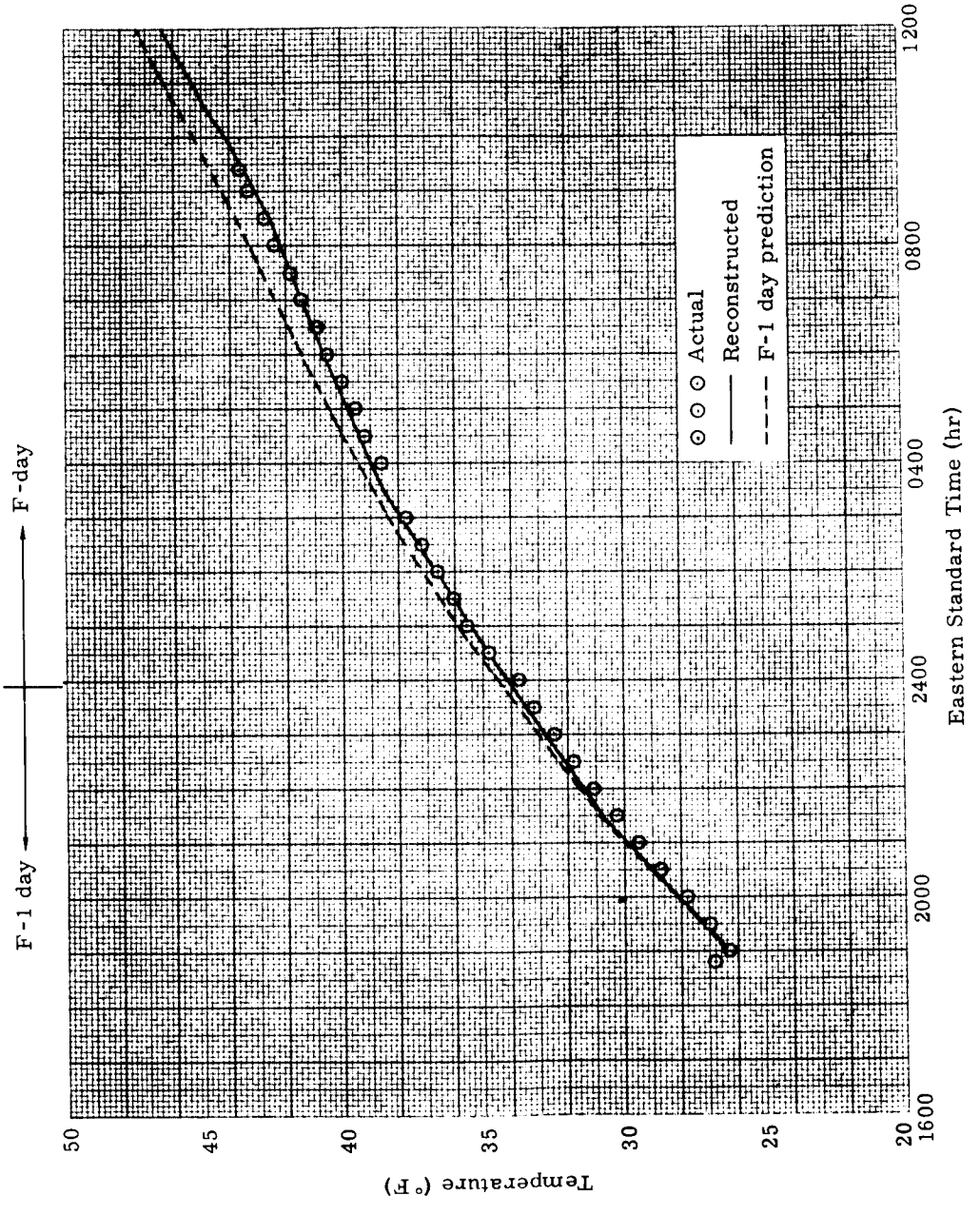


Fig. III-16. Stage II Oxidizer Tank Bottom Probe Temperature (Meas 4604)

[redacted]

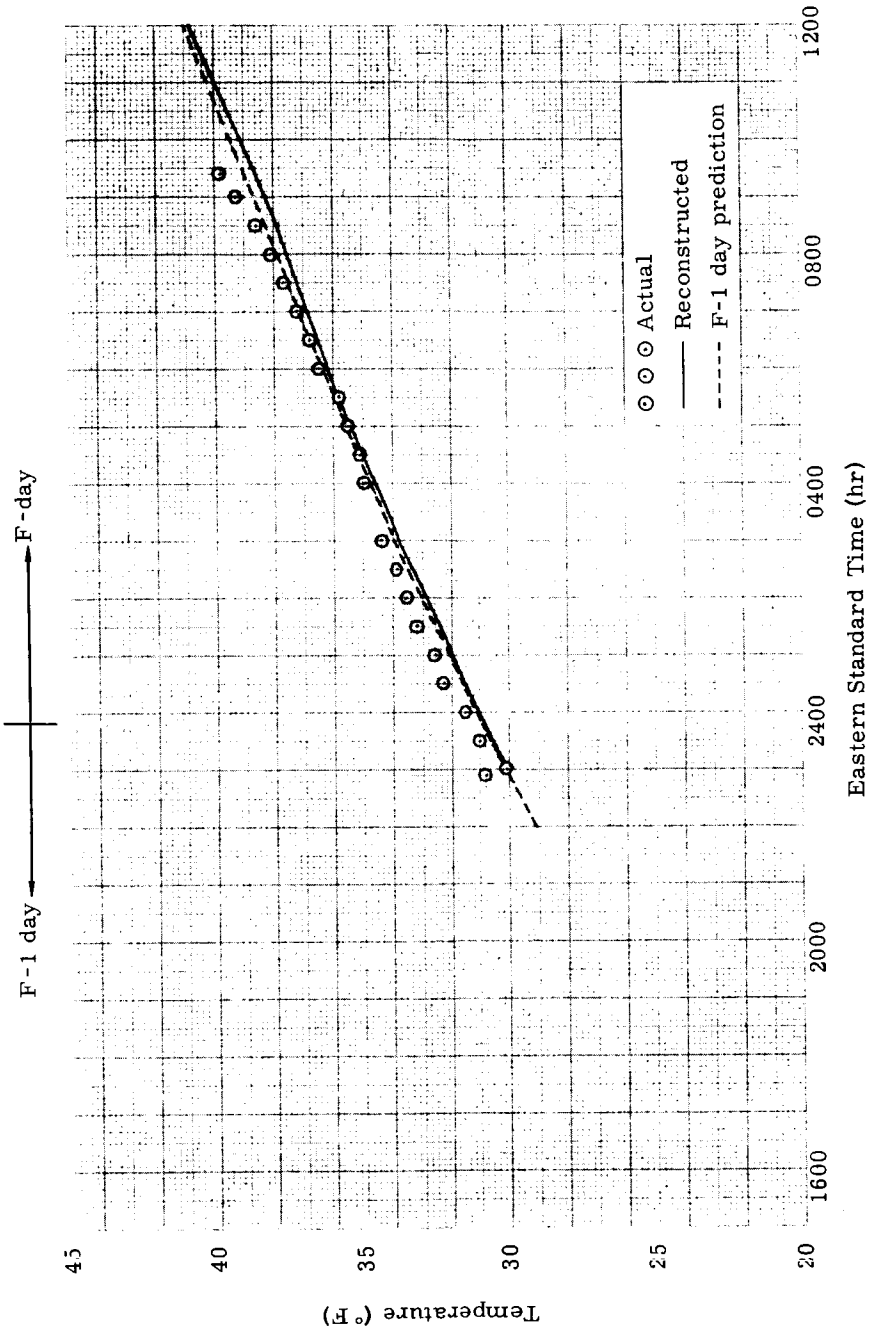


Fig. III-17. Stage II Fuel Tank Bottom Probe Temperature (Meas 4601)

[redacted]

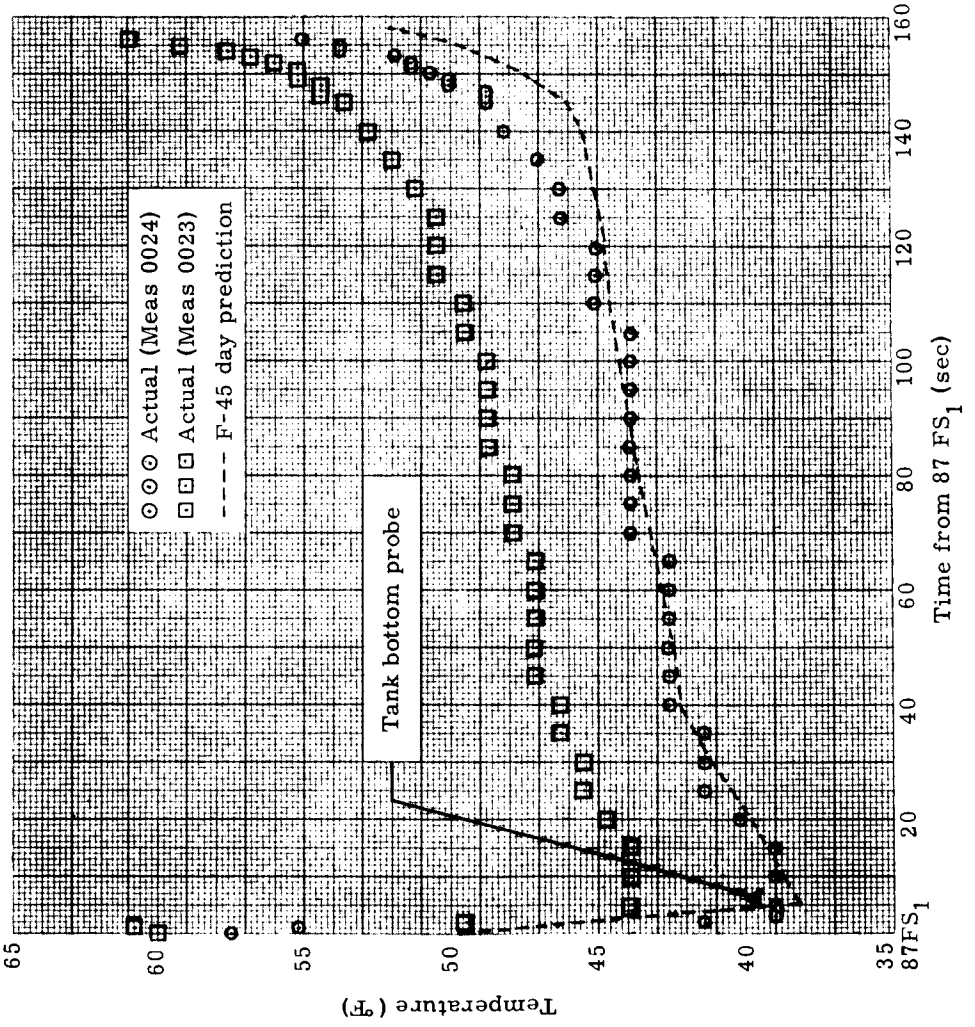


Fig. III-18. Stage I Oxidizer Pump Inlet Temperature (Meas 0023 and 0024)

[redacted]

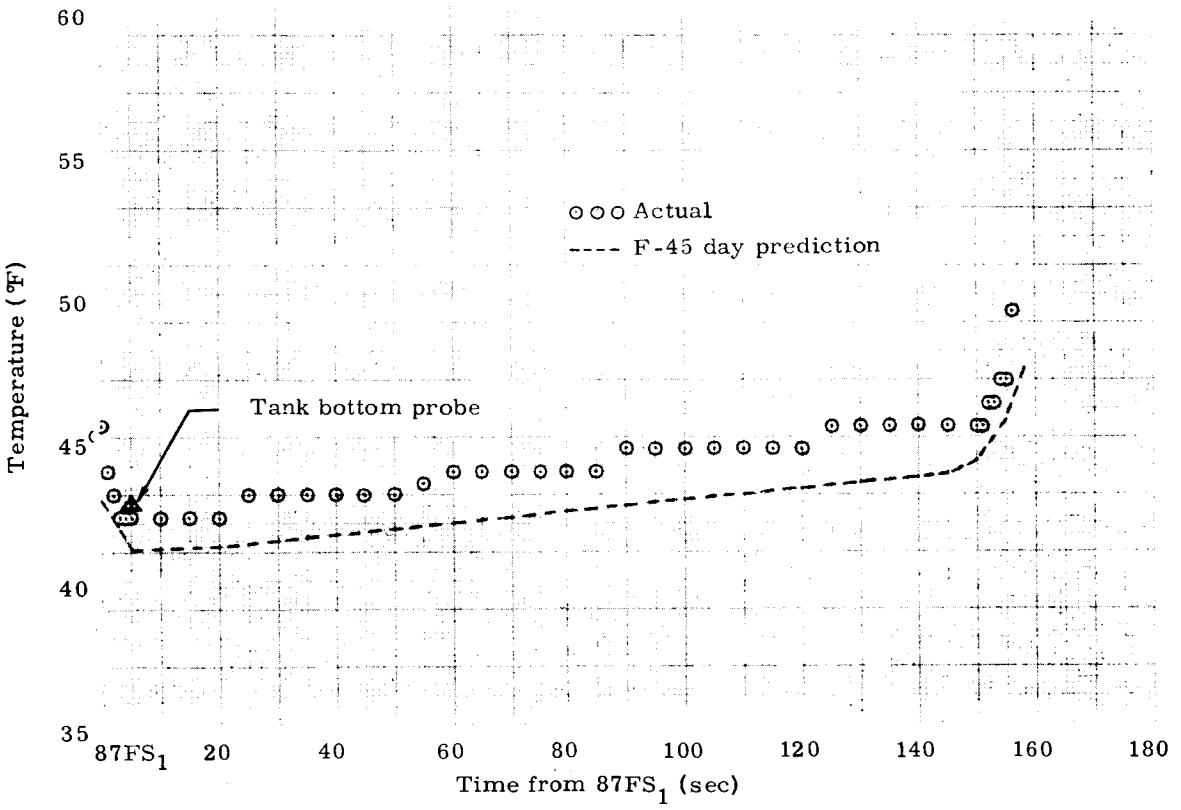


Fig. III-19. Stage I Fuel Pump Inlet Temperature (Meas 0013)

~~CONFIDENTIAL~~

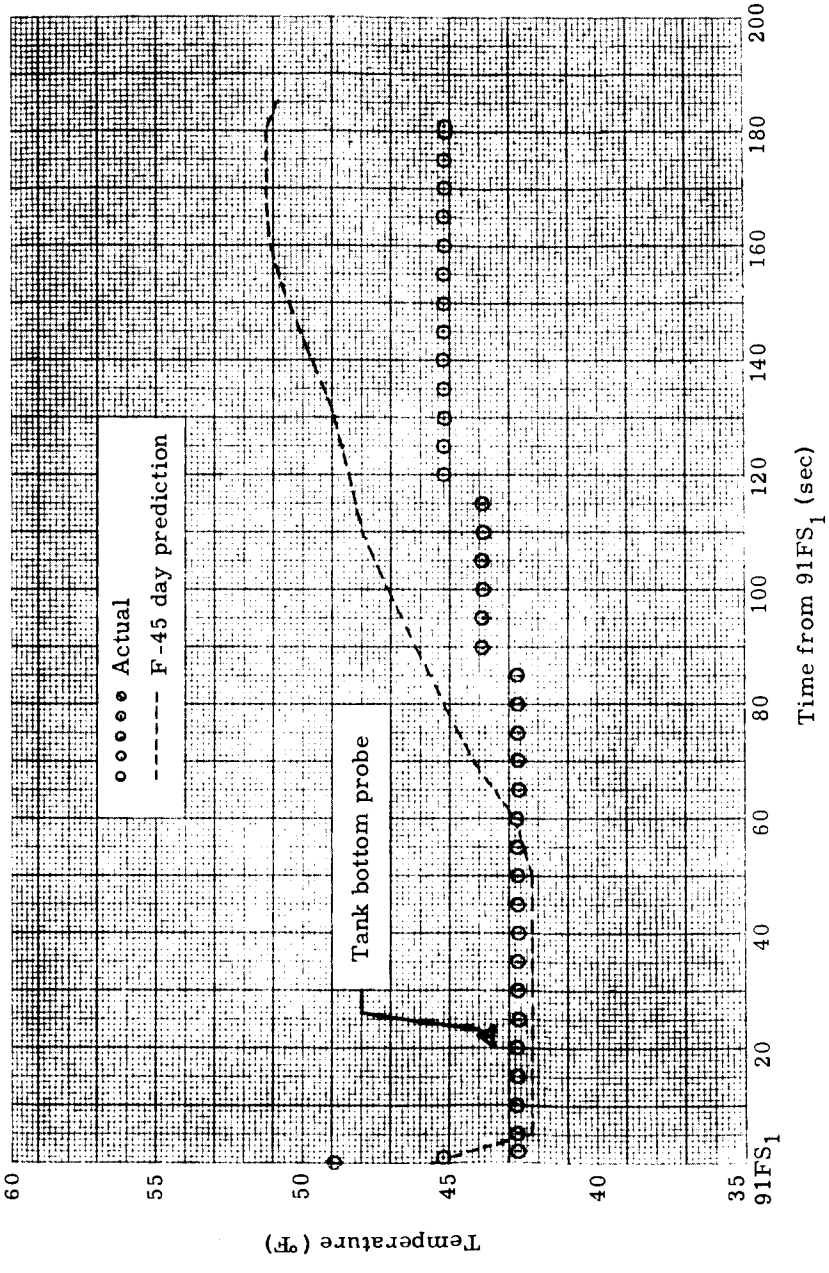


Fig. III-20. Stage II Oxidizer Pump Inlet Temperature (Meas 0514)

~~CONFIDENTIAL~~

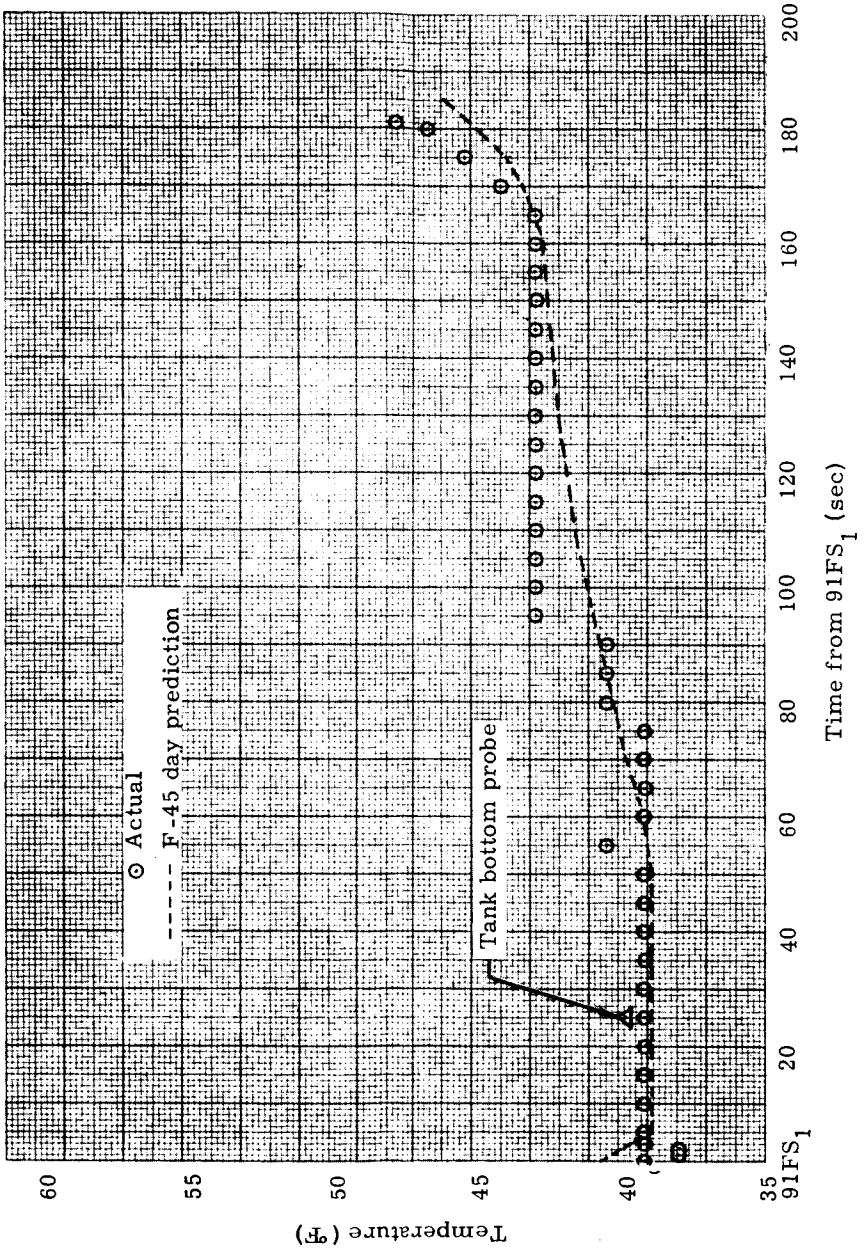


Fig. III-21. Stage II Fuel Pump Inlet Temperature (Meas 0508)

temperature than had been predicted. Since this also occurred on GT-2, the profile of the suction temperatures will be modified for future flights.

The tank bottom probes were in good agreement with the suction probes on all tanks. This vehicle incorporated and relocated a new pump inlet temperature probe (Meas 0024) in the Stage I oxidizer feedline, thereby correcting the discrepancy that has appeared on all previous flights. A comparison with data from the original suction temperature probe (Meas 0023) shows that the relocated probe is more indicative of the real propellant temperatures at the pump inlet.

A comparison has been made between the suction probes and the tank bottom probes temperatures at various times after $FS_1$. In this manner both probes tend to measure the same element of fluid, and a more realistic comparison is possible. The tank bottom probe temperatures and the pump inlet temperatures at these various times are shown in Table III-15.

TABLE III-15

Comparison of Tank Bottom Probe and Pump Inlet Temperatures

| Tank | Time (sec) | Suction Probe (°F) | Tank Bottom Probe (°F) | Delta Temperature (°F) |
|---|---|---|---|---|
| Stage I fuel | $87FS_1 + 5$ | 42.2 | 42.7 | -0.5 |
| Stage II fuel | $91FS_1 + 25$ | 39.1 | 39.8 | -0.7 |
| Stage I oxidizer | $87FS_1 + 6$ | 39.0 | 39.6 | -0.6 |
| Stage II oxidizer | $91FS_1 + 22$ | 42.7 | 43.6 | -0.9 |

3. Propellant Feed System

a. Feedline transients

The maximum transient pressures recorded at the pump inlet instrumentation bosses are presented in Table III-16.

TABLE III-16

Maximum Transient Pressures

| System | Meas | ΔT Prevalve Opening (psia) | Initial Pressure Wave | ΔT Ignition (psia) | ΔT TCV Closing | Design Operating Pressure (psia) |
|---|---|---|---|---|---|---|
| Stage I oxidizer | (0017) | No data | Negligible | 114 | Negligible | 215 |
| Stage I fuel | (0014) | 46.5 | Negligible | 38 | Negligible | 55 |
| Stage II oxidizer | (0510) | 72.0 | Negligible | * | Negligible | 260 |
| Stage II fuel | (0507) | Negligible | Negligible | * | Negligible | 80 |

*Not available due to telemetry blackout at staging.

Pressure data at the opening of the Stage I oxidizer prevalves were unavailable since these valves were opened prior to start of telemetry recording. Stage I ignition transient pressures were similar to those on GT-2. Telemetry blackout normally experienced during Stage II ignition inhibits receipt of data on sustainer engine ignition transients. Simultaneous propellant exhaustion resulted in no TCV closing spikes on Stage II.

b. Pump inlet suction pressures

Stages I and II static pressures at the suction line measurement location are shown in Figs. III-22 through III-25. These figures present the preflight predicted and post-flight reconstructed pressures, and the best estimate of actual flight pressures.

The post-flight reconstructed curves have been based on flight measured values of ullage gas pressure, axial load factors, propellant temperatures, and propellant loadings. The best estimate curves are considered to be the most indicative of the actual pressures. The Stage I oxidizer best estimate curve of the static suction pressures at the measurement boss represents an average of the measured pressure (Meas 0017) and the two oxidizer standpipe pressures (Meas 0033 and 0034) adjusted to the Meas 0017 transducer location. The Stage I fuel suction pressure best estimate at the transducer location is an average of the measured pressure (Meas 0014) and the two fuel accumulator pressures (Meas 0037 and 0038) adjusted to the Meas 0014 transducer location. The Stage II oxidizer and fuel best estimate suction pressures were obtained directly.

c. NPSH supplied

The NPSH supplied at the engine turbopump inlets during the start phase and steady-state operation is shown in Table III-17.

[redacted]

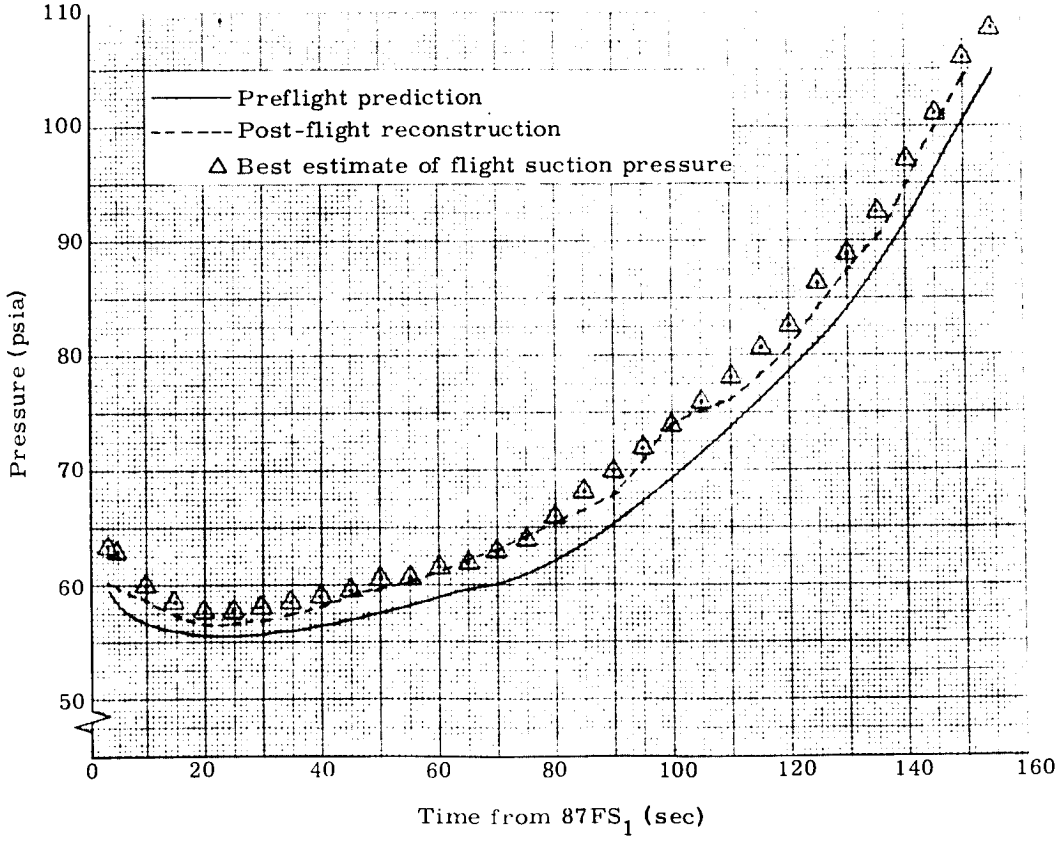


Fig. III-22. Stage I Oxidizer Suction Pressure (Meas 0017)

[redacted]

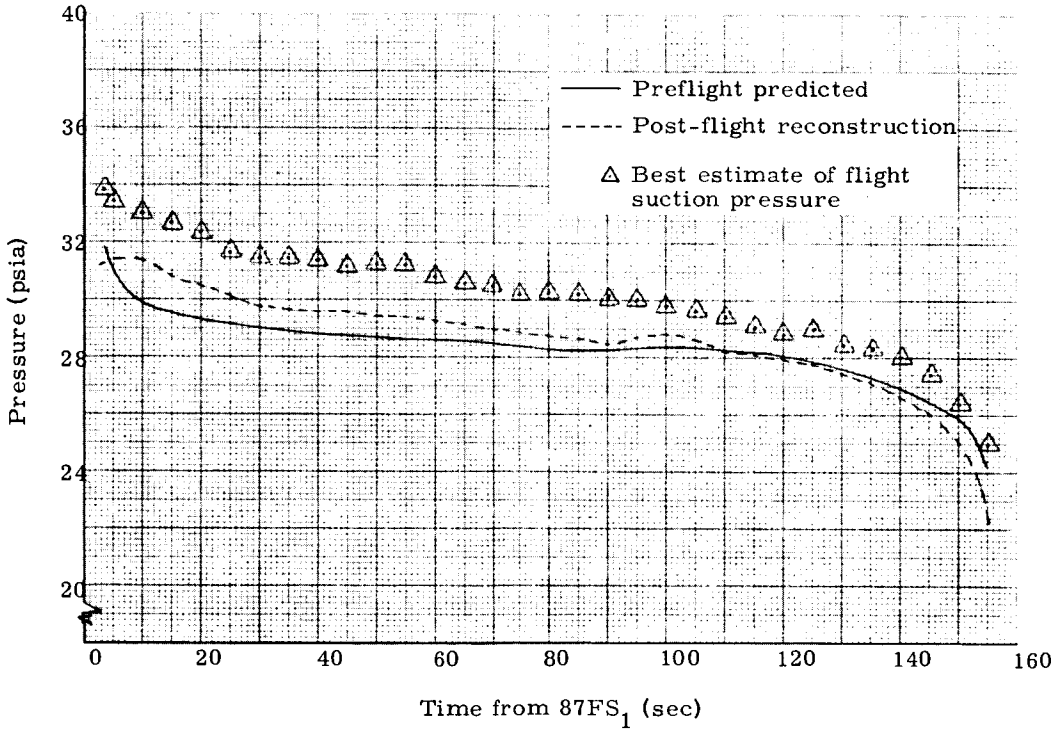


Fig. III-23. Stage I Fuel Suction Pressure (Meas 0014)

~~CONFIDENTIAL~~

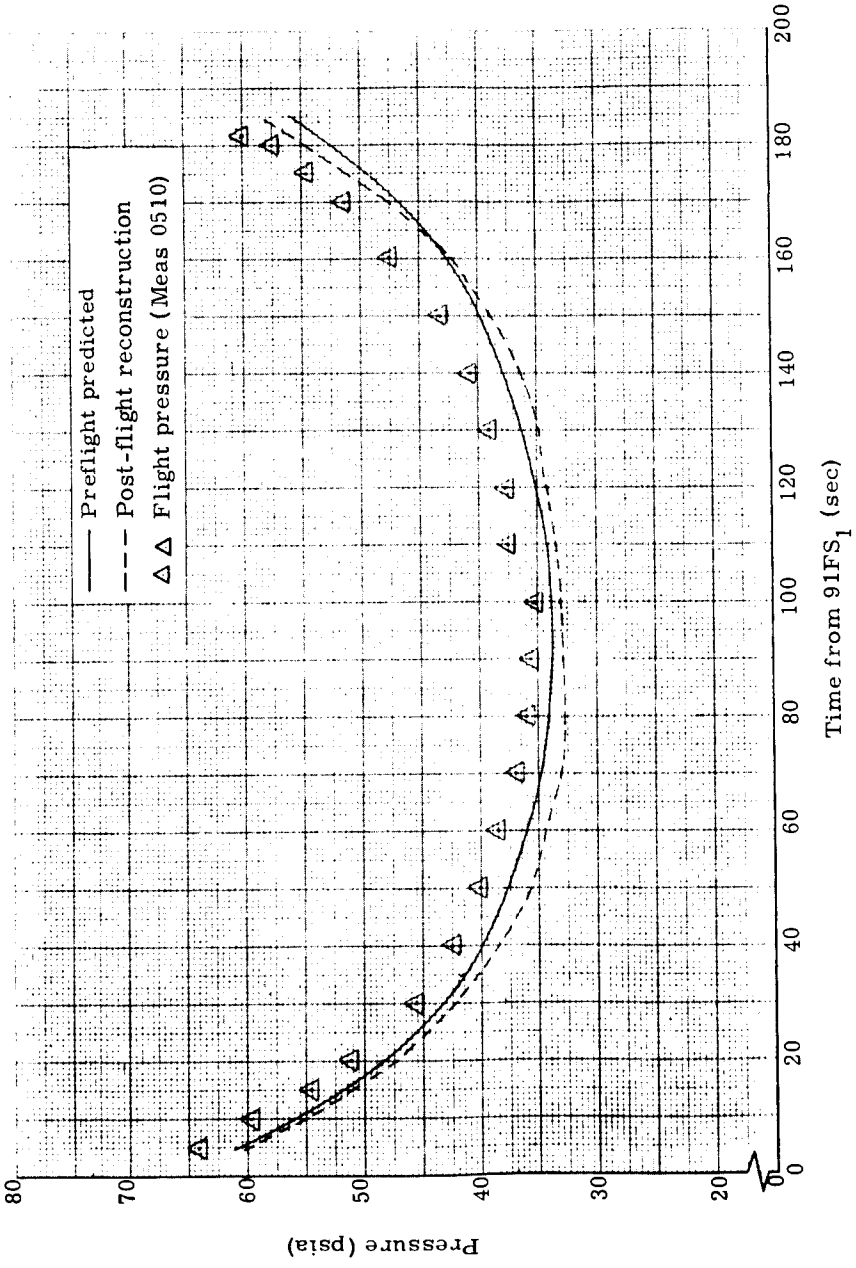


Fig. III-24. Stage II Oxidizer Suction Pressure (Meas 0510)

~~CONFIDENTIAL~~

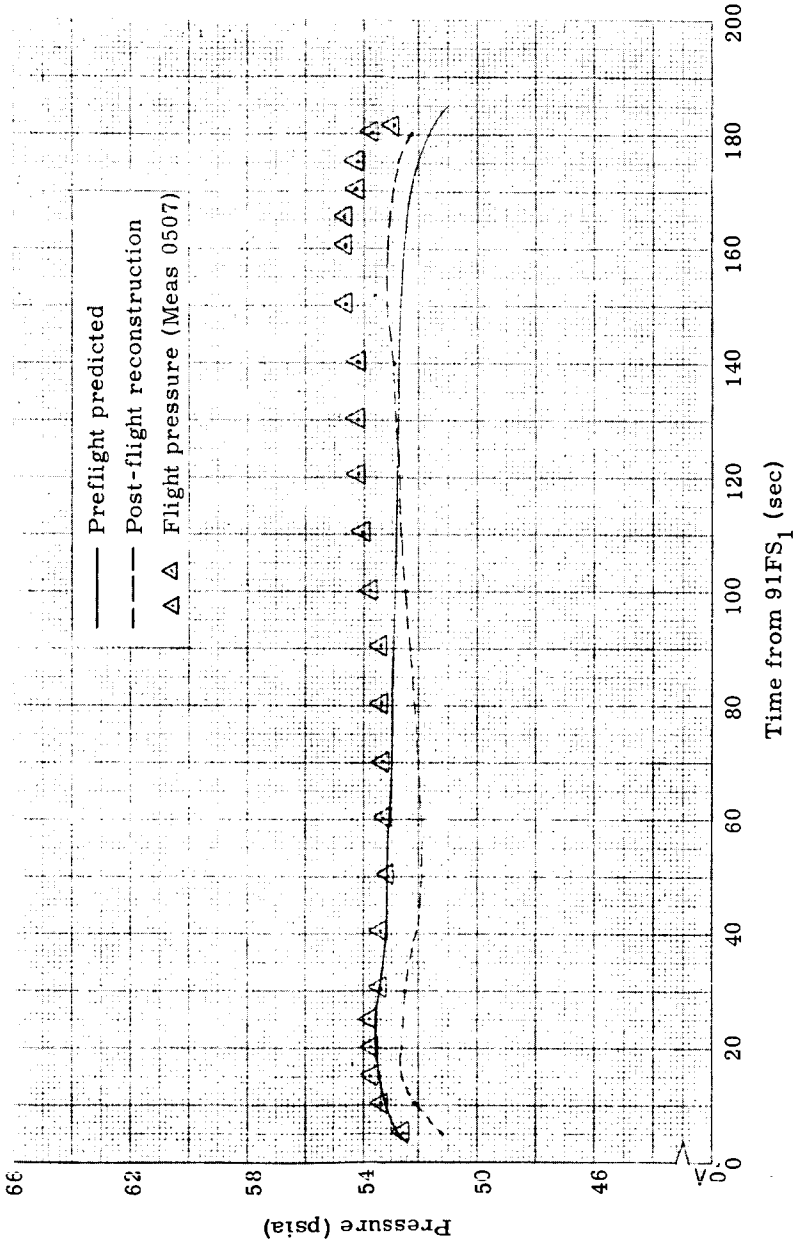


Fig. III-25. Stage II Fuel Suction Pressure (Meas 0507)

CONFIDENTIAL

TABLE III-17

Minimum NPSH Supplied

| System | Minimum NPSH Supplied During Start Transient (psia) | Starting NPSH Required (psia)* | Limited Operation NPSH Required (psia)** | Minimum Steady State NPSH Supplied (psia) | Unlimited Operation NPSH Required (psia)* |
|---|---|---|---|---|---|
| Stage I oxidizer | 26.8 | 38.4 | 28.2 for 135 sec | 55.4 | 46.1 |
| Stage I fuel | 28.9 | 17.1 | 17.1 for 120 sec | 31.2 | 23.1 |
| Stage II oxidizer | *** | 38.4 | 19.2 for 120 sec | 28.2 | 22.4 |
| Stage II fuel | *** | 39.8 | 39.8 for 120 sec | 46.4 | 43.4 |

*Oxidizer values represent NPSH required at $FS_1$, fuel values at engine start.

**Time given in table represents maximum cumulative operating time from engine acceptance, at the given NPSH levels.

***Not available due to telemetry blackout.

CONFIDENTIAL

4. Propellant Utilization

a. Level sensor operation

Figures III-26 and III-27 show the predicted, actual and reconstructed level sensor uncover times for Stages I and II. Measured level sensor uncovering times appear in Table III-18. The relationship of the predicted to the actual times of sensor uncover reflects the higher-than-predicted flow rates seen on Stages I and II.

Reconstructed level sensor uncover times show closer agreement to the actuals and reflect a reconstruction using actual engine nominal values of thrust and flow rate.

Slosh (indicated by on and off signals near the uncovering of two Stage II oxidizer sensors, one Stage II fuel sensor, and one Stage I oxidizer high level sensor) was less than that noted on GT-1, GT-2 and on many Titan II flights. The longest duration of slosh was 0.85 second as indicated by the Stage II fuel high level sensor. To obtain uncover times with slosh present, the time halfway from first uncover to last uncover was chosen as best representing the actual uncover time. All recover indications on the unshielded fuel sensors occurred long enough from uncover so as not to prevent proper interpretation of the data.

b. Best estimate level sensor uncover times

Table III-19 contains the best estimate of average level sensor uncover times for the GT-3 flight. The adjustments to the measured average uncover times of Table III-18 were as follows:

(1) All times decreased by 0.06 second to allow for the built-in level sensor delay of 0.033 second and the telemetry sampling tolerance of 0.05 second.

(2) Stage II fuel tank high level sensor uncover times were decreased by 0.213 second to allow for the apparent delay in uncover time, probably due to unsymmetrical surface waves occurring at the tank walls during slosh. Similar delays were evident on GT-1, GT-2 and on all Titan II flights. The magnitude of the time adjustment was much less on GT-3 because of two factors:

(a) Duration of slosh on GT-3 was much less than that experienced on previous flights.

(b) Reanalysis of propellant tank stretch has shown that the stretch below the level sensor is approximately 0.5 $ft^3$ less than previously calculated.

[redacted]

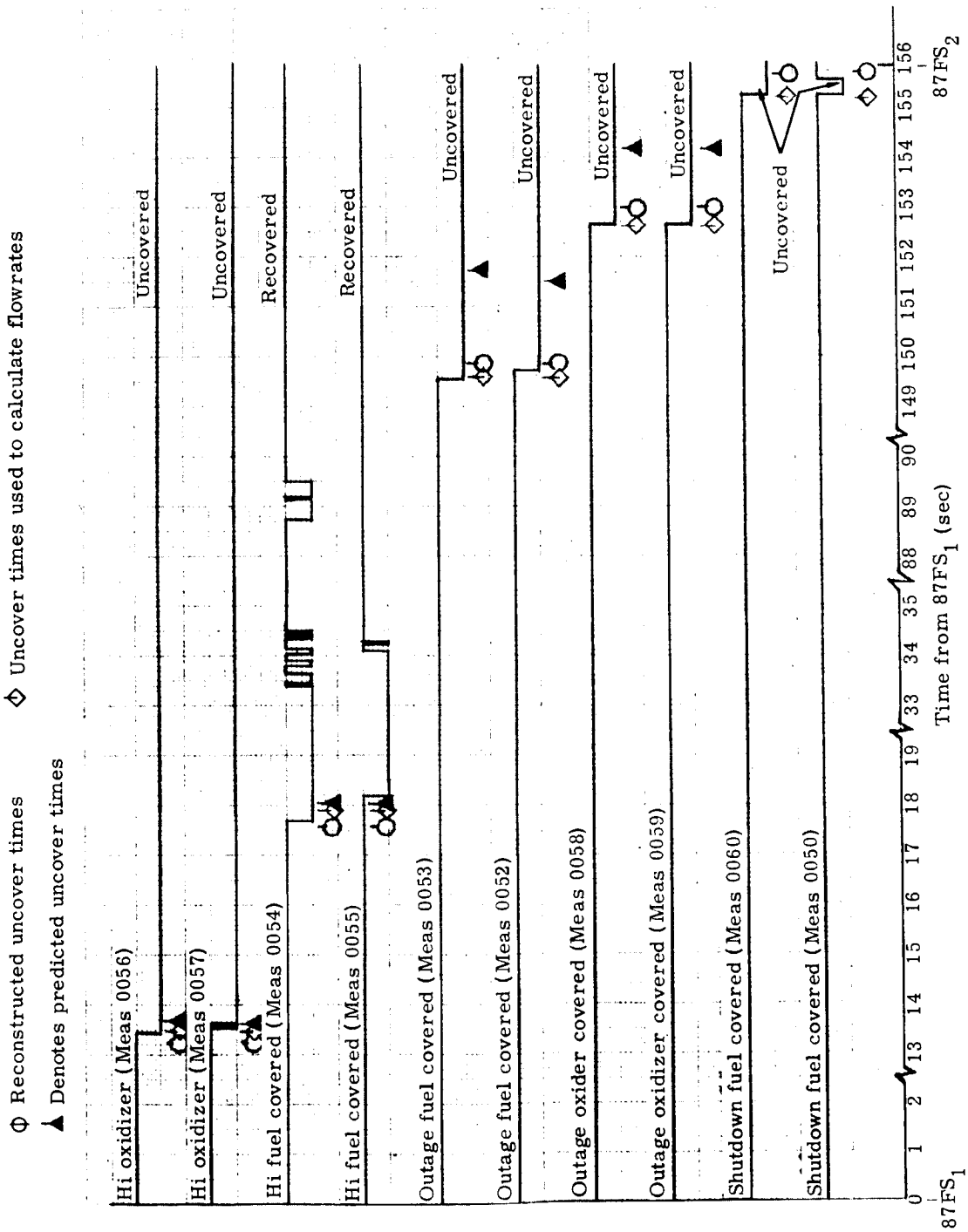


Fig. III-26. Stage I Level Sensor Operation

[redacted]

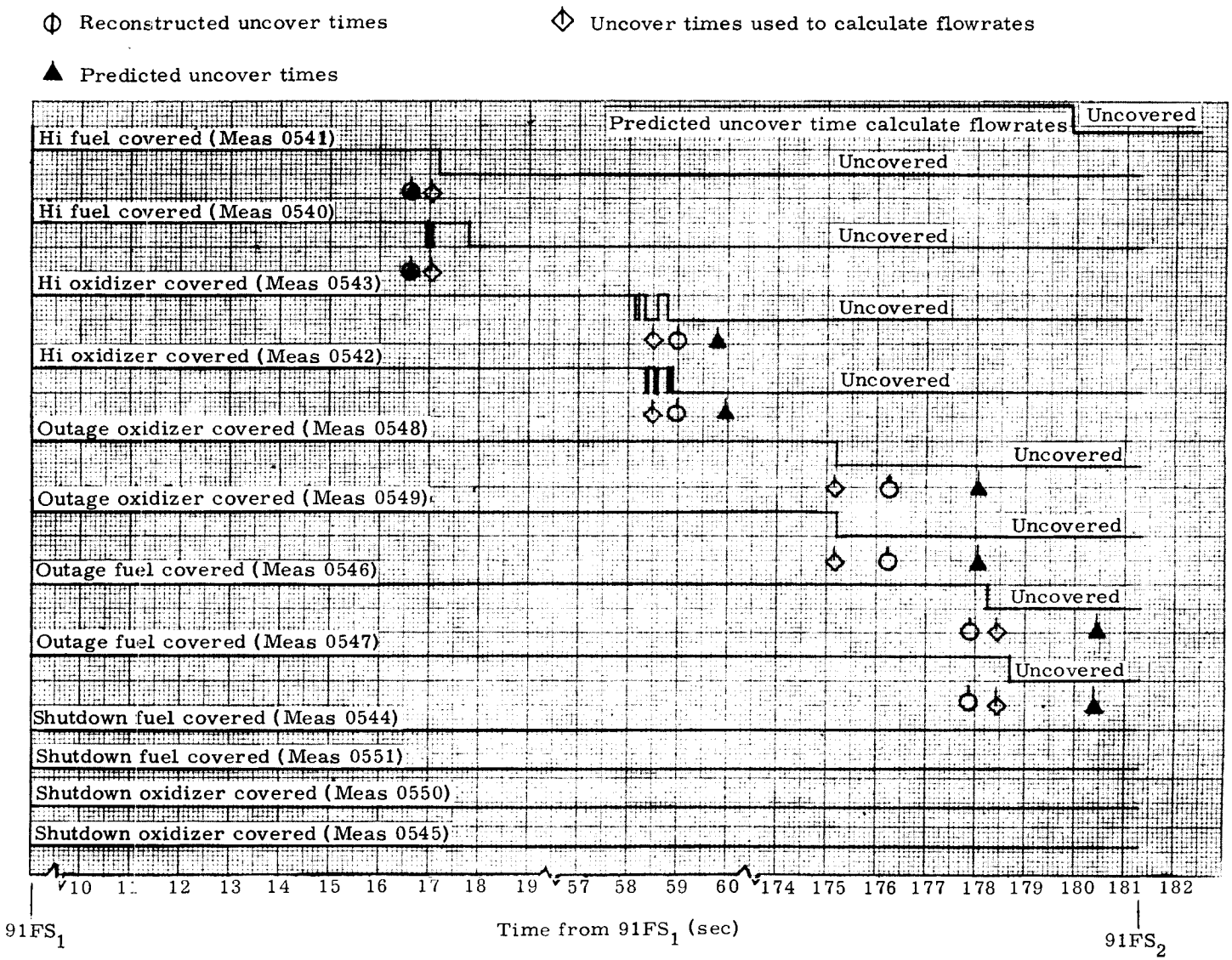


Fig. III-27. Stage II Level Sensor Operation

[redacted]

TABLE III-18

Measured Level Sensor Uncover Times

| Meas | Sensor | Uncover Time (GMT) | Average Uncover Time (GMT) | Remarks |
|---|---|---|---|---|
| 0056 | Stage I oxidizer high | 1424:10.128 | 1424:10.203 | Clean |
| 0057 | Stage I oxidizer high | 1424:10.278 | | Single slosh cycle, 0.1 sec |
| 0058 | Stage I oxidizer outage | 1426:29.330 | 1426:29.330 | Clean |
| 0059 | Stage I oxidizer outage | 1426:29.330 | | Clean |
| 0054 | Stage I fuel high | 1424:14.378 | 1424:14.628 | Clean, but re-covered after 15.7 sec |
| 0055 | Stage I fuel high | 1424:14.878 | | Clean, but re-covered after 15.9 sec |
| 0052 | Stage I fuel outage | 1426:26.420 | 1426:26.325 | Clean |
| 0053 | Stage I fuel outage | 1426:26.230 | | Clean |
| 0050 | Stage I fuel shutdown | 1426:31.920 | 1426:31.925 | Clean, but re-covered after 0.3 sec |
| 0060 | Stage I fuel shutdown | 1426:31.930 | | Clean |
| 0542 | Stage II oxidizer high | 1427:31.116 | 1427:31.041 | Three slosh cycles, 0.55 sec |
| 0543 | Stage II oxidizer high | 1427:30.966 | | Two slosh cycles, 0.65 sec |
| 0548 | Stage II oxidizer outage | 1429:27.704 | 1429:27.704 | Clean |
| 0549 | Stage II oxidizer outage | 1429:27.704 | | Clean |
| 0540 | Stage II fuel high | 1426:49.865 | 1426:49.778 | Single slosh cycle, 0.85 sec |
| 0541 | Stage II fuel high | 1426:49.690 | | Clean |
| 0546 | Stage II fuel outage | 1429:30.744 | 1429:30.969 | Clean |
| 0547 | Stage II fuel outage | 1429:31.194 | | Clean |
| 0545 | Stage II oxidizer shutdown | -- | -- | Did not uncover |
| 0550 | Stage II oxidizer shutdown | -- | -- | Did not uncover |
| 0544 | Stage II fuel shutdown | -- | -- | Did not uncover |
| 0551 | Stage II fuel shutdown | -- | -- | Did not uncover |

[redacted]

TABLE III-19

Best Estimate Average Level Sensor Uncover Time

| Quadrant | Meas | Tank Sensor | Average Uncover Time (GMT) | Δt (sec) | Remarks |
|---|---|---|---|---|---|
| I<br>III | 0056<br>0057 | Stage I oxidizer hi-level<br>Stage I oxidizer hi-level | 1424:10.145 | 139.127 | |
| I/IV<br>II/III | 0058<br>0059 | Stage I oxidizer outage<br>Stage I oxidizer outage | 1426:29.272 | | |
| I<br>III | 0054<br>0055 | Stage I fuel hi-level<br>Stage I fuel hi-level | 1424:14.570 | 131.697 | |
| III<br>I | 0052<br>0053 | Stage I fuel outage<br>Stage I fuel outage | 1426:26.267 | | |
| -- | -- | Stage I oxidizer shutdown | | -- | |
| I<br>III | 0050<br>0060 | Stage I fuel shutdown<br>Stage I fuel shutdown | 1426:31.867 | | |
| IV<br>II | 0542<br>0543 | Stage II oxidizer hi-level<br>Stage II oxidizer hi-level | 1427:30.983 | 116.663 | |
| I/IV<br>II/III | 0548<br>0549 | Stage II oxidizer outage<br>Stage II oxidizer outage | 1429:27.646 | | |
| I<br>III | 0540<br>0541 | Stage II fuel hi-level<br>Stage II fuel hi-level | 1426:49.507* | 161.404 | *Result of decreasing by an additional time of 0.213 second |
| I<br>III | 0546<br>0547 | Stage II fuel outage<br>Stage II fuel outage | 1429:30.911 | | |
| II<br>IV | 0545<br>0550 | Stage II oxidizer shutdown<br>Stage II oxidizer shutdown | -- | -- | |
| II<br>IV | 0544<br>0551 | Stage II fuel shutdown<br>Stage II fuel shutdown | -- | | |

| | Average Temperatures Between Uncoverings (°F) | Corresponding Density ($lb/ft^3$) |
|---|---|---|
| Stage I oxidizer | 44.0 | 92.076 |
| Stage I fuel | 44.1 | 57.155 |
| Stage II oxidizer | 45.2 | 91.982 |
| Stage II fuel | 41.4 | 57.241 |

[redacted]

Also shown in Table III-19 are the integrated average temperatures between level sensor uncoverings, and the corresponding liquid densities.

Table III-20 contains the level sensor volumes and incremental volumes used in the level sensor flow rate analysis.

TABLE III-20

Averaged Volumes at Level Sensor Locations

| Tank | Sensor | Averaged Volumes, Stretch Included (cu ft) | Incremental Volumes (cu ft) |
|---|---|---|---|
| Stage I oxidizer | Hi-level<br>Outage | 1711.870<br>38.33 | 1673.540 |
| Stage I fuel | Hi-level<br>Outage | 1406.345<br>67.24 | 1339.105 |
| Stage II oxidizer | Hi-level<br>Outage | 285.635<br>23.47 | 262.165 |
| Stage II fuel | Hi-level<br>Outage | 351.350<br>18.45 | 332.90 |

c. Flow rates

Table III-21 presents the predicted and actual volumetric flow rates between level sensors.

TABLE III-21

Propellant Volumetric Flow Rate

| Tank | Predicted ($ft^3$/sec) | Actual ($ft^3$/sec) |
|---|---|---|
| Stage I oxidizer | 11.916 | 12.029 |
| Stage I fuel | 10.038 | 10.168 |
| Stage II oxidizer | 2.211 | 2.247 |
| Stage II fuel | 2.032 | 2.063 |

This tabulation also reflects the higher-than-predicted flow rates of Stages I and II engines.

d. Mixture ratio

The following tabulation shows the Stages I and II predicted and actual engine mixture ratios between level sensors for GT-3. Also

[redacted]

shown are the mixture ratios predicted on F-0 day as part of the propellant temperature monitoring procedure.

| System | Predicted Mixture Ratio* | Actual Mixture Ratio | Predicted Mixture Ratio (F-0 day) |
|---|---|---|---|
| Stage I | 1.9121 | 1.9058 | 1.9136 |
| Stage II | 1.7490 | 1.7508 | 1.7515 |

*From LV-326-3.

e. Outage and trapped propellants

The statistical mean and maximum (99%) outages predicted for GT-3 for both the F-45 day preflight report (Ref. 19) and the F-0 day propellant temperature monitoring procedure are given in Table III-22. Also shown are the actual outages as calculated using the information contained in the reconstructed propellant inventories (Tables III-26 and III-27 presented later in this chapter).

TABLE III-22

Mean and Maximum Outages

| | Predicted (F-45 day) | | Predicted (F-0 day) | | |
|---|---|---|---|---|---|
| | Mean | Maximum (99%) | Mean | Maximum (99%) | Actual |
| Stage I | 0.159%<br>408 lb | 0.465%<br>1197 lb | 0.155%<br>400 lb | 0.467%<br>1201 lb | 0%<br>0 lb |
| Stage II | 0.325%<br>194 lb | 0.973%<br>580 lb | 0.319%<br>190 lb | 0.986%<br>588 lb | 0.357% fuel<br>213 lb |

All outages are presented in pounds and as a percent of total steady state propellants. The value used for total steady-state propellants for Stage I was 257,405 pounds, and for Stage II was 59,610 pounds.

The predicted and actual trapped propellants for Stages I and II are shown in Table III-23.

TABLE III-23

Trapped Propellants

| | | Oxidizer (lb) | | Fuel (lb) | |
|---|---|---|---|---|---|
| | | Predicted | Actual | Predicted | Actual |
| Stage I | Above interface | 0 | 0 | 73 | 20 |
| | Below interface | 138 | 235 | 309 | 309 |
| Stage II | Above interface | 0 | 0 | 0 | 0 |
| | Below interface | 20 | 20 | 14 | 14 |

The differences in trapped propellants are due to recent re-evaluation of trapped propellants which will be incorporated on future flights.

f. Start and holddown propellant consumptions

The predicted and actual propellant consumptions during the Stage I start and holddown transients are presented in Table III-24.

TABLE III-24

Start and Holddown Propellant Consumption

| | Oxidizer | | Fuel | |
|---|---|---|---|---|
| Stage I | Predicted (lb) | Actual (lb) | Predicted (lb) | Actual (lb) |
| Start consumption ($87FS_1$ to TCPS) | 223 | 204 | 43 | 40 |
| Holddown (TCPS to liftoff) | 2149 | 2168 | 1127 | 1127 |

The predicted start consumptions listed in Table III-24 were selected from AGC Report 521-3.15-Q-10 (Ref. 20) after modification to allow for the difference between propellant out of the tanks (as listed in Ref. 20) and propellant overboard. The actual values were selected from the later AGC Report 521-3.15-Q-15 (Ref. 21). The predicted holddown consumption was derived from the engine analytical model and previous flight test data, while the actual was derived from the PRESTO engine performance reconstruction program.

For Stage II, the predicted and actual propellant consumptions for the time from $91FS_1$ to $91FS_1$ + 1.2 seconds are listed below.

| | Oxidizer | | Fuel | |
|---|---|---|---|---|
| | Predicted (lb) | Actual (lb) | Predicted (lb) | Actual (lb) |
| Start consumption ($91FS_1$ to $91FS_1$ + 1.2 sec) | 168 | 131 | 72 | 51 |

The predicted consumptions were obtained from Ref. 20 and modified as on the Stage I start consumption. Analysis of the GLV-3 flight data, however, revealed that the Stage II engine would have had to consume propellants at the steady-state flow rate during the start transient to equal the predicted values. Evaluation of a later AGC report (Ref. 21) indicated that the original start consumption prediction was in error. The actual value was therefore selected from the latter AGC report.

This difference was also reported for GLV-2 but was discovered too late to change the GLV-3 loading. It has been changed for GLV-4 and up.

g. Vapor retained

The predicted and actual values of vapor retained in the tanks as a result of pressurization gases and vaporization during flight are shown in Table III-25.

TABLE III-25

Pressurization Gas Inventory

| | Oxidizer | | Fuel | |
|---|---|---|---|---|
| | Predicted (lb) | Actual (lb) | Predicted (lb) | Actual (lb) |
| Stage I | | | | |
| Vapor retained: | | | | |
| Oxidizer tank | 331 | 326 | | |
| Fuel tank | 8 | 8 | 98 | 103 |
| Vaporized | 6 | 6 | 0 | 0 |
| Stage II | | | | |
| Vapor retained: | | | | |
| Pressurization (fuel tank) | 4 | 4 | 50 | 53 |
| Vaporization (oxidizer tank) | 20 | 20 | -- | -- |

The actual values were taken from the reconstructed flight pressure profile of the pressurization computer program runs.

h. Shutdown

The Stage I shutdown was due to an oxidizer exhaustion. However, the remaining fuel was consumed during the shutdown phase to yield zero outage. This resulted in essentially a simultaneous propellant exhaustion shutdown. The predicted and actual values for the propellants consumed during shutdown are shown in the tabulation which follows. The actual values were obtained by integrating a curve (derived from PRESTO) of flight flow rate versus time after $87FS_2$.

The Stage II shutdown was initiated by a guidance command. Therefore, the propellants were not exhausted as in Stage I. The predicted and actual values for the propellants consumed during shutdown are shown below. The actual values were computed from actual data in the same manner as Stage I.

| | Propellant Shutdown Consumption | | | |
|---|---|---|---|---|
| | Oxidizer | | Fuel | |
| | Predicted (lb) | Actual (lb) | Predicted (lb) | Actual (lb) |
| Stage I | 110 | 0 | 66 | 44 |
| Stage II | 86 | 87 | 69 | 70 |

i. Propellant inventory

The GT-3 reconstructed propellant inventories for Stages I and II are presented in Tables III-26 and III-27. This inventory consists of both nonusable and usable propellants. The burning time margin for Stage II was 3.719 seconds.

5. Components

a. Prevalves

All prevalve functions were performed without incident. GLV-3 was shipped from Baltimore to Cape Kennedy with dummy prevalves (solid cups welded back-to-back with appropriate prevalve flanges). Following the wet mock simulated launch test, all six dummy prevalves were replaced with new flight valves. Prevalves installed for the flight are identified in Chapter XVII.

TABLE III-26

Stage I Reconstructed Propellant Inventory

| | | | | |
|---|---|---|---|---|
| I. | Predicted average inflight engine mixture ratio: | | | 1.909 ± 1.05% |
| II. | Actual average inflight engine mixture ratio: | | | 1.9003 ± 1.71% |
| III. | Outage (% of predicted total usable propellants): | | | 0 |
| | | Oxidizer (lb) | Fuel (lb) | Total (lb) |
| IV. | Nonusable propellants | | | |
| | A. Fuel bleed | | 11 | 11 |
| | B. Start consumption ($87FS_1$ to TCPS) | 204 | 40 | 244 |
| | C. Holddown (TCPS to blow bolts) | 2,168 | 1,127 | 3,295 |
| | D. Trapped above interface at separation | 0 | 20 | 20 |
| | E. Trapped below interface at separation | 235 | 309 | 544 |
| | F. Vapor retained at shutdown | | | |
| | 1. For pressurization | | | |
| | a. Oxidizer tank | 326 | 0 | 326 |
| | b. Fuel tank | 8 | 103 | 111 |
| | 2. Vaporized | 6 | 0 | 6 |
| | G. Total nonusable propellants | 2,947 | 1,610 | 4,557 |
| V. | Usable propellants | | | |
| | A. Steady-state overboard (blow bolts to $87FS_2$) | 168,527 | 88,791 | 257,318 |
| | B. Shutdown transient ($87FS_2$ to separation) | 0 | 44 | 44 |
| | C. Outage | 0 | 0 | 0 |
| | D. Total usable | 168,527 | 88,835 | 257,362 |
| VI. | Total propellant loaded | 171,474 | 90,445 | 261,919 |
| VII. | Propellant load at LO | 168,893 | 89,132 | 258,025 |
| VIII. | Weight of initial pressurizing gas | | | |
| | A. Fuel tank ($N_2$) | | | 8 |
| | B. Oxidizer tank | | | |
| | 1. $N_2$ | | | 11 |
| | 2. $NO_2$ | | | 9 |

CONFIDENTIAL

TABLE III-27

Stage II Reconstructed Propellant Inventory

| | |
|---|---|
| I. Predicted average inflight engine mixture ratio: | 1.748 ± 2.38% |
| II. Actual average inflight engine mixture ratio: | 1.754 ± 1.55% |
| III. Outage (% of predicted total usable propellants): | 0.354 (fuel) |
| IV. Burning time margin (time to command shutdown) (sec): | 3.719 |

| | Oxidizer (lb) | Fuel (lb) | Total (lb) |
|---|---|---|---|
| V. Nonusable propellants | | | |
| A. Fuel bleed | | 11 | 11 |
| B. Trapped above interface at $91FS_2$ + 20 sec (0% thrust) | 0 | 0 | 0 |
| C. Trapped below interface at $91FS_2$ + 20 sec (0% thrust) | 20 | 14 | 34 |
| D. Vapor retained at shutdown | | | |
| 1. For pressurization (fuel tank) | 4 | 53 | 57 |
| 2. Vaporized (oxidizer tank) | 20 | -- | 20 |
| E. Total nonusable propellants | 44 | 78 | 122 |
| VI. Usable propellants | | | |
| A. Start consumption ($91FS_1$ to $91FS_1$ + 1.2 sec) | 131 | 51 | 182 |
| B. Steady-state overboard ($91FS_1$ + 1.2 sec to $91FS_2$) | 37,175 | 21,147 | 58,322 |
| C. Shutdown consumption ($91FS_2$ to 0% thrust) | 87 | 70 | 157 |
| D. Steady-state residuals (after $91FS_2$) | | | |
| 1. Burning time margin | 788 | 432 | 1,220 |
| 2. Outage | -- | 213 | 213 |
| E. Total usable propellants | 38,181 | 21,913 | 60,094 |
| VII. Total propellants loaded | 38,225 | 21,991 | 60,216 |
| VIII. Weight of initial pressurizing gas | | | |
| A. Fuel tank ($N_2$) | | | 4 |
| B. Oxidizer tank | | | |
| 1. $N_2$ | | | 21 |
| 2. $NO_2$ | | | 10 |

CONFIDENTIAL

In the process of replacing one Stage I oxidizer dummy prevalve with the flight prevalve, contamination was detected in the dummy prevalve. The tank was flushed one time, no further contamination was found, and the flight prevalve was installed.

b. Level sensors

GLV-3 was flown with 22 Bendix optical-type propellant level sensors of the Martin 424-7491004-009 configuration. These sensors included a modification which incorporated a chip seal, a device designed to prevent chips from the glass seal of the sensor from contaminating the propellants should the glass seal produce chips. Identification and other configuration and installation data of all the level sensors used on this flight are shown in Table III-28.

All propellant level sensors functioned satisfactorily in providing data used to determine propellant flow rates. Three of the fuel level sensors exhibited extraneous covered signals after normal uncovering. The two Stage I high level fuel sensors (Meas 0054 and 0055) signaled normal uncovering as the propellant level completely passed the sensor locations: however, approximately 16 seconds later, each of these sensors returned to the covered signal condition accompanied by one or more cycles of covered-uncovered signals. Each one finally ended up with a covered signal which remained until the end of Stage I flight. The Stage I shutdown level fuel sensor (Meas 0050) signaled normal uncovering but returned to and remained in a covered signal condition approximately 0.3 second later.

The reappearance of covered signals on fuel level sensors after normal uncovering was reported on previous Titan II flights and on the GT-1 and GT-2 flights, and has been attributed to contamination of the sensor optical prism by autogenous gas products. Shields (not available for the GT-3 flight), designed to prevent this contamination, were successfully demonstrated on GLV-2. During the GT-2 flight, 6 of the 12 fuel sensors were shielded, and none of the shielded sensors generated covered signals after the propellant level completely passed the sensor. By contrast, three of the unshielded fuel sensors returned falsely to the covered signal condition.

c. Ball valves

Performance of the AGE ball valves was completely satisfactory during the launch efforts for GT-3.

d. Oxidizer suction line standpipes

The standpipes were charged with nitrogen gas at approximately T-125 minutes. No problems were encountered during the charging procedure. The configuration of the GLV-3 standpipe was unchanged from that flown on GLV-1 and GLV-2. Standpipe pressure data were normal.

~~CONFIDENTIAL~~

TABLE III-28

Propellant Level Sensor Serial Numbers and Locations

| Stage I | | | | |
|---|---|---|---|---|
| Function | Meas | Location (quadrant) | Volume (cu ft)* | Serial No. |
| Oxidizer tank | | | | |
| High level | 0057<br>0056 | III<br>I | 1712.42<br>1711.32 | 000360<br>000264 |
| Outage | 0059<br>0058 | II/III<br>I/IV | 38.38<br>38.28 | 000315<br>000432 |
| Shutdown | --<br>-- | --<br>-- | --<br>-- | --<br>-- |
| Fuel tank | | | | |
| High level | 0054<br>0055 | I<br>III | 1406.25<br>1406.44 | 000340<br>000405 |
| Outage | 0052<br>0053 | III<br>I | 67.13<br>67.35 | 000396<br>000411 |
| Shutdown | 0060<br>0050 | III<br>I | 8.19<br>8.29 | 000320<br>000371 |
| | Stage II | | | |
| Function | Meas | Location (quadrant) | Volume (cu ft)* | Serial No. |
| Oxidizer tank | | | | |
| High level | 0543<br>0542 | II<br>IV | 285.80<br>285.47 | 000424<br>000408 |
| Outage | 0549<br>0548 | II/III<br>I/IV | 23.42<br>23.52 | 000362<br>000385 |
| Shutdown | 0545<br>0550 | II<br>IV | 5.41<br>5.37 | 000364<br>000397 |
| Fuel tank | | | | |
| High level | 0541<br>0540 | III<br>I | 351.37<br>351.33 | 000376<br>000363 |
| Outage | 0547<br>0546 | III<br>I | 18.63<br>18.27 | 000333<br>000319 |
| Shutdown | 0544<br>0551 | II<br>IV | 1.99<br>2.13 | 000380<br>000394 |

*Volume to interface including tank stretch at uncover time.

~~CONFIDENTIAL~~

e. Fuel suction line accumulators

The fuel accumulator assemblies used on GLV-3 incorporated a number of modifications as a result of the piston displacement instrumentation problems encountered on the GT-2 flight. The changes were as follows:

(1) Spectral Electronics potentiometer incorporated heavier gage wire in the critical area between coil and case, complete potting of the volume around the heavier wires, and a greater wiper force.

(2) Heavier bracket at the end of the piston shaft.

(3) Addition of a heat shield completely surrounding the extended piston and potentiometer assembly.

(4) Use of an electrical connector mounted on the heat shield to pick up the potentiometer leads and shorten their unsupported length.

The response of piston displacement Meas 0035 and 0036 was excellent throughout the flight; this excellent performance is attributed to the aforementioned modifications.

Figure III-28 is a plot of indicated accumulator piston displacement during Stage I flight. Figure III-29 presents high speed traces at various times of interest during flight.

Piston displacement data can be matched to the estimated flight pressure at the accumulator piston shown in Fig. III-28 (dashed curve). The general amplitude of S/A 1 was much greater than that of S/A 2 as indicated by the high speed traces in Fig. III-29. Using accumulator measurements only would indicate that the high S/A 1 amplitudes were caused by the 6-cps motion superimposed on the predominantly 22-cps motion (the measured piston frequencies, 6 and 22 cps, are the resonant frequencies of the fuel system).

Dynamic friction levels for dry accumulators were measured prior to installation of the accumulator assemblies, and again prior to flight. A summary of these friction measurements follows. Friction levels are measured as peak-to-peak values (twice the equivalent friction force in one direction).

[redacted]

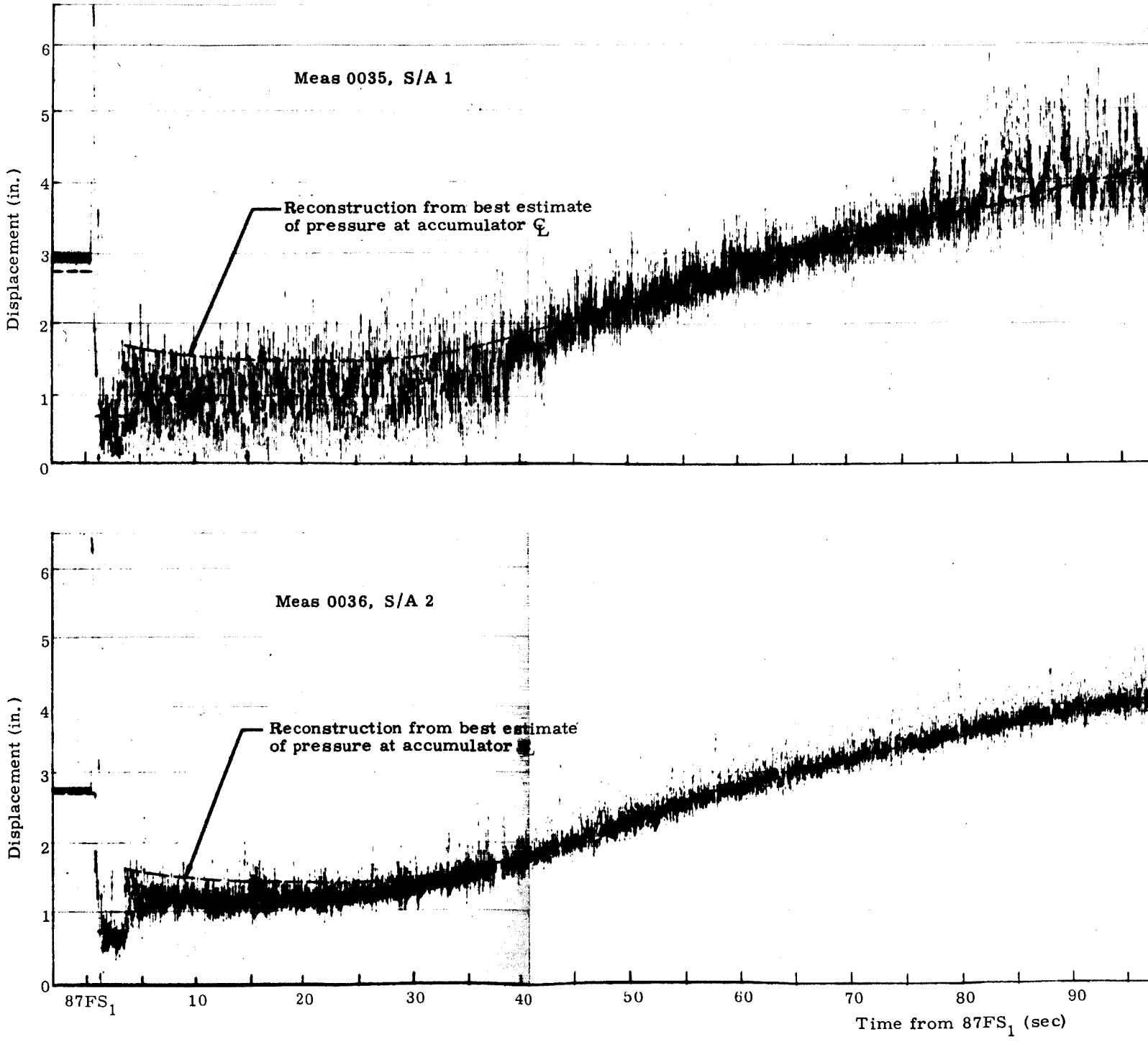


[redacted]

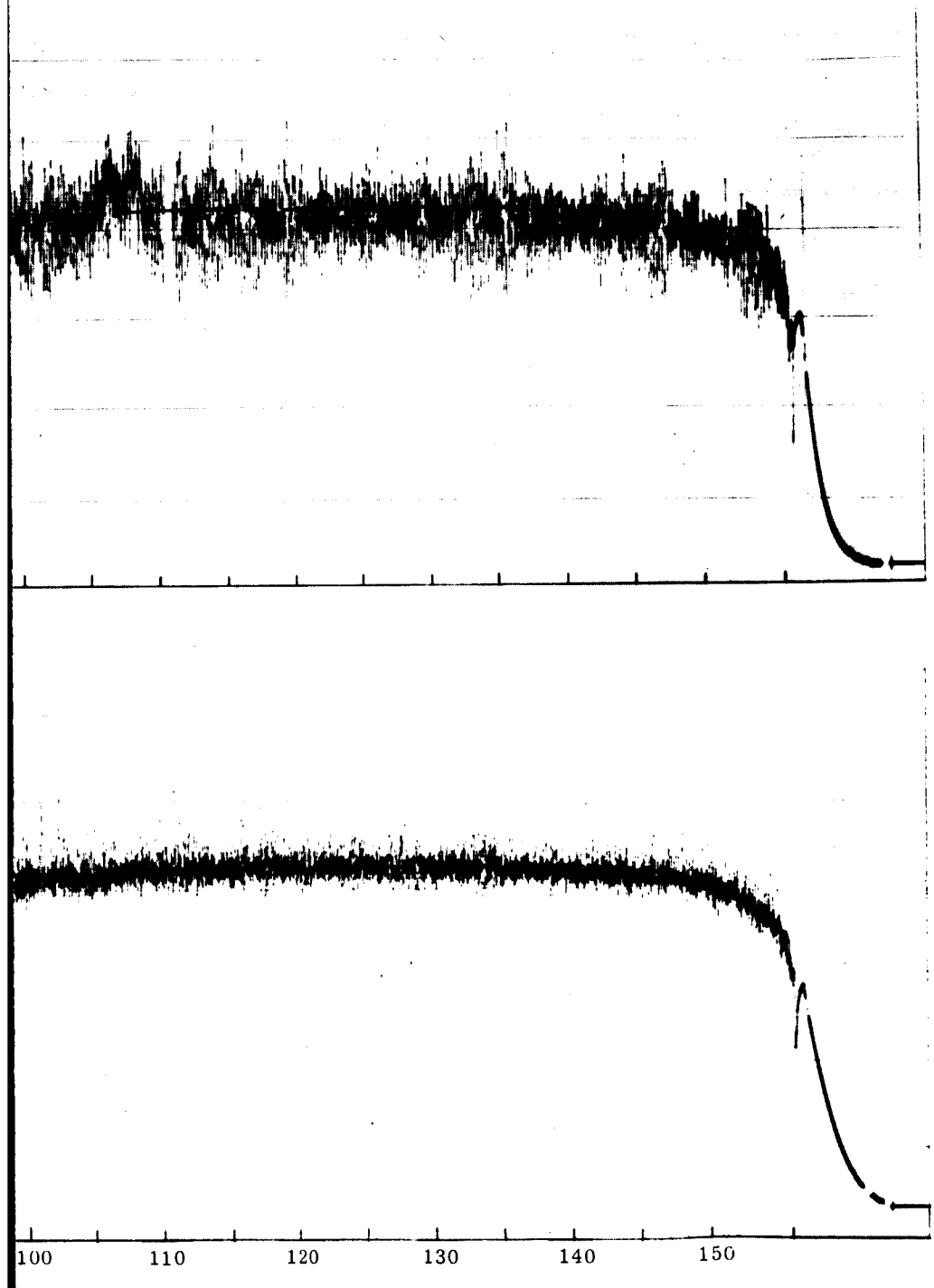


Fig. III-28. GT-3 Fuel Accumulator Piston Travel

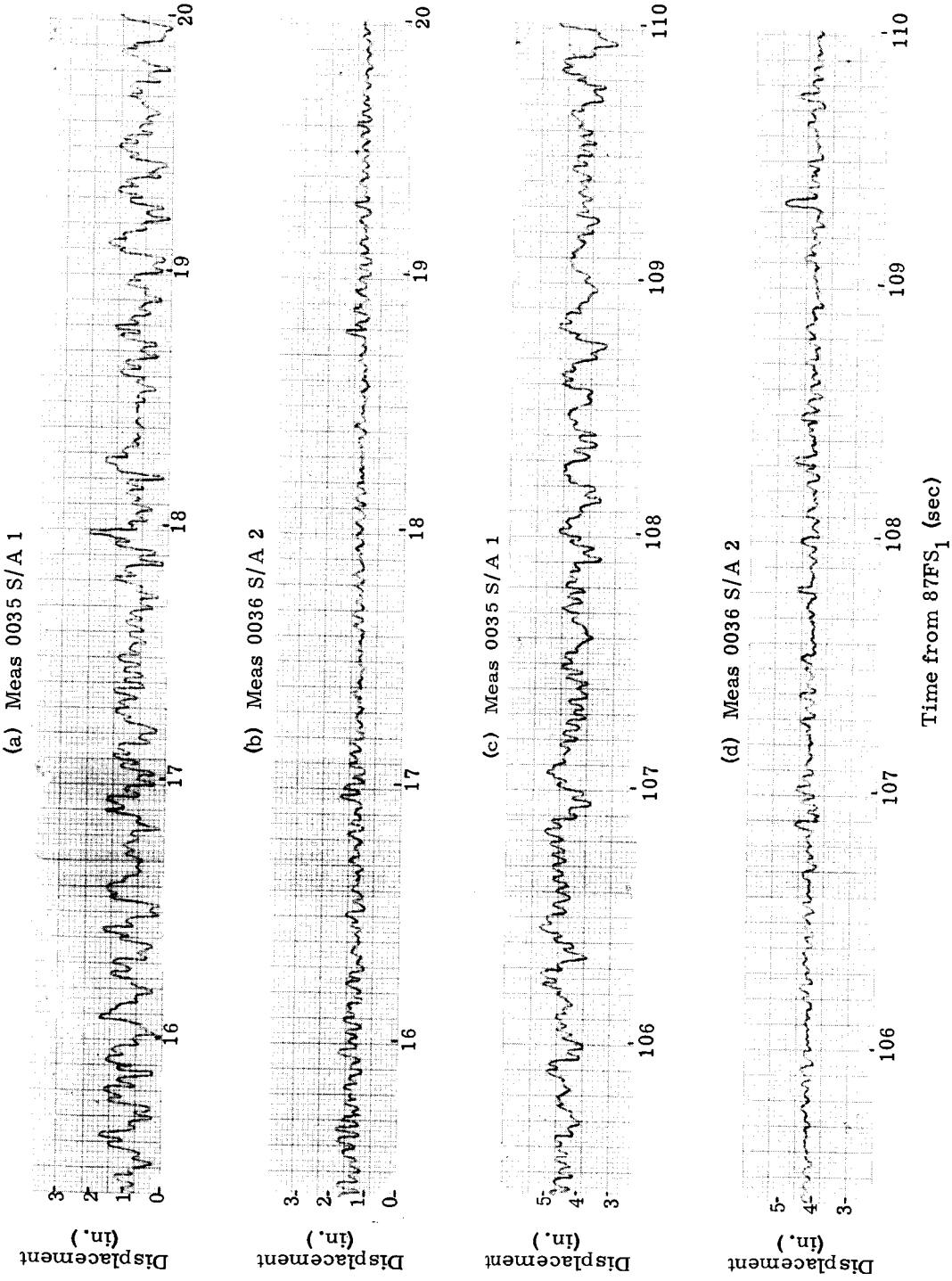


Fig. III-29. Fuel Accumulator Displacement Dynamic Measurements

~~CONFIDENTIAL~~

| Engine Subassembly | Peak-to-Peak Friction (psi) | |
|---|---|---|
| | Bench | Preflight |
| 1 | 1.6 | 1.4 |
| 2 | 1.3 | 1.2 |

Observed flight data do not indicate significant differences in friction levels between accumulators.

f. POGO performance

A detailed description of the Stage I longitudinal vibrations which occurred on GT-3 appears in Chapter XII. Both steady-state and dynamic levels of pertinent propulsion system parameters (including pump suction, pump discharge, and thrust chamber pressures) are presented.

Propulsion measurements other than standpipe pressures did not exhibit significant POGO structural frequency responses (10 to 18 cps). Pressure amplitudes were somewhat lower than GT-2 data, particularly in the standpipes, a good indication of low POGO activity. Table III-29 presents pressure amplitudes at various flight times. By comparison, at the maximum POGO time, GT-2 zero-to-peak pressure amplitudes for Meas 0033 and 0034 were 22 and 20 psi, respectively.

TABLE III-29

Propulsion POGO Parameters

| Time from $87FS_1$ (sec) | Oxidizer Standpipe Maximum Pressure Amplitude (zero-to-peak)* (psi) | | Fuel Accumulator Maximum Pressure Amplitude (zero-to-peak)* (psi) | |
|---|---|---|---|---|
| | S/A 1 Meas 0033 | S/A 2 Meas 0034 | S/A 1 Meas 0037 | S/A 2 Meas 0038 |
| 100 | 2 | 2 | 9 | 6 |
| 120 | 3 | 3 | 7 | 4 |
| 140 | 5 | 4 | 8 | 5 |
| 145** | 8 | 7 | 9 | 5 |
| 150 | 8 | 4 | 8 | 5 |

*Unfiltered data

**Maximum POGO

~~CONFIDENTIAL~~

Fuel and oxidizer cavitation indices are shown in Fig. III-30. These parameters have a partial correlation with POGO levels and are provided for reference only. These data are referenced to the pump inlet stations, with impeller velocities calculated on the basis of a 7-inch oxidizer impeller diameter and a 6-inch fuel impeller diameter. The results are similar to GLV-1 and GLV-2 results, as indicated in Table III-30.

TABLE III-30

Comparison of Cavitation Indices

| Flight | Burn Time (sec) | Burn Time (%) | Oxidizer Cavitation Index ($k_o$) | Fuel Cavitation Index ($k_f$) |
|---|---|---|---|---|
| GLV-1 | 157.5 | 70<br>80<br>90 | 0.101<br>0.115<br>0.132 | 0.084<br>0.085<br>0.086 |
| GLV-2 | 155.5 | 70<br>80<br>90 | 0.106<br>0.120<br>0.137 | 0.082<br>0.083<br>0.085 |
| GLV-3 | 155.8 | 70<br>80<br>90 | 0.107<br>0.120<br>0.138 | 0.080<br>0.079<br>0.079 |

## C. PRESSURIZATION SUBSYSTEM

### 1. Prelaunch Pressurization

At approximately T-185 minutes, all propellant tanks were pressurized through the AGE from blanket pressure level to flight pressure levels. The resultant time-pressure profiles (Fig. III-31) indicate that the process was normal. The tank ullage lock-up pressures from land-line measurements made at T-0 and the related normal operating pressure ranges are as follows:

| Meas | Parameter | Normal Range (psia) | Measured (psia) |
|---|---|---|---|
| 4125 | Stage I fuel tank pressure | 27.5 to 31.5 | 27.6 |
| 4129 | Stage I oxidizer tank pressure | 30.5 to 34.5 | 34.2 |
| 4602 | Stage II fuel tank pressure | 49.5 to 54.5 | 51.5 |
| 4605 | Stage II oxidizer tank pressure | 53.5 to 57.5 | 55.2 |

[redacted]

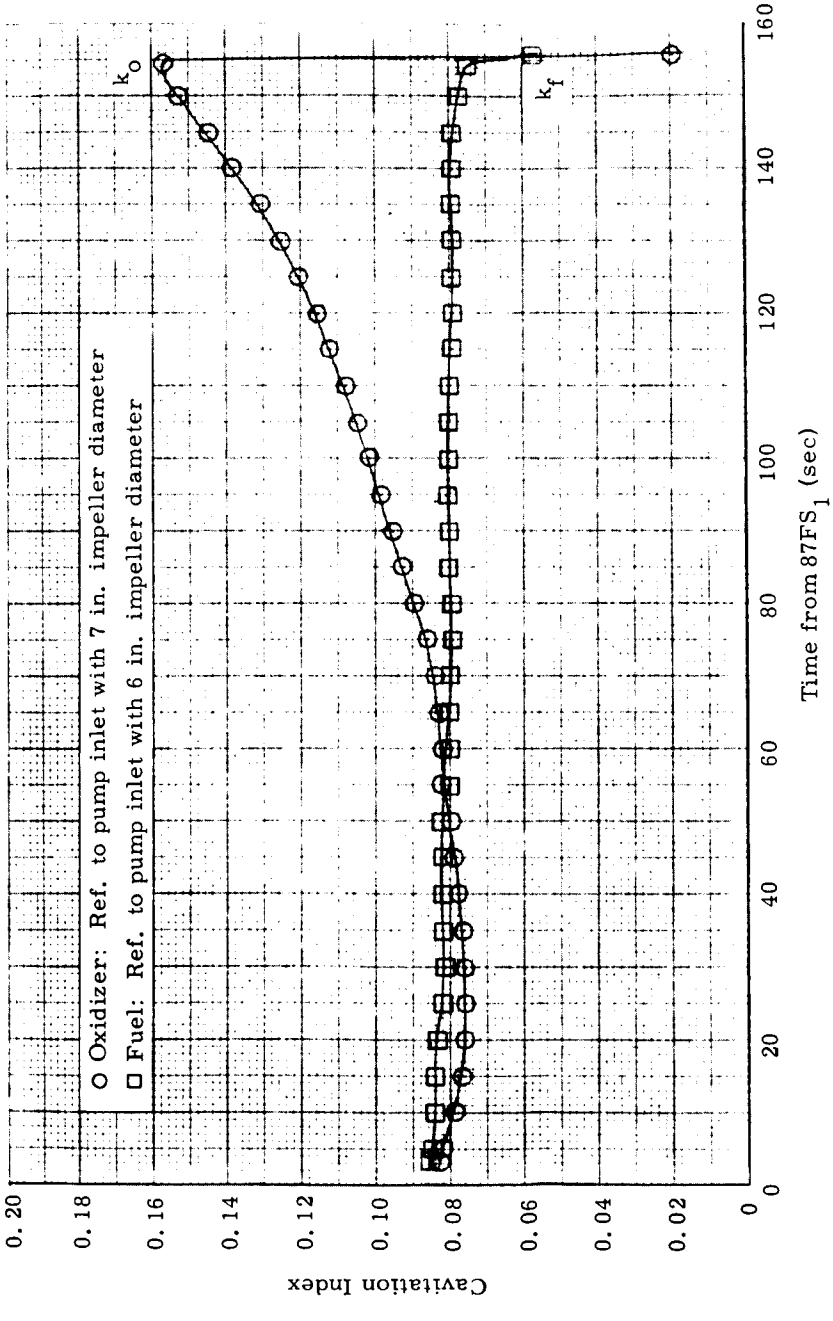


Fig. III-30. GT-3 Cavitation Indices (quasi-steady state)

[redacted]

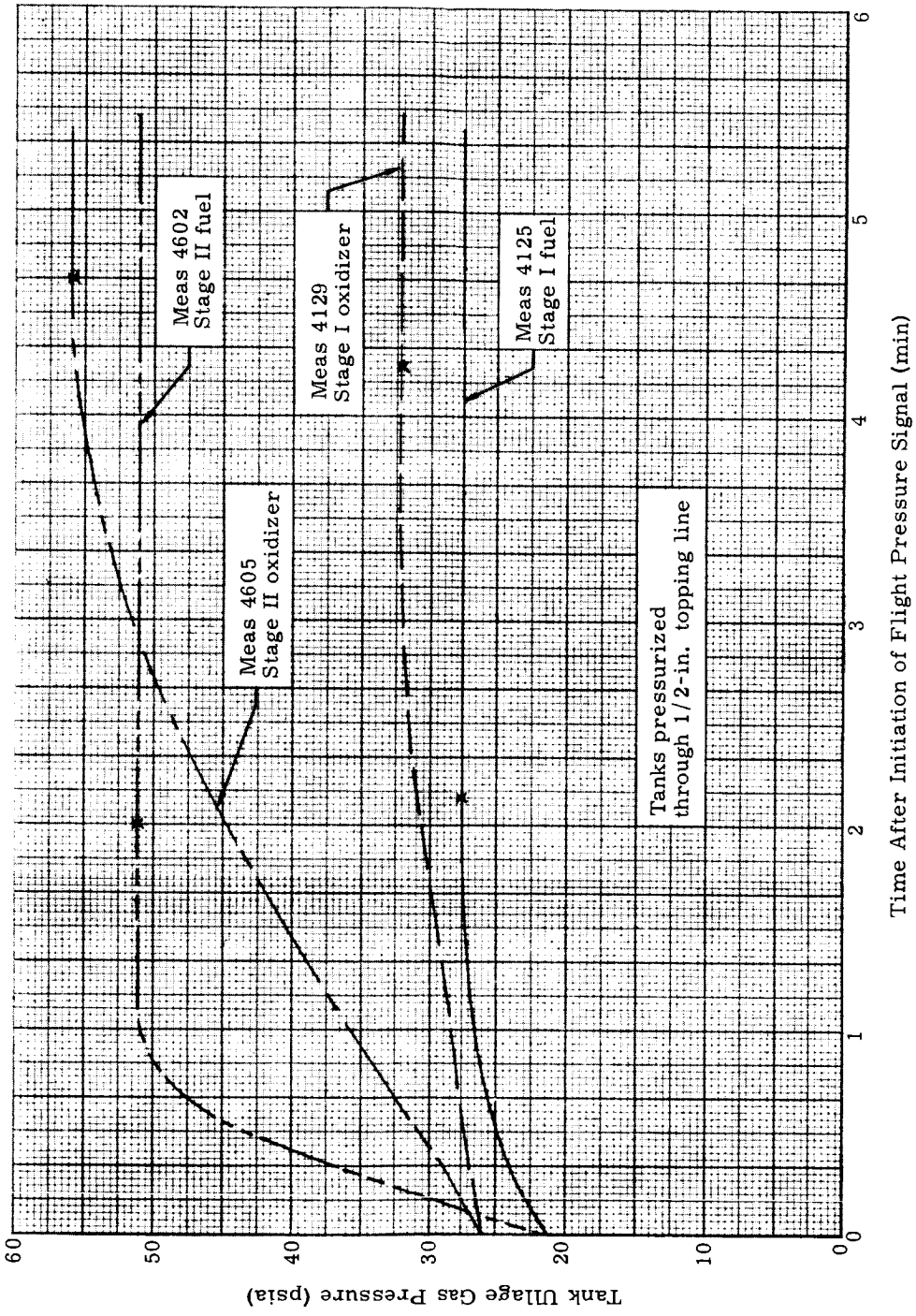


Fig. III-31. Tank Pressurization Cycle (blanket to flight pressure)

2. Flight Pressurization

Stages I and II ullage gas pressure time histories are shown in Figs. III-32 through III-35. These figures show flight-measured pressures, preflight-predicted pressures and post-flight reconstructed pressures. The flight-measured pressures shown were obtained by averaging the telemetered output from each pair of pressure transducers in the individual tanks. The preflight predicted curves are from Ref. 19. The post-flight reconstruction was based on flight-measured values of engine performance, propellant temperatures and propellant loadings. A comparison of significant pressurization system parameters taken at $FS_1$ + 100 seconds is given in Table III-32.

Figures III-36, III-37 and III-38 present the preflight-predicted and the inflight-measured pressurization parameters for the autogenous-gas pressurized tanks.

3. Component Performance

All pressurization subsystem components functioned normally. The previously troublesome Stage I oxidizer tank pressurization disconnect poppet and cap, incorporating (for the first time) a Kynar seal, did not leak. The Stage II oxidizer tank sensor pairs (A and B) exhibited none of the erratic behavior shown on the GT-2 flight. The maximum and mean pressure differences between pairs of sensors in each of the individual propellant tanks are shown in Table III-31.

TABLE III-31

Pressure Differences Between Tank Pressure Transducer Pairs

| Tank | Maximum Difference (psi) | Mean Difference (psi) | Maximum Allowable Difference (psi) |
|---|---|---|---|
| Stage I oxidizer | 0.64 | 0.15 | 1.50 |
| Stage I fuel | 0.37 | 0.11 | 1.50 |
| Stage II oxidizer | 0.87 | 0.54 | 2.25 |
| Stage II fuel | 0.73 | 0.33 | 2.25 |

D. ENVIRONMENTAL

1. GLV Air-Conditioning System

The air-conditioning system which serves launch vehicle Compartment 2 and all engine start cartridges was operative continuously during

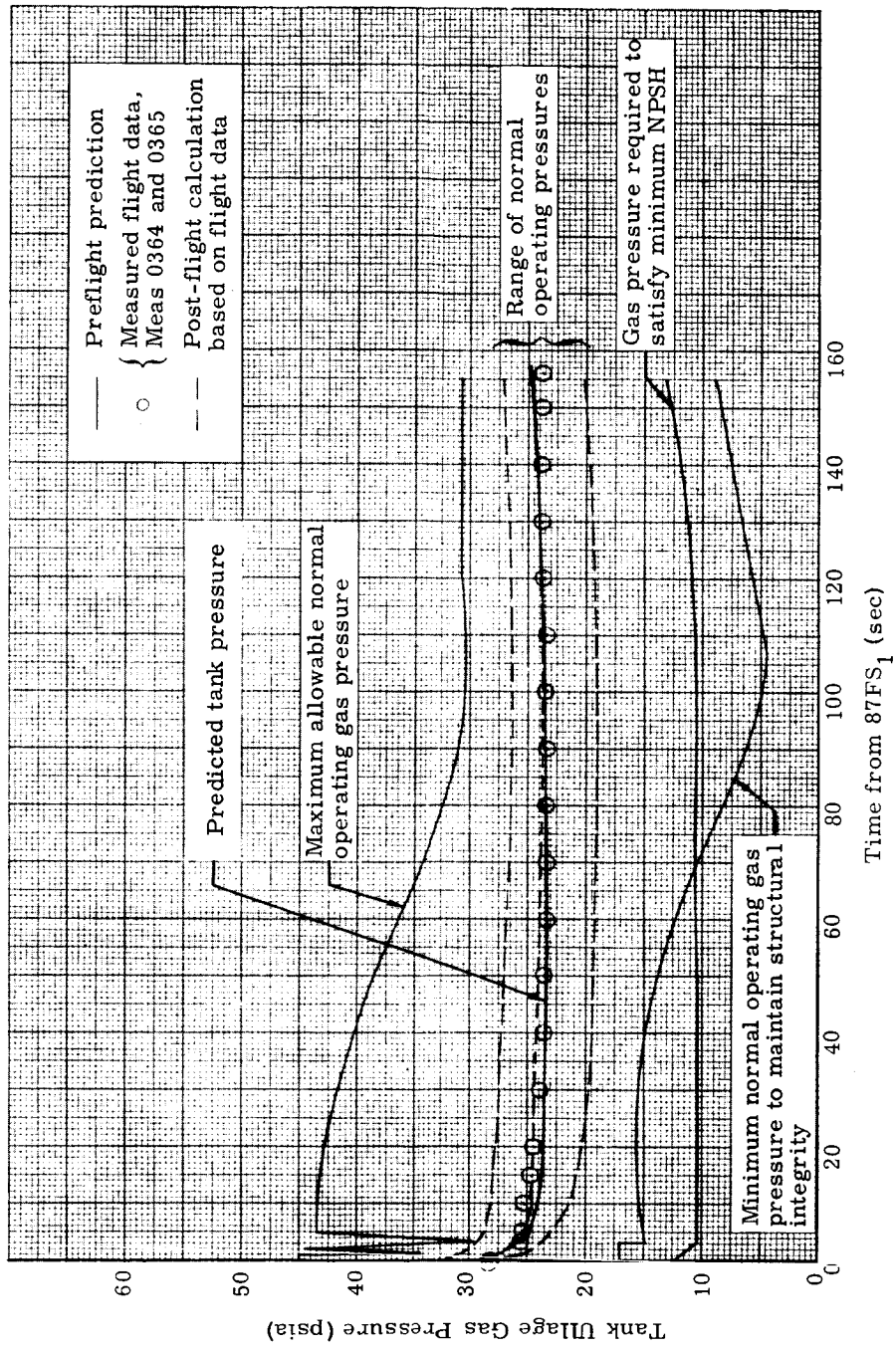


Fig. III-32. Stage I Fuel Tank Ullage Pressure History

CONFIDENTIAL

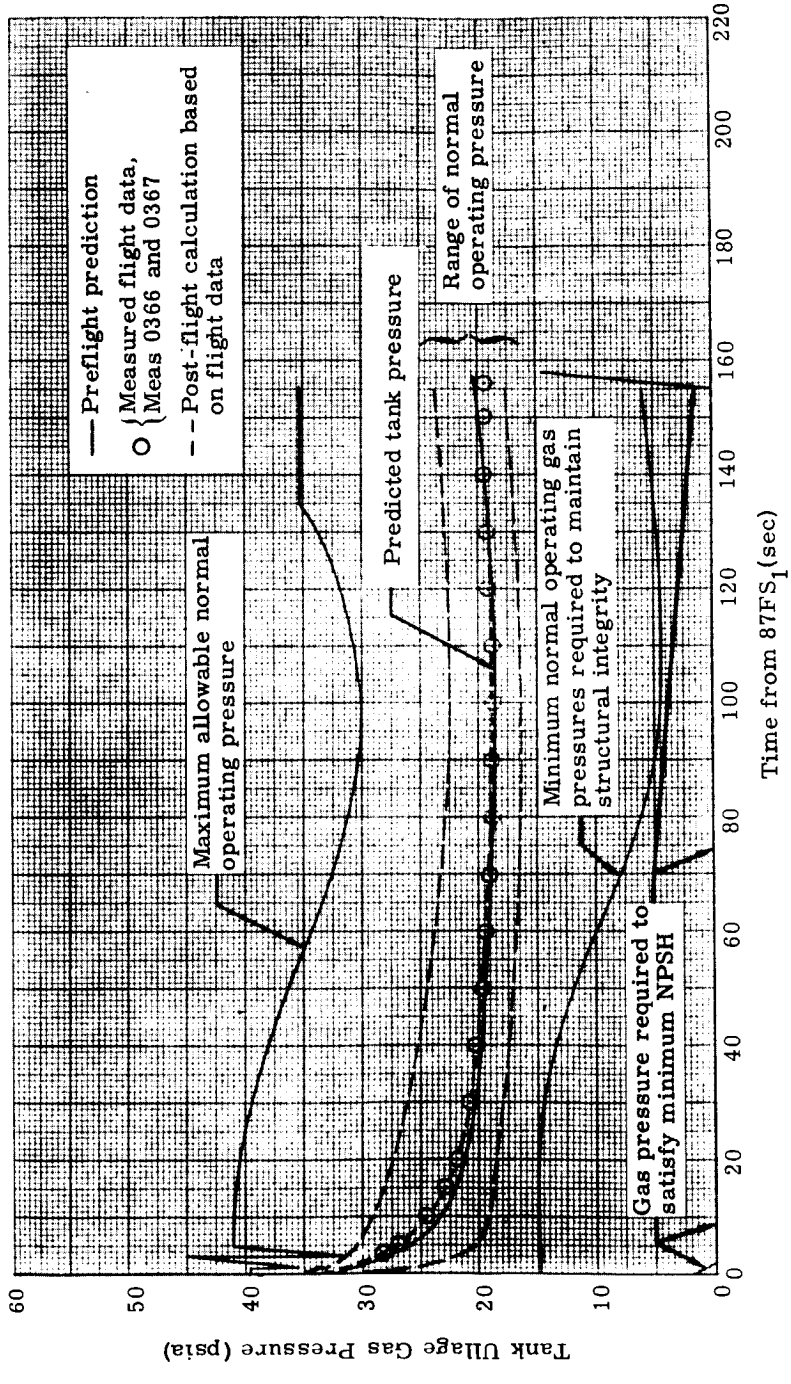


Fig. III-33. Stage I Oxidizer Tank Ullage Pressure History

CONFIDENTIAL

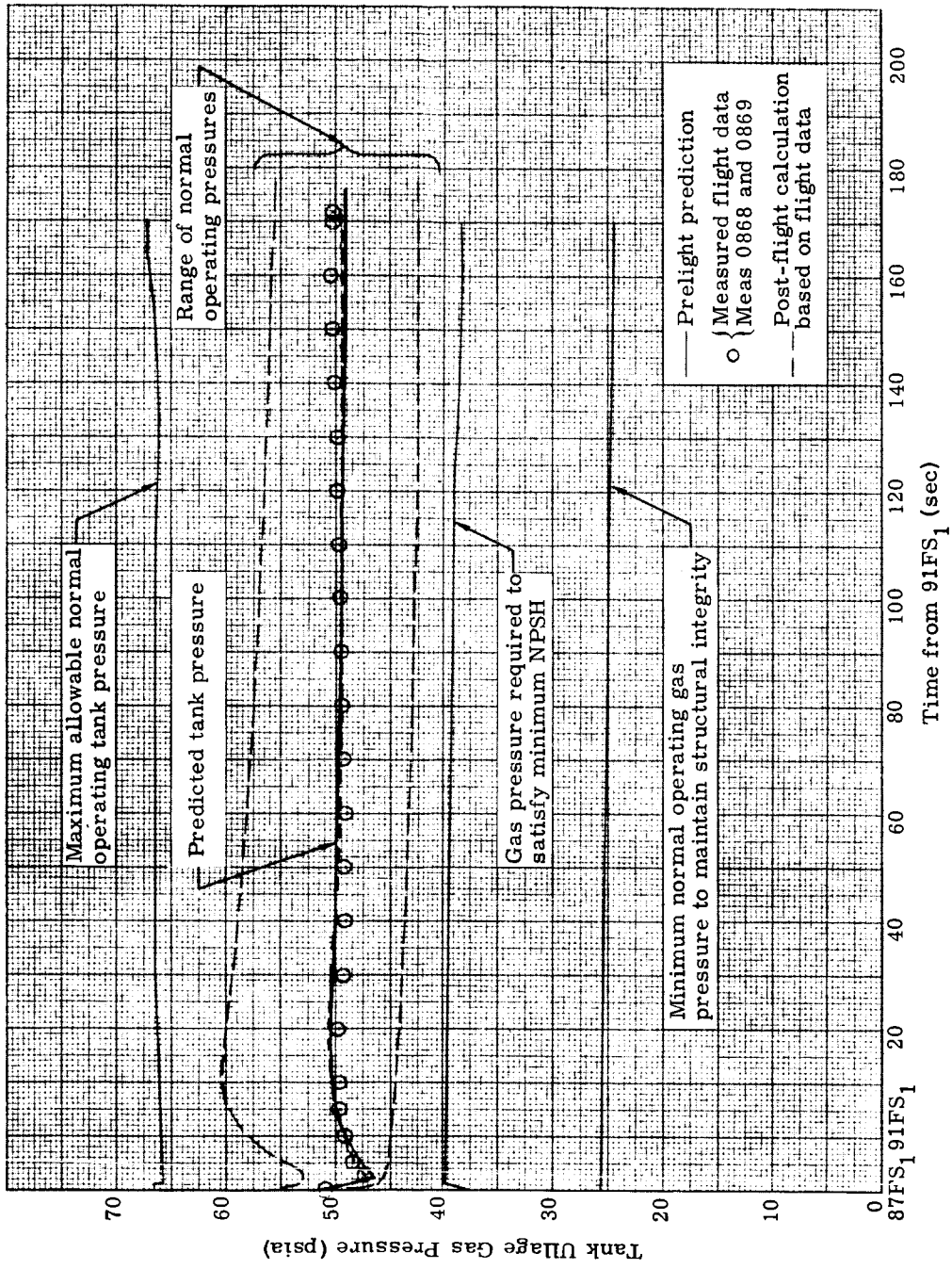


Fig. III-34. Stage II Fuel Tank Ullage Pressure History

~~CONFIDENTIAL~~

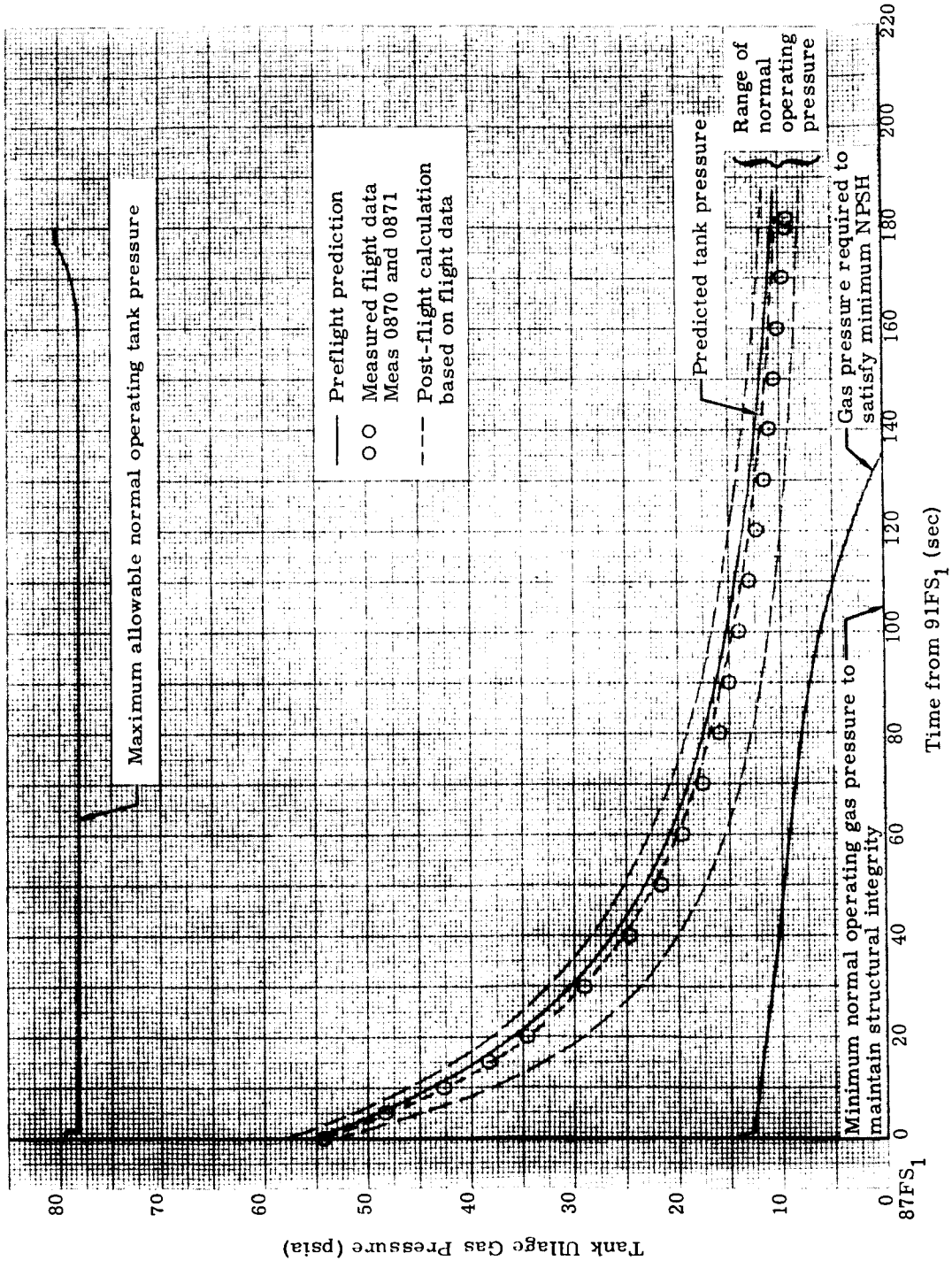


Fig. III-35. Stage II Oxidizer Tank Ullage Pressure History

~~CONFIDENTIAL~~

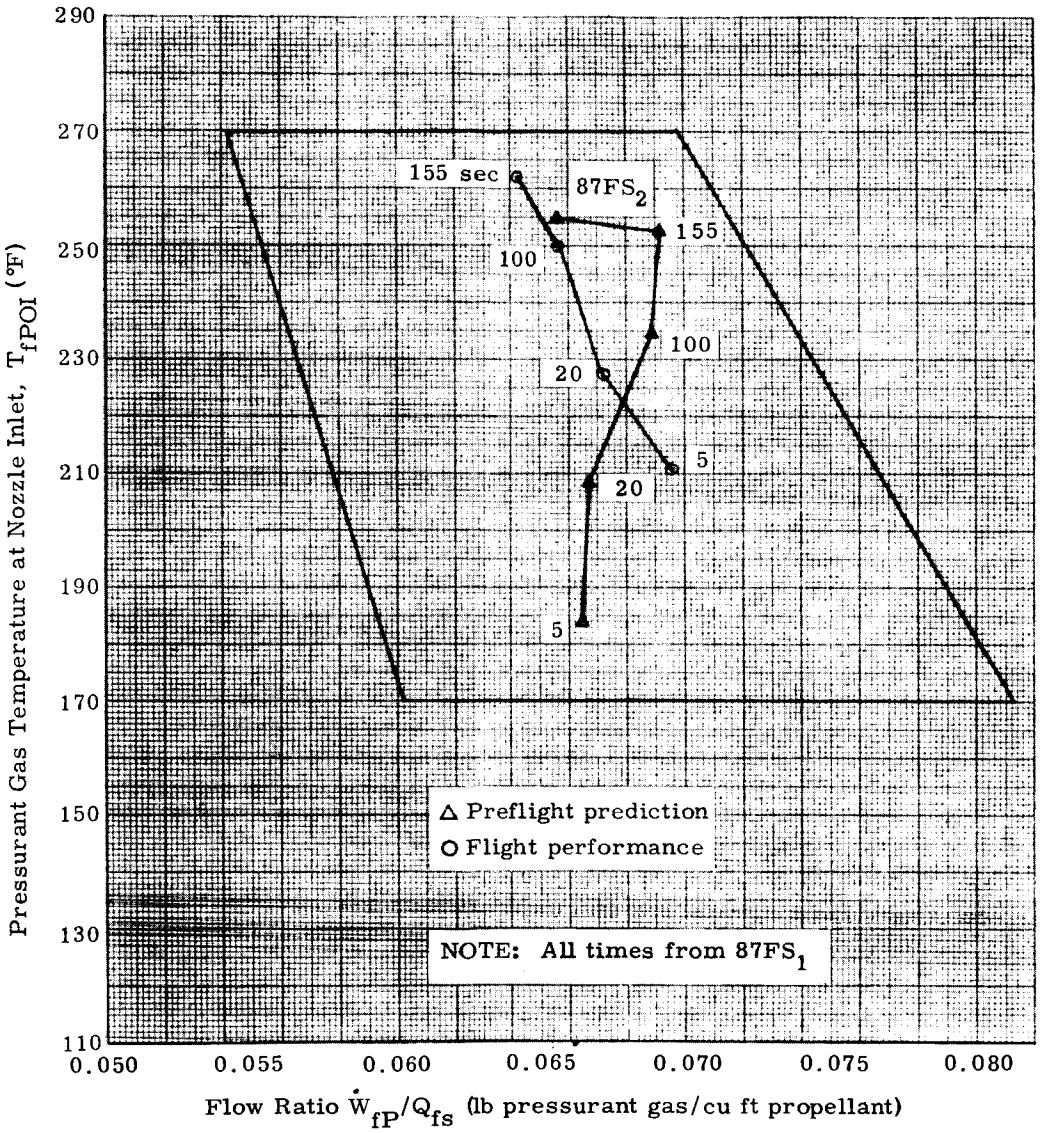


Fig. III-36. Stage I Fuel Tank Pressurant Performance

[redacted]

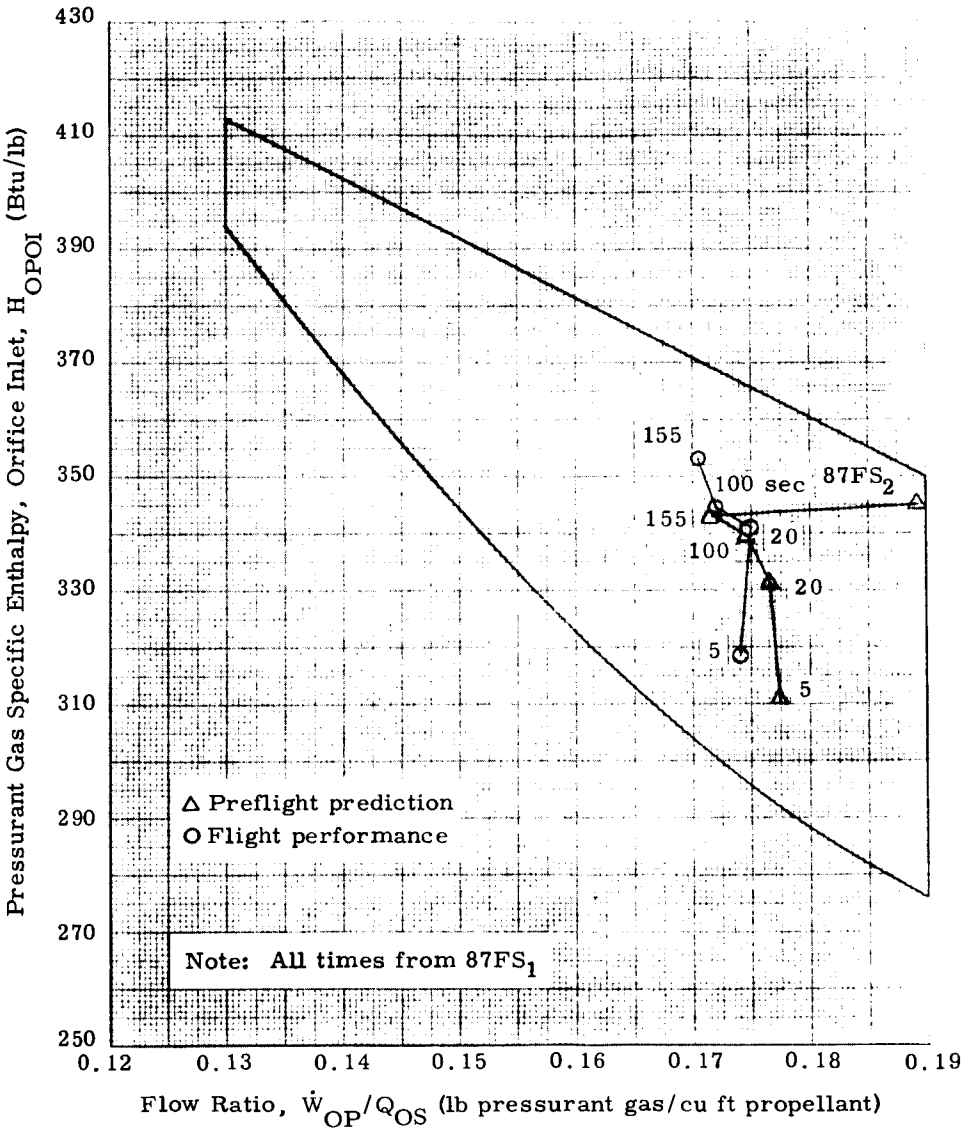


Fig. III-37. Stage I Oxidizer Tank Pressurant Performance

[redacted]

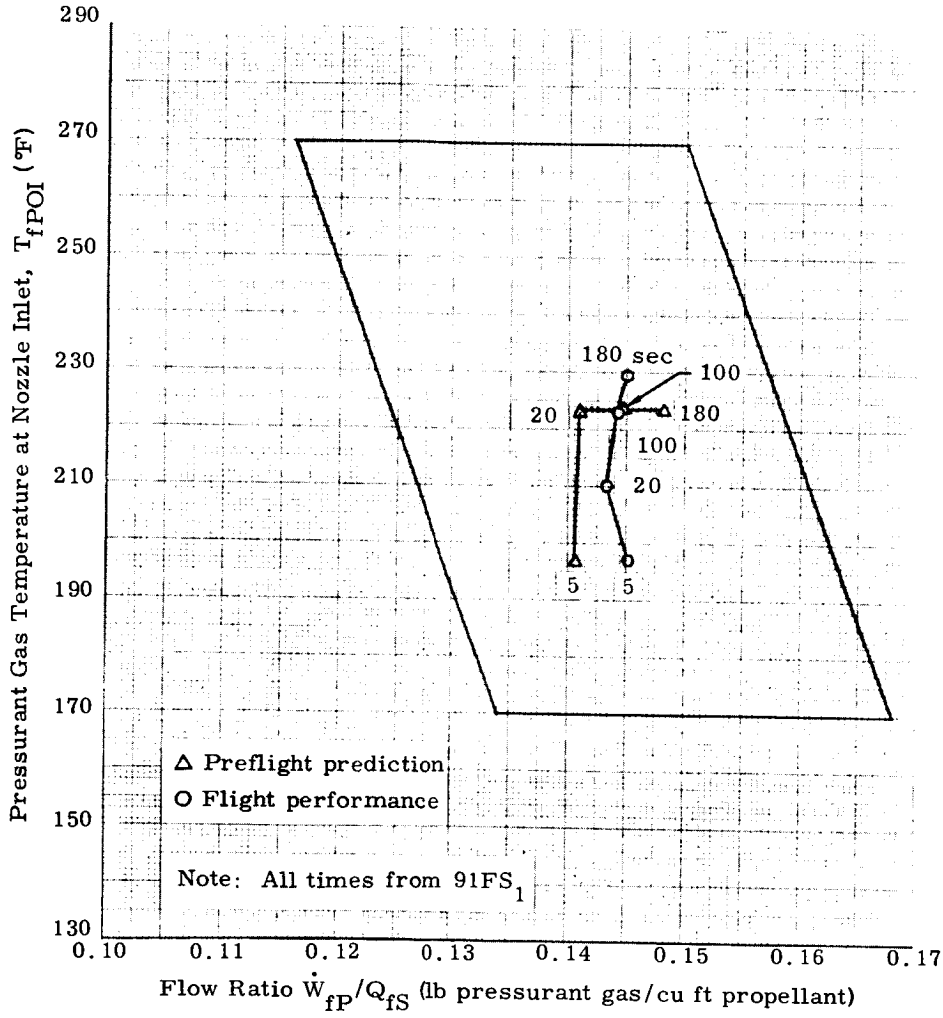


Fig. III-38. Stage II Fuel Tank Pressurant Performance

[redacted]

TABLE III-32

Significant Pressurization System Parameters at $FS_1$ + 100 Seconds

| Parameters | Preflight Predicted | Flight | Post-flight Reconstructed |
|---|---|---|---|
| Stage I fuel tank | | | |
| Tank pressure, $P_{FT}$ (psia) | 23.60 | 23.28 | 23.68 |
| Nozzle inlet pressure, $P_{FPOI}$ (psia)* | 259.9 | 265.1 | 265.1 |
| Nozzle inlet temperature, $T_{FPOI}$ (°F) | 234 | 249 | 249 |
| Flow ratio, $W_{FP}/Q_{FS}$ (lb/cu ft) | 0.0688 | 0.0657 | 0.0657 |
| Stage I oxidizer tank** | | | |
| Tank pressure, $P_{OT}$ (psia) | 18.61 | 18.81 | 18.69 |
| Orifice inlet pressure, $P_{OPOI}$ (psia) | 529.8 | 511.1 | 511.1 |
| Orifice inlet specific enthalpy, $H_{OPOI}$ (Btu/lb) | 340 | 345 | 345 |
| Flow ratio, $W_{OP}/Q_{OS}$ (lb/cu ft) | 0.1794 | 0.1770 | 0.1770 |
| Stage II fuel tank | | | |
| Tank pressure, $P_{FT}$ (psia) | 49.70 | 49.46 | 49.66 |
| Nozzle inlet pressure, $P_{FPOI}$ (psia)*** | 398.6 | 404.2 | 404.2 |
| Nozzle inlet temperature, $T_{FPOI}$ (°F) | 223 | 223 | 223 |
| Flow ratio, $W_{FP}/Q_{FS}$ (lb/cu ft) | 0.1448 | 0.1443 | 0.1443 |
| Stage II oxidizer tank | | | |
| Tank pressure, $P_{OT}$ (psia) | 15.22 | 13.70 | 14.75 |
| Propellant flow rate, $Q_{OS}$ (cu ft/sec) | 2.2005 | 2.2303 | 2.2303 |

*Nozzle diameter, FPN Stage I fuel--0.48 in.
**Flow control venturi coefficient--0.0513
***Nozzle diameter, FPN Stage II fuel--0.26 in.

[redacted]

the prelaunch activities until vehicle liftoff. The system performed satisfactorily. Table III-33 presents a summary of the system parameters.

TABLE III-33

Air-Conditioning System Summary Performance

| Meas | Description | Observed Range | Specified Range | Remarks |
|---|---|---|---|---|
| 4403 | GLV supply air temperature | 52° to 55° F | 48° to 56° F (Compartment 2) 48° to 58° F (engine start cartridges) | Temperature of air supplied to GLV Compartment 2 and engine start cartridges |
| 4405 | Compartment 2 supply air mass flow rate | Approximately 90 lb/min | 82 lb/min (minimum) | -- |
| 4418 | Compartment 2 exhaust air temperature | 56° to 61° F | 40° to 75° F | Manual hold parameter |

2. Stage I Oxidizer Tank Dome Pressure at Staging

Pressure rise on the exterior of the Stage I oxidizer tank dome during the staging sequence was measured by one high-frequency pressure transducer (Meas 1085) located on the tank dome surface at Station 607, WL 58 and BL 27R. This location was identical to that on GLV-2. Figure III-39 presents the recorded pressure-time profile which was generally similar to that noted on GLV-2. The observed maximum pressure peak of 66 psia, while in excess of the 40 psia recorded on GLV-2, is below the value used in designing the tank dome.

~~CONFIDENTIAL~~

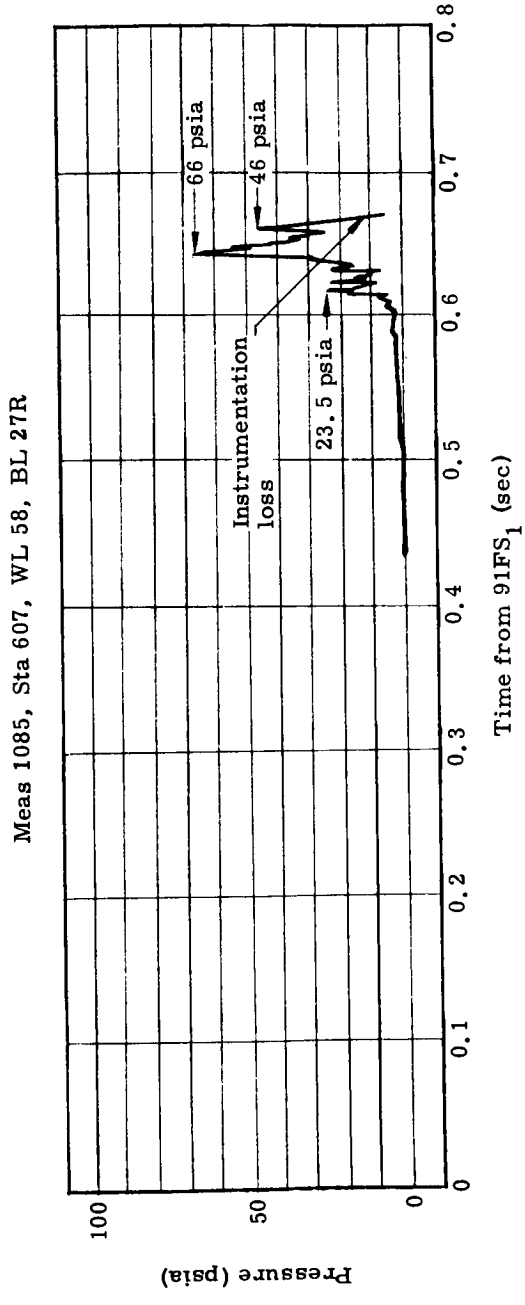


Fig. III-39. Stage I Oxidizer Tank Dome Pressure During Staging

~~CONFIDENTIAL~~

# IV. FLIGHT CONTROL SYSTEM

## A. STAGE I FLIGHT

### 1. Ignition and Liftoff Transients

Peak actuator travels and rate gyro disturbances recorded during the holddown period are presented in Table IV-1. A 0.5-cps oscillation was observed on the pitch and yaw axes rate gyro signals before the vehicle lifted off; this frequency corresponds to the first bending mode which was excited by winds.

TABLE IV-1

Transients During Stage I Holddown Period

| Actuator Designation | Maximum Peak During Ignition: Travel (in.) | Maximum Peak During Ignition: Time from $87FS_1$ (sec) | Maximum During Holddown Null Check (in.) |
|---|---|---|---|
| Pitch, $1_1$ | -0.140 | 0.86 | +0.030 |
| Yaw/roll, $2_1$ | +0.270 | 0.88 | -0.020 |
| Yaw/roll, $3_1$ | +0.090 | 0.81 | ±0.010 |
| Pitch, $4_1$ | -0.060 | 0.79 | -0.030 |

| Axis | Maximum Rate Stage I Gyro (deg/sec) | Maximum Rate Stage II Gyro (deg/sec) |
|---|---|---|
| Pitch | ±0.4 | ±0.9 |
| Yaw | ±0.3 | ±0.2 |
| Roll | ±1.0 | -- |

The combination of thrust misalignment and engine misalignment at full thrust initiated a roll transient at liftoff. The response of the flight control system (FCS) to correct the offset kept the roll rate to a maximum of 1.53 deg/sec CW at 0.3 second after liftoff (Fig. IV-1). The rate oscillation had a basic frequency of 4.4 rad/sec, damping out in 1.5 seconds--exactly as predicted in prelaunch stability studies. The roll rigid body oscillatory mode of approximately 15.5 rad/sec can also be seen on the rate trace.

CONFIDENTIAL

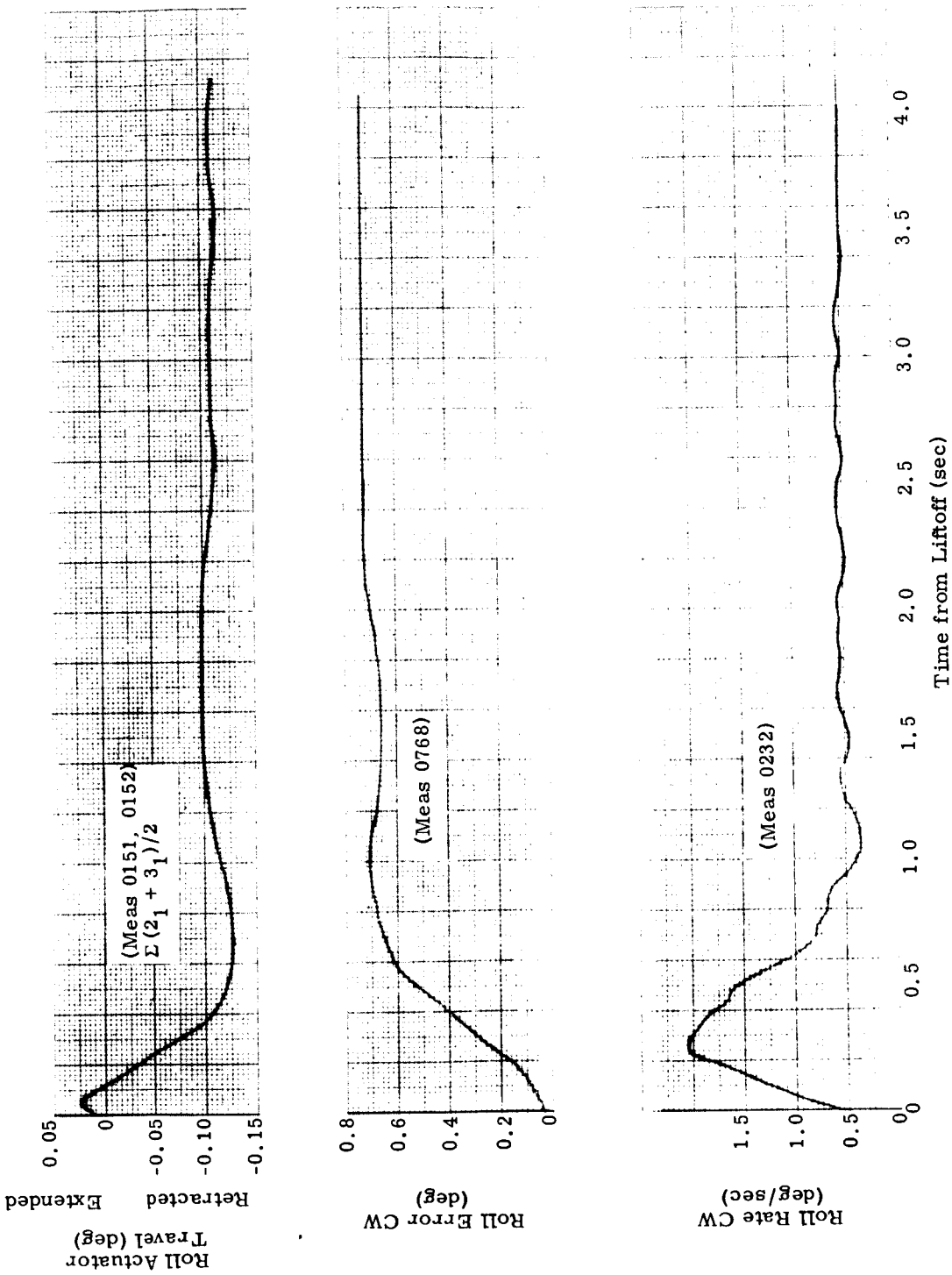


Fig. IV-1. Liftoff Roll Transients

CONFIDENTIAL

As shown on the error roll curve in Fig. IV-1, a roll bias of 0.73 degree CW was introduced at liftoff by the equivalent engine misalignment of 0.13 degree.

## 2. Roll and Pitch Programs

The measured flight results of the TARS roll and pitch programs are shown in Table IV-2. The rate gyros indicate that proper roll and pitch programs were executed during flight. The maximum roll and pitch rates, which occurred at the start of their respective programs, were 1.4 deg/sec CW for roll and 0.9 deg/sec pitch-down.

TABLE IV-2

TARS Roll and Pitch Programs

| Program | Flight Time (sec) | Nominal Time (sec) | Flight Data-- Stage I Rate Gyros (deg/sec) | | Torquer Monitor Rate (deg/sec) | Nominal Rate (deg/sec) |
|---|---|---|---|---|---|---|
| | | | Primary | Secondary | | |
| Roll<br>Start<br>Stop | <br>LO + 10.14<br>LO + 20.42 | <br>10.16<br>20.48 | 1.14 CW | 1.12 CW | 1.16 CW | 1.25 CW |
| Pitch Step I Start | LO + 23.01 | 23.04 | -0.70 | -0.58 | -0.70 | -0.697 |
| Pitch Step II Start | LO + 88.22 | 88.32 | -0.49 | -0.39 | -0.51 | -0.493 |
| Pitch Step III<br>Start<br>Stop | <br>LO + 118.84<br>LO + 162.32 | <br>119.04<br>162.56 | -0.20 | -0.20 | -0.25 | -0.246 |

## 3. TARS-IGS Comparison

The TARS and IGS attitude signals during Stage I flight for pitch, yaw and roll are presented in Figs. IV-2, IV-3 and IV-4.

The dispersion between the TARS and IGS attitude signals is caused by TARS and IGS gyro drifts, errors in open-loop guidance programs, and reference axis cross-coupling. The dispersions at BECO and the contributing factors are given in Table IV-3.

~~CONFIDENTIAL~~

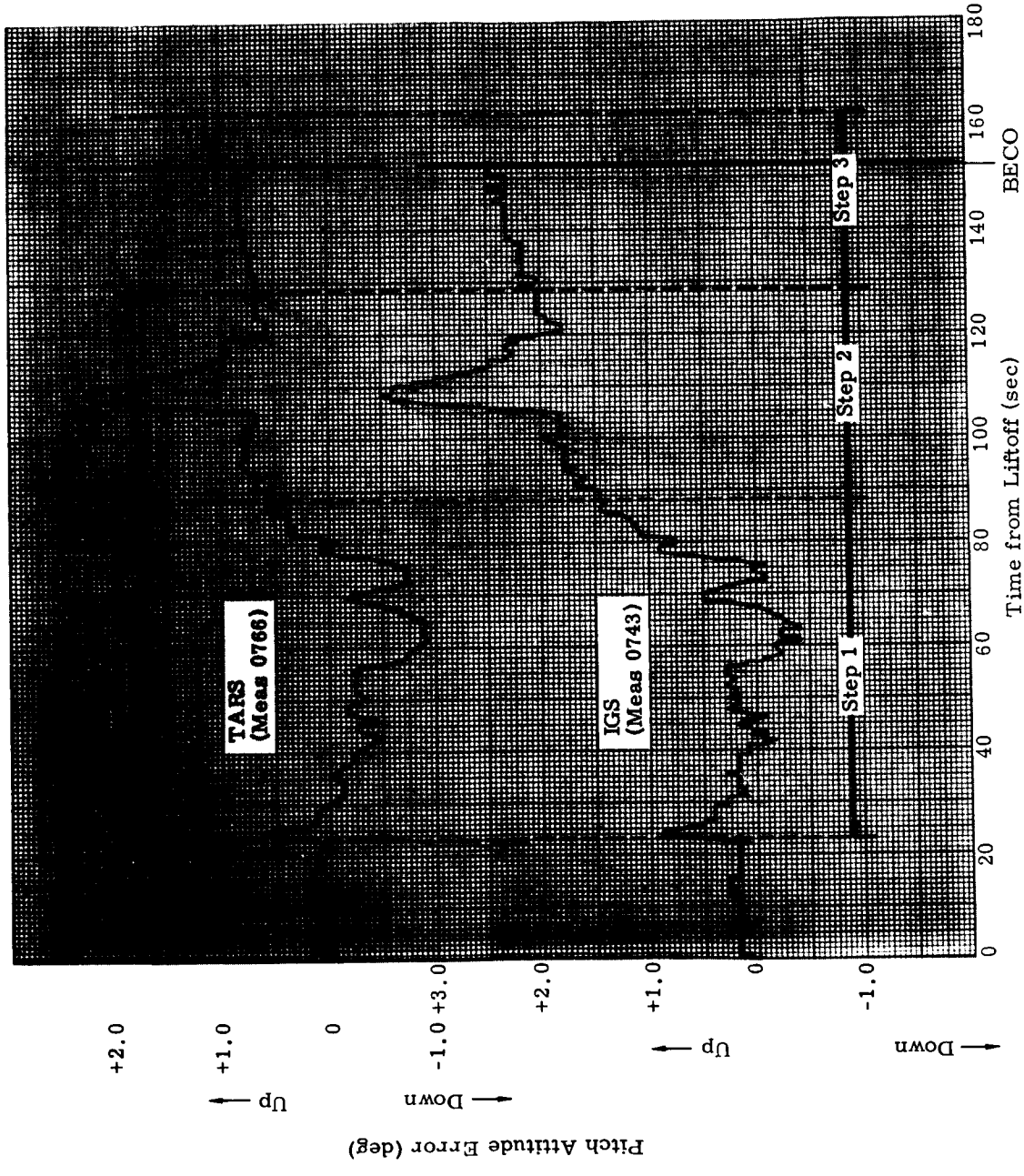


Fig. IV-2. Pitch Attitude Error History During Stage I Flight

~~CONFIDENTIAL~~

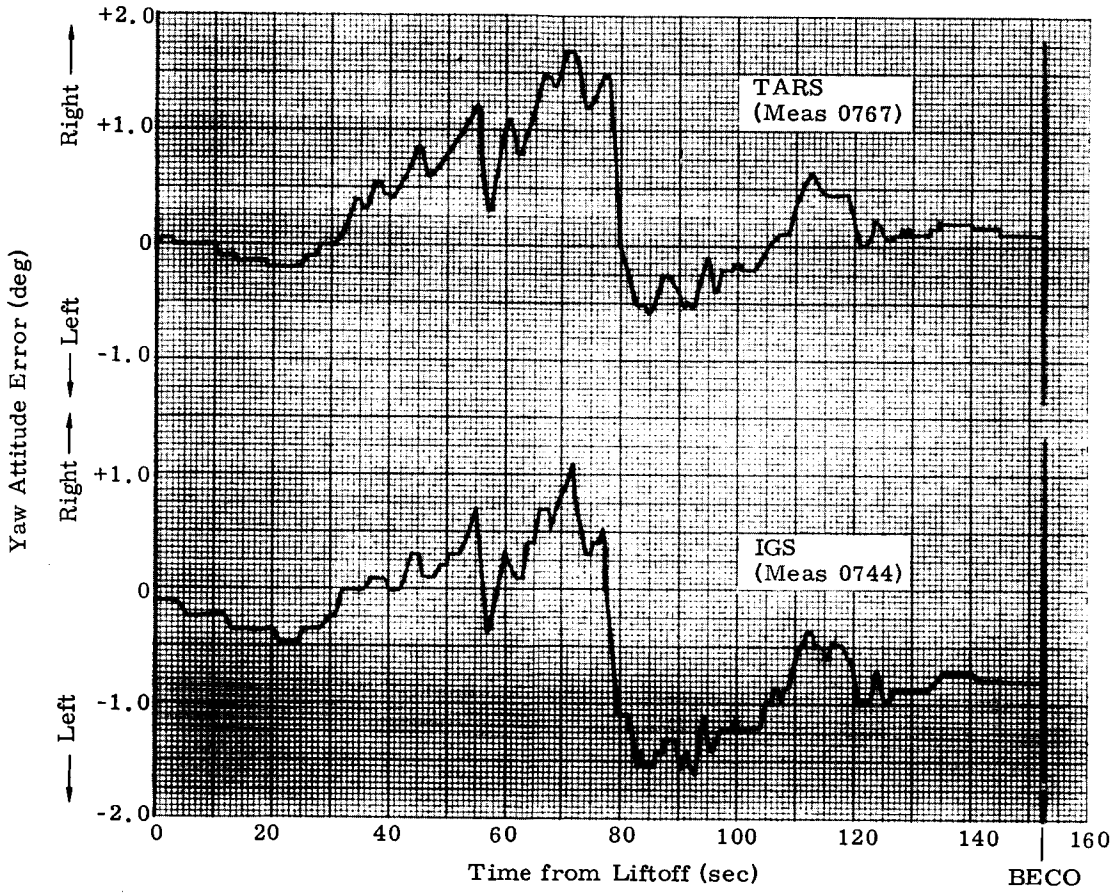


Fig. IV-3. Yaw Attitude Error History During Stage I Flight

~~CONFIDENTIAL~~

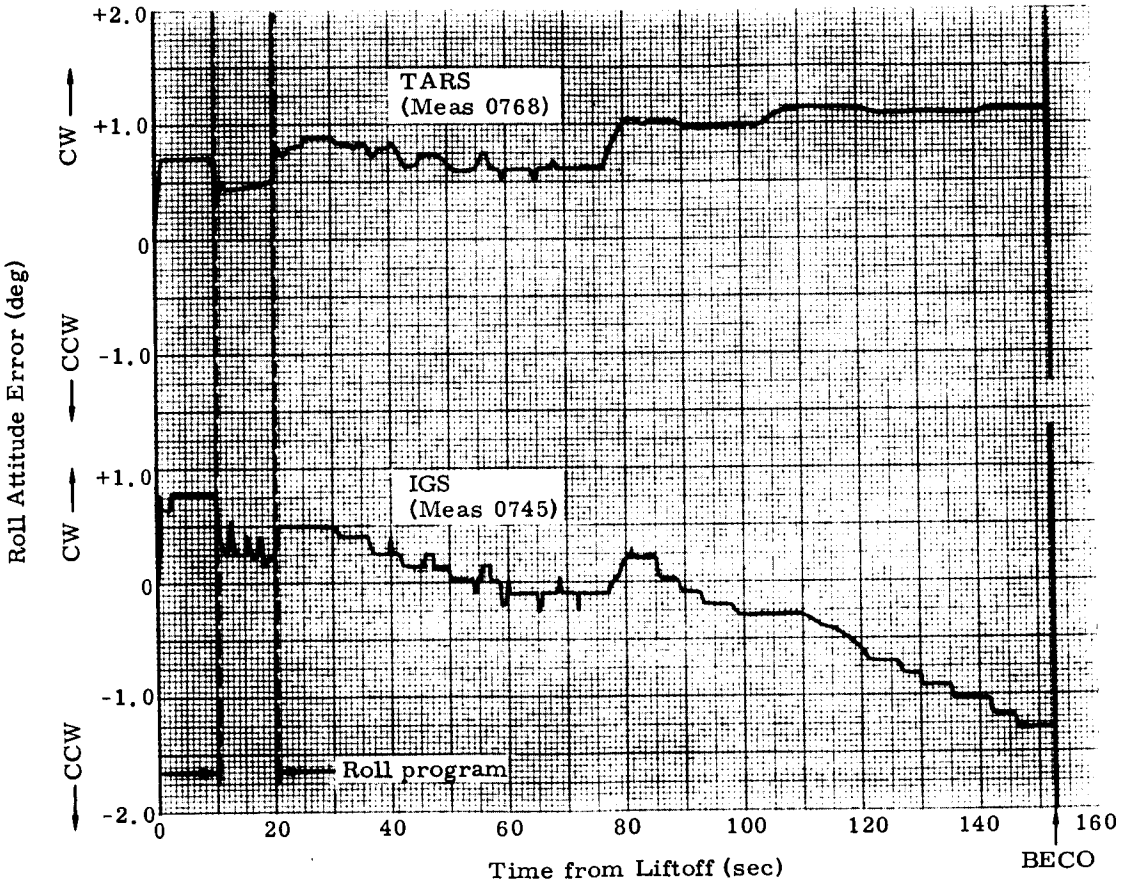


Fig. IV-4. Roll Attitude Error History During Stage I Flight

~~CONFIDENTIAL~~

TABLE IV-3

TARS-IGS Dispersion at BECO

| Axis | Total Dispersions (deg) | Contributing Factors | | | |
|---|---|---|---|---|---|
| | | TARS Drift | | TARS Guidance Program Errors (deg) | Uncertain Dispersions (deg) |
| | | Anticipated Drift at BECO (deg) | Hourly Drift Rate | | |
| Pitch | +1.60 | +0.15 | +3.60 deg/hr | +0.83 | +0.62 |
| Yaw | -0.90 | -0.22 | -5.13 deg/hr | -- | -0.68 |
| Roll | -2.40 | -0.72 | 14.00 deg/hr/g | -0.20 | -1.48 |

The uncertain dispersions are attributed to cross-coupling effects in IGS, IGS gyro drifts, IGS guidance program errors, and additional TARS gyro drifts.

4. Stage I Flight Disturbances

The primary FCS operated properly during Stage I flight as shown by the TARS attitude signals in Figs. IV-2, IV-3 and IV-4. These attitude signals reflect response to wind disturbances and to the guidance programs.

Analysis indicates that the speed and direction of the winds aloft are the causes of the vehicle disturbance. The control system response to these disturbances was normal and well controlled. During wind disturbances, oscillations occurred in both pitch and yaw at the predicted rigid body oscillatory mode frequency of 1.6 rad/sec with an average peak-to-peak amplitude of 0.2-degree attitude error. In roll, the oscillations occurred at the roll rigid body natural frequency of approximately 1 cps with an average peak-to-peak amplitude of 0.1 degree. These oscillations were similar in nature to those experienced during the GT-1 and GT-2 flights due to wind disturbances. During the wind disturbances, the vehicle rates never exceeded 1 deg/sec and a maximum recorded attitude of 1.68 degrees.

At the time of gain change (LO + 105 seconds), there was a noticeable, but very highly damped, pitch transient reaching a maximum of 2.26 degrees attitude error.

Due to the nature of the winds aloft combined with the pitch rate program, the attitude and rate pitch errors command an engine deflection. The reduction of attitude and rate gains reduces the amount of engine de-

flection. Therefore, the attitude error increases rapidly causing an increase in engine deflection. The proper system response is indicated by the following equation:

$$\delta = K_D \theta \left(\frac{1}{1 + \tau S}\right) + K_R \dot{\theta} \left(\frac{1}{1 + \tau S}\right)^2$$

where

$\tau$ = 1/22 second

$S = j\omega$

$\omega$ = 0.314 rad/sec (value obtained by measuring first half of transient overshoot)

Table IV-4 presents a comparison of GT-3 in-flight attitude errors with the theoretical calculated errors before and after gain change flight conditions. The small difference between theoretical and actual can be attributed to minor variations in gains and/or wind effects during the transient period. Analyses indicate that the control system reacted properly to the flight conditions which existed before and after gain change.

TABLE IV-4

Gain Change Calculations

| Parameter | Before Gain Change (LO +104.5 sec) | After Gain Change (LO +108.5 sec) |
|---|---|---|
| Flight data | | |
| Engine deflection ($\delta$) | 0.242 deg | 0.348 deg |
| Pitch rates ($\dot{\theta}$) | -0.55 deg/sec | -0.45 deg/sec |
| Design gains | | |
| Displacement ($K_D$) | 0.65 deg/deg | 0.21 deg/deg |
| Rate ($K_R$) | 0.40 deg/deg/sec | 0.165 deg/deg/sec |
| Pitch attitude error ($\theta$) | | |
| Theoretical | 0.71 deg | 2.18 deg |
| Measured | 0.68 deg | 2.26 deg |

The maximum rates and attitude errors recorded during the wind disturbance and gain change periods of Stage I flight are noted in Table IV-5.

TABLE IV-5

Stage I Maximum Rates and Attitude Errors

| Axis | Stage I Rates (deg/sec) | Time from Liftoff (sec) |
|---|---|---|
| Pitch | -0.90<br>+0.18 | 71.5<br>106. |
| Yaw | -0.95<br>+0.45 | 79.<br>93.5 |
| Roll | -0.55<br>+0.45 | 58.5<br>59. |
| **Axis** | **Attitude Error (deg)** | **Time from Liftoff (sec)** |
| Pitch | -0.95<br>+2.26 | 62.<br>108.5 |
| Yaw | +1.68<br>-0.58 | 71.<br>85. |
| Roll | +1.14<br>+1.14 | 107.<br>152. |

5. Static Gains

The primary FCS static gains (as determined from telemetry data) were within the instrumentation inaccuracy of preflight evaluations, and indicate that no static gain deterioration was experienced during Stage I boost flight.

## B. STAGE II FLIGHT

1. Stage Separation

During the staging event, moderate rates and attitude errors of the sustainer vehicle were observed. The maximum attitude errors recorded were as follows:

| | |
|---|---|
| Pitch | -0.59 deg at BECO + 2.2 sec |
| Yaw | +1.8 deg at BECO + 2.4 sec |
| Roll | -0.48 deg at BECO + 1.2 sec |

The maximum sustainer vehicle rates recorded were as follows:

| | |
|---|---|
| Pitch | -1.5 deg/sec at BECO + 1.2 sec |
| Yaw | +1.5 deg/sec at BECO + 1.6 sec |
| Roll | -2.0 deg/sec at BECO + 0.7 sec |

These were also the maximum recorded rates for the entire Stage II flight except for a guidance-induced pitching rate of -2.0 deg/sec about 3.25 seconds after guidance initiation.

In general, all staging-induced sustainer rate transients were completed by BECO +5 seconds; however, a 17-second lightly-damped yawing rate oscillation of approximately 0.8 cps was observed with a maximum peak-to-peak rate of about 0.47 deg/sec and an accompanying peak-to-peak displacement error of about 0.12 degree. From linear analysis, this frequency is in agreement with that of the Stage II oxidizer slosh mode. The probable cause of the excitation of this mode was the yawing motion of the vehicle in adjusting for a yaw attitude bias error which was immediately evident when the separation transient disappeared.

2. Pitch and Yaw Attitude Bias

The FCS indicated an attitude bias in both pitch and yaw during Stage II flight, which was well within predicted limits. The attitude error signals for pitch and yaw are shown in Figs. IV-5 and IV-6. The attitude biases are mainly caused by engine thrust vector misalignment due to structural deformation at the engine gimbal assembly, center-of-gravity travel off the vehicle longitudinal axis, and the position of the roll thrust vector off the longitudinal axis. The GT-3 yaw bias of +1.4 degrees is similar to the biases experienced on GT-1 and GT-2 flights. The GT-3 pitch bias of -0.6 degree is the same order of magnitude as that on GT-2. The pitch actuator length adjustment incorporated on GT-2 and GT-3 greatly reduced the pitch bias from that experienced on GT-1. The deviation of the pitch and yaw attitude errors from the predicted values (which assumed fixed bias, center-of-gravity shift and roll thrust bias) toward the end of Stage II flight is similar to that experienced on GT-1 and GT-2 flights.

3. Guidance Initiate

The guidance enable command was generated by the TARS timer at LO + 162.30 seconds. The first pitch guidance command was received at LO + 168.68 and was a full 2.0 deg/sec pitch-down command for 12.3 seconds. Low magnitude pitch commands existed during the remainder of flight. The first yaw command was received at LO + 169.6 seconds.

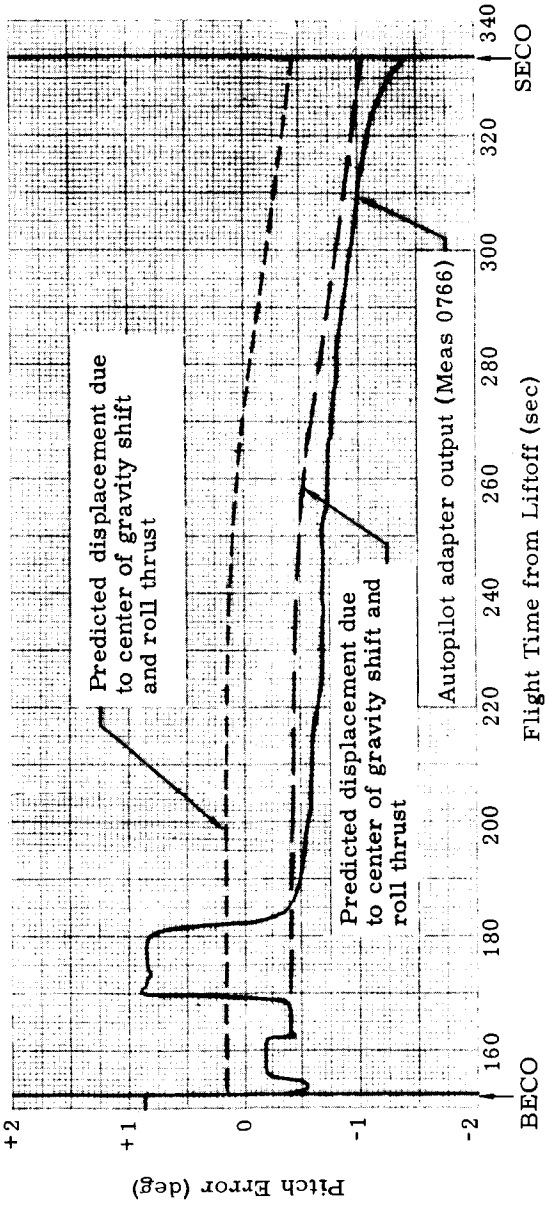


Fig. IV-5. Pitch Axis Displacement Error During Stage II Flight

~~CONFIDENTIAL~~

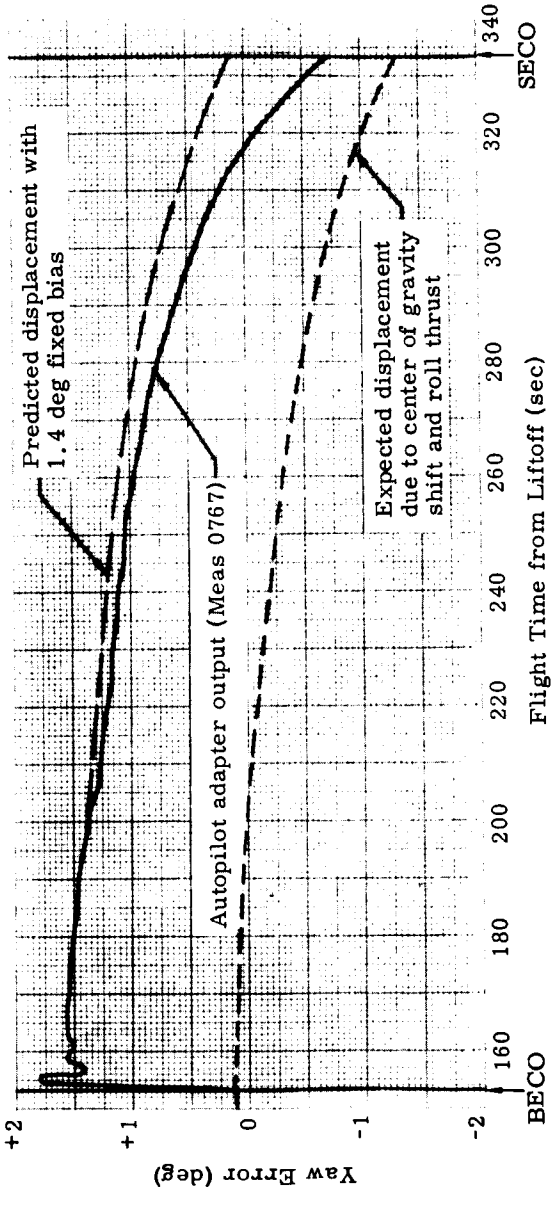


Fig. IV-6. Yaw Axis Displacement Error During Stage II Flight

~~CONFIDENTIAL~~

All yaw commands during Stage II flight were low magnitude, and never exceeded 0.06 deg/sec. The rate gyro signals substantiated the correct response to the guidance commands.

4. Static Gains

The primary FCS static gains determined from telemetry data were within the instrumentation inaccuracy of preflight evaluations.

## C. POST-SECO FLIGHT

1. Vehicle Motions

Prior to SECO, telemetry data indicated that the pitch actuator was retracted, producing a sustainer engine gimbal deflection of 0.332 degree to correct for a pitch error of -1.424 degrees nose-down. In yaw, the error was -0.727 degree with an equivalent engine gimbal deflection of 0.143 degree. At SECO, the roll error was less than 0.1 degree counterclockwise.

Pitch, yaw and roll attitude errors and rates during the period from SECO through spacecraft separation are shown in Fig. IV-7. Significant vehicle rates measured during this period appear in Table IV-6.

TABLE IV-6

Vehicle Rates Between SECO and Spacecraft Separation

| Pitch Axis | Rate (deg/sec) |
|---|---|
| Max positive rate ($91FS_2$ + 2.4 sec) | +0.9 |
| Max negative rate ($91FS_2$ + 17.2 sec) | -0.4 |
| Rate at $91FS_2$ + 20 sec | -0.4 |
| Rate at spacecraft separation ($91FS_2$ + 25.6 sec) | -0.1 |
| **Yaw Axis** | |
| Max positive rate ($91FS_2$ + 13.3 sec) | +0.2 |
| Max negative rate ($91FS_2$ + 0.34 sec) | -0.2 |
| Rate at $91FS_2$ + 20 sec | +0.2 |
| Rate at spacecraft separation ($91FS_2$ + 25.6 sec) | +0.5 |

[redacted]

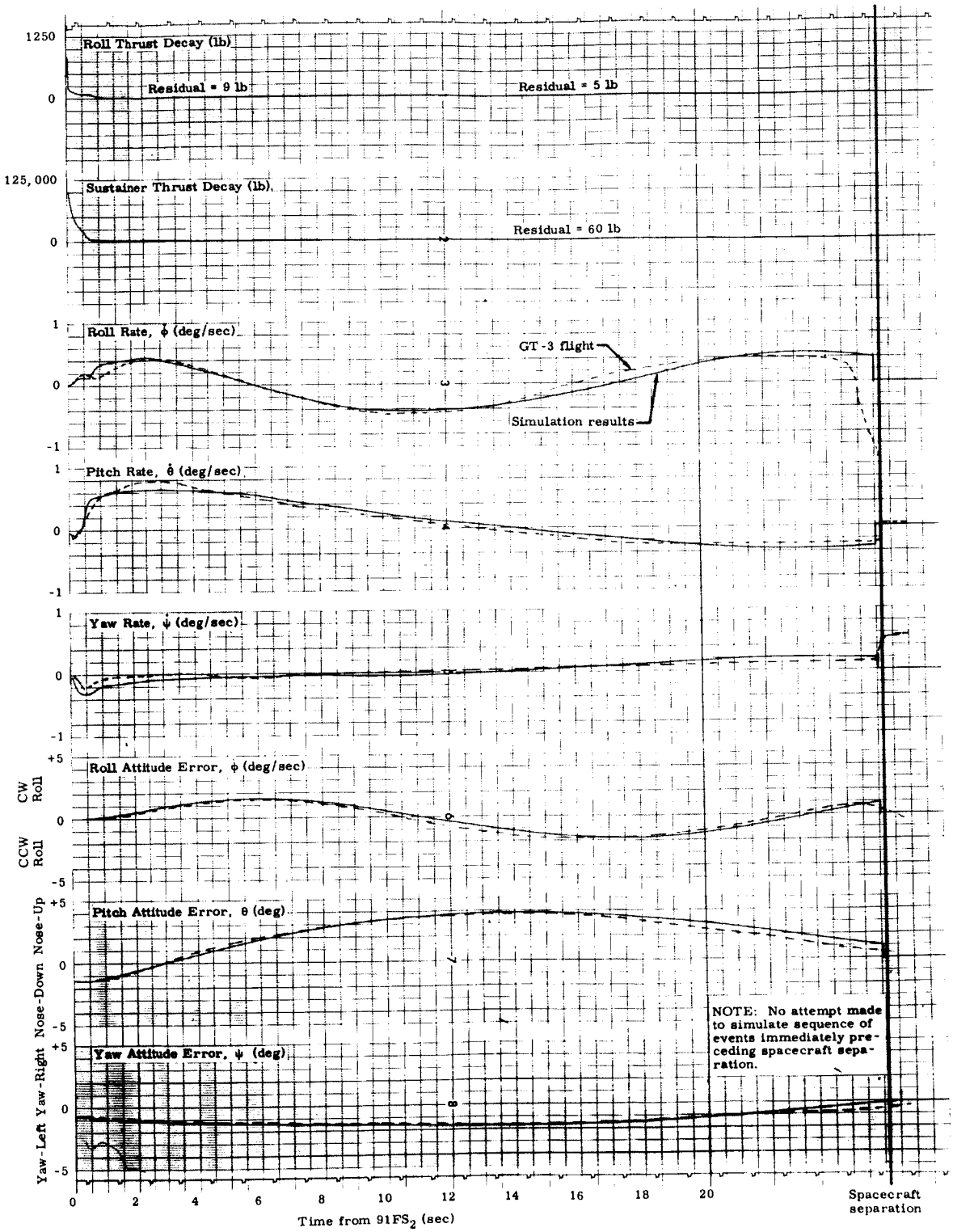


Fig. IV-7. Reconstructed GT-3 Post-SECO Motion

[redacted]

TABLE IV-6 (continued)

| Roll Axis | Rate (deg/sec) |
|---|---|
| Max positive rate ($91FS_2$ + 2.1 sec) | +0.4 |
| Max negative rate ($91FS_2$ + 10.4 sec) | -0.6 |
| Rate at $91FS_2$ + 20 sec | +0.3 |
| Rate at spacecraft separation (91 $FS_2$ + 25.6 sec) | -1.2 |

The Stage II redundant engine shutdown system was used for the first time on the GT-3 flight. With this type of shutdown, the roll nozzle thrust decay precedes the sustainer thrust decay. Also, the initial portion of the sustainer engine and gas generator nozzle thrust decay as experienced on GT-3 was very rapid in comparison to the same GT-2 parameters with the normal thrust chamber valve shutdown. These two factors caused the vehicle's post-SECO rates to be less severe than those experienced on the GT-1 and GT-2 flights.

## 2. Post-SECO Simulations

The vehicle motions observed beyond SECO on the GT-3 flight have been reconstructed via the current analog post-SECO simulation. The initial conditions and engine thrust decay characteristics were obtained from the flight telemetry data. Preflight autopilot gains and compensating dynamics were utilized. These data (as well as the factors which were introduced in the initial portion of the subject period in order to obtain the vehicle motions) are shown in Figs. IV-7 and IV-8. A comparison of flight with simulation results appears in Fig. IV-7.

The biases assumed for thrust vector position and magnitude can be explained as follows:

a. Pitch

The transient at SECO + 0.1 second appears to be caused by the removal of propellant line bias loads during shutdown.

The second step at SECO + 0.4 second appears to be caused by the removal of a thrust dependent bias (such as structural deformation) experienced during Stage II flight under full thrust conditions.

~~CONFIDENTIAL~~

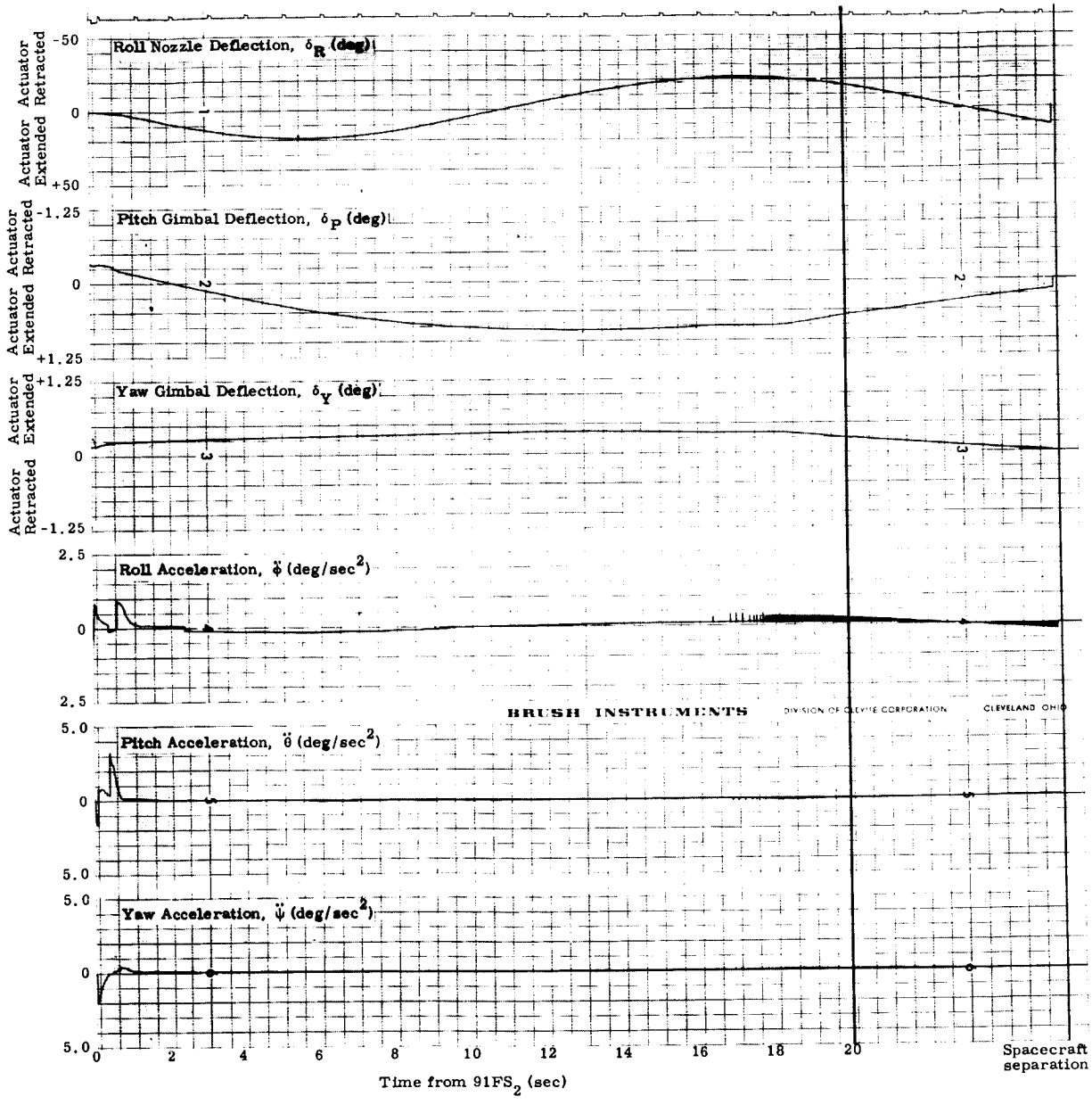


Fig. IV-8. Reconstructed GT-3 Post-SECO Motion

~~CONFIDENTIAL~~

Bias Steps Required to Reconstruct GT-3 Flight Data

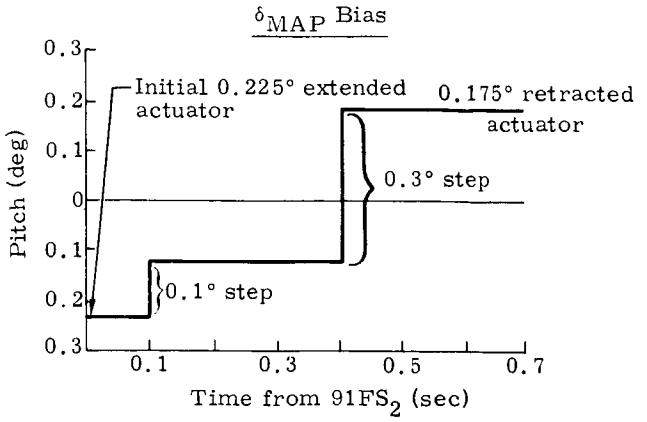


Initial Conditions

$\theta$ = -1.424°
$\dot{\theta}$ = -0.05 deg/sec
$\ddot{\theta}$ = -0.000745 deg/sec$^2$
$\psi$ = -0.727°
$\dot{\psi}$ = -0.0485 deg/sec
$\ddot{\psi}$ = -0.0414 deg/sec$^2$
$\phi$ = -0.062°
$\dot{\phi}$ = 0
$\ddot{\phi}$ = +0.0494 deg/sec$^2$
$\delta_P$ = 0.332° actuator retracted
$\delta_Y$ = 0.143° actuator extended
$\delta_R$ = 0.731° actuator retracted

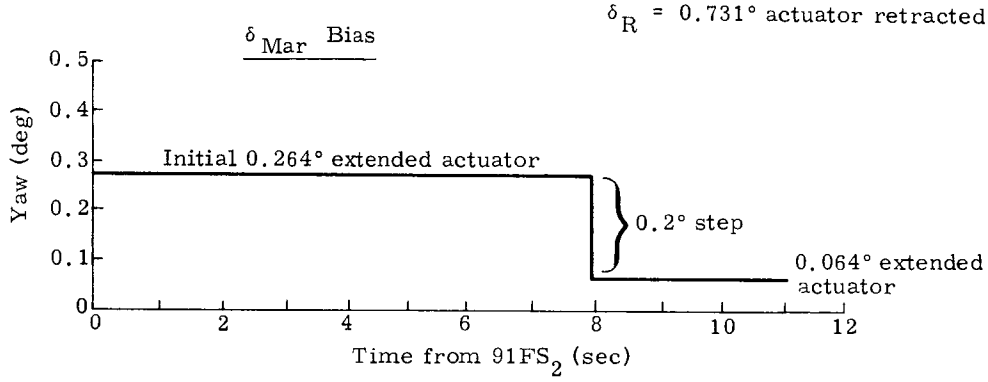


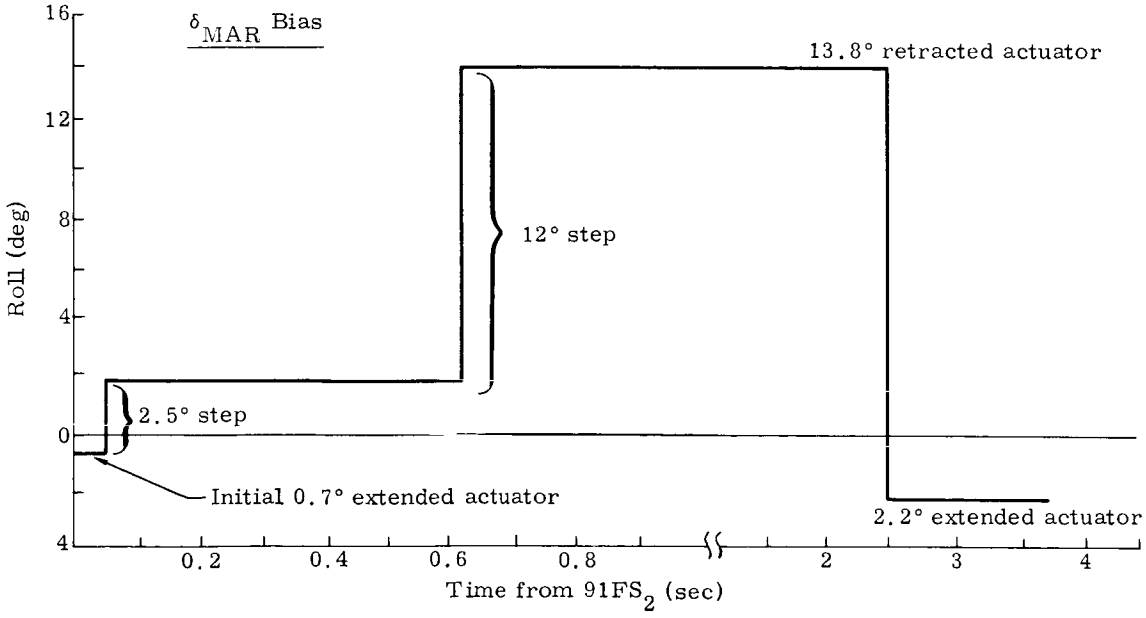


Fig. IV-8. (continued)

b. Yaw

The small transient in yaw at SECO + 8 seconds can be attributed to one of these factors:

(1) Due to the large quantity of propellant remaining at SECO, the vehicle lateral, horizontal and vertical center of gravity offsets could have shifted an amount equivalent to the assumed bias when the vehicle reached a condition close to zero g loading.

(2) A small change in the thrust vector position could have occurred. Existing telemetry instrumentation does not detect the direction of the thrust vector.

c. Roll

The small transient at SECO + 0.05 second appears to be caused by the removal of propellant line bias loads during shutdown.

The second roll bias step (12°) becomes effective at SECO + 0.625 second and remains so until SECO + 2.5 seconds when a step of the same approximate magnitude is removed. The large bias step is similar in magnitude to the one required to reconstruct the GT-1 post-SECO motions. Even though the nozzle deflection required appears to be large, the equivalent actuator and structural deformation of the roll nozzle supporting structure is only 1/2 inch. The most probable cause of this transient is a change in the roll nozzle thrust vector position. However, it could be caused by perturbations in the main sustainer engine thrust decay. These perturbations can be small enough to be ineffective in pitch and yaw, but large enough to cause the required roll nozzle transient.

Contrary to preflight predictions, the GT-3 flight post-SECO pitching rates were higher than the yawing rates. On this flight, the total Stage II pitch thrust misalignment in pitch (including the actuator null length adjustment as well as the bias recorded in flight) exceeded the yaw thrust dependent bias. With the rapid sustainer engine thrust decay, the removal of the thrust dependent biases largely determine the resulting vehicle rates. No attempt has been made to simulate the sequence of events immediately preceding spacecraft separation. Therefore, the GT-3 flight data and the simulation results only indicate correlation for the period from SECO to SECO + 20 seconds.

# V. HYDRAULIC SYSTEM

Analysis of the telemetered data revealed that the GLV-3 hydraulic systems performed satisfactorily during Stages I and II flight.

Shortly before the launch of GT-3, the engine-driven hydraulic pumps were replaced with units that had been recently cleaned by the vendor, thereby minimizing the probability of contamination being present prior to start of vehicle systems tests requiring hydraulic power. The newly installed pumps were checked with a Gauss meter to verify free motion of the compensator. The pump response during engine start was normal (Fig. V-1) and there was no evidence of stiction as occurred on the GT-2 launch.

## A. STAGE I

### 1. Primary Subsystem

The output of the Stage I electric motor pump was automatically switched from the secondary subsystem to the primary subsystem at T-110 seconds. This event pressurized the primary subsystem and resulted in normal system operation. The indicated accumulator precharge was 1820 psia. Electric motor pump pressure was a normal 3265 psia at T-0. Engine start transients starting at $87FS_1$ + 0.76 second produced flow demands which dropped primary pressure to 2580 psia at $87FS_1$ + 0.96 second. Pressure recovery occurred immediately, indicating proper pump compensator response. The pressure overshoot on recovery peaked at 3340 psia at $87FS_1$ + 1.18 seconds. A steady-state pressure of 3079 psia was reached at $87FS_1$ + 1.8 seconds. There were no significant pressure perturbations at liftoff or during flight. Pressure decayed normally during flight to 2900 psia at staging.

The static reservoir level was 61.7% full prior to T-110 seconds, decreasing to 38.9% full at T-0. The level increased during flight to 52.3% full at staging. This level increase of 13.4% is consistent with the observed fluid temperature rise from 90° F at T-0 to 161° F at staging.

The steady-state reservoir levels and the level changes during system pressurization were normal.

Primary and secondary system pressures and switch closure periods are shown in Fig. V-1. A comparison of primary system pressure history from GT-1, GT-2 and GT-3 launches during engine start and hold-down is presented in Fig. V-2.

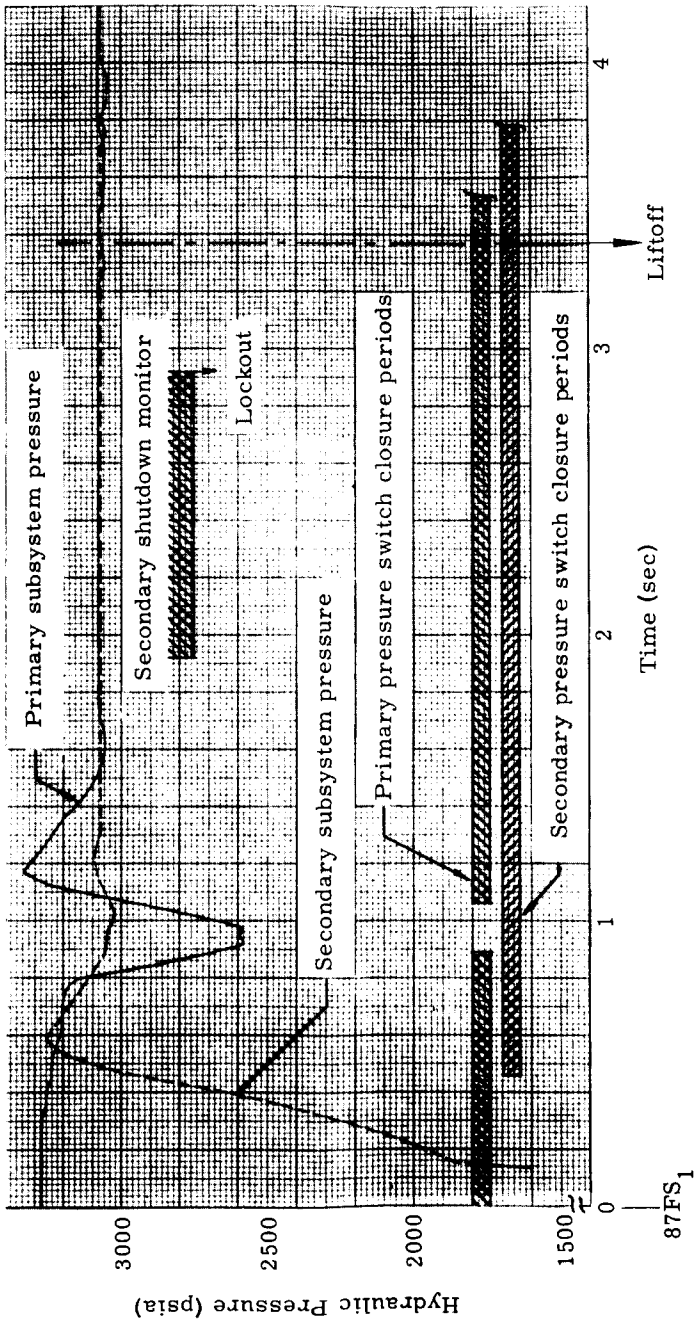


Fig. V-1. Stage I Hydraulic System Pressure Variation During Engine Start and Holddown

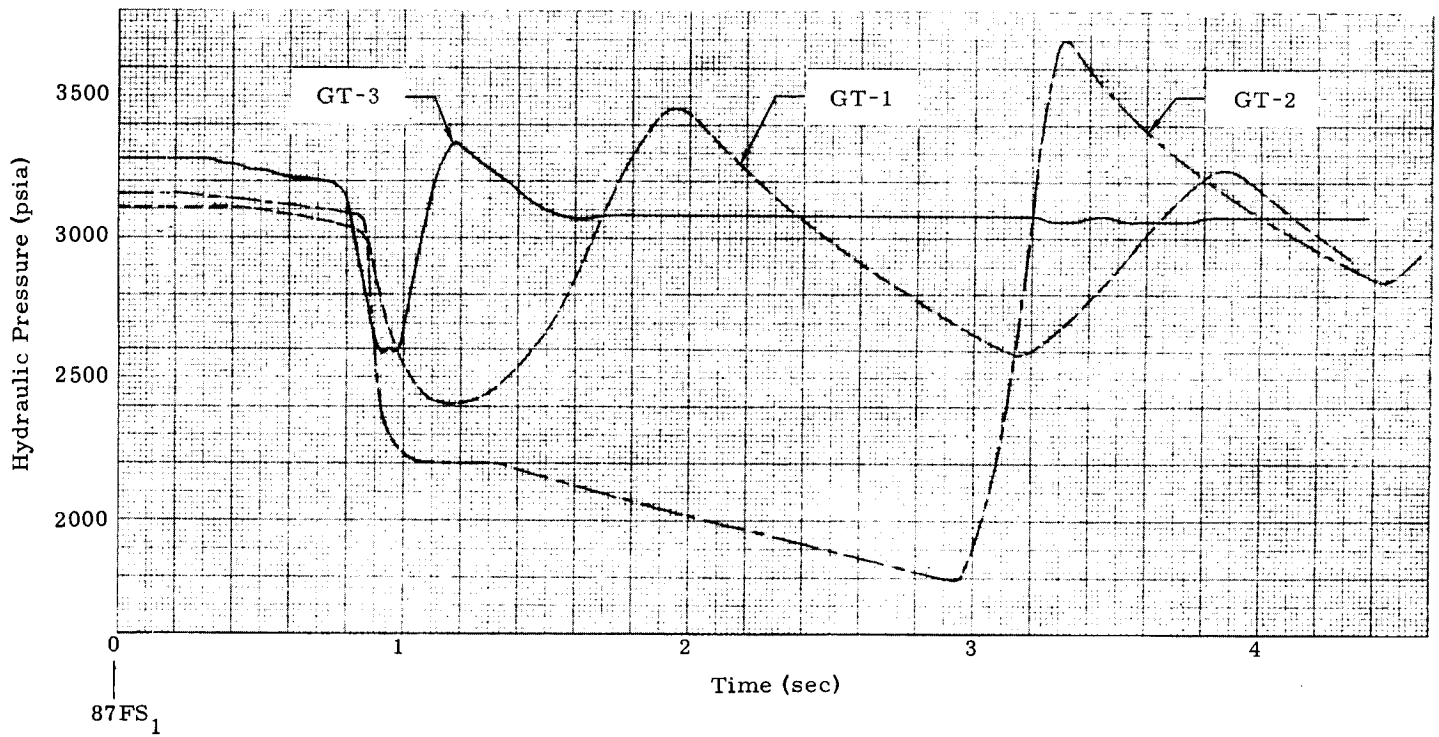


Fig. V-2. Comparison of Primary System Hydraulic System Pressure During Engine Start and Holddown

2. Secondary Subsystem

The secondary subsystem was pressurized by the electric motor pump from T-180 to T-110 seconds. The indicated accumulator precharge was 1850 psia. Motor-pump pressure was a normal 3160 psia at T-110 seconds.

The static reservoir level was a normal 55.2% full prior to pressurization at T-3 minutes, and had decreased to 29.5% full at T-110 seconds. These levels and the level changes during pressurization and depressurization of the system were normal.

At T-0 the system was unpressurized or "soft." Pressure began to develop immediately as the start cartridge rotated the engine turbine. Pressure overshoot reached a maximum of 3180 psia, indicating very good pump compensator response. A steady-state pressure of 2980 psia was reached at $87FS_1$ + 1.31 seconds. During the pressure shutdown monitor period from T + 2 seconds to shutdown lockout, the pressure remained at a steady 2980 psia.

There were no pressure perturbations during flight as the system remained in a stand-by condition. Pressure decayed normally during flight to 2800 psia at staging.

The reservoir level stabilized at 34.2% full after engine start, increasing during flight to 44.2% full at staging. This level increase of 10% was consistent with the observed fluid temperature rise from 87° F at T + 10 seconds to 159° F at staging.

The pressure values quoted were obtained from Sanborn playbacks and digital printouts of telemetered data. It has been determined that the secondary pressure data quoted are low by approximately 100 psi. The error was due to a change in the transducer output subsequent to calibration by the vendor. Such changes are attributed to aging of the transducer. The amount of error was determined by comparing vendor acceptance data on the Stage I pumps with telemetered data. The electric motor-pump pressure at a flow of 1 gpm was 3250 psig when tested by the vendor. This agrees with the value of 3265 psia read from Sanborn records of primary subsystem operation prior to engine start. The primary pressure indication after engine start was 3079 psia which also agrees with the vendor data on the engine pump of 3080 psia at 1 gpm. The secondary system pressure indications were 3160 psia from the electric motor pump and 2972 psia from the engine-driven pump. The vendor secondary system test readings were 3265 psia for the electric motor pump (105 psi higher) and 3080 psia (108 psi higher) for the engine-driven pump.

In Figs. V-1 and V-3, a correction of +100 psi has been applied to the values of GT-3 secondary pressure during the holddown period to depict the true pressure margin over the operating range of the pressure switch used for the shutdown monitor. This margin was 230 to 240 psi, which is more than adequate to cover normal pressure perturbations in the system. A comparison of secondary system pressure from GT-1, GT-2 and GT-3 launches during engine start and holddown is presented in Fig. V-3.

## B. STAGE II

Prelaunch checkout of Stage II hydraulics was initiated at T-4 minutes and was followed by normal system operation. The indicated accumulator precharge was 1850 psia. Electric motor-pump pressure stabilized at a normal 3155 psia. The static reservoir level was 60.6% full, decreasing to 36.7% full after pressure application, and again increasing to 60.3% full upon removal of pressure at T-3 minutes.

During engine startup at staging, the indicated precharge was 1875 psia and the pressure overshoot was to 3655 psia. Steady-state pressure after engine start was 2980 psia, decreasing to 2890 psia, at SECO. No significant pressure perturbations occurred during flight. After SECO, the pressure recovered temporarily and fluctuated with the turbine speed, a normal reaction to the low and variable turbine speeds occurring during this period.

The reservoir level was a normal 60.3% full prior to staging. After staging, the level stabilized at 38.2% full, gradually increasing to 40.0% full at SECO. This level increase of 1.8% is normal and consistent with the fluid temperature rise from 69.5° F at staging to 105° F at SECO.

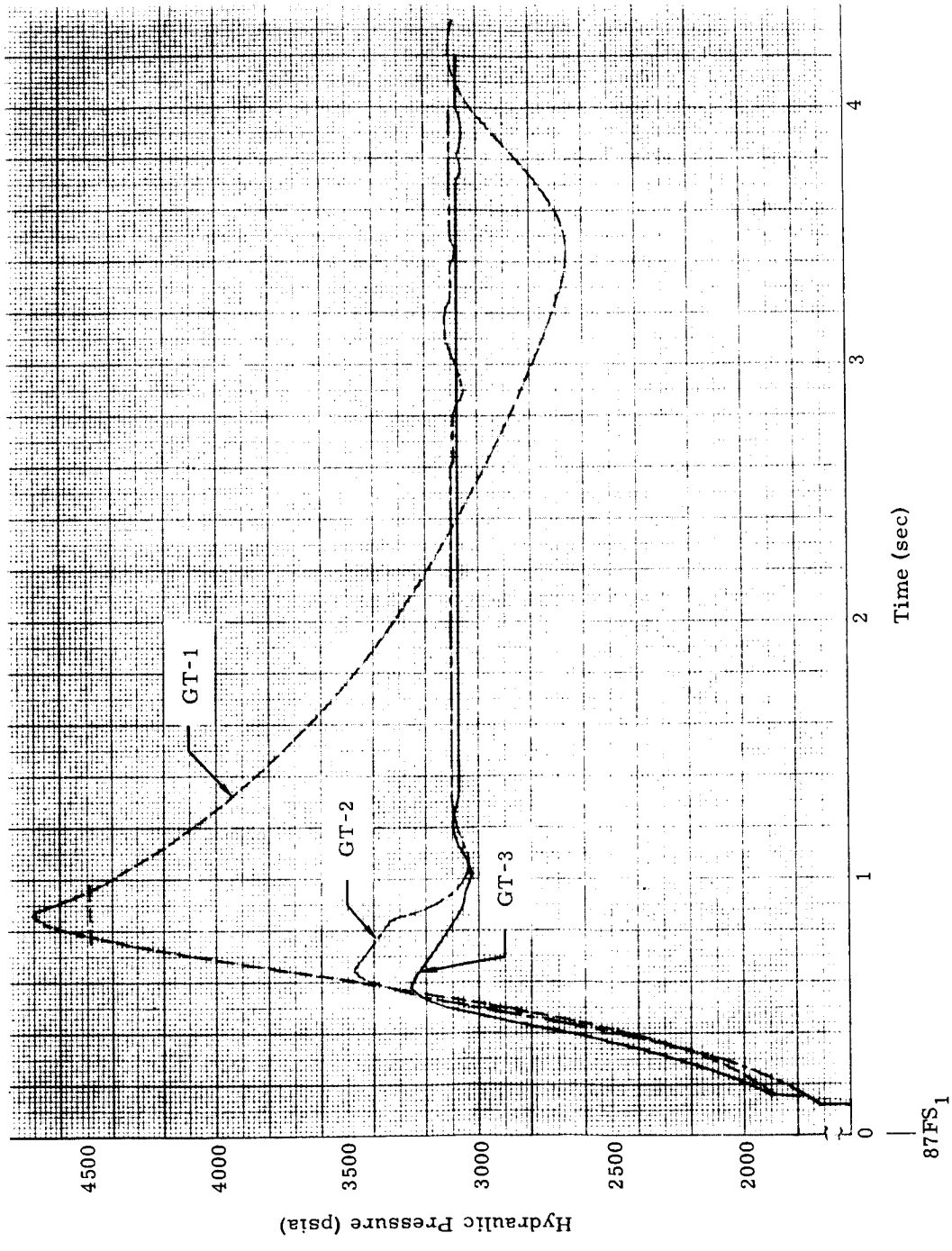


Fig. V-3. Comparison of Secondary System Hydraulic System Pressure During Engine Start and Holddown

# VI. GUIDANCE SYSTEMS

## A. RADIO GUIDANCE SYSTEM PERFORMANCE

### 1. Rate Beacon

The rate beacon performed satisfactorily on the GT-3 flight. Good lock was maintained up to engine ignition, and from approximately LO + 46 to SECO + 50 seconds. Momentary loss of lock at engine ignition is considered normal. Relock occurs as the primary antenna is brought into favorable ground station view.

Values of the rate beacon telemetered functions are presented in Table VI-1.

TABLE VI-1

Rate and Pulse Beacon Parameters

| Function | Measurement | Maximum Value | Minimum Value |
|---|---|---|---|
| Rate Beacon | | | |
| Received signal No. 1 | 0750 | 3.78 | 3.75 |
| Phase detector | 0751 | 3.00 | 2.45 |
| Power out | 0752 | 4.15 | 4.08 |
| Power supply | 0746 | 2.90 | 2.80 |
| Pulse Beacon | | | |
| Magnetron current | 0753 | 2.80 | 2.75 |
| AGC | 0754 | -10 dbm | -53.3 dbm |
| Power supply | 0747 | 4.19 | 4.10 |

The values in Table VI-1 are applicable from prior to liftoff through approximately SECO + 50 seconds. Rate beacon values do not include the momentary unlock at engine ignition, nor values until good lock was acquired at LO + 46 seconds. Pulse beacon values do not include oscillations during antenna crossover period. All values are in telemetry volts except pulse beacon AGC.

## 2. Pulse Beacon

The pulse beacon performed satisfactorily throughout GT-3 flight. Good lock was maintained through engine ignition and up to approximately SECO + 50 seconds.

Normal oscillations during the antenna crossover period were observed in AGC from approximately LO + 41 seconds to LO + 75 seconds. During this period, the minimum signal level received by the beacon was -54.7 dbm.

The ground station signal level increase occurred at LO + 85.2 seconds. The increase was observed to be approximately 15 db.

Values of pulse beacon telemetered functions are listed in Table VI-1.

## 3. Decoder

Proper performance was observed throughout flight. Telemetry data indicate that pitch and yaw steering signals, and the SECO discrete signal were properly executed. No noticeable decoder null drift in pitch or yaw was observed. The decoder power supply maximum and minimum readings (in telemetry volts) were 4.49 and 4.29 volts, respectively, and are applicable from prior to liftoff to approximately SECO + 50 seconds.

## 4. Guidance Commands

### a. Pitch steering

A profile of closed-loop pitch steering in terms of computer commands, decoder pitch telemetry, TARS gyro torquer monitor, and primary Stage II rate gyro is given in Fig. VI-1.

RGS enable. TARS discrete No. 3 (RGS enable) was issued at LO + 162.30 seconds, thereby energizing the airborne guidance initiate relay. Simultaneously, TARS pitch program No. 3 was terminated. This effect can be observed on plots (c) and (d) of Fig. VI-1.

Guidance initiate. At computer guidance initiate (LO + 168.18 seconds for GT-3 flight), a radar validity check was performed to differentiate between bad radar data and actual vehicle dispersions in velocity and altitude. During this check, a preprogrammed pitch-down command was issued. For this flight, the command was 0.2 deg/sec. The duration of the command is a function of magnitude of the altitude and velocity dispersions; however, it is issued for at least 1 computer cycle (0.5 second) and not for more than 8 cycles (4.0 seconds). For this flight, the duration was 0.5 second.

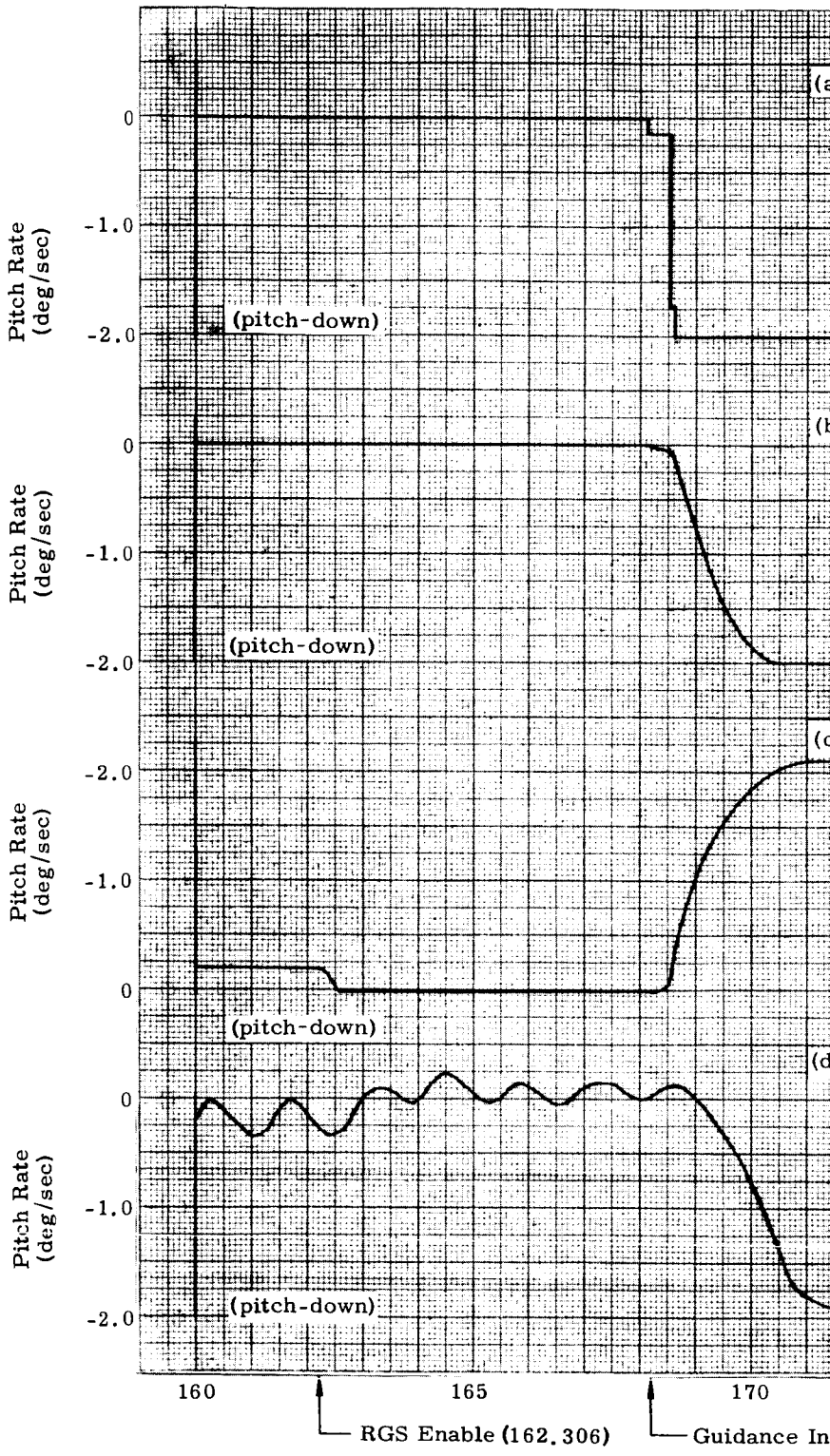
Pitch Rate (deg/sec)
0
-1.0
-2.0
(pitch-down)
Pitch Rate (deg/sec)
0
-1.0
-2.0
(pitch-down)
Pitch Rate (deg/sec)
-2.0
-1.0
0
(pitch-down)
Pitch Rate (deg/sec)
0
-1.0
-2.0
(pitch-down)
160
165
170
RGS Enable (162.306)
Guidance In

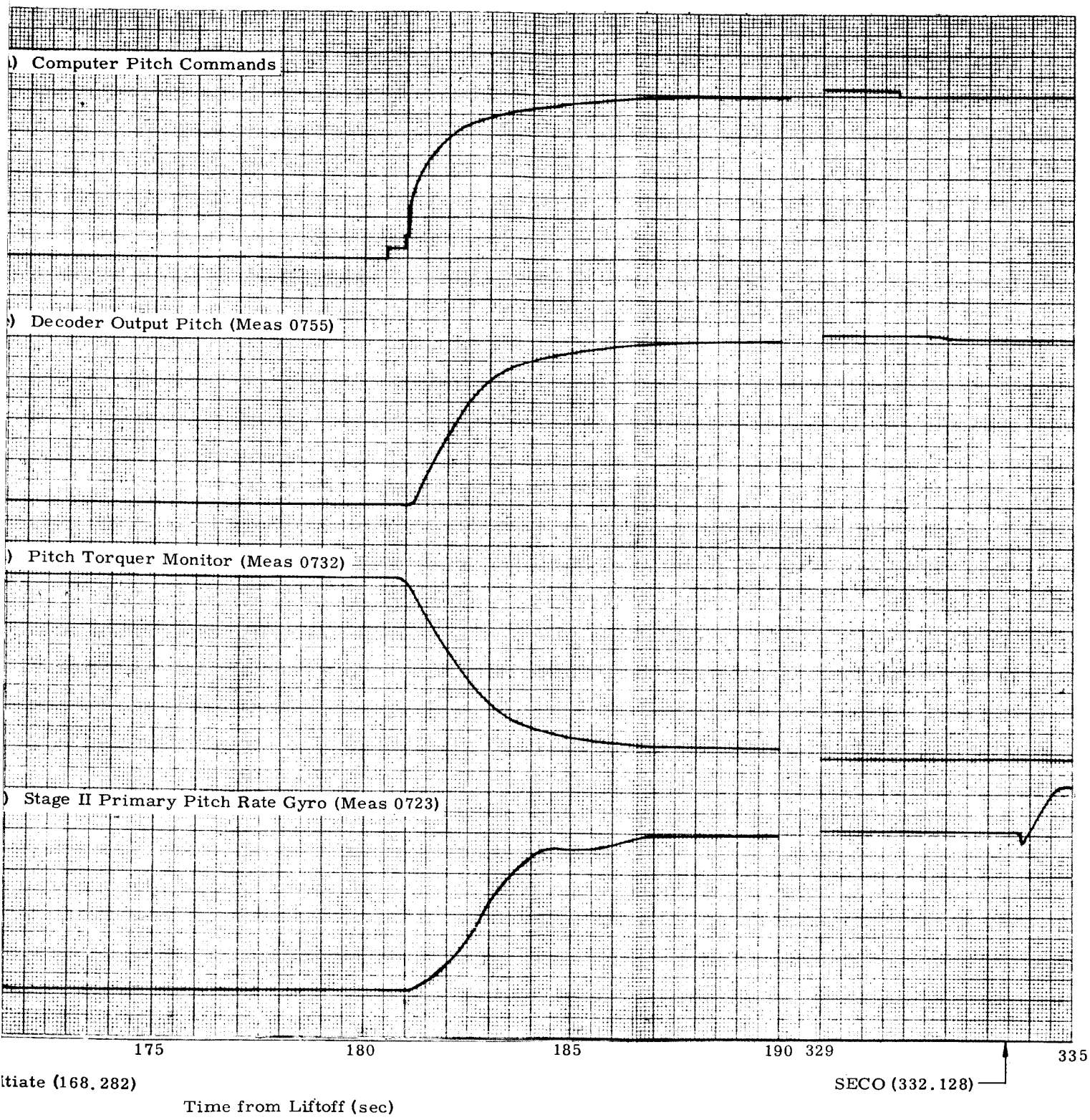


Fig. VI-1. Stage II Pitch Guidance Flight History

Following the 0.2 deg/sec pitch-down command, a 2.0 deg/sec pitch-down command was issued for 12 seconds. A nominal Gemini trajectory requires a 2.0 deg/sec pitch-down command because the Stage I trajectory is purposely lofted to ensure favorable primary antenna look angles in the pitch plane. (The duration of this command is a function of BECO dispersions, primarily in velocity and altitude.)

Throughout the remainder of flight, the computer commands were small, with slow variations from about 0.1 deg/sec pitch-up to about 0.1 deg/sec pitch-down. Guidance was terminated at SECO - 2.8 seconds.

The decoder output, torquer monitor and rate gyro reactions were proper for the computer commands, and are shown in Fig. VI-1.

b. Yaw steering

A profile of closed-loop yaw steering in terms of decoder yaw telemetry is given in Fig. VI-2. The yaw torquer monitor and rate gyro are not shown since the small yaw commands issued resulted in signal variations smaller than the respective resolution of the telemetry of these measurements.

Computer yaw commands were initiated at LO + 169.68 seconds, or 1.5 seconds after the initial pitch-down command of 0.2 deg/sec. The decoder yaw outputs were small, ranging from approximately 0.01 deg/sec yaw-right to 0.02 deg/sec yaw-left for the first 30% of closed-loop guidance, and between zero and 0.025 deg/sec yaw-right for the remaining 70% (approximately). Yaw guidance was terminated at SECO - 2.8 seconds.

c. Discrete commands

The time for the computer-generated ASCO/SECO command and vehicle reactions is presented in the following tabulation.

| Signal | Measurement | GMT Time of Signal | Time from Liftoff (sec) |
|---|---|---|---|
| Ground station ASCO/SECO | * | 1429:33.764 ± 16 ms | 333.700 ± 16 ms |
| Decoder discrete output | 0777 | 1429:33.791 ± 5 ms | 333.727 ± 5 ms |
| $91FS_2$ | 0519 | 1429:33.811 ± 5 ms | 333.747 ± 5 ms |
| ASCO | 0799 | 1429:33.853 ± 25 ms | 333.789 ± 25 ms |

*Time obtained from Burroughs Corporation report.

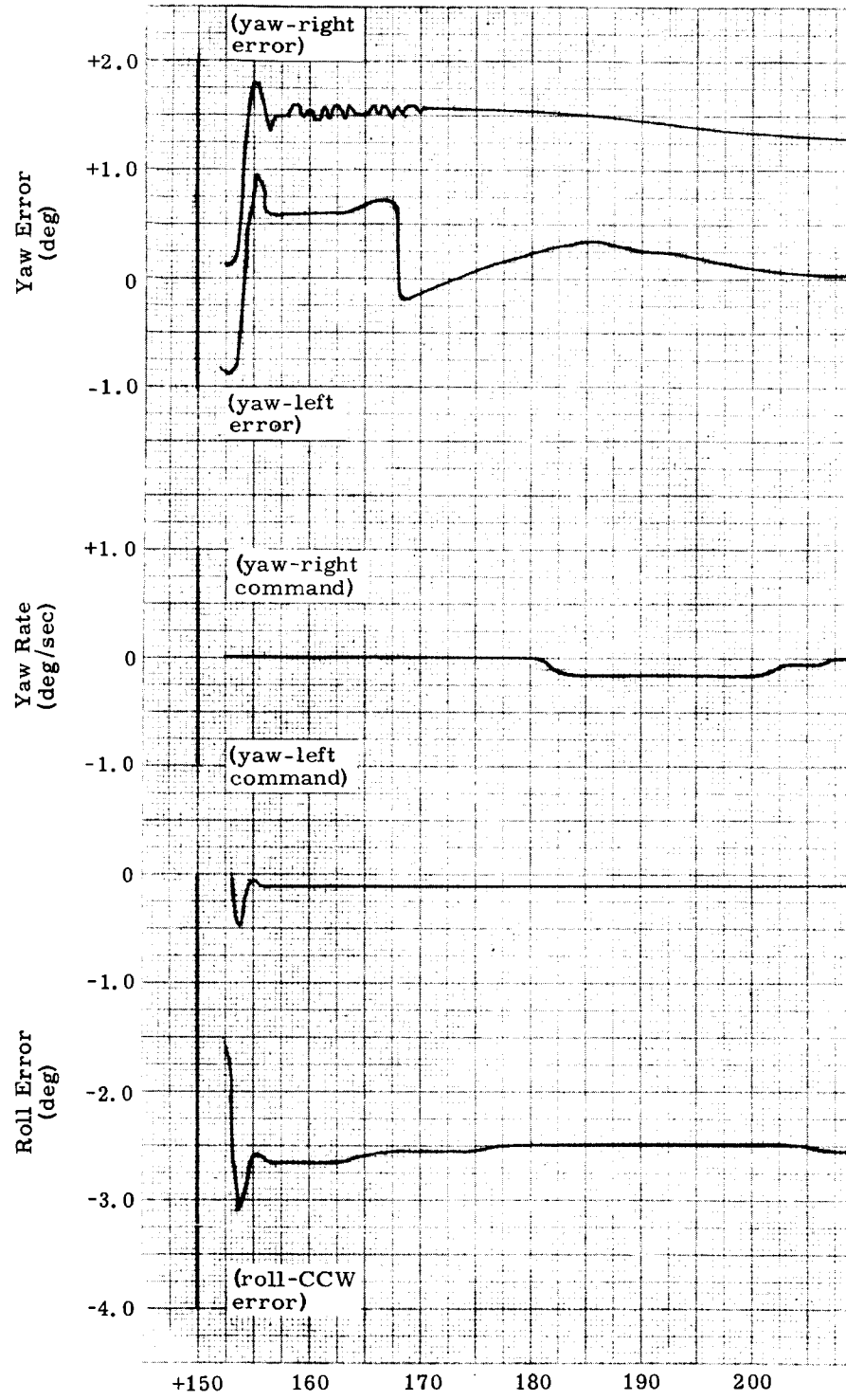
(yaw-right error)
+2.0
+1.0
0
-1.0
Yaw Error (deg)
(yaw-left error)
+1.0
(yaw-right command)
0
Yaw Rate (deg/sec)
-1.0
(yaw-left command)
0
-1.0
-2.0
Roll Error (deg)
-3.0
(roll-CCW error)
-4.0
+150
160
170
180
190
200

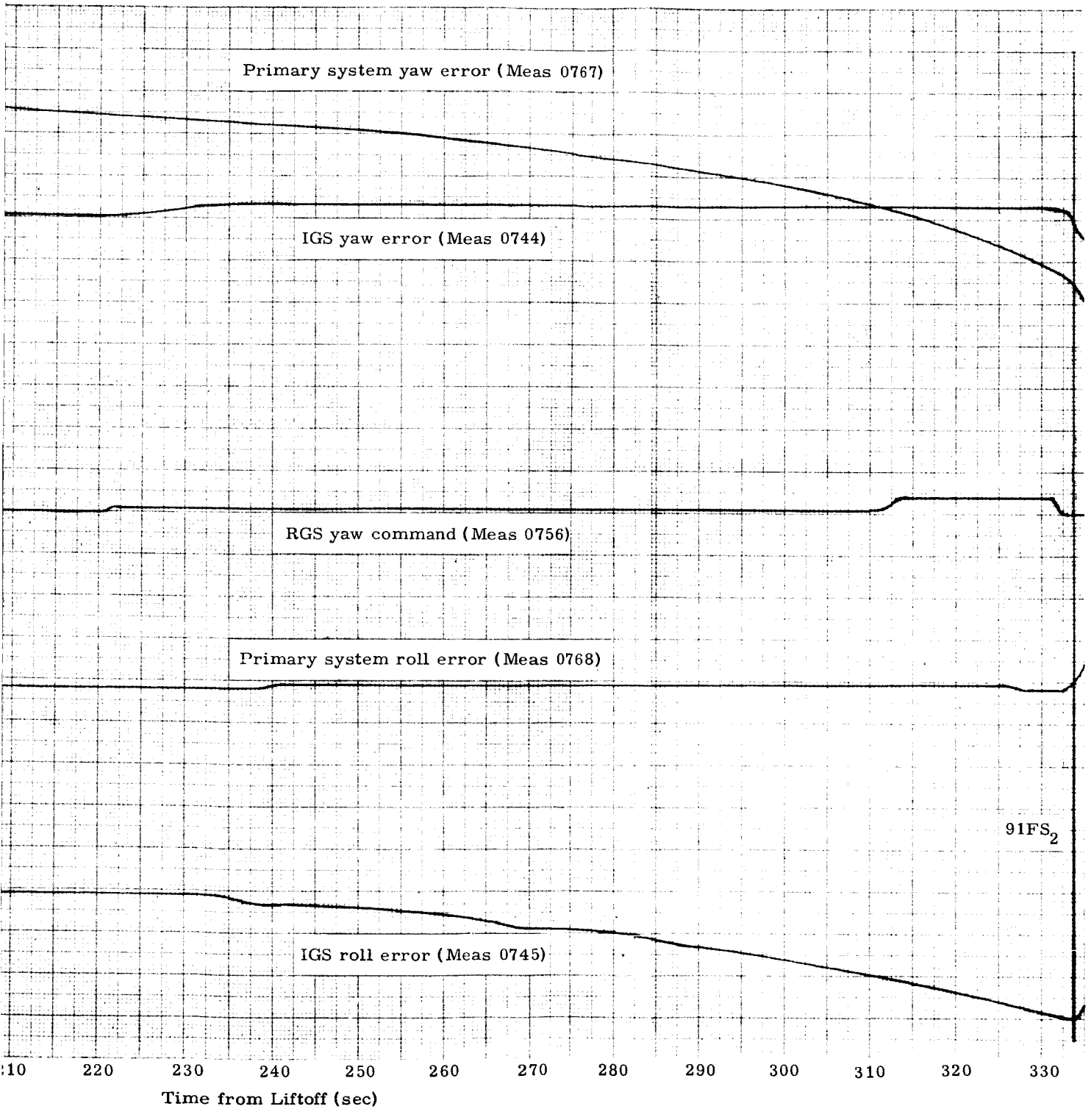


Fig. VI-2. Stage II IGS Yaw/Roll Guidance Flight History

These data indicate that the SECO time delay from ground station issuance to $91FS_2$ was 47 ± 21 milliseconds. The time delay between $91FS_2$ and ASCO reception was 42 ± 30 milliseconds. The time delay between $91FS_2$ and ASCO reception was 42 ± 30 milliseconds.

5. Vibration Environment

Two vibration transducers located in Compartment 2 near the pulse beacon on the rigid intermediate mount were used to measure lateral and vertical vibrations (Meas 1697 and 1698, respectively). The maximum vibration levels observed during the ignition and liftoff period were 1.45 g rms for Meas 1697, and 3.0 g rms for Meas 1698. The maximum lateral vibration level during Stage I flight was 1.25 g rms, and occurred at LO + 53 seconds. The maximum Stage I vertical vibration level was 3.25 g rms, and occurred at LO + 58 seconds.

A detailed analysis, including a power spectra, is given in Chapter XII. These measurements were telemetered during Stage I flight only.

6. Conclusions

The rate and pulse beacons operated properly throughout flight. Pitch and yaw commands were received by the decoder and properly transmitted to the flight control system. The SECO signal was properly transmitted by the decoder. Lateral vibrations during Stage I flight were well within the maximum allowable for Compartment 2 (14.3 g rms).

## B. SPACECRAFT INERTIAL GUIDANCE SYSTEM ASCENT PERFORMANCE

1. Prelaunch Nulls

The prelaunch IGS attitude error nulls were as follows:

| | |
|---|---|
| Pitch (deg) | + 0.056 |
| Yaw (deg) | - 0.135 |
| Roll (deg) | + 0.028 |

These nulls were well within the specification values of ± 0.37 degree in pitch and yaw and ± 0.25 degree in roll.

2. Stage I

IGS performance during Stage I flight was generally good, as determined by a comparison of IGS attitude errors and the corresponding primary system attitude errors.

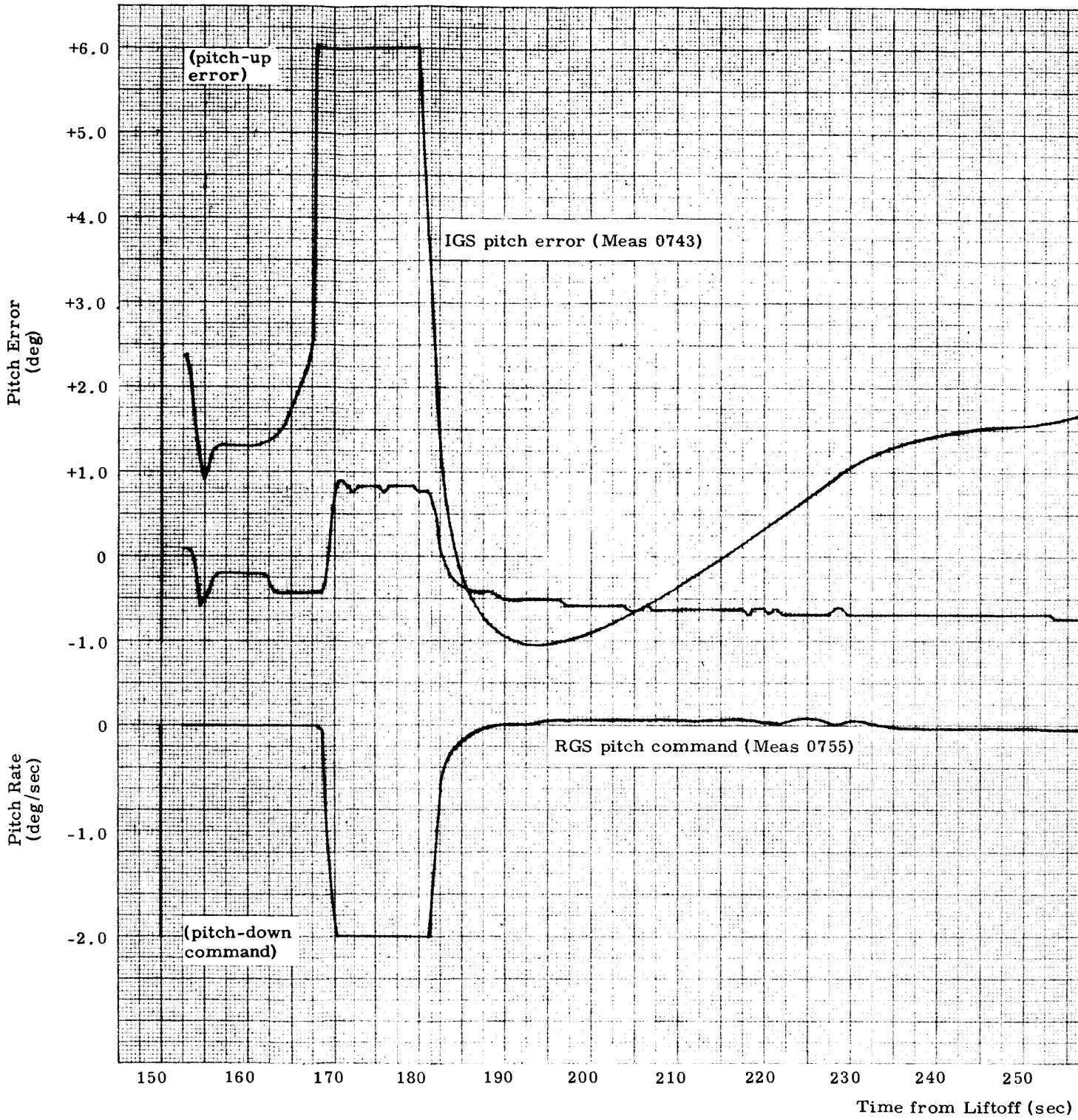
+6.0
+5.0
+4.0
+3.0
+2.0
+1.0
0
-1.0
Pitch Error (deg)
(pitch-up error)
IGS pitch error (Meas 0743)
0
-1.0
-2.0
Pitch Rate (deg/sec)
RGS pitch command (Meas 0755)
(pitch-down command)
150
160
170
180
190
200
210
220
230
240
250
Time from Liftoff (sec)

ER 13227-3

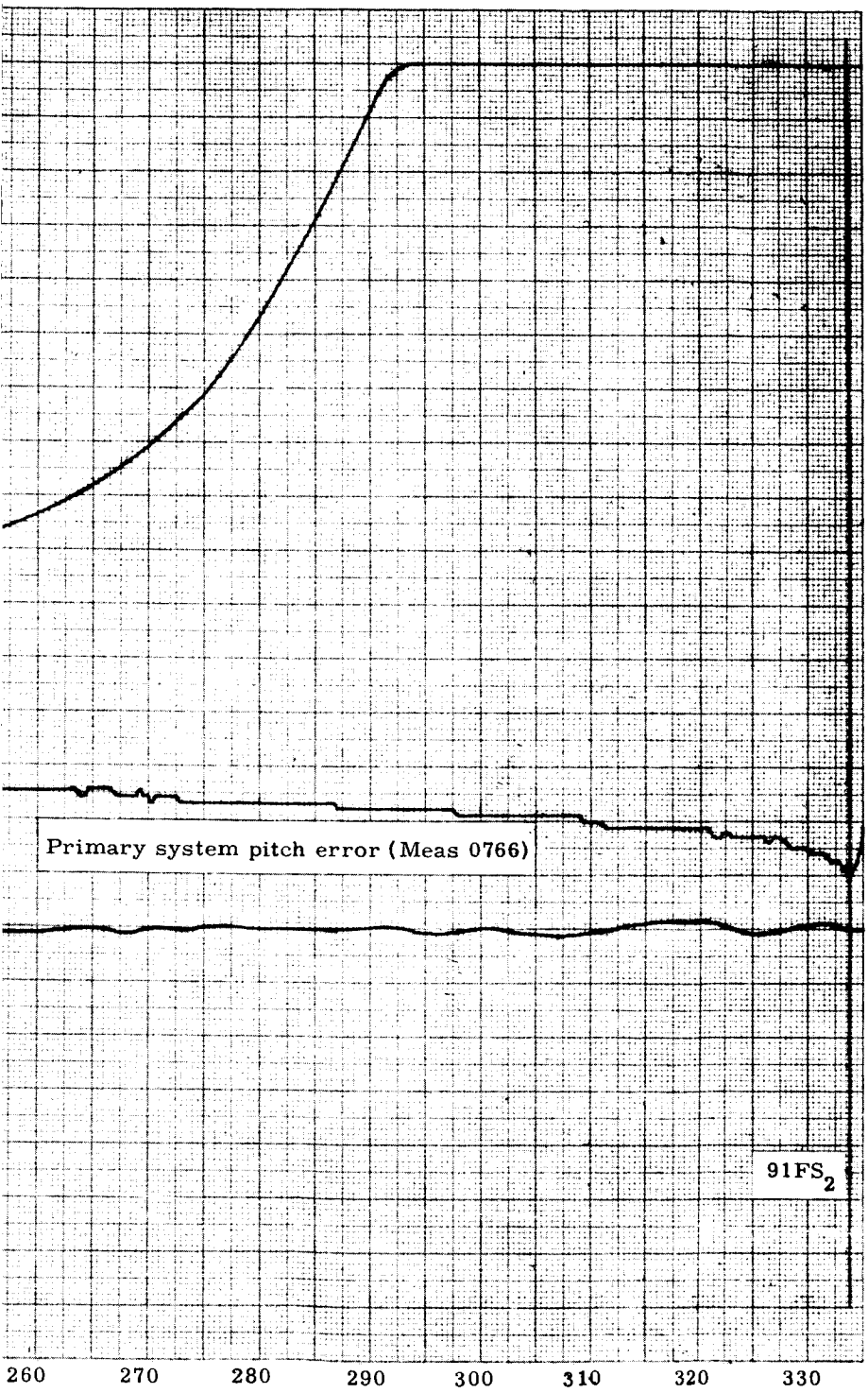


Fig. VI-3. Stage II IGS Pitch Flight History

The Stage I IGS pitch, yaw and roll attitude errors are shown in Figs. IV-2, IV-3 and IV-4, respectively. The BECO dispersions between TARS and IGS are shown in Table IV-3, and are discussed in Chapter IV.

The IGS Stage I gain change discrete was issued at LO + 105.213 ± 0.025 seconds, which is well within the specification time of LO + 104.96 ± 1% seconds.

3. Stage II

IGS yaw and roll performance during Stage II flight appeared normal. Pitch also appeared normal until sometime after start of closed-loop guidance. The attitude error dispersions which had built up between IGS and TARS pitch, yaw and roll during Stage I flight were carried over into the early portion of Stage II flight as shown in Figs. VI-2 and VI-3.

a. Pitch

The ramp buildup of IGS pitch attitude error between approximately LO + 162.5 and LO + 168 seconds is due to the fact that primary system pitch rate No. 3 ended at LO + 162.5 seconds, while the IGS third pitch rate remained until the start of closed-loop guidance.

IGS closed-loop pitch guidance commenced at LO + 168 seconds as expected. IGS pitch attitude error saturated at +6 degrees shortly after LO + 168 seconds, and remained on saturation for approximately 12 seconds. Figure VI-3 shows that the TARS pitch attitude error built up during this time period to approximately +0.85 degree due to the RGS pitch rate command. The reason for the large difference in IGS and TARS attitude errors is due to the fact that, in the primary system, the steering command is limited to a rate of ±2.0 deg/sec, while the IGS limits attitude error only to a nominal 6 degree value. Therefore, IGS pitch behavior during this period appeared normal and compared well with primary system behavior in correcting the vehicle for the high Stage I trajectory.

For the remainder of Stage II flight, the IGS pitch behavior does not correlate with the primary system as depicted in Fig. VI-3. The attitude error built up to the 6 degree limit at LO + 293 seconds, and remained on limit for the remainder of Stage II flight. The expected normal pitch IGS behavior would be to operate near zero attitude error during this period of Stage II flight, assuming normal RGS performance.

An inspection of the IGS unlimited pitch attitude error data, obtained from the spacecraft telemetry system, shows that the attitude error signal would have peaked at approximately 9.4 degrees at LO + 300 seconds (approximate). The attitude error signal decreased to about

6.3 degrees at LO + 322 seconds, then increased to approximately 12.7 degrees at LO + 331 seconds. Inspection of the IGS pitch gimbal angle data, obtained from spacecraft telemetry, indicated that the GLV did not experience such motions. This is confirmed by the TARS output (Fig. VI-3).

Since primary closed-loop guidance operation was normal (as evidenced by the fact that insertion conditions were well within specification), it appears that the IGS was in error in pitch. Had a switchover to IGS occurred prior to SECO, where IGS was indicating a 6 degree positive limited attitude error, the IGS would have inserted the GLV at a more negative flight path angle.

b. Yaw

IGS yaw performance during Stage II flight appeared normal. The IGS yaw attitude error buildup between approximately LO + 168.5 and LO + 180 seconds is due to GLV pitch-down rate (commanded by RGS) coupling into the IGS yaw gimbal. The RGS pitch rate is shown in Fig. VI-3. This type of coupling exists because the IGS roll gimbal is approximately 2.5 degrees off-nominal, as evidenced by the -2.5 degree IGS roll attitude error which exists during this time period (Fig. VI-2).

The reduction in IGS yaw attitude error between approximately LO + 180 and LO + 205 is due to the GLV response to the RGS rate command, as shown in Fig. VI-2. IGS performance for the remainder of the flight correlates with the primary system.

c. Stage II roll

Relative drift between TARS and IGS roll attitude error was in evidence during Stage II flight (Fig. VI-2) and was in the same direction (CCW, TARS with respect to IGS) as the relative drift observed during Stage I flight. The average relative drift rate during Stage II was approximately -36 deg/hr. The relative drift rate increased during Stage II flight, as would be expected due to a g sensitive drift. TARS $3\sigma$ roll drift rates for GT-3 are documented in Ref. 8 which shows that TARS Stage II roll drift alone could exceed the -36 deg/hr average seen on GT-3 flight, even allowing no drift for the IGS.

d. IGS SECO

The IGS SECO discrete was issued at LO + 333.628 ± 0.008* seconds. This compares to the RGS SECO time of 333.727 ± 0.005 seconds. Had a switchover to IGS occurred just prior to SECO, the IGS would have inserted the vehicle approximately 23 ± 3 fps slower than it was inserted by the primary guidance system.

---

*IGS SECO time obtained from NASA source

## 4. Conclusions

IGS yaw and roll performance for the entire GLV flight appeared normal. IGS pitch performance appeared normal for the open-loop portion of flight; however, IGS closed-loop pitch performance was questionable in that the pitch attitude error signal to the GLV autopilot drifted to the 6-degree limit at approximately LO + 293 seconds, and remained on saturation for the remainder of Stage II flight. Also, the IGS SECO discrete was issued earlier than RGS SECO.

Had a switchover to IGS occurred, the vehicle would have been inserted with less velocity and at a more negative flight path angle than was attained by the RGS.

The data reviewed, including IGS gimbal angle and unlimited attitude error data, indicated that it would have been safe to switchover to the IGS from the standpoint of safety-of-flight.

# VII. ELECTRICAL SYSTEM

## A. CONFIGURATION

The GLV-3 airborne electrical system components installed for the GT-3 mission were similar to those employed for GT-2 except for the addition of the shutdown squib relay assembly.

## B. COUNTDOWN AND FLIGHT PERFORMANCE

The airborne electrical system functioned as designed throughout the seven-hour prelaunch countdown and during flight, and all parameters were within specification. Power transfer to airborne batteries was comparatively smooth, and liftoff occurred without incident.

During the staging event, examination of the APS and IPS current traces indicated no ordnance squib shorts to structure. Data from the GT-2 flight indicated that the Stage II engine start squib on the APS bus and one separation nut on the IPS bus had shorted to structure at staging.

At spacecraft separation, the launch vehicle/spacecraft electrical interface was cut by a guillotine in the adapter. This caused a momentary rise in APS and IPS bus currents, indicating transient shorting of the normal GLV interface signals to the adapter structure. The APS bus current rose approximately 11 amperes and the IPS current rose 9 amperes for less than 150 milliseconds. This transient effect is an expected phenomenon, since several active signals are normally maintained across the launch vehicle/spacecraft interface up to separation.

The shutdown squib relay assembly (used in the Stage II redundant shutdown system) functioned as designed. A summary of the electrical system parameters prior to liftoff and during significant flight phases appears in Table VII-1.

## TABLE VII-1

### GLV-3 Electrical System Parameters

| Meas | Description | At Power Transfer | | | At Liftoff | At $87FS_2/91FS_1$ (Staging) | | | At Spacecraft Separation | | |
|---|---|---|---|---|---|---|---|---|---|---|---|
| | | Before | During | After | | Before | During | After | Before | Peak | After |
| 0800 | IPS (volts) | 28.9 | 28.1 | 29.7 | 29.7 | 29.3 | 29.0 | 29.4 | 29.6 | 29.3 | 29.6 |
| 0804 | IPS (amp) | 36.3 | 35.3 | 36.3 | 35.5 | 37.9 | 42.1 | 33.7 | 33.7 | 42.7 | 33.7 |
| 0801 | APS (volts) | 29.1 | 29.4 | 30.1 | 29.7 | 29.6 | 29.3 | 30.1 | 29.7 | 29.4 | 29.9 |
| 0805 | APS (amp) | 31.5 | 31.5 | 31.5 | 35.8 | 30.4 | 36.4 | 19.4 | 24.9 | 36.4 | 21.3 |
| 0802 | 400 cycle Phase A (volts) | 114.4 | 114.4 | 114.4 | 114.4 | 114.3 | 114.3 | 114.3 | 114.1 | 114.1 | 114.3 |
| 0803 | 400 cycle Phase A (cps) | 400.7 | 400.7 | 400.7 | 400.7 | 400.5 | 400.5 | 400.5 | 400.5 | 400.5 | 400.5 |
| 0726 | 25 vdc power supply (volts) | 25.3 | 25.3 | 25.3 | 25.3 | 25.3 | 25.3 | 25.3 | 25.3 | 25.3 | 25.3 |

# VIII. INSTRUMENTATION SYSTEM

## A. AIRBORNE INSTRUMENTATION

### 1. Prelaunch and Countdown Status

Between simulated flight test on 18 March 1965 and launch day, the PCM/FM transmitter was replaced because of a loose pressurization valve. During countdown, the system operated within specified limits.

### 2. Data Acquisition

The entire airborne telemetry and instrumentation system operated in a satisfactory manner throughout countdown and flight. The measurement program for this launch consisted of 184 PCM analog signals, 46 PCM bilevel signals, and 12 FM/FM analog signals. All channels functioned throughout flight resulting in 100% data acquisition.

### 3. Instrumentation System Parameters

Instrumentation system parameters, as measured in-flight, are compared with required values for significant events in Table VIII-1.

### 4. Anomalies

Measurement 0517 (bootstrap fuel venturi inlet pressure--S/A 3) exhibited 41 dropouts lasting up to 1/2 second during second-stage powered flight. Each dropout had similar characteristics, i.e., a rapid drop in level and an overshoot before the signal returned to normal running level. This behavior appears to be indicative of a transducer malfunction. The balance of the data from this measurement, when compared with GT-2 flight data, is considered valid.

Measurement 0029 (bootstrap fuel venturi inlet pressure--S/A 2) dropped below its nominal operating level at LO + 92.55 seconds, returning to a normal value at LO + 93.6 seconds, and functioned satisfactorily thereafter. The signal decay was too rapid to be the filter capacitor discharge through the encoder, thus indicating that the transducer was still connected to the encoder channel. The momentary signal drop probably occurred within the transducer; however, all other data from this measurement were valid.

### 5. Telemetry Signal Strength (237.0 and 244.3 mc)

Telemetry signal strength records indicated satisfactory signal levels from the launch vehicle from liftoff to approximately SECO + 83 seconds. The anticipated staging blackout occurred and lasted approximately 250 milliseconds.

TABLE VIII-1

Instrumentation System Parameters

| Meas | Description | Required PCM Count | Required Value Engineering Units | PCM Count and Engineering Units | | | |
|---|---|---|---|---|---|---|---|
| | | | | Liftoff | $87FS_2$ $91FS_1$ | $91FS_2$ | SECO + 20 sec |
| 0810 | 5 volt power supply | 204 ±1 | 5.000 v ±0.025 | 204 5.029* | 204 5.029* | 204 5.029* | 204 5.029* |
| 0811 | 40 volt power supply | 229 ±3 | 40.00 v +0.51 -0.18 | 229 40.15 | 229 40.15 | 229 40.15 | 229 40.15 |
| 0812 | Signal conditioner package temperatures | N/A | 104° to 126° F | 107 116.7 | 104 114.1 | 103 113.4 | 103 113.4 |
| 0813 | PCM mercury battery | 72 to 74 | 1.315 v to 1.355 v | 73 1.355 | 73 1.355 | 72 1.335 | 72 1.335 |
| 0814 | PCM mercury battery | 72 to 74 | 1.315 v to 1.355 v | 73 1.355 | 73 1.355 | 72 1.335 | 72 1.335 |
| 0815 | PCM mercury battery | 72 to 74 | 1.315 v to 1.355 v | 74 1.375* | 74 1.375* | 73 1.355 | 73 1.355 |
| 0816 | +30 volt power supply | 174 ±3 | 29.91 v to 30.02 v | 175 29.99 | 175 29.99 | 175 29.99 | 175 29.99 |
| 0817 | -30 volt power supply | 199 ±3 | -29.91 v +30.05 v | 199 -29.99 | 199 -29.99 | 199 -29.99 | 199 -29.99 |

*Reading high due to encoder resolution. The encoder counts in 1-bit steps; each bit = 20.08 mv.

Cape Kennedy Tel II and Tel III ground stations monitored the entire flight of the launch vehicle. The Grand Bahama Island station acquired data from approximately LO + 45 seconds to the end of flight. The Grand Turk station acquired data during Stage II flight beginning at approximately LO + 173 seconds.

Review of playbacks made from the data recorded on magnetic tape at Tel II indicates that a dropout of less than one second occurred at approximately LO + 69.2 seconds. This dropout did not appear on records made from the Tel III or Hangar T ground stations' magnetic tapes.

## B. LANDLINE INSTRUMENTATION

### 1. Countdown Status

The entire landline instrumentation system functioned satisfactorily prior to and up to liftoff. All airborne instrumentation hold functions monitored in the blockhouse remained within specification limits throughout the countdown.

### 2. Data Acquisition

Data acquisition was 100% on 51 channels programmed as follows:

14 propellant temperatures on Bristol multipoint recorder No. 2.

3 start cartridge temperatures on Bristol multipoint recorder No. 1.

2 air-conditioning system temperature on Bristol strip chart recorders.

1 air-conditioning system pressure measurement on Bristol strip chart recorder.

4 launch vehicle tank pressures on Bristol strip chart recorders

8 event signals on a 78-channel Brush events recorder.

9 a-c and d-c electric power source measurements on oscillograph recorder.

6 BLH base reaction load measurements on magnetic tape via voltage-controlled oscillators.

1 BLH total vehicle weight measurement on a digital printout.

2 hydraulic pressure switch signals on magnetic tape via voltage-controlled oscillators.

1 d-c electric power source measurement on a Sanborn analog recorder.

In addition, landline measurements were observed or recorded on the following backup channels:

16 voltage-controlled oscillator channels for recording on magnetic tape.

14 digital voltmeter channels.

1 vehicle total weight visual digital display.

# IX. RANGE SAFETY AND ORDNANCE SYSTEMS

## A. COMMAND CONTROL RECEIVERS

### 1. Countdown

The command receivers ASCO checkout between T-280 and T-270 minutes, the shutdown and destruct checkout at T-235 minutes, and the final ASCO check at T-15 minutes were performed satisfactorily. The command receiver telemetry data indicated a signal level greater than 100 microvolts from T-5 minutes through liftoff.

### 2. Flight Results

Advanced Communications Incorporated (ACI) command control receivers (S/N 31 and 32) were installed in GLV-3. Telemetered command control receiver parameters monitored during powered flight showed that receiver operation was satisfactory. Receiver RF input signal ranged from a maximum level of approximately 5000 microvolts (experienced when the Cape transmitter went to high power) to a minimum of approximately 20 microvolts at the end of Stage II flight. The receivers successfully responded to the Mod III ASCO signal at LO + 333.789 ± 0.025 seconds which was within the expected time interval. When the ASCO signal was transmitted to the receiver by the command transmitter at Grand Bahama Island, the RF signal level was approximately 20 microvolts.

A ground station problem with the Cape transmitter occurred shortly after the switch from low to high power. The DRUL system sampling of DCS data quality indicated an improper level, and the transmitters were automatically switched from primary to standby. It was determined that the problem was not with the transmitter and a manual switchback from secondary to primary was performed. The transmitter switching appears on the receiver relative signal strength trace as a loss of signal. The approximate times for the switching events were as follows:

(1) Start DRUL transmitter switch (primary to secondary) at LO + 76.738 seconds; end at LO + 77.138 seconds.

(2) Start manual switchback (secondary to primary) at LO + 87.338 seconds; end at LO + 87.488 seconds.

It has been reported that the problem with the ground station was improper operation of the NASA QUAD steerable antenna when the transmitting system was switched from low to high power. The problem will be corrected by the responsible agency.

## B. MISTRAM SYSTEM

### 1. Countdown

The MISTRAM open loop checks with the MACK station from T-390 to T-330 minutes and from T-30 to T-10 minutes were performed without incident. A review of MISTRAM telemetry showed that the transponder was locked on to the MACK station signals from T-5 minutes until LO - 0.513 ± 0.025 seconds. The MACK station transmit signal is manually turned off at liftoff so that it will not interfere with the downrange tracking stations.

### 2. Flight Results

a. Airborne transponder

The GE transponder (S/N 95) was installed in GLV-3. Analysis of the MISTRAM telemetry records for Stages I and II boost flight indicates that the overall performance of the airborne MISTRAM system was very good. The MISTRAM I station started to sweep the calibrate CW signal at about LO + 30 seconds, and from this period until SECO there were no unlocks of either the range or calibrate channel. This is an unusual occurrence since the ionization caused by the Stage II engine plume will usually attenuate the incoming signal to a point below the threshold of the transponder. The transponder telemetry shows that the calibrate channel acquired the Valkaria signal at LO + 1.5 seconds and the range channel was acquired at LO + 4.6 seconds.

### 3. Ground Stations Operation

a. Valkaria station (MISTRAM I)

Valkaria station started active tracking at approximately LO + 41 seconds and continued until LO + 153.5 seconds. Valkaria picked up active track again at LO + 164 seconds and continued until LO + 384 seconds. The handover from MISTRAM I (Valkaria) to MISTRAM II (Eleuthera) took place at LO + 389 seconds. MISTRAM I was used as a data source for the range safety impact predictor for 69% of the time during launch vehicle powered flight. The source data for primary and secondary range safety plot boards are included in Table IX-1.

b. Eleuthera station (MISTRAM II)

The Eleuthera station performed in active track mode from LO + 389.4 seconds until LO + 401.4 seconds and continued intermittently in active track until LO + 435.8 seconds. MISTRAM II was not used as source data for the range safety plot boards on this launch.

TABLE IX-1

Range Safety Plot Board Data Source

| Primary Plot | | Secondary Plot | |
|---|---|---|---|
| Data Source | Total Time Source Used (sec) | Data Source | Total Time Source Used (sec) |
| MISTRAM I | 290.9 | GE Mod III | 330.6 |
| Merritt Island TPQ18 radar | 38.2 | Merritt Island TPQ18 radar | 106.3 |
| Patrick AFB TPQ18 radar | 67.6 | Patrick AFB TPQ18 radar | 18.4 |
| Grand Bahama Island TPQ18 radar | 16.7 | Grand Bahama Island TPQ18 radar | 71.6 |
| Grand Bahama Island FPS16 radar | 23.4 | Grand Bahama Island FPS16 radar | 22.7 |
| Grand Turk Island TPQ18 radar | 113.7 | Grand Turk Island TPQ18 radar | |
| Total | 549.6 | Total | 549.6 |

## C. ORDNANCE SYSTEM

All ordnance systems associated with the dropweight and engine prevalves operated as required during the GLV-3 countdown and launch operations.

The eight launch nuts actuated as required at launch. This fact was established when all four lower nuts and interconnecting studs were found on the pad after the launch.

The airborne staging system operated as required during the staging sequence. The TARS issued a staging arm signal at LO + 144.431 seconds, and the staging arm timer issued a staging arm signal at LO + 145.133 seconds. Both times were within specification limits and consistent with the trend data from previous GLV-3 tests.

# X. MALFUNCTION DETECTION SYSTEM

## A. CONFIGURATION

The malfunction detection system (MDS) and associated hardware performed satisfactorily during the GT-3 countdown and flight. Significant MDS components appear in Table XVII-1.

Table X-1 presents the MDS hardware change-out history for GLV-3.

## B. SYSTEM PERFORMANCE

### 1. Engine Pressure Switches

Operation of the Stage I engine malfunction detection thrust chamber pressure switches (MDTCPS) and the Stage II engine malfunction detection fuel injector pressure switches (MDFJPS) is summarized in Table X-2. These switches are required to "make" in a pressure range of 540 to 600 psia and "break" in a pressure range of 585 to 515 psia. The Stage I engine start transient was of sufficient amplitude and time duration to cause the S/A 1 MDTCPS switches to momentarily respond to the thrust chamber pressure. All MDS engine pressure switches operated properly and within the specification requirements.

TABLE X-2

MDS Engine Pressure Switch Operation

| Operation | S/A 1 (Meas 0356) | S/A 2 (Meas 0357) | S/A 3 (Meas 0855) |
|---|---|---|---|
| Make | 1423:57.609 GMT at 590 psia | 1423:57.700 GMT at 585 psia | 1426:33.148 GMT* |
| Break | 1426:32.441 GMT at 525 psia | 1426:32.442 GMT at 523 psia | 1429:33.952 GMT* |

* S/A 3 fuel injector pressure was not instrumented on GLV-3; hence, make and break pressures were not available.

### 2. Switchover

The MDS switchover circuitry responded properly throughout the flight. There were no switchover commands and no switchover was executed, indicating proper performance of the switchover circuitry.

# TABLE X-1

## MDS Hardware History

| Component | Installed and Tested Configurations | | | | | | | | | | |
|---|---|---|---|---|---|---|---|---|---|---|---|
| | VTF Testing | | | | | ETR Testing | | | | | |
| | SSFVT | Data Acquisition | Run No. 1 CSAT | Partial SSFVT | Run No. 2 CSAT | SSFVT | CST | JCST | EIIV | FCMT | WMSL |
| Rate switch package PS830600015 | -023 | -023 | -023 | [3] -027 | -027 | [5] -027 | -027 | -027 | -027 | -027 | -027 [1] |
| Malfunction detection package 424-7569205 | -169 | -169 | -169 | -169 | -169 | [2] -189 | -189 | -189 | -189 | -189 | -189 |
| Staging disconnect Plug | -5 | -5 | -5 | -5 | -5 | -5 | -5 | -5 | -5 | -5 | -5 |
| Receptacle 8119A1 | -6 | -6 | -6 | -6 | -6 | -6 | -6 | -6 | -6 | -6 | -6 |
| Tank pressure sensor Stage I PS746000002 | -013 | -013 | -013 | -013 | -013 | [4] -023 | -023 | -023 | -023 | -023 | -023 |
| Stage II PS746000002 | -015 | -015 | -015 | -015 | -015 | [4] -025 | -025 | -025 | -025 | -025 | -025 |
| Engine MDS sensors Stage I | 284321 | 284321 | 284321 | 284321 | 284321 | 284321 | 284321 | 284321 | 284321 | 284321 | 284321 |
| Stage II | 284321 | 284321 | 284321 | 711049 [3] | 711049 | 711049 [5] | 711049 | 711049 | 711049 | 711049 | 711049 |

NOTES:

1. Changed out due to elapsed calibration check periods.
2. Same package was modified and reinstalled, and the revisions included RSP noise suppression, switchback capability and improved wiring insulation.
3. Removed the 40-second shutdown lockout timers, rate switch package and Stage II MDTCPS change-out.
4. Incorporation of ECP 426, Revise Wiring Identification Procedure on MDS Tank Pressure Transducers.
5. Incorporation of ECP 424, MDS Stage I Engine and Staging Signal Circuit Revision.

## 3. Vehicle Rate Detection

The spin motor rotation detectors (SMRDs) contained in the malfunction detection package (MDP) functioned properly. The SMRDs monitor rate switch package (RSP) gyro speed and, thereby, rate sensing capability.

The RSP operated properly throughout the countdown and flight. There were no vehicle overrates detected by the MDS (rate switch operations) and none occurred during flight from liftoff through SECO + 20 seconds. Table X-3 compares the maximum launch vehicle rates (measured during the period from liftoff through SECO + 20 seconds) with the RSP switch settings.

TABLE X-3

Maximum Vehicle Rates Versus Rate Switch Settings

| | | Stage I Flight | Flight Event | Stage II Flight | Flight Event |
|---|---|---|---|---|---|
| Rate switch settings (deg/sec) | Pitch | +2.5; -3.0 | N/A | ±10 | N/A |
| | Yaw | ±2.5 | N/A | ±10 | N/A |
| | Roll | ±20.0 | N/A | ±20 | N/A |
| Maximum vehicle rates (deg/sec) | Pitch | -0.97 | Pitch program | -1.90 | Guidance command |
| | Yaw | -0.87 | Wind disturbance | +1.44 | Staging |
| | Roll | +1.53 | Liftoff | -2.08 | Staging |

Following spacecraft separation (SECO + 25.6 seconds), there were two operations of the yaw rate switches. The yaw rate gyro outputs verified that the rate switch performance was in agreement with the RSP calibration data. Table X-4 summarizes the yaw rate switch operation.

TABLE X-4

Yaw Rate Switch Operation

| Specification Operation Limits (deg/sec) | RSP Calibration Data | | Time of Rate Switch Operation | Rate Gyro Output | |
|---|---|---|---|---|---|
| | Primary (deg/sec) | Redundant (deg/sec) | | Primary (deg/sec) | Redundant (deg/sec) |
| Closed 2.08-2.92 | 2.40 | 2.57 | SECO + 35.534 sec | 2.57 | 2.43 |
| Open 2.57-1.80 | 2.31 | 2.28 | SECO + 38.584 sec | 2.28 | 2.23 |

4. Tank Pressure Sensors

All MDS tank pressure transducers operated properly throughout the countdown and flight. The maximum differences between the transducer pairs on each tank are presented in Table X-5.

Figure X-1 presents the calibration curves for the Stage I fuel tank pressure transducer pairs (A and B) to clarify the percentage variations between voltage and psi as shown in Table X-5. The maximum difference of 1.40% of transducer full-range output voltage is well within the transducer and telemetry system errors.

TABLE X-5

Maximum Voltage and Pressure Differences Between Tank Pressure Transducer Pairs

| | Maximum Difference | | | |
|---|---|---|---|---|
| | ΔVolts (telemetry) | Percent of Transducer Full Range | ΔPSI | Percent of Transducer Full Range |
| Stage I fuel | 0.040 | 0.80 | 0.43 | 0.86 |
| Stage I oxidizer | 0.060 | 1.20 | 0.50 | 1.00 |
| Stage II fuel | 0.060 | 1.20 | 0.67 | 0.89 |
| Stage II oxidizer | 0.070 | 1.40 | 1.07 | 1.43 |

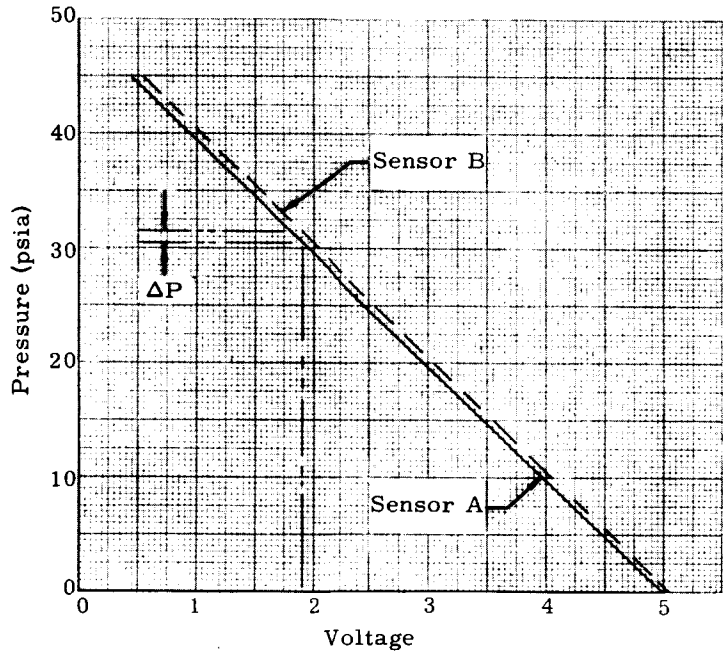


Fig. X-1. Calibration Curves for Stage I Fuel Tank Pressure Transducers

# XI. CREW SAFETY

GT-3 was the first manned flight in the Gemini Program and, as such, constituted the first "operational" test of the crew safety program; however, the crew safety program had been exercised on the unmanned GT-1 and GT-2 missions. On GT-3 the operations were performed satisfactorily and without incident.

## A. PRELAUNCH SIMULATIONS

Preflight wind measurements from Cape Kennedy were data-card transmitted to Martin-Baltimore and used as inputs to three computer programs. One digital program evaluated the wind conditions by comparing actual measurements against specification wind speeds and wind shears. A second digital program was used to compute the wind-affected trajectory. A third analog program determined the vehicle bending loads and the control system transients for the wind-affected trajectory. Subroutines were then used to establish the first-stage propellant tank underpressure constraints and the slow malfunction action thresholds for flight control system (FCS) switchover. The results were sent periodically by phototelegraphy to Martin-Canaveral prior to launch.

All portions of the program worked smoothly. Balloon soundings, data-card transmissions, IBM 1620 wind computations, IBM 7094 trajectory computations, analog flight load simulations, the communications network, the phototelegraphy of documents to Cape Kennedy, and the delivery of these documents to Complex 19 and to the Mission Control Center (MCC) were accomplished on schedule. A brief summary of all computer runs is presented in Table XI-1.

### 1. Trajectory Simulation

Of the six wind profiles (Figs. XI-1, XI-2 and XI-3), the soundings released by the Air Force at T-12, T-5, T-3, and T-1 hour (Figs. XI-2 and XI-3) were programmed into the IBM 7094 Gemini trajectory program. Results of the first three trajectory simulations were delivered to the MCC for use in plotboard revisions of the nominal trajectory as affected by winds. The results of the T-1 hour run were sent to Cape Kennedy after the launch.

The T-3 hour simulation indicated a peak lateral velocity of +82 fps at LO + 83 seconds, and a peak $\gamma$ of 26.5 degrees at LO + 75 seconds. The wind effect was to depress the nominal trajectory.

TABLE XI-1

Summary of Prelaunch Wind Monitoring Operations

| Run Schedule | Time of Data Release to Martin-Baltimore | Type of Operation |
|---|---|---|
| First | F-2 day | Wind evaluation; sent to Martin-Canaveral (M-C) |
| Second | F-1 day | Wind evaluation; sent to M-C |
| Third | T-12 hr* | Computed wind evaluation, load, analog and trajectory simulations and constraints; data sent to M-C; winds were GO |
| Fourth | T-5 hr* | Computed wind evaluation, load, analog and trajectory simulations and constraints; data sent to M-C; winds were GO |
| Fifth | T-3 hr* | Computed wind evaluation, load, analog and trajectory simulations and constraints; data sent to M-C; winds were GO |
| Sixth | T-1 hr* | Computed wind evaluation and updated wind status by telephone to M-C before liftoff; winds were GO; load, analog and trajectory simulations were then sent to M-C for reference |

*Based upon T-0 at 0900 hours EST.

## 2. Loads Simulation

The winds-aloft launch recommendations for the GT-3 flight were based upon the results obtained from analog computer load simulation runs at Baltimore. Four simulations were run using winds data released at T-12, T-5, T-3 and T-1 hours. Computed ratios of equivalent axial load to equivalent axial limit strength at launch vehicle Station 935 were 0.83, 0.81, 0.79 and 0.82, respectively. These loads were below limit strength; thus, all recommendations were GO. The simulations showed that peak loads would occur from 72 to 78 seconds after liftoff.

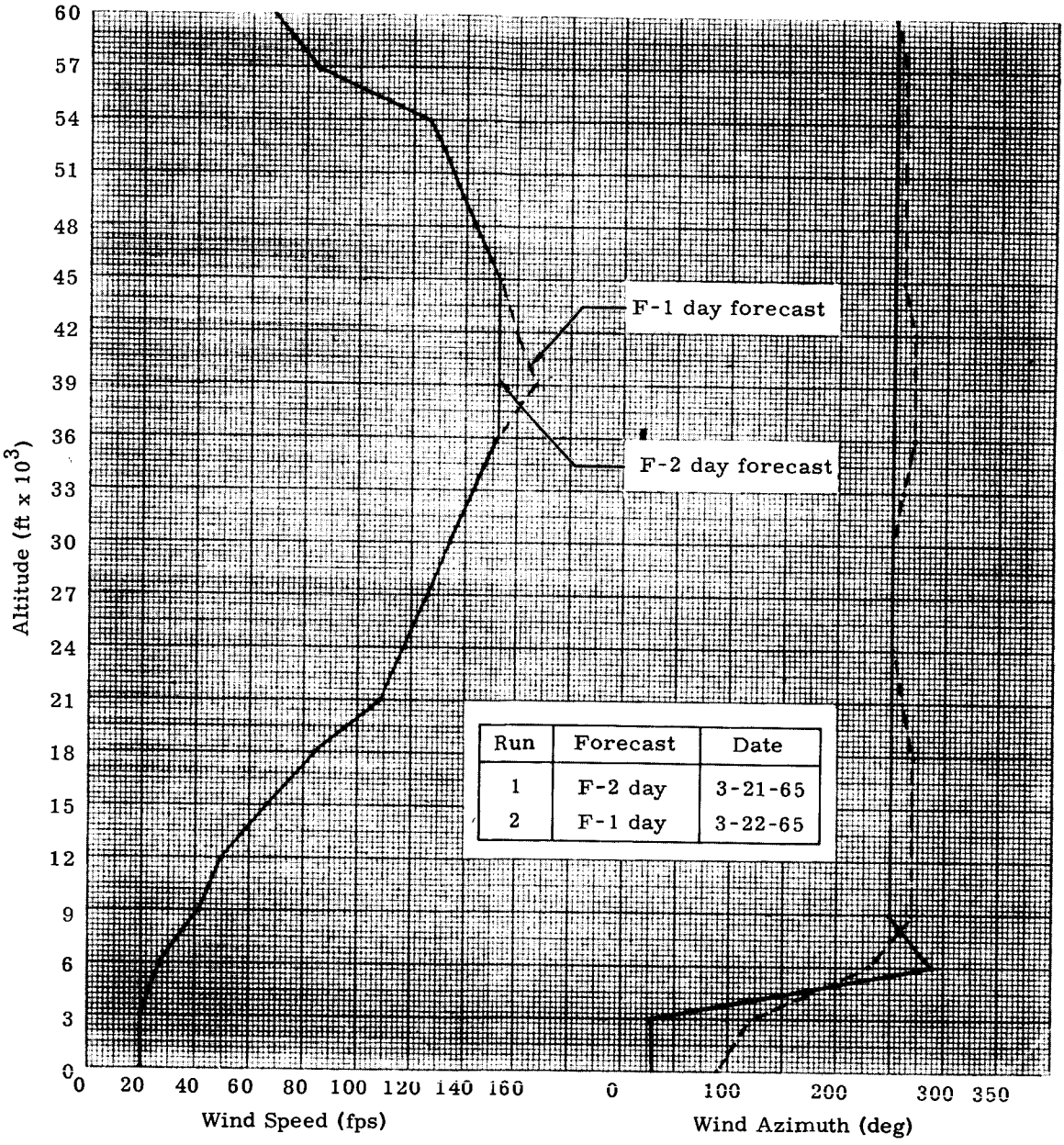


Fig. XI-1. Launch Winds Forecast for T + 0

~~CONFIDENTIAL~~

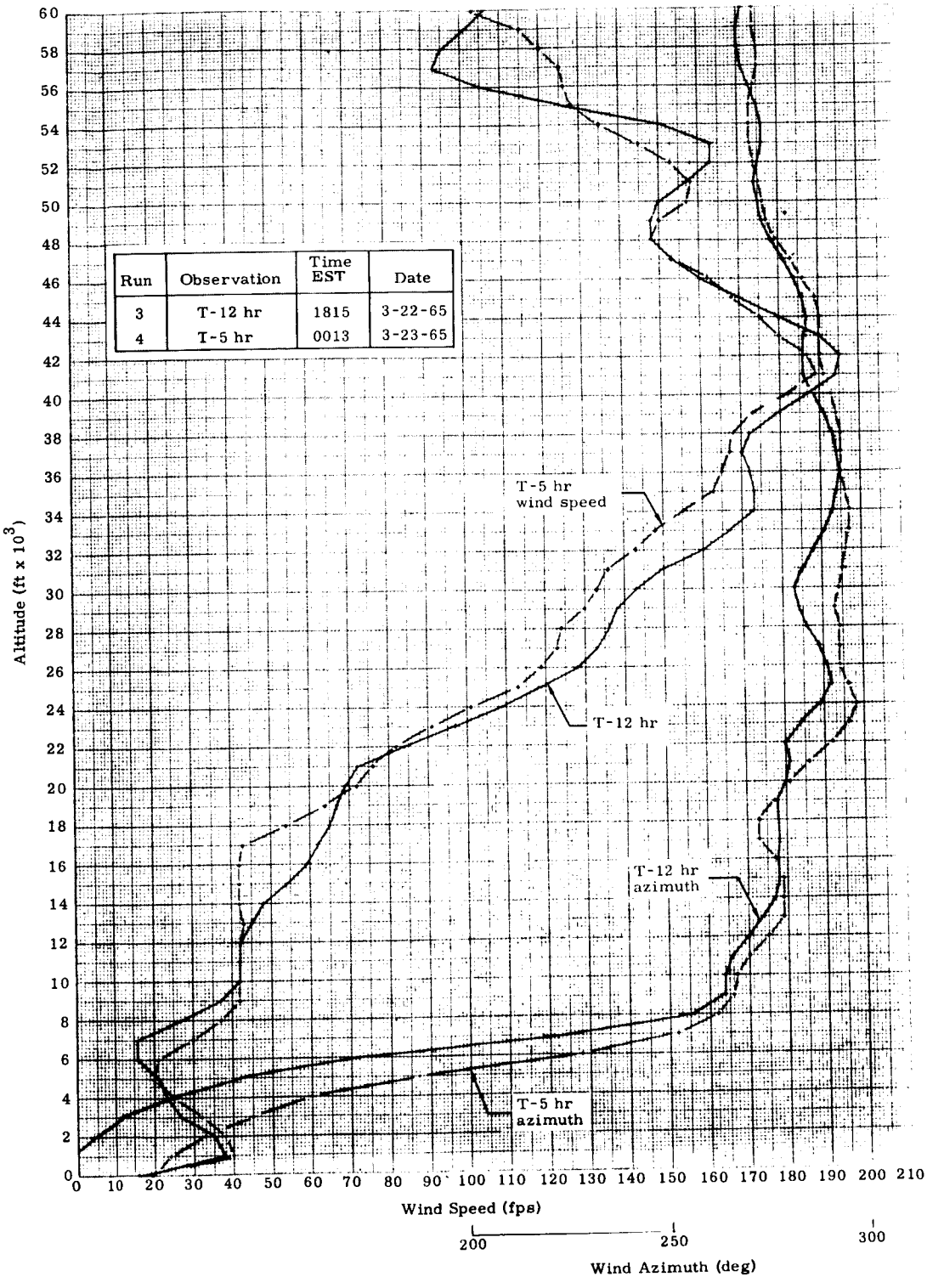


Fig. XI-2. Winds-Aloft Observations

~~CONFIDENTIAL~~

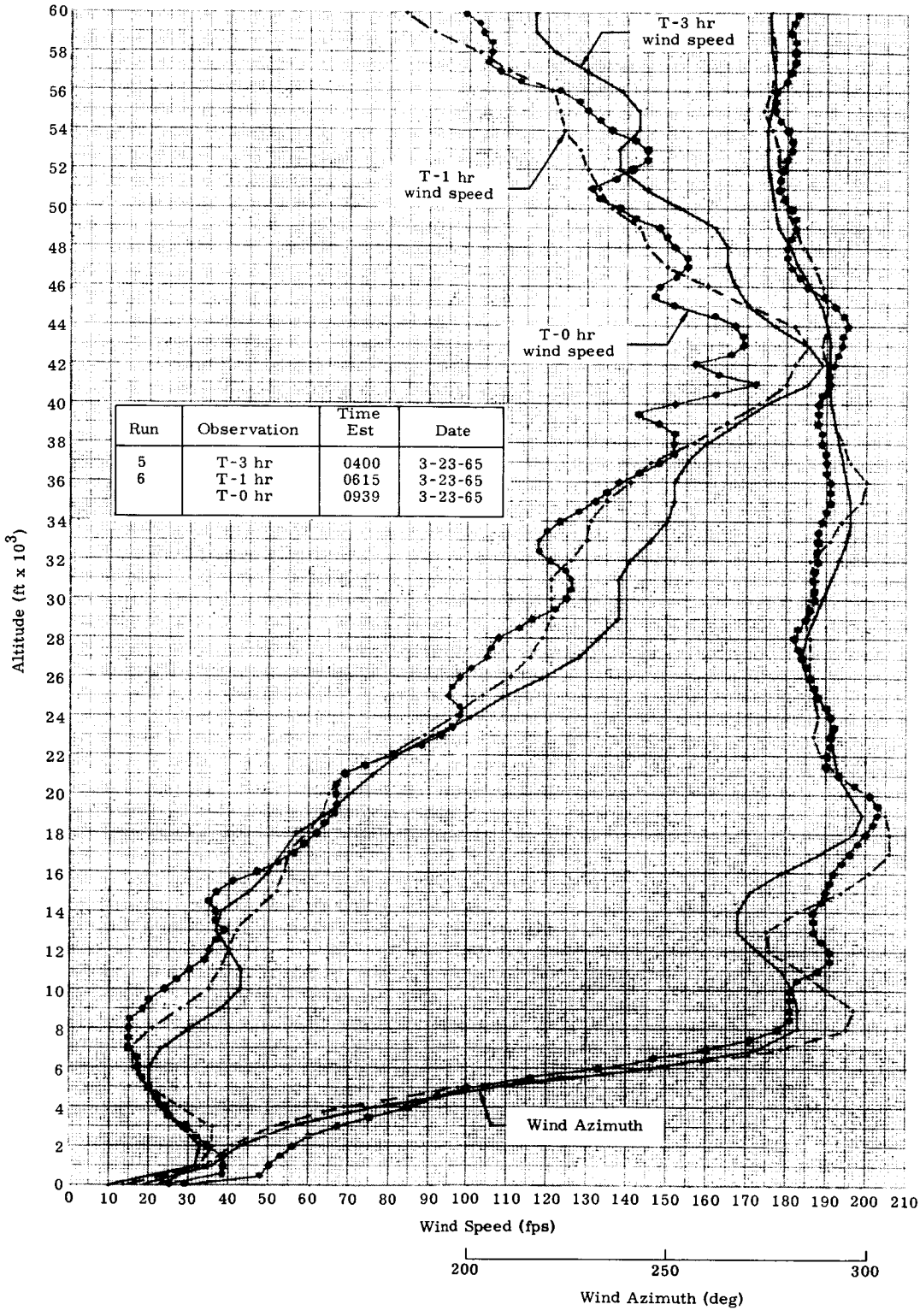


Fig. XI-3. Winds-Aloft Observations

3. Analog Transient Simulations

The engine gimbal outputs, the attitude errors, and the pitch and yaw angles of attack from the wind load analog simulations were sent to the Monitors in the MCC for use as a preview of vehicle and control system responses to the winds aloft. These are long wavelength responses since the wind data are averaged in 1000-foot altitude layers; also, the analog input is a smoothed function of the averaged values.

4. First-Stage Propellant Tank Underpressure Constraints

The Stage I tank underpressure constraints for GT-3 were selected on the basis of minimum tank pressure required to maintain structural integrity for the simulated flight loads. The constraints used (Table XI-2) were lower than the constraints required to withstand design winds which are more severe than those used for the GT-3 prelaunch simulations. The selected constraints were transmitted in timely fashion to the MCC.

TABLE XI-2

Stage I Tank Pressure Constraints

| Oxidizer Tank | | Fuel Tank | |
|---|---|---|---|
| Time from 87 $FS_1$ (sec) | Pressure (psia) | Time from 87$FS_1$ (sec) | Pressure (psia) |
| 50 | 9.4 | 50 | 9.4 |
| 61.8 | 8.0 | 61.8 | 7.0 |
| 75 | 4.5 | 75 | 3.8 |
| 80 | 2.9 | 86 | 2.0 |
| | | 90 | 1.5 |

NOTE: Pressures selected to withstand T-12, T-5, T-3 and T-1 hour winds.

5. Slow Malfunction Switchover Action Threshold

The slow malfunction switchover action threshold was sent to Cape Kennedy in the form of inertial velocity (EUVTIL) and inertial flight path angle (GPTIL) (Table XI-3). The V-$\gamma$ threshold was selected from an original set of six functions using average wind velocity increase with altitude and average wind direction, and interpolating to

TABLE XI-3

Slow Malfunction Switchover Action Threshold in Pitch Plane
Structural and Temperature Constraints of Stage I Flight

| Inertial Velocity (EUVTIL) (fps x $10^3$) | Inertial Flight Path Angle, GPTIL* | | | | | |
|---|---|---|---|---|---|---|
| | T-12 hr Wind Sounding | | T-5, T-3 hr Wind Sounding | | T-1 hr Wind Sounding | |
| | Structural (GPTIL)* | Temperature (GPTIL)* | Structural (GPTIL)* | Temperature (GPTIL)* | Structural (GPTIL)* | Temperature (GPTIL)* |
| 1.90 | 20.3 | | 20.5 | | 20.5 | |
| 2.00 | 20.9 | | 21.1 | | 21.1 | |
| 2.25 | 21.5 | | 21.6 | | 21.7 | |
| 2.50 | 21.6 | | 21.8 | | 21.8 | |
| 2.75 | 21.2 | | 21.3 | | 21.4 | |
| 3.00 | 20.5 | 20.5 | 20.7 | 20.6 | 20.7 | 20.7 |
| 3.25 | | 20.9 | | 21.0 | | 21.0 |
| 3.50 | 18.4 | 20.8 | 18.6 | 20.9 | 18.7 | 21.0 |
| 3.75 | | 20.6 | | 20.7 | | 20.7 |
| 4.00 | 15.3 | 20.2 | 15.4 | 20.2 | 15.4 | 20.3 |
| 4.25 | | 19.7 | | 19.7 | | 19.8 |
| 4.50 | | 19.2 | | 19.2 | | 19.2 |
| 4.75 | | 18.6 | | 18.7 | | 18.7 |

*GPTIL = sin $\gamma_I$ x 57.3

produce the operational threshold. This threshold (in the trajectory pitch plane) was transmitted to the Martin Guidance Monitor at the MCC.

6. Wind Comparison

The six prelaunch winds-aloft data are shown graphically in Figs. XI-2 and XI-3. These plots were transmitted to Cape Kennedy for use as a gage of existing wind conditions and as an indicator of the wind trend. The winds-aloft forecasts for launch made on F-2 and F-1 days are shown in Fig. XI-1. A peak speed of 168 fps (115 mph) at a 39,000-foot altitude was forecast from an azimuth of 270 degrees (18 degrees left of tail). The launch day winds-aloft observations are shown in Figs. XI-2 and XI-3. These plots show the wind profile varying from a double spike to a single spike with a maximum speed of 172 fps (117 mph) at a 41,000-foot altitude at launch. The peak wind was predicted within 4 fps, 20 degrees in direction and 2000 feet in altitude.

Table XI-4 lists definitive parameters of the four GT-3 simulations and the measured winds-aloft. The T-3 and T-1 hour updating information sent to the Monitors was comparable to the T-12 and T-5 hour simulations that had been used to revise the plotboards in the MCC. The launch wind (liftoff) parameters listed in Table XI-4 also compare well with the prelaunch winds. This agreement is indicative that the prelaunch winds were representative of the actual conditions which existed at the time of launch.

Table XI-5 shows that the GT-3 wind situation was almost the same magnitude as the GT-2 mission except that the GT-3 winds were essentially a mirror image of the GT-2 tail winds. The GT-2 and GT-3 winds were more severe than the GT-1 winds, and produced structural loads slightly over 80% of limit strength.

TABLE XI-4

Summary of GT-3 Simulations

| Item | T-12 hr | T-5 hr | T-3 hr | T-1 hr | Liftoff Balloon |
|---|---|---|---|---|---|
| Time of sounding (EST) | 1815* | 0013 | 0400 | 0615 | 0939 |
| Time of data release (EST) | 2100* | 0400 | 0600 | 0800 | No simulations |
| Peak wind speed (fps) | 195 | 189 | 189 | 185 | 172 |
| Wind speed/spec wind (%) | 86 | 83 | 84 | 84 | 76 |
| Altitude of peak (ft) | 42,000 | 41,000 | 42,000 | 43,000 | 41,000 |
| Wind azimuth at peak (deg) | 286 | 291 | 291 | 289 | 291 |
| Wind degrees off tail | 34 left | 39 left | 39 left | 37 left | 39 left |
| $\frac{\text{Structural load}}{\text{Limit strength}}$ (%) | 83 | 81 | 79 | 82 | No simulations |
| Wind shear downward, 3000 ft from peak ($sec^{-1}$) | 0.0078 | 0.0079 | 0.0073 | 0.0044 | 0.0068 |
| Wind shear/spec (%) | 20 | 21 | 19 | 11 | 18 |
| Launch recommendation | GO | GO | GO | GO | -- |
| Max GPTIL (nominal 27.78 deg) | 26.41 | 26.56 | 26.53 | 26.65 | 27.9 (flight value) |
| Max VYTIL (nominal zero) (fps) | 75.28 | 85.04 | 82.09 | 77.86 | 48.3 (flight value) |

* 22 March 1965

TABLE XI-5

Comparison of Mission Simulations

| Item | GT-1 | GT-2 | GT-3 |
|---|---|---|---|
| Sounding data | T-2 hr | T-1 hr | T-1 hr |
| Launch azimuth (deg) | 72 | 105 | 72 |
| Date of launch | 8 April 1964 | 19 January 1965 | 23 March 1965 |
| Peak wind speed (fps) | 107 | 195 | 185 |
| Altitude of peak speed (ft) | 44,000 | 39,000 | 43,000 |
| Wind azimuth of peak speed (deg) | 310 | 243 | 289 |
| Wind off tail (deg) | 58 left | 42 right | 37 left |
| $\frac{\text{Structural load}}{\text{Limit strength}}$ (%) | 74 | 83 | 82 |

## B. SLOW MALFUNCTION MONITORING

### 1. Countdown

Prelaunch trajectory simulations performed at Martin-Baltimore, based on T-12, T-15 and T-3 hour upper air wind soundings at Cape Kennedy, were used to predict and evaluate the effect on wind-sensitive MCC plotboard and strip chart recorder parameters. Based on the T-3 hour simulation, a peak flight path angle ($\tilde{\gamma}_P$) of 26.53 degrees and a maximum lateral velocity of 82 fps were predicted. The plotboard sheets that incorporated the prelaunch wind information were completed and installed by T-1 hour.

The countdown appeared nominal as monitored from the guidance console displays. The 24-minute hold at T-35 minutes required no Monitor action.

### 2. Stage I Flight

Both the primary and secondary guidance systems were in a GO condition at T-0.

A slight roll thrust misalignment was noted at liftoff, requiring approximately 0.73 degree of roll CW error to compensate. The primary and secondary roll programs were within specified limits. The IGS roll error signal displayed an apparent drift rate of approximately 33 deg/hr CCW. The roll drift rate is a combination of IGS roll gyro drift and a roll displacement caused by the thrust misalignment coupled with the unequal thrust developed by the two subassemblies. The build-up in the negative lateral velocity that occurred between LO + 80 seconds and BECO appears to be the result of the pitch program cross coupling into the yaw axis through the roll misalignment.

Stage I yaw-roll performance was within acceptable mission limits. RETRO was informed of the lateral velocity anomaly and its impact on the Stage I ground track; no other Monitor action was required.

The velocity versus elapsed time from liftoff display on plotboard IIIA was indicative of a higher-than-nominal thrust causing an increase in the nominal BECO velocity of approximately 95 fps; however, this was within the 3-sigma tolerance of ±143 fps.

The primary and secondary pitch program initiation times were within specified limits. The IGS pitch attitude error signal displayed an increasing nose-down command starting with pitch program initiation and continuing until BECO. This was apparently caused by a combination of TARS pitch gyro drift-up, TARS cross coupling into the yaw axis caused by roll misalignment, and the 1.2% low primary pitch program. The pitch axis inertial velocity ($\tilde{V}$) versus flight path angle ($\tilde{\gamma}_P$) display on plotboard VA depicted a lofted trajectory with the flight path angle increasing to approximately 2.5 degrees above the predicted BECO nominal. Stage I pitch performance was within acceptable mission limits and no Monitor action was required.

3. Stage II Flight

RGS steering was initiated on time, and pitch steering commands were as expected for the dispersed trajectory conditions at BECO. IGS and RGS yaw steering commands were in agreement throughout the closed-loop guidance portion of the flight.

The IGS roll attitude error displayed a CCW drift throughout second-stage flight of approximately 40 deg/hr. The roll drift rate was well within the specified tolerance and no Monitor action was required.

Both RGS and IGS pitch steering commands were saturated nose-down (2 deg/sec) for 12 seconds; this was due to the high dispersed initial conditions at guidance start. The RGS pitch altitude component ($\omega_{PS}$) reflected the high dispersed altitude present at guidance start.

At the completion of the initial (2 deg/sec) pitch-down steering command, the IGS pitch attitude error started diverging in the command-nose-down direction until the maximum signal of 6 degrees was attained at approximately LO + 293 seconds. The signal remained at 6 degrees nose-down command for the remainder of the flight. The flight path angle versus velocity ($\tilde{\gamma}$ versus $\tilde{V}$) display and the RGS steering commands depicted nominal primary system operation; hence, no Monitor action was required. On plotboard VA, the SECO ($\delta_7$) velocity display was 319 fps below SECO + 20 VR.

Figures XI-4 and XI-5 are the pitch axis and the yaw-roll axis real-time plotboard displays as recorded at the MCC. Figures XI-6 and XI-7 are the pitch axis and the yaw-roll axis strip chart recorder traces as were displayed in real time at the MCC.

4. Recommendations

The ±0.25 degree scaling on the RGS $\omega_{PS}$ signal appears too sensitive for diagnostic use under non-nominal conditions. It would appear that a scaling change to ±0.5 degree full-scale would greatly benefit the real-time evaluation of RGS performance in the pitch axis. $\omega_{PS}$ is also utilized to predict the resulting flight path angle recovery maneuvers required by the IGS for Stage II dispersed trajectory switchover cases.

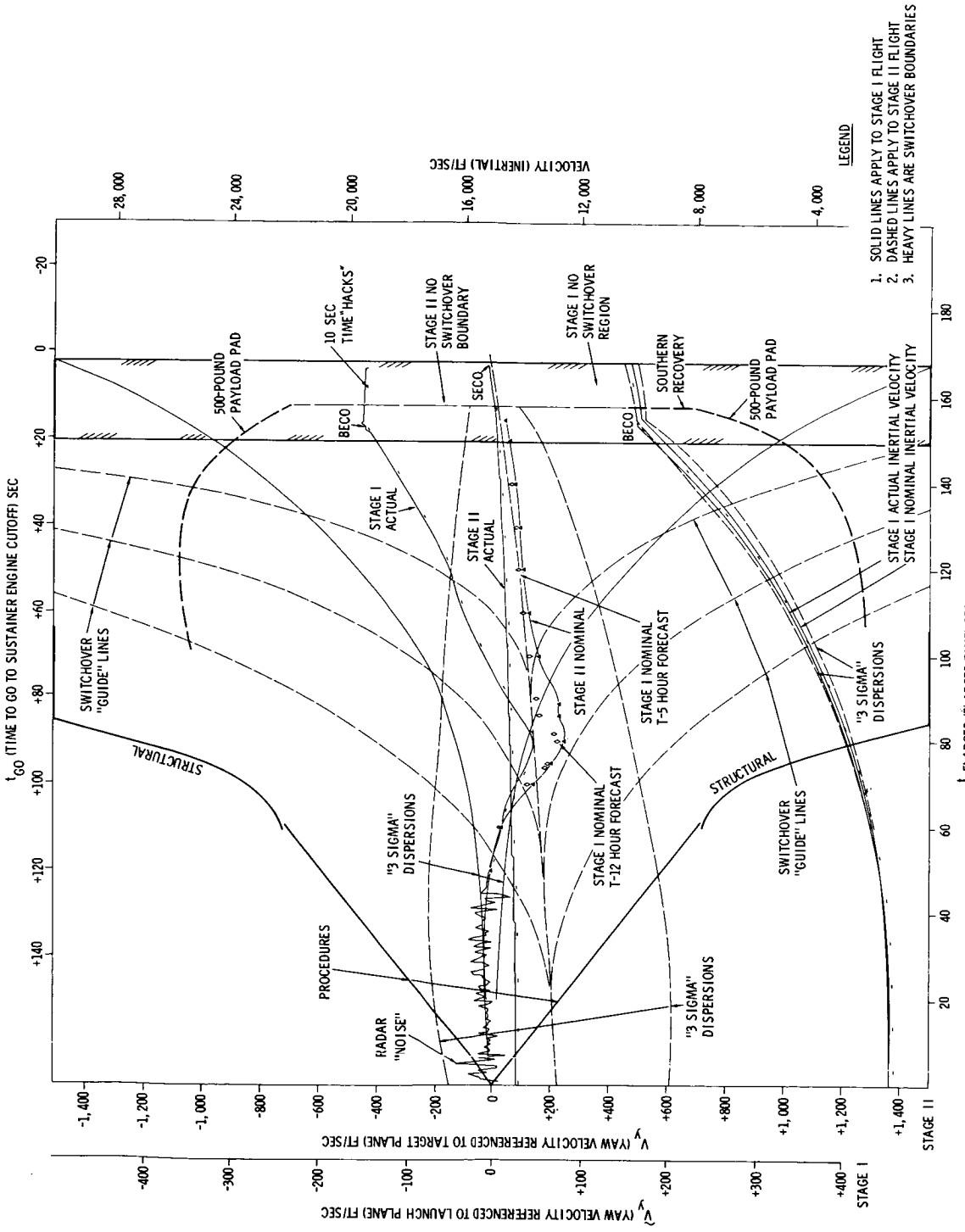


Fig. XI-4. GT-3 MCC Lateral Velocity Plot

CONFIDENTIAL

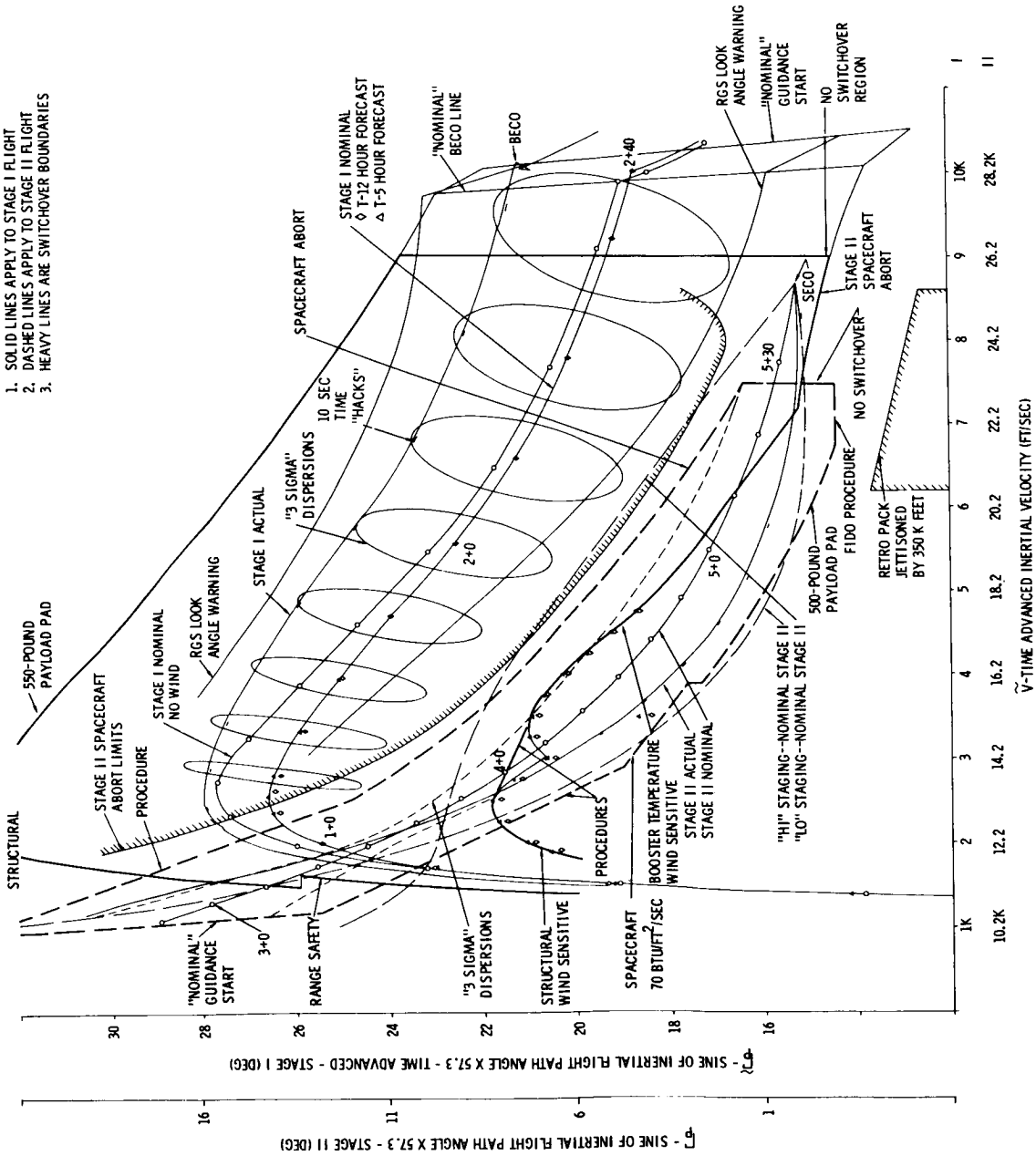


Fig. XI-5. GT-3 MCC Pitch Plane Plot

CONFIDENTIAL

| | Stage II | Stage I | |
|---|---|---|---|
| | 10-Sec Marks from Liftoff | | 1 |
| Nose Down | $\theta_{e_s}$ 743 ±6° | $\theta_{e_s}$ 743 ±6° | 1 |
| | SWO 872 or 874 | | 2 |
| — | Diff $\theta_{e_s} - \theta_{e_p}$ 743 - 766 | Diff $\theta_{e_s} - \theta_{e_p}$ 743 - 766 | 2 |
| | GCP 728 | | 3 |
| ↑ | $\delta\beta_p$ GE/B ±5° | $\dot{\theta}_c$ 732 MSB | 3 |
| | GCS 773 | | 4 |
| Pitch Axis | ↑ 2°/sec $\omega_{pN}$ GE/B 2°/sec ↓ | $\delta\theta_1$ 153 ±5° | 4 |
| | Guid Init TARS 740 | | 5 |
| ↓ | ↑ 2°/sec $\dot{\theta}_g$ 755 2°/sec ↓ | $AP\theta_1$ 770 MSB | 5 |
| | $\delta_6$ Guid Start GE/B | | 6 |
| ↑ ↓ | $\omega_{ps}$ GE/B ±1°/sec ↓ | $\delta\theta_2$ 150 ±5° | 6 |
| | $\delta_7$ SSCO GE/B | | 7 |
| ↓ | $\delta\theta$ 651 ±3° | $AP\theta_2$ 771 MSB | 7 |
| | SWO Command | | 8 |
| | — | | 8 |
| | 1-Sec Marks from Liftoff | | 9 |

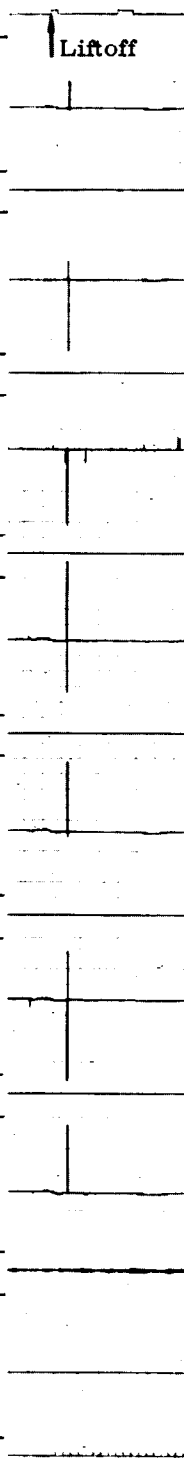

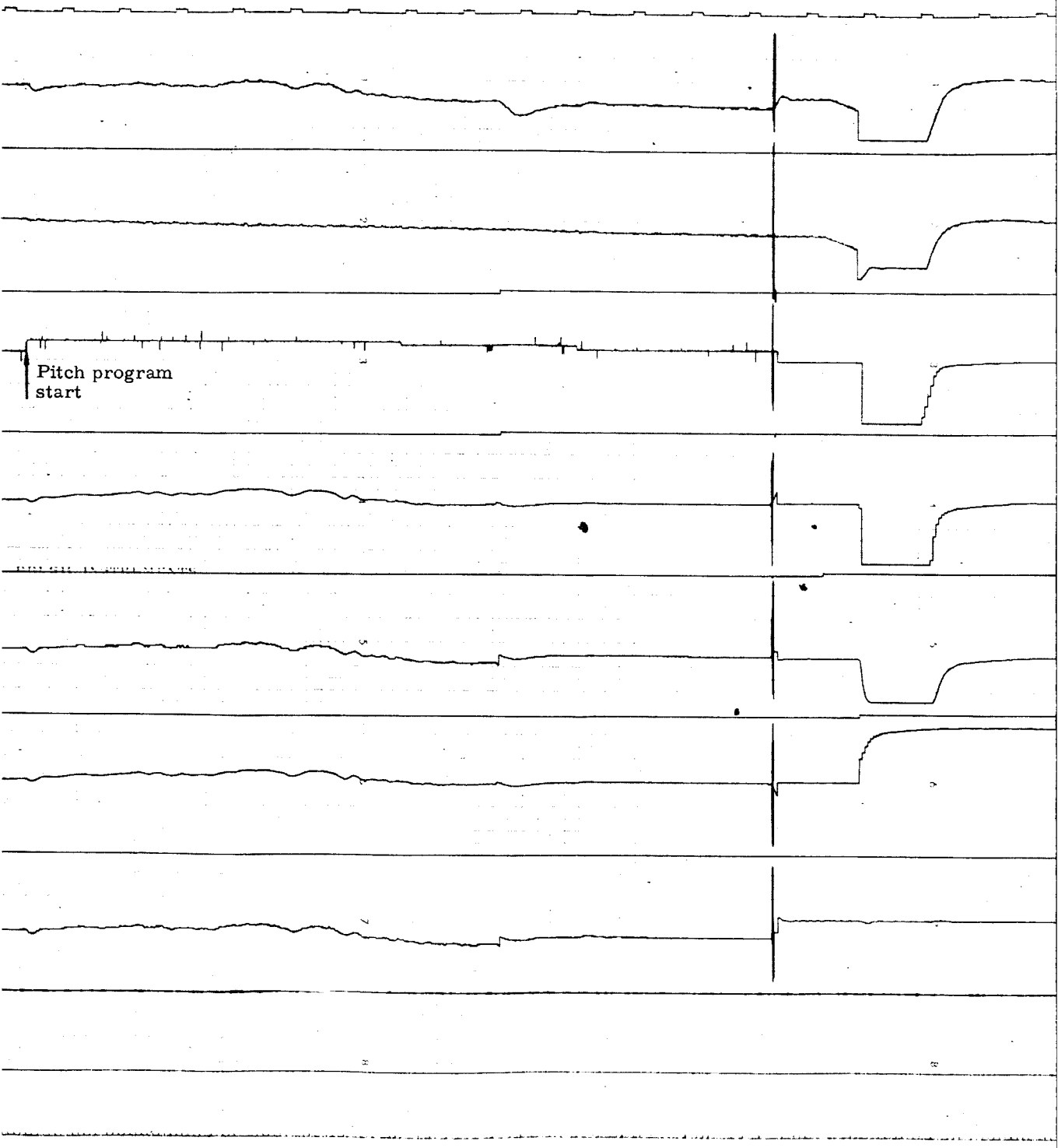


Stage I

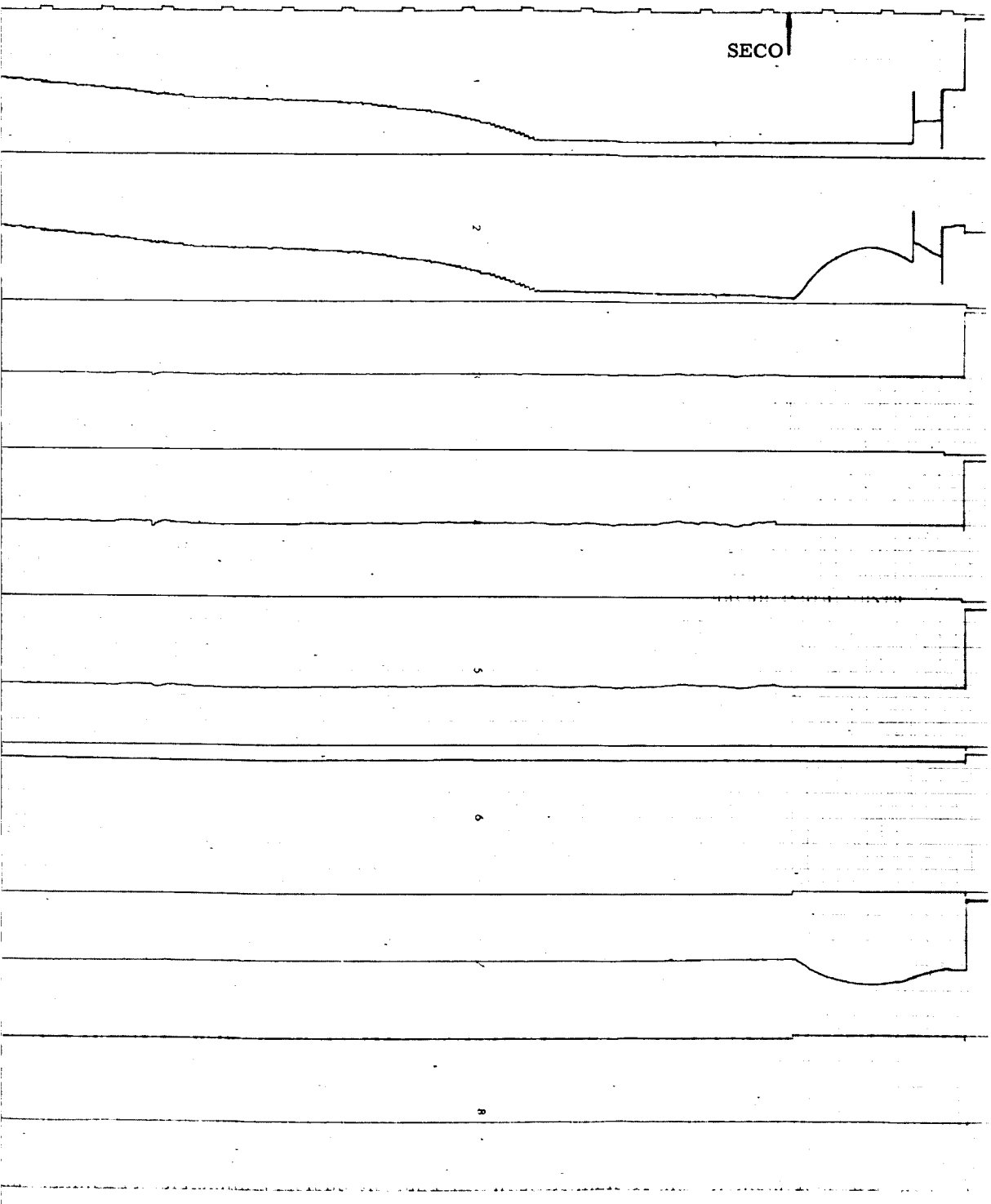


Stage II

Fig. XI-6. Telemetry II Recording (pitch axis)

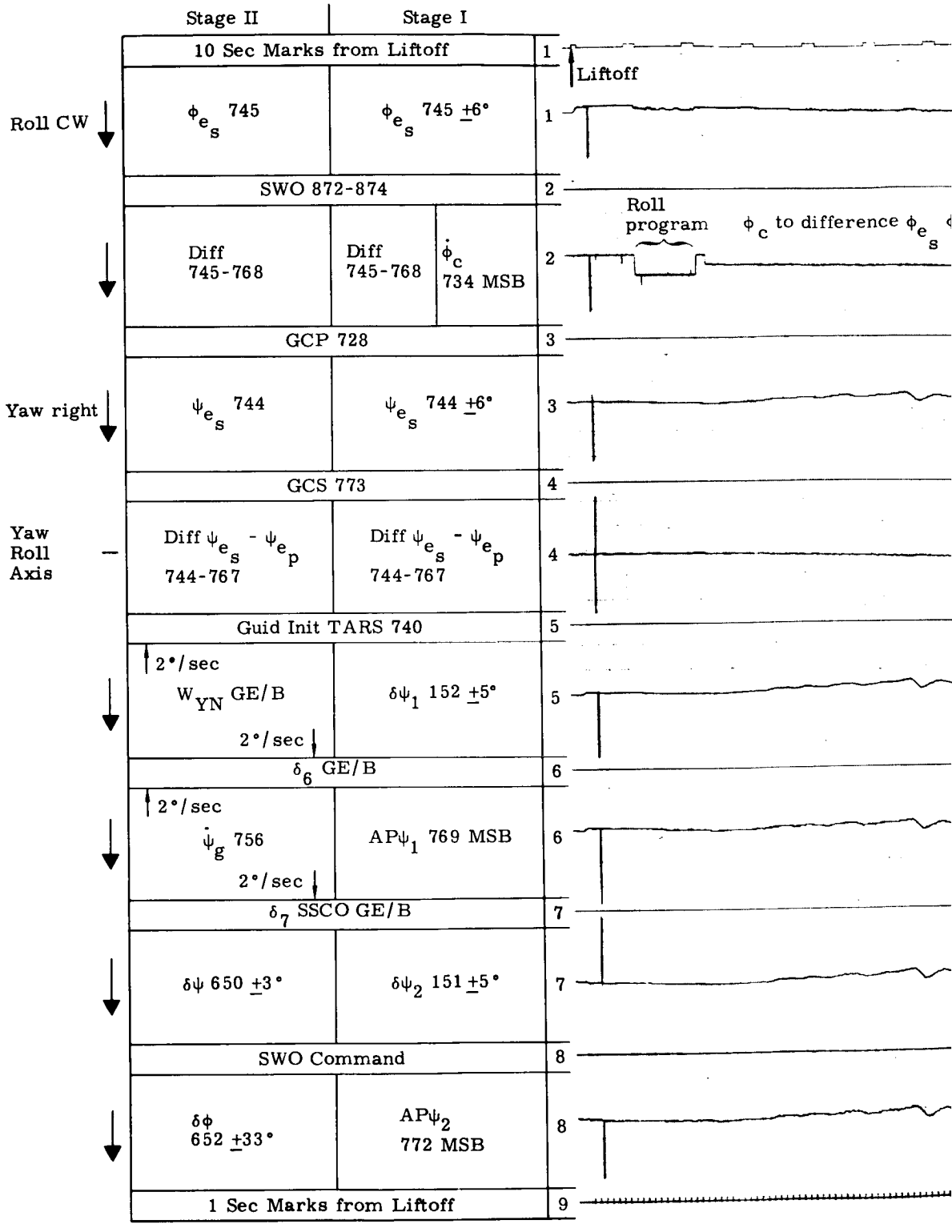
Stage II
Stage I
10 Sec Marks from Liftoff
1
Liftoff
Roll CW
$\phi_{e_s}$ 745
$\phi_{e_s}$ 745 ±6°
1
SWO 872-874
2
Roll program
$\phi_c$ to difference $\phi_{e_s}$
Diff 745-768
Diff 745-768
$\dot{\phi}_c$ 734 MSB
2
GCP 728
3
Yaw right
$\psi_{e_s}$ 744
$\psi_{e_s}$ 744 ±6°
3
GCS 773
4
Yaw Roll Axis
Diff $\psi_{e_s}$ - $\psi_{e_p}$ 744-767
Diff $\psi_{e_s}$ - $\psi_{e_p}$ 744-767
4
Guid Init TARS 740
5
2°/sec
$W_{YN}$ GE/B
2°/sec
$\delta\psi_1$ 152 ±5°
5
$\delta_6$ GE/B
6
2°/sec
$\dot{\psi}_g$ 756
2°/sec
$AP\psi_1$ 769 MSB
6
$\delta_7$ SSCO GE/B
7
$\delta\psi$ 650 ±3°
$\delta\psi_2$ 151 ±5°
7
SWO Command
8
$\delta\phi$ 652 ±33°
$AP\psi_2$ 772 MSB
8
1 Sec Marks from Liftoff
9

[redacted]

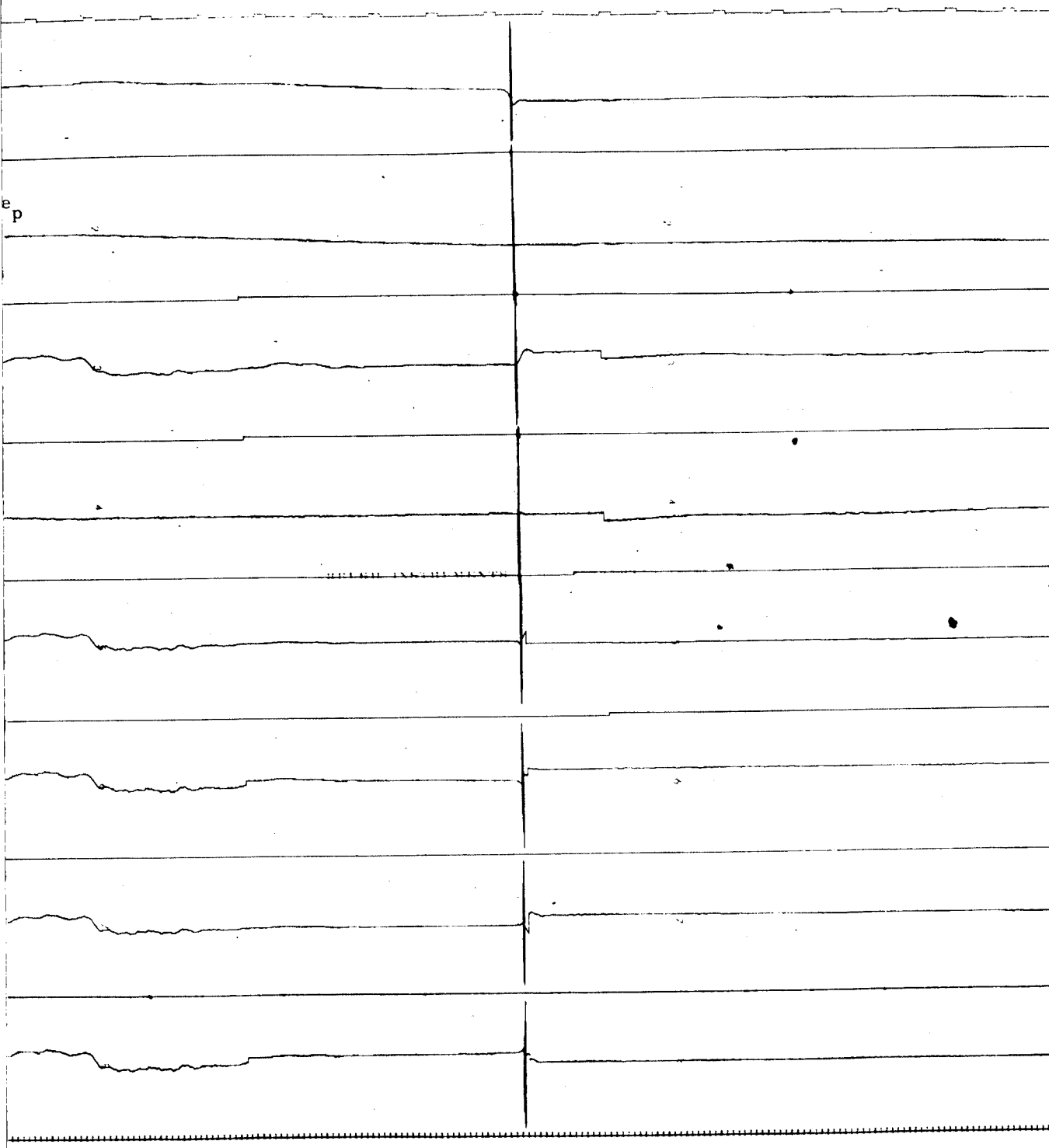


Stage I

[redacted]

ER 13227-3

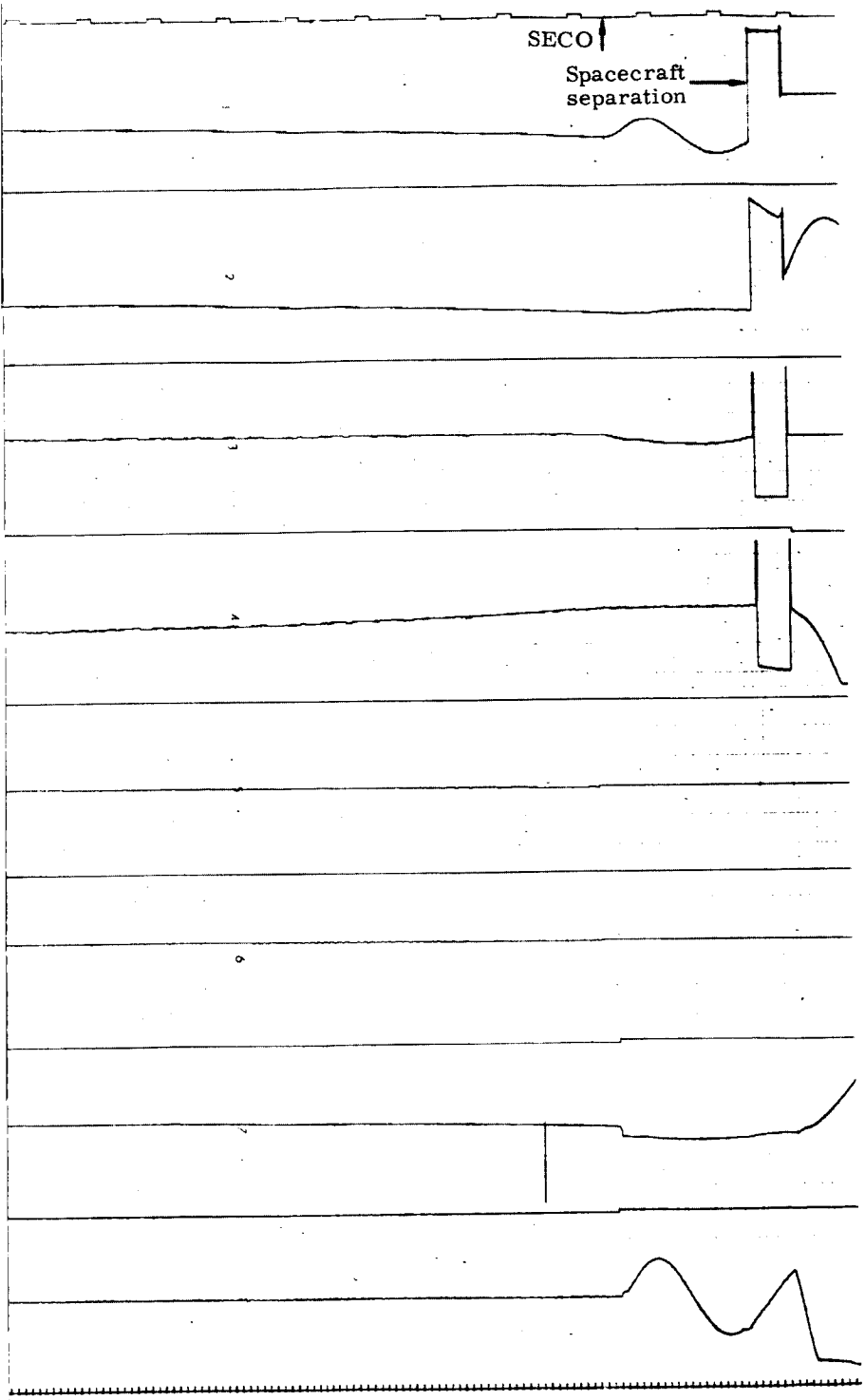


Stage II

Fig. XI-7. Telemetry II Recording (yaw-roll axis)

# XII. AIRFRAME SYSTEM

## A. STRUCTURAL LOADS

Analysis of the GT-3 flight data indicates that the structural loads imposed on the vehicle were within its structural capability. The most critical loading condition occurred at BECO where the load aft of Station 320 reached 97% of the design limit. This, however, was only 71% of the tested strength. Flight data analysis also indicates that dynamic response signals from the rate gyros can be used for lateral dynamic load analyses. The details of the loads associated with specific periods of interest are discussed in the following sections. [a]

### 1. Preignition--Axial

The static axial load consists of the 1 g deadweight distribution only (Fig. XII-1). Strong axial transients occurred due to the sudden displacements of the propellants when the engine prevalves were opened. Although these responses have been typical on all vehicles (Titan II and GLV), the dynamic response amplitude of the structure in its fundamental axial mode (4 cps) was 30% greater than that induced by the thrust start transient. The high frequency vibration pickup located on the tandem actuator (Meas 1191) responded much the same as it did during the ignition period which was greater than it had been on previous vehicles. Its duration of response was approximately 1 second.

### 2. Preignition--Lateral

The preignition lateral dynamic loads consisted primarily of the first structural mode response to ground winds. The maximum response occurred at LO - 170 seconds, and resulted in loads at Station 1224 as follows:

| | |
|---|---|
| Pitch plane moment (in.-lb) | $0.540 \times 10^6$ |
| Yaw plane moment (in.-lb) | $0.255 \times 10^6$ |
| Resultant moment (in.-lb) | $0.540 \times 10^6$* |
| Predominant direction of motion (deg from N) | 85 to 265 |
| Wind speed (mph) | 14 |
| Wind direction (deg from N) | 150 |

* At the time this maximum response occurred, the pitch and yaw plane motions were 90 degrees out of phase.

[a] Whenever possible, flight loads should be compared with tested strength in order to provide some concept of criticality. (Note by NASA GT-3 Mission Evaluation Team, August 11, 1965.)

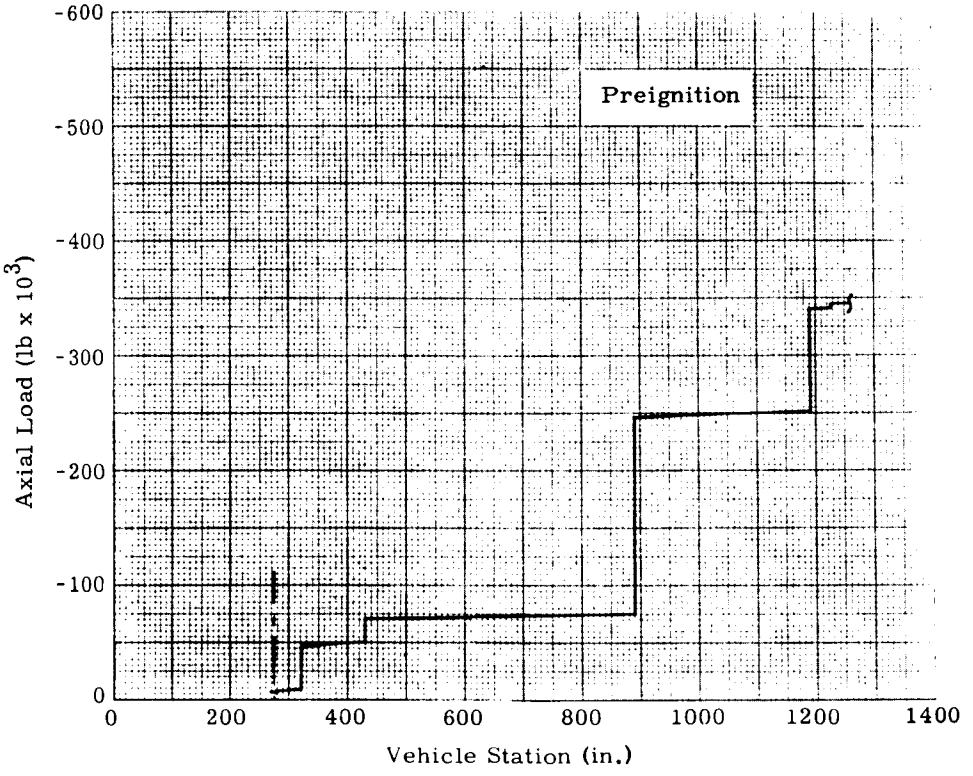


Fig. XII-1. Steady 1 g Axial Load

The frequency of the oscillation was 0.4 cps which corresponds to the computed frequency of 0.404 cps. (See Table XII-1 for additional frequency correlation.) The resulting envelope of dynamic bending moment along the vehicle is shown in Fig. XII-2.

Pitch plane strain gage data (Meas 0180) were also reviewed for evidence of wind-induced oscillation loads. These indicated a load of 175,000 in.-lb (based on the unbuckled effective area of 33.44 in.$^2$) at Station 937 which corresponds to 150,000 in.-lb (at that station) using the BLH and vibration modal data (Fig. XII-3).

The winds caused a steady load at Station 1224 of 124,000 in.-lb as determined from ground wind load analyses using the Tower 702 wind data (velocity, direction and profile). These steady ground wind loads are also shown in Fig. XII-2.

3. Launch Prerelease--Axial

The prerelease axial dynamic loads were obtained using the time history of the total thrust buildup (Fig. XII-4) and the response indicated by the BLH axial load measurements (Fig. XII-5). The GT-3 weight and thrust values were used to calculate the static portion of the total loads. The resulting envelope of static plus dynamic axial loads is shown in Fig. XII-6. The corresponding propellant tank bottom dome loads for the prerelease condition are shown in Table XII-2. These loads were lower than those induced on previous flights because the response of the fundamental axial mode (4 cps) was less.

4. Launch Prerelease--Lateral

The prerelease lateral dynamic loads were due primarily to the response of the first four structural modes to the combined action of the ground winds and the engine start transients. These responses were obtained from the BLH (Fig. XII-7) and the thrust differential pressure measurements as shown in Fig. XII-4. The resulting loads are presented in Fig. XII-8.

It should be noted that engine displacements due to wind-induced oscillations occurred prior to ignition, and that ignition appears to have taken place at the peak displacement thereby causing higher loads than would normally be encountered due to the induced engine displacement. This was apparent in both pitch and yaw planes. The resulting loads, although higher than on the previous vehicles, were not excessive.

5. Launch Post-Release--Axial

Axial responses at vehicle release for structural loads determination were primarily obtained from the axially oriented accelerometers. However, the accelerometer responses were associated specifically with an

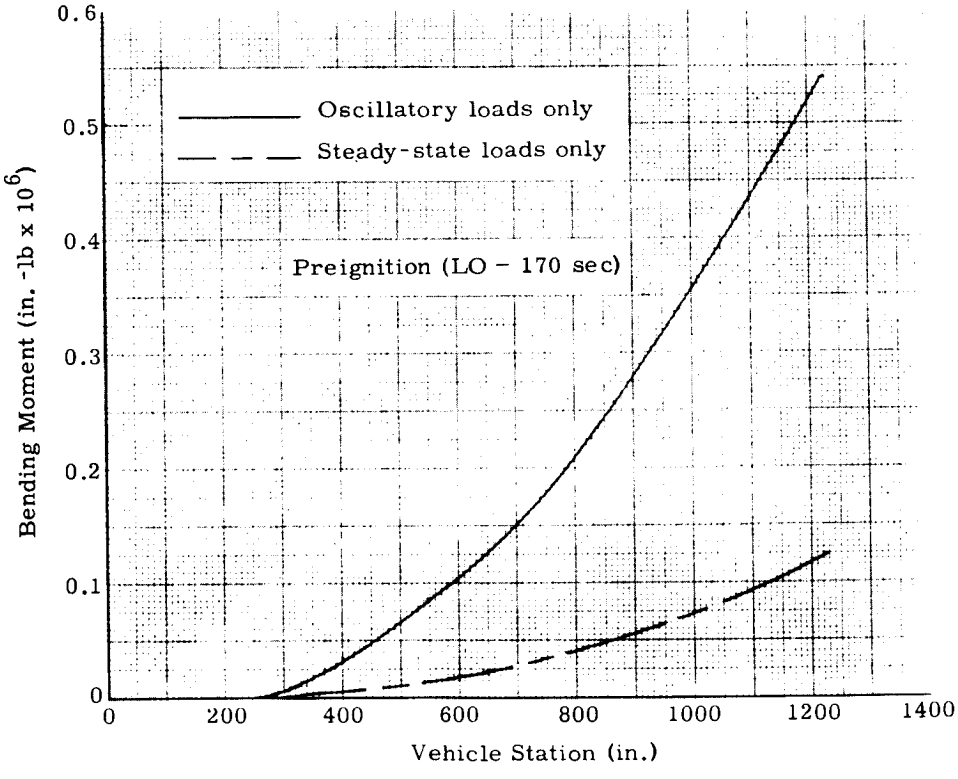


Fig. XII-2. Bending Moments Due to Ground Winds

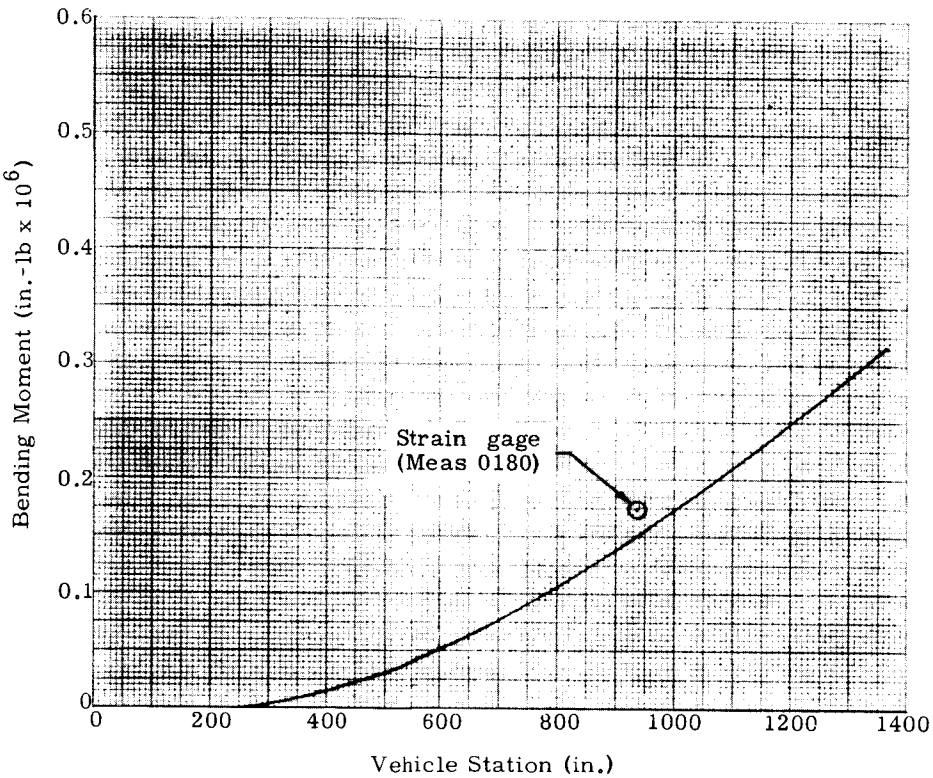


Fig. XII-3. Correlation of WIO Bending Moment as Determined from BLH and Strain Gage (Preignition: LO - 4 sec) in Pitch Plane

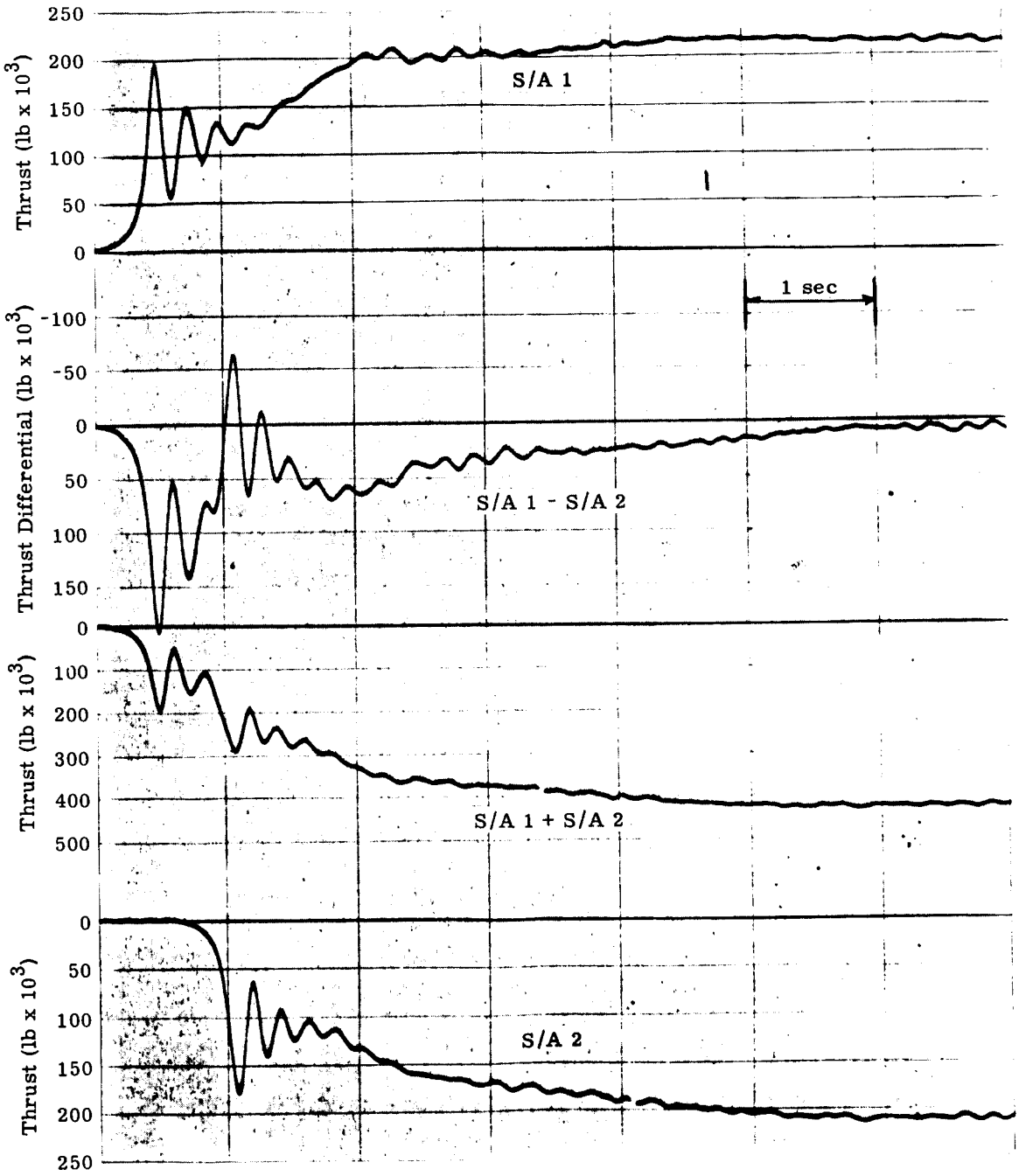


Fig. XII-4. GT-3 Ignition Transient

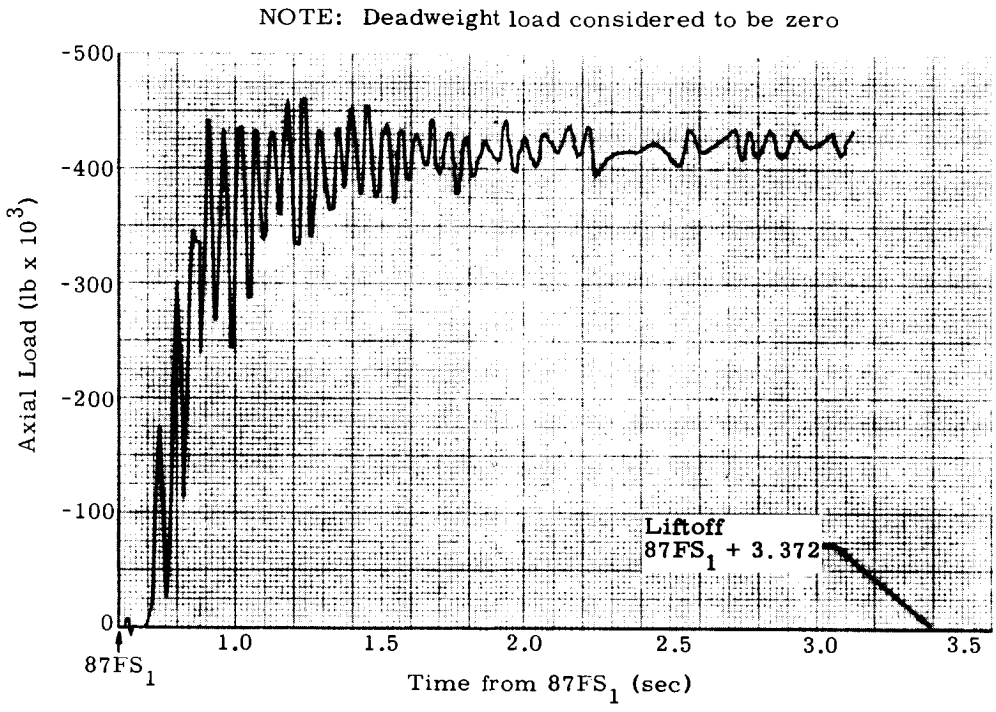


Fig. XII-5. BLH Axial Load During Hold-down

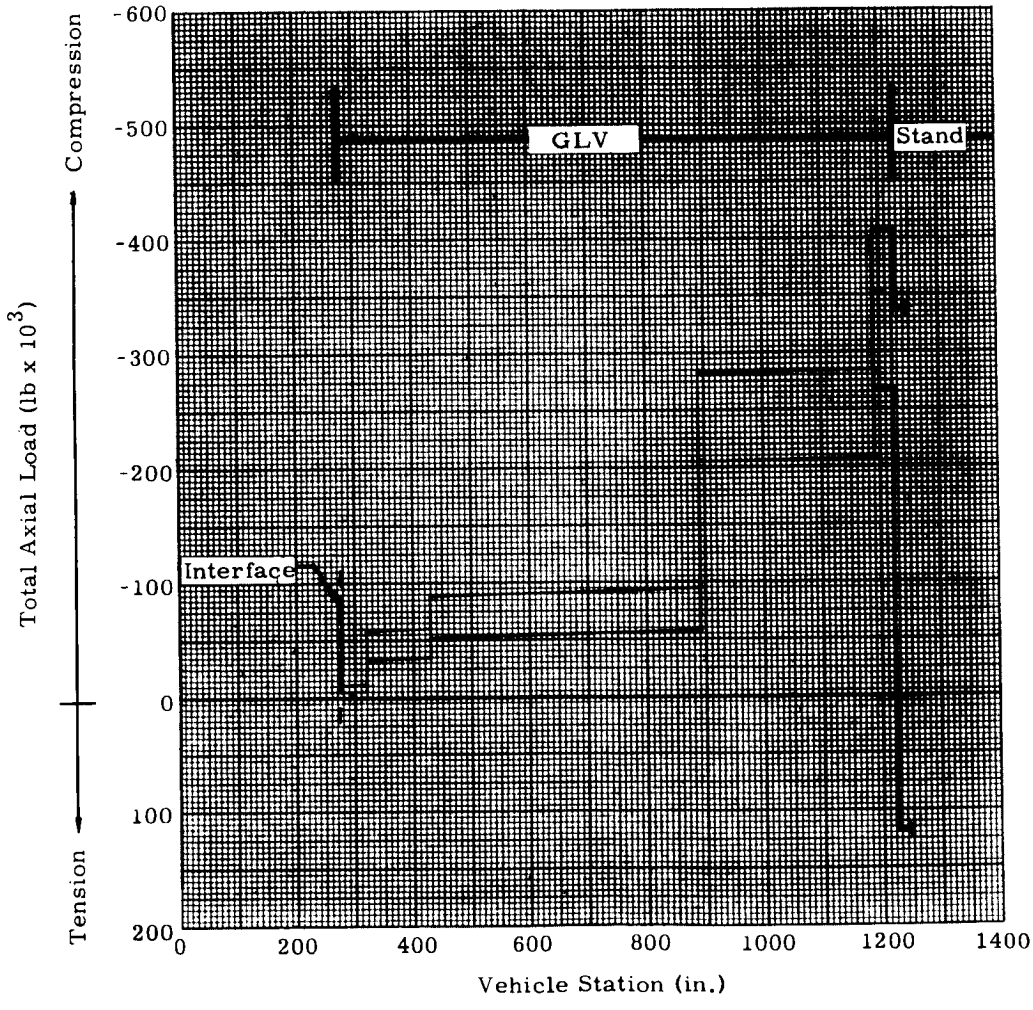


Fig. XII-6. Total Axial Load Envelope: Prelaunch Condition

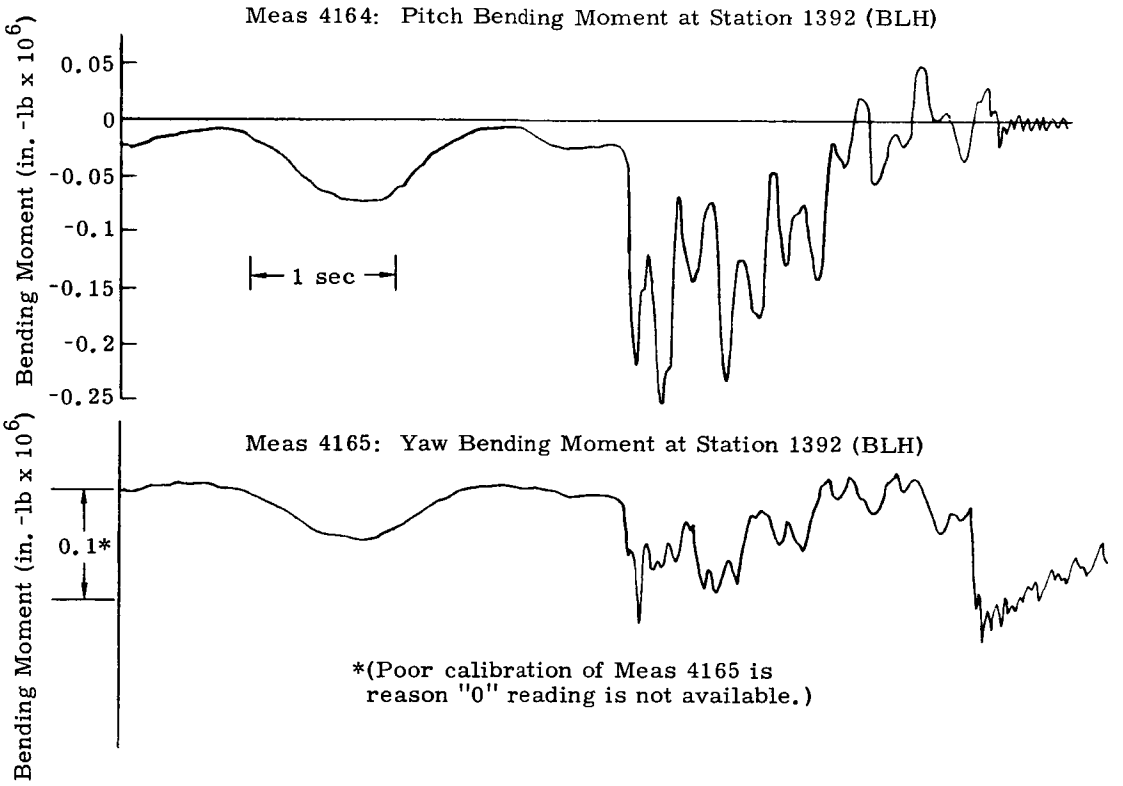


Fig. XII-7. GT-3 Bending Moment at Station 1392: Prerelease

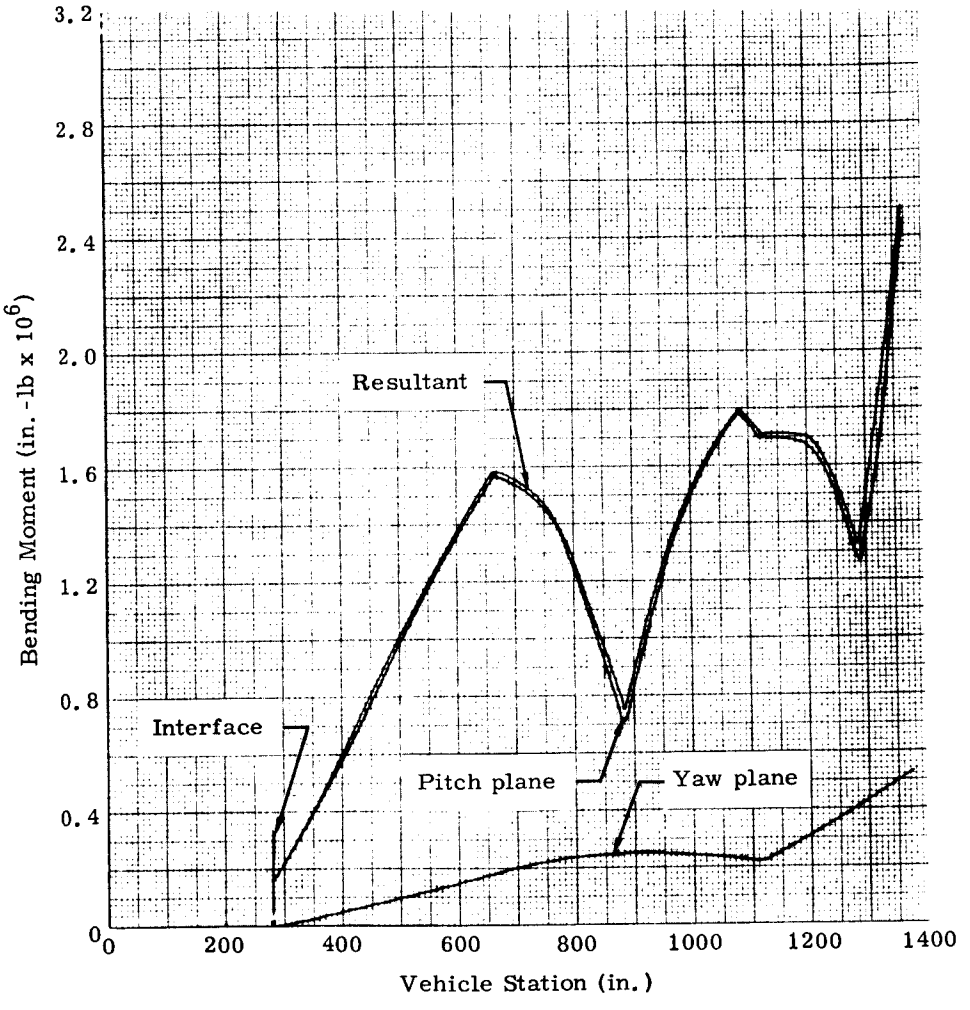


Fig. XII-8. Lateral Dynamic Bending Moment Envelope: Prerelease

TABLE XII-1

Frequency Correlation (preflight conditions)

| Condition | Calculated Frequency (cps) | | GT-3 Measured Frequency (cps) | | |
|---|---|---|---|---|---|
| | Lateral | Axial | Pitch | Yaw | Axial |
| Prerelease | Slosh | | | | |
| | 0.582 Stage I fuel | | | | |
| | 0.585 Stage I oxidizer | | | | |
| | 0.677 Stage II oxidizer | | 0.67 | | |
| | 0.801 Stage II fuel | | | | |
| | Structural | | | | |
| | 0.404 | | 0.40 | 0.40 | |
| | 1.78 | | 1.78 | 1.75 | |
| | 4.39 | | 4.8 | 4.8 | |
| | 7.53 | | 7.7 | | |
| | 9.88 | | | | |
| | 12.90 | | | | |
| | 17.91 engine | | | | |
| | | 4.2 | | | 4.0 |
| | | 8.1 | | | 8.8 |
| | | 17.9 | | | 18.3 |
| Post-Release | Slosh | | | | |
| | 0.627 Stage I fuel | | | | |
| | 0.651 Stage I oxidizer | | | | |
| | 0.723 Stage II oxidizer | | | | |
| | 0.862 Stage II fuel | | | | |
| | Structural | | | | |
| | 2.4 | | 2.5 | 2.5 | |
| | 6.75 | | | | |
| | 9.45 | | | 9.0 | |
| | 12.32 | | | | |
| | 15.79 | | | | |
| | 17.46 engine | | | | |
| | | 7.12 | | | |
| | | 7.78 | | | |
| | | | | | 18.5 |

TABLE XII-2

Maximum Axial Loads in Propellant Tank Domes

| Configuration | Prerelease | | Post-Release | | Design Load Factor (g)[a] |
|---|---|---|---|---|---|
| | Load (lb) | Load Factor** | Load* (lb) | Load Factor** | |
| Stage II oxidizer dome | 47,023 | 1.230 | 48,464 | 1.268 | 2.76 |
| Stage II fuel dome | 35,624 | 1.620 | 30,169 | 1.372 | 3.54 |
| Stage I oxidizer dome | 174,781 | 1.019 | 215,016 | 1.254 | 1.91 |
| Stage I fuel dome | 190,732 | 2.109 | 113,388 | 1.254 | 2.85 |

*Load due to steady acceleration only; known structural modes not excited.
**Based on actual loaded propellant weight.

[a]Design load factor for Stage II fuel and oxidizer tank domes should be at least 5.81 g. (Note by NASA GT-3 Mission Evaluation Team, August 11, 1965.)

18.5-cps oscillation which is not related to a primary structural mode. The strain gage responses were associated only with the fundamental lateral modes. Therefore, axial post-release dynamic loads of significant amplitudes were, in all probability, very low or nonexistent except those related to the undefined 18.5-cps mode.

The post-release steady axial load was calculated by simply applying the 1.27 liftoff factor to the deadweight release load.

6. Launch Post-Release--Lateral

The post-release lateral loads were entirely dynamic with the primary response being in the first structural mode. This was noted on the accelerometers, rate gyros and strain gages. The Mode I pitch plane loads as determined from each of these measurements are compared in Fig. XII-9, with reasonably good agreement indicated. The total dynamic loads (based on rate gyro signals) are presented in Fig. XII-10. Although the loads due to the second mode are not shown, it cannot be presumed that they did not exist since the Compartment 1 accelerometers were located near the node and the Stage II rate gyros were located near the anti-node of the second mode. Spacecraft accelerometers have been the primary measurements used for lateral dynamic response analysis on GT-1 and GT-2. No such instrumentation was available on GT-3.

7. Stage I Flight--Axial

Low amplitude axial oscillations occurred intermittently throughout Stage I flight and increased with flight time with maximum amplitude occurring at LO + 141 seconds (Fig. XII-35). The response frequency, as it varied with flight time, is shown in Fig. XII-11. The maximum dynamic loads resulting from this axial oscillation were only ±4200 pounds in the Mach 1-Max q region.

The steady axial loads resulted from the combined effects of thrust, aerodynamic drag and compartment pressures.

8. Stage I Flight--Lateral

The dynamic responses of the accelerometers located in Compartment 1 (Meas 1671 and 1672), and the Stage II rate gyros (Meas 0723 and 0724) were converted through vibration analytic parameters to lateral dynamic bending moments along the launch vehicle. The observed frequencies of the various structural modes are shown in Fig. XII-11. The variation of the peak modal bending moments is shown in Figs. XII-12 and XII-13 as obtained from the accelerometer and rate gyro signals, respectively. These data are presented to confirm the feasibility of utilizing rate gyro dynamic responses for determining

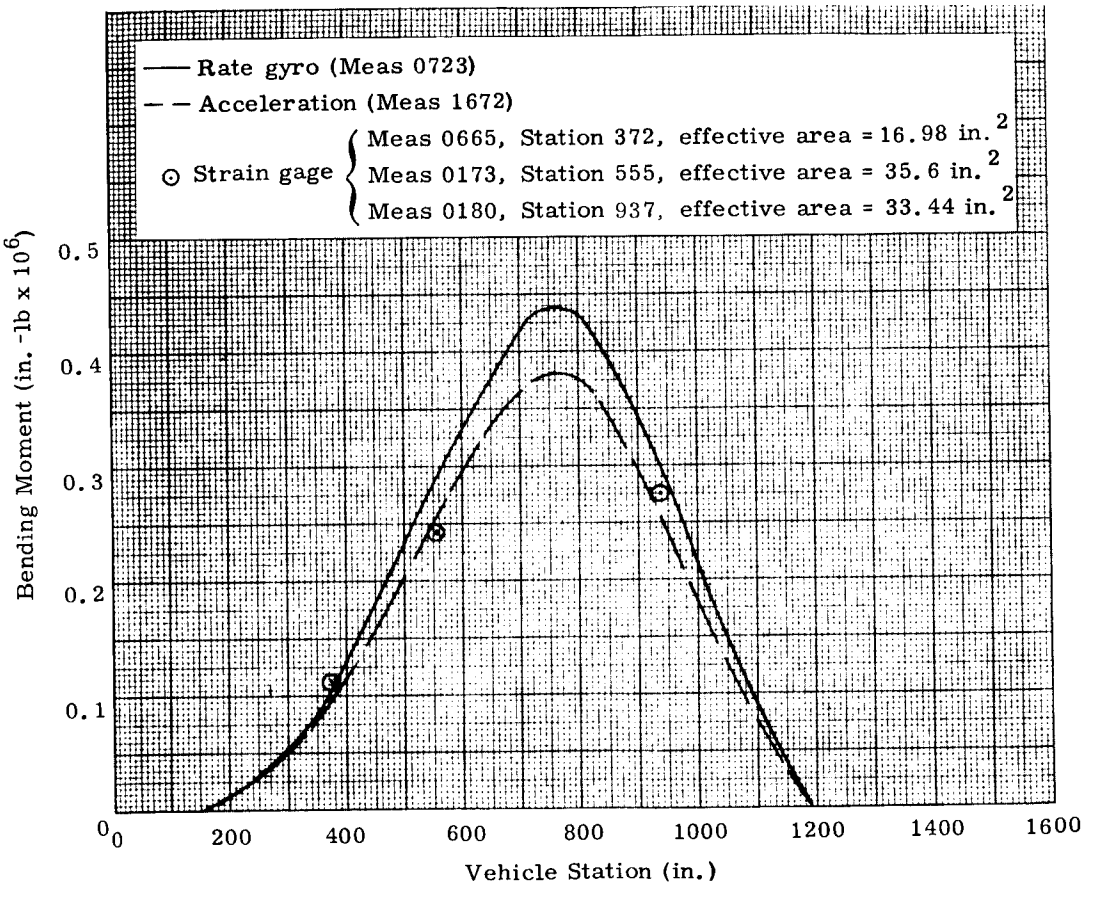


Fig. XII-9. Correlation of Mode 1 Bending Moments from Various Measurements: Post-Release Pitch Plane Response

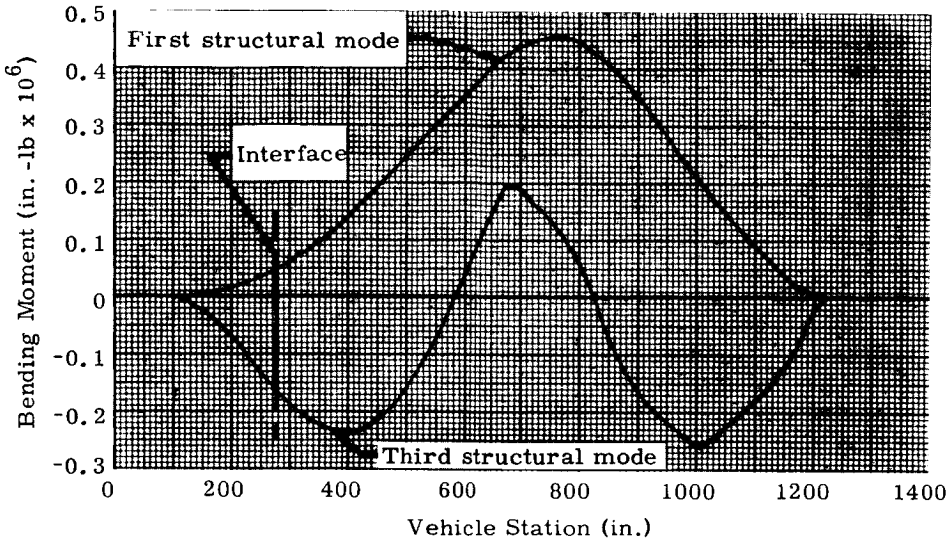


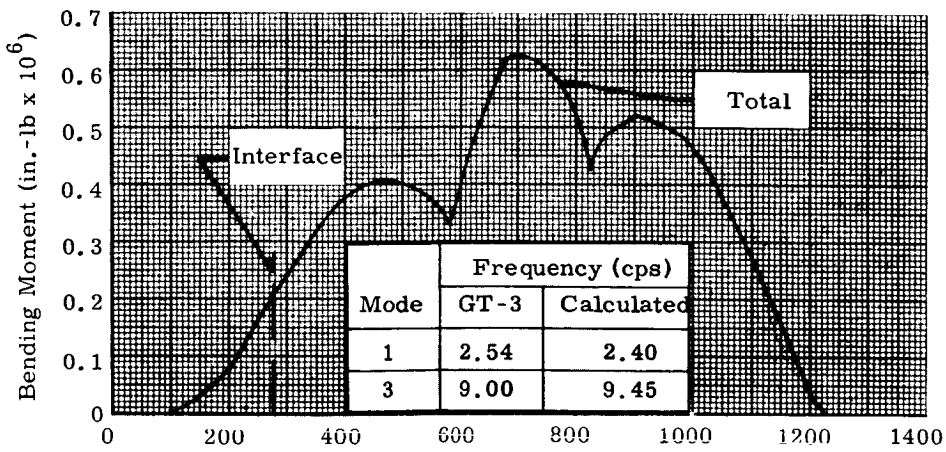


| Mode | Frequency (cps) GT-3 | Frequency (cps) Calculated |
|---|---|---|
| 1 | 2.54 | 2.40 |
| 3 | 9.00 | 9.45 |

NOTE: Data based upon rate gyro response.

Fig. XII-10. Total Lateral Load Envelope--Post-release

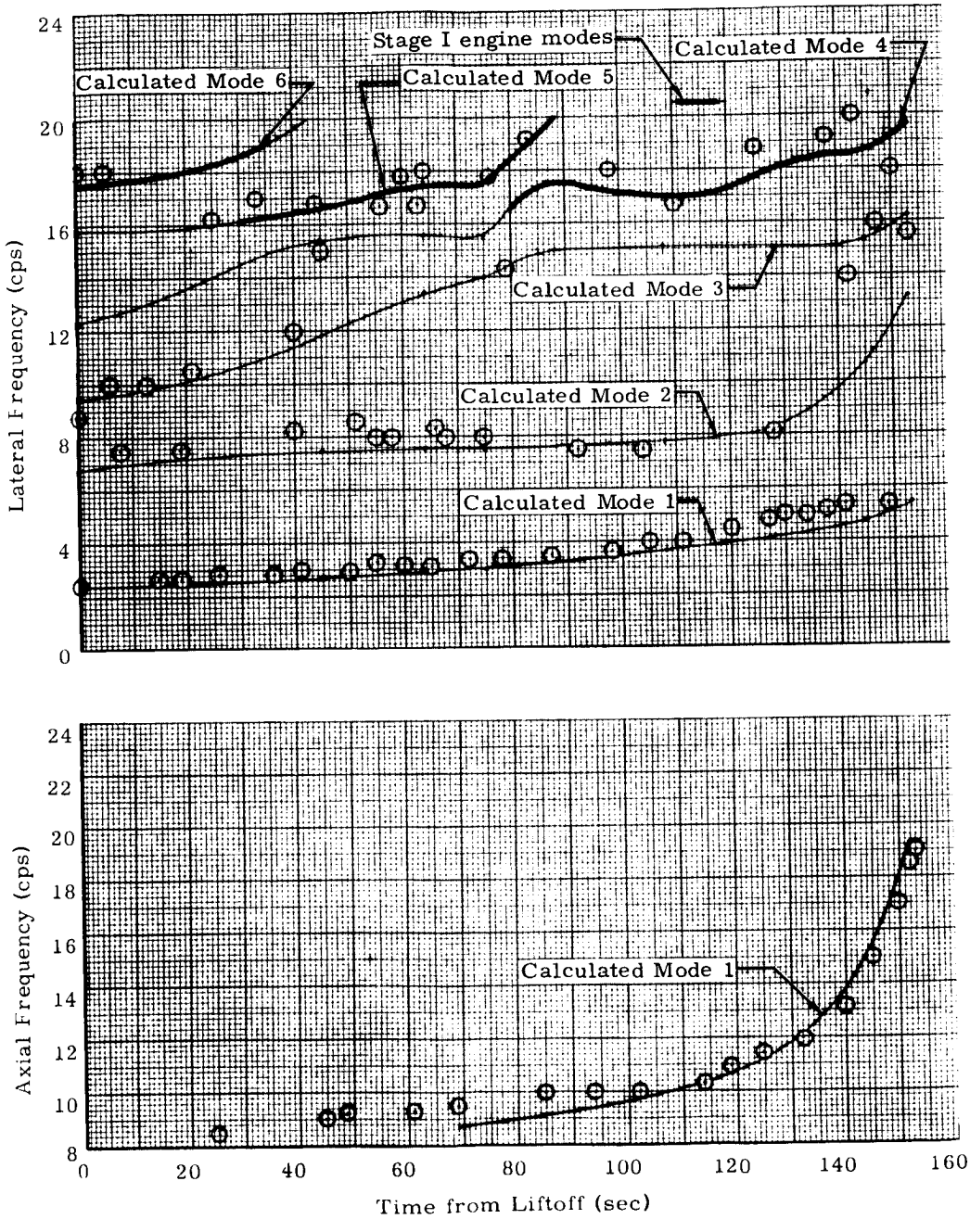


Fig. XII-11. Stage I Flight Vibratory Modes

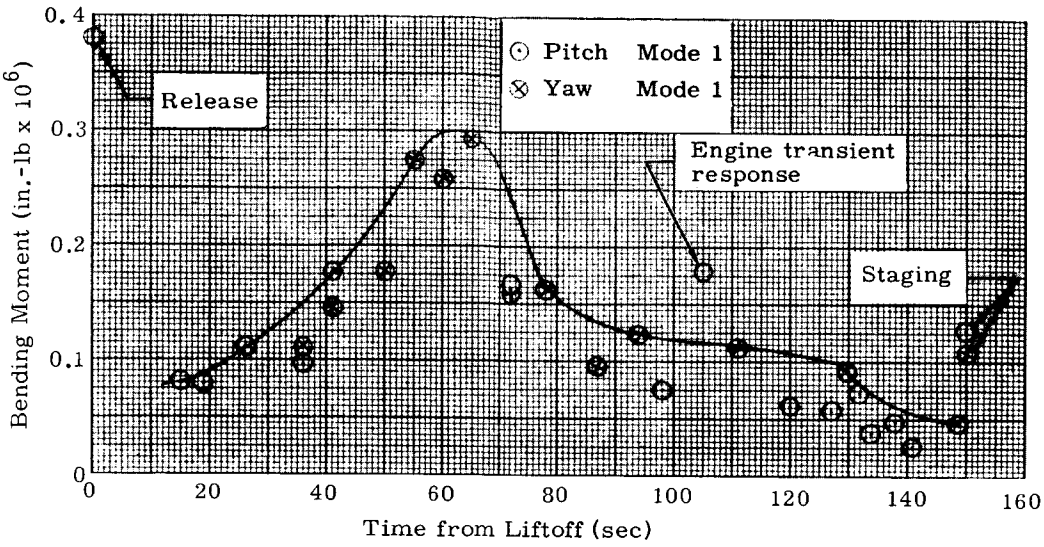


Fig. XII-12. Peak Modal Bending Moment as Determined by Compartment 2 Accelerometers

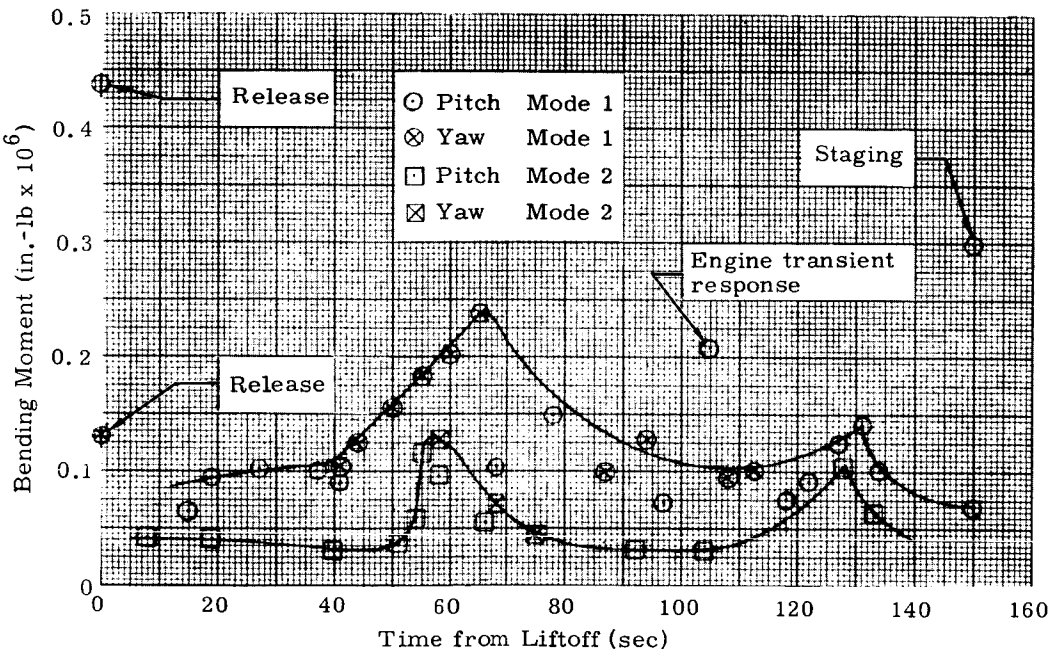


Fig. XII-13. Peak Modal Bending Moment as Determined by Stage II Rate Gyros

lateral dynamic loads, particularly since GLV-5 and up will not be equipped with lateral accelerometers. The general trends show good agreement.

Maximum dynamic responses occurred in the transonic region as in previous flights and the amplitudes were approximately the same as those which occurred on GT-2 (Fig. XII-14). The total Mach 1 and Max $C_{N_\alpha}$ q $\alpha$ dynamic loads are shown in Figs. XII-15 and XII-16, respectively.

Strain gage data were not used to assess the flight dynamic responses in the 4- to 10-cps frequency range because of the superposition of extraneous responses which are not attributable to the structural system.

Low amplitude slosh mode oscillations occurred throughout the time period from approximately LO + 90 seconds to BECO. Figure XII-17 presents the observed frequency and its correlation with calculated slosh mode vibration frequencies. Although the amplitude of these oscillations was low (approximately ±0.1 inch at the crew station and a maximum load of ±48,000 in.-lb), the motion did occur as a limit cycle oscillation with a beat period of 3 to 5 seconds.

The quasi-steady lateral loads resulted primarily from winds during Stage I flight. The T-0 wind profile is shown in Fig. XI-3. The Max $C_{N_\alpha}$ q $\alpha$ condition occurred at LO + 68 seconds and resulted in a peak bending moment of $1.96 \times 10^6$ in.-lb at Station 935. The peak bending moment at Mach 1 (LO + 60 seconds) was $1.52 \times 10^6$ in.-lb.

At LO + 105 seconds (gain change), a small step change in the engine angle took place (only 0.2 degree), apparently due to winds. This step induced a low amplitude oscillation in the fundamental bending mode (peak bending moment of 210,000 in.-lb) at 4.0 cps (Fig. XII-13). Although this was of little significance to the total GT-3 flight loads, it serves as an experimental indication of the loads induced by an engine step change for use in malfunction and abort studies. This engine step change resulted in a peak modal moment of $1.05 \times 10^6$ in.-lb/deg of engine deflection.

9. Pre-BECO--Axial

The oscillatory axial loads reached a maximum at pre-BECO. This resulted in loads at the critical Station 320 of only ±6400 pounds based on the Compartment 1 axial accelerometer response at the fundamental

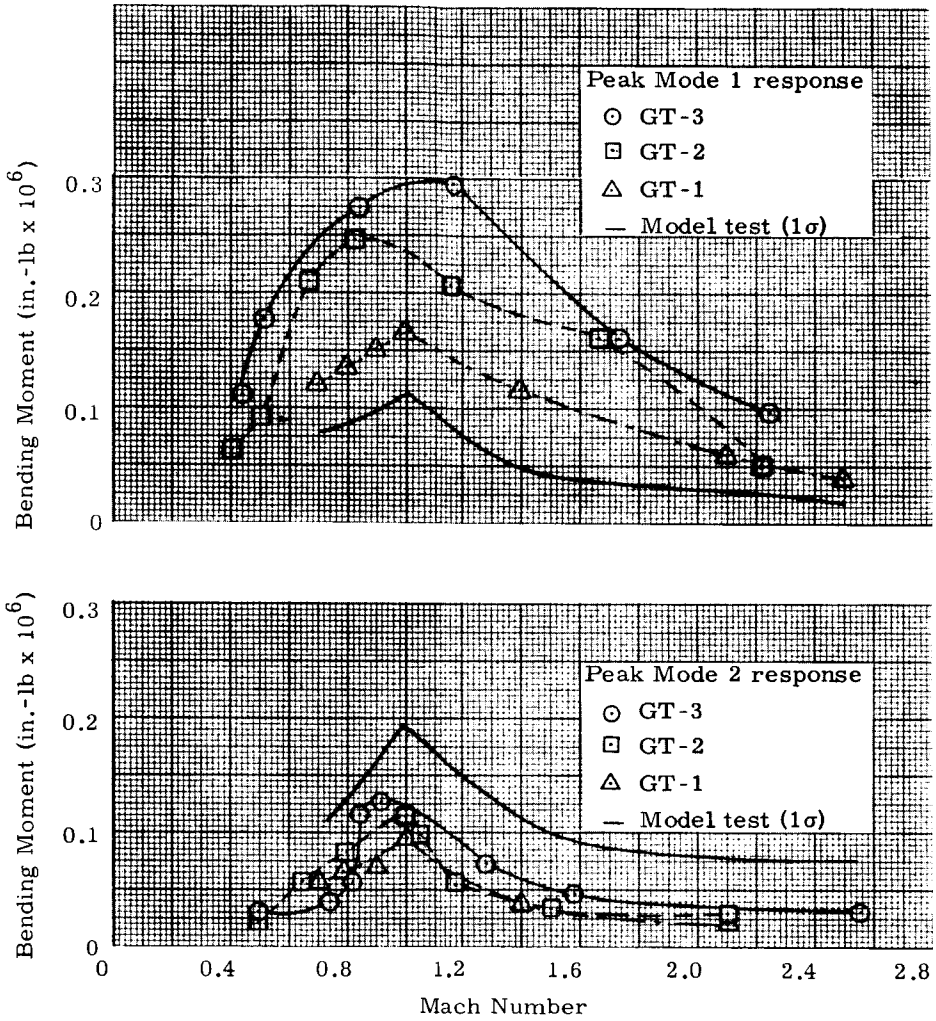


Fig. XII-14. Peak Modal Bending Moment Response to Transonic Buffet: Lateral

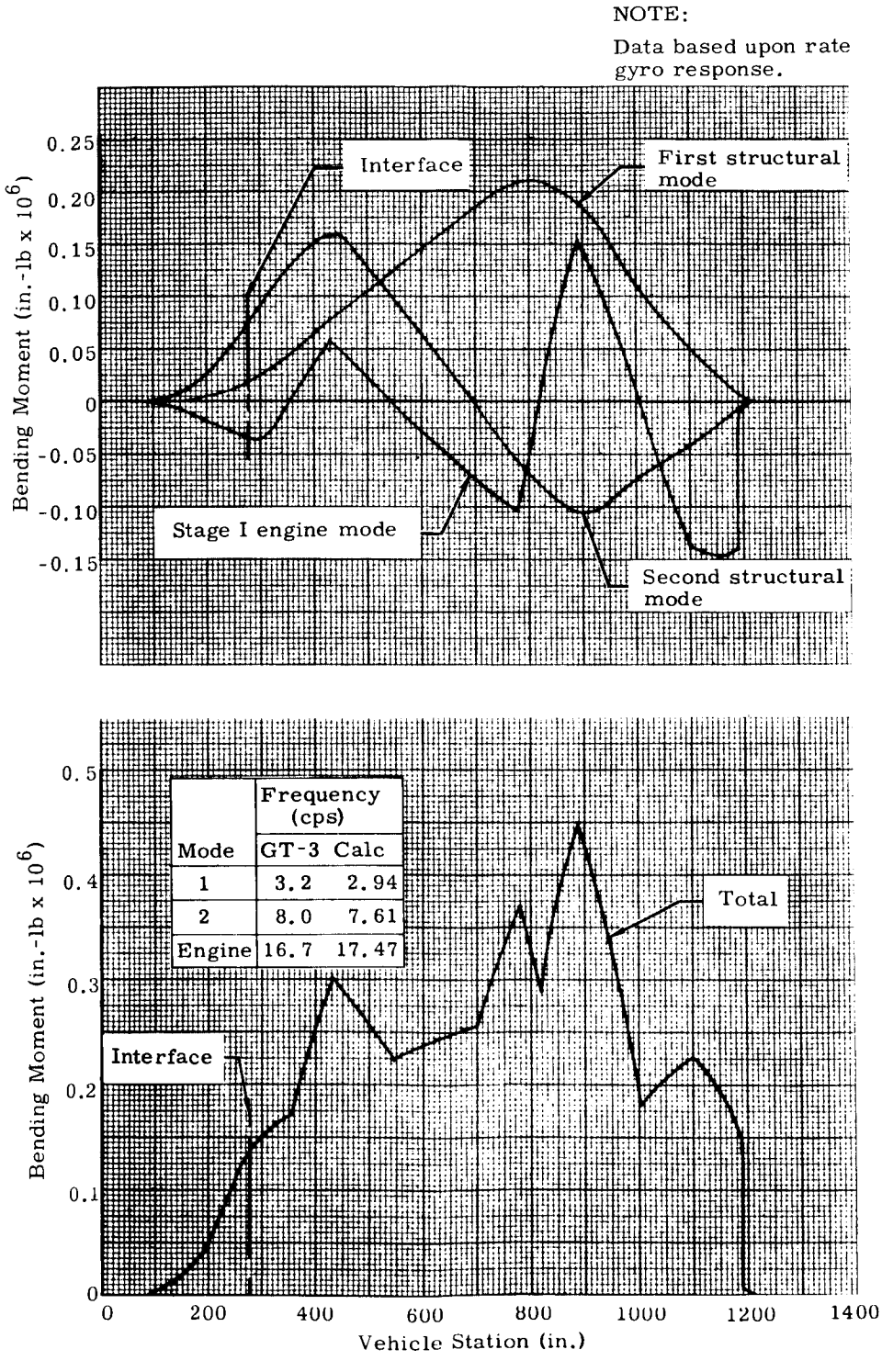


| Mode | Frequency (cps) GT-3 | Calc |
|---|---|---|
| 1 | 3.2 | 2.94 |
| 2 | 8.0 | 7.61 |
| Engine | 16.7 | 17.47 |

Fig. XII-15. Total Lateral Load Envelope--Transonic Buffet

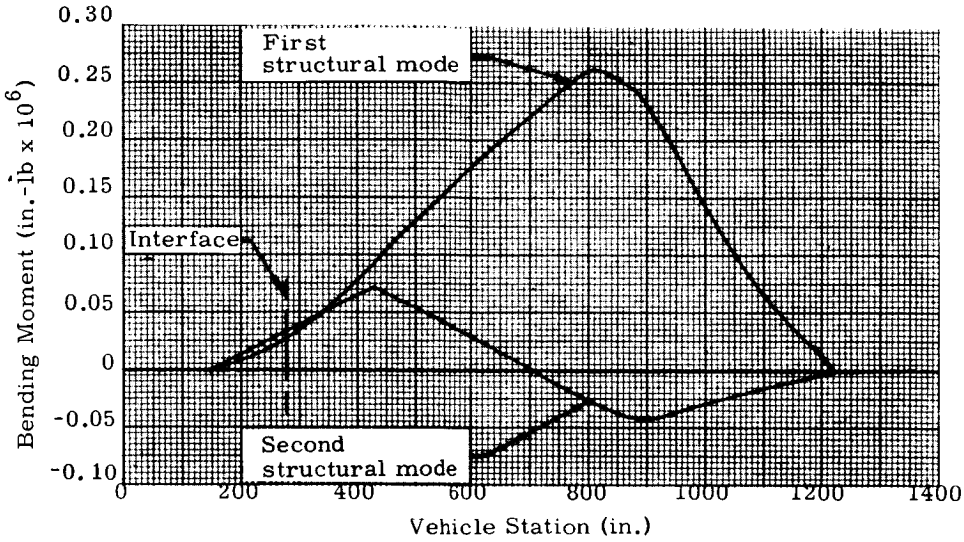


NOTE:

Data based upon rate gyro response.

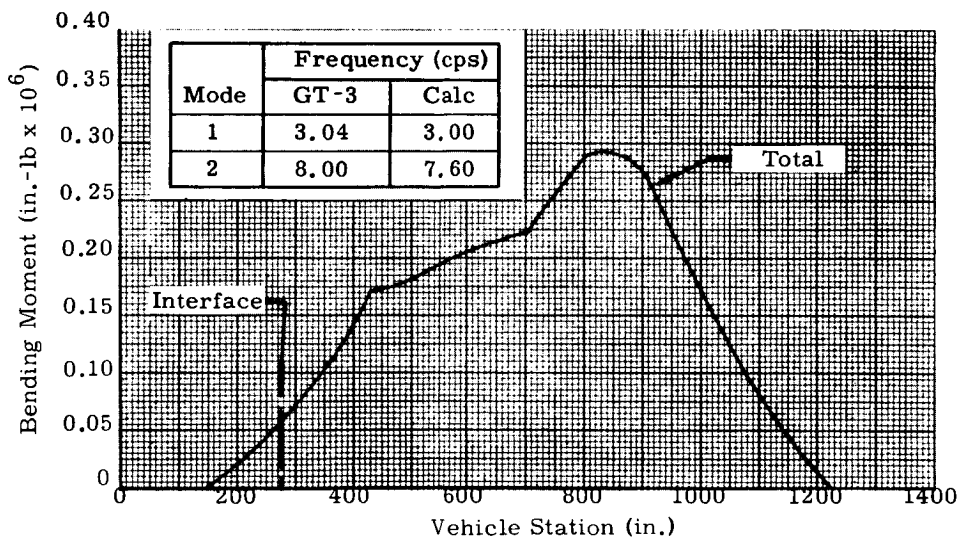


| Mode | Frequency (cps) GT-3 | Frequency (cps) Calc |
|---|---|---|
| 1 | 3.04 | 3.00 |
| 2 | 8.00 | 7.60 |

Fig. XII-16. Total Lateral Load Envelope--Max $C_{N_\alpha} q_\alpha$

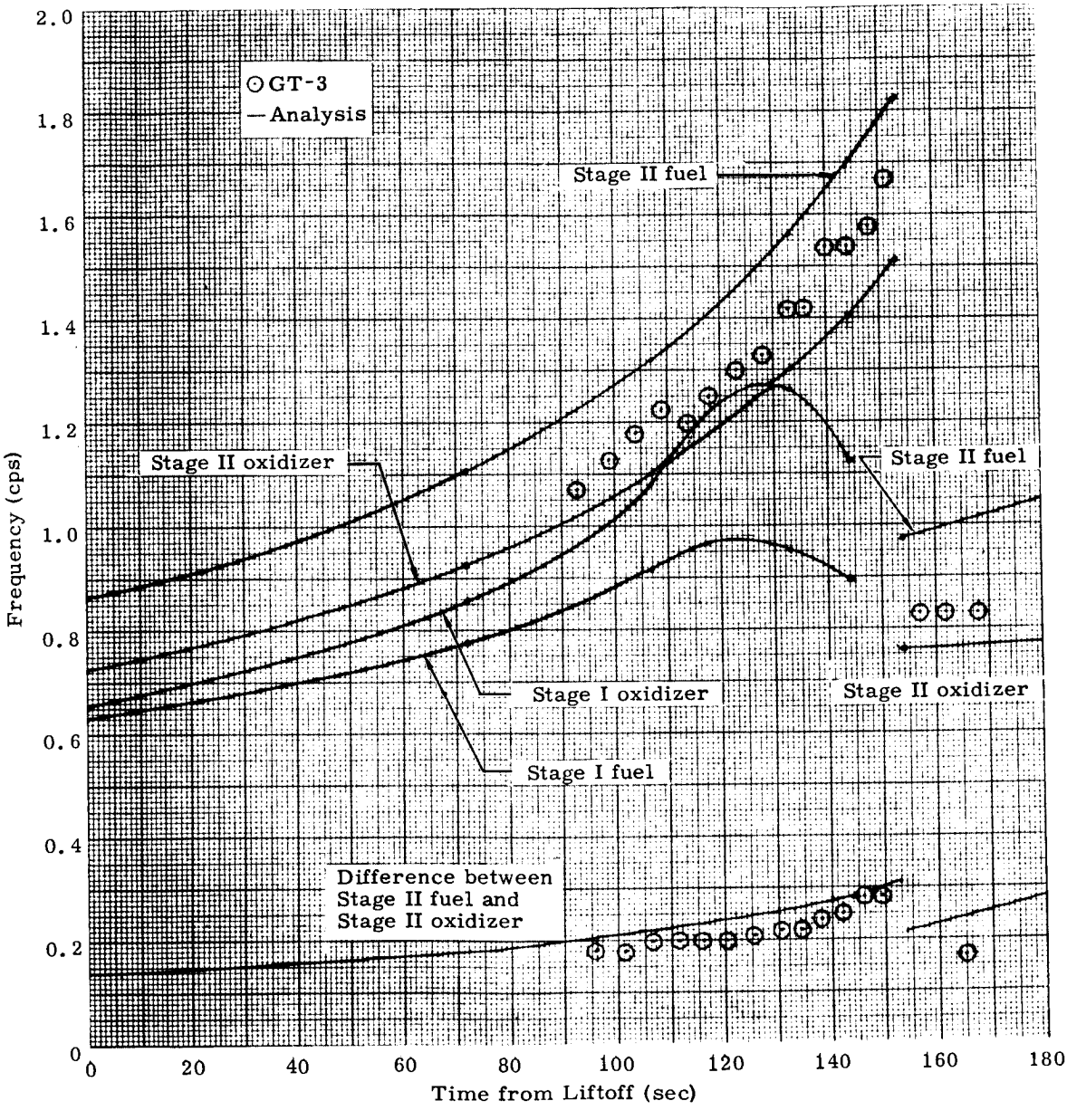


Fig. XII-17. Correlation of Observed Slosh Frequencies with Analysis

axial mode (19 cps). The resulting loads at Station 372 correlated with strain gage response loads as follows:

| Type | Meas | Load (lb) |
|---|---|---|
| Axial accelerometer | 0670 | 6400 |
| Strain gage | 0665 | 9660 |
| Strain gage | 0666 | 7245* |

* Based on an effective area of 13.0 in.$^2$

The greatest component of structural loading at pre-BECO is due to the steady axial load. Loads analysis using measured thrust values produced a maximum load of 261,000 pounds at Station 320. The axial acceleration as determined from the loads analysis (using measured thrust values) was 5.63 g which was the same value directly measured from the Compartment 1 axial accelerometer.

10. Pre-BECO--Lateral

Lateral dynamic responses during the pre-BECO period were observed primarily on the first, third and engine structural modes, and in the Stage II fuel slosh mode. The load distribution from these responses is shown in Fig. XII-18. The second mode responses are presumed to exist, but their existence was not evidenced on the Compartment 1 accelerometers and on the Stage II rate gyros because of the peculiar location of these transducers with respect to the second mode node and antinode.

A correlation of the load due to slosh mode responses at Station 372, as determined from various transducers, is as follows:

| Type | Meas | Load (in.-lb) |
|---|---|---|
| Rate gyro | 0723 | 31,200 |
| Accelerometer | 0672 | 32,700 |
| Strain gage | 0665 | 36,000* |

* Based on an effective area of 13.0 in.$^2$

11. Stage II Flight

The steady axial acceleration reached a value of 7.5 g at the end of Stage II flight. The various dynamic responses which occurred during this portion of the flight were low in magnitude. At Stage II ignition,

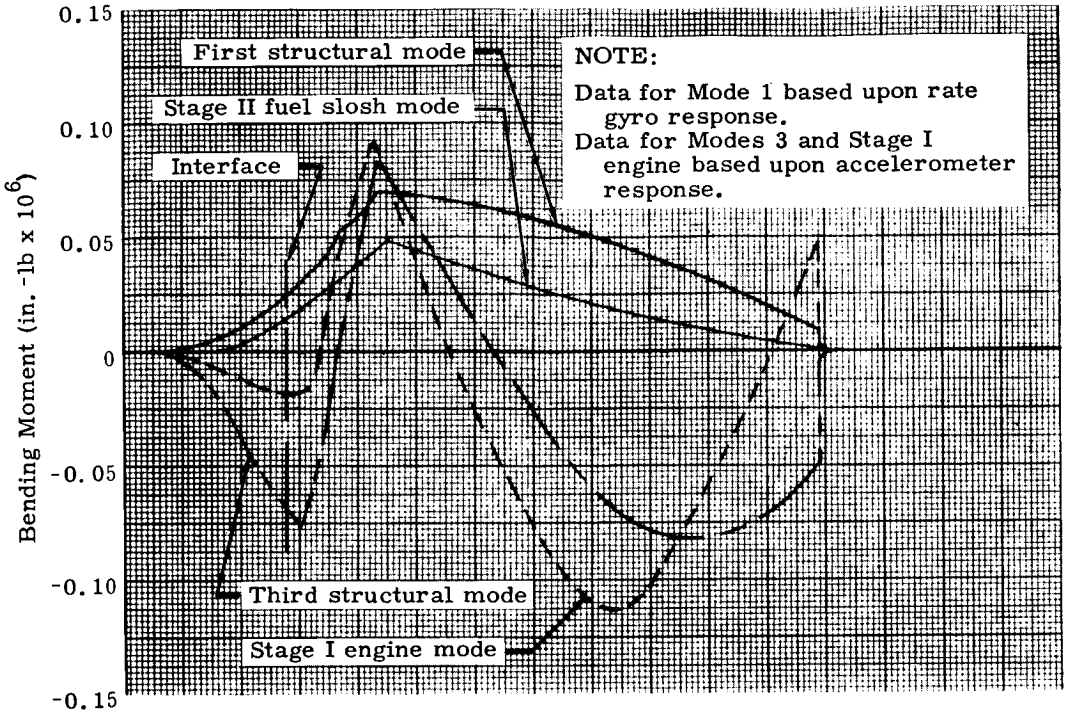


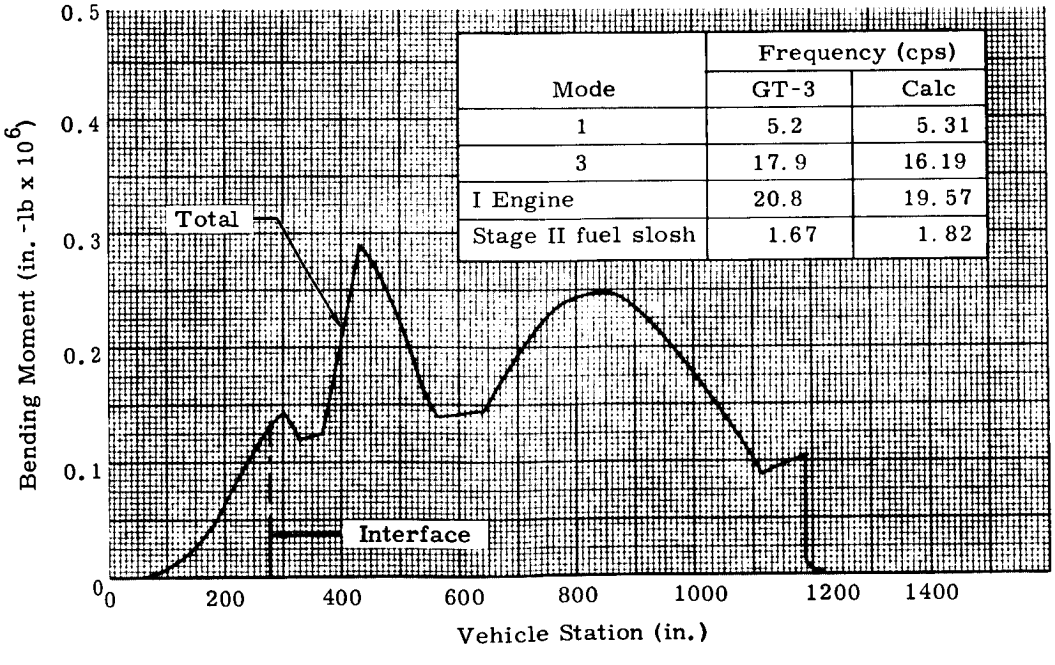


| Mode | Frequency (cps) | |
|---|---|---|
| | GT-3 | Calc |
| 1 | 5.2 | 5.31 |
| 3 | 17.9 | 16.19 |
| I Engine | 20.8 | 19.57 |
| Stage II fuel slosh | 1.67 | 1.82 |

Fig. XII-18. Total Lateral Load Envelope--Pre-BECO

the 24-cps axial mode was excited by the hypergolic ignition spike and resulted in a ±31,000-pound load at Station 372 as indicated by strain gage Meas 0666. The total load at this time was low relative to that experienced at pre-BECO.

A low frequency oscillation (0.83 cps) was induced by the staging process, which corresponds to the Stage II oxidizer slosh mode (Fig. XII-17). This resulted in a displacement at the crew station of approximately ±1.5 inches.

The only observed post-SECO transients were those induced by spacecraft separation. The resulting effect on the structure was negligible.

12. Total Airframe Loads

a. Launch prerelease

The prerelease total equivalent axial loads shown in Fig. XII-19 reflect the following considerations:

(1) Axial deadweight plus axial dynamic loads caused by engine ignition (Fig. XII-6)

(2) Lateral steady wind load (Fig. XII-2)

(3) Lateral oscillatory loads (Fig. XII-8)

(4) Stage I tank pressure.

The equivalent axial loads in all parts of the structure were well below the design limit. Aft of Station 1188, GT-3 experienced loads which were only 78% of design limit.

b. Launch post-release

The post-release total equivalent axial loads shown in Fig. XII-20 reflect the following:

(1) Axial acceleration

(2) Lateral bending moment transients induced by the sudden release from the launch stand (Fig. XII-10)

(3) Stage I tank pressure.

c. Transonic

The maximum total equivalent axial load at Mach 1.0, where the lateral dynamic loads are greatest, is shown in Fig. XII-21. This

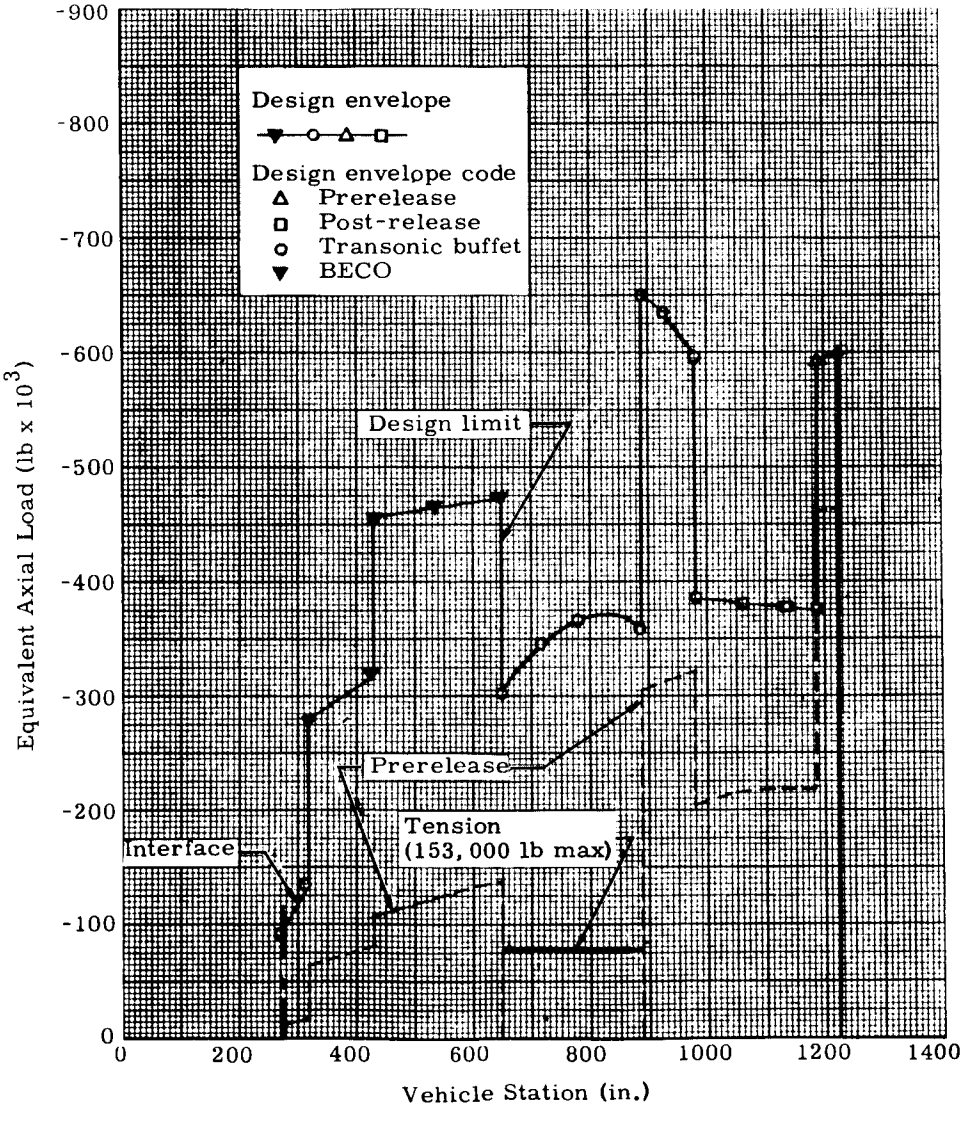


Fig. XII-19. Equivalent Axial Load: Prerelease Condition

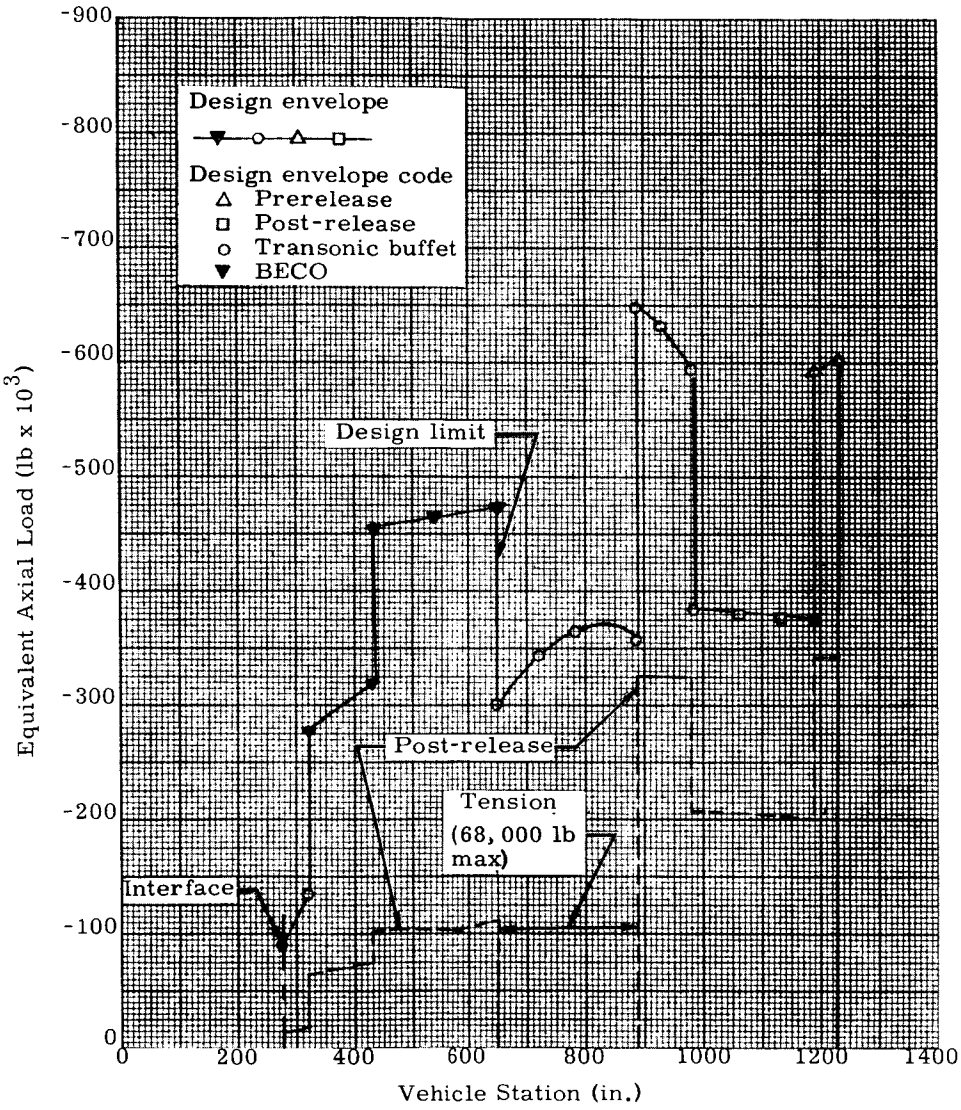


Fig. XII-20. Equivalent Axial Load: Post-release Condition

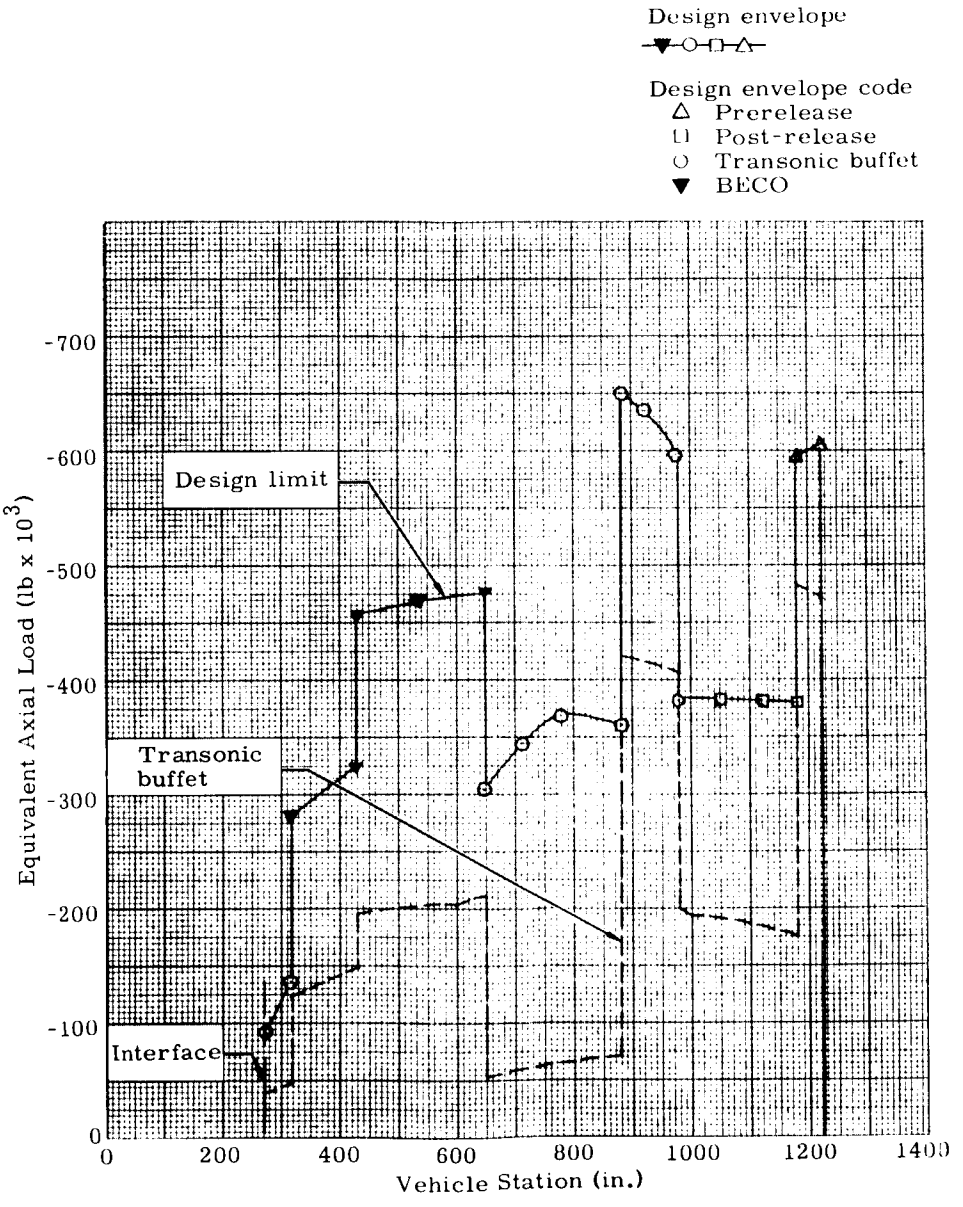


Fig. XII-21. Equivalent Axial Loads: Transonic Buffet

load includes the following:

(1) Axial acceleration applied to the deadweight load and axial air drag

(2) Axial oscillatory loads

(3) Quasi-steady lateral bending moment due to aerodynamic loading

(4) Lateral dynamic bending moments (Fig. XII-15)

(5) Stage I tank pressures.

The largest equivalent axial load occurred just aft of Station 1188, amounting to 81% of the design limit load.

d. Max $C_{N_\alpha} q \alpha$

The maximum total equivalent axial load during Stage I flight (Fig. XII-22) includes the following:

(1) Axial acceleration applied to the deadweight load and axial air drag

(2) Axial oscillatory loads

(3) Quasi-steady lateral bending moment due to aerodynamic loading

(4) Dynamic lateral bending moments (Fig. XII-16)

(5) Stage I tank pressures.

The largest equivalent axial load occurred just aft of Station 1188, and was 83% of the design limit load.

e. Pre-BECO

The time of maximum Stage I acceleration was considered. The pre-BECO total equivalent axial load shown in Fig. XII-23 comprises the following:

(1) Axial acceleration applied to the deadweight load

(2) Axial (POGO) oscillatory loads

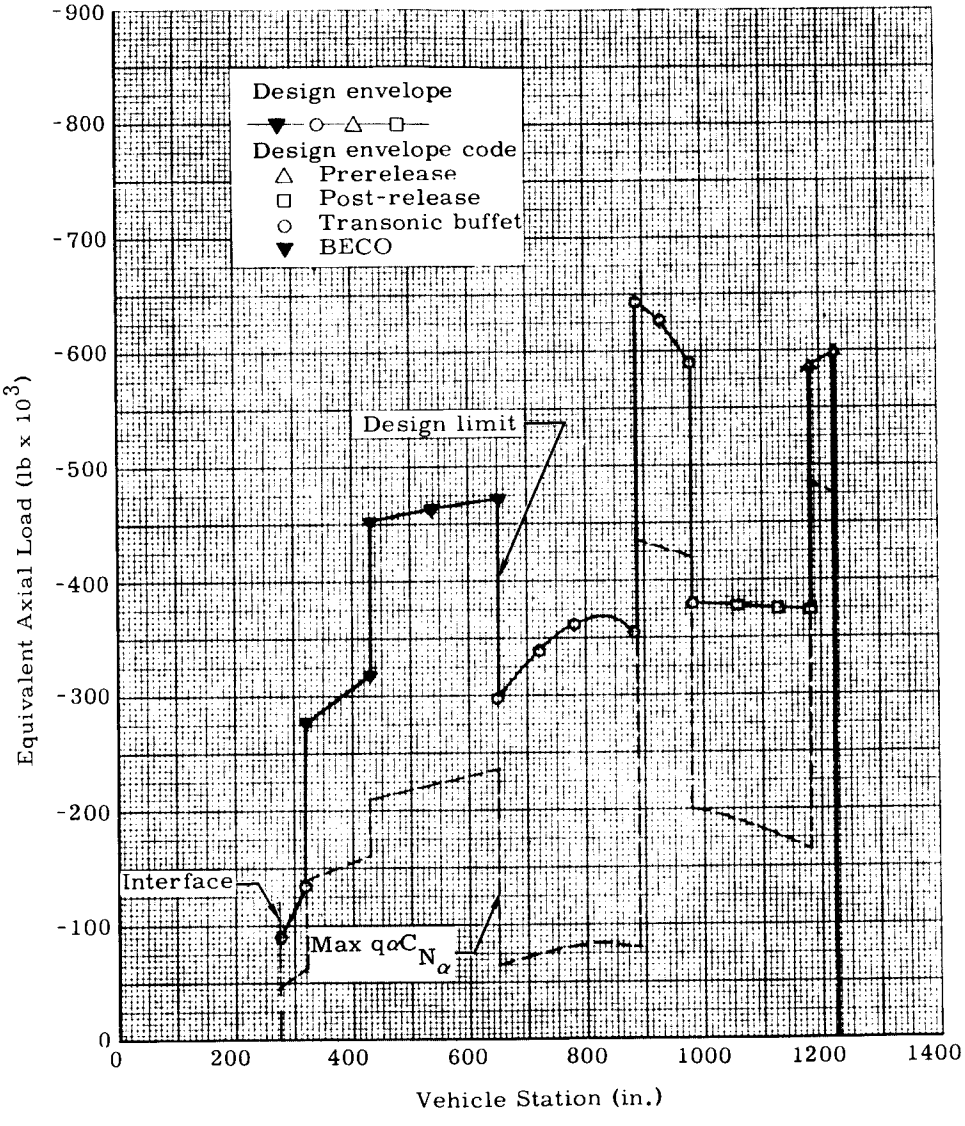


Fig. XII-22. Equivalent Axial Load--Maximum $C_{N_\alpha}$ q $\alpha$ Condition

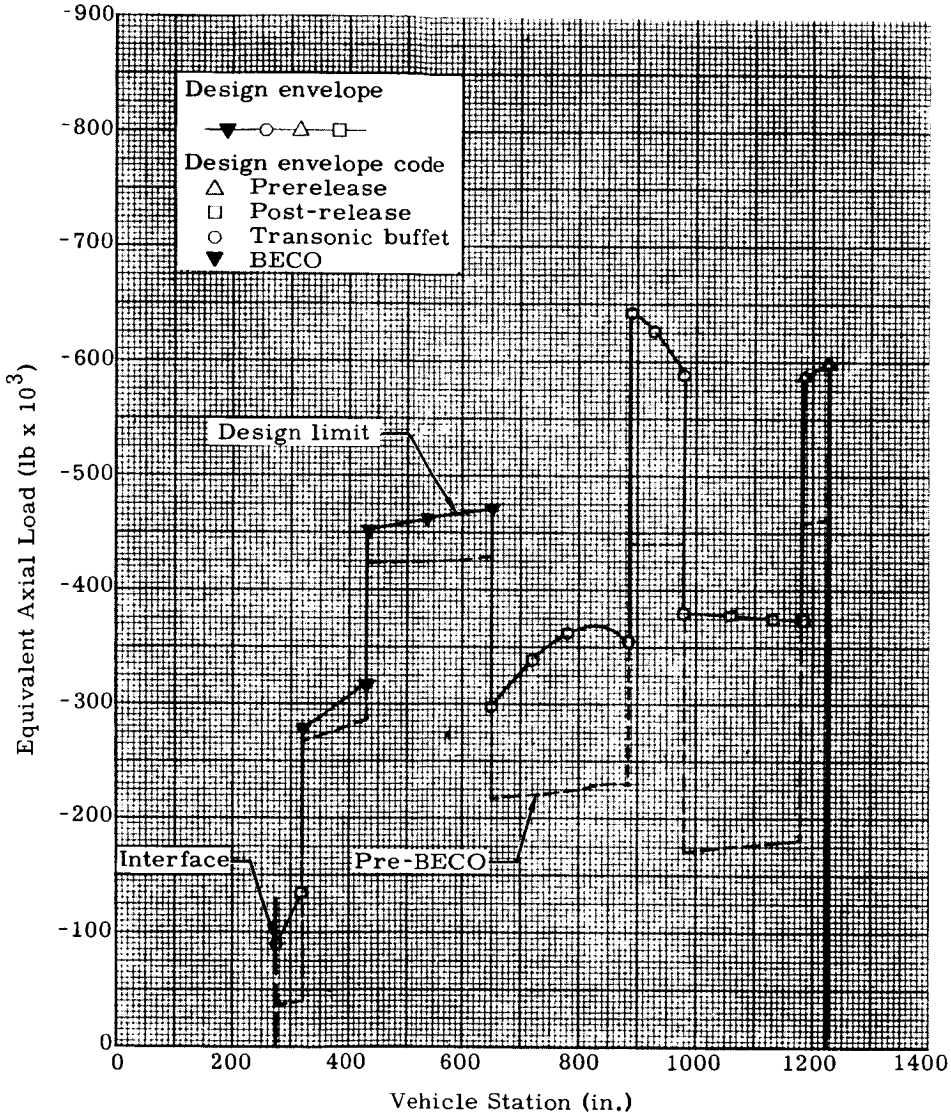


Fig. XII-23. Equivalent Axial Load: Pre-BECO

(3) Quasi-steady lateral bending moment

(4) Dynamic lateral bending moments (Fig. XII-18)

(5) Stage I tank pressures.

Just aft of the Stage II oxidizer lower dome tangency point (Station 320), the GT-3 axial equivalent load was equal to 97% of the design limit load. It must be realized, however, that this equivalent axial load was only 71% of the tested load. The apparent decrease in lateral dynamic loads on GT-3 is due to the inability to obtain loads attributed to dynamic responses in the second structural mode. Location of instrumentation was the cause for this inability of measurement.

f. Stage II flight

The maximum total equivalent axial load which occurred at SECO is shown in Fig. XII-24. It was due solely to the axial load caused by acceleration. The greatest equivalent axial load was only 59% of the design limit at Station 277.

## 13. Overall Load Envelope Comparison

The maximum flight equivalent axial loads from all loading conditions experienced by GT-3 are shown in Fig. XII-25; the limit design curve has been included for reference. Although the load at Station 320 was nearly equal to the limit design value, this condition was not considered critical since it represents only 71% of the tested strength.

As shown in Fig. XII-25, the flight conditions which caused the maximum equivalent axial loads were prerelease, Max $C_{N_\alpha} q \alpha$, and BECO. Table XII-3 summarizes the net interface (Station 276) loads experienced on this flight. These are comparable to loads occurring on the GT-2 flight and are well within design requirements.

## 14. Structural Anomalies

On previous flights (GT-1 and GT-2), structural integrity of the launch vehicle transportation section (Compartment 3B) during booster staging was not ascertainable. Astronaut debriefing from the GT-3 mission, however, indicated that particles classed as debris were sighted for a short period of time after stage separation. It is most likely that these particles were, in fact, debris resulting from the usual breakup of the transportation section; this has been substantiated by examination of tracking films. Based on similar occurrences on Titan II flights and on subsequent analytical studies, there is no hazard to Stage II from

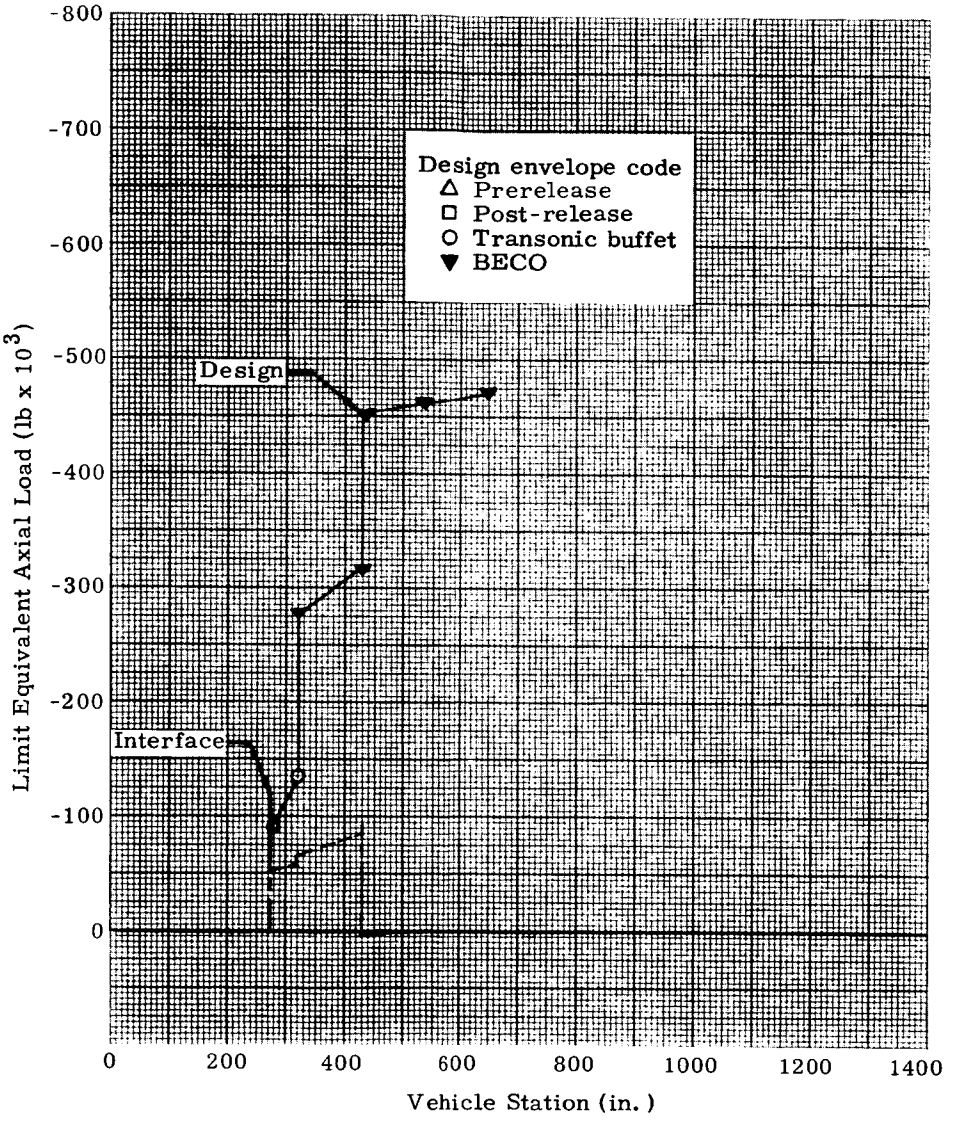


Fig. XII-24. Equivalent Axial Load: SECO Condition

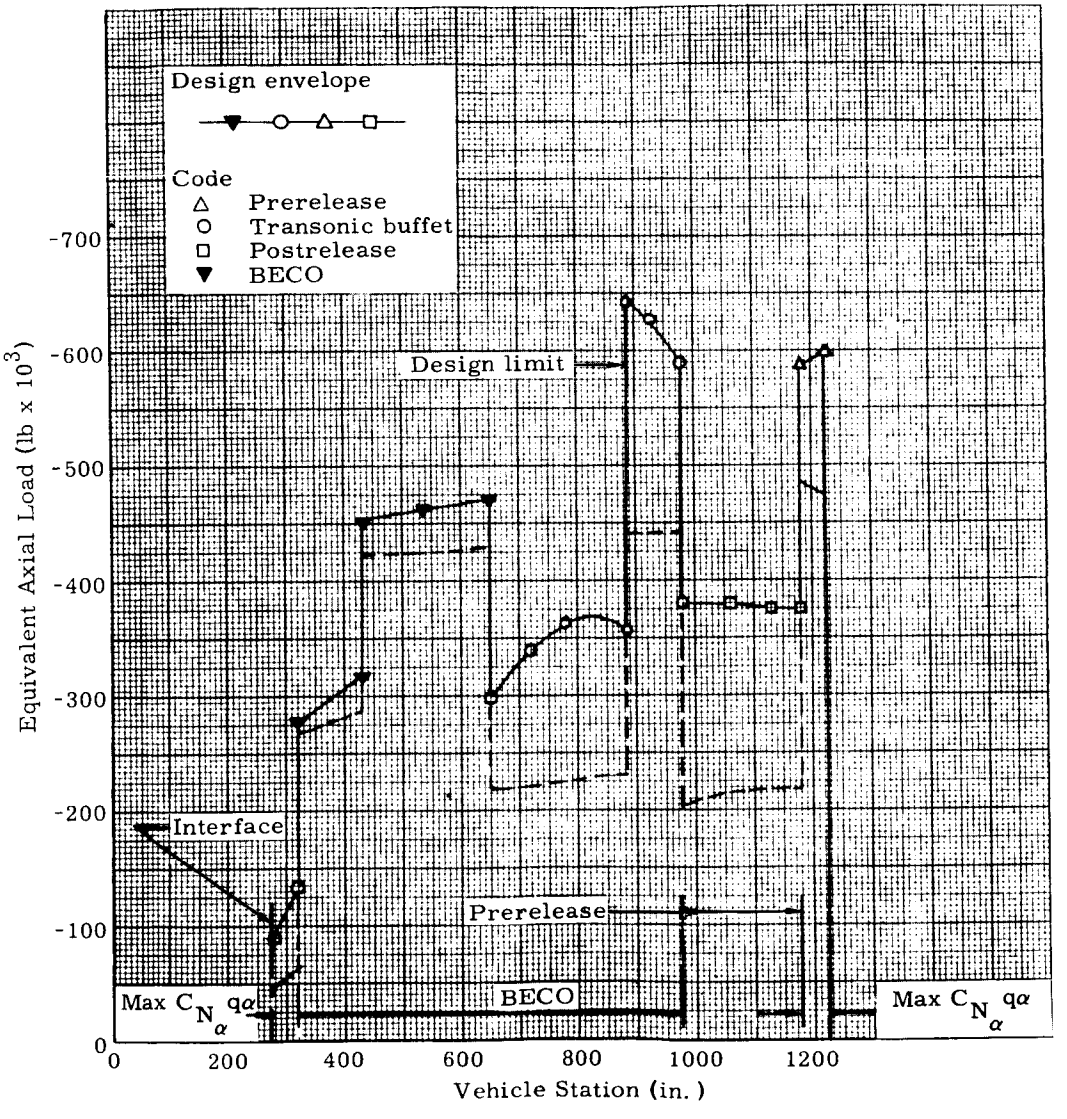


Fig. XII-25. Maximum Structural Load Envelope

this debris. Motion of the debris is normally directed radially outward from the vehicle and, since some forward velocity can be imparted to the particles, a momentary glimpse is possible.

## B. VIBRATION ENVIRONMENT

Three vibration transducers were incorporated on GLV-3 to obtain environmental data on the GT-3 flight. The primary results are shown in Fig. XII-26 and are listed in the following tabulation.

| Meas | Location | Orientation | Valid System Frequency Range (cps) | g rms | |
|---|---|---|---|---|---|
| | | | | Maximum | Spec 0 to 2000 cps |
| 1191 | Tandem Actuator $2_1$, Compartment 5 | Vertical (actuator axes) Lateral (GLV axes) | 1200 | 7.0 at LO | 54 |
| 1697 | RGS equipment mount | Lateral (GLV axes) | 660 | 1.45 at LO + 4 sec | 14.3 |
| 1698 | Compartment 2 truss | Vertical (GLV axes) | 2000 | 3.0 at LO + 58 sec | 14.3 |

Although the maximum g rms values listed are with respect to power spectrum analyses covering the frequency range up to twice the valid system frequency range, the actual values for Meas 1191 and 1697 may be somewhat lower than those shown because of the limitation of the system frequency range of these measurements. Conversely, data from Meas 1698 may be conservative. Data were not obtained during Stage II flight.

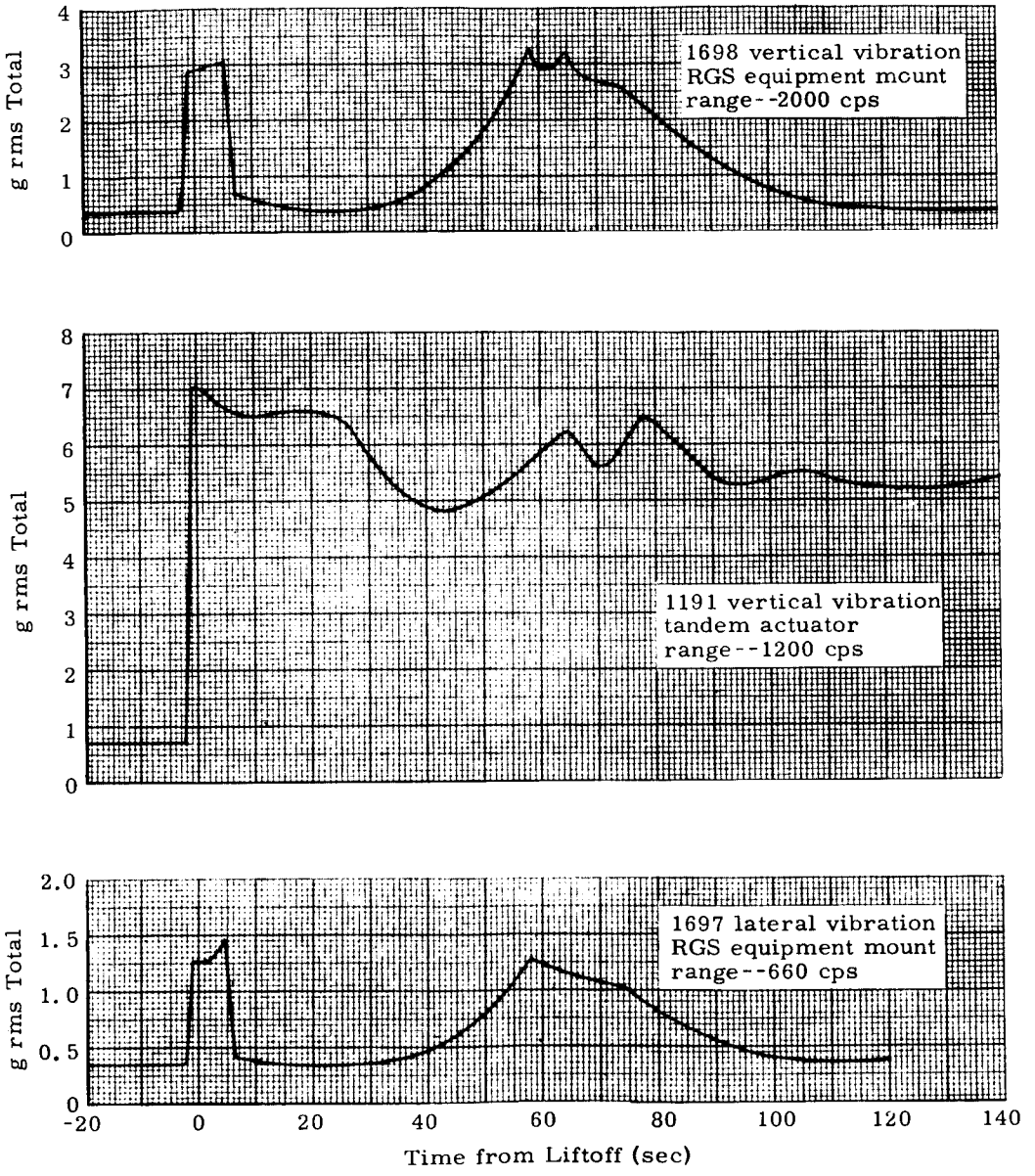


Fig. XII-26. Vibration--g rms

TABLE XII-3

GT-3 Spacecraft/Launch Vehicle Interface Net Loads Comparison

| Condition | Compartment Pressure | | Compressive Equivalent Axial Load (lb) | |
|---|---|---|---|---|
| | Differential (psi) | Load (lb) | Pressure Neglected | Pressure Included |
| Transonic Max $C_{N_\alpha} q\alpha$ | +1.05<br>+1.82 | +11,875<br>+20,584 | -40,002<br>-46,374 | -28,127<br>-25,790 |
| BECO Design | --<br>+3.0 | --<br>+33,930 | -42,917<br>-94,300* | --<br>-60,400 |

| Condition | Compartment Pressure | | Tensile Equivalent Axial Load (lb) | |
|---|---|---|---|---|
| | Differential (psi) | Load (lb) | Pressure Neglected | Pressure Included |
| Transonic Max $C_{N_\alpha} q\alpha$ | +1.05<br>+1.82 | +11,875<br>+20,584 | -2,669<br>-11,827 | +9,206<br>+8,757 |
| BECO Design | --<br>+3.0 | --<br>+33,930 | -33,912<br>+52,430 | --<br>+86,230* |

*The data in this table indicate the effect of a positive compartment pressure on interface axial loads. The reduction in axial compressive loading due to this positive compartment pressure is not included in the compression design loading but is included in the tensile design loading. GT-3 experienced interface loads amounting to 29.8% of design compression and 10.7% of design tension. Measurement of compartment pressure differential was available on GT-1 and GT-2 only. The differential used for GT-3 was data from GT-2; BECO Compartment 1 pressure was not available from GT-2 for this analysis.

Interface design loads shown in this table were obtained from Ref. 13.

## C. STRUCTURAL INTEGRITY PROGRAM

The structural integrity flight evaluation program carried out on the GT-2 and GT-3 flights was comprised of the following:

(1) A calorimeter to measure heat input to the Stage I oxidizer tank dome due to cross-flow of boundary layer air in the

transportation section (Compartment 3B) in the event of high angles of attack during Stage I flight.

(2) Temperature measurements to determine the degree of aerodynamic heating resulting from trajectory dispersions or from a slow drift-type malfunction.

(3) Strain gage measurements for evaluation of structural loads in the event of a switchover and the effect of total angle of attack during flight.

Instrument locations appear in Fig. XII-27. The calorimeter was mounted on the Stage I oxidizer tank forward dome at Station 608.

1. Calorimeter Data

Temperature measurements from the calorimeter (Meas 0176) indicate that cross-flow heating in Compartment 3B on this flight was virtually nonexistent. This has been substantiated by the post-flight reconstructed trajectory which indicated angles of attack on the order of four degrees. An angle of attack of this magnitude would produce very little cross-flow through the compartment. The calorimeter did experience a rapid temperature rise upon ignition of the Stage II engine (approximately 600° F in a fraction of a second) which was expected due to the impingement of hot exhaust gases on the tank dome. Tank dome temperature history is as follows:

| Stage I Oxidizer Tank Dome Temperature (Meas 0176) | | | | | | | | | | | |
|---|---|---|---|---|---|---|---|---|---|---|---|
| Time (sec) | 0 | 20 | 35 | 45-85 | 90 | 95 | 100 | 105 | 110 | 120-153 | 153+ |
| Temperature (° F) | 79.7 | 76.8 | 74 | 71.1 | 74 | 76.8 | 79.7 | 82.6 | 85.4 | 88.3 | 603.5* |

*Gage limit.

2. Temperature Measurements

The temperatures recorded by the transducers had to be corrected to account for a small lag due to the thermal capacity of the transducer according to the relationship:

$$T_c = T_i + K\Delta T \qquad (1)$$

where

$T_c$ = corrected temperature (° F)

$T_i$ = temperature at start of heating (° F)

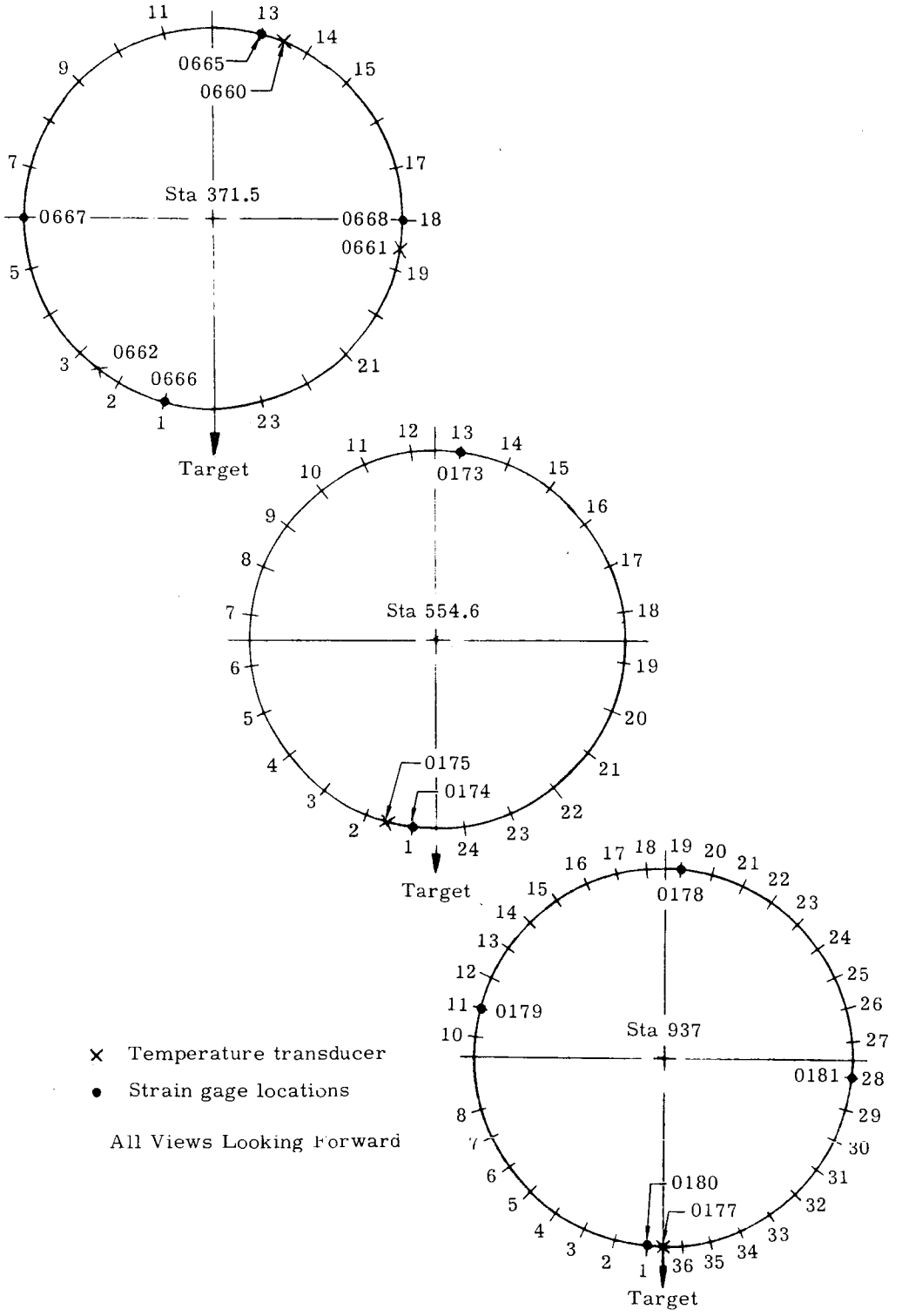


Fig. XII-27. Structural Integrity Instrumentation Locations

$\Delta T$ = measured temperature rise from $T_i$ (° F)

K = 1.09

The corrected temperatures are shown in Fig. XII-28 for the three transducers at Station 377 and in Fig. XII-29 for Stations 564 and 935. These skin temperature measurements were taken as far as possible from large heat sinks such as stringers or other internal structural members. For loads analyses, it is necessary to arrive at temperatures of strain-gaged members in order that the material properties can be adjusted. It was found that at the peak skin temperature the corresponding stringer temperature was low enough such that the degradation of the stringer modulus of elasticity was less than 1%. Therefore, stringer temperature increases above ambient have been neglected.

3. Strain Gage Evaluation

Strain measurements recorded at Stations 371 and 937 on the GT-3 flight are presented in Tables XII-4 and XII-5. Strain history for Stations 371, 555 and 937 are plotted in Figs. XII-30, XII-31 and XII-32.

A basic assumption necessary in the strain gage data evaluation is that the launch vehicle bending planes remain planar. This is reasonable since the basic structure is generally stability-critical, and for the anticipated flight loads no plastic deformation of structure is expected. The measured strains were therefore expected to fall within a defined plane; however, this condition was not indicated by the flight data.

Since three points determine a plane, load planes for Stations 371 and 937 were determined by utilizing combinations of the four recorded strains at these stations. Thus, for any flight condition examined, the test data indicate that four load planes are possible at each station. The calculated strain for any one of the four gage locations at Stations 371 and 937 was obtained by assuming that the remaining three measured strains were planar. The comparison between measured and calculated strains appears in Tables XII-4 and XII-5.

The axial loads calculated from strain data (internal measurements) were generally lower than those derived from the reconstructed trajectory (external measurement). As may be seen in Tables XII-4 and XII-5, the loads obtained from strain data indicate that all skin panels were buckled. One manner in which more realistic loads can be derived from the strain data would be to apply a modified panel buckling and effective skin criteria.

The strain measurement loads digital program used in calculating the GT 2 loads (Ref. 1), and the original GT-3 loads (Tables XII-4 and

Sta 377

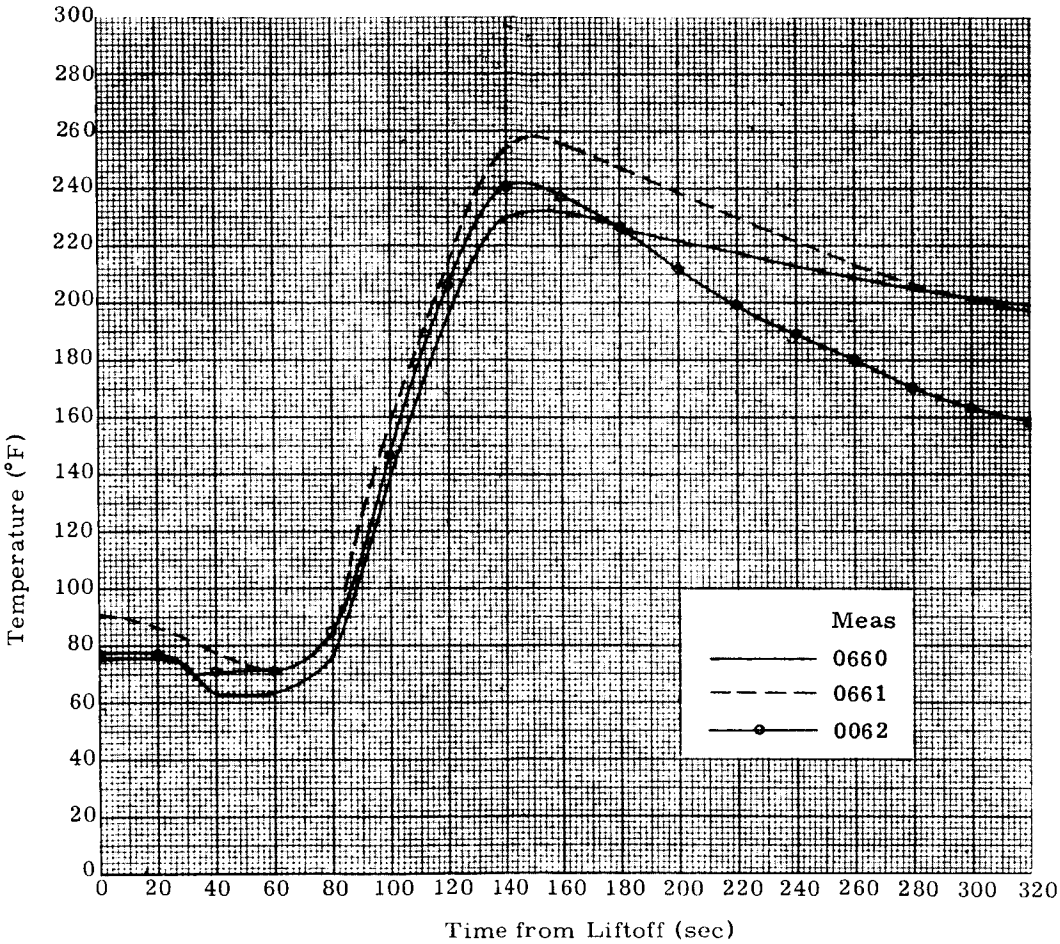


Fig. XII-28. Skin Temperatures Versus Time

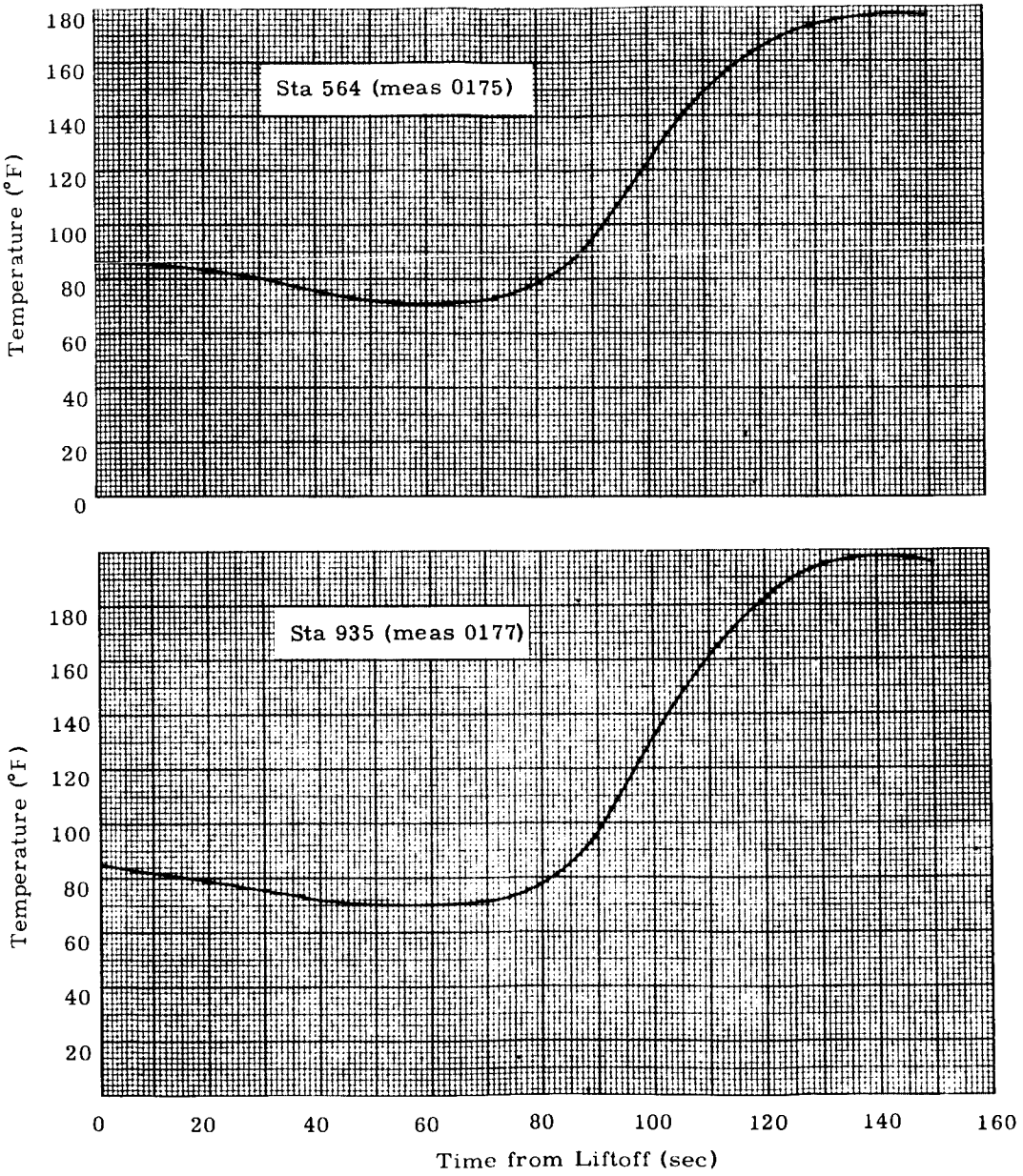


Fig. XII-29. Skin Temperatures Versus Time

## Station 371 Measured Strains Versu

| Time (sec) | Meas $\epsilon_{0665}$ | Calculated $\epsilon_{0665}$ | Meas $\epsilon_{0666}$ | Calculated $\epsilon_{0666}$ | Meas $\epsilon_{0667}$ | C |
|---|---|---|---|---|---|---|
| -3.0 | -0.000247 | | -0.000244 | | -0.000278 | |
| | | -0.000283 | | | | |
| | | | | -0.000280 | | |
| | | -0.000242 | | | | |
| | | | | -0.000239 | -0.000278 | |
| | | | | | -0.000238 | |
| | | -0.000243 | | | | |
| | | | | -0.000240 | | |
| | | -0.000202 | | | | |
| -3.0 | -0.000247 | | -0.000244 | -0.000199 | -0.000238 | |
| 70 | -0.000660 | | -0.000945 | | -0.000480 | |
| | | -0.000447 | | | | |
| | -0.000660 | | | -0.000732 | -0.000480 | |
| | -0.000701 | | | | -0.000520 | |
| | | -0.000528 | | | | |
| | -0.000701 | | -0.000945 | -0.000772 | -0.000520 | |
| | -0.000660 | | -0.000986 | | -0.000480 | |
| | | -0.000447 | | | | |
| | | | | -0.000773 | | |
| | | -0.000406 | | | | |
| 70 | | | | | -0.000480 | |
| 80 | | | | | -0.000720 | |
| | | -0.000479 | | | | |
| | | | | -0.000805 | -0.000720 | |
| | | | | | -0.000759 | |
| | | -0.000518 | | | -0.000759 | |
| 80 | -0.000660 | | -0.000986 | -0.000844 | -0.000759 | |
| 150 | -0.001524 | | -0.001997 | | -0.001719 | |
| | | -0.001660 | | | | |
| 150 | -0.001524 | | -0.001997 | -0.002133 | -0.001719 | |

*P does not include 1 g deadweight of empty booster plus payload; Sta
**Dynamic loads included.

TABLE XII-4

Computed Strains and Strain Derived Loads Versus Trajectory Derived Loads

| lculated $\epsilon_{0667}$ | Meas $\epsilon_{0668}$ | Calculated $\epsilon_{0668}$ | $\omega$ (deg) | $\overline{Y}$ (in.) | Panels Buckled | Strain P Axial* (lb) | Strain Moment (in.-lb) | Trajectory P Axial (lb) | Trajectory Moment (in.-lb) |
|---|---|---|---|---|---|---|---|---|---|
| | -0.000249 | -0.000213 | 72.47 | 2.73 | 2,4,7,9,15,20 | -33,116 | -47,583 | -48,000 | -16,000 |
| | | | 31.06 | 0.14 | 2,4,7,9,15,20 | -35,176 | -97,402 | | |
| 000242 | | | -80.04 | -3.06 | 2,4,7,9,15 | -33,080 | -116,332 | | |
| | -0.000249 | | -47.70 | 3.62 | 2,4,7,9,15,20 | -35,135 | -42,688 | | |
| | -0.000208 | | 76.58 | 3.02 | | -32,827 | -49,019 | | |
| 000283 | -0.000208 | | 72.80 | 2.85 | | -33,113 | -65,061 | | |
| | -0.000208 | | 68.87 | 2.63 | 2,4,7,9,15,20 | -32,833 | -64,631 | | |
| | -0.000249 | -0.000253 | 86.50 | -2.60 | 2,4,7,9,15 | -33,071 | 117,350 | | |
| | -0.000249 | | 70.09 | -1.99 | | -32,842 | 88,649 | | |
| | -0.000249 | | -68.66 | -3.22 | | -32,848 | -131,831 | | |
| | -0.000208 | | -40.25 | 4.18 | | -30,469 | -25,290 | | |
| | -0.000208 | | 27.46 | 0.15 | 2,4,7,9,15 | -30,540 | -115,947 | -48,000 | -16,000 |
| | -0.000912 | -0.001125 | 54.04 | 0.90 | 2,4,7,9,15,18,20 | -93,005 | 1,277,412 | -110,488 | -902,216 |
| | | | 34.38 | 1.39 | | -81,708 | 1,182,240 | | |
| 000693 | | | 31.76 | 0.75 | | -93,178 | 622,931 | | |
| | -0.000912 | | 66.22 | 0.34 | | -81,910 | 800,891 | | |
| | -0.000953 | -0.001126 | 55.59 | 0.75 | | -95,214 | 1,181,836 | | |
| | | | 38.33 | 1.09 | | -86,064 | 1,083,949 | | |
| 000693 | | | 38.89 | 0.58 | | -95,346 | 635,578 | | |
| | | | 66.35 | 0.30 | | -86,209 | 799,787 | | |
| | | -0.001166 | 52.76 | 0.98 | | -95,132 | 1,374,503 | | |
| | | | 34.63 | 1.45 | | -83,842 | 1,287,060 | | |
| 000693 | | | 32.56 | 0.79 | | -95,314 | 728,482 | | |
| | -0.000953 | | 62.73 | 0.48 | | -84,052 | 886,388 | | |
| | -0.000912 | | 31.10 | 1.62 | | -81,651 | 1,286,494 | | |
| 000734 | -0.000912 | | 24.80 | 0.90 | | -95,330 | 619,354 | -110,488 | -902,216 |
| | -0.000745 | -0.000926 | 27.68 | 0.86 | | -95,325 | 654,937 | -120,564 | -360,748 |
| | | | 26.93 | 1.86 | | -85,698 | 753,907 | | |
| 000901 | | | -27.82 | 1.90 | | -95,342 | 411,731 | | |
| | | | 9.06 | 1.02 | | -85,869 | 180,207 | | |
| | | -0.000887 | 10.00 | 1.00 | | -95,337 | 559,127 | | |
| | | | -1.67 | 1.83 | | -87,786 | 666,898 | | |
| | -0.000745 | | -4.29 | 1.33 | | -87,917 | 204,017 | -120,564 | -360,748 |
| | -0.001938 | -0.001802 | 9.21 | 0.67 | | -192,702 | 702,184 | -258,923; -265,323** | -6030; -131,030** |
| | | | 28.25 | 0.40 | | -199,737 | 657,546 | | |
| 001583 | | | 31.26 | 0.46 | | -192,697 | 1,004,501 | | |
| | -0.001938 | | 17.63 | 0.62 | 2,4,7,9,15,18,20 | -199,670 | 1,030,205 | -258,923; -265,323** | -6030; -131,030** |

tion 371 1 g deadweight = 10,400 lb.

# TABLE XII-5

## Station 937 Measured Strains Versus Computed Strains and Strain Derived Loads Versus Trajectory Derived Loads

Station 937 Measured Strains Versus Computed Strains and Strain Derived Loads Versus Trajectory Derived Loads

| Time (sec) | Meas $\epsilon_{0178}$ | Calculated $\epsilon_{0178}$ | Meas $\epsilon_{0179}$ | Calculated $\epsilon_{0179}$ | Meas $\epsilon_{0180}$ | Calculated $\epsilon_{0180}$ | Meas $\epsilon_{0181}$ | Calculated $\epsilon_{0181}$ | $\omega$ (deg) | $\bar{Y}$ (in.) | Panels Buckled | Strain P Axial* (lb) | Strain Moment (in.-lb) | Trajectory P Axial (lb) | Trajectory Moment (in.-lb) |
|---|---|---|---|---|---|---|---|---|---|---|---|---|---|---|---|
| -3.0 | -0.000724 | | -0.000788 | | -0.000705 | | -0.000546 | -0.000642 | 77.56 | 1.97 | All | -197,997 | -216,000 | -247,000 | -240,000 |
| | | -0.000637 | | | | | | | -79.77 | 2.35 | | -188,050 | 650,243 | | |
| | | | | -0.000882 | | | | | 81.77 | 2.81 | | -197,470 | -848,080 | | |
| | | | | | | -0.000601 | -0.000546 | | 57.18 | 2.70 | | -186,203 | -607,000 | | |
| | | -0.000591 | | | | | -0.000496 | | -74.46 | 2.67 | | -182,733 | 899,000 | | |
| | | | | -0.000931 | | | -0.000496 | | 82.51 | 3.28 | | -197,111 | -1,179,000 | | |
| -3.0 | -0.000724 | | -0.000788 | | -0.000705 | -0.000547 | -0.000496 | | 52.58 | 3.14 | | -179,936 | -842,000 | -247,000 | -240,000 |
| 70 | -0.001012 | | -0.000836 | | -0.001417 | | -0.001284 | -0.001563 | 54.84 | 0.74 | | -304,601 | 2,803,000 | -352,713 | -1,917,522 |
| | | -0.000757 | | | | | | | 25.81 | 1.16 | | -277,529 | 2,650,000 | | |
| | | | | -0.001111 | | | | | 13.93 | 0.32 | | -304,502 | 1,520,000 | | |
| 70 | -0.001012 | | -0.000836 | | -0.001417 | -0.001113 | -0.001284 | | 72.14 | -- | | -273,120 | 1,729,000 | -352,713 | -1,917,522 |
| 80 | -0.001062 | | -0.001082 | | -0.001467 | | -0.000988 | -0.001414 | 31.45 | 0.21 | | -314,958 | 1,813,000 | -362,624 | -746,124 |
| | | -0.000673 | | | | | | | -16.68 | 2.03 | | -273,217 | 2,619,000 | | |
| | | | | -0.001502 | | | | | -58.80 | 2.10 | | -313,978 | 1,931,000 | | |
| | | | | | -0.001467 | -0.001004 | | | 52.10 | 1.41 | | -266,577 | -36,000 | | |
| | | | | | -0.001417 | | | -0.001368 | 30.91 | 0.09 | | -309,804 | 1,613,000 | | |
| | | -0.000715 | | | -0.001417 | | | | -17.54 | 1.79 | | -272,584 | 2,323,000 | | |
| 80 | -0.001062 | | -0.001082 | -0.001456 | -0.001417 | | -0.000988 | | -59.77 | 2.00 | | -308,891 | 1,711,417 | -362,624 | -746,124 |
| 150 | -0.001541 | | -0.001324 | | -0.001567 | | -0.001284 | -0.001785 | 81.77 | -0.29 | | -374,740 | 1,766,000 | -430,837; -435,977** | -1,489; -211,489** |
| | | -0.001084 | | | | | | | -14.70 | 0.83 | | -327,056 | 1,563,000 | | |
| | | | | -0.001812 | | | | | 87.79 | 1.76 | | -373,544 | -1,271,000 | | |
| 150 | -0.001541 | | -0.001324 | | -0.001567 | -0.001022 | -0.001284 | | -5.56 | 1.31 | All | -318,495 | -1,550,000 | -430,837; -435,977** | -1,489; -211,489** |

*P does not include 1 g deadweight of empty booster plus payload; Station 937 1 g deadweight = 14,200 lb.
**Dynamic loads included.

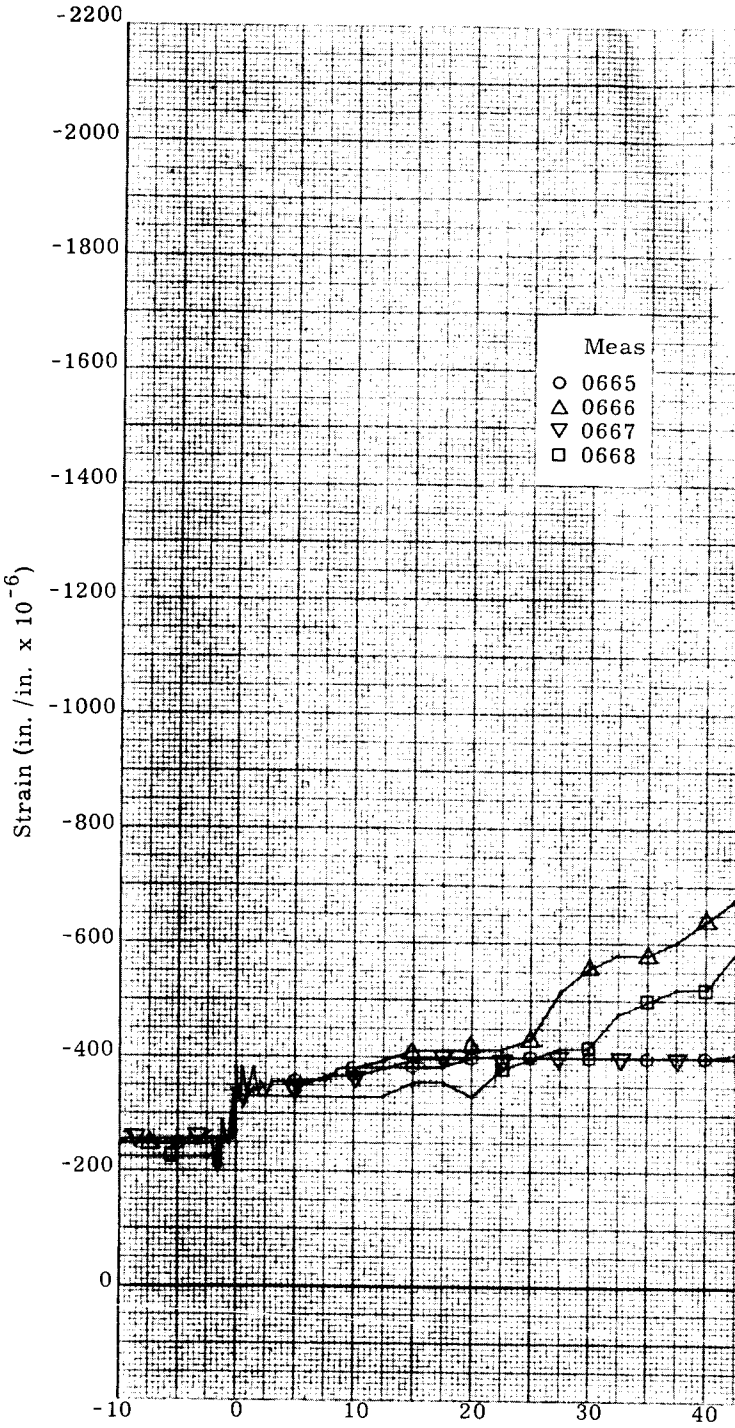
Meas
0665
0666
0667
0668
Strain (in. /in. x 10^-6)
-2200
-2000
-1800
-1600
-1400
-1200
-1000
-800
-600
-400
-200
0
-10
0
10
20
30
40

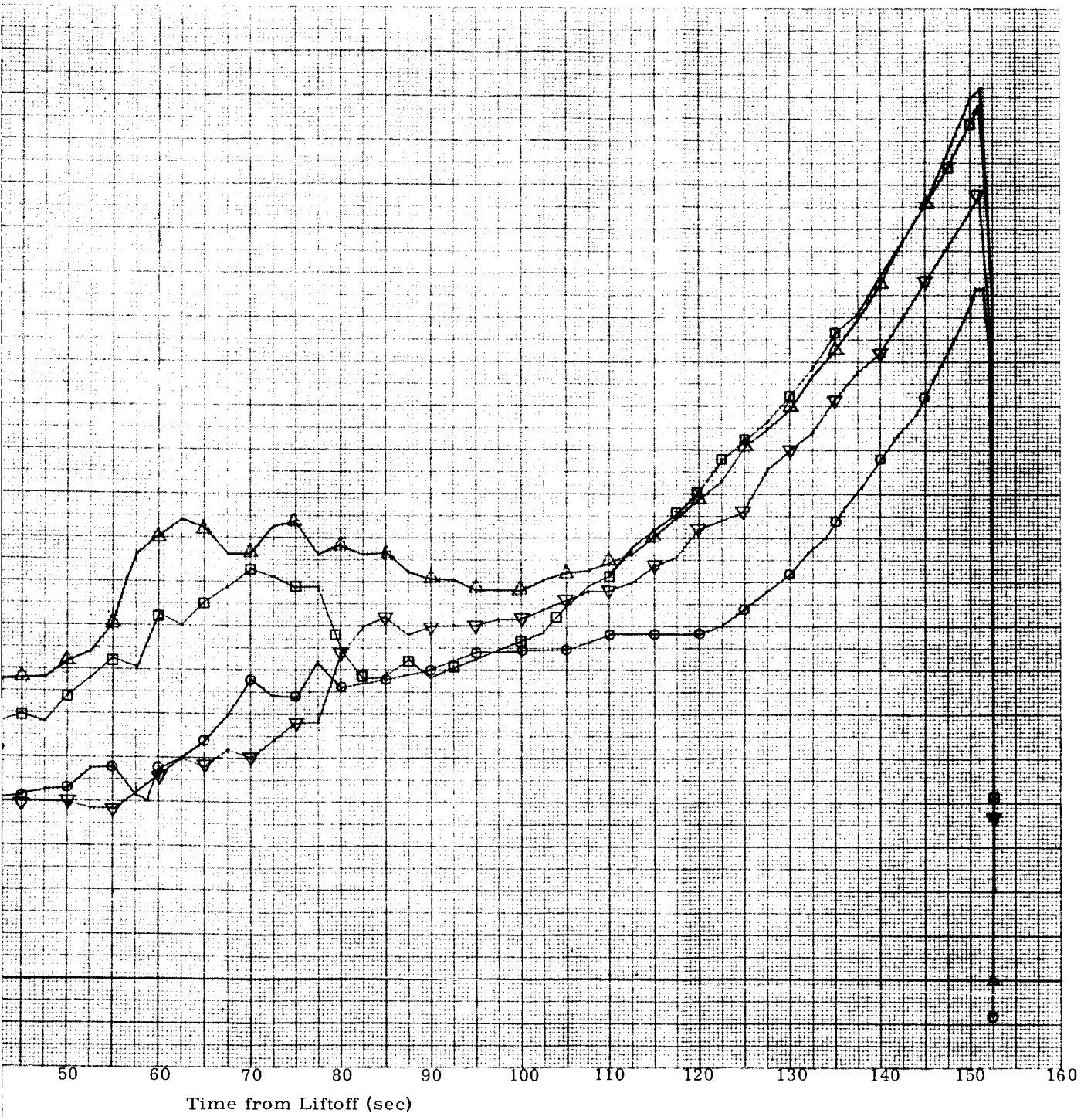


Fig. XII-30. Station 371 GT-3 Strain History

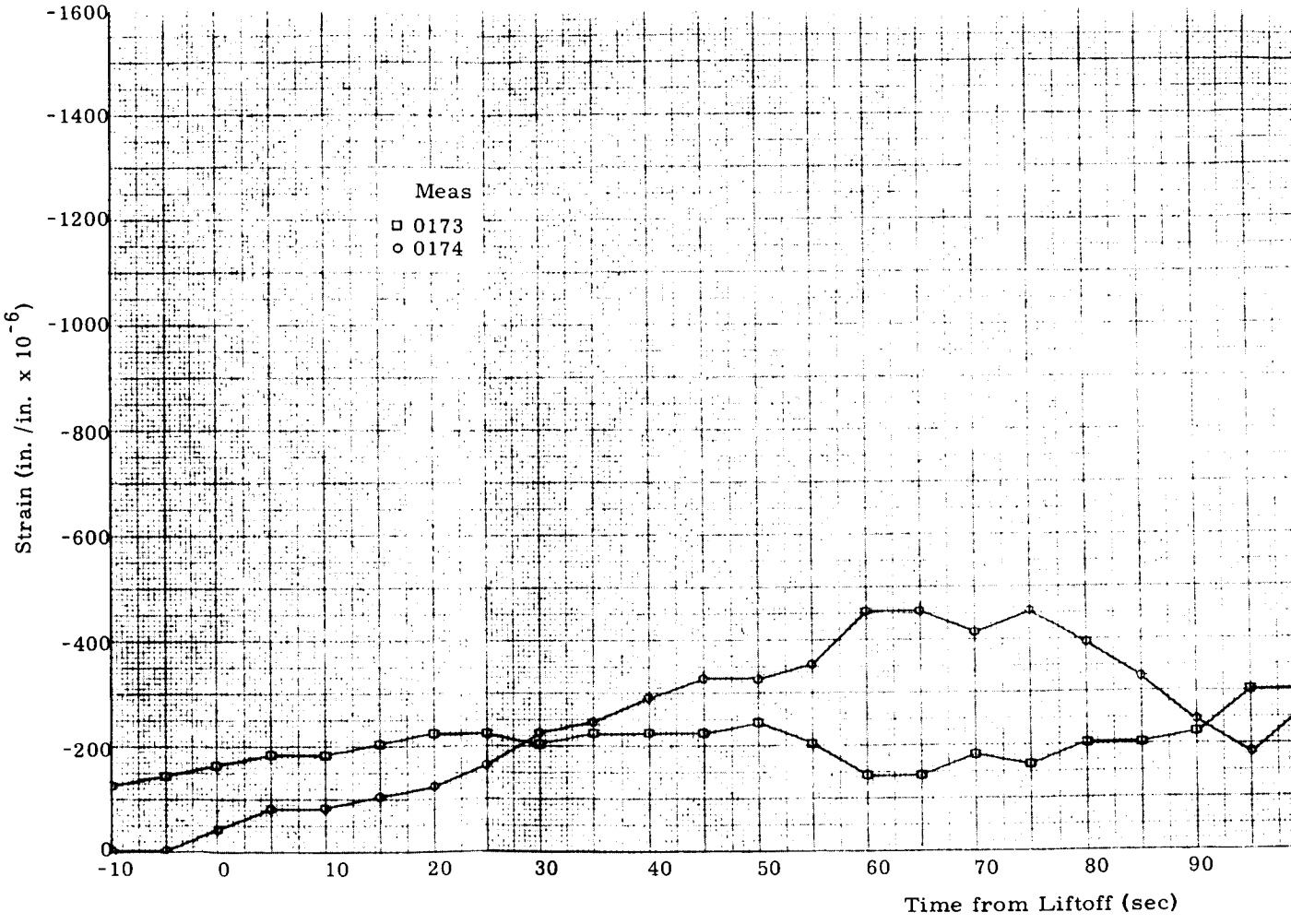
Meas
0173
0174
Strain (in. /in. x 10^-6)
-1600
-1400
-1200
-1000
-800
-600
-400
-200
0
-10
0
10
20
30
40
50
60
70
80
90
Time from Liftoff (sec)

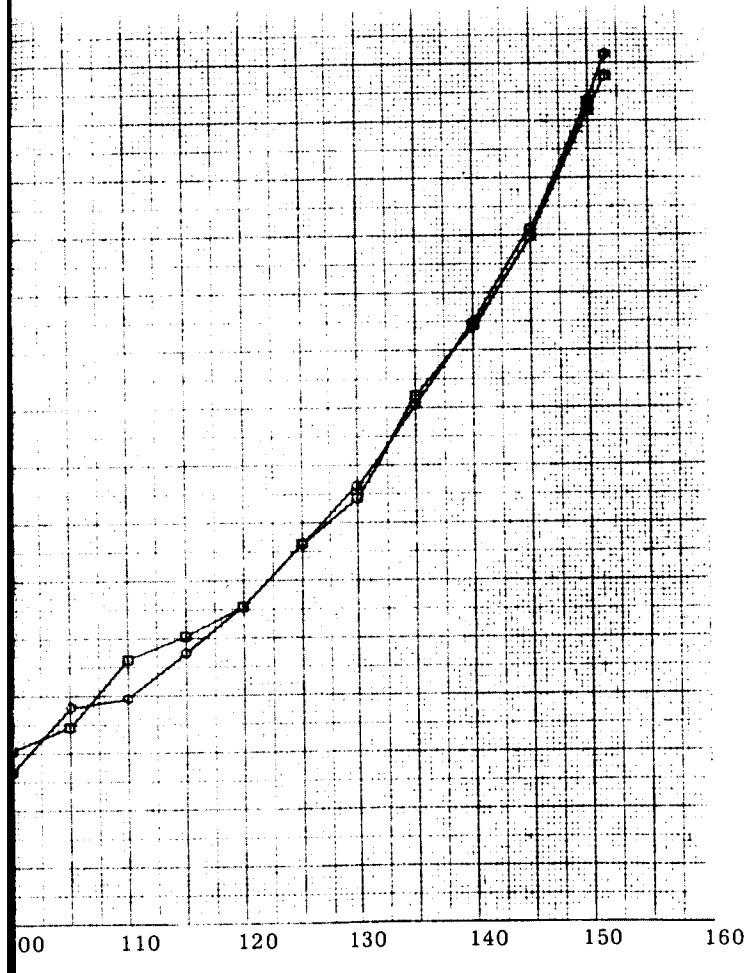


Fig. XII-31. Station 555 GT-3 Strain History

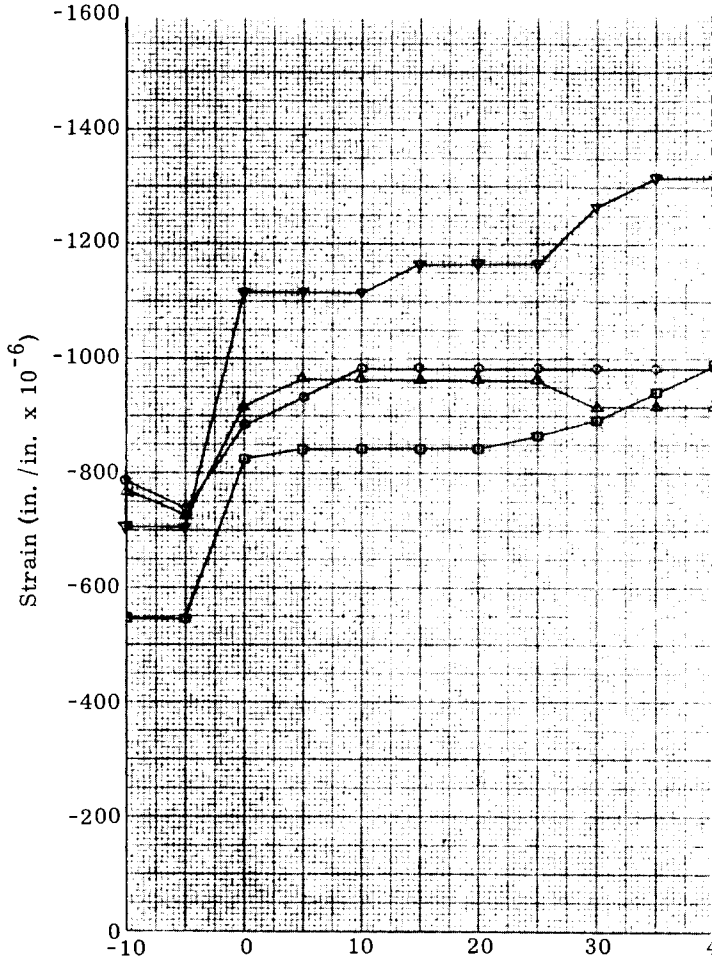
-1600
-1400
-1200
-1000
-800
-600
-400
-200
0
Strain (in. /in. x 10^-6)
-10
0
10
20
30

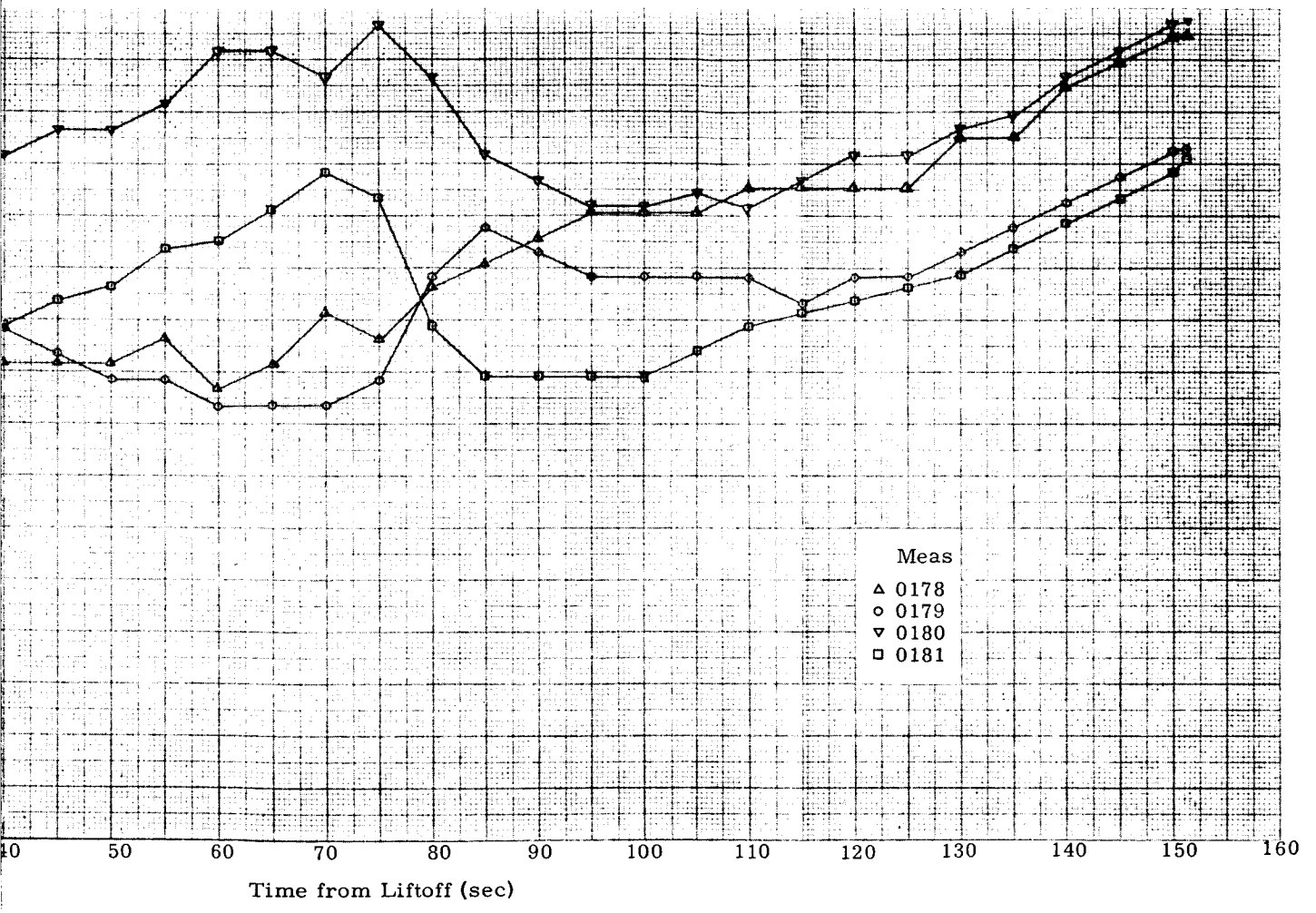


Fig. XII-32. Station 937 GT-3 Strain History

XII-5) used skin panel buckling criteria based on skin panel simply supported on all edges. These criteria were revised to a clamped, clamped, simple, simple panel. Also, the stress distribution assumed across a panel from axial compression loads as found in Sketch A was revised as shown in Sketch B.

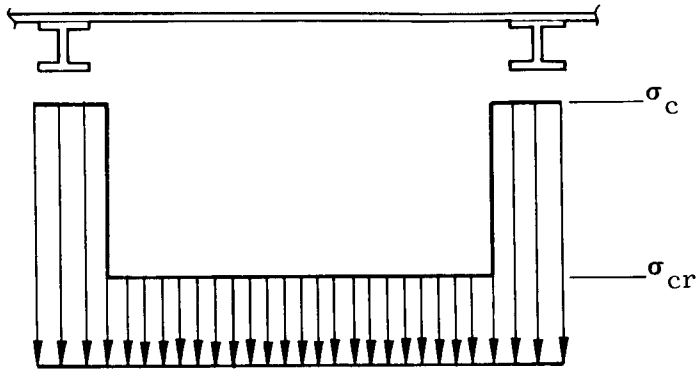


Sketch A

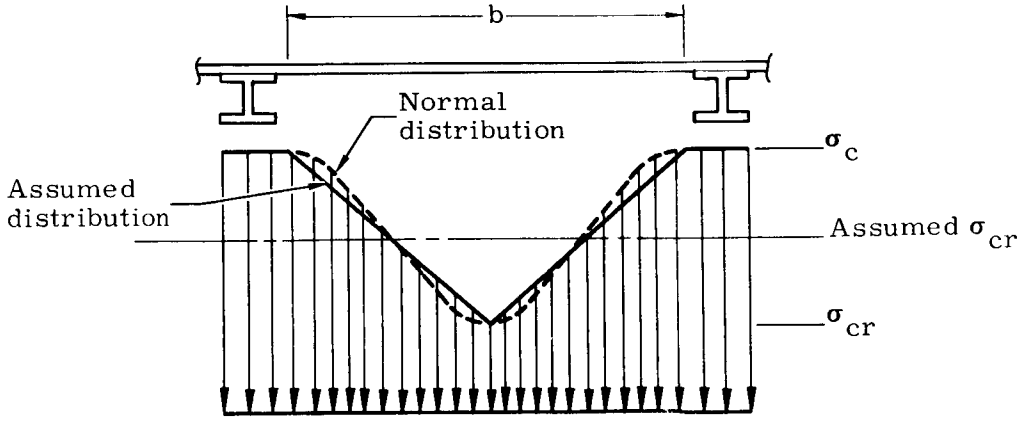


Sketch B

Using these revised criteria, checks were made for Station 371 and Station 937--one at LO - 3.5 seconds and one at LO + 150 seconds. The comparisons are shown in Table XII-6. These comparisons show that the revised buckling criteria brings the calculated strain loads into a much better comparison with the calculated GT-3 trajectory loads.

Another factor affecting the loads as calculated from strain data is the gaps at the manufacturing splices which are close to the strain gages. The measured gaps are shown in Fig. XII-33. Reading No. 1 of this figure was made by passing a feeler gage completely through the splice frames. Reading No. 2 was made by inserting a feeler gage between the splice frames to a depth of one inch. The influence of these measured gaps cannot be readily evaluated but it is felt that they definitely contribute to mismeasurement of loads.

## 4. Conclusions

Discrepancies between the trajectory-derived loads and the strain-derived loads are attributed to the tolerances in the strain measurements and the validity of associated criteria used in the strain loads analysis. Primary reasons for inconsistent out-of-plane readings appear to be unknown factors associated with the following:

(1) The actual stress distribution across a structure composed of stringers and buckled skin is not well defined in tests. Present design distribution (Sketch A) was used in the strain loads digital program. While this method is satisfactory for sizing in the design phase, it is not satisfactory for analysis of load distribution. A revised distribution similar to Sketch B is needed and very little published data or test data are available on the subject.

(2) The actual area of structural members comprising a cross section varies with the manufacturing tolerances to the amount of 16% between maximum and minimum values. For the strain loads digital program, nominal values were used since the vehicles (GT-2 and GT-3) were already assembled.

(3) It was assumed that the skirt removable doors were nonload carrying both in this analysis and in design; however, these doors do have some load capacity and their actual load would be a function of the overall load because attachment slop would have to be taken up before these doors could, in fact, carry any load.

(4) Gaps at the stringer fittings at the manufacturing splices were considered nonexistent both in this analysis and in design. Figure XII-33 shows that gaps do exist and engineering drawings permit gaps of specific magnitudes. Splice gaps can be attributed to at least two things:

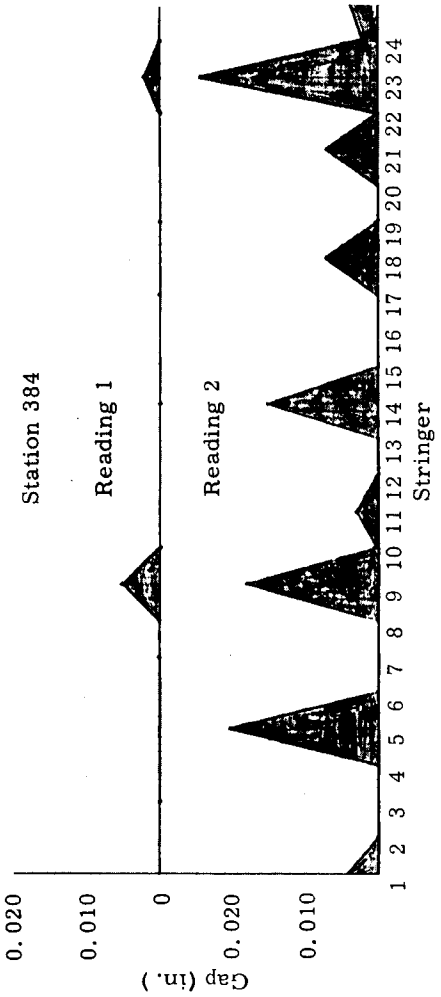


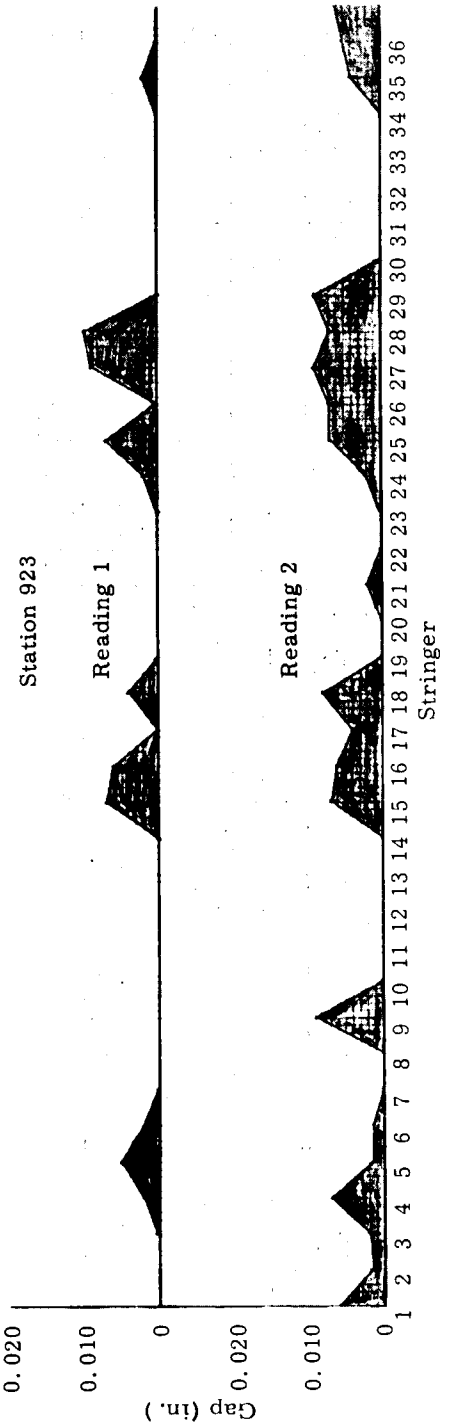


Fig. XII-33. Splice Gap Measurements

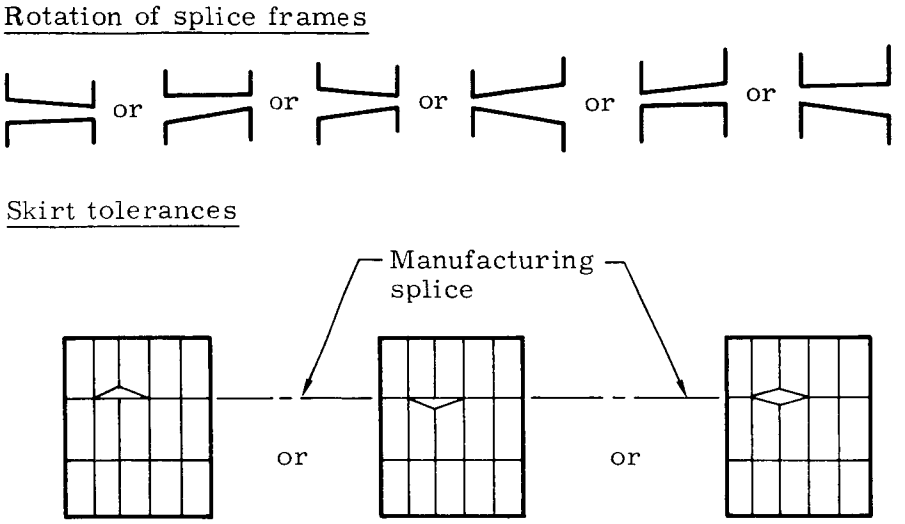


Sketch C

(5) The calibration of the strain gages was accomplished by checking the zero load condition on the vehicle and the full load (during WMSL) condition on the vehicle. However, these gages were checked for accuracy from Sanborn data rather than digital data (which are not taken during WMSL).

(6) Insufficient strain instrumentation created the possibility of off readings or, in fact, loss of the gage. For the limited instrumentation available, it would have been better to concentrate all the instrumentation at one station to get a better picture of strain distribution, to better establish the load plane, to eliminate bad readings and to possibly answer the effect of the gap problem.

The recorded strains on GT-3 followed the same general trend of those recorded on GT-2. The comparison of the loads derived from using standard design buckling criteria versus that of using a more realistic load carrying criteria indicates that very good correlation of axial strain loads versus trajectory axial loads is possible. Poor correlation of bending moments still exists. GT-3 was the last vehicle scheduled to have structural integrity instrumentation onboard. The results, while possibly within the "generally accepted limits" for tests using strain gages, could have been better. The test articles (GT-2 and GT-3) could have been treated more like laboratory specimens in the area of the instrumentation by incorporating the following:

(1) Monitor one vehicle station and therefore have a concentration of instrumentation at that one station (preferably Station 935). This would give a better load picture, especially if one or two gages are read erroneously.

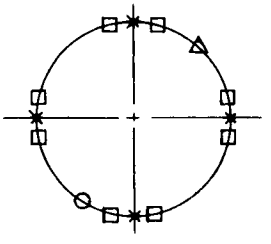

✱ Strain gages on GT-2 and GT-3

Δ Strain gages removed from other stations and replaced at this station

O Existing temperature transducers

Δ Added temperature transducers from other station

(2) Lower the range and increase the sensitivity of the strain gages. The original purpose of the strain gages was for evaluation of structural loads in the event of a switchover and the effect of total angle of attack during flight. Based on this purpose, the range of the gages was established to cover the ultimate strength of the vehicle at the monitored stations. Since normal flight loads are generally well below design values, the range of the gages could be lowered and their sensitivity increased if, in fact, the main purpose would be to cover only normal flight loads.

(3) Eliminate the splice gap problem by shimming (laminated) at every stringer at the manufacturing splice whether the stringer is physically spliced or not.

(4) Use a more realistic skin load carrying criteria even if not established by test. The normal distribution used for design purposes is too conservative for this type of analysis.

(5) Load calibrate the strain gages during WMSL and check the calibration by digital printout rather than analog paper records.

(6) Establish the actual areas of the structural members in the monitored section. Skin thickness tolerance affects both the total area used for load carrying capacity and the skin buckling stress level. Skin thickness tolerance alone at Station 935 could vary the skin area between 17.34 and 20.36 square inches. Thirty-one of the thirty-five stringers at Station 935 could each have an effective area of 0.383 to 0.447 square inch. Since articles GT-2 and GT-3 were already fabricated, getting the actual dimensions of all the components at a particular station was not possible.

(7) Use thrust chamber differential (Stage I engine) versus flight time and actual actuator displacements in the calculation of trajectory loads. Calculate actual pitch-yaw loads rather than total plane loading. Trajectory derived loads were computed by the existing design loads program which at this time did not have the aforementioned factors incorporated.

TABLE XII-6

Comparison of Loads Using Revised Buckling Criteria

| Vehicle Station | Time (sec) | Method | Axial Load (lb) | Bending Moment (in.-lb) | Pitch Axis Rotation ($\omega$) (deg) | Centroidal Axis Shift ($\overline{Y}$) (in.) |
|---|---|---|---|---|---|---|
| 371 | -3.5 | Original | -35,176* | -97,402 | 31.06 | 0.14 |
| | -3.5 | Revised | -37,093* | -90,800 | 31.06 | 0.458 |
| | -3.5 | GT-3 trajectory | -48,000 | -16,000 | | |
| | 150 | Original | -199,737* | 657,546 | 28.25 | 0.40 |
| | 150 | Revised | -229,681* | 660,300 | 28.25 | 0.612 |
| | 150 | GT-3 trajectory | -258,923 | -6,030 | | |
| | | | -265,323** | -131,030** | | |
| 937 | -3.5 | Original | -197,997* | -216,000 | 77.56 | 1.97 |
| | -3.5 | Revised | -231,289* | -153,700 | 77.56 | 2.39 |
| | -3.5 | GT-3 trajectory | -247,000 | -240,000 | | |
| | 150 | Original | -327,056* | 1,563,000 | -14.70 | 0.83 |
| | 150 | Revised | -406,322* | 1,868,700 | -14.70 | 1.006 |
| | 150 | GT-3 trajectory | -430,837 | -1,489 | | |
| | | | -435,977** | -211,489** | | |

*Does not include 1 g deadweight of empty booster plus payload.
Station 371 1 g deadweight = 10,400 lb.
Station 937 1 g deadweight = 14,200 lb.
**Dynamic loads included.

## D. LONGITUDINAL VIBRATIONS (POGO)

It has been determined analytically and verified on all three Gemini-Titan flights that the longitudinal oscillation instability that characterized the Titan II configuration can be suppressed by the use of tuned hydraulic resonators inserted into the Stage I propellant feedlines. These suppression devices (piston-type fuel accumulators and oxidizer line standpipes) were incorporated on GLV-3.

1. Flight Longitudinal Vibration Levels

A review of telemetry data indicates that a sustained launch vehicle longitudinal vibration in excess of the prescribed criterion of 0.25 g zero-to-peak at Station 280 did not occur. The suppression system operated satisfactorily, and successfully eliminated the POGO instability from GT-3. Figure XII-34 shows a comparison of the acceleration levels observed on GT-3 with those measured on the GT-1 and GT-2.

No unusual or unanticipated oscillations were noted on any of the pressure transducers or axial accelerometers. Although pressure responses of all measurements on S/A 1 were somewhat larger than those observed on S/A 2, it was apparent that this occurrence had no noticeable effect on the performance of the POGO hardware or on the amplitude response of the structure at POGO frequencies. The signals from the launch vehicle axial accelerometers located at Station 280 on the Compartment 1 skirt near the spacecraft interface, and at Station 1209 on the aft fuel tank longeron of Compartment 5 were analyzed by narrow band analog filtering to determine the magnitude and frequency of the primary oscillation.

Figure XII-35 presents a comparison of filtered data from the two launch vehicle accelerometers. The general filtered level of response near the spacecraft interface was less than 0.15 g zero-to-peak. At Station 280, a peak value of 0.13 g zero-to-peak at a frequency of 13.5 cps occurred at LO + 140 seconds. An additional intermittent response was also noted at LO + 132 seconds, with a maximum value of 0.125 g zero-to-peak.

At Station 1209, a peak value of 0.26 g zero-to-peak occurred at LO + 132 seconds, while intermittent higher peaks of 0.33 g zero-to-peak occurred at LO + 140 seconds and 0.49 g zero-to-peak at LO + 150 seconds.

Correlation of calculated and measured values of frequency and amplitude ratios was good. The vibration levels in Compartment 1, as shown in Fig. XII-36, were the lowest values obtained on the GT flights.

2. POGO Parameters

Accelerations and propulsion system pressure data associated with the POGO phenomenon were monitored, using both PCM and FM techniques. Figure XII-36 presents the telemetry traces of significant system parameters during the period of Stage I flight between LO + 128 seconds and BECO.

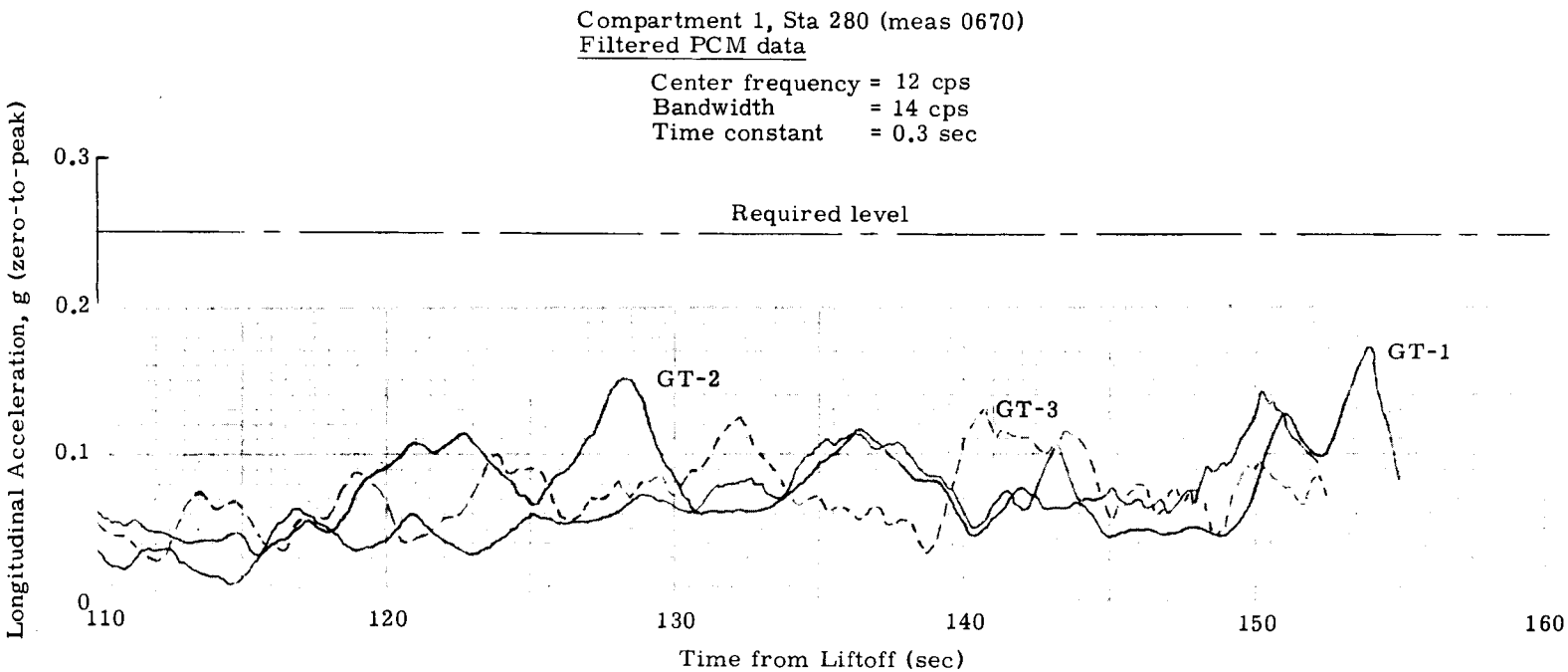


Fig. XII-34. Comparison of Longitudinal Oscillations at Sta 280 for All Flights

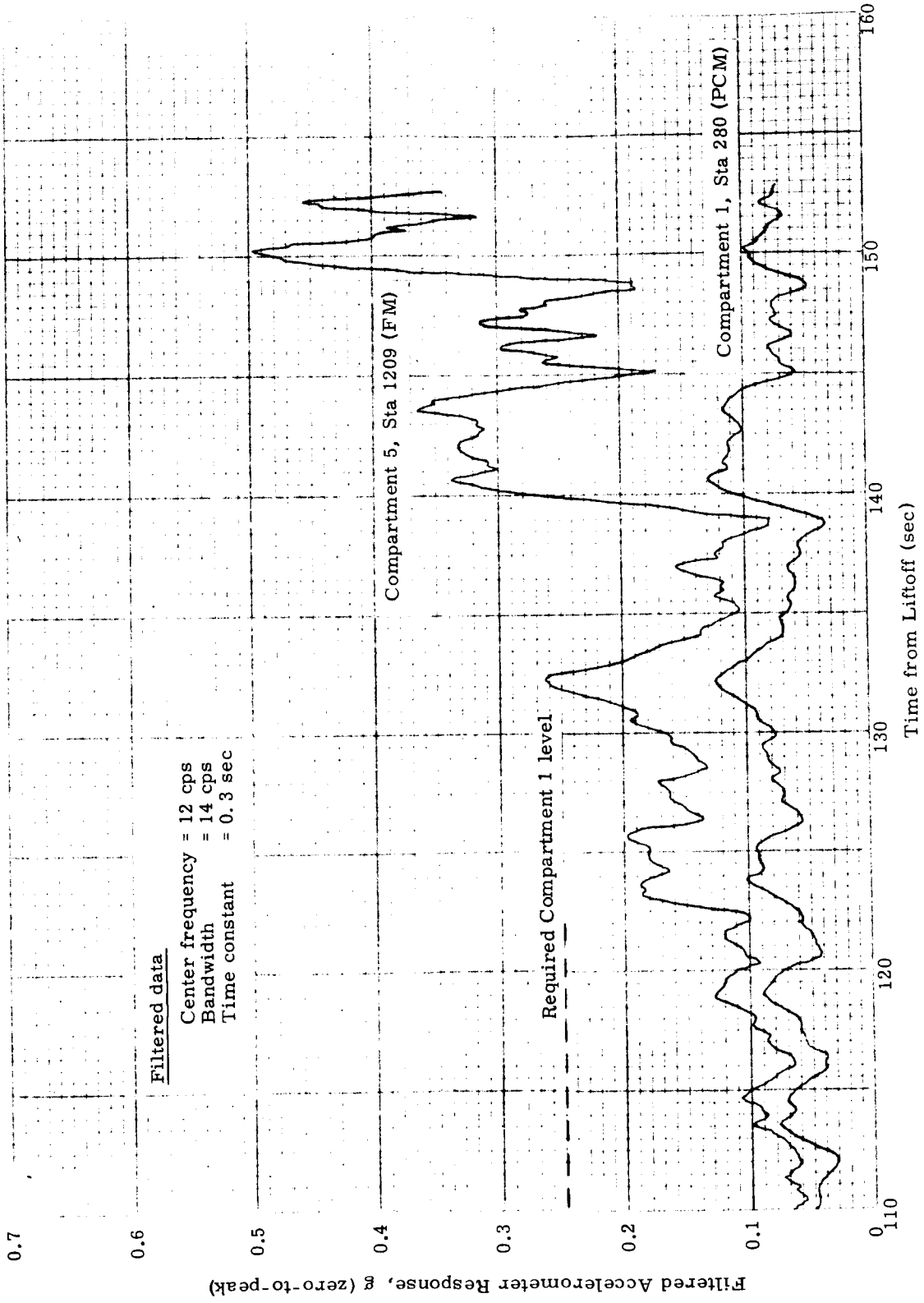


Fig. XII-35. GT-3 Longitudinal Oscillations

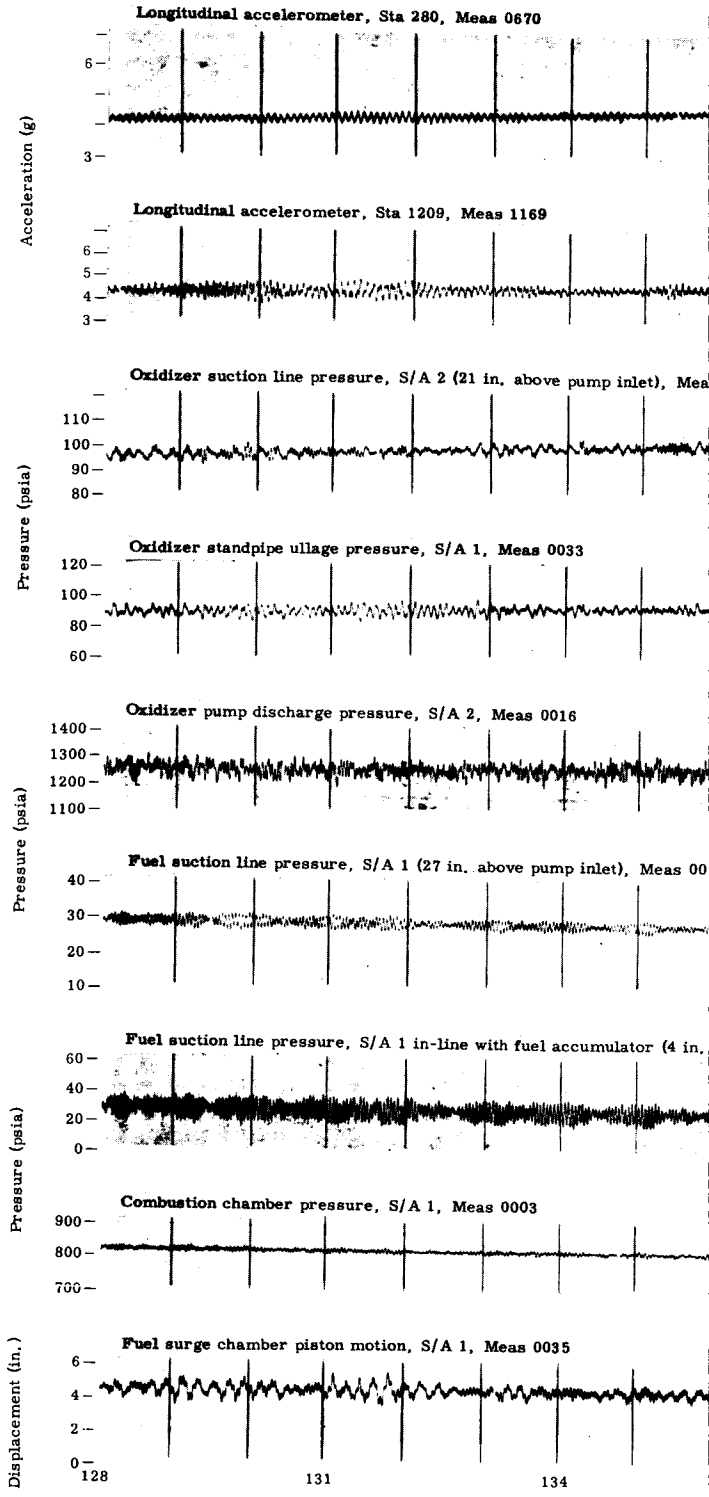
Longitudinal accelerometer, Sta 280, Meas 0670
Acceleration (g)
6
3
Longitudinal accelerometer, Sta 1209, Meas 1169
6
5
4
3
Oxidizer suction line pressure, S/A 2 (21 in. above pump inlet), Mea
Pressure (psia)
110
100
90
80
Oxidizer standpipe ullage pressure, S/A 1, Meas 0033
120
100
80
60
Oxidizer pump discharge pressure, S/A 2, Meas 0016
Pressure (psia)
1400
1300
1200
1100
Fuel suction line pressure, S/A 1 (27 in. above pump inlet), Meas 00
40
30
20
10
Fuel suction line pressure, S/A 1 in-line with fuel accumulator (4 in.
Pressure (psia)
60
40
20
0
Combustion chamber pressure, S/A 1, Meas 0003
900
800
700
Fuel surge chamber piston motion, S/A 1, Meas 0035
Displacement (in.)
6
4
2
0
128
131
134

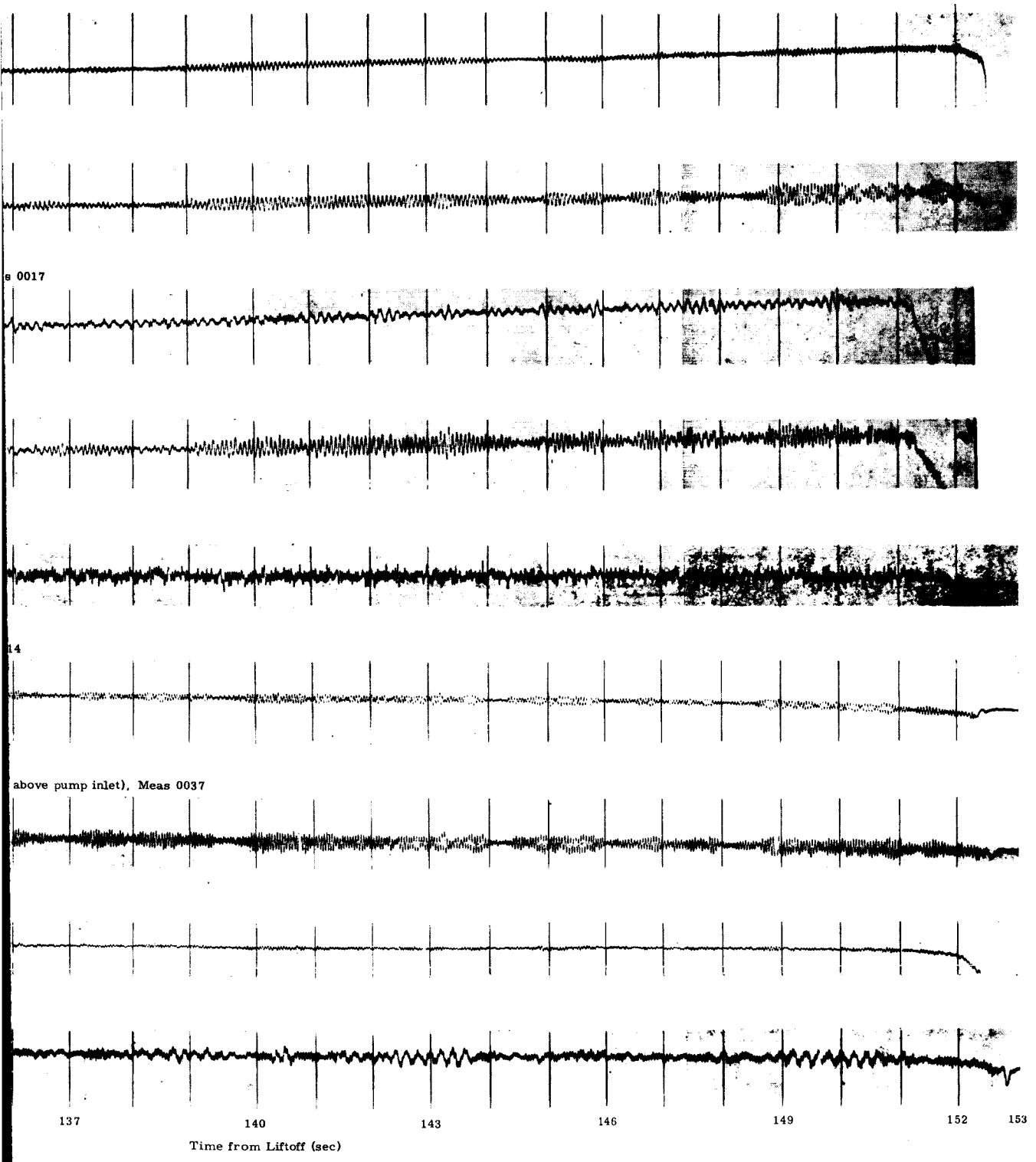


Fig. XII-36. Oscillogram of Selected Parameters (LO + 128 sec to BECO)

The major propulsion system parameters (oxidizer suction line pressure, $P_{os}$, fuel suction line pressure, $P_{fs}$, oxidizer pump discharge pressure, $P_{od}$, and engine thrust chamber pressure, $P_c$) were relatively free of first structural mode frequency POGO-type pressure oscillations. The oxidizer standpipes operated to suppress vibrations, and clearly showed responses to the first mode longitudinal vibrations. It is difficult to ascertain the degree of efficiency of the fuel accumulators to motion at structural frequencies due to the large steady-state response at the fuel line resonance of 23 cps. However, this response indicates that the systems responded well to pressure oscillations and operated as intended.

# XIII. AGE AND FACILITIES

## A. MECHANICAL AGE

Launch vehicle mechanical AGE functioned properly during precount, countdown and launch operations.

### 1. Precount Operations

The mechanical AGE equipment used during precount activities is primarily utilized during transport and erection of the launch vehicle stages. One Stage I trailer was modified after GLV-2 to permit transporting GLV-3 from Baltimore to Cape Kennedy by the B-377PG aircraft. Stages I and II were airlifted on separate flights without incident. Stage I was transferred from the modified trailer to a conventional trailer at Cape Kennedy to permit entry into the erector for vertical erection. No other design revisions were made to the AGE items following the GT-2 launch. All equipment functioned as designed.

### 2. Countdown Operations

All mechanical AGE used during the countdown functioned properly. One design revision was incorporated from GLV-2 to GLV-3. Passage holes for umbilicals 3D1E and 3D2E were made in the lower curtains.

### 3. Launch Operations

Spacecraft umbilical disconnect system. The dropweight system was released simultaneously with the firing of the launch holddown explosive nuts and retracted the three spacecraft umbilicals as intended.

Launch vehicle umbilical sequence. Review of the landline recordings plus film coverage confirmed that all seven umbilicals separated cleanly and in the planned sequence. The first umbilical disconnected at 1424:00.240 GMT and the last separated at 1424:00.870 GMT.

## B. ELECTRICAL AGE

The launch and checkout equipment operated satisfactorily during prelaunch and launch operations, and no problems were encountered.

### 1. Power Distribution Control Set (PDCS)

The PDCS equipment functioned properly throughout prelaunch and launch operations. The APS, IPS, 25 vdc and inverter monitors did not indicate a hold or shutdown condition, thereby verifying satisfactory

operation of the transformer/rectifiers and associated equipment before, during and after power transfer. The interface cabling and umbilicals also functioned satisfactorily.

2. Propellant Loading

All electrical counters on the propellant loading system operated properly with no discrepancies noted.

## C. MASTER OPERATIONS CONTROL SET (MOCS)

Analysis of the MOCS automatic sequence records shows that all functions were performed properly. At T-35 minutes, a hold was called due to a leak in the oxidizer line. After this condition was rectified, the automatic sequence was initiated and proceeded through a successful liftoff. MOCS T-0 occurred at 1423:56.6 GMT followed by TCPS 1.2 seconds later. The following MOCS generated time functions occurred as specified:

TCPS + 1.6 seconds

TCPS + 1.8 seconds

TCPS + 2.0 seconds--fire launch nuts 1423:59.8 GMT.

The launch operation was completed in 3.2 seconds.

During the launch holdfire, E-8 (primary hydraulic system shutdown) was monitored although its shutdown capability was removed. However, had E-8 been a shutdown parameter for this launch, a shutdown would have occurred at T+1 second due to a below-limit pressure drop in the primary system. Approximately 0.1 second later, the primary system pressure returned within limits and remained there until E-8 was timed off at TCPS + 1.8 seconds.

The recorders were changed to high speed at T-2 minutes. During the remainder of the count, the operation of the sequencer was compared to the real-time trace. All traces were checked for time of occurrence, proper sequence and coincidence of occurrence, and found to be correct and consistent with the planned operation of the sequencer.

## D. PAD DAMAGE

The damage to AGE and facilities caused by engine blast and heat was minor. The damage was less than that for the GT-2 launch. All damaged items will be refurbished to their original configuration. The most significant damaged items are as follows:

(1) Complete Vehicle Erector (CVE)

(a) Corrugated aluminum siding (east side of CVE). Panels from the deck to the 26 foot 7 inch level loosened and two pieces were blown off.

(b) Launch vehicle personnel elevator (west side). The elevator guard screen from the pivot point to the 9 foot 8 inch level was blown loose and bent. The weld between the weight/sheave guide bracket and track support channel on the overspeed governor cable tensioning device was broken, and the elevator guide track channel was twisted.

(c) Spacecraft service elevator (east side). The button conduit was torn out from the deck level to the 9 foot 8 inch level.

(d) Ground strap at the west pivot point was damaged.

(e) Electrical items. The flexible 1-1/2 inch conduit at the east pivot point pulled loose from the connector. The MITOC unit became inoperative and burned above the west pivot point.

(f) Safety showers. The sides on the 9 foot 8 inch level were blown loose and bent.

(2) Complete Vehicle Umbilical Tower (CVUT)

(a) Deck level. The nitrogen purge conduit to the portable erector controller J-box (east face) was broken off.

(b) Level No. 1. The camera was broken loose from bracket.

(c) Level No. 2. The spray header was damaged and the elevator cable guard screen was broken loose.

(d) Level No. 3. The elevator cable guard screen was broken loose.

(e) Level No. 4. The nitrogen pressure reducing station was blown apart and the piping was badly bent.

(f) Level No. 7. The safety chains for slide wire No. 2 were broken, the handrail on the north side was bent, and the support bracket for lights and cameras at the top of the tower collapsed.

(3) Second-Stage Umbilical Tower (SSUT)

(a) Light and conduit support brackets at the south side of the top level were bent down.

(4) CVE Thrust Mount Area

(a) Flame shields. A-frame shields were missing and damaged. The inner thrust ring shields (one section) were missing and (one section) damaged.

(5) Launch Deck Area

(a) Structural. The blast cover for the Aerojet cleaning unit on the north side of CVE thrust ring was damaged. The second-stage erector leg lock blast cover at the west leg was damaged. The spacecraft elevator ramp was torn loose from the deck at hoistway. The spacecraft elevator hoistway gate posts were bent.

(b) Electrical. The MITOC unit near J-box "C" became inoperative. The conduit was broken loose from the MOPS J-box mounted on the spacecraft elevator ramp. The spacecraft elevator control conduit was bent and broken. The conduit pulled loose from the transfer crane J-box at base of the crane.

(c) Mechanical. The safety shower at the base of the CVUT stairway (ground level west of ramp) was distorted, and eyewash piping was broken.

(d) Miscellaneous. The CCTV camera No. 3 tilt mechanism was damaged.

# XIV. RELIABILITY

## A. ENVIRONMENTAL CRITERIA

GT-3 flight data, pertinent to GLV environmental criteria, have been reviewed and found to be lower than the qualification test levels. A comparison of the flight data with qualification test limits, analysis data, GT-1 and GT-2 data and with Titan II flight data appears in Table XIV-1.

### 1. Compartment Temperatures

Compartment 2 and engine start cartridge air-conditioning system exhaust temperatures were recorded prior to liftoff. These temperatures ranged from 56° to 61° F and were within the specified 40° to 75° F range.

In-flight compartment temperature measurements were made in Compartment 3B to measure heat input to the Stage I oxidizer tank dome from the boundary layer air cross flow during high angles of attack. Temperature measurements varied from 71° to 88° F on this flight indicating that cross flow heating was virtually nonexistent.

### 2. Skin Temperatures

Skin temperatures were measured at three locations on GT-3. The thermocouples were mounted as far as possible from large heat sinks, such as stringers and other internal structure, in order to minimize their effect on the true readings. All temperature readings were well within specified limits.

### 3. Random Vibration

Vibration measurements were obtained on the Compartment 2 truss next to the RGS and on the tandem Actuator $2_1$ in Compartment 5. The maximum lateral (yaw axis) vibration (g rms) of the truss occurred at liftoff. The maximum vertical (pitch axis) vibration (g rms) of the tandem actuator occurred at liftoff, and the maximum vertical vibration of the truss occurred 58 seconds after liftoff. No axial (longitudinal axis) vibration measurements were made. All measurements were well below the qualification test levels.

### 4. Steady-State Accelerations

Longitudinal accelerations on the GT-3 flight were comparable to those measured on the GT-2 flight, and were well below the qualification test level.

The maximum Stage I measured steady-state acceleration was 5.63 g, just prior to BECO.

The maximum Stage II measured steady-state acceleration reached a peak of 7.50 g at the end of the Stage II flight.

5. Shock

No separate shock measurements were made; however, the vibration data include transient responses of the structure during release, staging and at the time of spacecraft separation.

No detrimental effects were experienced or expected from these transients.

6. Acoustic Noise

GLV-3 was not instrumented to record levels of acoustic noise environment. This environment is considered to be adequately represented by Titan II test data. GLV-4 will be instrumented to measure sound pressure levels in Compartments 1 and 2.

## B. PROBABILITY ESTIMATES

1. Countdown Probabilities

Based on GLV countdown experience, the average number of holds per countdown ($\bar{h}$) was calculated to be 0.25. $\bar{h}$ is based on the countdown period from T-420 to T-0. Spacecraft holds and SCF data are not counted. Countdown experience was gained on the following:

(1) One countdown (GLV-1), including engine ignition

(2) One countdown (GLV-2), countdown completed, tandem actuator failed

(3) One countdown (GLV-2), including engine ignition

(4) One countdown (GLV-3), with one hold

From Ref. 13, the probability of GLV-4 completing the countdown without a hold was predicted to be:

$$P_{c/d}\,(\bar{h} = 0.33) = 0.75$$

The estimate for GLV-3 was 0.82 and was based on both SCF, and GLV-1 and GLV-2 data.

## 2. Flight Probabilities

No failure nor significant anomaly was observed in any GLV-3 system during this flight. Therefore, the only reliability conclusion drawn is a slight overall increase in the estimate arising from the increased hours accumulated.

The system of obtaining reliability assessments of engines, IGS and RGS units is presently under review with SSD. Consequently, no re-evaluation of these systems with respect to the GT-3 flight results is presently available.

Modifications to the hazard model (Ref. 14) are therefore not included here. It is expected that an amended hazard model including these systems will be presented in the May Monthly Reliability Report (ER 12794) and in all future issues of the Flight Evaluation Report.

Based on the March Monthly Reliability Report (ER 12794-25), the current reliability of the complete launch vehicle, exclusive of the spacecraft, is 0.911.

# TABLE XIV-1

## Environmental Criteria Summary

| Parameter | Source | Compartment 1 | 2 | 3A | 3B | 4 | 5 |
|---|---|---|---|---|---|---|---|
| Compartment exhaust air temperature (°F) | Qualification test ① | 120 | 90 | 100 | 100 | 110 | 160 |
| | Analysis ② | 100 | 75 | 80 | 80 | 100 | 100 |
| | Flight data, GLV-1 | N/A | 60 (at T-0) | N/A | N/A | N/A | N/A |
| | Flight data, GLV-2 | N/A | 58 (at T-0) | N/A | N/A | N/A | N/A |
| | Flight data, GLV-3 | N/A | 61 (at T-0) | N/A | 88 (at T-150) | N/A | N/A |
| Maximum skin temperature (°F) | Qualification test | -- | -- | -- | -- | -- | -- |
| | Analysis ③ | 372 | 485 | 470 | 305 | 310 | 297 |
| | Flight data, GLV-1 | 153 | N/A | N/A | N/A | N/A | N/A |
| | Flight data, GLV-2 | 150 | 236 | N/A | 152 | 168 | N/A |
| | Flight data, GLV-3 | N/A | 258 | N/A | 177 | 198 | N/A |
| Random vibration (max g rms) | Qualification test ④ | 41 | 65 (truss 14.3) | 97 | 29 | 44 | 92.5 |
| | PMT level ④ | 20.5 | 32.5 (truss 9) | 48.5 | 14.5 | 22 | 46.3 |
| | Flight data, Titan II ④ | 10 | 15 (truss 6) | 22 | 21 | 33 | 37 |
| | Flight data, GLV-1 | 2.0 lateral | Truss 0.95 axial | N/A | N/A | N/A | 12 axial |
| | Flight data, GLV-2 | N/A | Truss 1.96 lateral | N/A | N/A | N/A | 8.5 axial |
| | Flight data, GLV-3 | N/A | Truss 1.45 lateral<br>Truss 3.30 vertical | N/A | N/A | N/A | 7.0 vertical |
| Steady-state acceleration (max g) | Qualification test ⑤ | 12 | 12 | 12 | 8 | 8 | 8 |
| | Flight data, GLV-1 | 7.35 | N/A | N/A | N/A | N/A | 5.61 |
| | Flight data, GLV-2 | 7.70 | N/A | N/A | N/A | N/A | 5.69 |
| | Flight data, GLV-3 | 7.50 | N/A | N/A | N/A | N/A | 5.63 |
| Maximum shock (g) | Qualification test ⑤ | None | None | 100 | None | None | 100 |
| | Flight data, GLV-1, 2 and 3 | N/A | N/A | N/A | N/A | N/A | N/A |
| Acoustics (db), average inside compartment noise level | Qualification test ⑤ | 154 | 151 | 159 | 151 | 154 | 159 |
| | Analysis | 154 | 151 | 159 | 151 | 154 | 159 |
| | Flight data, Titan II | 154 | 151 | 159 | -- | 154 | 159 |
| | Flight data, GLV-1, 2 and 3 | N/A | N/A | N/A | N/A | N/A | N/A |

① Ref. 16, page 49

② Ref. 17, page 3

③ Ref. 18

④ Ref. 15, Figs. 14, 15 and 16

⑤ Ref. 16, Table 3

N/A = not available

# XV. RANGE DATA

## A. DATA DISPOSITION

### 1. Quick-Look Data

Quick-look data supplied by ETR to Martin-Baltimore are summarized in Table XV-1.

A high quality PCM serial tape was used, and few drop-outs were exhibited during the flight. The formatted magnetic tape was of excellent quality and contained no redundancies. The Tel II formatted tape showed that, except for the 250-millisecond transmission blackout at staging, there were only 30 bad data words recorded. Station 3 also had a net data loss during the blackout of 250 milliseconds.

TABLE XV-1

Range Supplied Quick-Look Data

| Description | Time Requested | Time Received (ETR) | Time Received (Baltimore) |
|---|---|---|---|
| Telemetry magnetic tapes: | | | |
| Tel II, post-detection PCM/FM (1 roll) | T+1 hr | T+1 hr | T+9 hr |
| Tel II, FM/FM (2 rolls) | T+1 hr | T+1 hr | T+9 hr |
| Station 1 formatted (2 rolls) | T+1 hr | T+3.5 hr | T+9 hr |
| Range safety plots | T+1 hr | T+3.5 hr | |

### 2. Martin Data

Test data and records generated by Martin at Cape Kennedy were received in Baltimore within two days after launch. These data consisted of the following items:

(1) One set of quick-look records from RCA tape.

(2) Fast engine rolls.

(3) Landline records (events, Bristol, Multipoint and Sanborn records) with associated calibration sticks.

(4) BLH printouts.

(5) 2600 records (2650 and 2660, and events).

(6) Sequencer records with code sheets.

(7) Summary of flight events.

(8) Dub of C-19 landline magnetic tape.

3. Final Range Data

The data supplied by ETR are summarized in Table XV-2. The time requested for delivery to Martin (Canaveral) and the time received at Baltimore are also shown.

TABLE XV-2

Range-Supplied Final Data

| OD Item | Description | Time Requested (Canaveral) | Time Received (Baltimore) |
|---|---|---|---|
| 1 | Position velocity and acceleration, theodolite | 3 CD | 8 CD |
| 3 | Position velocity and acceleration, camera | 3 CD | 8 CD |
| 7 | Position velocity and acceleration, radar | 3 CD | 8 CD |
| 15 | Position velocity and acceleration, MISTRAM | 5 CD | 16 CD |
| 5 | Attitude, camera | 3 CD | 8 CD |
| 8 | Altitude, Mach No. and Dynamic pressure | 4 CD | -- |
| 9 | Special parameters, radar | 10 WD | 6 WD |
| 4.9/29.9 | MISTRAM function recordings | 3 WD | 7 WD |
| 21 | Best estimate of trajectory | 14 WD | |
| 22 | Best estimate of trajectory | 15 WD | |
| 1.5-2 | Serial PCM, post-detection magnetic tape | 1 hr | 1 hr |

CD = Calendar Days WD = Working Days

TABLE XV-2 (continued)

| OD Item | Description | Time Requested (Canaveral) | Time Received (Baltimore) |
|---|---|---|---|
| 1.5-1 | FM/FM, post-detection magnetic tape | 1 hr | 1 hr |
| 1.5-3 | PCM formatted, post-detection magnetic tape | 4 hr | 4 hr |
| 3.5-2 | Serial PCM, post-detection magnetic tape | 3 CD | 1 CD |
| 3.5-1 | FM/FM, post-detection magnetic tape | 3 CD | 1 CD |
| 3.5-3 | PCM formatted magnetic tape | 1 CD | 1 CD |
| 1.5-6 | Signal strength (center frequency) recordings | 1 hr | 8 CD |
| 1.5-7 | Antenna positions | 3 hr | 8 CD |
| 3.5-5 | Signal strength (center frequency) recordings | 3 CD | 6 CD |
| 1.5-11 | Oscillograph records, near real time | 3 hr | 1 WD |
| 1.18 | Range safety plot charts | 1 hr | 1 hr |
| 4 | Launch vehicle IP | 1 hr | 4 WD |
| 1.11-1 | Command control function records | 3 WD | 5 WD |
| -3 | Command control function records | 3 WD | -- |
| -4 | Command control function records | 3 WD | -- |
| -5 | Command control function records | 3 WD | -- |
| -6 | Command control function records | 3 WD | -- |
| 3.11-1 | Command control function records | 5 WD | 5 WD |
| -2 | Command control function records | 5 WD | -- |

TABLE XV-2 (continued)

| OD Item | Description | Time Requested (Canaveral) | Time Received (Baltimore) |
|---|---|---|---|
| -3 | Command control function records | 5 WD | 5 WD |
| 7.11-1 | Command control function records | 5 WD | -- |
| -2 | Command control function records | 5 WD | -- |
| -3 | Command control function records | 5 WD | -- |
| - | Range T-0 and time of liftoff | 1 CD | 2 CD |
| 1 | Preliminary estimate of data coverage | 3 hr | 1 WD |
| 1 | Weather surface, local terminal | 3 WD | 5 WD |
| 27 | Weather surface observations | 1 WD | 1 WD |
| | Weather upper theodolite | 1 WD | 1 WD |
| | Weather upper Rawinsonde | 3 WD | 1 WD |
| | Weather tower 700/702 | 1 WD | 5 WD |
| | Weather upper area sonde | 3 WD | 5 WD |
| - | TLM Operations Log Station 1 | 3 CD | 26 CD |
| - | TLM Operations Log Station 3 | 3 CD | 2 CD |
| - | TLM Operations Log Station 7 | 3 CD | 2 CD |
| - | TLM Operations Log Station 12 | 3 CD | 8 CD |
| - | TLM Operations Log Station 13 | 3 CD | 8 CD |
| - | TLM Operations Log Station 91 | 3 CD | 7 CD |
| 7.5-3 | Signal strength (center frequency), Station 7 | -- | 4 WD |
| 7.5-5 | Antenna position, Station 7 | -- | 4 WD |
| 3.5-6 | Antenna position, Station 3 | -- | 4 WD |
| 25 | QLAP Part 1--Stage I | -- | 4 WD |
| | QLAP Part 1--Stage II | -- | 4 WD |
| | QLAP Part 1--transient | -- | 4 WD |

TABLE XV-2 (continued)

| OD Item | Description | Time Requested (Canaveral) | Time Received (Baltimore) |
|---|---|---|---|
| 1.5-53 | Signal strength (center frequency) and antenna position Tel III | - | 6 WD |
| 1.5-54 | Signal strength (center frequency) and antenna position Tel III | - | 6 WD |

4. Agency/Contractor Supplied Data

Table XV-3 presents data received from associated contractors and NASA-MSC.

TABLE XV-3

Agency/Contractor Supplied Data

| Description | Associate Contractor | Received |
|---|---|---|
| Mod III, AMRO GMCF | GE ETR | 6 CD |
| Mod III, Radio guidance system | GE Syracuse | 6 CD |
| Special launch trajectory<br>Range trajectory<br>Impact predictor | NASA-MSC | 6 CD |
| Q 058 IGS ascent parameters | NASA-MSC | 8 CD |
| Power spectrum density, preliminary vibration (g rms) | NASA-MSC | 8 CD |

## B. FILM COVERAGE

Photographic conditions at the Cape Kennedy area during the GT-3 launch were excellent and motion picture coverage was very good. Table XV-4 contains a listing of the films from the fixed cameras and tracking cameras.

The 70mm tracking films (Items 1.2-38 and 1.2-40) and one 35mm film (Item 1.2-39) were reviewed for information pertinent to the booster staging event. Inspection of these films shows that the normal breakup of the first-stage transportation section occurred after Stage II had staged cleanly.

TABLE XV-4

Film Coverage and Disposition

| OD Item Number | Film Description | Footage | Time Received (Baltimore) |
|---|---|---|---|
| 1.2-4 16 mm Fixed | Launcher and Stand Centered | 1200 | 5 WD |
| 1.2-5 16 mm Fixed | Launcher and Stand Centered | 1175 | 6 WD |
| 1.2-6 16 mm Fixed | Launcher and Stand Centered | 1162 | 5 WD |
| 1.2-9 16 mm Fixed | MSL Centered, Movement at Launch | 400 | 4 WD |
| 1.2-10 16 mm Fixed | MSL Centered, Movement at Launch | 408 | 6 WD |
| 1.2-11 16 mm Fixed | MSL Centered, Movement at Launch | 409 | 6 WD |
| 1.2-12 16 mm Fixed | Spacecraft Centered, Evaluate Spacecraft at Launch | 121 | 9 WD |
| 1.2-13 16 mm Fixed | Spacecraft Centered, Evaluate Spacecraft at Launch | 118 | 7 WD |
| 1.2-14 16 mm Fixed | Explosive Bolts and First Motion | 219 | 6 WD |
| 1.2-15 16 mm Fixed | Explosive Bolts and First Motion | 227 | 7 WD |
| 1.2-16 16 mm Fixed | East Launch Ring Engine | 27 | 4 WD |
| 1.2-17 16 mm Fixed | West Launch Ring Engine | 148 | 6 WD |
| 1.2-18 16 mm Fixed | North Launch Ring Engine | 216 | 4 WD |
| 1.2-19 16 mm Fixed | South Launch Ring Engine | 216 | 7 WD |

TABLE XV-4 (continued)

| OD Item Number | Film Description | Footage | Time Received (Baltimore) |
|---|---|---|---|
| 1.2-20 16 mm Fixed | 3 D1E and 3 D2E Umbilical Plugs | 217 | 7 WD |
| 1.2-21 16 mm Fixed | 2 DFVT Umbilical Plug | 219 | 7 WD |
| 1.2-22 16 mm Fixed | 1 DOVT Umbilical Plug | 216 | 6 WD |
| 1.2-23 16 mm Fixed | 3 B1E and Associated Umbilical Plugs | 216 | 6 WD |
| 1.2-24 16 mm Fixed | 2 B1E and Associated Umbilical Plugs | 218 | 6 WD |
| 1.2-25 16 mm Fixed | Cable Cutters | 219 | 7 WD |
| 1.2-26 16 mm Fixed | Umbilical Boom 3, J-Bars and Lanyards | 216 | 7 WD |
| 1.2-27 16 mm Fixed | Spacecraft Upper Umbilical Plug | 216 | 6 WD |
| 1.2-28 16 mm Fixed | Spacecraft Upper Umbilical Plug | 216 | 6 WD |
| 1.2-29 16 mm Fixed | Lanyards and Release | 224 | 14 WD |
| 1.2-30 16 mm Tracking | LO to LOV, Pad Emergency Spacecraft Centered | 338 | 6 WD |
| 1.2-31 16 mm Tracking | LO to LOV, Pad Emergency Spacecraft Centered | Not required | |
| 1.2-32 16 mm Tracking | LO to LOV, Pad Emergency Spacecraft Centered | 400 | 7 WD |
| 1.2-33 16 mm Tracking | LO to LOV, Missile Centered | 265 | 7 WD |

TABLE XV-4 (continued)

| OD Item Number | Film Description | Footage | Time Received (Baltimore) |
|---|---|---|---|
| 1.2-34 16 mm Tracking | LO to LOV, Missile Centered | 321 | 6 WD |
| 1.2-37 16 mm Tracking | First Acquisition to LOV Missile Centered and Staging | 126 | 7 WD |
| 1.2-38 16 mm Tracking | First Acquisition to LOV Missile Centered and Staging | 133 | 7 WD |
| 1.2-39 16 mm Tracking | First Acquisition to LOV Missile Centered and Staging | 104 | 4 WD |
| 1.2-40 16 mm Tracking | First Acquisition to LOV Missile Centered and Staging | 126 | 4 WD |
| 1.2-42 16 mm Tracking | C-54 Aircraft, Launch and Liftoff | | |
| 1.2-43 16 mm Tracking | C-54 Aircraft, Launch and Liftoff | | |
| 1.2-35 35 mm Tracking | First Acquisition to LOV Missile Centered | 907 | 5 WD |
| 1.2-36 35 mm Tracking | First Acquisition to LOV Missile Centered | 830 | 5 WD |
| 1.2-39 35 mm Tracking | First Acquisition to LOV Missile Centered and Staging | 260 | 4 WD |
| 1.2-38 70 mm Tracking | First Acquisition to LOV Missile Centered and Staging | 100 | 16 CD |
| 1.2-40 70 mm Tracking | First Acquisition to LOV Missile Centered and Staging | 100 | 16 CD |

# XVI. PRELAUNCH AND COUNTDOWN OPERATIONS

## A. PRELAUNCH SUMMARY

### 1. Final Systems Test

The GT-3 simulated flight test (SFT) was performed successfully on 18 March 1965. The test was conducted in accordance with test procedure (Ref. 4). The flight crew was in the spacecraft during the primary run, and the backup crew was in the spacecraft during the secondary run for spacecraft monitoring and crew training.

The countdown for the secondary run was started at T-45 minutes, but the holdfire -B3 (launch mode check) was programmed on at T-34:59. This holdfire was caused by the launch panel not being reset. After properly resetting the launch panel, the countdown was resumed at T-34:59 and continued until T-20 minutes, at which time Spacecraft Test Conductor called a manual hold due to a UHF communication problem. After the communication problem was repaired, the countdown was resumed and continued until the run was completed.

The countdown for the primary run was started at T-6 minutes. After completion of the primary run, it was determined that the IMU counter-torquing values were incorrect for the secondary and the primary runs. Upon investigation, it was found that the AGE-spacecraft switch was improperly positioned. A rerun off the secondary run was required to satisfy data evaluation requirements.

Prior to picking up the count for the rerun of the secondary run, the flight control Console Operator noticed improper indications on the 2600 console. It was decided to shut down all AGE and replace the roll converter chassis. The new chassis was installed and reverification test of the chassis was performed by running a MOD III interface test and manual azimuth set-in check.

The countdown was picked up at T-6 minutes and continued to T+ 1:39 minutes when the Spacecraft Test Conductor reported he did not receive their event timer start signal nor any computer outputs. It was found that an AGE switch on the spacecraft console was in the "off" position; thus, the computer was turned "off." The switch was turned to the "on" position.

The Test Conductor recycled to T-6 minutes for another start of the secondary run (rerun No. 2). It was then noted that the White Room a-c overvoltage alarm went off. SRO confirmed an industrial power problem. Investigation showed that a bird had hit a power line which caused a momentary short and all evidence indicated the alarm was due to an overshoot during power recovery.

The alarm was reset, and the countdown was picked up at T-6 minutes and completed without incident.

2. Precountdown Operations

Precountdown preparations were initiated on 19 March 1965 and were completed without any problems. On 20 March, the mounting bolts on the spacecraft IMU were replaced. To replace the bolts, cabling on the IMU had to be disconnected. After completion of installation of the bolts and reconnecting of the cables, the interface was retested by performing an abbreviated IGS end-to-end phasing test.

On 22 March, the PCM/FM transmitter was replaced because of a loose pressurization valve. Oxidizer loading was started at 1821 hours EST and completed at 1959 hours EST. A vapor leak was found on the Stage II oxidizer airborne fill and drain disconnect. The pressure cap was removed and a new pressure cap installed and torqued. There was no evidence of the leak after installation of the new pressure cap. Fuel loading was started at 2235 hours EST and was completed at 2335 hours EST on 22 March 1965.

## B. COUNTDOWN SUMMARY

The launch countdown was picked up at 0200 hours EST on 23 March. The 420-minute countdown was performed in accordance with Martin test procedure (Ref. 3). The countdown progressed smoothly to T-35 minutes when a manual hold was initiated by the Test Conductor because of a leak on the S/A 1 oxidizer discharge pressure transducer sensing line fitting. The fitting "jam" nut was backed off and then retorqued, thus stopping the leak. The countdown was resumed at 0849 hours EST-T-35, and continued through liftoff for a very successful launch. It was noted that a communication problem existed on Channel No. 2 throughout the countdown.

# XVII. CONFIGURATION SUMMARY

## A. LAUNCH VEHICLE SYSTEMS DESCRIPTION

The Gemini Launch Vehicle (GLV) is a modified two-stage Titan II intercontinental ballistics missile (ICBM) which has been "man rated" for Gemini usage. The propulsion system in each stage uses hypergolic (self-igniting upon mixture) propellants. Modifications to the basic Titan II vehicle to achieve the "man rated" GLV follow:

(1) Addition of a completely redundant malfunction detection system (MDS).

(2) Replacement of the Titan II inertial guidance system (IGS) with the Mod III G radio guidance system (RGS).

(3) Addition of a three-axis reference system (TARS) to provide attitude reference and open-loop programming to the autopilot.

(4) Addition of a secondary flight control system (FCS).

(5) Addition of a secondary Stage I hydraulic system.

(6) Addition of the capability of switchover to the secondary guidance, flight control, and hydraulic systems.

(7) Provision of redundancy in electrical sequencing by APS and IPS power.

(8) Provision of an engine shutdown capability from the spacecraft.

(9) Provision of a 120-inch diameter cylindrical skirt forward of the Stage II oxidizer tank for mating the spacecraft to the launch vehicle.

(10) Removal of the retrorockets, vernier rockets and associated equipment.

(11) Addition of fuel line spring-piston accumulators and oxidizer line tuned standpipes for suppression of POGO vibrations.

(12) Capability for redundant Stage II engine shutdown (GLV-3 and up).

Significant GLV-3 changes from the GLV-2 configuration are listed in Table XVII-1.

TABLE XVII-1

GLV-3 Modifications

| System | Significant Changes Incorporated in GLV-3 from the GLV-2 Configuration |
|---|---|
| Stage I structure | Transportation section skin splice riveting changed from 1/2-in. pitch to 1 in. pitch.<br>Manhole cover installation changed from narrow to wide gasket on oxidizer and fuel tank. |
| Stage II structure | Manhole cover installation changed from narrow to wide gasket on oxidizer and fuel tank. |
| Propulsion | Contamination shields not incorporated on fuel tank level sensors.<br>Redundant shutdown system provided for Stage II engine through addition of squib-operated valve in oxidizer bootstrap line.<br>Heat shield added to fuel accumulator piston assembly to protect shaft and potentiometer. |
| Flight controls | Added capability for flight crew-initiated switch-back from secondary to primary guidance/flight control system during Stage II flight.<br>Pitch program in TARS package changed to accommodate GT-3 mission requirements.<br>Diodes susceptible to "gold flaking" replaced. |
| Radio guidance | Guidance equations revised for GT-3 insertion conditions.<br>Yaw velocity bias in guidance equation changed (function of spacecraft center of gravity). |
| Hydraulics | Stage I secondary system pressure monitored as shutdown parameter between $T_o$ + 2.0 seconds and TCPS + 1.8 seconds. Limits set at 2800 $\pm$50 psig. |
| Electrical | Added circuitry for guidance/flight control switch-back function. |

TABLE XVII-1 (continued)

| System | Significant Changes Incorporated in GLV-3 from the GLV-2 Configuration |
|---|---|
| Malfunction detection | MDP modified as follows:<br>(1) Provisions for switchback added;<br>(2) Wires shortened and bundle insulation improved;<br>(3) Better diode insulation provided;<br>(4) Three capacitors added to suppress RSP noise.<br>NOTE: These changes were effective on GLV-2; however, on GLV-2 the switchback function was not incorporated in the other systems.<br>Spacecraft display of staging removed. Separate spacecraft displays of Stage I engine S/A 1 and S/A 2 effective through staging now provided. |
| Instrumentation | Various FM/FM and PCM/FM measurements repatched. |
| Range safety | 3.5-second time delay between range safety engine shutdown and command destruct now incorporated in command receivers. |
| Ordnance | None |

## 1. Structure

The GLV is primarily of semi-monocoque shell construction (Stage II tank barrels are monocoque) with integral fuel and oxidizer tanks.

The basic diameter of the structural vehicle is 10 feet, and the length is 89.27 feet. Stage I, which includes the interstage transportation section, the fuel tank, and the oxidizer tank, is 70.67 feet long. The transportation section is assembled to the tank assembly by a manufacturing splice located at Vehicle Station 621.

Stage II consists of the fuel tank assembly and the oxidizer tank assembly, and is 28.27 feet in length.

The two stages are joined at Vehicle Station 500 by four studs and eight explosive nuts, the latter being used for staging.

On both Stage I and Stage II, external conduits are provided along the fuel and oxidizer tanks to house and support the propulsion and electrical lines which lead into the various vehicle compartments.

### a. Stage I

The Stage I structure consists of a fuel tank, an oxidizer tank, skirts at each end of the tanks, an interstage structure and external conduits. Channel-shaped, high strength longerons mounted externally on the fuel tank aft skirt provide separate interfaces for engine truss attachment and for launch stand tiedown. The propellant tanks are capable of withstanding ground and prelaunch loads with no internal pressure applied.

The fuel tank is a completely welded aluminum alloy structure. It consists of an ellipsoidal forward dome, a cylindrical barrel section and the aft cone assembly. An internal conduit, welded to the forward and aft domes, provides for passage of a single oxidizer line from the oxidizer tank through the fuel tank to the engine assembly. An outlet provides the channel for the fuel to pass from the tank to the engine.

The oxidizer tank consists of two end domes welded to a cylindrical section. During the staging event, the forward dome and the surrounding skirt structure are protected from the heat and blast of the Stage II engine exhaust by an ablative coating material.

The interstage section consists of the structure between the stage separation plane and the oxidizer tank forward skirt. A minimum of 7100 square inches of blast port area is provided at the aft end of this section for venting of the Stage II exhaust during staging.

b. Stage II

The Stage II structure includes an oxidizer tank, a fuel tank, skirts at the forward and aft ends of each tank, and external conduits. The tanks are capable of withstanding ground and prelaunch loads with no internal pressure applied.

The fuel tank consists of two ellipsoidal domes, each welded to an extruded aluminum alloy ring frame which forms the juncture of the dome, tank wall and skirt. The cap in the forward dome has a hole to accommodate the passage of the oxidizer line through the tank. The aft dome has provisions for a single fuel outlet. The aft skirt extends to the stage separation plane.

The between-tanks compartment consists of the forward section which is welded to the oxidizer tank aft dome ring frame and the aft section which is welded to the fuel tank forward dome ring frame. Aluminum alloy welded trusses are installed within this structure for support of subassembly components.

The oxidizer tank is similar to the fuel tank. It consists of two ellipsoidal domes, each welded to an extruded aluminum alloy ring frame which forms the juncture of the dome, tank wall and skirt. The aft dome contains the outlet for the oxidizer line. The forward skirt forms the interface between the spacecraft and the launch vehicle. Tension bolts are used in 20 external lugs, which are machined as part of the interface frame, to attach the spacecraft to the launch vehicle. An external 0.05-inch insulating coating is applied to the forward skirt for protection in the event of protuberance heating.

2. Propulsion System

The two-stage propulsion system for the GLV is adapted from the system used on the Titan II ICBM. Minor changes have been made to "man rate" the vehicle and to eliminate those elements of the Titan II system which are not required for the Gemini mission.

a. Stage I

The Stage I engine is comprised of two independently operated subassemblies mounted on a single engine frame. These subassemblies are designed to operate simultaneously. Each contains a thrust chamber, a turbopump and a gas generator.

The thrust chambers are gimbaled to permit vehicle control and stabilization in flight. Gimbal action is provided by tandem hydraulic actuators that operate in response to signals from the FCS.

Propellants are fed to the thrust chamber by turbopumps. Gas generators, used to drive the turbopumps, utilize the same propellants discharged by the pumps; this allows the engine to "bootstrap" during steady-state operation.

Propellants consist of fuel (50% hydrazine combined with 50% unsymmetrical-dimethyl hydrazine) and oxidizer (nitrogen tetroxide). This hypergolic mixture eliminates the need for combustion chamber igniters.

Solid propellant cartridges provide hot gas to start and drive the turbopumps during the engine start period. Shutdown is controlled by the override solenoid valve on the thrust chamber valve.

The thrust chambers are regeneratively cooled by circulating fuel through coolant tubes within the chamber walls. A dry jacket start is employed.

In-flight propellant tank pressurization is provided by an autogenous (self-generating) pressurization system. The fuel tank is pressurized by small portions of the gas generator exhaust gas output. A heat exchanger is provided to cool the gas generator exhaust before supplying it to the fuel tank for pressurization. The oxidizer tank is pressurized by oxidizer which has been heated to a gaseous state. Liquid oxidizer, supplied under pressure from the turbopump, is directed through a superheater where it is vaporized by the heat from the turbine exhaust.

b. Stage II

The Stage II engine is a single-chamber unit similar in operation to the Stage I engine. However, the engine is designed for maximum operating efficiency at high altitude. An ablative skirt is attached to the regeneratively cooled thrust chamber to increase the nozzle expansion ratio for high altitude performance improvement.

Like Stage I, the thrust chamber is gimbaled. Because only pitch and yaw control is provided in this manner, a roll nozzle is incorporated to permit roll control. The roll nozzle directs gas generator exhaust gas overboard, and roll control is obtained through swivel action of the nozzle.

A redundant means of shutdown is provided through a squib-operated valve in the oxidizer bootstrap line.

An autogenous pressurization system is provided for pressurizing the fuel tank in a manner similar to that of Stage I. The oxidizer tank, however, is pressurized before launch, and no additional pressurization is required.

3. Flight Control System

The redundant flight control system (FCS) consists of the (1) primary guidance and control system, (2) secondary guidance and control system and (3) switchover system.

The primary guidance and control system consists of a three-axis reference system (TARS), an adapter package, a Stage I rate gyro package, an autopilot, the primary servovalves in the Stage I tandem actuators, and the Stage II hydraulic actuators. The GE Mod III G radio guidance system (RGS) provides steering commands to the primary guidance and control system during Stage II flight.

The secondary guidance and control system consists of a duplicate Stage I rate gyro package, a duplicate autopilot, the secondary servovalve in the Stage I tandem actuators, and the Stage II hydraulic actuators. The spacecraft inertial guidance system (IGS) provides stabilization and steering commands to the secondary guidance and control system.

The switchover system consists of the redundant power amplifiers located in the malfunction detection package (MDP), the FCS switchover relays located in the adapter package, the Stage I tandem actuator switchover valve, pressure switches, hardover sensors, and the MDS rate switches.

The TARS is used to establish angular reference along the pitch, roll and yaw axes; to provide roll and pitch open-loop guidance programs during Stage I flight; to accept pitch and yaw radio guidance steering signals during Stage II closed-loop guidance operation; and to provide discrete timing functions.

The main function of the adapter package is to condition attitude outputs from the TARS for inputs to the autopilot. The package also houses the FCS switchover relays.

Two sets of rate gyros are utilized for GLV stabilization: the Stage I rate gyro package (one each for the primary and secondary systems) and the Stage II rate gyros located within the redundant autopilot assemblies. During Stage I flight, signals from both the Stage I and the Stage II pitch and yaw rate gyros are summed in a given proportion.

The autopilot contains an 800-cps static inverter, Stage II rate gyros, gain switching module, channel amplifiers and valve drive amplifiers (VDA). The rate and displacement gyro signals are suitably amplified, demodulated, mixed and dynamically compensated, with filtering, in the autopilot to provide vehicle stability. The autopilot output signals are used to drive the servovalves.

Both the primary and secondary FCS operate at all times during flight. During Stage I flight, each servovalve coil in the Stage I tandem actuators receives control signals. At switchover, control of the tandem actuator is switched from the primary to the secondary servovalve.

4. Radio Guidance System

The GE Mod III G RGS is used to guide the GLV Stage II/spacecraft combination in the proper trajectory. The RGS accomplishes this by using steering commands to torque the pitch and yaw attitude gyros in the TARS. The RGS also supplies the Stage II shutdown signal (SECO) in the primary mode.

The RGS airborne components are the pulse beacon unit, rate beacon unit, decoder unit and antenna system.

Vehicle rates are derived by means of the doppler principle, and position tracking radar is utilized to derive the vehicle position as a function of range, elevation and azimuth. The vehicle position and rate information are used by the ground-based guidance computer to generate the steering commands. The messages that contain the steering commands and SECO discrete are monitored by the decoder for validity. If the message is valid, the steering commands are supplied to the control system as pitch and yaw corrections and the SECO command, when present, is supplied to the engine shutdown circuitry.

5. Hydraulic System

The Stage I hydraulic system is redundant. Separate primary and secondary hydraulic circuits power the four tandem actuators for positioning the two thrust chambers in response to signals from the FCS. The system contains two engine-driven pumps; two accumulator-reservoirs; four tandem actuators; one electric motor pump; one test selector valve; one in-line filter; two coaxial disconnects; and instrumentation transducers. Each tandem actuator contains two hydraulically and electrically separated servo loops which can be switched from primary to secondary by external command or due to a pressure loss in the primary system. Each circuit is powered during engine operation by a variable displacement pressure-compensated pump driven through the accessory gearbox of each subassembly. For tests and during launch countdown, an electric motor pump powers the system.

The Stage II hydraulic system contains an engine-driven pump; two engine actuators, a roll nozzle actuator, an accumulator-reservoir, an electric motor pump, an in-line filter; a coaxial disconnect and instrumentation transducers. The system is not redundant and operation is the same as for a single system on Stage I.

## 6. Electrical System

The GLV electrical system is divided into a power distribution system and a sequencing system. The power distribution system consists of the accessory power supply (APS) and the instrumentation power supply (IPS).

The APS and IPS buses are provided with airborne power from separate 28 vdc silver-zinc rechargeable batteries.

The APS provides power to the static inverter, the malfunction detection system (MDS), the APS command receiver, the APS shutdown and destruct circuitry, the RGS, the FCS, the sequencing system and the Stage II engine start circuitry. Static inverter output is 115/200 volts, 400 cps at 750 va.

The IPS provides power to the MDS, MISTRAM, the IPS command receiver, the IPS shutdown and destruct circuitry, the FCS, the sequencing system, Stage II engine start circuitry and the airborne instrumentation system.

The sequencing system provides the proper sequencing of events from Stage I engine start to Stage II engine shutdown. Major functions are: reset Stage I prevalves switch; actuate APS and IPS staging switches; shut down Stage I engine; fire staging nuts; and start Stage II engine.

Redundancy in the form of dual power supplies, relays, motorized switches, diodes and wiring is used throughout the GLV electrical system. A separate battery is provided in Stage I to supply power to the engine shutdown and destruct system if inadvertent separation occurs.

## 7. Malfunction Detection System

The MDS is provided to monitor launch vehicle performance and to supply indications of potentially catastrophic malfunctions and certain significant flight events to the spacecraft. An automatic function is provided for switching from the primary Stage I flight control-guidance-hydraulic combination to the secondary system in the event of a failure in the primary system. Switchover can be initiated by pitch, yaw or roll overrate, Stage I engine hardover, loss of primary system hydraulic pressure or by the flight crew. Switchback to the primary system can be initiated by the flight crew during the Stage II flight.

The main components of the MDS are the malfunction detection package (MDP), the rate switch package (RSP), and the various bilevel

and analog sensors located throughout the launch vehicle. All circuits, components and wiring of the MDS are redundant to provide high reliability.

Functions monitored by the MDS include Stage I engine chamber pressure, Stage II fuel injector pressure, propellant tank pressures, excessive angular rates, staging, loss of Stage I primary hydraulic pressure, engine hardover, and switchover.

8. Instrumentation System

The airborne instrumentation system is comprised of various transducers or measuring points, signal conditioners, a PCM multiplexer, a PCM/FM telemetry unit, an FM/FM telemetry unit, a tape recorder-reproducer, and an antenna system.

The PCM telemetry is a time-multiplexed data system with an input capacity of 196 analog and 48 bilevel channels. The output is a serial pulse train. Samples of input data are as follows:

Analog

| Number of Channels | Samples per Second |
|---|---|
| 85 | 20 |
| 35 | 40 |
| 36 | 100 |
| 20 | 200 |
| 20 | 400 |

Bilevel

| Number of Channels | Samples per Second |
|---|---|
| 40 | 20 |
| 8 | 100 |

The major components of the FM telemetry are an FM multiplexer subcarrier oscillator assembly, an RF transmitter and a separate power amplifier. The system has a seven-channel data capacity.

Prior to staging, the seven FM channels are switched to monitor staging functions, and these signals are transmitted in real time and paralleled on the tape recorder. The recorder is programmed to play back its recording after completion of the staging event.

9. Range Safety System

The GLV range safety system is comprised of the MISTRAM system, command control system and ordnance destruct systems.

The primary tracking and impact prediction system employed in the GLV is the GE MISTRAM system. It consists of an airborne transponder, antennas and ground stations located at Valkaria, Florida and Eleuthera.

In operation, the airborne transponder receives two CW signals from the ground station, and displaces and retransmits them back to the ground station for computation of accurate position, velocity and impact prediction information.

Because line-of-sight transmission between the GLV and Valkaria is impossible, MISTRAM cannot lock in until the GLV attains an altitude of approximately 8000 feet. A beacon system in the spacecraft combined with an AN/FPS-16 radar is used to supply backup tracking information.

The command control system consists of two Advanced Communications, Inc. (ACI) receivers, four flush-mounted antennas, a six-port junction and an interconnecting cable. The redundant receivers each contain a decoder unit capable of receiving a coded FM signal from the ground station and converting this signal (or tones) into commands for (1) engine shutdown and warning to the spacecraft, (2) destruct (command No. 1 must be received 3.5 seconds before command No. 2 can take effect) and (3) ASCO which is a backup to RGS/IGS Stage II engine shutdown. The ASCO command originates at the Burroughs ground guidance computer.

The ordnance destruct system components consist of destruct initiators, primacord, and bidirectional destruct charges. The initiators are basically out-of-line explosive trains which are armed by AGE prior to liftoff. Each of the initiators is connected to two bidirectional destruct charges which are located 180 degrees apart midway between the fuel and oxidizer tanks in each stage. Upon receipt of command No. 2, the IPS and APS electrical signals cause the initiators to ignite the primacord, thus setting off the destruct charges which rupture the tanks.

The Stage I inadvertent separation destruct system is designed to function up to the time of staging enable (approximately LO + 145 seconds). This system consists of a separate destruct battery, lanyard switches between Stages I and II, and the same Stage I initiators, primacord and destruct charges used in the command control ordnance destruct system. Should Stage I inadvertently separate from Stage II

prior to staging enable, the lanyard switches would route the output of the Stage I destruct battery to Stage I engine shutdown and through a 5.5-second delay timer to the initiators, causing the destruct charges to explode.

10. Ordnance Separation System

The launch separation system uses ordnance devices at the four vehicle-to-pad attachment points. Each attachment point has one interconnecting stud with an explosive nut on each end. Each nut assembly contains a gas pressure cartridge with two independent bridgewires mounted internally. The circuits for these bridgewires are activated by a MOCS signal to the launch release control set two seconds after TCPS make.

The airborne separation system uses ordnance devices at the four Stage I and Stage II attachment points located at Vehicle Station 500. Each attachment point has one interconnecting stud with an explosive nut on either end. Each nut assembly is similar to that of the launch separation system. The cartridges are ignited electrically by the staging command (initiated by TCPS).

## B. MAJOR COMPONENTS

The major GT-3 components are as follows:

(1) Spacecraft

(a) Manufacturer: McDonnell Aircraft Corporation

(b) Serial Number: Spacecraft Number 3

(2) Gemini Launch Vehicle

(a) Manufacturer: Martin Company

(b) Serial Number: GLV-3

(c) Air Force Serial Number: 62-12558

(3) Gemini Launch Vehicle systems

The GLV systems and major components are listed in Table XVII-1. Figure XVII-1 shows the general arrangement of the GLV.

TABLE XVII-1

GLV Systems and Major Components

| System/Component | Part No. | Serial No. | Manufacturer |
|---|---|---|---|
| Powerplant | | | |
| Engine, Stage I | YLR87-AJ-7 | 1004 | Aerojet-General Corp. |
| Engine, Stage II | YLR91-AJ-7 | 2004 | Aerojet-General Corp. |
| Propellants | | | |
| Level sensor, propellant | PS830900012-009 | 264 | Bendix |
| Level sensor, propellant | PS830900012-009 | 315 | ↑ |
| Level sensor, propellant | PS830900012-009 | 319 | |
| Level sensor, propellant | PS830900012-009 | 320 | |
| Level sensor, propellant | PS830900012-009 | 333 | |
| Level sensor, propellant | PS830900012-009 | 340 | |
| Level sensor, propellant | PS830900012-009 | 360 | |
| Level sensor, propellant | PS830900012-009 | 362 | |
| Level sensor, propellant | PS830900012-009 | 363 | |
| Level sensor, propellant | PS830900012-009 | 364 | |
| Level sensor, propellant | PS830900012-009 | 371 | |
| Level sensor, propellant | PS830900012-009 | 376 | |
| Level sensor, propellant | PS830900012-009 | 380 | |
| Level sensor, propellant | PS830900012-009 | 385 | |
| Level sensor, propellant | PS830900012-009 | 394 | |
| Level sensor, propellant | PS830900012-009 | 396 | |
| Level sensor, propellant | PS830900012-009 | 397 | |
| Level sensor, propellant | PS830900012-009 | 405 | |
| Level sensor, propellant | PS830900012-009 | 408 | |
| Level sensor, propellant | PS830900012-009 | 411 | |
| Level sensor, propellant | PS830900012-009 | 424 | ↓ |
| Level sensor, propellant | PS830900012-009 | 432 | Bendix |
| Switch, pressure | PS718000100-011 | 0001 | Hydra Electric |
| Switch, pressure | PS718000100-013 | 0008 | ↑ |
| Switch, pressure | PS718000100-015 | 0014 | ↓ |
| Switch, pressure | PS718000100-017 | 0005 | Hydra Electric |

TABLE XVII-1 (continued)

| System/Component | Part No. | Serial No. | Manufacturer |
|---|---|---|---|
| Propellants (cont) | | | |
| Transducer, temperature | PS741000002-005 | 692 | Rosemount Engineering |
| Transducer, temperature | PS741000002-005 | 694 | ↕ |
| Transducer, temperature | PS741000002-005 | 696 | ↕ |
| Transducer, temperature | PS741000002-005 | 699 | Rosemount Engineering |
| Transducer, tank pressure | PS746000002-023 | 1091 | Servonics |
| Transducer, tank pressure | PS746000002-023 | 1093 | ↕ |
| Transducer, tank pressure | PS746000002-023 | 1094 | ↕ |
| Transducer, tank pressure | PS746000002-023 | 1095 | ↕ |
| Transducer, tank pressure | PS746000002-025 | 2089 | ↕ |
| Transducer, tank pressure | PS746000002-025 | 2090 | ↕ |
| Transducer, tank pressure | PS746000002-025 | 2091 | ↕ |
| Transducer, tank pressure | PS746000002-025 | 2099 | Servonics |
| Prevalve, 7 inch | PS475100007-159 | 0700014 | Thiokol, RMD |
| Prevalve, 7 inch | PS475100007-139 | 0700015 | ↕ |
| Prevalve, 4 inch | PS475100006-059 | 0400011 | ↕ |
| Prevalve, 6 inch | PS475100005-159 | 0600010 | ↕ |
| Prevalve, 6 inch | PS475100005-169 | 0600020 | ↕ |
| Prevalve, 6 inch | PS475100005-199 | 0600030 | Thiokol, RMD |
| Burst disc assembly | PS571300000-009 | 219 | Consolidated Controls |
| Burst disc assembly | PS571300000-009 | 220 | ↕ |
| Burst disc assembly | PS571300000-009 | 221 | Consolidated Controls |
| Hydraulics | | | |
| Tandem actuator, Stage I | PS460000008-149 | 023 | Moog Servocontrols, Inc. |
| Tandem actuator, Stage I | PS460000008-149 | 033 | ↕ |
| Tandem actuator, Stage I | PS460000008-159 | 030 | ↕ |
| Tandem actuator, Stage I | PS460000008-159 | 035 | ↕ |
| Actuator, Stage II | PS460000004-019 | 014 | ↕ |
| Actuator, Stage II | PS460000004-019 | 017 | ↕ |
| Actuator, roll nozzle | PS460000005-019 | 006 | Moog Servocontrols, Inc. |

TABLE XVII-1 (continued)

| System/Component | Part No. | Serial No. | Manufacturer |
|---|---|---|---|
| Hydraulics (cont) | | | |
| Filter, hydraulic | PS481000001-009 | B-010 | Aircraft Porous Media |
| Filter, hydraulic | PS481000001-009 | B-009 | Aircraft Porous Media |
| Valve, selector | PS470000029-009 | 013 | Sterer Engineering and Manufacturing Company |
| Accumulator-reservoir, secondary | PS480000013-009 | 120 | Cadillac Gauge |
| Accumulator-reservoir, primary | PS480000013-009 | 118 | ↑ |
| Accumulator-reservoir, Stage II | PS480000013-009 | 117 | Cadillac Gauge |
| Motor pump, electric | PS483100013-009 | C50954 | Vickers, Inc. |
| Motor pump, electric | PS483100013-009 | C50955 | Vickers, Inc. |
| Pump, Stage I engine, primary | PS483100010-019 | A0-14 | New York Air Brake |
| Pump, Stage I engine, secondary | PS483100010-019 | A0-02 | ↑ |
| Pump, Stage II engine | PS483100011-009 | A1-119 | New York Air Brake |
| Coaxial disconnect, primary | PS485000001-009 | 1050 | Aeroquip |
| Coaxial disconnect, secondary | PS485000001-009 | 1013 | ↑ |
| Coaxial disconnect, Stage II | PS485000001-009 | 1000 | Aeroquip |
| Flight Controls | | | |
| Package, TARS | PS640900235-079 | G010 | Honeywell |
| Package, TARS adapter | 424-7562601-059 | B-015 | Martin-Baltimore |
| Autopilot, primary | 424-7562200-079 | D-013 | Martin-Denver |
| Autopilot, secondary | 424-7562200-079 | D-012 | Martin-Denver |
| Rate gyro, primary | PS962000001-049 | 2015 | Giannini Controls |
| Rate gyro, secondary | PS962000001-049 | 2008 | Giannini Controls |
| Guidance | | | |
| Beacon, pulse | 66D802028G1 | G020 | General Electric |
| Beacon, rate | 66D802029G1 | G019 | ↑ |
| Decoder | 66D802030G3 | G021 | General Electric |

TABLE XVII-1 (continued)

| System/Component | Part No. | Serial No. | Manufacturer |
|---|---|---|---|
| Electrical | | | |
| Inverter, static | PS946000001-007 | R-22 | Bendix |
| Power supply, 25 volt | CCI 9401A11-1 | 166 | United Controls |
| Relay, time delay | PS722700003-002 | 3002 | Autronics |
| Relay, time delay | PS722700004-002 | 312 | ↕ |
| Relay, time delay | PS722700004-002 | 307 | |
| Relay, time delay | PS722700005-001 | 219 | Autronics |
| Relay | PS720200002-001 | 0036 | Leach Company |
| Relay | PS720200002-001 | 0039 | ↕ |
| Relay | PS720200002-001 | 0065 | |
| Relay | PS720200002-001 | 0070 | |
| Relay | PS720200002-001 | 0072 | |
| Relay | PS720200002-001 | 0108 | |
| Relay | PS720200002-001 | 0110 | |
| Relay | PS720200002-001 | 0128 | |
| Relay | PS720200002-001 | 0158 | |
| Relay | PS720200002-001 | 0165 | |
| Relay | PS720200002-001 | 0184 | Leach Company |
| Relay assembly (gain change) | 424-7567018-009 | B-004 | Martin-Baltimore |
| Relay assembly (RESS) | 424-7567050-009 | B-010 | Martin-Baltimore |
| Switch, motor-driven | CCI 7241B3-4 | 0002 | Kinetics Corporation |
| Switch, motor-driven | CCI 7241B3-4 | 0012 | ↕ |
| Switch, motor-driven | CCI 7241B2-8 | 0061 | |
| Switch, motor-driven | CCI 7241B2-8 | 0072 | |
| Switch, motor-driven | CCI 7241B2-8 | 0076 | |
| Switch, motor-driven | CCI 7241B2-8 | 0080 | |
| Switch, motor-driven | CCI 7241B2-8 | 0082 | |
| Switch, motor-driven | CCI 7241B2-8 | 0090 | |
| Switch, motor-driven | CCI 7241B2-8 | 0092 | |
| Switch, motor-driven | CCI 7241B2-8 | 0093 | |
| Switch, motor-driven | CCI 7241B2-8 | 0096 | |
| Switch, motor-driven | CCI 7241B2-8 | 0100 | |
| Switch, motor-driven | CCI 7241B2-8 | 0105 | |
| Switch, motor-driven | CCI 7241B2-8 | 0122 | Kinetics Corporation |

TABLE XVII-1 (continued)

| System/Component | Part No. | Serial No. | Manufacturer |
|---|---|---|---|
| Electrical (cont) | | | |
| Switch, motor-driven | CCI 7241B2-8 | 0124 | Kinetics Corporation |
| Switch, motor-driven | CCI 7241B2-8 | 0152 | ↕ |
| Switch, motor-driven | CCI 7241B2-14 | 0030 | ↕ |
| Switch, motor-driven | CCI 7241B2-14 | 0041 | ↕ |
| Switch, motor-driven | CCI 7241B2-14 | 0027 | ↕ |
| Vibration isolation assembly | CCI 7241B2-21 | 0032 | ↕ |
| Vibration isolation assembly | CCI 7241B2-21 | 0026 | ↕ |
| Vibration isolation assembly | CCI 7241B2-21 | 0027 | ↕ |
| Vibration isolation assembly | CCI 7241B2-21 | 0028 | ↕ |
| Vibration isolation assembly | CCI 7241B2-21 | 0029 | ↕ |
| Vibration isolation assembly | CCI 7241B2-21 | 0030 | ↕ |
| Vibration isolation assembly | CCI 7241B2-21 | 0031 | Kinetics Corporation |
| Connector, staging | CCI 8124B1-22 | 0002 | Cannon Electric |
| Connector, staging | CCI 8124B1-23 | 0004 | ↕ |
| Connector, staging | CCI 8124B1-32 | 0007 | ↕ |
| Connector, staging | CCI 8124B1-33 | 0003 | ↕ |
| Connector, staging | CCI 8124B1-34 | 0009 | ↕ |
| Connector, staging | CCI 8124B1-35 | 0013 | ↕ |
| Connector, staging | CCI 8124B1-36 | 0010 | ↕ |
| Connector, staging | CCI 8124B1-37 | 0018 | ↕ |
| Connector, staging | CCI 8124B1-38 | 0030 | ↕ |
| Connector, staging | CCI 8124B1-39 | 0013 | Cannon Electric |
| Disconnect, separation | CCI 8119A1-6 | 0027 | Cannon Electric |
| Disconnect, separation | CCI 8119A1-6 | 0029 | Cannon Electric |
| Switch, lanyard | CCI 7121B4-1 | 0004 | Kinetics Corporation |
| Switch, lanyard | CCI 7121B4-1 | 0010 | Kinetics Corporation |
| Capacitor | CCI 90B15-1 | 0012 | Sprague Electric Company |
| Capacitor | CCI 90B15-1 | 0014 | Sprague Electric Company |
| Diode, 5-amp | CCI 7920A7-2 | N/A | U.S. Semcor |

TABLE XVII-1 (continued)

| System/Component | Part No. | Serial No. | Manufacturer |
|---|---|---|---|
| Electrical (cont) | | | |
| Umbilical, disconnect | PS812400002-039 | 003 | Cannon Electric |
| Umbilical, disconnect | PS812400002-039 | 022 | ↕ |
| Umbilical, disconnect | PS812400002-049 | 031 | ↕ |
| Umbilical, disconnect | PS812400002-049 | 036 | ↕ |
| Umbilical, disconnect | PS812400002-049 | 007 | Cannon Electric |
| Diode box assembly | 424-7567020-009 | B-012 | Martin-Baltimore |
| Diode box assembly | 424-7567020-009 | B-057 | ↕ |
| Diode box assembly | 424-7567020-019 | B-012 | ↕ |
| Diode box assembly | 424-7567020-019 | B-050 | ↕ |
| Diode box assembly | 424-7567020-019 | B-052 | ↕ |
| Semiconductor package | 424-7567029-009 | B-006 | ↕ |
| Semiconductor package | 424-7567029-009 | B-013 | Martin-Baltimore |
| Battery, APS/IPS | PS940300011-001 | 064 | Yardney Electric |
| Battery, APS/IPS | PS940300011-001 | 063 | ↕ |
| Battery, disconnect | CCI 9401B15-1 | 031 | Yardney Electric |
| Microfuse | CCI 8609B7-3 | N/A | Littlefuse, Inc. |
| Microfuse post | CCI 8609B7-4 | N/A | Littlefuse, Inc. |
| Range Safety | | | |
| Command receiver, APS/IPS | R-423A | 31 | Advanced Communications, Inc. |
| Command receiver, APS/IPS | R-423A | 32 | Advanced Communications, Inc. |
| Transponder, MISTRAM | 764145061 | 95 | GFP |
| Malfunction Detection | | | |
| Package, rate switch | PS830600015-027 | 4012 | Giannini Controls |
| Package, malfunction detection | 424-7569205-189 | B-008 | Martin-Baltimore |
| Connector, stage separation | CCI 8119A1-5 | 0034 | Cannon Electric |
| Connector, stage separation | CCI 8119A1-6 | 0037 | Cannon Electric |

TABLE XVII-1 (continued)

| System/Component | Part No. | Serial No. | Manufacturer |
|---|---|---|---|
| Malfunction Detection (cont) | | | |
| MDTCPS, S/A 1 primary | 284321 | 618 | Aerojet-General Corp. |
| MDTCPS, S/A 1 redundant | 284321 | 863 | ↑ |
| MDTCPS, S/A 2 primary | 284321 | 806 | |
| MDTCPS, S/A 2 redundant | 284321 | 565 | |
| MDFJPS, S/A 3 primary | 711049-1 | 811 | ↓ |
| MDFJPS, S/A 3 redundant | 711049-1 | 809 | Aerojet-General Corp. |
| Instrumentation | | | |
| Multiplexer/encoder, PCM | PS640900237-039 | 012 | Epsco, Inc. |
| Telemetry unit, PCM-FM | 424-7565020-039 | D-003 | Martin-Denver |
| Signal conditioner | 424-7565006-019 | B-006 | Martin-Baltimore |
| Ordnance | | | |
| Initiator, destruct | PS601100013-015 | 36 | Thiokol Chemical Corp. |
| Initiator, destruct | PS601100013-015 | 33 | Thiokol Chemical Corp. |
| Nut, hold-down | PS335200000-001 | 14334 | High-Shear Corp. |
| Nut, hold-down | PS335200000-001 | 14335 | ↑ |
| Nut, hold-down | PS335200000-001 | 14337 | |
| Nut, hold-down | PS335200000-001 | 14338 | |
| Nut, hold-down | PS335200000-001 | 14339 | |
| Nut, hold-down | PS335200000-001 | 14341 | |
| Nut, hold-down | PS335200000-001 | 14342 | |
| Nut, hold-down | PS335200000-001 | 14343 | |
| Nut, separation | PS335200000-003 | 15070 | |
| Nut, separation | PS335200000-003 | 15072 | |
| Nut, separation | PS335200000-003 | 15073 | |
| Nut, separation | PS335200000-003 | 15075 | |
| Nut, separation | PS335200000-003 | 15077 | |
| Nut, separation | PS335200000-003 | 15079 | |
| Nut, separation | PS335200000-003 | 15080 | ↓ |
| Nut, separation | PS335200000-003 | 15084 | High-Shear Corp. |

TABLE XVII-1 (continued)

| System/Component | Part No. | Serial No. | Manufacturer |
|---|---|---|---|
| Ordnance (cont) | | | |
| Cartridge, gas pressure-prevalve | PS601100010-001 | N/A (12 used) | McCormick Selph |
| Cartridge, gas pressure-dropweight | PS601100010-001 | N/A (4 used) | ↕ |
| Cartridge, gas pressure-holddown nut | PS601100010-001 | N/A (8 used) | ↕ |
| Cartridge, gas pressure-separation nut | PS601100010-001 | N/A (8 used) | McCormick Selph |
| Primacord assembly | 424-14060001-009 | N/A | The Ensign-Bickford Co. |
| Primacord assembly | 424-14060001-039 | N/A | ↕ |
| Primacord assembly | 424-14060001-049 | N/A | ↕ |
| Primacord assembly | 424-14060001-059 | N/A | ↕ |
| Primacord assembly | 424-14060001-079 | N/A | ↕ |
| Primacord assembly | 424-14060001-089 | N/A | The Ensign-Bickford Co. |
| Destruct charge, bidirectional | PS601100009-001 | 9, 10, 11, 12 | Francis Associates |

LAUNCH VEHICLE UMBILICAL SYSTEMS INTERFACE

| CODE | FUNCTION | SYSTEM | LOCATION |
|---|---|---|---|
| 2BA | AIR COND | GUIDANCE AIR COND STG II | STA 371.522 QUAD I 82½° OFF BL O |
| S2BOV | OXID. VENT | OXID STG II | STA 371.522 QUAD. II 85° OFF BL O |
| 2B2E | ELECTRICAL | ELECTRICAL STG II | STA 402.472 QUAD II 82½° OFF BL O |
| 2B1E | ELECTRICAL | ELECTRICAL STG II | STA 402.472 QUAD II 65½° OFF BL O |
| 2BFVT | FUEL VENT TOPPING | FUEL STAGE II | STA. 406.491 QUAD II 36°20' OFF BL O |
| S2BFV | FUEL VENT | FUEL STG II | STA 404.472 QUAD II 37½° OFF BL O |
| S3BH | HYDRAULIC | HYDRAULIC STG II | STA 470.125 QUAD II 15° OFF BL O |
| 1 3BA | AIR CONDITIONING | ENGINE AREA STG II | STA 474.875 QUAD II 30° OFF BL O |
| S3BF | FUEL FILL AND DRAIN | FUEL STG II | STA 492.250 QUAD II 15° OFF BL O |
| 3BFD | FUEL PRESS. SEQ. VALVE DRAIN | FUEL STG II | STA 492.250 QUAD II 30° OFF BL O |
| S3BO | OXID. FILL AND DRAIN | OXID STG II | STA 492.250 QUAD II 72° OFF BL O |
| 3B1E | ELECTRICAL | ELECTRICAL STG II | STA 492.250 QUAD II 45° OFF BL O |
| 1C1FD | TUBO-PUMP FUEL DRAIN | FUEL STG I | STA 554.750 QUAD II 17½° OFF BL O |
| 1COD | TUBO-PUMP OXID. DRAIN | OXID STG I | STA 554.750 QUAD I 17½° OFF BL O |
| S1DOV | OXID. VENT | OXID. STG I | STA 630.727 QUAD I & II WL 60.0 |
| S2DFV | FUEL VENT | FUEL STG I | STA 963.326 QUAD II 40° OFF BL O |
| 3D1M | MALFUNCTION DETECTION SYS. | MALFUNCTION STG. I | STA. 214.873 QUAD I 38 3/4° OFF BL O |
| 3D2M | MALFUNCTION DETECTION SYS. | MALFUNCTION STG I | STA 1214.873 QUAD III 38½° OFF BL O |
| 3D1E | ELECTRICAL | ELECTRICAL STG. I | STA 1216.691 QUAD II 20° OFF BL O |
| S3DF | FUEL FILL AND DRAIN | FUEL STG. I | STA 1243.560 QUAD I |
| S3DFD | FUEL DRAIN - PRE-VALVE | FUEL STG I | STA. 1244.123 QUAD III |
| S3DOD | OXID. DRAIN - PRE-VALVE | OXID. STG I | STA 1250.560 QUAD II |
| S3D1H | HYDRAULIC SUPPLY AND RETURN | HYDRAULIC STG. I PRIMARY | STA 1255.835 QUAD I |
| S3DO | OXID. FILL AND DRAIN | OXID. STG I | STA 1249.560 QUAD IV |
| 2BOVT | OXID. VENT TOPPING | OXID. STG II | STA. 351.802 QUAD II 4° OFF WL 60 |
| 1DOVT | OXID. VENT TOPPING | OXID. STG. I | STA. 630.727 QUAD II 60° OFF BL O |
| 2DFVT | FUEL VENT TOPPING | FUEL STAGE I | STA 963.326 QUAD II 50° OFF BL O |
| 3D2E | ELECTRICAL | ELECTRICAL STG. I | STA 1216.691 QUAD II 10° OFF BL O |
| S3D2H | HYDRAULIC SUPPLY AND RETURN | HYDRAULIC STG. I SECONDARY | STA. 1255.835 QUAD. II |
| 2 3D1OC | OXID. REMOTE CHARGING SYSTEM | OXID. STG. I | STA. 1224.311 QUAD III 22½° OFF B.L.O. |
| 2 3D2OC | OXID. REMOTE CHARGING SYSTEM | OXID. STG. I | STA. 1224.311 QUAD III 17½° OFF B.L.O. |

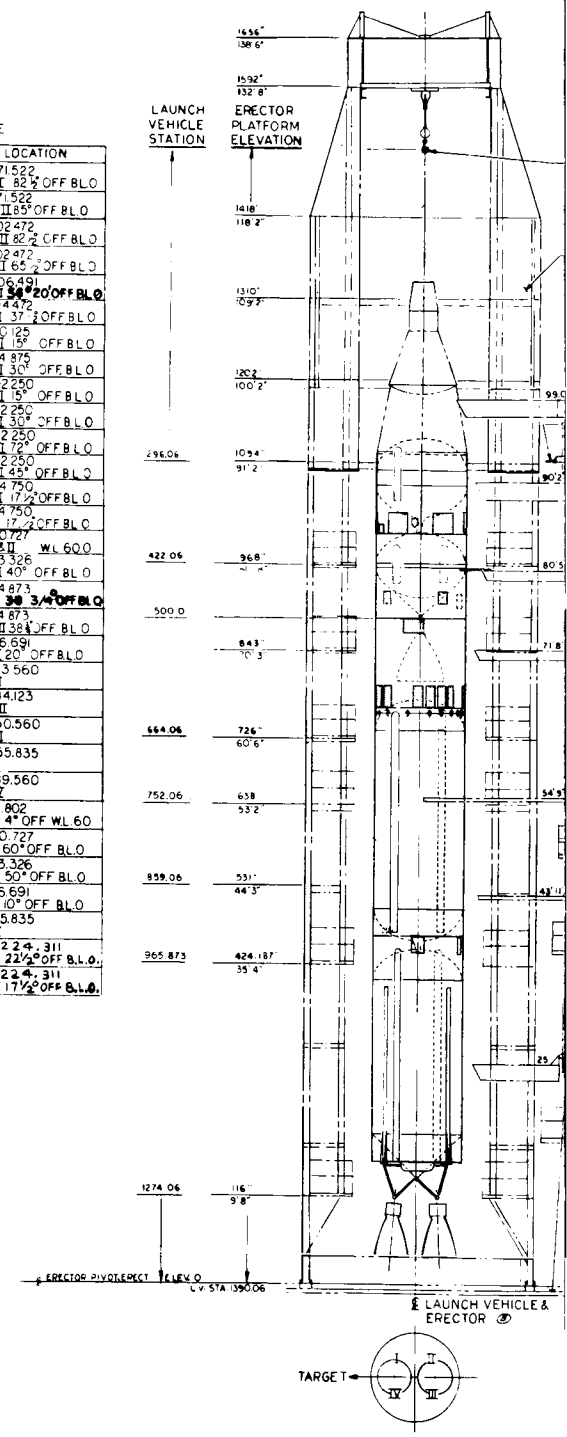

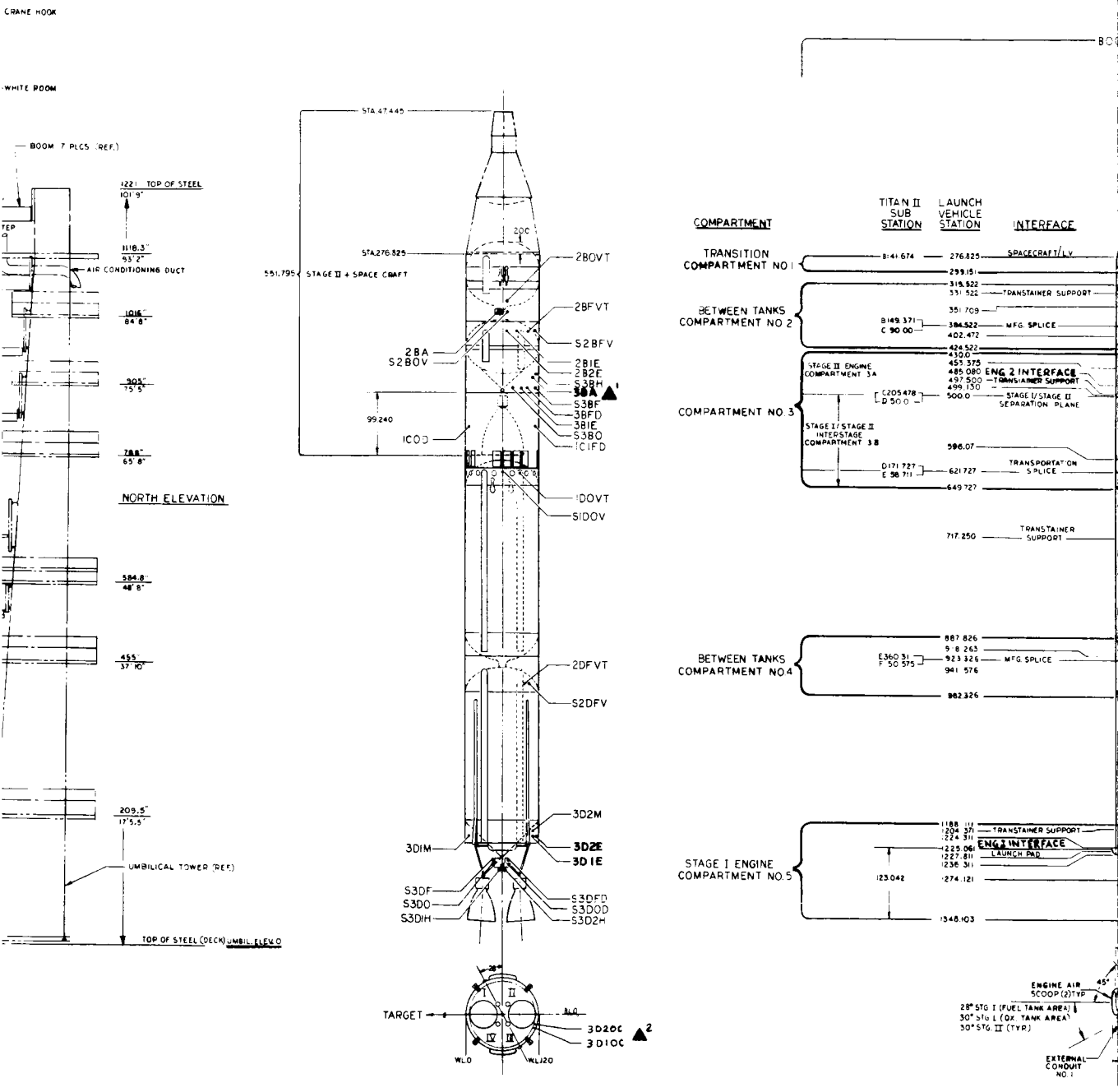
CRANE HOOK
WHITE ROOM
BOOM 7 PLCS (REF.)
1221 TOP OF STEEL
101' 9"
1118.3"
93' 2"
AIR CONDITIONING DUCT
1016"
84' 8"
905"
75' 5"
788"
65' 8"
NORTH ELEVATION
584.8"
48' 8"
455"
37' 10"
209.5"
17' 5.5"
UMBILICAL TOWER (REF.)
TOP OF STEEL (DECK) UMBIL. ELEV. 0
STA 47.445
STA 276.825
551.795
STAGE II + SPACE CRAFT
200
2BOVT
2BFVT
S2BFV
2BA
S2BOV
2BIE
2B2E
S3BH
3BA
S3BF
3BFD
3BIE
S3BO
1C1FD
99.240
1COD
1DOVT
S1DOV
2DFVT
S2DFV
3D2M
3DIM
3D2E
3D1E
S3DF
S3DO
S3DIH
S3DFD
S3DOD
S3D2H
TARGET
ALO
3D2OC
3D1OC
WLO
WL120
COMPARTMENT
TITAN II SUB STATION
LAUNCH VEHICLE STATION
INTERFACE
TRANSITION COMPARTMENT NO 1
8141.674
276.825
SPACECRAFT/LV
299.151
BETWEEN TANKS COMPARTMENT NO 2
315.522
351.522
TRANSTAINER SUPPORT
351.709
B149.371
C 90.00
384.522
MFG. SPLICE
402.472
424.522
COMPARTMENT NO 3
STAGE II ENGINE COMPARTMENT 3A
450.0
453.375
485.080
ENG 2 INTERFACE
497.500
TRANSTAINER SUPPORT
499.130
C205.478
D 50.0
500.0
STAGE I/STAGE II SEPARATION PLANE
STAGE I/STAGE II INTERSTAGE COMPARTMENT 3B
596.07
D171.727
E 58.711
621.727
TRANSPORTATION SPLICE
649.727
717.250
TRANSTAINER SUPPORT
BETWEEN TANKS COMPARTMENT NO.4
887.826
918.263
E360.31
F 50.575
923.326
MFG. SPLICE
941.576
982.326
STAGE I ENGINE COMPARTMENT NO.5
1188.311
1204.371
TRANSTAINER SUPPORT
1224.311
1225.061
ENG 1 INTERFACE
1227.811
LAUNCH PAD
1236.311
123.042
1274.121
1348.103
ENGINE AIR SCOOP (2) TYP
28" STG I (FUEL TANK AREA)
30" STG I (OX. TANK AREA)
30" STG. II (TYP.)
EXTERNAL CONDUIT NO. 1

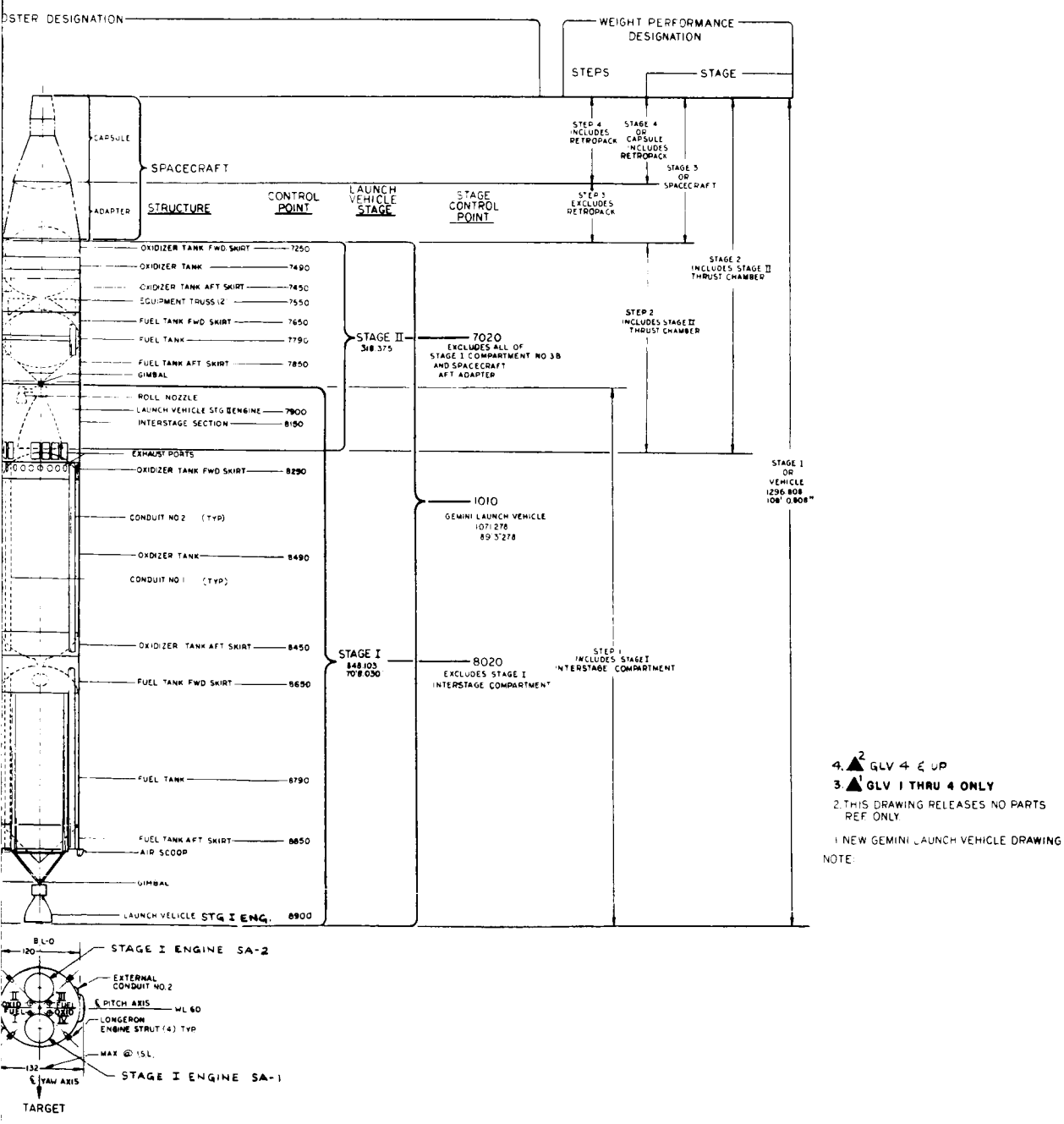


Fig. XVII-1. Gemini Launch Vehicle General Arrangement

# XVIII. REFERENCES


1. "Launch Vehicle No. 2 Flight Evaluation," Engineering Report 13227-2, Martin Company, [redacted]ltimore, Maryland, March 1965. [redacted]

2. "Launch Vehicle No. 2 Launch Attempt Evaluation," Engineering Report 13227-2X, Martin Company, Baltimore, Maryland, January 1965. [redacted]

3. "Launch Vehicle No. 1 Flight Evaluation," Engineering Report 13227-1, Martin Company, Baltimore, Maryland, May 1964. [redacted]

4. "Martin-Canaveral Test Procedure," 424-875-ETR, Revision H.

5. "Martin-Canaveral Test Procedure," 424-876-ETR, Revision C.

6. "Total Uncertainties on Fully Corrected and Smoothed MOD III Radio Guidance and Instrumentation System, Gemini III," letter from General Electric Company (Mr. G. D. Smith) to Martin Company (Mr. W. D. Smith), 8 April 1965, Syracuse, New York.

7. "Master Measurements List," LV-220, Revision H, Martin Company, Baltimore, Maryland, 15 February 1965.

8. "Revised GLV Trajectory Dispersion Analysis," LV-274-3, Martin Company, Baltimore, Maryland, February 1964.

9. "Flight Weight Coordination Report Post-Flight Weight, GT-3," LV-165-3B, Martin Company, Baltimore, Maryland, 7 April 1965.

10. "Gemini Launch Vehicle Performance Specification," MB-1046, SCN-6, Martin Company, Baltimore, Maryland, 15 March 1965.

11. "GT-3 Guidance Equations Accuracy Estimate," Aerospace Technical Memorandum No. ATM-65 (5126-40)-16, Aerospace Corporation, El Segundo, California, 18 February 1965. [redacted]

12. "GLV-3 Incentive Catalog," IM-103, Martin Company, Baltimore, Maryland, 1 February 1965.

13. "Gemini Launch Vehicle Structural Analysis (Interim) Report," Engineering Report 13028, Martin Company, Baltimore, Maryland, February 1964. [redacted]

14. "Flight Hazard Analysis," LV-378, Martin Company, Baltimore, Maryland, February 1965. [redacted]

15. "Gemini Launch Vehicle Acoustic and Vibration Environment," Part 1: Vibration and Part 2: Acoustics, Engineering Report 12414, Martin Company, Baltimore, Maryland, December 1963.

16. "GLV System Environmental Requirements and Tests," MB-1043, Martin Company, Baltimore, Maryland, September 1963.

17. "Analysis of Gemini Airborne Equipment Temperature Rise," LV-136, Revision A, Martin Company, Baltimore, Maryland, February 1963.

18. "Predicted Heating Rates and Structural Temperatures for the Gemini Launch Vehicle," LV-43, Martin Company, Baltimore, Maryland, September 1963.

19. "GT-3 Pre-flight Report," LV-326-3, Martin Company, Baltimore, Maryland, 1965. [redacted]

20. "Subsystem Engineering Analysis YLR 87-AJ-5 and YLR 91-AJ-5 Rocket Engines," AGC-521-3.15 Q-10, Aerojet-General Corporation, Sacramento, California, 29 March 1963. [redacted]

21. "Subsystem Engineering Analysis YLR 87-AJ-5 and YLR 91-AJ-5 Rocket Engines," AGC 521-3.15 Q-15, Aerojet-General Corporation, Sacramento, California, 22 July 1964. [redacted]